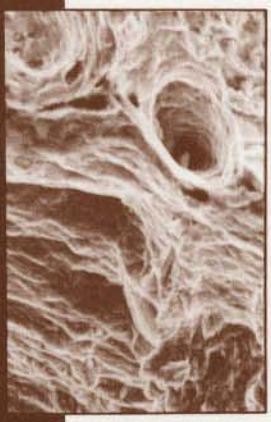

Elastic-Plastic Fracture Test Methods

The User's Experience

Wessel/Loss, *editors*

ASTM STP 856

ELASTIC-PLASTIC FRACTURE TEST METHODS: THE USER'S EXPERIENCE

A symposium sponsored by
ASTM Committee E-24 on
Fracture Testing
Louisville, KY, 20–22 April 1983

ASTM SPECIAL TECHNICAL PUBLICATION 856
E. T. Wessel, Westinghouse R&D
Center, and F. J. Loss, Materials Engineering
Associates, editors

ASTM Publication Code Number (PCN)
04-856000-30

1916 Race Street, Philadelphia, PA 19103

Library of Congress Cataloging in Publication Data

Elastic-plastic fracture test methods.

(ASTM special technical publication; 856)
Papers presented at the Symposium on User's Experience with Elastic-Plastic Fracture Toughness Test Methods.
Includes bibliographies and index.
"ASTM publication code number (PCN) 04-856000-30."
1. Fracture mechanics—Congresses. 2. Materials—Testing—Congresses. 3. Elasticity—Congresses. 4. Plasticity—Congresses. I. Wessel, E. T. II. Loss, F. J. III. ASTM Committee E-24 on Fracture Testing. IV. Symposium on User's Experience with Elastic-Plastic Fracture Toughness Test Methods (1983: Louisville, KY) V. Series.
TA409.E423 1985 620.1'126 84-70607
ISBN 0-8031-0419-7

Library of Congress Catalog Card Number: 84-70607

Printed in Ann Arbor, MI
April 1985

Foreword

The symposium on User's Experience with Elastic-Plastic Fracture Toughness Test Methods was presented at Louisville, KY, 20–24 April 1983. The symposium was sponsored by ASTM Committee E-24 on Fracture Testing. E. T. Wessel, Westinghouse R&D, and F. J. Loss, Materials Engineering Associates, presided as chairmen of the symposium and are editors of the publication.

Related ASTM Publications

Fracture Mechanics: Fifteenth Symposium, STP 833 (1984), 04-833000-30

Elastic-Plastic Fracture: Second Symposium—Volume I: Inelastic Crack Analysis and Volume II: Fracture Curves and Engineering Applications, STP 803 (1983), 04-803000-30

Crack Arrest Methodology and Applications, STP 711 (1980), 04-711000-30
Elastic-Plastic Fracture, STP 668 (1979), 04-668000-30

A Note of Appreciation to Reviewers

The quality of the papers that appear in this publication reflects not only the obvious efforts of the authors but also the unheralded, though essential, work of the reviewers. On behalf of ASTM we acknowledge with appreciation their dedication to high professional standards and their sacrifice of time and effort.

ASTM Committee on Publications

ASTM Editorial Staff

Janet R. Schroeder
Kathleen A. Greene
Helen M. Hoersch
Helen P. Mahy
Allan S. Kleinberg
Susan L. Gebremedhin

Contents

Introduction

Interest in elastic-plastic fracture has increased significantly over the past decade. New approaches to analyze structural performance under elastic-plastic conditions have been accompanied by the development of test methods to characterize material behavior in a manner compatible with the analysis. Key issues that must be addressed in test method development are characterization of geometry factors in the structure with respect to crack-tip constraint, specimen size effects, crack initiation, stable crack extension, and fracture mode. A rational test method should provide information from a laboratory specimen, which lends itself to a standard approach with due regard to these key issues such that useful information can be developed for the assessment of structural integrity.

Several test methods have been developed as a result of advances in elastic-plastic fracture mechanics, for example, J-integral R-curve, tearing instability, and crack-tip opening displacement (CTOD) approaches. A few of these methods have been standardized in the United States and other countries, and other methods are under development. A critical review of these procedures was considered necessary for others to benefit from the experience gained to date. This information will lead to improvements in existing standards and provide the basis for new test methods. The Symposium on User's Experience with Elastic-Plastic Fracture Toughness Test Methods was held in Louisville in April 1983 to provide a forum for an exchange of ideas among scientists and engineers who are actively engaged in test method development and application. This symposium provided a unique opportunity for representatives from several countries to present and discuss their views relating to experimental characterization of elastic-plastic fracture behavior in terms of laboratory specimens. Primary objectives were to define the problems and limitations associated with current test methods as a means to assess the state of the art, to describe new experimental techniques, and to highlight areas requiring further investigation.

The content of this publication will be particularly useful to experimentalists working in the field of elastic-plastic fracture. This should include researchers involved in material property studies, test laboratories, and organizations involved with structural safety and licensing. The contents of this book represent the current status of the elastic-plastic test methods that are in widespread use. Emphasis is placed on techniques used by different laboratories in measuring the parameters required by the various test methods. Since many of these tech-

niques are new, it is expected that some will be refined and perhaps incorporated in appropriate test methods. This symposium was meant to provide a report of progress aimed at focusing investigations in this field worldwide.

Four major areas were addressed by the symposium: comparison of standards in various countries; problems encountered with test methods; improvements in techniques and methods; and problems associated with material characterization in the brittle-to-ductile transition region. The symposium concluded with a workshop that provided the participants with an opportunity to critique the papers. Emphasis in the presentations was on application of the methods to characterize material behavior in terms of the J integral, R curve, and CTOD approaches. Methods to measure stable crack initiation and growth were also discussed with emphasis on the compliance and electric potential drop techniques.

The collection of papers from this symposium represents the first of its kind in the United States and provides an assessment of the state of the art in many of the elastic-plastic test procedures in current use or under development. Reviews of developments on this topic in Europe and Japan are provided. It is hoped that this volume will encourage further progress in the field and provide the basis for future symposia on this topic.

The editors would like to acknowledge the assistance of J. D. Landes, J. P. Gudas, W. R. Andrews, and M. E. Lieff in planning and organizing the symposium. We also express our appreciation to all of the attendees for their open and fruitful presentations and discussion at the symposium, and for their subsequent suggestions and recommendations pertinent to improvement of the test methods; to the authors for submitting the formal papers that comprise this publication; and to the many reviewers whose high degree of professionalism ensured the quality of the publication. The editors also wish to express their appreciation to the ASTM Publications staff for their contributions in preparing the STP.

F. J. Loss
Materials Engineering Associates, Lanham, MD 20706; symposium co-chairman and co-editor.

E. T. Wessel
Westinghouse R&D Center, Pittsburgh, PA 15235; symposium co-chairman and co-editor.

Hideo Kobayashi,[1] *Haruo Nakamura,*[1] *and Hajime Nakazawa*[1]

Comparison of J_{Ic} Test Methods Recommended by ASTM and JSME

REFERENCE: Kobayashi, H., Nakamura, H., and Nakazawa, H., **"Comparison of J_{Ic} Test Methods Recommended by ASTM and JSME,"** *Elastic-Plastic Fracture Test Methods: User's Experience, ASTM STP 856,* E. T. Wessel and F. J. Loss, Eds., American Society for Testing and Materials, 1985, pp. 3–22.

ABSTRACT: The elastic-plastic fracture toughness J_{Ic} test method recommended by the Japan Society of Mechanical Engineers (JSME) Standard Method of Test for Elastic-Plastic Fracture Toughness J_{Ic} S001-1981 is outlined. Its applicability and utility compared with the ASTM Test for J_{Ic}, a Measure of Fracture Toughness (E 813) are discussed in this paper. It appears that JSME Standard S 001-1981 offers a superior approach to ASTM J_{Ic} determination in some aspects.

KEY WORDS: ductility, tearing, fracture tests, elastic-plastic fracture toughness, J integral, J_{Ic} test, blunting line, *R* curve, stretch zone, ductile tearing, tearing modulus, plane strain, metallic materials

In Japan, the Japan Society of Mechanical Engineers (JSME) Committee S781 on Standard Method of Test for Elastic-Plastic Fracture Toughness J_{Ic} (Chairman: H. Miyamoto, Vice-chairman: H. Kobayashi) standardized a J_{Ic} test method, which was published in October 1981 under the designation JSME S 001-1981.

The objective of the J_{Ic} test method recommended by JSME is to determine J_{Ic}, the value of J integral at the onset of Mode I, plane-strain, ductile tearing for metallic materials. The recommended test specimens are compact (CT) or three-point bend types that contain deep fatigue cracks. The JSME standard includes two multiple-specimen techniques and three single-specimen techniques. In the former, the J_{Ic} value is determined by the stretch zone width *SZW* technique or the *R*-curve technique. In the latter, the electrical potential, ultrasonic, or acoustic emission techniques can be applied. This method is not recommended in cases where unstable cleavage fracture occurs before the determination of the *R* curve. Under small scale yielding conditions, however, the JSME standard includes the modified ASTM Test for Plane-Strain Fracture Toughness of Metallic Materials (E 399) as a special case.

[1] Associate professor, research associate, and professor, respectively, Department of Physical Engineering, Tokyo Institute of Technology, Ohokayama, Meguro, Tokyo, Japan 152.

On the other hand, ASTM Test for J_{Ic}, a Measure of Fracture Toughness (E 813) was published in August 1981. A J_{Ic} criterion and its test method were developed by Begley and Landes [*1*] and ASTM Task Group E24.01.09 [2]. Their test method was adopted into ASTM E 813. In ASTM E 813, attention is directed mainly to processes of ductile tearing, and the following J versus Δa blunting line is assumed

$$\Delta a = \delta/2 = J/2\sigma_{fs} \tag{1}$$

where δ is the crack-tip opening displacement, and σ_{fs} is the average of the yield stress σ_{ys} in uniaxial tension (offset = 0.2%) and the tensile strength σ_B. The R curve is determined by the multiple-specimen technique or the single-specimen technique (unloading compliance). The J_{Ic} value is defined as a J value at the intersection of the blunting line and the R curve. There are several differences between the two methods recommended by ASTM and JSME.

The purpose of this paper is to give a brief description of the J_{Ic} test method recommended by JSME and to discuss its applicability and usefulness with special attention given to a comparison of this method with that recommended by ASTM.

Stretched Zone Width Technique

The stretched zone width *SZW* technique has been proposed by the present authors [*3*]. This technique is the most important one recommended in the JSME Standard. The procedure is summarized as follows.

1. Statically load two or more specimens to selected different displacement levels that are lower than those at the onset of ductile tearing. Calculate the J integral of each specimen by a modified Merkle-Corten equation [*4*] in terms of an area under load versus load-line displacement record.
2. Unload each specimen and mark the crack extension caused by plastic blunting that occurred during loading by an appropriate method such as subsequent fatigue cycling. Then, break each specimen open to reveal the fracture surface.
3. Measure microscopically the subcritical *SZW* from the fatigue precrack tip to the tip of the marked crack at three or more locations spaced evenly from 3/8 to 5/8 of the specimen thickness as shown in Fig. 1. Determine the average SZW.
4. Plot all *J*-SZW data points, and determine a best-fit blunting line through an original point as shown in Fig. 2.
5. Pull three or more identical specimens apart by overload.
6. Measure microscopically the critical stretched zone widths (SZW_c) by the same method as the measurement of *SZW*. Determine the average SZW_c.
7. Mark J_{in} as a J value at the intersection of the line $SZW = SZW_c$ and the blunting line as shown in Fig. 2.

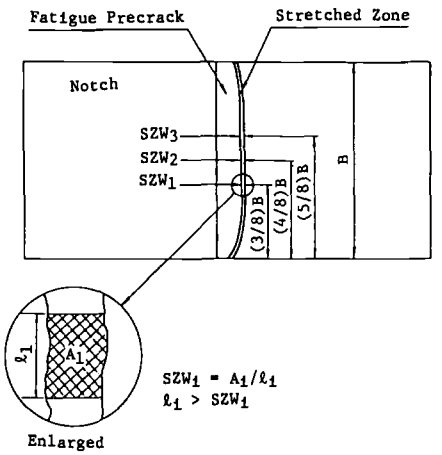

FIG. 1—*Schematic illustration of SZW measurements in the JSME standard.*

8. $J_{in} = J_{Ic}$ if the requirements on fatigue precracking, and the following validity requirements are satisfied

$$b_0 = W - a_0 \geq 25(J_{in}/\sigma_{fs}) \tag{2}$$

$$B \geq 25(J_{in}/\sigma_{fs}) \tag{3}$$

where b_0 is the initial uncracked ligament, W is the specimen thickness, and a_0 is the original crack size. Equation 2 is not necessarily required if J_{In} is confirmed to be constant irrespective of B by an additional test for specimens that have a different B from the original B. It is desired to change B to more than twice as large or less than half as small as the original B.

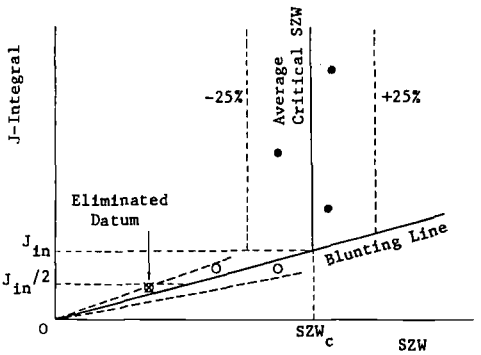

FIG. 2—*Schematic illustration of SZW technique in the JSME standard.*

R-Curve Technique

The *R*-curve technique recommended by JSME is almost identical to that recommended by ASTM except for the following four points.

1. The blunting line is determined experimentally in the same method as the *SZW* technique.
2. Four or more specimens are loaded up to displacement levels so as to cause ductile tearing. By following the procedure described in the *SZW* technique, the physical crack extension Δa is determined as the average of the measurements that are made at three or more locations spaced evenly from 3/8 to 5/8 of the specimen thickness as shown in Fig. 3.
3. Using a method of least squares, a linear regression line of J upon Δa is determined as shown in Fig. 4. All data points that do not fall within $\Delta a < 1$ mm are eliminated, and at least four data points must remain. This linear regression line represents the beginning stage of material resistance to ductile tearing (R curve). The intersection of the R curve with the blunting line marks J_{in} as shown in Fig. 4.
4. $J_{in} = J_{Ic}$ if the following validity requirement is satisfied in addition to the requirements of Item 8 in the *SZW* technique.

$$(dJ/da)_R \leq (1/2)\ (dJ/da)_B \tag{4}$$

where $(dJ/da)_R$ is the slope of the regression line and $(dJ/da)_B$ is the slope of the blunting line.

Single Specimen Techniques

The JSME standard includes three single-specimen techniques. The electrical potential, ultrasonic, or acoustic emission techniques can be used to make the following measurement nondestructively and continuously during loading: (1) the difference of electrical potential, (2) the variation of ultrasonic signal amplitude, or (3) the variation of acoustic-emission event count, accumulated energy

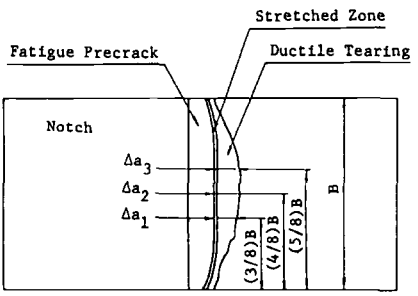

FIG. 3—*Schematic illustration of* Δa *measurements in the JSME standard.*

count, or amplitude distribution of event. The procedure is summarized as follows.

1. Each single-specimen technique actually requires three specimens, namely, A, B, and C, to compensate for the uncertainty of the technique.
2. Determine a load-line displacement, $\delta_{in}(A)$, of the first specimen A at the onset of ductile tearing by one of the single-specimen techniques.
3. Load the second specimen B up to a displacement level that is larger than $\delta_{in}(A)$ but is smaller than $1.1\delta_{in}(A)$.
4. Load the third specimen C up to a displacement level that is larger than $0.9\delta_{in}(A)$ but is smaller than $\delta_{in}(A)$.
5. Monitor the specimens B and C during loading by one of the single-specimen techniques so as to confirm the onset of ductile tearing on the specimen B but no onset on the specimen C.
6. Determine a load-line displacement $\delta_{in}(B)$ of the specimen B at the onset of ductile tearing.
7. Unload, mark, and break each specimen by following the procedure described in Item 2 of the *SZW* technique. Examine fractographically the fracture surface of the three specimens and confirm the onset of ductile tearing on the specimens A and B but not on the specimen C.
8. Determine J_{in} as an average of two J values corresponding to $\delta_{in}(A)$ and $\delta_{in}(B)$.
9. $J_{in} = J_{Ic}$ if the requirements of Item 8 in the *SZW* technique are satisfied.

The comparison of the J_{Ic} test methods recommended by ASTM and JSME is summarized in Table 1.

Evaluation of Blunting Line

For an "ideal crack" (a saw-cut crack or a fatigue precrack where the previous fatigue loading effect can be considered negligible compared with the following

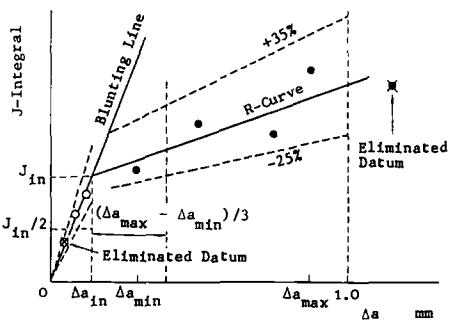

FIG. 4—*Schematic illustration of* R-*curve technique in the JSME standard.*

TABLE 1—*Comparison of J_{Ic} test methods recommended by JSME and ASTM.*

Item	JSME Standard S001-1981	ASTM E 813
Specimen thickness B	$B \geq 25\, J_{in}/\sigma_{fs}$[a]	$B \geq 25\, J_Q/\sigma_{fs}$
Applicable multiple-specimen techniques	*SZW* technique or *R*-curve technique	*R*-curve technique
Blunting line	to be determined experimentally[b]	$\Delta a = J/2\sigma_{fs}$
Location for measurement of Δa	midthickness average at 3 or more locations	through-thickness average at 9 or more locations
Limit of Δa	$\Delta a \leq 1.0$ mm	between 0.15 and 1.5 mm offset lines
Applicable single-specimen techniques	electrical potential, ultrasonic, or acoustic emission technique	unloading compliance technique

[a]Not necessarily required if J_{in} is confirmed to be constant irrespective of B.
[b]Recommended equations on blunting line can be used without experimental determination for some specified materials.

monotonic load), a relation between the crack-tip opening displacement δ and the stress intensity factor K, or the J-integral of the form

$$\delta = (1 - \nu^2)\, K^2/\lambda E\sigma_{fs} \tag{5}$$

in the linear elastic fracture mechanics case or

$$\delta = J/\lambda\sigma_{fs} \tag{6}$$

in the elastic-plastic fracture mechanics case under the plane-strain conditions has been found, where ν is Poisson's ratio, E is Young's modulus, and λ is about 2. A schematic section profile of the subcritical stretch zone is shown in Fig. 5. The geometric relation between Δa or *SZW* and δ is given by

$$\Delta a = SZW = \delta/2\tan\beta = J/2\lambda\sigma_{fs}\tan\beta \tag{7}$$

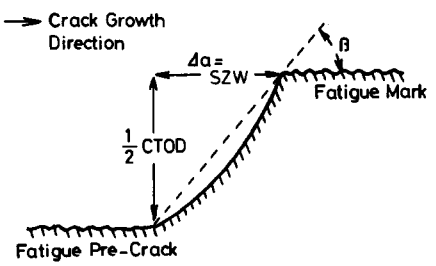

FIG. 5—*Schematic section profile of subcritical stretch zone.*

where 2β is the crack-tip blunting angle, and the quantity $2\tan\beta$ has a value between 1.4 and 2.

In recent years, many experimental data of *SZW* have been accumulated in the results of the J_{Ic} tests carried out by the present authors [*5*] and other researchers [*6*] in Japan. Figures 6 and 7 present all the results on a double-logarithmic plot of *SZW* for various materials as functions of J/σ_{fs} and J/E. If we assume relationships of two types of form

$$SZW = C_1 (J/\sigma_{fs}) \tag{8}$$

$$SZW = D_1 (J/E) \tag{9}$$

the values of C_1 and D_1 are as shown in Table 2. As the present authors [*5,6*] have shown, the *J-SZW* blunting line of the ideal crack depends not on σ_{ys} or on σ_{fs} but on E.

A specific examination in Fig. 6 shows that the values of C_1 for alloy steels ($0.23 < C_1 < 0.57$) and aluminum alloys ($0.23 < C_1 < 0.44$) have a tendency to become larger as σ_{fs} becomes larger [*7*]. It should be noted that if J/σ_{ys} instead of J/σ_{fs} is taken as a parameter, dependence on σ_{ys} becomes more remarkable. Therefore, it is evident that the relation between δ or Δa and J does not obey Eqs 5 or 6. For intermediate-strength materials (σ_{fs} = from 500 to 800 MPa for

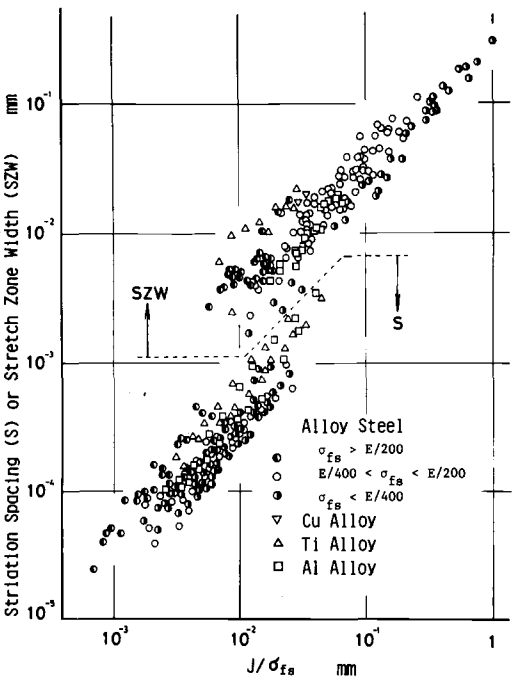

FIG. 6—*Comparison of* SZW *and* S *as functions of* J/σ_{fs} *and* $\Delta J/\sigma_{fs}$.

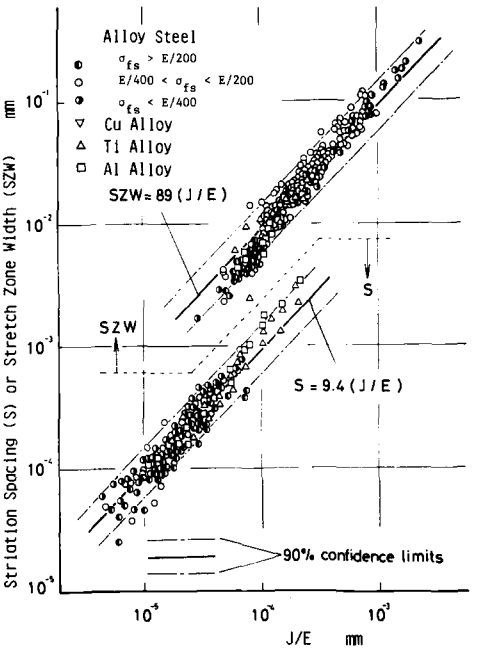

FIG. 7—*Comparison of* SZW *and* S *as functions of* J/E *and* ΔJ/E.

alloy steels, and σ_{fs} = 200 ~ 400 MPa for aluminum alloys), however, Eqs 5 or 6 can stand, and the value of C_1 is [7]

$$C_1 = 1/4 \tag{10}$$

This value is plausible, since it can be obtained assuming that $\lambda = 2$ and $\beta = 45°$ in Eq 7. In the JSME standard, Eq 10 is recommended as the blunting line and can be used without experimental determination for some specified materials. On the other hand, the value of D_1 shows the structure-insensitive property as stated earlier. Metallurgical variables, such as heat treatments [5], anisotropies [7] and weldments [8], and test temperatures [3,9] have little influence on the value of D_1, although they have a large influence on σ_{fs}. This is the reason why the experimentally determined *J-SZW* blunting line is utilized in the JSME standard. It may be concluded that Eq 1 in the ASTM standard generally should not be used as the blunting line.

TABLE 2—*Values of* C_1 *and* D_1 *with assumed relationships of Eqs 8 and 9.*

Mean Values	Deviations for 90% Confidence Limits
$\bar{C}_1 = 0.37$	$0.152 < C_1 < 0.90$
$\bar{D}_1 = 89$	$54.7 < D_1 < 143$

For comparison, the striation spacing S in fatigue crack growth when the stress ratio R is about 0 are plotted in Figs. 6 and 7 as functions of $\Delta J/\sigma_{fs}$ and $\Delta J/E$, where ΔJ is the cyclic J integral converted from the stress intensity factor range ΔK. Note that the use of ΔJ does not mean the elastic-plastic fracture mechanics case, as all the data on S satisfy small-scale yielding conditions. If we assume relationships of two types of form

$$S = C_2(\Delta J/\sigma_{fs}) \tag{11}$$

$$S = D_2(\Delta J/E) \tag{12}$$

the values of C_2 and D_2 are as shown in Table 3. The values of C_2 show the same tendency as C_1. It should be noted that not C_1, but ratio C_2/C_1 or D_2/D_1 becomes the structure-insensitive property.

From the structure-insensitive property of C_2/C_1, it is clear that the values of *SZW* and S for the same J value are as different as approximately one order of magnitude. The reason for the smaller width of the striation should be attributed to plasticity-induced crack closure under the cyclic load [*10*]. A specific examination in Fig. 6 shows that the values of C_2/C_1 are 0.12, 0.18, and 0.11 for the alloy steels, the aluminum alloys and a Ti-6Al-4V alloy, respectively [*7*]. The mean values of C_2/C_1 for the three alloys become about 0.13. The present authors have shown that the fatigue crack acceleration during a single peak overload can be exactly evaluated from the ratio C_2/C_1 [*11*]. The result is given by the following expression in the case that R of the previous fatigue load is about 0

$$GS/S = [(C_2/C_1)J_2 + (J_1 - J_2)]/[(C_2/C_1)J_1] \tag{13}$$

where

GS = giant striation spacing formed during single peak overload,
S = striation spacing formed by previous fatigue load,
J_1 = experimentally determined J integral for single peak overload,
$J_2 = (1 - \nu^2)(K_2^2/E)$, and
K_2 = stress-intensity factor for previous fatigue load.

For $J_1 >> J_2$, GS would become *SZW*, and the crack can be considered as the ideal crack. The comparison of predictions and experiments for the three alloys is shown in Fig. 8.

TABLE 3—*Values of* C_1 *and* D_1 *with assumed relationships of Eqs 11 and 12.*

Mean Values	Deviations for 90% Confidence Limits
$\bar{C}_2 = 0.039$	$0.0179 < C_2 < 0.085$
$\bar{D}_2 = 9.4$	$6.0 < D_2 < 14.8$

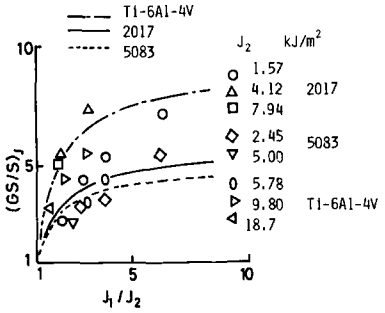

FIG. 8—*Fatigue crack acceleration during a single peak overload.*

The fatigue precrack requirement in the JSME standard is almost identical to that of the ASTM E 399 and is given by

$$K_f < 0.6[EJ/(1 - \nu^2)]^{1/2} \tag{14}$$

where K_f is the maximum stress-intensity factor at fatigue precracking and can be converted into J_f. Upon the substitutions of J_2 and J_1 for J_f and J, respectively, Eq 14 becomes

$$J_1/J_2 > 2.8 \tag{15}$$

As shown by Fig. 8, Eq 15 prescribes a reasonable range for the ideal crack from the engineering viewpoint.

Evaluation of *R* Curve

A comparison of the *J-R* curves based on Δa_{avg} and Δa_{max} obtained by the multiple-specimen technique was made for the ½ CT, 1 CT, and 2 CT specimens of an A533B-1 (Unified Number System [UNI] K12539) steel (quenched and tempered, σ_{fs} = 585 MPa), where Δa_{avg} is the average physical crack extension in the ASTM E 813 and Δa_{max} is the maximum physical crack extension near the midthickness of the specimens. These two different measurement techniques result in markedly differing Δa-values caused by crack tunneling near the midthickness of the specimens (see Fig. 9).

The tearing modulus [*12*]

$$T_J = (E/\sigma_{fs}^2)(dJ/da) \tag{16}$$

was evaluated by making a statistical curve-fitting to the *R*-curve data. The equation form is

$$\Delta a = \sum_{k=0}^{n} C_k J^k \tag{17}$$

where C_k is a constant. Changing n from 2 to 15, the value of n to give the best fit was chosen. Differentiating and substituting Eq 17 into Eq 16, T_J was obtained as shown in Figs. 10 and 11. In Fig. 10, the plateaus of T_J exist in the early stage of crack extension. The value of ½ CT is larger than those of 1 CT and 2 CT. This arises because the data of ½ CT did not satisfy the following validity criterion of J

$$B,\ b > 25(J/\sigma_{fs}) \tag{18}$$

It is clear that the Δa_{avg} range of the plateau decreases with decreasing specimen sizes. On the other hand, T_J becomes constant for a wide range of Δa_{max} as shown in Fig. 11.

Figure 12 shows a relation between Δa_{avg} and Δa_{max} for each specimen. In the early stage of crack extension, the following equation stands

$$\Delta a_{avg} = 0.38\ \Delta a_{max} \tag{19}$$

As the crack extends, Eq 19 ceases to hold, and the data approach the line of $\Delta a_{avg} = \Delta a_{max}$. The deviation points from Eq 19 correspond to occurrence of

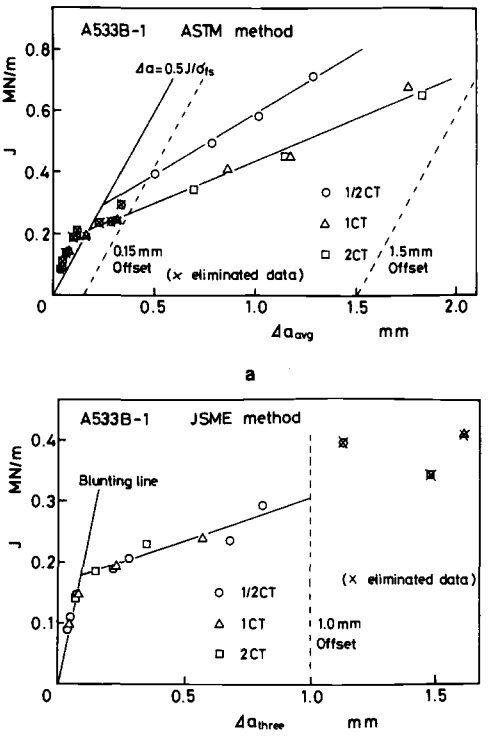

FIG. 9—J-Δa *curves in A533B-1 steel:* (a) *ASTM method and* (b) *JSME method.*

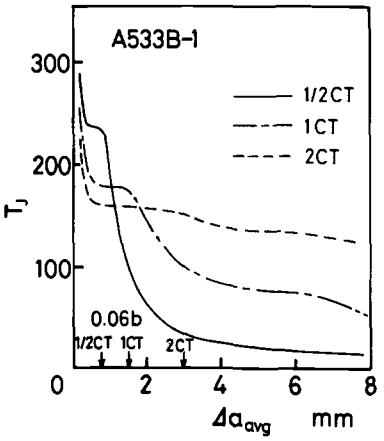

FIG. 10—*Tearing modulus* T_J *as a function of* Δa_{avg}.

shear lips at the specimen surfaces. So, mixed mode fracture appears thereafter. Moreover, these points agree well with those where the plateaus of T_J end. On the other hand, the relation between $\Delta a_{avg}/b$ and $\Delta a_{max}/b$ shows little influence on b or a/W as shown in Fig. 13. The Δa range where Eq 19 stands is given by

$$\Delta a_{avg}/b \leq 0.23$$
$$\Delta a_{max}/b \leq 0.09 \tag{20}$$

And Eq 20 also prescribes the plateau range in Fig. 10. Within the range of Eq 20, the following equation stands between T_J based on Δa_{max} and Δa_{avg}

$$T_J(\Delta a_{max}) = 0.38\, T_J(\Delta a_{avg}) \tag{21}$$

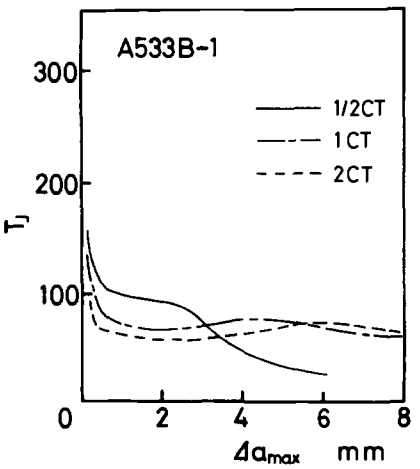

FIG. 11—*Tearing modulus* T_J *as a function of* Δa_{max}.

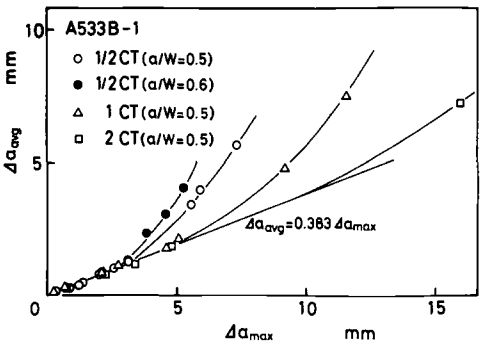

FIG. 12—*Relation between* Δa_{avg} *and* Δa_{max}.

Figure 14 shows the effect of the side groove on the plateau of T_J. It is clear that the side groove has no effect on the plateau if T_J is evaluated from the J-Δa_{max} curve. So, the Mode I, plane-strain, ductile tearing resistance can be obtained not from the J-Δa_{avg} curve but from the J-Δa_{max} curve.

In the J_{Ic} test, the linear regression line of J upon Δa should represent the beginning stage of the J-R curve. So, it may be concluded that the J-Δa_{max} curve is more useful than the J-Δa_{avg} curve because the former becomes a straight line over a wider range of Δa compared with the latter.

Evaluation of J_{Ic} Test Methods

SZW *Technique*

Figure 15 shows the J-Δa_{avg} curve in an HT60 steel (T-L orientation, σ_{fs} = 617 MPa), where the blunting line is determined experimentally [7]. After the onset of ductile tearing, a scatter is observed reflecting the wide variation of J_{Ic} of each specimen. In this case, it is not reasonable to determine one R-curve using multiple specimens. Furthermore, it was difficult to control the Δa value because of the low value of dJ/da, which resulted in insufficient data being obtained

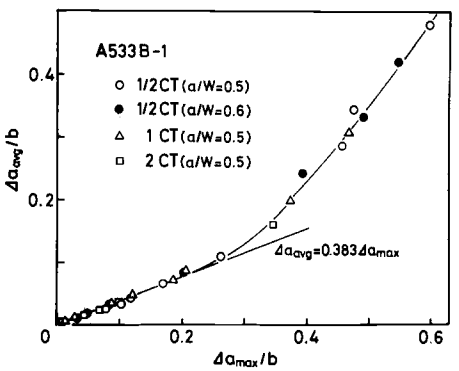

FIG. 13—*Relation between* $\Delta a_{avg}/b$ and $\Delta a_{max}/b$.

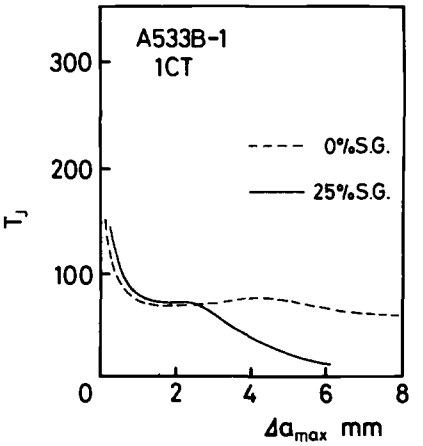

FIG. 14—*Effect of side groove on plateau of* T_J.

within the offset line. The *R*-curve method can not be applied for this kind of material.

The relation between *SZW* and *J* in HT60 is shown in Fig. 16 [7]. Open and solid symbols in Fig. 16 represent data of *SZW* and SZW_c, respectively. All the data before *SZW* reaches SZW_c fall on a *J-SZW* blunting line with little variation. On the other hand, a fair amount of scatter on SZW_c exists. Fractographic observation revealed that splitting by elongated and pancaked dimples occurred along the alloy-rich band oriented at right angles to the crack front. Accordingly, the critical stretched zone is divided into several parts. Also, its width, SZW_c, for each specimen has a wide variation caused by the material inhomogeneity. The J_{Ic} value for each specimen, however, can be evaluated exactly at the intersection of the blunting line and each SZW_c.

Figure 17 shows the relation between *SZW* and *J* in A533B-1 (Q and T). The data include the results in the longitudinal (L-T), long transverse (T-L), and

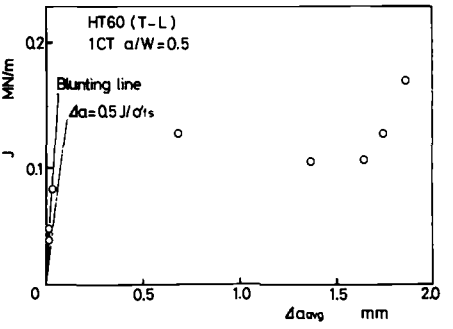

FIG. 15—J-Δa_{avg} *curve in HT60 (T-L).*

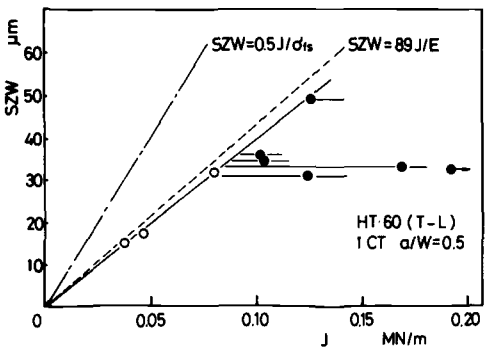

FIG. 16—*Relation between* SZW *and* J *in HT60 (T-L).*

short transverse (S-L) orientations. All the data before *SZW* reaches SZW_c fall on a *J-SZW* blunting line regardless of the orientation. On the other hand, a fair amount of differences on SZW_c exists. So, the J_{Ic} value for each orientation can be evaluated at the intersection of the blunting line obtained for the L-T orientation and each SZW_c.

Figure 18 shows the relation between *SZW* and *J* in an A533B-1 steel (normalized and tempered, σ_{fs} = 597 MPa) [9]. The data include the results over a high-temperature range from room temperature to 573 K. All the data before *SZW* reaches SZW_c fall on a *J/E-SZW* blunting line regardless of the temperature. So, the J_{Ic} value for each temperature can be evaluated at the intersection of the blunting line obtained for the room temperature and each SZW_c. In this temperature range, however, the SZW_c values show the temperature-insensitive property, and an upper shelf J_{Ic} value exists.

The temperature-insensitive property of the blunting line has been found in a 4340 (UNS G 43370) steel (σ_{fs} = 1100 MPa) over a low-temperature range

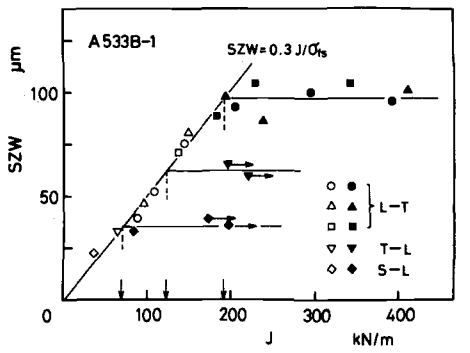

FIG. 17—*Relations between* SZW *and* J *in A533B-1 steel (L-T, T-L, S-L).*

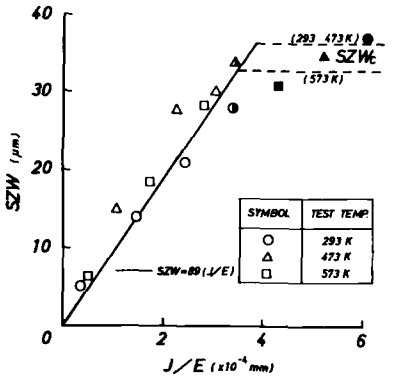

FIG. 18—*Relations between* SZW *and* J/E *in A533B-1 steel (N and T) over a high-temperature range.*

from 133 K to room temperature as shown in Fig. 19 [*3*]. In this case, the J_{Ic} value increases with increasing the temperature.

Figure 20 shows the relation between *SZW* and *J* in weldment of a 304 steel (σ_{fs} = 431 MPa) [*8*]. It also includes the result of base metal. All the data before *SZW* reaches SZW_c fall on a *J-SZW* blunting line. So, the J_{Ic} value for the weldment can be evaluated at the intersection of the blunting line obtained for the base metal and SZW_c for the weldment. It should be noted that the J_{Ic} value in the weldment is considerably low compared with the conservative J_{Ic} value in base metal where the transitional stage of crack extension exists.

The blunting line shows the structure-insensitive property as stated earlier. The *SZW* technique is useful for the establishment of this property. If the property is established for a wide range of metallic materials, there is a possibility of evaluating J_{Ic} more simply by measuring SZW_c from a few specimens broken by overload. Also, the *SZW* technique is useful for the partial confirmation of the statistical J_{Ic} test results obtained by the single-specimen techniques.

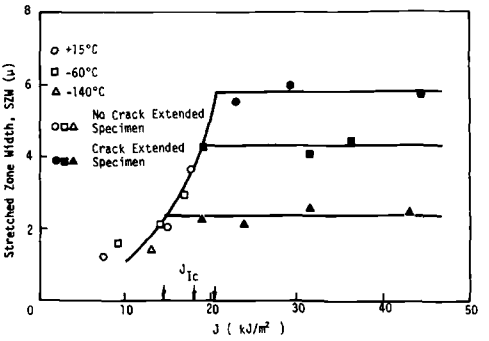

FIG. 19—*Relations between* SZW *and* J *in 4340 steel over a low-temperature range.*

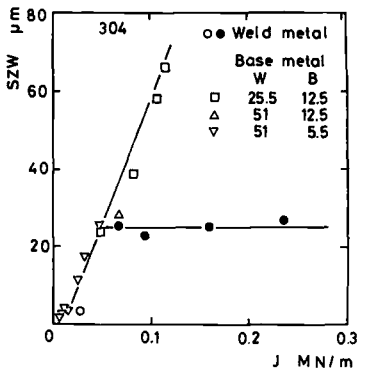

FIG. 20—*Relations between* SZW *and* J *in weldment and base metal of 304 steel.*

R-*Curve Technique*

The relation between J and Δa in 304 steel is shown in Fig. 21 [7]. The assumed blunting line given in Eq 1 does not represent the experimentally derived one. The slope of the J-Δa curve after the onset of ductile tearing ($J > 490$ kN/m) is almost identical to that of the blunting line. So, it is not possible to determine J_{Ic} by the R-curve technique.

The total average Δa_{avg} (ASTM E 813), the midthickness average Δa_{three} (JSME standard), and the maximum Δa_{max} physical crack extensions were measured in an HT80 steel (σ_{fs} = 789 MPa). A comparison of the R-curves for three measurement techniques is shown in Fig. 22 [7]. It is clear that the three different techniques result in markedly differing Δa values caused by crack tunneling near the midthickness of the specimens. However, this difference has little influence on the J_{Ic} value. Figure 23 shows the relation between *SZW* and J in this material [7]. The J_{Ic} value obtained from the *SZW* technique is in good agreement with that obtained from the R-curve technique, because the misfit of Eq 1 for the actual blunting line is not so large.

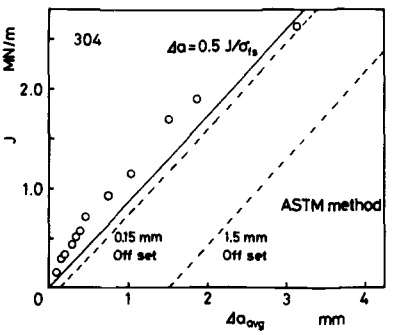

FIG. 21—J-Δa_{avg} *curve in steel 304.*

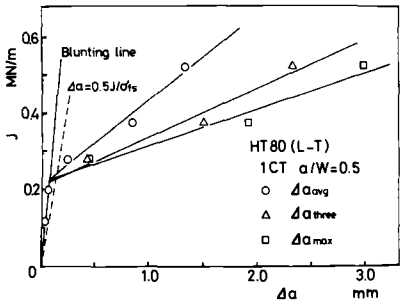

FIG. 22—J-Δa_{avg}, Δa_{three}, *and* Δa_{max} *curves in HT80 steel.*

Figure 9 shows the results of the *R*-curve techniques in A533B-1 steel (Q and T) where (a) and (b) represent the ASTM and JSME methods, respectively. The JSME method utilizes the data just after the onset of ductile tearing. So, all the valid data in the JSME method are regarded as invalid in the ASTM method because of the data limitation of 0.15-mm lower offset line. However, the difference between these two methods has little influence on the valid J_{Ic} values, which are almost identical to those obtained by the *SZW* technique (see Fig. 24). Strictly, the J_{Ic} value of the ASTM method is somewhat larger than that of the JSME method. The reason may be attributed to the misfit of Eq 1 for the actual blunting line in the ASTM method.

In the ASTM method, the valid J_{Ic} value of the ½ CT specimen was not obtained because of the following specimen size restriction

$$B,\ b > 15(J/\sigma_{fs}) \tag{22}$$

where b is the uncracked ligament. If the restriction of Eq 22 is neglected, the conditional value J_Q of the ½ CT specimen becomes larger than the valid J_{Ic} values of the 1 CT and 2 CT specimens.

On the other hand, according to the JSME method, the J_{Ic} value of the ½

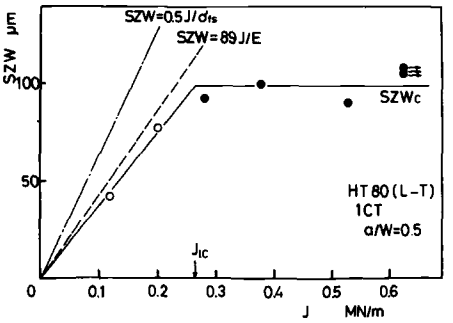

FIG. 23—*Relation between* SZW *and* J *in HT80 steel.*

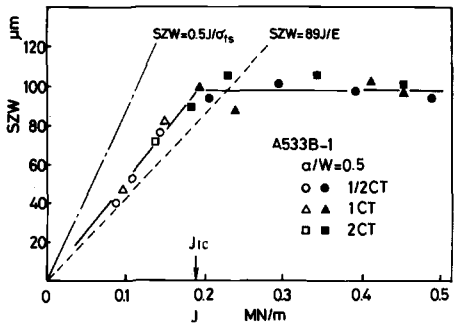

FIG. 24—*Relation between* SZW *and* J *in A533B-1 steel.*

CT specimen can be obtained, because the Δa_{three} data near J_{Ic} are utilized. The R-curves for different specimen sizes obtained in this method have a pivot point at J_{Ic}, although the specimen size influences the dJ/da value. In the JSME method, the restriction of Eq 22 is not needed necessarily for the R-curve data if the J_{Ic} value satisfies the restrictions of Eqs 2 and 3. So, it may be concluded that, according to the JSME method, the J_{Ic} value can be evaluated using smaller specimen size compared with the ASTM method. Furthermore, the dJ/da value for Δa_{three} is smaller than that for Δa_{avg}, and this gives a sharp intersection of the R curve and the blunting line, which results in the clear determination of J_{Ic}.

As shown by Figs. 9 and 10, the J-Δa_{avg} being nonlinear, the slope of the curve decreases with increasing Δa_{avg} and tends to show the plateau. Therefore, in some materials, the use of the linear regression line of J upon Δa_{avg} for large values of Δa_{avg} between the two offset lines in the ASTM method can overestimate J_{Ic}. Also, it should be noted that the use of Eq 1 instead of the experimentally determined blunting line in the R-curve technique can overestimate J_{Ic} for some low- and intermediate-strength materials as stated earlier.

Single-Specimen Techniques

The JSME standard accepts three single-specimen techniques. The electrical potential and ultrasonic techniques yield fairly good results in some intermediate- and high-strength materials. The acoustic emission technique is affected strongly by the microstructure of materials, so that the applicability of the technique to the J_{Ic} test depends on the material type [*13*]. The unloading compliance technique in ASTM E 813 is not particularly recommended in the JSME standard because of the inaccuracy of the technique for small values of Δa.

Conclusion

The elastic-plastic fracture toughness J_{Ic} test method recommended by JSME S001-1981 is outlined. Its applicability and utility compared with ASTM E 813 are discussed in this paper. It appears that JSME S001-1981 offers a superior approach to ASTM J_{Ic} determination in some aspects.

Acknowledgment

The authors wish to express their thanks to Prof. Hiroshi Miyamoto, Science University of Tokyo, Dr. Naotake Ohtsuka, Chiyoda Chemical Engineering and Construction Co., Ltd., and Norio Takashima, a graduate student at Tokyo Institute of Technology, for their help and contribution to this work.

References

[1] Begley, J. A. and Landes, J. D., *Fracture Toughness, Proceeding of the 1971 Symposium on Fracture Mechanics Part II, STP 514*, American Society for Testing and Materials, Philadelphia, 1972, pp. 1–23.

[2] Clarke, G. A., Andrews, W. R., Begley, J. A., Donald, J. K., Embley, G. T., Landes, J. D., McCabe, D. E., and Underwood, J. H., *Journal of Testing and Evaluation*, Vol. 7, No. 1, Jan. 1979, pp. 49–56.

[3] Kobayashi, H., Hirano, K., Nakamura, H., and Nakazawa, H., *Advances in Research on the Strength and Fracture of Materials, Proceedings*, Fourth International Conference on Fracture, Vol. 3, Pergamon Press, New York, 1977, pp. 583–592.

[4] Clarke, G. A. and Landes, J. D., *Journal of Testing and Evaluation*, Vol. 7, No. 5, Sept. 1979, pp. 264–269.

[5] Kobayashi, H., Nakamura, H., and Nakazawa, H., *Recent Research on Mechanical Behavior of Solids*, University of Tokyo Press, Tokyo, Japan, 1979, pp. 341–357.

[6] Kobayashi, H., Nakamura, H., and Nakazawa, H., *Mechanical Behaviour of Materials, Proceedings*, Third International Conference on Materials, Vol. 3, Pergamon Press, New York, 1979, pp. 529–538.

[7] Kobayashi, H., Nakamura, H., and Nakazawa, H., *Elastic-Plastic Fracture: Second Symposium, Vol. II—Fracture Resistance Curves and Engineering Applications, STP 803*, American Society for Testing and Materials, Philadelphia, 1983, pp. II-420–II-438.

[8] Kobayashi, H., Nakamura, H., and Nakazawa, H., *Proceedings of the Fourth International Conference on Pressure Vessel Technology*, Vol. I, Institution of Mechanical Engineers, London, 1980, pp. 251–256.

[9] Hirano, K., Kobayashi, H., and Nakazawa, H., *Mechanical Behaviour of Materials, Proceedings*, Third International Conference on Materials, Vol. 3, Pergamon Press, New York, 1979, pp. 457–467.

[10] Kobayashi, H., Nakamura, H., and Nakazawa, H., *Mechanics of Fatigue*, AMD-Vol. 47, American Society of Mechanical Engineers, New York, 1981, pp. 133–150.

[11] Kobayashi, H., Nakamura, H., Hirano, A., and Nakazawa, H., *Materials, Experimentation and Design in Fatigue, Proceedings, Fatigue '81*, Westbury House, Surrey, United Kingdom, 1981, pp. 318–327.

[12] Paris, P. C., Tada, H., Zahoor, A., and Ernst, H., *Elastic-Plastic Fracture, STP 668*, J. D. Landes, J. A. Begley, and G. A. Clarke, Eds., American Society for Testing and Materials, Philadelphia, 1979, pp. 5–36.

[13] Ohtsuka, N., Nakano, M., and Ueyama, H., *Fracture Mechanics of Ductile and Tough Materials and Its Application to Energy Related Structures, Proceedings*, USA-Japan Joint Seminar, Martinus Nijhoff Publishers, The Hague, Netherlands, 1981, pp. 139–148.

Oliver L. Towers[1] *and Michael G. Dawes*[1]

Welding Institute Research on the Fatigue Precracking of Fracture Toughness Specimens

REFERENCE: Towers, O. L. and Dawes, M. G., **"Welding Institute Research on the Fatigue Precracking of Fracture Toughness Specimens,"** *Elastic-Plastic Fracture Test Methods: The User's Experience, ASTM STP 856*, E. T. Wessel and F. J. Loss, Eds., American Society for Testing and Materials, 1985, pp. 23–46.

ABSTRACT: Three techniques are described for growing uniform fatigue cracks in fracture toughness specimens originally containing welding residual stresses. These are local compression, reverse bending, and the use of a high R-ratio in the fatigue cycle. The possible effects of the techniques on the subsequent measurements of fracture toughness are assessed. The relative merits of the three techniques are summarized, and the main conclusion reached is that local compression is the best defined technique at present, and that reverse bending and high R-ratio, although probably more convenient, require further research and development.

KEY WORDS: welded joints, residual stresses, cracking (fracturing), test specimens, standards, fracture toughness, K_{κ}, crack-tip opening displacement

Nomenclature

a	Crack length
B	Specimen thickness
CTOD	Crack-tip opening displacement
HAZ	Heat-affected zone
K	Mode I stress intensity factor
K_c	Critical value of K
K_{Fmax}	Maximum value of K imposed during fatigue
K_{Ic}	Plane strain fracture toughness for Mode I loading
K_{ISCC}	Threshold value of K for stress corrosion cracking
P	Load
P_L	Limit load
R-ratio	Ratio of minimum to maximum applied K during fatigue
S	Loading span

[1] Senior research engineer and principal fracture consultant, respectively, The Welding Institute, Abington Hall, Abington, Cambridge, England CB1 6AL. Mr. Towers is now a principal mechanical research engineer, Rolls-Royce Ltd., P.O. Box 31, Derby, England DE2 8BJ.

SMA Shielded metal arc
W Specimen width
ΔK_F Range of K applied during fatigue cycle
$\delta_c, \delta_u, \delta_m, \delta_i$ Measured values of the crack-tip opening displacement (CTOD) as defined in British Standard Methods for Crack Opening Displacement (COD) Testing (BS 5762-1979)
σ_{YS} Material yield, or 0.2% proof, strength

Introduction

As a general rule fracture toughness tends to decrease with increased notch acuity. It is therefore normal to use fatigue precracked specimens for fracture toughness tests. Fatigue precracking however involves considerable expense. This results from the capital invested in test equipment, the necessary labor, and the occasional requirement for retests because of invalid fatigue crack shapes. The cost of testing weldments tends to be higher than that for plates because of complications caused by weld profiles, distortion, and the presence of residual stresses.

Research on precracking at The Welding Institute has been directed towards maximizing the number of valid fracture toughness tests results. For weldments this involves two main issues. First, how can the effects of welding residual stresses on fatigue crack shape be dealt with? Second, when fatigue cracks are obtained that are of unacceptable shape to the criteria of the present standards, what should be done with the results? This paper describes the research performed to help solve the first of these issues. Work carried out at The Welding Institute to help answer the second issue has recently been described elsewhere by Towers [*1*].

Effects of Welding Residual Stresses on Fatigue Crack Shape

Figure 1 shows the most common orientation of a fracture toughness specimen used for testing weldments. When this orientation is used for a weldment in the as-welded condition, that is, without stress relief, it is common for the welding

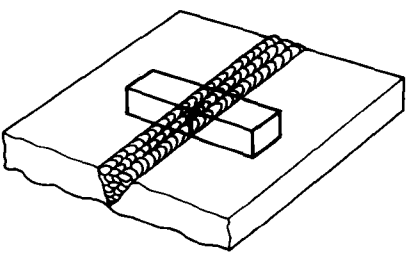

FIG. 1—*Common specimen orientation for fracture toughness tests on weldments.*

residual stresses to adversely affect the fatigue crack front shape. Figure 2 gives a comparison between fatigue crack front shapes in specimens that

(1) are virtually free from residual stresses (Fig. 2*a*) and
(2) contain welding residual stresses (Figs. 2*b* and *c*).

The most common problem is that illustrated in Fig. 2*b*, where little or no growth of the fatigue crack occurs in the center of the specimen. This general shape, which is characteristic of specimens with through-thickness notches in multipass weldments [*2–9*], is consistent with the residual stresses present in the specimen as a result of welding [*2,8,9*]. The situation depicted in Fig. 2*c*, where excessive fatigue crack growth occurs in the center of the specimen and little or no growth

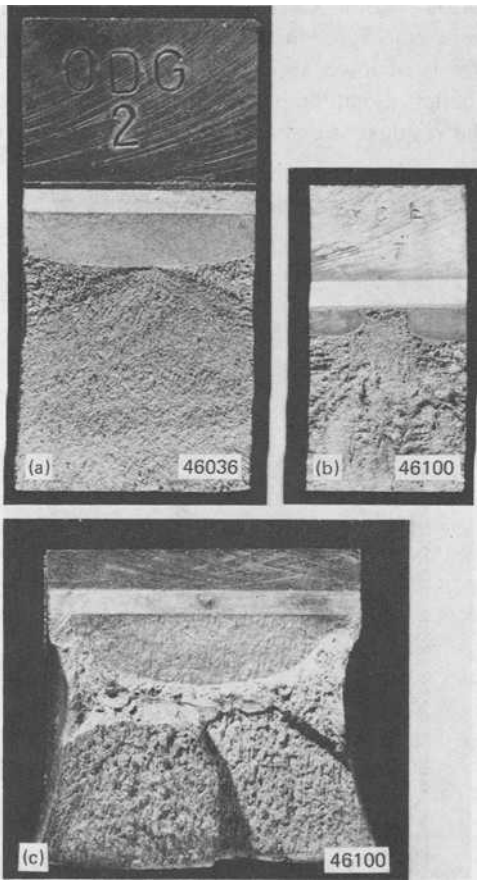

FIG. 2—*Fatigue crack front shapes for various situations:* (a) *residual stress free parent material,* (b) *through-thickness crack in as-welded multipass weldment, and* (c) *through-thickness crack in as-welded single-pass electron-beam weld.*

occurs at the edges, is less commonly experienced. Here the through-thickness notch is sampling a single-pass electron beam weld in an austenitic stainless steel. The crack front shape in Fig. 2*c* is consistent with tensile residual stresses being present at the center of the specimen. This is not unexpected for a single-pass weld because the molten pool will solidify last at the mid-thickness.

The fatigue crack front shape is not unduly affected by welding residual stresses when they are approximately constant across the notch front. Thus, it is unusual for there to be problems with fatigue crack shapes for fracture toughness specimens with surface notches into weldments. In addition, it is unusual for problems to occur because of welding residual stresses for specimen thicknesses less than 15 mm.

In weldments there can be a wide variety of microstructures present, including the parent material, heat-affected zone (HAZ), and weld metal. Also, the yield strengths of the various regions can differ markedly. Dawes [2] showed, however, that the type of crack growth shown in Fig. 2*b* occurs if the material in the specimen center is of lower or higher strength than the material near the edges. Thus, it is believed that the prime cause of variable fatigue crack shapes in weldments is the residual stresses rather than being caused by variable mi-

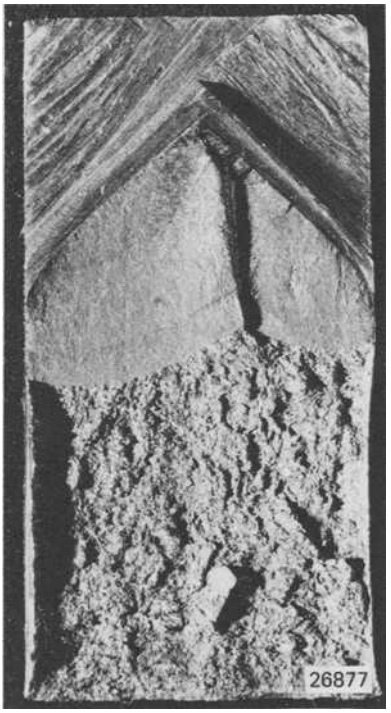

FIG. 3—*Fatigue crack growth in chevron notched specimen with through-thickness notch into a 25-mm thickness butt weld* [2].

crostructures or yield strength. In addition, it should be remembered that unwelded materials can also contain residual stresses (for example, caused by uneven cooling or plastic deformation), which on occasions can lead to uneven fatigue crack shapes, for example, for aluminum alloy forgings in Ref *10*.

The use of chevron notches might be expected to obviate the problem illustrated in Fig. 2*b*. Various investigations have however shown that the welding residual stresses for through-notches cause crack growth to be more pronounced from the sides of the chevron than from the tip [*2,4,7*]. In the extreme, Dawes [*2*] found that crack growth could occur on two different planes, one originating on each side of the chevron, as illustrated in Fig. 3.

The slightly bowed fatigue crack front obtained with through-thickness notches in nominally residual stress free parent material is consistent with theoretical predictions and numerical computations, as reviewed in Ref *1*. This crack front is relatively close to straight fronted and is thus not far removed from the assumption of a straight fronted crack that is implicit in most fracture toughness testing standards. The fatigue crack shapes of Figs. 2*b* and *c* are clearly undesirable. Also, work performed by Dawes [*5*] showed that elevated values of fracture toughness could be obtained with a crack front shape similar to that in Fig. 2*b* when compared to a uniform crack front, as illustrated in Fig. 4.

Methods for Relief of Residual Stresses

One of the most well established means of relaxing residual stresses is thermal stress relief, which when required is usually performed at around 600°C for

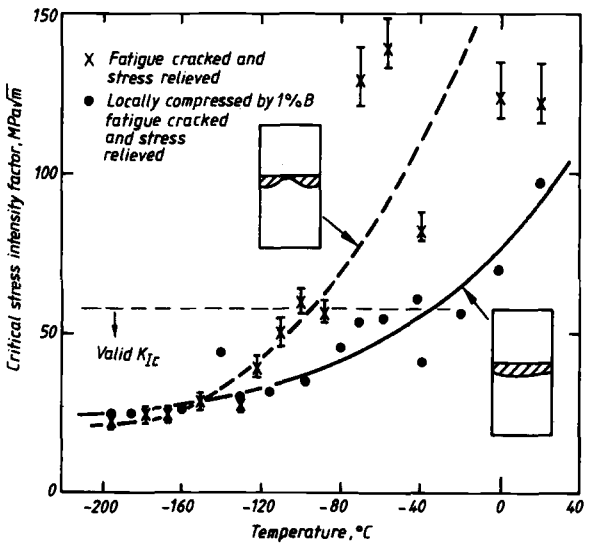

FIG. 4—*Effect of fatigue crack shape on fracture toughness of a 38-mm thick double-V multipass SMA weld metal measured using three-point bend specimens to BS 5447:1977 procedures* [5].

welded structural steels. Although thermal stress relief can relax the residual stresses sufficiently to prevent the problems with nonuniform fatigue crack shape [*2*], it is not desirable when an attempt is being made to measure the fracture toughness appropriate to a weldment in an as-welded structure. This is because the thermal stress relief can markedly affect the fracture toughness because of metallurgical changes, some of these being described in Refs *11* and *12* for weld metals and HAZs, respectively.

An alternative method for relieving residual stresses is to load the section containing residual stresses so that plastic straining occurs. When the load is removed, the residual stress levels will be reduced. The greater the load is, the greater is the reduction in residual stress levels, as shown, for example, by Kihara et al [*13*]. In principle, if a uniform stress of yield stress magnitude is applied the residual stresses remaining on unloading should be negligible. Applying a tensile load to a test specimen and unloading before notching should reduce the residual stresses in as-welded specimens. However, early work performed at The Welding Institute indicated that insufficient stress relief could be achieved in the weld metal without inducing unacceptable deformation in the adjoining parent material, which generally has a lower yield strength than the weld metal. Instead, techniques have evolved whereby the strain is concentrated in the notched region, so that effective residual stress relief, or redistribution, is achieved. One of these techniques is "local compression," others include "reverse bending" and the use of a high R-ratio and high loads in the fatigue cycle during precracking (where R-ratio is the minimum load in the fatigue cycle divided by the maximum load). These techniques and various studies on them are described in turn.

Local Compression

Development of Effective Technique

Local compression is a technique whereby mechanical stress relief is achieved at the weldment by pressing a platen into the local region in front of the machined notch before fatigue precracking [*2,5,6*]. For this "local compression" technique to be effective in relieving residual stresses sufficiently for uniform fatigue cracks to be obtained, a total plastic strain applied across the specimen thickness of 1% of the specimen thickness was found to be the minimum practical [*2,5*]. This can be performed using a variety of platen shapes and sizes, as indicated in Fig. 5. The approximate loads P required to indent material of yield strength σ_{YS} and thickness B are given in Fig. 5.

Research has been performed to assess the effectiveness of the various techniques illustrated in Fig. 5 in relieving residual stresses [*8*]. Experiments performed on 25-mm thick double-V multipass weldments showed that the residual stress levels are reduced to lower levels when a single cylindrical pattern of diameter equal to the section thickness B is used for local compression than they are if the multiple-indent technique is used with a platen diameter equal to half

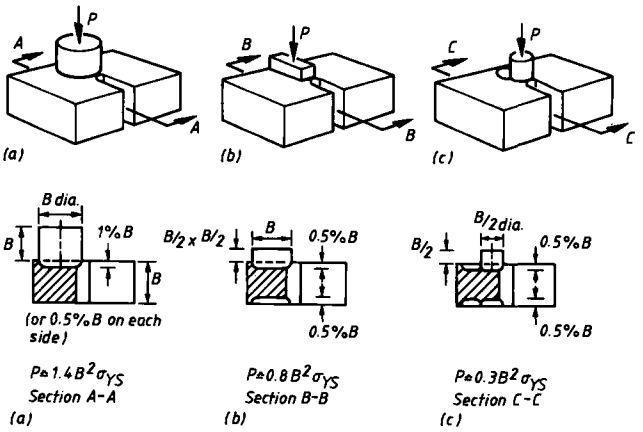

FIG. 5—*Alternative local compression treatments for as-deposited steel weldments.* σ_{YS} *is the weld metal yield strength.*

of B, as in Fig. 5*c*. (The measured residual stress distributions are given in Fig. 6.) Despite this, after local compression using either technique, uniform fatigue cracks were obtained that were a considerable improvement on fatigue cracks obtained in the as-welded specimens [*8*]. In this study the sequence of the multiple-indent procedure (Fig. 5*c*) had little apparent effect on the reduction in residual stress levels.

The above research indicates that local compression relieves residual stresses more effectively when it is performed using one large platen than if multiple indents with a smaller size platen are used. Unfortunately, the limited load capacity available in most laboratories forces one to use the multiple indent procedure (Fig. 5*c*) if the section thickness is large. However, a survey of the shapes of fatigue cracks in fracture toughness specimens (with widths W equal

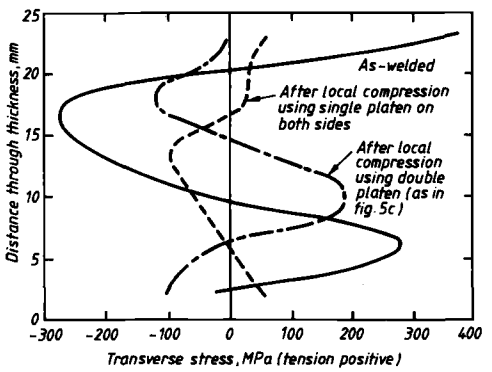

FIG. 6—*Transverse residual stress distributions measured before and after local compression for 25- by 50-mm notched CTOD specimens sampling a double-V multipass weldment* [8].

to twice the thickness B) tested at The Welding Institute has indicated that where a multiple-indent procedure is used for as-welded specimens of large thicknesses, far more unacceptable fatigue cracks are obtained than for a "general" sample of specimens including a mixture of plain materials and stress relieved and as-welded (and locally compressed) weldments. The data are plotted in terms of the rate of rejection of fatigue cracks to current fracture toughness testing standards versus specimen thickness in Fig. 7. The following features are apparent from these data.

1. The rates of rejection of specimens according to the requirements of ASTM Test Method for Plane-Strain Fracture Toughness of Metallic Materials (E 399) and British Standard Methods of Test for Plane Strain Fracture Toughness (K_{Ic}) of Metallic Materials (BS 5447-1977) are generally much greater than the rejection rates to British Standard Methods for Crack Opening Displacement (COD) Testing (BS 5762-1979). This is because the former have more stringent limits on the amount by which the crack front can deviate from being straight. (The limits in the current ASTM K_{Ic} standard E 399-83 are however more lenient than those in ASTM E 399-78 and are in principle quite close to those of BS 5762: 1979.)
2. For specimen thicknesses where a single platen can be used for local compression, that is, for thicknesses less than the maximum platen diameter in Fig. 7, the rejection rates appear to be slightly lower for as-welded specimens than for the general sample. This may, in fact, be due to the occurrence of residual stresses in the plain materials and stress relieved weldments which in part made up the general sample [*1*]. Poorly shaped fatigue cracks have been shown to occur in some plain materials [*1,10*], presumably because of residual stresses resulting from rolling, heat treatment, or plastic bending.
3. If the data are ignored for specimens where the local compression is apparently less effective, that is, for specimen thicknesses larger than the maximum platen size, there is a general trend for the fatigue crack shapes to be relatively better in thicker specimens. This can be considered to be due to there being relatively larger plane stress regions for the smaller specimens for the same maximum stress intensity factor K_{Fmax} in the fatigue cycle [*1*]. Fatigue crack growth is retarded in the plane stress regions because these are more compliant than the central, near-plane-strain, region or because of crack closure effects or both [*1*].

The most important implication of the data of Figs. 6 and 7 to the local compression technique is that the platen size for local compression should be comparable to the specimen thickness, and multiple indents using a platen smaller than the section thickness should be avoided if possible. This observation is not surprising for two reasons. First, for a platen size comparable to the specimen thickness B, the whole uncracked ligament can be locally compressed without reverting to a multiple-indent procedure. Second, with a platen size comparable

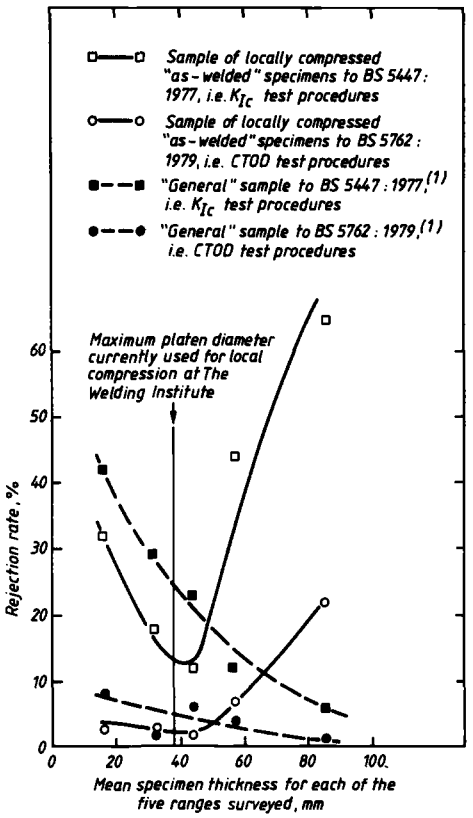

FIG. 7—*Rate of rejection of specimens because of fatigue crack shape to requirements of current British* K_{Ic} *and CTOD standards. (Total number of specimens included in general sample is 534, and the data given is found in Ref* 1*; total number in as-welded sample is 943, that is, approximately 189 specimens per specimen thickness range.)*

to the section thickness the through-the-thickness yielding induced by a 1% local plastic compression (which occurs as slip lines that are orientated at an angle of approximately 45° to the specimen surface) reaches the opposite surface of the specimen to that which is being indented. An example of this is shown in Fig. 8. Unfortunately, high loads become necessary to indent large thickness specimens when using a platen with a diameter equal to the specimen thickness. For instance, the load of approximately $1.4\,\sigma_{YS}B^2$ (Fig. 3*a*) is 175 000 kg (175 tonnes) for B = 50 mm and σ_{YS} = 500 MPa. Thus, one probably would require a 200 000-kg (200-tonne) load capacity test machine in this instance. For larger thicknesses and higher strength materials the load requirements are correspondingly greater. These machine load capacities are in fact somewhat higher than is required for fatigue precracking and testing. For instance, an approximate calculation indicates that the loads required for local compression using a cylindrical platen of diameter equal to the specimen thickness B are eight times the

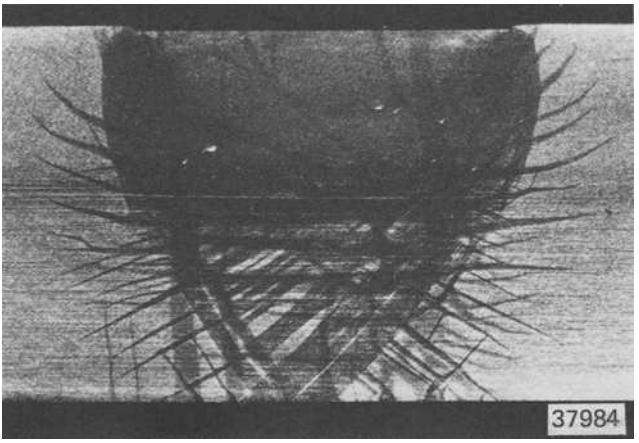

FIG. 8—*Yielding patterns on a 25-mm thick block of high nitrogen steel after 1% B local compression from one side using a 25-mm diameter platen, sectioning, and finally etching using Fry's reagent* [5].

limit load, which is expected in fracture toughness tests on the preferred geometry ($2B \times B$) three-point bend or compact tension specimens. This requirement for large load capacity test machines is one of the major disadvantages of local compression.

Another problem arises with local compression of full-thickness specimens when geometric discontinuities are present, such as those illustrated in Fig. 9.

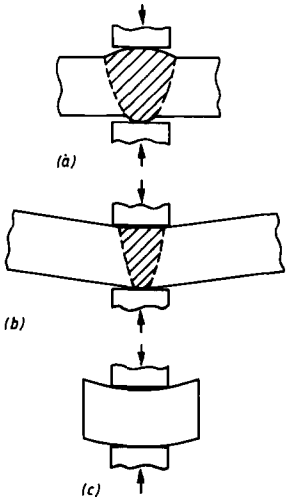

FIG. 9—*Three specimen shapes that impede local compression:* (a) *weld overfill,* (b) *weld distortion (despite removal of overfill), and* (c) *pipe curvature, such as is present when testing girth welds.*

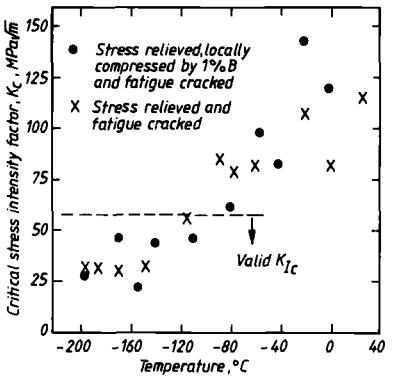

FIG. 10—*Influence of local compression on the fracture toughness of a 38-mm thick double-V SMA weldment (tests on compact tension specimens to BS 5447:1977)* [5].

Effects of Local Compression on Fracture Toughness

An important consideration is the extent to which the plastic strains induced by local compression affect the fracture toughness. The effects of local compression by 1% of B on fracture toughness for a range of test temperatures are shown in Figs. 10 and 11, for a 38-mm thick double-V weld and for a 25-mm thick low alloy steel plate, respectively. Results of tests on compact tension specimens at −20 and −100°C test temperatures are given in Tables 1 and 2, respectively. In general, local compression appears to reduce the fracture toughness for the materials tested, for example, for the specimens tested at −100°C the mean of the critical values of stress intensity factor K_c was 28% lower for locally compressed specimens (Table 2). However, tests performed by Dawes [2] on specimens with machined notches having a 0.075-mm radius tip sampling mild steel bar and a submerged arc weld in a 25-mm plate, together with the results of

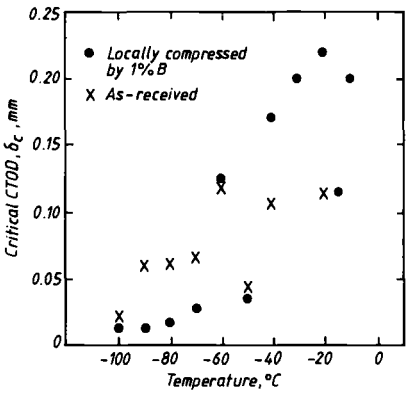

FIG. 11—*Influence of local compression on fracture toughness of 25-mm thick normalized NiCrMoV plate, Grade 281 to BS 1501:Part 2:1970 (tests performed to DD 19:1972 procedures)* [5].

TABLE 1—*Results of fracture toughness tests at −20°C on compact tension specimens sampling double-V SMA welds in 38 mm thickness produced using American Welding Society (AWS) E7016 electrodes* [5].[a]

Thermally Stress Relieved and Fatigue Cracked		Thermally Stress Relieved, Locally Compressed by 1% B and Fatigue Cracked	
Specimen Identification[b]	Critical Stress Intensity Factor K_c, MPa · $m^{1/2}$	Specimen Identification[b]	Critical Stress Intensity Factor K_c, MPa · $m^{1/2}$
8-55	93.6	8-58	61.2
8-61	105.5	8-62	49.7[c]
8-63	83.8	7-54	67.6
9-66	127.9	9-65	90.4
9-68	118.5	9-67	78.6
9-72	55.3[c]	9-71	104.0
Mean = 97.4 MPa · $m^{1/2}$		Mean = 75.3 MPa · $m^{1/2}$	

[a] Tests performed and analyzed to BS 5447:1977 procedures.
[b] Panel number and specimen number, respectively.
[c] Valid K_{Ic}.

Fig. 10, indicate little consistent effect of local compression on fracture toughness. Although there is a tendency in the data presented in Fig. 10 for the scatter in fracture toughness values to be greater after local compression than without, this is not expected to be generally the case. Indeed, the opposite trend occurred for the tests on specimens with a machined notch sampling mild steel bar, that is, local compression tended to reduce scatter. Dawes argued that different materials have different sensitivities to embrittlement caused by the 1% of B plastic strain applied at room temperature [5]. He also made the point that strains of this order can occur in the manufacture of welded structures, and it is not unreasonable to include the effects of small strains in the fracture toughness test, particularly if the material is susceptible to room temperature embrittlement at such relatively low strains. Finally, it is preferable to measure fracture toughness in a specimen that has a fatigue crack that is close in shape to the straight front implied by the testing standards, albeit with the fracture toughness at times reduced by local compression, rather than to measure fracture toughness values that may be inaccurate and indeed not conservative (see Fig. 4).

A final area of study on the effects of local compression on fracture toughness has been to assess the effects of the different local compression techniques (Fig. 5). Research reported by Bramat and Doucet [3] indicated that for two separate multipass submerged arc welds (single V and double V) the fracture toughness was lower after local compression by 1% of B on one specimen side than it was after local compression by ½ of 1% of B on each side (making a total of 1% of B). In another study, reported by Leggatt and Kamath [8], there was little apparent difference between fracture toughness values measured after multiple-indent local compression (Fig. 5*c*) and those measured after a single-platen procedure (Fig. 5*a* with ½ of 1% of B applied to each side). The results are given in Table 3. The application of ½ of 1% of B to each side of the specimen

TABLE 2—*Results of fracture toughness tests at −100°C on compact tension specimens sampling single-V SMA welds in 38 mm thickness produced using AWS E7016 electrodes* [5].[a]

Thermally Stress Relieved and Fatigue Cracked		Thermally Stress Relieved, Locally Compressed by 1% *B* and Fatigue Cracked	
Specimen Identification[b]	Critical Stress Intensity Factor K_c, MPa · $m^{1/2}$	Specimen Identification[b]	Critical Stress Intensity Factor K_c, MPa · $m^{1/2}$[c]
3-25	61.2	3-34	52.7
4-27	60.7	4-26	55.5
4-32	63.2	4-31	49.1
5-35	40.5[c]	5-34	45.9
5-37	53.0[c]	5-36	45.0
5-40	81.2	5-38	54.3
5-42	77.1	5-41	33.4
6-44	65.6	6-43	46.4
6-46	71.8	6-45	38.0
6-48	61.1	6-47	39.4
6-51	69.9	6-49	49.9
Mean = 64.1 MPa · $m^{1/2}$		Mean = 46.3 MPa · $m^{1/2}$	

[a] Tests performed and analyzed to BS 5447:1977 procedures.
[b] Panel number and specimen number, respectively.
[c] Valid K_{Ic}.

rather than 1% of *B* to one side only has been the preferred and the usual practice at The Welding Institute in recent years.

Reverse Bending

Development of Effective Technique

It is understood that many laboratories, particularly in the United States and Japan, use "reverse bending" before fatigue cracking as a means of redistributing welding residual stresses in specimens. There are however relatively few pub-

TABLE 3—*Results of fracture toughness tests at 5°C on three-point bend specimens tested to BS 5762:1979 and sampling a SMA double-V weld metal* [8].

Local Compression Technique (with 0.5% *B* plastic strain applied to each side)	Specimen	CTOD Value, mm	Type of Instability[a]
Using a platen diameter equal to the specimen thickness (Fig. 5*a*)	1200-2	0.27	δ_u
	1196-1	0.35	δ_u
	1200-1	0.54	δ_m
		Mean: 0.39	
Using multiple-indent procedure with platen diameter equal to half the specimen thickness (Fig. 5*c*)	1200-9	0.27	δ_u
	1196-7	0.38	δ_u
	1200-8	0.44	δ_m
		Mean: 0.36	

[a] δ_u and δ_m being to BS 5762:1979 definitions.

lished reports on the use of the technique for weldments [*4,14*], and most of the background work has seemingly been done "in-house" and has not been reported. Reverse bending is performed before fatigue cracking by loading the notched specimen in the opposite mode to a conventional fracture toughness test; so that the notch tip is loaded in compression, and residual tensile stresses are induced at the notch tip when the specimen is unloaded. Reverse bending is in fact allowed by such fracture toughness testing standards as ASTM E 399-83 and BS 5447:1977 for K_{Ic} testing, and BS 5762:1979 for CTOD testing, as a means of speeding up initiation of fatigue crack growth from the machined notch. The reverse bending loads allowed by these codes are however generally not high enough to create sufficient residual stress redistribution in as-welded specimens. This was demonstrated in tests on a single-V multipass shielded metal arc (SMA) butt weld in a 25-mm thick section where single reverse bending loads were applied at two levels, and the fatigue cracks obtained were compared with specimens for which no reverse bending was performed. As seen in Fig. 12, for the specimens reverse bent at loads low enough for it to be possible to subsequently measure valid K_{Ic} values, only a small amount of fatigue crack growth was induced in the center of the specimen. Presumably the tensile residual stresses induced by reverse bending initially aided growth across the whole front, but as soon as the crack reached the edge of this zone of tensile residual stresses the crack was again influenced by the welding residual stresses. Thus, a greater improvement in fatigue crack shape would be expected for higher reverse bending loads. This appears to be in part demonstrated in Fig. 12, because the fatigue crack shapes obtained are slightly improved for a higher reverse bending load, although the increased fatigue load itself (to the maximum permitted by the standard for CTOD testing BS 5762:1979) may also have improved matters.

Cycling the load during reverse bending has been reported to be effective in improving fatigue crack shape in as-welded test pieces [*4*]. Experiments on weld metal specimens from a 25-mm thick single-V SMA multipass weld have indicated, however, that there is no noticeable difference between the fatigue crack shapes obtained when the reverse bending is applied only once or 10 000 times (Fig. 13). In the same series of tests it was shown that local compression was effective in producing a uniform fatigue crack despite a much lower fatigue cracking load level (Fig. 13). What seems to be important is that the reverse bending load should be effective in redistributing residual stresses over the complete distance of fatigue crack propagation in order to obtain uniform fatigue crack shapes. To do this, it is expected that reverse bending loads need to be applied that are a significant proportion of the limit load. The tests performed at The Welding Institute and those described elsewhere [*14*] indicate that to be effective in producing a uniform fatigue crack, the reverse bending load needs to be around 60 to 90% of the limit load P_L. For a three-point bend single-edge notched specimen [*15*], this can be estimated as

$$P_L = [1.3\sigma_{YS}B(W - a)^2]/S$$

where

P_L = limit load,
σ_{YS} = yield strength,
B = specimen thickness,
W = specimen width,
a = notch depth, and
S = loading span.

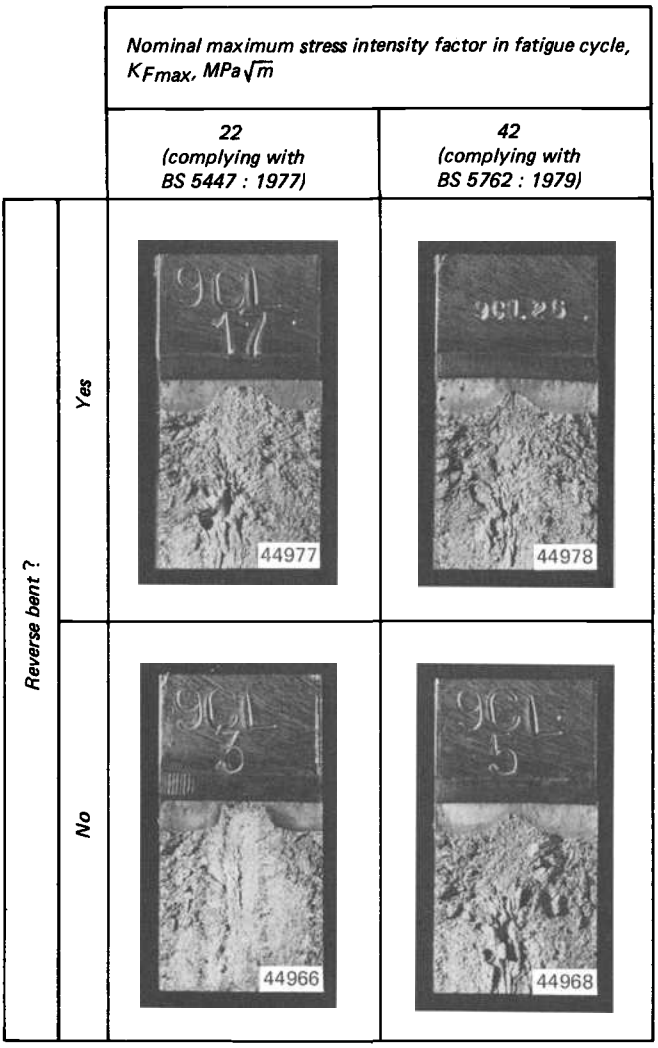

FIG. 12—*Influence of reverse bending on fatigue crack shapes in bend specimens sampling a single-V multipass weld in 25-mm thickness. (Note: reverse bending was performed at a load level equivalent in magnitude, though opposite in sign, to the* K_{Fmax} *level subsequently applied in the fatigue cycle.)*

Pre-fatigue cracking treatments					
One reverse bending cycle at a nominal K of -36MPa $\sqrt{m}$ ($P \sim 43\% P_L$)	10,000 reverse bending cycles at a nominal K of -36MPa $\sqrt{m}$ ($P \sim 43\% P_L$)	One reverse bending cycle at a nominal K of -44MPa $\sqrt{m}$ ($P \sim 53\% P_L$)	10,000 reverse bending cycles at a nominal K of -44MPa $\sqrt{m}$ ($P \sim 53\% P_L$)	None	Local compression to 1%B
Nominal K_{Fmax} in fatigue cracking, MPa $\sqrt{m}$					
42	42	26	26	22	22
 48400	 48401	 48398	 48397	 49130	 49133

FIG. 13—*Effect of load cycling in reverse bending and local compression on fatigue crack shapes. (For 25-mm thick specimens sampling multipass single-V SMA weldments.)*

This load is much higher than existing standards allow for reverse bending. For instance 75% of P_L, calculated using the above relationship, is approximately 50% higher than the maximum fatigue cracking load, and therefore reverse bending load, allowed by the CTOD testing standard BS 5762:1979, and this is less stringent than K_{Ic} standards.

An interesting variation on the reverse bending technique is to reverse bend notched specimens sampling ferritic steels at a very low temperature, say −196°C [*14,16,17*], which can induce short cleavage cracks when the specimen is unloaded. This is an alternative method to fatigue precracking for producing sharp cracks in a test piece before the fracture toughness test. It is important to note, however, that the tensile residual stresses induced at the notch tip by the reverse bending that cause the short arrested cleavage crack at low temperature are still present at a reduced level at the tip of the arrested cleavage crack, and it is necessary to apply a subsequent tensile, or "opening," load at the low temperature so that the subsequent fracture toughness is similar to that for fatigue precracked specimens [*14,17*]. Thus, although the technique can be used to obtain relatively straight fronted arrested cleavage cracks, even in as-welded specimens [*16,17*], it is important to ensure that the effects on the fracture toughness of residual stresses caused by the reverse bending itself and those remaining from the original welding residual stresses are carefully considered.

Effects of Reverse Bending on Fracture Toughness

The available data on the effects of reverse bending treatments on fracture toughness appear to be very limited. Fujii and Metzbower [*4*] noted that, for a quenched and tempered steel, specimens cyclically reverse bent before conventional fatigue cracking resulted in identical values of the threshold stress intensity factor for stress corrosion cracking K_{ISCC} to specimens precracked using conventional procedures. Underwood and Kapp [*18*] found little difference for high-strength steel forgings between K_{Ic} values measured after the use of reverse bending before precracking relative to specimens precracked without reverse bending. The loads applied in reverse bending in this case were however low relative to the limit load for the specimens and indeed were low relative to the subsequently measured K_{Ic} values, the nominal K applied during reverse bending being between 49 and 64% of the K_{Ic} values. As already noted, cleavage cracks induced at low temperature using reverse bending result in lower values of fracture toughness than fatigue cracked specimens unless a subsequent tensile load is applied at low temperature, presumably because of the tensile residual stresses induced by reverse bending [*14,17*].

Tests have been performed at The Welding Institute on 38-mm thick three-point bend specimens taken from a structural steel plate to the BS Specification for Weldable Structural Steels (BS 4360-1979) Grade 50E specification. The results are summarized in Table 4. Three sets of three specimens were tested.

TABLE 4—*Results of fracture toughness tests on 38-mm thick plain plate to assess the influence of local compression and reverse bending. (Bend tests to BS 5762:1979 on BS 4360 Grade 50E steel.)*

Treatments to Notched Specimen Blanks Before Fatigue Cracking	Fatigue Cracking Condition		Specimen	Values of CTOD at −90°C, δ_c, mm		Values of K_c at −90°C, MPa · $m^{1/2}$	
	Average K_{Fmax}, MPa $m^{1/2}$	R-ratio					
None	24	0.1	ODG7	0.086	mean	109	mean
			ODG8	0.069	0.082	102	108
			ODG9	0.092		112	
Local compression to 0.5% *B* plastic strain each side using 38 mm diameter platens	23	0.1	M6-5	0.058	mean	87	mean
			M6-6	0.068	0.082	95	98
			M6-7	0.119		113	
Reverse bent to 75% of limit load	24	0.1	M6-1	0.137	mean	116	mean
			M6-2	0.023	0.068	71	92
			M6-3	0.045		89	

One set was locally compressed before fatigue cracking, one set was reverse bent to 75% of the limit load before fatigue cracking, and the last set was fatigue cracked without a pretreatment. In all cases, the fatigue cracking loads applied at room temperature were at levels appropriate to the subsequent measurement of K_{Ic}. Although the specimen behavior at the −90°C fracture test temperature was too ductile for measurement of valid K_{Ic} values, the values of fracture toughness all corresponded to unstable cleavage fractures with no macroscopic evidence of prior tearing. As summarized in Table 4, the average fracture toughness values measured in specimens that were locally compressed appear to be little different from those for untreated specimens, although the scatter in the test results is somewhat higher for the locally compressed specimens. For the reverse bent specimens, the fracture toughness is on average 17% lower (based on the CTOD values) than it is for untreated specimens. The scatter in the test results is also greater for the reverse bent specimens. It is not unexpected that the average fracture toughnesses measured in reverse bent specimens are the lowest (Table 4) because reverse bending not only induces plastic strains (which it must do to achieve effective residual stress redistribution in as-welded specimens), but also is likely to leave residual tensile stresses at the crack tip. The observation that reverse bending lowers the fracture toughness is consistent with the measurements of fracture toughness in specimens with cleavage cracks induced by reverse bending at a low temperature [*14,17*]. Local compression also induces plastic strains that may reduce the fracture toughness, but the residual stresses present will be at low enough levels not to affect the measured fracture toughness, provided a suitable procedure is used.

High R-Ratio

Development of an Effective Technique

The use of a high R-ratio in the fatigue cycle can be effective in improving the fatigue crack shapes in test pieces sampling weldments in the as-welded condition [*3,9*].

Initial trials [*9*] at The Welding Institute using 25-mm thick specimens sampling a single-V multipass SMA weld indicated that R-ratios as high as 0.5 were not fully effective in producing uniform fatigue cracks in the as-welded test pieces unless the maximum load in the fatigue cycle was higher than that permitted by either the K_{Ic} or CTOD fracture toughness testing standards. However, later tests on specimens taken from a similar welded joint indicated that uniform fatigue cracks could be obtained using an R-ratio of 0.7 with a maximum stress intensity in the fatigue cycle K_{Fmax} being the maximum permitted for CTOD testing to BS 5762:1979 [*9*]. Furthermore, uniform fatigue cracks could be obtained at an R-ratio of 0.5 if higher values of K_{Fmax} were used. The general trend displayed by the data is that the effects of welding residual stresses on fatigue crack shape are reduced by an increased R-ratio and an increased K_{Fmax} level.

The time taken for fatigue cracking is usually a very important practical consideration. Unfortunately, for a given K_{Fmax}, a higher R-ratio will reduce the stress intensity factor range ΔK_F and thereby increase the time necessary to grow a finite-size crack. Thus, K_{Fmax} levels in excess of those permitted by the standards may be necessary to shorten the times for fatigue cracking when high R-ratios are used.

R-ratios greater than 0.1 are not permitted by the current fracture toughness testing standards. Although the reason for this is probably to maximize the range in the stress intensity factor ΔK_F during fatigue cracking, and thereby obtain the most rapid crack growth rate for practical purposes; the reason for the mandatory imposition of the limit on R-ratio is unknown. Nevertheless, it is clearly important to consider the effects of both higher R-ratios than 0.1 and higher K_{Fmax} values on fracture toughness.

Effects of High R-Ratio on Fracture Toughness

Fracture toughness values measured in weldment specimens after the use of a high R-ratio in the fatigue cycle have been compared with results for locally compressed specimens by Bramat and Doucet [*3*], Towers [*9*], and Wildschut [*19*]. The study by Bramat and Doucet [*3*] indicated different trends for a single-V weld than for a double-V weld. For the single-V weld the lowest fracture toughness values were obtained after fatigue cracking at an R-ratio of 0.5. For the double-V weld, however, the locally compressed specimens produced results similar to those specimens for which a high R-ratio had been adopted. There

were few obvious trends in the data for single-V welds obtained by Towers [*9*], though the fracture toughness values measured in specimens prepared using the combination of a high K_{Fmax} and a high R-ratio (which was most conducive to uniform fatigue cracks) were generally higher than the results for locally compressed specimens. Wildschut [*19*], in another study on a double V-weld, reported higher fracture toughness values for specimens prepared using a high R-ratio than for locally compressed specimens. The general trend for these data appears to be for higher fracture toughnesses to be measured in specimens prepared using a high R-ratio, which may be due to the high R-ratio elevating the fracture toughness or local compression lowering it or both. Alternatively, the fatigue crack front shapes may have been important, since these were not always ideal after the use of high R-ratio [*3,9*], with a cusp sometimes occurring in the center of the specimen as shown in Fig. 14.

In order to remove the effects of local compression and crack shape from the above comparisons, Towers reported results for a parent steel where specimens were fatigue cracked using R-ratios of 0.1 and 0.5 and different K_{Fmax} levels [*9*]. The results are shown in Fig. 15. The results for an R-ratio of 0.1 display the trend for the fracture toughness to increase with increased K_{Fmax}, which is consistent with other published data [*20,21*]. However, for an R-ratio of 0.5 the tendency for the fracture toughness to initially increase, peak, and fall off again with increased K_{Fmax} was unexpected. The tendency for fracture toughness to be higher, the higher the R-ratio, for a given K_{Fmax} level, appears to be consistent with a simple (linear elastic) model of the effects of R-ratio suggested by Towers [*20*] based on the premise that crack closure is an important effect. If, however, crack blunting is the main cause of the increased fracture toughness with increased K_{Fmax} (for given R-ratio), which has been suggested by many authors [*20*], it is not surprising that the fracture toughness is less sensitive to the effect of increased K_{Fmax} for a high R-ratio, because at a given K_{Fmax} level ΔK_F is lower for a high

FIG. 14—*Cusp shape sometimes observed in fatigue cracks of specimen precracked with high R-ratio (in this case* R = *0.5)* [9].

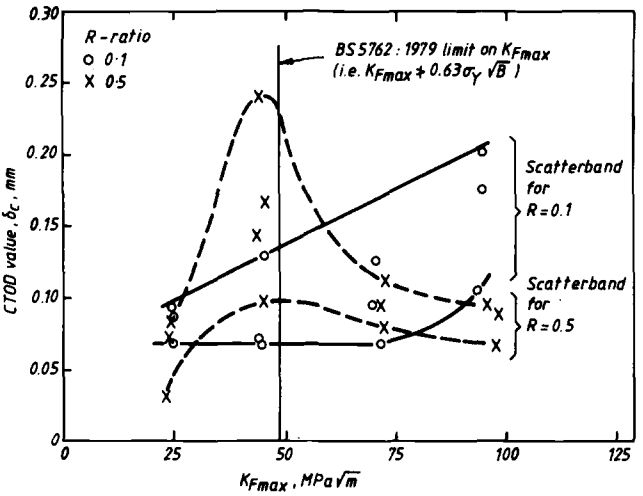

FIG. 15—*Influence of R-ratio on fracture toughness of 38-mm thick BS 4360:50E plate tested at −90°C* [9].

R-ratio and the fatigue crack surface appearance is far smoother and the crack tip presumably sharper [*9*]. The data given in Fig. 15 would support the latter hypothesis for the two relatively high levels of K_{Fmax}. Limited published data however are available, which indicate that for a high-strength steel the critical value of stress intensity factor K_c in the fracture toughness test was not significantly affected by the R-ratio used during fatigue cracking [*21*]. Further work is clearly required to understand the competing effects influencing the fracture toughness when different R-ratios are used in fatigue precracking.

Relative Merits of Techniques Used To Obtain Satisfactory Fatigue Cracks

It is clear that three techniques have been developed to the stage where they are capable of producing uniform fatigue cracks in as-welded specimens despite the original presence of welding residual stresses. Table 5 provides a summary of the relative merits of the three techniques, namely, local compression, reverse bending, and high R-ratio. In our experience, local compression to a plastic strain of 1% of B has been found to be generally reliable in producing uniform fatigue cracks in specimens sampling weldments in the as-welded state without special fatigue cracking procedures having to be used. For the technique to be fully effective, however, the platen size needs to be comparable to the section thickness, and this can mean for thick specimens that high load capacity machines are required. Reverse bending at room temperature should not require any greater load capacity machines than are already needed for the fracture toughness test. For this reason the technique is attractive, but there appears to be very little work published on the most suitable load to use for reverse bending. Furthermore,

TABLE 5—*Relative merits of three techniques used to obtain uniform fatigue cracks in as-welded specimens.*

Advantages	Disadvantages
LOCAL COMPRESSION TECHNIQUE	
1. Relatively large amount of development work published.	1. Extra operation, and equipment (for example, platens) required.
2. Method used for approximately ten years and has proved reliable, with plastic strains of 1% B being applied across the ligament beneath the notch.	2. Higher load capacity machines are required for effective local compression than for the fracture toughness test.
3. Can use conventional fatigue cracking procedures that meet requirements of current standards.	3. Fracture toughness values may be lower for materials that are sensitive to 1% plastic strain at room temperature.
4. Effect on fracture toughness, if any, results in conservative measurements.	4. Local compression is awkward for specimens without flat surfaces.
REVERSE BENDING TECHNIQUE	
1. Can use conventional fatigue cracking procedures that meet requirements of current standards.	1. An extra operation is required.
2. Effects on fracture toughness are expected to result in conservative measurements.	2. Fracture toughness values may be significantly lower because of tensile residual stresses and plastic strains.
3. No special equipment is needed over and above that already required (for the fracture toughness test).	3. Relatively little information published on the development of technique and no unified method.
HIGH R-RATIO TECHNIQUE	
1. No extra operation or equipment is required.	1. For effective use the fatigue cracking loads and R-ratio are likely to contravene the requirements of current standards.
	2. Fracture toughness values may be affected, possibly giving unsafe results.
	3. Relatively little development work published and no unified technique.

the effects of the treatment on fracture toughness need to be clarified. On this point, it is felt that the effects are probably crucially dependent on the amount of crack growth following reverse bending. This is because the crack is being grown into steep gradients of residual stresses and plastic strains. Finally, using a high R-ratio is potentially the most convenient technique of all, requiring no extra equipment than is already required for fracture toughness tests, and involving no extra operation for specimen preparation. At the same time, however, the fatigue cracking conditions that need to be used will be nonstandard, since the R-ratio needs to exceed 0.1, and the maximum fatigue load probably has to be higher than currently permitted. The effects of high R-ratio on fracture toughness do not appear to be clearly understood and, until there is more information, the technique is not recommended.

Probably the most important point to emphasize is that any techniques used

to obtain uniform fatigue cracks in specimen sampling weldments should be documented and preferably should appear on the test results sheets. If this is not done, results of tests on weldments may be compared, and incorrect judgements made of the relative merits of the fracture toughness values, because it was not realized that different techniques were used to obtain uniform fatigue cracks.

Summary and Conclusions

A description is given of three techniques that may be used to ensure that uniform fatigue cracks are obtained in specimens initially containing residual stresses. These techniques are especially relevant to specimens that are extracted from multipass welded joints in the as-welded condition. The three techniques are local compression, reverse bending, and the use of high R-ratios in the fatigue precracking procedure. A review is made of the development, limitations, and relative merits of the three techniques; these being summarized in Table 5.

At present, local compression is the most reliable and well defined technique, and it can be used with the fatigue precracking restrictions in the current fracture toughness testing standards. Reverse bending and high R-ratios, while attractive, require further research and development and also changes in the fracture toughness testing standards.

Acknowledgments

The authors wish to thank the Materials and Chemicals Requirements Board (MCRB) and Research Members of The Welding Institute for providing the financial support for this research.

References

[1] Towers, O. L., "Fatigue Crack Front Shape and Its Effect on Fracture Toughness Measurements," *Journal of Testing and Evaluation*, Vol. 11, No. 1, Jan. 1983, pp. 34–45.

[2] Dawes, M. G., "Fatigue Pre-Cracking Weldment Fracture Mechanics Specimens," *Metal Construction and British Welding Journal*, Vol. 3, No. 2, Feb. 1971, pp. 61–65.

[3] Bramat, M. and Doucet, J. P., "Present Aspects of the Application of Fracture Mechanics to Welded Joints," *Soudage et Techniques Connexes*, Vol. 31, No. 9/10, Sept.–Oct. 1977, pp. 331–352.

[4] Fujii, C. T. and Metzbower, E. A., "Stress-Corrosion Cracking of Steel Weldments," *Metals Engineering Quarterly*, Vol. 16, No. 4, Nov. 1976, pp. 15–20.

[5] Dawes, M. G., "The Application of Fracture Mechanics to Brittle Fracture in Steel Weld Metals," PhD thesis, Council for National Academic Awards, London, England, Dec. 1976.

[6] Pisarski, H. G. and Dawes, M. G., "Measurement of Crack Opening Displacement in Weldments with Particular Reference to Offshore Structures," *Proceedings of an International Conference on Analytical and Experimental Fracture Mechanics*, G. C. Sih and M. Mirabile, Eds., Sijthoff and Noordhoff, Alphen aan den Rijn, The Netherlands, 1981, pp. 595–614.

[7] Nelson, F. G. and Kaufman, J. G., "Fracture Toughness of Plain and Welded 3-in. Thick Aluminum Alloy Plate," *Progress in Flaw Growth and Fracture Toughness Testing, STP 536*, American Society for Testing and Materials, Philadelphia, 1973, pp. 350–376.

[8] Leggatt, R. H. and Kamath, M. S., "Residual Stresses in 25 mm Thick Weld Metal COD Specimens in the As-welded and Locally Compressed States," Report 145/1981, The Welding Institute, Cambridge, England, June 1981.

[9] Towers, O. L., "The Use of High R-ratio for Growing Fatigue Cracks in Fracture Toughness Specimens," *Proceedings of an International Conference on Fracture Toughness Testing*, Paper 25, The Welding Institute, Cambridge, England, 1982.

[10] Bucci, R. J., "Effect of Residual Stress on Fatigue Crack Growth Rate Measurement," *Fracture Mechanics: Proceedings of the Thirteenth National Symposium on Fracture Mechanics, STP 743*, R. Roberts, Ed., American Society for Testing and Materials, Philadelphia, 1981, pp. 28–47.

[11] Pargeter, R. J. and Abson, D. J., "Factors Influencing the Toughness of Weld Metals in Pipeline, Structural and C-Mn Pressure Vessel Steels," *Proceedings of an International Conference on Fitness-for-purpose Validation of Welded Constructions*, The Welding Institute, Cambridge, England, 1982, pp. P42-1–P42-12.

[12] Dolby, R. E., "HAZ Toughness of Structural and Pressure Vessel Steels—Improvement and Prediction," *Welding Journal Research Supplement*, Vol. 59, No. 8, Aug. 1979, pp. 225-s–238-s.

[13] Kihara, H., Masubuchi, K., Kusuda, T., and Iida, K., "Initiation and Propagation of Brittle Fracture in Residual Stress Field," IIW Document X-219-59, International Welding Society, Paris, France, June 1959.

[14] Sakano, K., "Precompression Cracking Method for Fracture Toughness Test—2nd Report," Ishikawijima-Harima Heavy Industries (IHI) Engineering Review, Vol. 13, No. 3, July 1980, pp. 1–7.

[15] Towers, O. L. and Garwood, S. J., "Ductile Instability Considerations and Prediction of Driving Force Curves for Six Test Geometries," *Welding Research International*, Vol. 9, No. 6, 1979, pp. 56–103.

[16] Sakano, K., "Precompression Cracking Method for Fracture Toughness Test," *Transactions of the Japan Welding Society*, Vol. 8, No. 2, Sept. 1977, pp. 22–28.

[17] Sakai, K. and Sakano, K., "Precompression Effects on Brittle Crack Initiation and Growth," *Fracture Tolerance Evaluation*, K. Kanazawa, A. S. Kobayashi, and K. Iida, Eds., Toyoprint Company Limited, Japan, 1981, pp. 57–64.

[18] Underwood, J. H. and Kapp, J. A., "Benefits of Overload for Fatigue Cracking at a Notch," *Fracture Mechanics: Proceedings of the Thirteenth National Symposium on Fracture Mechanics, STP 743*, Richard Roberts, Ed., American Society for Testing and Materials, Philadelphia, 1981, pp. 48–62.

[19] Wildschut, H., "COD Measurements and Wide Plate Tests on Welded Material with Thicknesses of 50 and 30 mm," *Proceedings of an International Conference on Steel in Marine Structures*, Paper ST.3.2, Commission of the European Communities, Luxembourg, 1981.

[20] Towers, O. L., "Review of the Effects of Fatigue Cracking Loads on Plane Strain Fracture Toughness," *Journal of Testing and Evaluation*, Vol. 11, No. 1, Jan. 1983, pp. 27–33.

[21] Clark, G., "Fracture Toughness and Critical Crack Length Parameters in Fatigue Failure," *Strength of Metals and Alloys*, Vol. 2, R. C. Gifkin, Ed., Pergamon Press, Oxford, England, 1983, pp. 773–779.

Terence Ingham[1]

The Interpretation and Analysis of Upper Shelf Toughness Data

REFERENCE: Ingham, T., **"The Interpretation and Analysis of Upper Shelf Toughness Data,"** *Elastic-Plastic Fracture Test Methods: The User's Experience, ASTM STP 856*, E. T. Wessel and F. J. Loss, Eds., American Society for Testing and Materials, 1985, pp. 47–67.

ABSTRACT: The paper outlines the problems encountered in attempting to define a self-consistent upper shelf toughness data base for use in a generic study of the integrity of a light water reactor (LWR) pressure vessel. Multiple-specimen resistance curve J_R data were examined to provide "best estimates" of static initiation fracture toughness K_i at temperatures corresponding to fully ductile upper shelf behavior. In some cases, this involved reassessment of published data. To provide information that should be typical of current commercial steel making practice, K_i temperature relationships were developed from a statistical analysis of those data for A533B-1 and A508-3 steels containing less than 0.010 weight % sufur.

Relatively few data exist for weld metals, but the available results indicated that the K_i temperature relationships derived for base metals should also be applicable when assessing the significance of defects located in welds of a modern LWR pressure vessel.

Lower bound slopes $(dJ/da)_{LB}$ to the available J_R data for A533B-1 and A508-3 steels were also defined. These can be used in conjunction with the K_i temperature relationships to derive post-initiation toughness data for up to 2-mm crack growth. The data base was derived from linear J_R analyses, and its relevance to upper shelf initiation toughness data derived from nonlinear (power law) J_R analyses is considered. Different methods of estimating initiation toughness are discussed and proposals are made to simplify the interpretation of upper shelf toughness data.

KEY WORDS: ductility, crack propagation, temperature, welded joints, sulfur, upper shelf, fracture toughness (initiation), J_R curve, pressure vessel steels

Nomenclature

- a Crack length
- a_o Initial crack length
- b Ligament length
- B Specimen thickness
- E Young's modulus
- J J integral
- J_i "best estimate" value of J at initiation

[1]Senior scientific officer, Risley Nuclear Laboratories, UKAEA-Northern Division, Warrington WA3 6AT, Cheshire, England.

$J_{i2\sigma f}$, $J_{i4\sigma f}$	Initiation toughness values defined using $2\sigma_f\Delta a$ and $4\sigma_f\Delta a$ blunting lines
J_{io}	Initiation toughness value at $\Delta a = O$ where Δa includes crack-tip blunting
$J_{i\Delta a} = O$	Initiation toughness value at $\Delta a = O$ where Δa excludes crack-tip blunting
J_{Ic}	Initiation toughness value defined using ASTM E 813
J_L	Lower bound value of J
J_R	Measure of J in the presence of ductile crack growth
J_{RL}	Reference lower bound value of J in the presence of ductile crack growth
K	Stress intensity factor
K_i	A "best estimate" initiation toughness value
$K_{i2\sigma f}$, $K_{i4\sigma f}$	Initiation toughness values calculated using $J_{i2\sigma f}$, $J_{i4\sigma f}$
K_{io}	Initiation toughness value calculated from J_{io}
$K_{i\Delta a=O}$	Initiation toughness value calculated from $J_{i\Delta a=o}$
K_{Jc}	Initiation toughness value calculated from J_{Ic}
W	Specimen width
dJ/da	Measure of resistance to crack growth
$(dJ/da)_{LB}$	Lower bound resistance to crack growth
Δa	Ductile crack growth
$\Delta a_{(3)}$, $\Delta_{a(7)}$, $\Delta_{a(9)}$	Average measurements of ductile crack growth from 3, 7, and 9 measurements across the crack front
Δa_{max}	The maximum amount of ductile crack growth (usually measured at specimen mid-thickness)
σ_y	Yield stress
σ_u	Ultimate tensile stress
σ_f	Flow stress
SD	Standard deviation

Introduction

The main purpose of this paper is to present the methodology adopted by the United Kingdom Atomic Energy Authority (UKAEA) to provide "best estimate" reference values of start of life upper shelf fracture toughness properties for "modern" light water reactor pressure vessel materials. Such reference values of both initiation toughness and resistance to crack growth were used by a UKAEA study group in a generic assessment of the integrity of a pressurized water reactor (PWR) pressure vessel [*1*]. In their assessment "modern materials" were considered by the study group to be those whose fracture properties reflect the advances that have been made in both steelmaking and fabrication practices over the past decade.

One important distinction between the assessment performed by the study group and those performed using the more traditional routes of American Society

of Mechanical Engineers (ASME) III Appendix G and ASME XI Appendix A is that the former calculations involved best estimate physical/mechanical/fracture properties as well as lower bound values. Neither ASME III Appendix G nor ASME XI Appendix A are strictly applicable at operating temperatures where failure will occur by a ductile mechanism. By convention, however, lower bound toughness values corresponding to fully ductile behavior are usually taken as the upper limit to the respective reference K_{IR} or K_{Ic} fracture toughness/temperature curve, irrespective of upper shelf temperature. It has been recognized for a number of years that, on the upper shelf, fracture toughness decreases with increasing temperature [*2*]. Thus, a key requirement when specifying the data base was to define fracture resistance as a function of temperature from the onset of fully ductile upper shelf conditions to the normal operating temperature of ~288°C.

Ductile crack initiation and propagation involves the nucleation, growth, and coalescence of microvoids and the eventual formation of a macroscopic ductile tear. This is a continuous process, and consequently it is difficult to define precise values of "initiation" toughness. In an engineering context, "initiation" was taken to correspond with the onset of macroscopic ductile crack extension, but even this condition is difficult to define from much of the published upper shelf toughness data. Published data fell into two classes: those derived using the multi-specimen, interrupted test technique and those derived using suitably instrumented single-specimen techniques. When the study group began its deliberations, in 1980, available published data on the single-specimen methods based on either AC or DC potential drop were still considered to be less reliable than data from multi-specimen methods for defining initiation toughness and crack growth resistance. At this time, the unloading compliance technique was being actively developed as a viable alternative to multi-specimen testing. Apart from published unloading compliance data for materials where multi-specimen results were already available, published work by the key practitioners of this technique was devoted almost exclusively to the low upper shelf toughness materials used in early U.S. reactors. Such materials are not typical of current commercial practices, and the data were not included in the analysis. In view of the relative novelty of the unloading compliance method and possible unreliability of other single-specimen methods only data from multi-specimen tests were used to define reference upper shelf toughness values.

The multi-specimen method offered, in principle, the least ambiguous route for defining "best estimate" initiation toughness values but difficulties arose in producing a consistent data base because of significant differences in resistance curve J_R construction procedures that have been adopted by the technical community. In most cases it was necessary to reassess the original J-Δa data. The methods used to define a data base will be described briefly and the final results presented. The paper also comments on current methods of estimating upper shelf toughness, particularly where greater emphasis is being placed on defining nonlinear crack growth resistance data. Finally, some ideas will be outlined that

would allow a more consistent interpretation of upper shelf toughness data derived using current test procedures.

J_R *Construction Methods*

Relevant data available in 1980 and 1981 were based almost exclusively on linear J-Δa analyses. J_R constructions involved different methods of estimating the amount of ductile crack growth Δa and different procedures for defining initiation toughness. These were as follows:

1. Measurements where Δa includes the contribution caused by crack-tip blunting. These are, for example, the ASTM Test for J_{Ic}, a Measure of Fracture Toughness (E 813) which defines J_{Ic} as the intersection of a $J = 2\sigma_f \Delta a$ blunting line and a linear regression to data points within the Δa range 0.15 to 1.5 mm offset from the blunting line. Variants have been suggested on this method, which involve the use of lower crack growth data in conjunction with either a $J = 4\sigma_f \Delta a$ blunting line [2] or an experimentally defined blunting line [3].
2. Measurements where Δa does not include the blunting component before macroscopic ductile crack extension. In this method initiation is defined by extrapolating the J-Δa regression line to $\Delta a = 0$.

Initiation values defined by either method depend markedly on the crack growth range used to define the J-Δa regression line. Figure 1 shows examples of different J_R constructions for data where Δa includes crack-tip blunting. This comprehensive series of results, which was obtained by Carlson and Williams [4], refers to tests on nonside-grooved 25-mm-thick compact specimens extracted from an A533B-1 (Unified Numbering System [UNS] K12539) plate (Heavy

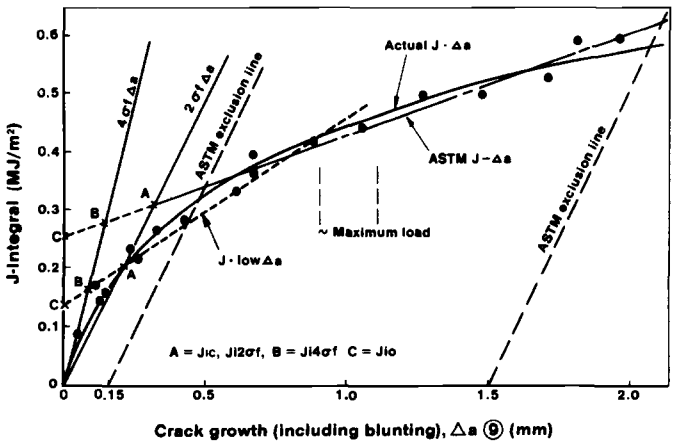

FIG. 1—*Comparison of different* J-Δa *constructions for defining initiation toughness. HSST-02 steel, 25-mm CS, T-L orientation tested at 149°C* [4].

Section Steel Technology [HSST]-02) notched to various depths (a/W = 0.5, 0.6, and 0.8). As pointed out by the authors, the data are better represented by a nonlinear fit than by a straight line, but the immediate point is the significant difference in estimates of initiation toughness that can arise from the two linear J_R constructions. Examples of J_R analyses where the Δa measurement excludes blunting are shown in Fig. 2, which presents results obtained by the author for plane sided and side-grooved 40-mm-thick compact specimens of a typical modern A533B-1 steel. Crack extension was measured as the average of the seven internal measurement positions recommended in ASTM E 813. These results illustrate that, within the limits of experimental accuracy, side-grooving has no effect on either initiation toughness or resistance to crack growth associated with the first increment (< 1 mm) of ductile crack extension.

Development of the Upper Shelf Data Base

The strategy adopted to define a consistent upper shelf data base was to reassess all published and "in-house" J_R data where Δa included blunting to provide toughness estimates corresponding to the intersection of the J-Δa line with $J = 2\sigma_f \Delta a$ and $J = 4\sigma_f \Delta a$ blunting lines and the value of J at Δa = O. These values were designated as J_{Ic} (or $J_{i2\sigma_f}$ if invalid according to E 813) $J_{i4\sigma_f}$ and J_{io} (examples are shown in Fig. 1), respectively. The data sets used for each J_R construction were designated as either "high Δa" or "low Δa." The former designation was applied when the crack growth range was as specified in ASTM E 813 or higher, and the latter designation was applied where all Δa values were less than ≈1 to 2 mm depending on specimen size and specifically when results

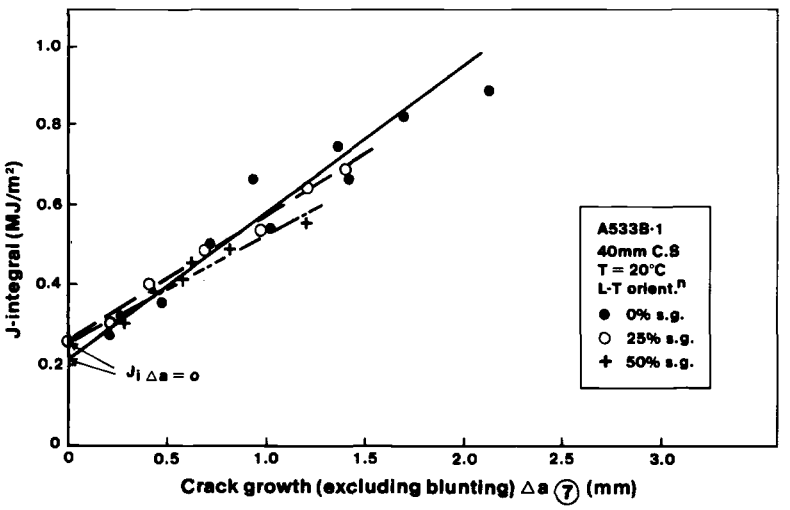

FIG. 2—*The effect of side-grooving on initiation toughness values defined when* Δa *excludes crack tip blunting.*

were obtained between the $J = 4\sigma_f\Delta a$ blunting line and the 0.15-mm data exclusion line parallel to $J = 2\sigma_f\Delta a$ (Fig. 1). The majority of results available were from tests on 20 to 40 mm-thick specimens and low Δa data conformed, in general, with the requirement $\Delta a \leq 6\%b$ where b is the remaining ligament. Similar guidelines in terms of crack growth ranges were applied to analyses where Δa data excluded crack-tip blunting.

J_R data from the United States [*4–8*], Europe [*2,3,9–16*][2–5] and Japan [*18,19;*] were examined to provide values of initiation toughness, which were defined in the following way:

1. Δa *Measurements Including Crack-tip Blunting*—The intersection of a "*J*-low Δa" regression line with a $J = 4\sigma_f\Delta a$ blunting line ($J_{i4\sigma_f}$). Where only "*J*-high Δa" data were available, the initiation value was taken to be the value of J at $\Delta a = O$ (J_{io}).
2. Δa *Measurements Excluding Crack-tip Blunting*—The value of J at $\Delta a = O$ for a "*J*-low Δa" regression line ($J_{i\Delta a} = O$).
3. *Experimental Determination of Crack-tip Blunting*—The intersection of a "*J*-low Δa" regression line with a metallographically defined blunting line [*3*].
4. *A Definition of Initiation From a Finite-Element Analysis*—The value of J at 0.2-mm crack growth from a nonlinear J-Δa regression analysis based on the maximum extent of crack growth, inclusive of blunting Δa_{max} [*16*].

In many cases, definition of Types 1 and 2 initiation toughness values involved a reevaluation of the published J-Δa data. This was deemed necessary to account for those differences in published initiation values that could be directly attributable to differences in *R*-curve construction procedure. Defining initiation toughness by Methods 1, 2, 3, or 4 should provide a more consistent date base, and such results were termed "best estimate" values.

These analyses yielded 82 initiation toughness measurements for A533B-1/A508-2, A508-3 (where A508-2 and A508-3 are UNS K12766 and K12042) base materials and associated welds/HAZs, which were expressed in terms of the equivalent stress intensity factor K using

$$K^2 = EJ/(1-\nu^2)$$

Best estimate toughness values for A533B-1 and A508-3 steels, and from tests on welds/HAZs are presented in Tables 1 through 3, respectively. Also given are the corresponding values of K_{Jc} (from J_{Ic}) or $K_{i2\sigma_f}$ (from $J_{i2\sigma_f}$). Most of the data were obtained before the requirements of ASTM E 813 were finalized, and consequently relatively little information is available to relate K_{Jc} (from valid J_{Ic}

[2]CEA Saclay, private communication.
[3]Ingham, T., UKAEA unpublished work, Warrington, Cheshire, England.
[4]Lidbury, D. P. G., UKAEA unpublished work, Warrington, Cheshire, England.
[5]Druce, S. G., UKAEA unpublished work, Harwell, Oxon, England.

TABLE 1—*Best-estimate* K_i *and* K_{Jc} (K_{i2af}) *toughness values for A533B-1 steel.*

Plate Origin [Ref]	Sulfur Content, Weight %	Test Temperature, °C	Best-Estimate K_i, MPa · $m^{1/2}$	K_{Jc} (K_{i2af}), MPa · $m^{1/2}$	Orientation
HSST-01 [2]	0.018	60	199	(282)	LT
HSST-01 [2]	0.018	250	155	ND	LT
HSST-02 [5]	0.014	23	203	(218)	TL
HSST-02 [5]	0.014	71	249	(284)	TL
HSST-02 [7]	0.014	121	199	(227)	TL
HSST-02 [4,8]	0.014	149	191	255, 239	TL
HSST-02 [7]	0.014	343	157	(175)	TL
EPRI-D [5]	0.009	54	221	(267)	TL
EPRI-D [5]	0.009	88	213	(243)	TL
EPRI-E [5]	0.015	49	206	(239)	TL
EPRI-E [5]	0.015	82	217	(240)	TL
EPRI-F [5]	0.021	38	233	(261)	TL
EPRI-F [5]	0.021	71	227	(248)	TL
EPRI-M [5]	0.013	177	168	(187)	TL
United States[3]	0.011	20	165	(191)	TL
Japan [27]	0.007	20	213	(261)	TL
France[2]	...	20	213	(278)	L-T
France[3]	0.005	20	228	320	LT
France[3]	0.005	288	202	220	LT
France[5]	0.005	290	172	(192)	TS
France[5]	0.005	290	172	ND[a]	TL
France [16]	0.007	24	215	ND	LT
France [16]	0.007	100	233	ND	LT
France [16]	0.007	150	209	ND	LT
France [16]	0.007	200	188	ND	LT
France [16]	0.007	250	174	ND	LT
France [16]	0.007	300	175	ND	LT
France [16]	0.007	275	177	177	LS
France [16]	0.005	70	238	ND	LS
France[2]	...	20	208	252	TL
United Kingdom [2]	0.013	20	191	(282)	LT
United Kingdom [2]	0.013	250	148	(163)	LT

[a]ND = not determined.

TABLE 2—*"Best-estimate," K_i, and K_{Jc} ($K_{i2\alpha f}$) toughness values for A508-3 steels.*

Forging Origin [Ref]	Sulfur Content, weight %	Test Temperature, °C	"Best-Estimate" K_i, MPa · $m^{1/2}$	K_{Jc} ($K_{i2\alpha_f}$), MPa · $m^{1/2}$	Specimen Orientation[a]
Japan [*19*]	0.005	10	265	(337)	A-R
Japan [*19*]	0.005	20	228	(346)	C-R
Japan [*15*]	0.003	290	260	305	A-R
Japan [*14*]	0.003	100	239	...	C-R
Japan [*14*]	0.003	280	256	...	C-R
Japan [*14*]	0.003	100	276	...	A-R
Japan [*14*]	0.003	280	210	...	A-R
Japan[4]	0.002	20	265	(363)	C-R
Japan[4]	0.002	20	238	323	A-R
Japan[4]	0.002	288	207	296	C-R
France [*10*]	0.006[b]	100	210	(227)	C-A
France [*10*]	0.005[b]	100	247	(278)	A-C, C-A
France [*10*]	0.006[b]	85	208	(227)	A-C
France [*10*]	0.005[b]	70	216	(232)	A-C
France [*10*]	0.007[b]	100	203	(222)	A-C
France [*10*]	0.015[b]	100	174	(180)	A-R
France [*3*]	0.010	100	217	(252)	C-A
France [*3*]	0.020	100	188	(199)	A-C
France [*3*]	0.005	100	217	(252)	C-A
France [*9*]	...	20	208	(275)	A-C

[a]A = axial (≡T), C = circumferential (≡L), and R = radial (≡S).
[b]S levels estimated from Ref 1.

TABLE 3—*"Best estimate"* K_i $K_{i2\sigma_f}$ *toughness values for welds/HAZs in A533B-1 and A508 steels.*

Weld Origin [Ref]	Material Sampled	Sulfur Content, weight %	Test Temperature, °C	"Best Estimate" K_i, MPa · $m^{1/2}$	$K_{i2\sigma_f}$, MPa · $m^{1/2}$
EPRI[a] Ht P [5]	MMA weld	0.010	10	329	376
EPRI Ht P [5]	MMA weld	0.010	43	335	385
EPRI Ht Q [5]	MMA weld	0.010	10	252	325
EPRI Ht Q [5]	MMA weld	0.010	43	297	344
EPRI Ht R [5]	MMA weld	0.010	16	244	296
EPRI Ht R [5]	MMA weld	0.010	49	223	301
EPRI Ht U [5]		0.024	177	199	214
EPRI Ht V [5]	S/A weld	0.009	10	232	279
EPRI Ht V [5]	S/A weld	0.009	43	257	293
EPRI Ht X [5]	S/A weld	0.010	10	244	270
EPRI Ht X [5]	S/A weld	0.010	43	270	296
EPRI Ht X [5]	S/A weld	0.010	177	212	238
EPRI Ht Y [5]	S/A weld	0.010	43	258	290
EPRI Ht K [5]	MMA weld	0.017	177	239	275
EPRI Ht L [5]	S/A weld	0.013	177	152	162
Japan [20]	S/A HAZ	0.004	0	214	269
United Kingdom [13]	S/A HAZ	0.008	70	228	...
United Kingdom [13]	S/A HAZ	0.008	280	200	...

[a]EPRI is the Electric Power Research Institute.

data) with best estimate data. This aspect will be discussed after presenting best estimate upper shelf toughness/temperature relationships for the data base.

Best Estimate Initiation Toughness/Temperature Relationships

Figure 3 shows initiation toughness data for base metals as a function of test temperature. The data have been subdivided on the basis of sulfur content and it can be seen that, in general, initiation toughness is higher for the low sulfur containing steels. The level of sulfur provides a good indication of the quality of steel making practice. Thus data for steels containing <0.010 weight % of sulfur were used to derive the best estimate upper shelf toughness/temperature relationships that would be applicable to modern A533B-1 and A508-3 steels.

The results of a linear regression analysis using toughness data for those A533B-1 and A508-3 steels containing less than 0.010 weight % sulfur are shown in Fig. 4. Taking the data to be normally distributed at upper shelf temperatures, the temperature dependence of upper shelf toughness of these base materials (in MPa · m $\frac{1}{2}$) is given by

$$K_i \text{ (mean)} = 231 - 0.096\,T°C$$
$$K_i \text{ (}-95\%\ CL\text{)} = 182 - 0.096\,T°C$$
$$K_i \text{ (}+95\%\ CL\text{)} = 282 - 0.096\,T°C$$

The available data base for weld metals/HAZs (Table 3) was too limited to justify independent statistical analysis of these data, and the results have been included in Fig. 4 to allow direct comparison with those for low sulfur base metals. Most of the data lie well above the mean line for base metals. The only data point lying below the lower 95% confidence limit refers to a submerged

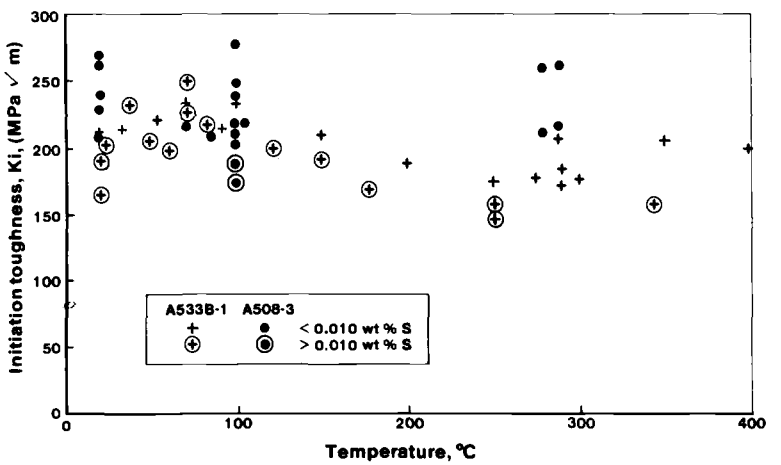

FIG. 3—*"Best estimate" initiation toughness data for A533B-1 and A508-3 steels.*

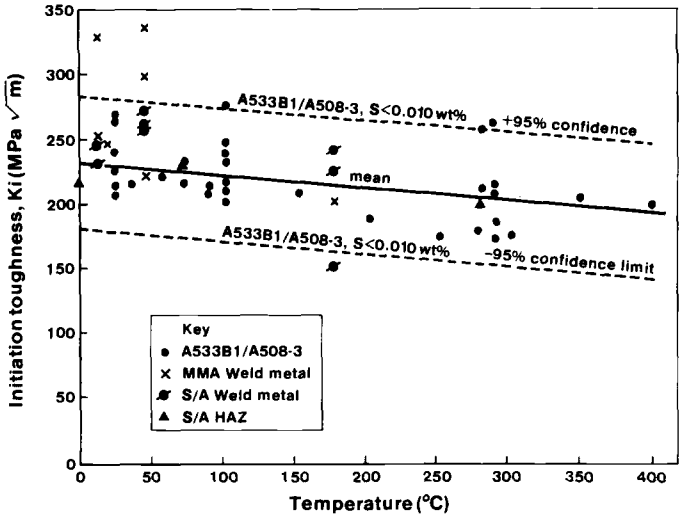

FIG. 4—*Comparison of initiation toughness data for weld metals/HAZ's with "best estimate" K_i-temperature relationships for A533B-1 and A508-3 steels containing less than 0.010 weight % sulfur.*

arc weld produced using a high heat input and a Linde 80 flux, neither of which are representative of current commercial welding practice as used in LWR fabrication. The results indicate that the mean and lower 95% confidence limit K_i temperature limits, which were derived for base metals, can also be used for weld metals produced to modern commercial practice.

Lower Bound Resistance to Crack Growth

The main problems when assessing the available data to define post-initiation toughness values were as follows:

1. The J_R slope dJ/da depends upon specimen orientation, the method used to estimate Δa, and on the Δa range over which dJ/da was estimated.
2. The majority of upper shelf toughness tests were made using plane-sided small scale specimens (25 mm thick) for which the increment of J-controlled crack growth [*21*] was relatively small (that is, $\leq$1 mm).

These factors introduced considerable uncertainties when assessing the available data. In particular, the differences in crack growth measurement procedures precluded the determination of a consistent data base. Consequently a statistical assessment of all dJ/da data was not attempted. Instead, an approach was adopted whereby reference lower bound J_R slopes $(dJ/da)_{LB}$, were defined, which were intentionally conservative with respect to all the available data for modern steels. Separate lower bound slopes were defined for both A533B-1 and A508-3 steels

tested at both the onset of upper shelf and at ~288°C; the onset of shelf conditions being defined as the temperature at which fully ductile behavior first occurs.

Comparison of the upper shelf initiation toughness analyses of the previous section with similar analyses relating to the fracture toughness transition region has shown that, for modern materials, ductile crack initiation should commence at temperatures below approximately 40°C [*1*]. Reference slopes for resistance to crack growth at the onset of upper shelf conditions were defined using the J_R data obtained from test at or close to ambient temperature.

Reference Slopes $(dJ/da)_{LB}$ *for A533B-1 and A508-3 Steels*

Lower bound slopes were derived for each material and test temperature in the following manner. Using a J-Δa data set of known pedigree, a J-Δa relationship was defined by reducing both the slope and intercept of the best fit linear J-Δa regression analysis by three standard deviations (-3SD) This '-3SD' slope was then compared with the slopes of J_R relationships from all other specimens of the same steel tested at the appropriate temperature. The '3 – SD' slopes were found to be lower bounds to all available results. To compensate for effects of crack growth averaging procedure and specimen orientation, reference lower bound slopes $(dJ/da)_{LB}$ were defined by reducing the '-3SD' slopes by a factor of two.

Examples of this approach are given in Figs. 5 and 6. The reference slope for A508-3 steel at the onset of upper shelf, is compared in Fig. 5, with other

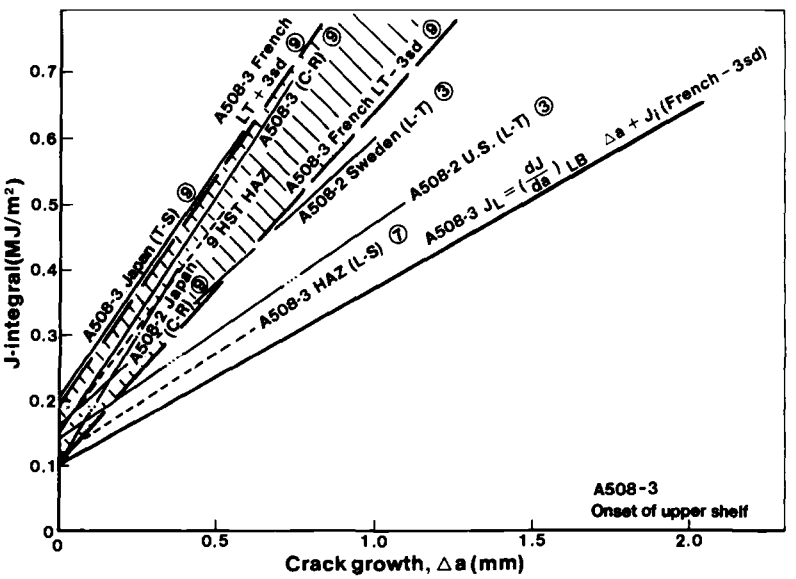

FIG. 5—*Initial resistance to crack growth for A508-2 and A508-3 steels tested at onset of upper shelf.*

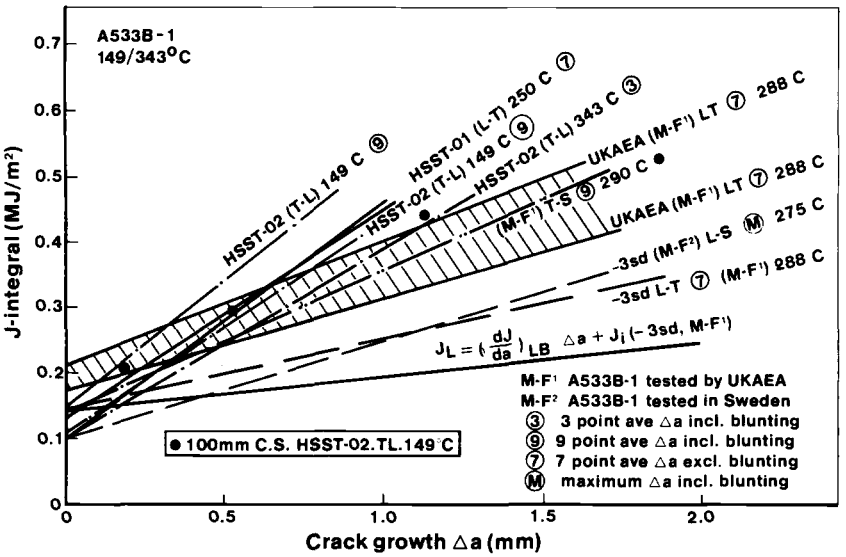

FIG. 6—*Initial resistance to crack growth for A533B-1 steels tested at 149 to 343°C.*

results for both A508-3 and A508-2 steels tested at or close to ambient temperature. In this case the lower bound J-Δa relationship J_L is defined by the reference slope and the intercept of the "$-3SD$" J_R line for an A508-3 steel produced and tested in France. This material was thought to represent a lower bound fracture toughness for forgings used in the French PWR program [*9*].[2] Figure 6 compares the lower bound slope for A533B-1 (UNS K12539) steel at 288°C with representative results for other A533B-1 steels, including the bounding data, which were obtained over the temperature range 149 to 343°C. This reference slope was derived using data for a French A533B-1 steel (M-F′) tested by the author.

The reference lower bound slopes derived for A533B-1 and A508-3 steels are given by

$$\text{A533B-1: onset of upper shelf: } (dJ/da)_{LB} = 0.130 \text{MJm}^{-2}/\text{mm and}$$

$$288°\text{C: } (dJ/da)_{LB} = 0.053 \text{MJm}^{-2}/\text{mm}$$

$$\text{A508-3: onset of upper shelf: } (dJ/da)_{LB} = 0.273 \text{MJm}^{-2}/\text{mm and}$$

$$288°\text{C: } (dJ/da)_{LB} = 0.125 \text{MJm}^{-2}/\text{mm}$$

Reference slopes for A533B-1 steel were derived using results from testing 40-mm-thick compact specimens whereas those for A508-3 steels were obtained from tests on 25-mm-thick specimens. No significant difference in resistance to crack growth was observed by the UKAEA when testing 25- and 40-mm-thick specimens of the French A533B-1 steel (M-F′). It was concluded therefore that the reference slopes for both A533B-1 and A508-3 steels could be used to define

post-initiation toughness data satisfying the requirements for J-controlled growth providing crack growth was limited to a maximum value of 2 mm. This limit on crack growth corresponds to approximately 6% of the ligament for a 40-mm compact specimen.

Reference Upper Shelf Data for A533B-1/A508-3 Steels

The reference slopes $(dJ/da)_{LB}$ are intended to be used with either +95% CL, mean, or −95% CL "best estimate" initiation values. Examples when the slopes are indexed to mean initiation values are shown in Fig. 7 where the reference J-Δa relationships are termed J_{RL} (R = reference initiation and L = reference lower bound slope). Although separate J_{RL} lines were derived for A533B-1 and A508-3 steels, the similarity in chemical composition and use of nominally equivalent heat treatments for these two materials suggests that they should exhibit no generic difference in resistance to crack growth. The differences in $(dJ/da)_{LB}$ may be attributable to increased purity of the A508-3 steels, which were generally of more recent origin.

Discussion

Comparison of "Best Estimate" Toughness Values with Data Derived Using a $J = 2_{\sigma f}\Delta a$ *Blunting Line*

The difference between best estimate K_i values and either the K_{Jc} values (derived from J_{Ic}) or $K_{i2\sigma_f}$ values (from nonvalid E 813 data) increases with increasing resistance to crack growth. The derivation of any relationship between these toughness measurements should therefore take account of factors that in-

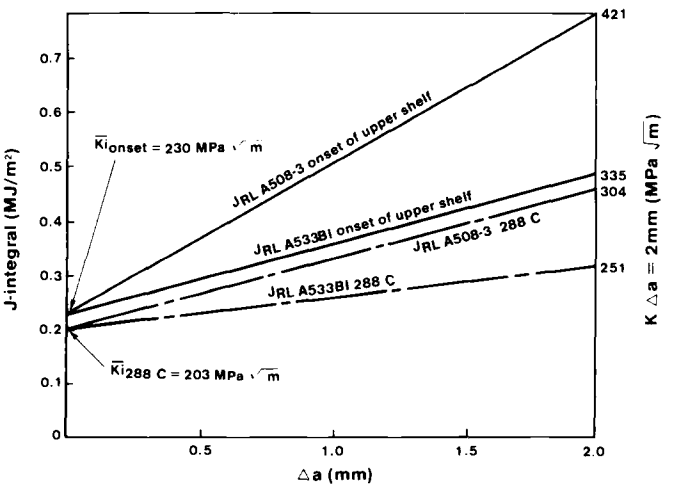

FIG. 7—*Proposed lower bound* J_R *relationships indexed to mean initiation toughness values, applicable for 2-mm maximum crack growth.*

fluence resistance to crack growth; for example, inclusion/impurity element content, specimen orientation, and test temperature. The available data base was too small to quantify each of these factors. Furthermore a strict comparison of the two methods of estimating initiation was complicated by the different crack growth ranges (low Δa and high Δa), which had to be used when defining the data base. This aspect was reflected by the unacceptably low correlation coefficients found ($r \approx 0.75$) in attempts to correlate K_i values in the range 165 to 265 MPa · m $\frac{1}{2}$ with corresponding K_{Jc} or $K_{i2\sigma_f}$ values. Nevertheless, a comparison of mean toughness values indicated that, at the onset of upper shelf conditions, K_{Jc} or $K_{i2\sigma_f}$ values for A533B-1 and A508-3 steels would have to be reduced by aproximately 20 and 25%, respectively, to provide mean best estimate, K_i, toughness values. The decrease in resistance to crack growth with increasing upper shelf temperature will result in a smaller difference between the two types of measurement at 288°C and to a first approximation the mean K_{Jc} or $K_{i2\sigma_f}$ data at 288°C for both A533B-1 and A508-3 steels would need to be reduced by 10 to 15%. These approximations are based on all available K_{Jc} or $K_{i2\sigma_f}$ data. In general, $K_{i2\sigma_f}$ provides an underestimate of K_{Jc}, and the assessment will not fully reflect the larger differences between K_i and K_{Jc} (from valid J_{Ic}), which will arise in steels of very high toughness.

If blunting should be represented by $J = 4\sigma_f \Delta a$ rather than $J = 2\sigma_f \Delta a$ [2,10] then J_{Ic} values for such steels will be associated with a significant amount of crack growth and the difference between K_i and K_{Jc} will increase accordingly. Figure 8 compares ASTM E 813 J_R analyses for two high quality, high toughness steels and the two steels tested in the round-robin programs used to develop the

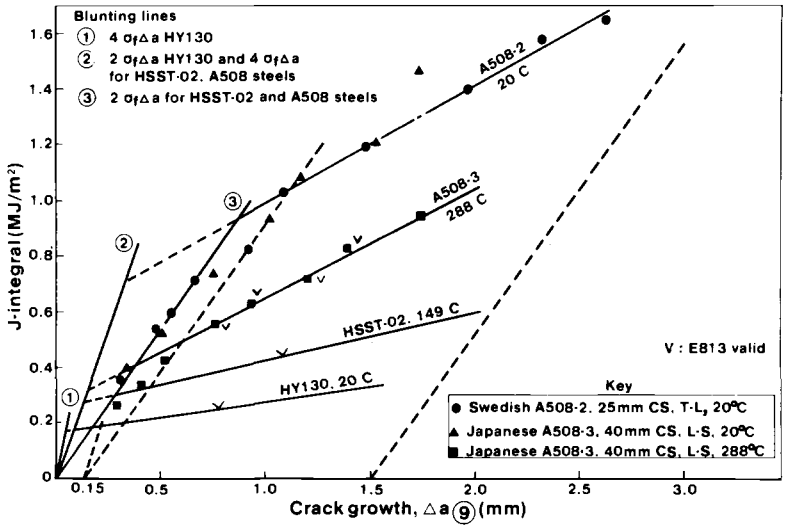

FIG. 8—*Comparison of ASTM E 813 J_R constructions for steels exhibiting different resistance to crack growth.*

ASTM E 813 test method. The increments of crack growth (including blunting) associated with J_{Ic} increases from approximately 0.1 mm for HY130 steel tested at 20°C to approximately 0.4 mm for the high purity Japanese A508-3 steel tested at 288°C. The specimen size requirements of ASTM E 813 preclude a determination of J_{Ic} at 20°C using 25-mm-thick specimens of the A508-2 steel and 40-mm-thick specimens of the Japanese A508-3 steel. It is clear, however, that J_{Ic} values for these steels would be associated with ~0.8-mm crack growth. J_{Ic} (J_Q) values for the data shown in Fig. 8 are compared (Table 4) with best estimate J_i values derived using a $J = 4\sigma_f\Delta a$ blunting line and "low Δa" data ($\Delta a \lesssim$ 0.6b). Conversion of these initiation J values to equivalent K values indicates that the E 813 procedure can overestimate the toughness at the onset of macroscopic crack growth by 25% at 288°C. The discrepancy will be larger at 20°C where resistance to crack growth is higher. Assuming the J_R curves for A508 steels to be essentially independent of size for the increase in thickness necessary to produce valid J_{Ic} measurements at 20°C then the resultant increase in K_{Jc} over K_i could be as high at 50%.

Developments in J_R Testing/Analysis

The ASTM E 813 procedure would be improved by replacing the $J = 2\sigma_f\Delta a$ blunting line with a $J = 4\sigma_f\Delta a$ line and defining a linear J_R relationship for data lying between 0.15 and 1.5 mm offsets from the modified blunting line. This would provide a better estimate of initiation toughness and would allow "valid" data to be derived from smaller specimens. The modified procedure would allow the testing of 25-mm-thick specimens of high toughness forging steels (see Fig. 8) but could still pose problems when testing smaller scale specimens that are more suited to reactor pressure vessel surveillance programs. Size-independent initiation data will be obtained from linear analyses only when (1) the specimen size satisfies a requirement of the form b, $B < xJ/\sigma_f$ where $x = 15$ in E 813, and (2) J_R relationships for different specimen sizes are defined using the same crack growth range. The need to satisfy the size requirement will impose a limit on the allowable crack growth range, which will decrease with specimen size. Thus, particular care must be taken when comparing results from surveillance programs with those obtained using larger scale specimens.

Linear analyses can only be used to define realistic estimates of initiation toughness and resistance to crack growth when J_R is defined for a small increment of crack growth. Consequently, such analyses provide only limited information concerning resistance to crack growth.

The development of J_R testing techniques has been stimulated by the need to provide a more accurate interpretation of resistance to crack growth rather than to define methods for identifying initiation toughness values. This is a consequence of the advances that have been made in methods of analyzing ductile instability. In this type of analysis, resistance to crack growth rather than initiation is the relevant material property. The latter is, however, a necessary input to a

structural instability analysis. Single-specimen unloading compliance testing is now well established, and a tentative testing procedure has been developed [*22*]. These developments have led to the more widespread use of nonlinear J_R analyses, which provide a better description of resistance to crack growth over a larger crack growth range than can be adequately accommodated in a linear analyses. A comparison of J_R data for a range of specimen sizes (10 to 100 mm thick) for A533B-1 steel [*23*] demonstrated that nonlinear (power law) J_R analyses provide a more consistent interpretation of specimen size effects than linear analyses. It would seem appropriate, therefore, to consider the development of a unified method for testing compact or bend specimens to determine both initiation toughness and extended amounts of resistance to growth from a nonlinear J_R construction. Initiation values could be adequately defined by the intersection of the J_R curve and some blunting line relationship. For example, good correspondence with the onset of ductile crack growth was defined in Refs *23* and *24* by the intersection of a power law J_R curve and a 0.1-mm offset from a $J = 4\sigma_f\Delta a$ blunting line whereas in Ref *4* the best estimate of initiation was identified as the intersection of a best fit polynomial J_R curve and a $J = 2\sigma_f\Delta a$ blunting line. These definitions must, to some extent, be material and therefore crack growth dependent.

Thus it may be expedient to eliminate the anomalies associated with different blunting line interpretations by defining an "initiation" toughness value at a specified small increment of crack growth (including crack-tip blunting). For engineering application the value of J at $\Delta a = 0.2$ mm could provide an ap-

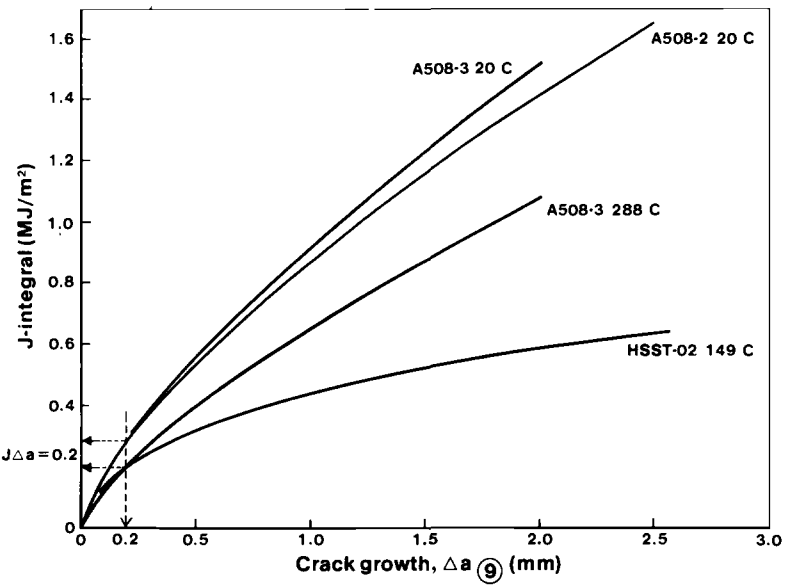

FIG. 9—*Power law J_R interpretations for the A508 and A533B-1 steels considered in Fig. 8.*

TABLE 4—*Comparison of initiation toughness estimates from linear and power law J_R analyses for steels exhibiting different resistance to crack growth.*

Material	Specimen Size, mm	Test Temperature, °C	Initiation Value J, MJ/m^2		
			Linear Analysis		Power Law
			J_{Ic} (J_Q)	$J_{0.4\sigma_{fl}}$	$J_{\Delta a=0.2\ mm}$
HY130	25	20	0.19	0.15	0.19
HSST-02	25	149	0.255	0.165	0.21
A508-2	25	20	(0.94)	0.19	0.28
A508-3	40	20	(>0.75)	0.31	0.28
A508-3	40	288	0.43	0.21	0.22

[a]Using J-low Δa ($\Delta a \leq 0.06\ b$).

propriate definition. This approach is illustrated in Fig. 9, which presents power law interpretations for the J_R data plotted in Fig. 8. Comparison of J at $\Delta a = 0.2$ mm from the power law analyses with best estimate ($J_{i4\sigma_f}$) values from linear analyses (Table 4) indicates that the $J_{\Delta a=0.2}$ data satisfactorily characterize the differences in initiation toughness of the four steels.

While it is perfectly acceptable for an initiation toughness testing procedure to use plane-sided specimens it is suggested that a unified initiation toughness/resistance to crack growth procedure should require that side-grooved specimens be tested. The total amount of side-grooving should be about 25% of the specimen thickness. If the specimen size requirements of ASTM E 813 and [*22*] are combined then the requirements for a unified procedure would be b, $B_N > 25J_i/\sigma_f$ and $20J/\sigma_f$ for an allowable crack growth range $\Delta a \leq 10\%$ of the remaining ligament. However, data obtained at the author's laboratory [*23*] indicate that these requirements may be unduly restrictive for defining nominally size independent J_i/J_R data from power law interpretations of the upper shelf toughness of A533B-1 steel. Within the limits of experimental accuracy, tests on 25% side-grooved 20-, 40-, and 100-mm-thick specimens produced size independent J_i and J_R data when b, B_N exceed $20J_{\Delta a=0.2}/\sigma_f$ and $15J/\sigma_f$ for crack growths of at least 15% b or 5 mm whichever is the smaller.

General Conclusions

"Best estimate" initiation toughness-temperature relationships and lower bound resistance to crack growth data have been defined, which are considered to be typical of the upper shelf fracture toughness properties of modern light water reactor pressure vessel materials. The results can be used in fracture analyses providing the pressure vessel is operating in the fully ductile upper shelf condition.

The relationships were derived from linear J_R analyses of multi-specimen test data, the majority of which were produced by testing nonside-grooved specimens.

Difficulties were encountered in defining consistent initiation toughness and resistance to crack growth data; the development of a tentative procedure for unloading compliance testing and the consequent publication of more comprehensive J_R data will eliminate these difficulties and allow further refinements to be made to the data base.

The progress in J_R testing and analysis since the data base was prepared indicates that continued pursuit of a precise definition of initiation toughness is inappropriate. Nonlinear J_R analyses provide a better representation of overall resistance to crack growth than linear analyses, and the former could be used in conjunction with an "engineering" definition of initiation toughness as the value of J at $\Delta a = 0.2$ mm, to develop a unified test procedure for determining J_i and resistance to crack growth using side-grooved specimens. This suggestion is based on results for A533B-1/A508-3 ferritic pressure vessel steels and should be tested against data for other materials.

Acknowledgments

The reference upper shelf toughness data were derived by a UKAEA Working Group acting under the chairmanship of Mr. S. F. Pugh (AERE Harwell). The author wishes to acknowledge the contributions made by Mr. Pugh and members of the group, Dr. A. Cowan and Mr. B. W. Pickles (RNL, Risley) and Drs. J. A. Hudson and S. G. Druce (AERE Harwell). The opinions expressed concerning the development of a power law interpretation of J_R data are those of the author and do not necessarily represent the view of the UKAEA or other organizations involved in the United Kingdom nuclear industry.

References

[*1*] Marshall, W., "An Assessment of the Integrity of PWR Pressure Vessels," summary report, UKAEA, Warrington, Cheshire, England, June 1982.

[2] Ingham, T. and Morland, E., *Proceedings of CSNI Specialist Meeting on Plastic Tearing Instability*, NUREG/CP-0010, St. Louis, MO, 1979, pp. 330–358.

[*3*] Lautridou, J. C. and Pineau, A., *Engineering Fracture Mechanics*, Vol. 15, No. 1/2, 1981, pp. 55–71.

[*4*] Carlson, K. W. and Williams, J. A., "A More Basic Approach to the Analysis of Multiple Specimen R-Curves for Determination of J_c, *"Fracture Mechanics Proceedings of the Thirteenth National Symposium on Fracture Mechanics, STP 743*, American Society for Testing and Materials, Philadelphia, 1981, pp. 503–524.

[*5*] Fracture Control Corporation, "Nuclear Pressure Vessel Data Base," Electric Power Research Institute Topical Report NP 933, Palo Alto, CA, Dec. 1978.

[*6*] Combustion Engineering Inc., "Subcritical Crack Growth in Ferritic Materials for Light Water Nuclear Reactor Vessels," final report, Electric Power Research Institute NP-304, Palo Alto, CA, Aug. 1976.

[*7*] Logsdon, W. A., "Static and Dynamic Fracture Toughness of ASTM A508 C1-2 and ASTM C1.1 Pressure Vessel Steels at Upper Shelf Temperatures," MPC-8 ASME Winter Annual Meeting, San Francisco, Dec. 1978, pp. 149–165.

[*8*] Clarke, G. A., *Journal of Testing and Evaluation*, Vol. 8, No. 5, Sept. 1980, pp. 213–220.

[*9*] Ponsot, J., Gauthier, J. P., Petrequin, P., Houssin, B., and Barrachim, B., "Effect of Specimen Size on Toughness Measurement on a SA 508 C1.3 Steel in the Transition-Evaluation of K_{Ic} with Sub-Size Specimens, *"Proceedings of the CSNI Specialists Meeting on Elastic-Plastic Fracture Mechanics*, CSNI Report 32, Vol. 1, Daresbury, England, May 1978.

[*10*] Houssin, B. and Ponsot, A., *Transactions of the 6th International Conference on Structural Mechanics in Reactor Technology*, Paper G6/4, Paris, Aug. 1981.

[*11*] Garwood, S. J., Welding Institute Research Report 98/1979, Abington, Cambridge, England.

[*12*] Garwood, S. J., Welding Institute Research Report 114/1980, Abington, Cambridge, England.

[*13*] Threadgill, P. L. and Garwood, S. J., Welding Institute Contract Report 3542/5/80, Abington, Cambridge, England.

[*14*] Garwood, S. J. and Threadgill, P. L., Welding Institute Report 3600/1/81.

[*15*] Belcher, W. P. A. and Druce, S. G., "Micromechanisms of Ductile Stable Crack Growth in Nuclear Pressure Vessel Steels, *"Elastic-Plastic Fracture: Second Symposium Volume II Fracture Resistance Curves and Engineering Applications, STP 803*, American Society for Testing and Materials, Philadelphia, 1983, pp. II-739–II-762.

[*16*] Ostensson, B. and Westin, R., Aktiebolaget Atomenergie Report S-536, Studsvik, Sweden, 1976.

[*17*] Nilsson, F. and Ostensson, B., *Engineering Fracture Mechanics*, Vol. 10, No. 2, 1978, pp. 223–323.

[*18*] Tsudada, H., Iawadate, T., Tanaka, Y., and Ono, S., Japan Steel Works Report MS79-4-17, April 1979; also *Fourth International Conference on Pressure Vessel Technology*, Paper C55/80, Institute of Mechanical Engineering, London, 1980.

[19] Japan Welding Engineering Society 7HST Committee on the Fracture Toughness of Heavy Section Steel for Reactor Pressure Vessels," Report of the 1977 Program, JWES-AE-7806, Nuclear Power Engineering Department, Tokyo University, Tokyo, Japan. main text in Japanese.

[20] Tanaka, M., Sano, K.-I., Nakano, Y., Kusuhara, Y., Yoshimura, S., and Ohashi, N., "Mechanical Properties and Fracture Toughness of Heavy Section Steel Welds for Nuclear Pressure Vessels," Kawasaki Steel Corporation Report, Mizushima Works, Kurashiki, Japan, 1981.

[21] Hutchinson, J. W. and Paris, P. C., "The Theory of Stability Analysis of *J*-Controlled Crack Growth," *Elastic-Plastic Fracture, STP 668,* American Society for Testing and Materials, Philadelphia, 1972, pp. 37–64.

[22] Albrecht, P., Andrews, W. R., Gudas, J. P., Joyce, J. A., Loss, F. L., McCabe, D. E., Schmidt, D. W., and VanDerSluys, W. A., "Tentative Test Procedure for Determining the Plane Strain J_I-R Curve," *Journal of Testing and Evaluation,* Vol. 10, No. 6, Nov. 1982, pp. 245–251.

[23] Ingham, T., Bland, J. T., and Wardle, G., "The Influence of Specimen Size on the Upper Shelf Toughness of SA533-1 Steel," Paper G2/3, SMIRT 7, Chicago, Aug. 1983.

[24] Davies, L. M., Ingham, T., and Squires, R. L., "Evaluation of Advanced Reactor Pressure Vessel Steels Under Neutron Irradiation," *Effects of Radiation on Materials Proceedings of the Eleventh International Symposium, STP 782,* American Society for Testing and Materials, Philadelphia, 1982, pp. 433–463.

W. Alan Van Der Sluys,[1] *Robert H. Emanuelson,*[1] *and Robert J. Futato*[1]

Elastic-Plastic Properties of Submerged Arc Weld Metal

REFERENCE: Van Der Sluys, W. A., Emanuelson, R. H., and Futato, R. J., **"Elastic-Plastic Properties of Submerged Arc Weld Metal,"** *Elastic-Plastic Fracture Toughness Test Methods: The User's Experience, ASTM STP 856,* E. T. Wessel and F. J. Loss, Eds., American Society for Testing and Materials, 1985, pp. 68–83.

ABSTRACT: The results of a study conducted over a number of years to characterize the elastic-plastic fracture properties of submerged arc weld metal are presented in this paper. The fracture properties of four different weldments were investigated at temperatures ranging from 24 to 288°C (75 to 550°F). Tests were conducted using both the conventional multiple-specimen J_{Ic} procedure as well as an automated single-specimen unloading compliance technique capable of generating the material J_I-R curve.

Test results obtained using the two different procedures are compared. The comparison indicates that while both test techniques generate comparable J-Δa data for a given test condition, J_{Ic} values from the respective sets of data can differ. This is attributed largely to the sparsity of data generated by the multiple-specimen technique and the nonlinearity of the J_I-R curves as revealed by the single-specimen technique.

Welding procedure was found to have a significant effect on measured toughness. A wide range of fracture behavior was observed. The welding parameters responsible for the observed behavior are discussed. The applicability of the current J_{Ic} and J_I-R curve test procedures over the wide range of crack growth behavior observed is discussed.

KEY WORDS: elastic properties, plastic properties, fracture tests, fracture strength, fracture toughness, fracture properties, weldments, weld metal, submerged arc welding, impact tests, impact strength, J tests, J integral

A study into the elastic-plastic fracture properties of submerged arc weld metals will be described. This study has taken place over the last six years, and a number of different laboratory procedures have been used to evaluate the toughness of the weld metals studied.

Submerged arc welding is one of the most common joining procedures in use today. Since manufacturing defects are most likely to occur in the weld area, the fracture properties of the weld metal are of major interest in the assessment of the integrity of a welded structure. The study reported in this paper was initiated to characterize the fracture properties of submerged arc weld metals.

[1]Technical advisor and research metallurgists, respectively, Babcock & Wilcox, McDermott Company Research and Development Division, P.O. Box 835, Alliance, OH 44601.

The four weld metals chosen for this study represented a cross section of welding practices commonly used in the pressure vessel industry.

When this study was initiated, the elastic-plastic fracture toughness procedure in use was an early version of the multiple-specimen procedure. As the test procedure evolved, the older test results had to be reanalyzed using the improved J expressions or crack length measuring technique. Many of these older data sets were found to not meet the requirements of ASTM Test for J_{Ic}, a Measure of Fracture Toughness (E 813) upon this reevaluation and are therefore not included in this report.

During the progress of this study, the configuration of J specimens changed from a straight-sided to a side-grooved specimen. Some of the multiple-specimen tests were therefore conducted using straight-sided specimens and some using side-grooved specimens. The most significant change that occurred during this time was the change to the unloading compliance method of crack length measurement and the development of the single-specimen test method.

A completely automated single-specimen test procedure was developed by the Research and Development Division of Babcock & Wilcox, (B&W), a McDermott company, and in 1980, because the preferred method of conducting J_I-R curve tests at B&W. The majority of the test results reported in this study have been conducted by this method.

Material Description

Weldments and Properties

The single-wire submerged arc process was used to fabricate the four weldments. All were fabricated from various heats of manganese-molybdenum-nickel weld wire. Different lots of Linde 80 flux were used for weldments W-A, W-B, and W-C. Linde 124 flux was used for weldment W-D. All received basically the same post weld heat treatment, representative of standard commerical practice:

Heat at 56°C (100°F)/h above 316°C (600°F) to 593°C (1100°F) −621°C (1150°F), hold 48 to 50 h, cool 8°C (15°F)/h to 316°C (600°F).

A detailed description of the four weldments is given in Table 1. Room temperature tensile properties are presented in Table 2, and impact data are shown in Table 3.

Specimens

Location—Fracture toughness measurements were made using 2.54-cm (1.0-in.) thick (1T) compact specimens (CT), as illustrated in Fig. 1, prepared in compliance with the specimen recommendations of ASTM Test for Plane-Strain Fracture Toughness of Metallic Materials (E 399). The earliest tests did not have the optional side grooves.

TABLE 1—*Characteristics of weldments.*

Characteristic	Weldment			
	W-A	W-B	W-C	W-D
Flux	Linde 80	Linde 80	Linde 80	Linde 124
Base metal	SA 508 Cl 2	SA 508 Cl 2	SA 533 Gr B Cl 1	SA 508 Cl 2
Thickness, cm (in.)	30.5 (12)	36.8 (14.5)	17.5 (6.9)	36.8 (14.5)
Wire diameter, cm (in.)	0.318 (1/8)	0.397 (5/32)	0.397 (5/32)	0.397 (5/32)
Wire chemistry, weight %				
carbon	0.088	0.080	0.089	0.071
manganese	1.5	1.47	1.41	1.20
phosphorus	0.019	0.018	0.016	0.01
sulfur	0.010	0.020	0.014	0.01
silicon	0.45	0.53	0.54	0.42
chromium	0.11	0.07	0.11	0.03
nickel	0.71	0.56	0.69	0.60
molybdenum	0.33	0.46	0.45	0.37
copper	0.29	0.29	0.049	0.02
Volts	34	35	35	35
Amperes (AC)	500	450 to 800	650	400 to 800
Travel speed, cm (in.)/min	30.5 (12)	30.5 (12)	30.5 (12)	30.5 (12)
Preheat, °C (°F)	149 (300)	149 (300)	149 (300)	93 (200)
Interpass, °C (°F)	260 (500)	163 to 232 (325 to 450)	260 (500)	260 (500)

TABLE 2—*Room temperature tensile properties.*

Property	Weldment			
	W-A	W-B	W-C	W-D
0.2% yield strength, MPa (psi)	489.9 (71 000)	517.5 (75 000)	496.8 (72 000)	427.8 (62 000)
Ultimate tensile strength, MPa (psi)	607.2 (88 000)	614.1 (89 000)	621 (90 000)	545.1 (79 000)

TABLE 3—*Impact properties.*

Property	Weldment							
	W-A		W-B		W-C		W-D	
NDTT, °C (°F)[a]	−40	(−40)	−51	(−60)	−18	(0)	−12	(10)
RT_{NDT}, °C (°F)[b]	−15	(5)	−23	(−10)	−18	(0)	−12	(10)
$T_{40.7J}$, °C (°F) (30 ft-lb)[c]	−12	(10)	−29	(−20)	−37	(−35)	−54	(−65)
CVN,USE, J (ft-lb)[d]	94.9	(70)	81.3	(60)	94.9	(70)	203.4	(150)

[a]NDTT is the nil-ductility transition temperature as determined from drop weight impact tests described in ASTM Conducting Drop Weight Test to Determine Nil-Ductility Transition Temperatures of Ferritic Steels (E 208).

[b]RT_{NDT} is the reference temperature nil-ductility transition temperature. The method for establishing this temperature is outlined in detail in Section III, Division I and Subsection NB-2331 of the ASME Boiler and Pressure Vessel Code [*1*].

[c]$T_{40.7J}$ (30 ft-lb) is the temperature at which 40.7 J (30 ft-lb) is absorbed in the Charpy V-notch impact test and is based on average curve through energy test temperature data.

[d]CVN,USE is the upper shelf energy level as determined by Charpy V-notch impact tests based on average curve through energy test temperature data.

Orientation—All specimens were taken from the weldments in the T-L orientation. Weld root passes and surface regions were avoided, and care was taken to ensure that specimens were centered on the centerline of each weld.

In addition to specimens taken from all of the weldments in a T-L orientation, a special series of 1T CT specimens with a T-S orientation were taken from weld W-C. These specimens were used to measure toughness when a crack was through the thickness in the weldment rather than in the welding direction.

Test Procedure

The fracture toughness tests conducted in this study were performed to either a single-specimen *J*-test procedure or to a multiple-specimen J_{Ic}-test procedure.

The single-specimen *J*-test procedure makes use of an interactive digital computer system, which both conducts the test and analyzes the results. This system,

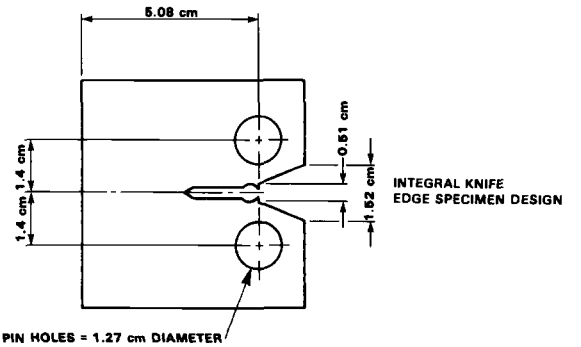

FIG. 1—*Compact tension specimen.*

described previously in Ref 2, uses unloading compliance to determine the crack length. The J value is determined using the J expression found in ASTM E 813. The test procedure follows the recommendation found by Albrecht et al [3]. The J_{Ic} value was determined by applying the procedures found in ASTM E 813 to the J_I-R curve determined by the above procedure.

The multiple-specimen test procedure required that five specimens be fatigue precracked to the same crack length. Two of these specimens were then tested. The first specimen was loaded to the maximum load point and unloaded. The second specimen was loaded to one-half of the displacement measured on the first specimen at maximum load. These two specimens were then heat tinted, the crack length determined, and the applied J calculated. A J_I-R curve was then constructed using these two points and the displacements that the remaining three specimens should be loaded to, in order to complete the J_I-R curve and meet the ASTM E 813 criterion. These three specimens were tested, analyzed, and the final J_I-R curve constructed. J_{Ic} was determined from this R curve and the validity criterion checked. Using this procedure, it is possible to achieve high success rates in determining J_{Ic} in accordance with ASTM E 813 with five specimens.

The specimen temperatures for both test procedures were achieved by enclosing the specimen, loading clevises and displacement gage in a hot air oven, and heating the specimen assembly to the desired test temperature. The specimen temperature was held to 2.8°C (±5°F) of the desired test temperature for the duration of the test. For tests above 260°C (500°F) additional heaters were added to the loading clevises in the hot air oven in order to achieve the desired specimen temperature without overheating the crack opening displacement gage.

Results

The results and significance of the fracture toughness tests conducted on the four weld metals of interest will be presented and a comparison of the properties between the four welds will be discussed in this section. Since this study has taken place over the last six years, the early fracture toughness tests were conducted by the multiple-specimen method while the more recent tests were conducted by the single-specimen test method using unloading compliance to determine the crack length.

The results of the fracture toughness tests on weld W-A in terms of the J_{Ic} value versus test temperature are presented in Fig. 2. The solid points in this figure represent tests in which the specimens fractured without measurable stable crack extension. For these tests, J_{Ic} was estimated to be the maximum J value attained. The circles in Fig. 2 represent J_{Ic} values calculated from multiple-specimen test results as prescribed in ASTM E 813. In performing these calculations, the total crack extension in each specimen was defined as the average of nine individual crack extension measurements across the crack front. In addition to these values, a second J_{Ic} value was calculated from the set of multiple-specimen data obtained at 24°C (75°F) using the maximum crack extension

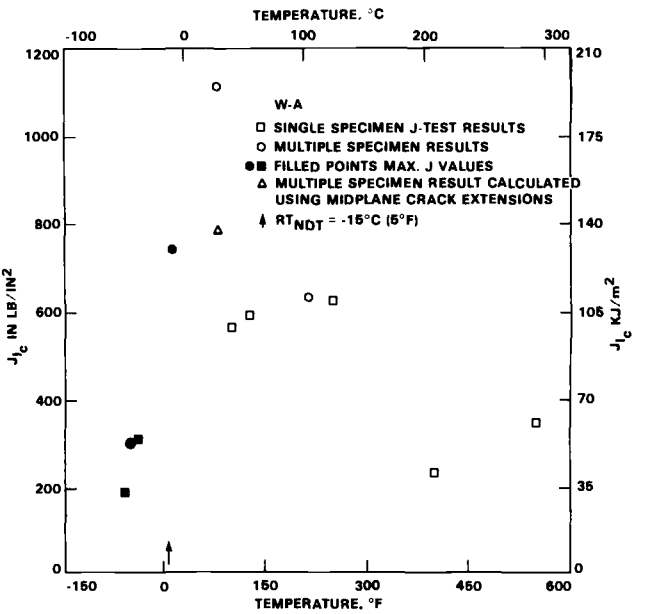

FIG. 2—*Fracture toughness as a function of test temperature for weld metal W-A.*

measured at the center of the specimens rather than the nine-point averages. That J_{Ic} value is represented by a triangle in Fig. 2. None of the specimens used in the multiple-specimen tests were side grooved. In addition, the *J* formulations used for the multiple-specimen tests and the *J* formulation used for the single specimen test, while both presented in ASTM E 813, are slightly different.

The toughness of this material is a strong function of temperature in the temperature ranges associated with both lower shelf and upper shelf Charpy behaviors. The maximum fracture toughness is around room temperature with a significant drop in toughness with temperature reaching a minimum around 204°C (400°F). The minimum at 204°C (400°F) suggests a dynamic strain aging mechanism to explain the drop in toughness properties. The RT_{NDT} temperature appears to be a conservative estimate of the transition temperature since it appears to represent a temperature in the upper portion of the transition region.

Figure 3 shows the *J-R* curves for the 38°C (100°F) single-specimen test and the 24°C (75°F) multiple-specimen test plotted using both the average and maximum crack extension in each specimen. The slopes of the multiple-specimen *R* curves are so steep that they appear to be almost parallel to the stretch line. The J_{Ic} value from the *R* curve produced using the average crack length does not meet the ASTM E 813 validity requirements because there are only three points between the exclusion lines. The *R* curve produced using the maximum crack extension does not meet ASTM E 813 requirements only because of the crack extension definition used. They are shown here, however, to illustrate the difference between the results from side-grooved and smooth-sided specimens

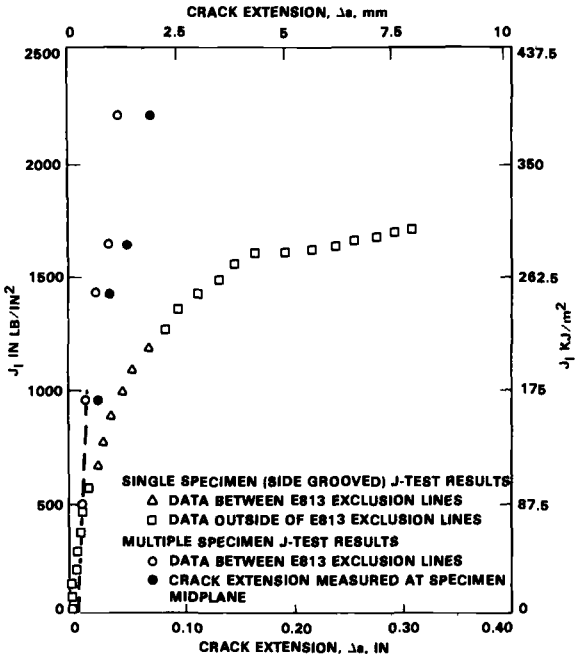

FIG. 3—J_I-R *curve for weld metal W-A with the single-specimen curve determined at 38°C (100°F) and the multiple-specimen curve at 24°C (74°F).*

and the average crack length versus the maximum crack length crack extension definitions. Even though the slope of the multiple-specimen *R* curve appears to be close to that of the stretch line, they are different enough to meet the ASTM E 813 slope requirements. The J_{Ic} value obtained from such an *R* curve is questionable. The confidence in the measured crack length values is not high enough to place much confidence in such results. The multiple-specimen test result in Fig. 2 at 99°C (210°F) appears to agree closely with the 121°C (250°F) single-specimen result, but this agreement is more coincidence than anything else because the two *R* curves for those tests are very similar to those in Fig. 3, and the values just happen to coincide.

Figure 4 shows all the single-specimen J_I-*R* curves obtained for material W-A. These *R* curves are ordered in the same way, as a function of temperature, as the J_{Ic} values were ordered. The 38°C (100°F) curve represents the highest toughness condition while the 204°C (400°F) curve represents the lowest toughness condition. The 288°C (550°F) result falls between the 121 and the 204°C (250 and 400°F) result. The −40 and −51°C (−40 and −60°F) results cannot be observed in the figure since the specimen was unstable and fractured while the *R* curve was still on the stretch line.

The results of the fracture toughness tests conducted on weld W-B are presented in Fig. 5 in terms of J_{Ic} versus test temperature. The fracture properties of this weld metal are again a function of the test temperature. However, the behavior

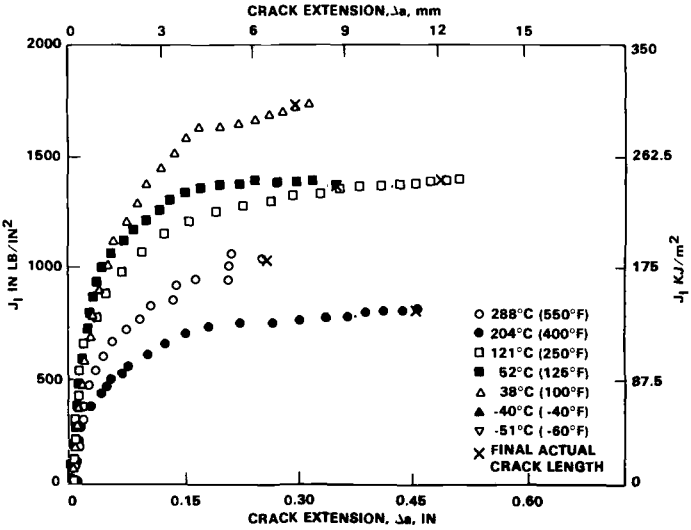

FIG. 4—J_I-R *curves determined over a range in test temperatures for weld metal W-A.*

of this weld metal is different from that of weld metal W-A (Fig. 2). The drop in fracture toughness with temperature in the upper shelf temperature region does not appear to be as dramatic as in weld W-A where the minimum toughness is observed at the 288°C (550°F) test temperature. The RT_{NDT} temperature for this weld metal, W-B, is again close to the upper shelf temperature for the J_{Ic} versus temperature relationship.

For this weld metal, the only fracture toughness result obtained by the multiple-

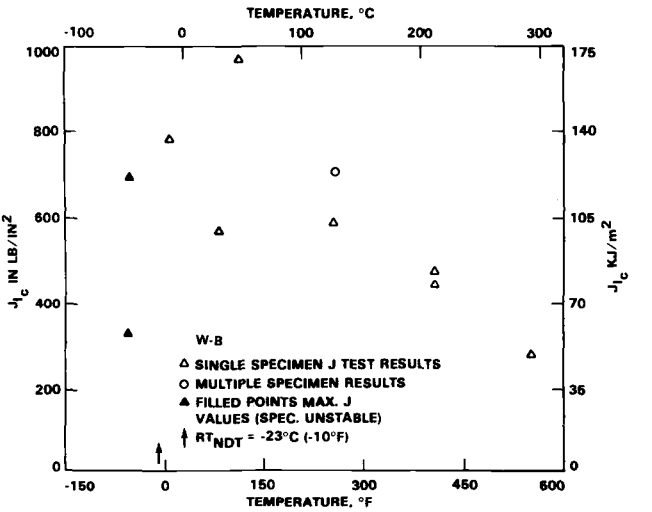

FIG. 5—*Fracture toughness as a function of test temperature for weld metal W-B.*

specimen procedure was at 121°C (250°F). Both a single- and a multiple-specimen test result were obtained at this temperature, and the two resulting R curves are shown in Fig. 6. In this case, the specimens used in the multiple-specimen techniques were side grooved so there should be good agreement between the two R curves. As shown in Fig. 6, there was very good agreement. The only difference between these two curves is caused by the two J formulations used. The multiple-specimen data were analyzed using the Merkle and Corten formulation in ASTM E 813 and the single-specimen results were obtained using the J formulation, corrected for a moving crack, which is also found in E 813.

For the amount of crack growth obtained in the multiple-specimen tests, it does not appear that differences in J formulation had any impact on the result. The J_{Ic} values obtained from these two R curves show reasonably good agreement, and the two R curves show very good agreement.

Figure 7 shows all the J_I-R curves obtained in this program on weld metal W-B using the single-specimen test technique. Here again the curves fall in the same order as the J_{Ic} values presented in Fig. 5; the 288°C (550°F) result being the lowest R curve and the −18°C (0°F) curve the highest. In this figure, there are three tests shown that were conducted at 204°C (400°F) while there are only two data points shown in Fig. 5 at 204°C (400°F). One of the three R curves did not meet the ASTM E 813 validity criterion because there were only three data points between the exclusion lines. There is good agreement, however, between the two J_{Ic} values obtained and the three J_I-R curves.

The results obtained during this study on weld W-C are shown in Fig. 8. In this weld, the T-S orientation as well as the T-L orientation, was investigated.

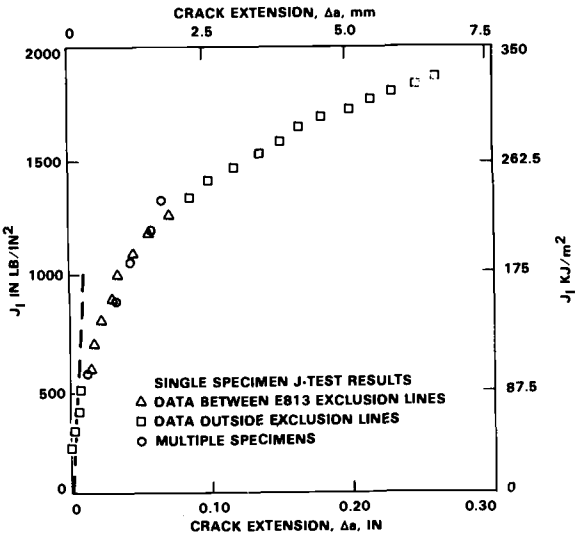

FIG. 6—J_I-R *curves determined at 121°C (250°F) by both the single-specimen and the multiple-specimen technique on weld metal W-B.*

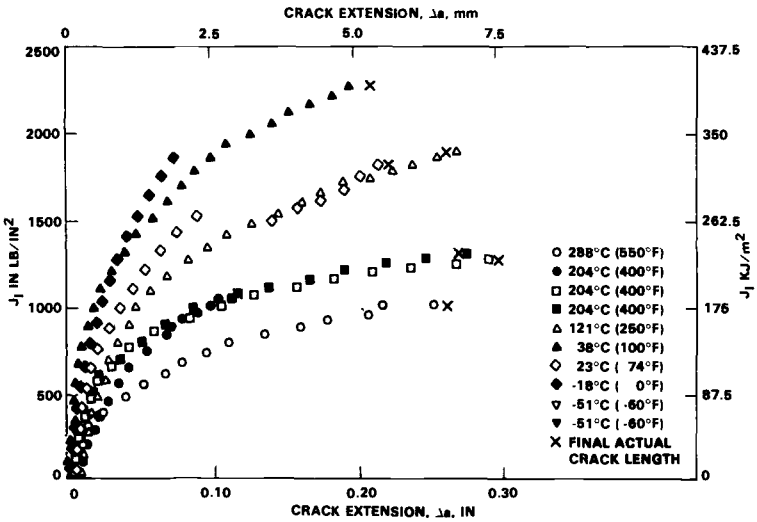

FIG. 7—J_I-R *curves determined over a range in test temperatures for weld metal W-B.*

As seen in Fig. 8, there was a substantial difference in J_{Ic} values between the two orientations. The T-S orientation exhibited substantially higher toughness values than the values obtained from specimens with the T-L orientation. It appears that the J_{Ic} values are a strong function of temperature for both orientations tested in this weld metal. This effect is more clearly seen in the results from specimens with the T-S orientation than those with the T-L orientation

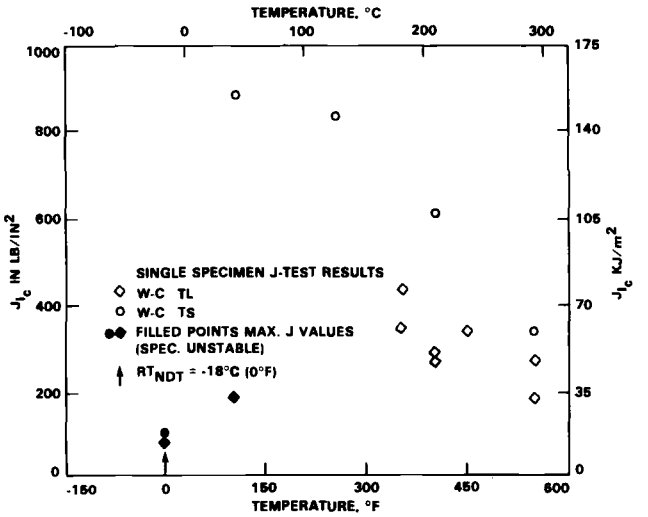

FIG. 8—*Fracture toughness as a function of test temperature for weld metal W-C.*

because test values are missing at temperatures between RT and 176°C (350°F) for this orientation.

The RT_{NDT} temperature for this material appears to be a better estimate of the start of the brittle to ductile transition. It is interesting to note from the data in Table 3 that the RT_{NDT} temperature for this material was established by the NDTT while it was established from the Charpy test results for the earlier two weld metals. Figures 9 and 10 present the J_I-R curve results from this weld metal. These J_I-R curves show trends similar to those seen in the results on the two weld metals W-A and W-B discussed earlier. The reproducibility of J_I-R curves from specimen to specimen is however not as good with this material as it was with weld W-B (Fig. 7). There are substantial differences between the two 176°C (350°F), two 232°C (450°F), and three 288°C (550°F) R curves presented in Fig. 9. There is no explanation at this time for this difference in test reproducibility. A microstructural and fractographic study of these weld metals and fracture specimens has not been performed but would seem needed in order to explain these differences.

Figure 10 presents the J_I-R curve for weld metal W-C with specimens in the T-S orientation. As noted in Fig. 8, T-S orientation specimens show higher J_{Ic} values than those with the T-L orientation. The reproduciblity of the 204°C (400°F) specimen is poor, however. As was the case for the poor reproducibility of W-C specimens in the T-L direction, there is no explanation at this time for this phenomenon.

The results obtained on the fourth weld metal W-D are presented in terms of J_{Ic} versus temperature in Fig. 11. In contrast to the earlier three weld metals, the J_{Ic} values for this weld metal exhibit little sensitivity to test temperature in

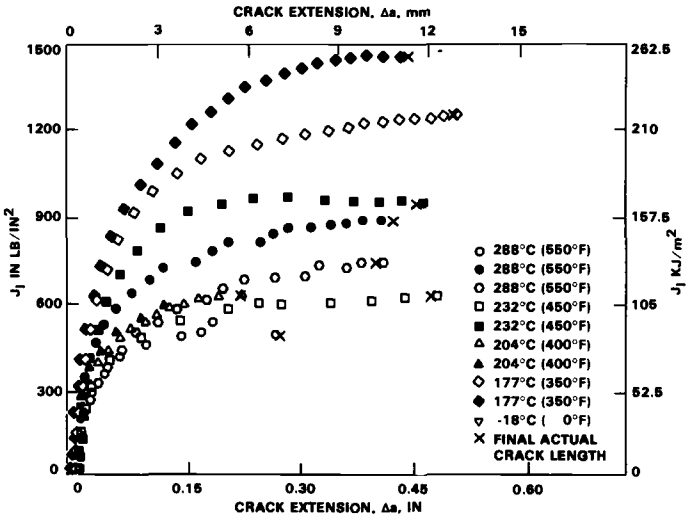

FIG. 9—J_I-C *curves determined over a range in test temperatures for weld metal W-C with a T-L orientation.*

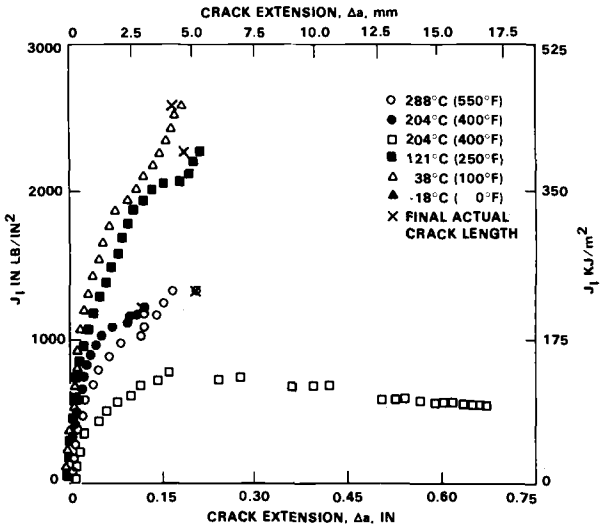

FIG. 10—J_I-R *curves determined over a range in test temperatures for weld metal W-C with a T-S orientation.*

the "upper shelf" temperature region. Not only is there little drop in toughness with temperature, but the overall toughness values are significantly higher. The RT_{NDT} temperature indicated on this figure is a conservative estimate of the temperature for the ductile to brittle transition since it almost represents the upper shelf temperature.

Figure 12 presents the J_I-R curves obtained from the specimens tested from weld metal W-D. This R curve shows the same trends as shown in Fig. 11; there is little effect of test temperature on the J_I-R curve properties at upper shelf

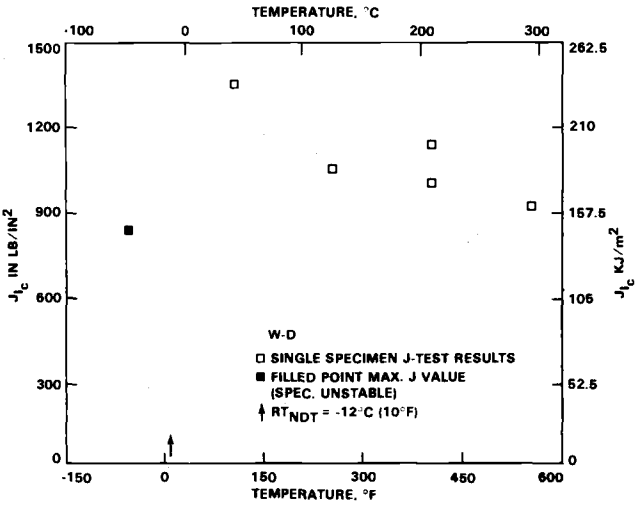

FIG. 11—*Fracture toughness as a function of test temperature for weld metal W-D.*

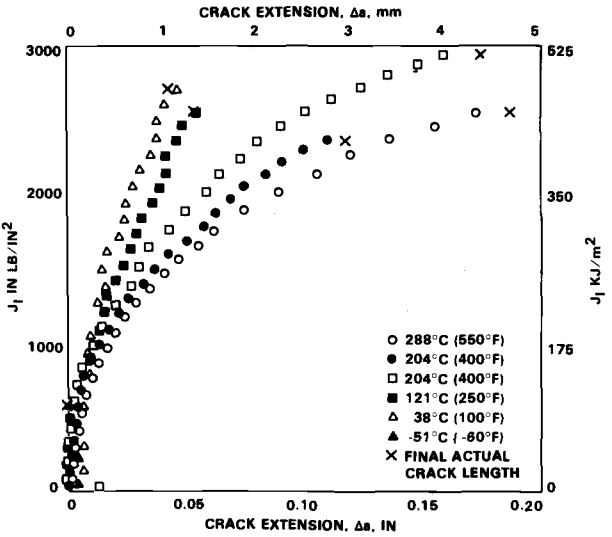

FIG. 12—J_I-R *curve determined over a range in test temperatures for weld metal W-D.*

temperature. In addition, the slopes of these *R* curves are significantly different than those shown in Figs. 4, 7, 9, and 10 for the other weld metals. The high-temperature R curves of the other metals are approaching a horizontal line ($dJ/da \rightarrow 0$) while the *R* curves for this weld metal still have a substantial slope (high tearing modulus) after a large amount of crack extension.

Discussion

There are a number of interesting comparisons that can be made based on the results of the experimental test program reported. There is a substantial difference in the fracture toughness properties of the four weld metals studied. The largest difference observed is between the two welding fluxes (Linde 80 and 124), but there are also substantial differences between the three weld metals in which the same flux (Linde 80) was used and which were fabricated essentially by the same practice.

The effect of test temperature on the upper shelf fracture toughness properties, whether measured by the J_{Ic} value, the height of the *R* curve, or the slope of the *R* curve (tearing modulus) appeared to take three forms. The upper shelf fracture properties of weld metal W-D varied little with test temperature. The properties of W-B dropped gradually with temperature, with the lowest values observed at the highest temperature tests. The properties of W-C appear to be similar to those of W-B only less well defined because of data scatter and limited upper shelf temperature range studies. The observed properties of W-A appear to be quite different, however, with a rapid drop in properties with increasing test temperature reaching a minimum at a temperature around 204°C (400°F). There is only one test at this temperature, however, and it may be questioned if the suggested trend is real, or only a result of data scatter. It is felt in this

case that the trend is real for the following reasons. First, the trend has been seen in weld metals before; Miglin et al report other weld metal data in which this same trend was seen.[2] In addition, Miglin et al report that the drop in *R*-curve properties is associated with serration in the load displacement record. This phenomenon was also observed in the 204°C (400°F) test of a W-A weldment. As a last point, concerning data scatter in general, there is much less data scatter in single-specimen J_I-R curve testing than was observed in multiple J_I-R curve tests. It appears that scatter in the J_I-R curves is usually associated with instabilities or uneven crack extension while the 204°C (400°F) R curve obtained on weldment W-A was smooth and well behaved. It appears that the drop in fracture toughness properties with test temperature is caused by more than one mechanism. At this time there appear to be three mechanisms that contribute to the drop in properties.

The first mechanism is a drop in the J_I-R curve properties because of a drop in the tensile properties of the material. This mechanism will be present in all weld metals of this type and is the most likely explanation for the gradual drop in J_I-R curve properties observed in weldment W-D.

The second mechanism is a drop in toughness caused by static strain aging that occurs during the unloads in the single-specimen J tests. This causes the reloading peaks that have been observed[2] in these tests. This mechanism, in addition to the first mechanism, appears to cause the more rapid drop in J_I-R curve properties observed in weld metals W-B and W-C. The third mechanism is dynamic strain aging, which occurs during the loading of the specimen. When this mechanism is active, serrations can be observed in the load displacement curves. When all three of these mechanisms are active, the dramatic drop in J_I-R curve properties, such as observed in weld W-A, can be observed. A more detailed discussion of the effect of dynamic strain aging on the load displacement curve and the J_I-R curves can also be found.[2]

From the elastic-plastic fracture toughness testing standpoint, if the strain aging mechanisms suggested above are true, there are some questions that should be answered concerning the effect of test method on J_I-R curve results. The specimen loading rate both during the loading and during the unloads may have a significant influence on the test result. The effect of loading rate on the J_I-R curve properties of a material, such as weld W-A, should be studied to determine if loading rate has a significant effect.

Based on the limited amount of data available in this study comparing the multiple-specimen method with the single-specimen method, it appears that they produce comparable J_I-R curves if the test specimens are side grooved in both procedures. Nonside-grooved specimens produce R curves that are substantially different from side-grooved specimens, and the J_{Ic} values obtained from such tests may be more difficult to interpret.

The J_{Ic} values obtained from the ASTM E 813 procedure appear to be quite

[2]Miglin, M. T., Van Der Sluys, W. A., Futato, R. J., and Domian, H. A., this publication, pp. 150–165.

useful in evaluating the fracture properties of a material. The J_{Ic} value, the J_I-R curve itself, and the slope of the J_I-R curve all seem to order the fracture properties of a material in the same way. It appears from this that J_{Ic} values should be useful from a quality control and material selection standpoint even if the whole J_I-R curve is more valuable from an analysis standpoint. It appears that J_{Ic} is a more sensitive measure of a material's fracture toughness than tests, such as the Charpy test, since the Charpy test does not produce the radical differences in upper shelf fracture properties observed in these four weld metals.

From the standpoint of the design of a structure, it is difficult to determine the significance of the differences in upper shelf fracture toughness properties observed in this study. There is no question that W-A has a lower fracture toughness and lower resistance to ductile tearing than the other three weld metals studied. What is not known at this time is if that difference is significant from a structural reliability standpoint. Have structures ever failed because of a low resistance to ductile tearing in the 204°C (400°F) temperature region? If there are examples of this type of failure in the literature, they are not known to the authors of this report.

Conclusions

The following conclusions can be reached based on the results of the studies reported:

1. The fracture toughness parameter J_{Ic} as defined by ASTM E 813 is useful in evaluating the toughness of the weld metals studied.

2. The J_{Ic} parameter orders the relative fracture properties of the four weld metals studied in the same order as the overall height of the J_I-R curves.

3. The single-specimen unloading compliance technique produces the same J_I-R curve as the multiple-specimen procedure as long as the specimens are side grooved.

4. The fracture toughness of a weld metal in the upper shelf temperature region can be a strong function of the test temperature.

References

[1] *ASME Boiler and Pressure Vessel Code*, Section III, Rules for Construction of Nuclear Power Plant Components, Division 1—Subsection NB—Class 1 Components, American Society for Mechanical Engineers, New York, 1980.

[2] Van Der Sluys, W. A., Futato, R. J., "Computer-Controlled Single-Specimen *J*-Test," *Elastic-Plastic Fracture, Vol. II, Fracture Resistance Curves, and Engineering Applications, ASTM STP 803*, American Society for Testing and Materials, Philadelphia, 1983, pp. II-464–II-482.

[3] Albrecht, P., Andrews, W. R., Gudas, J. P., Joyce, J. A., Loss, F. J., McCabe, D. E., Schmidt, D. W., and Van Der Sluys, W. A., "Tentative Test Procedure for Determining the Plane Strain J_I-R Curve," *Journal of Testing and Evaluation*, Vol. 10, No. 6, Nov. 1982, pp. 245–251.

Robert J. Futato,[1] *John D. Aadland,*[2] *W. Alan Van Der Sluys,*[1] *and Arthur L. Lowe*[2]

A Sensitivity Study of the Unloading Compliance Single-Specimen *J*-Test Technique

REFERENCE: Futato, R. J., Aadland, J. D., Van Der Sluys, W. A., and Lowe, A. L., **"A Sensitivity Study of the Unloading Compliance Single-Specimen *J*-Test Technique,"** *Elastic-Plastic Fracture Test Methods: The User's Experience, ASTM STP 856,* E. T. Wessel and F. J. Loss, Eds., American Society for Testing and Materials, 1985, pp. 84–103.

ABSTRACT: A sensitivity analysis of the unloading compliance single-specimen *J*-test technique was performed to determine the effect of errors in test parameters on calculated ductile fracture toughness J_{Ic} values and the shape of the *J-R* curve. Systematic errors in measured specimen dimensions, material properties, and load and displacement transducer calibration were considered. In addition, the effect of extensometer nonlinearity on the test results was modeled. The results of the study indicate that the shape of the *J-R* curve and the calculated J_{Ic} value are relatively insensitive to errors in parameters in the magnitudes allowed by the ASTM Test Method for J_{Ic}, a Measure of Fracture Toughness E 813 and the Tentative Procedure for Determining the Plane Strain J_I-*R* curve. However, the J_{Ic} calculation appears to be quite sensitive to the location and spacing of *J*-Δa data points along the *J-R* curve. Means for desensitizing the J_{Ic} calculation to the manner in which the test is run are discussed.

KEY WORDS: unloading, sensitivity, errors, unloading compliance, *J*-integral test

Nomenclature

- a Crack length
- $A_{i,i+1}$ Area under specimen load-displacement curve between unloads i and $i + 1$
- B Specimen thickness
- b_i Remaining ligament $= w - a_i$
- C Specimen compliance
- E Young's modulus
- J Value of J integral
- J_{Ic} Ductile fracture toughness value

[1]Research engineer and technical advisor, respectively, Babcock and Wilcox Co., Alliance Research Center, 1562 Beeson St., Alliance, OH 44601.

[2]Engineer and advisory engineer, respectively, Babcock and Wilcox Co., Nuclear Power Generation Division, Lynchburg, VA.

L_i Coefficients from linear transducer calibration equation
P Load
ΔP Change in load during unloading
Q_i Coefficients from quadratic transducer calibration equation
r_i Load or displacement value at start of transducer calibration
r_f Load or displacement value at end of transducer calibration
V Load or displacement transducer output voltage
V_i Transducer output voltage at start of calibration
V_f Transducer output voltage at end of calibration
w Specimen width
ϵ_x Error in measured parameter x (load, displacement, and so forth)
δ Specimen load-line displacement
$\Delta\delta$ Change in specimen load-line displacement during unload
σ_f Flow stress = average of yield and ultimate strengths

Introduction

To guarantee the accuracy of the results from any experimental program, it is necessary to understand the sensitivity of the test technique to errors in input data. Sensitivity analyses of experimental procedures should be performed to determine the effect of unavoidable or undetectable errors during the execution of the test on the obtained results. This type of analysis is particularly important for the single-specimen J test in which the relation of the final results to the raw test data is obscured by a long series of calculations. Errors in input data can propagate and accumulate in the J test in a manner difficult to trace without a careful analysis of the test procedure.

This paper will present the results of a study conducted to determine the effect of errors in input data on results obtained using the elastic unloading compliance single-specimen J-test technique. The effect of systematic errors in measured specimen dimensions, material properties, and transducer calibration on calculated crack lengths, crack extension, and J values will be modeled. Calibration errors caused by both systematic differences between the assumed and actual transducer calibration coefficients (transducer accuracy) as well as by the use of a linear curve fit to nonlinear calibration data (transducer nonlinearity) will be considered. In addition, the sensitivity of the J_{Ic} calculation (as specified in ASTM Test for J_{Ic}, a Measure of Fracture Toughness Standard [E 813]) to test parameters will be examined.

The remainder of this paper is divided into five sections. In the first section, a model is developed to simulate transducer response with varying degrees of accuracy and nonlinearity. This model is then used to study the effect of calibration errors as well as errors in other test parameters on calculated crack lengths and crack extension and to study the effect of these errors on calculated J values. The sensitivity of the J_{Ic} calculation to the manner in which the J test is conducted is then investigated. Finally, the significance of the results is discussed.

Transducer Calibration Model

Changes in load and displacement during a test cannot be measured directly in any convenient way but rather must be inferred from other more easily obtainable information. Generally, transducers are attached to the test specimen to convert the load and displacement into electric signals, which are in turn read and recorded by some electronic monitoring device. Before calculations can be performed, however, these electric signals must be converted back into load and displacement. That conversion is done using the relation between the physical quantity and the transducer output voltage predetermined during the transducer calibration. The simplest of such relations and the one most commonly used is a linear equation of the form

$$P \text{ or } \delta = L_1 V + L_0 \tag{1}$$

where L_1 and L_0 are determined from a linear regression analysis of the calibration data.

Transducers are seldom truly linear as illustrated in Table 1, which shows the calibration data for a typical extensometer as well as the residuals between the observed and calculated displacements for a linear curve fit to the data. The smooth change in polarity of the residuals from positive to negative and back to positive with increasing displacement suggests that the actual relation of the transducer output voltage to changes in displacement is in fact nonlinear. Significant errors between the actual and predicted load or displacement can therefore result from using the linear equation if the transducer response deviates substantially from true linearity. Consequently, the linear calibration equation should not be used for convenience without a clear understanding of the consequences to the test results.

TABLE 1—*Extensometer calibration data displacement = 0.0157776 × (volts) + 0.301239.*

Volts	Observed Displacement, in.[a]	Calculated Displacement, in.	Residual, in.
−9.59941	0.15000	0.149784	2.16037E-04
−8.01661	0.17500	0.174757	2.43336E-04
−6.42404	0.20000	0.199884	1.16482E-04
−4.82658	0.22500	0.225088	−8.75294E-05
−3.24377	0.25000	0.25006	−6.03795E-05
−1.64631	0.27500	0.275264	−2.64406E-04
−0.0635076	0.30000	0.300237	−2.37167E-04
1.52418	0.32500	0.325287	−2.86967E-04
3.09722	0.35000	0.350106	−1.05679E-04
4.68002	0.37500	0.375078	−7.84099E-05
6.25794	0.40000	0.399974	2.58684E-05
7.83586	0.42500	0.42487	1.30147E-04
9.40401	0.45000	0.449611	3.88592E-04

[a]Observed displacement values are ±0.00005 in. 1 in. = 25.4 mm.

In order to determine the effect of use of the linear equation on test results, it will be necessary to analytically simulate transducer nonlinearity. This can be done by first assuming some (nonlinear) functional form for the actual calibration data, and then adjusting the coefficients in that equation to produce the desired response. A candidate function to describe the actual transducer response can be determined by performing a nonlinear curve fit to the data in Table 1. Tables 2 and 3 show the results of fitting a quadratic and cubic equation, respectively, to the data. As can be seen, both the quadratic and cubic equations eliminate the systematic changes in the polarity of the residuals previously observed, with no apparent gains in accuracy resulting from use of the cubic fit. Consequently, it may be assumed for simplicity that the quadratic equation is sufficient to describe the true response of the transducer. Assuming this is true in general, the following model is proposed

$$\text{True response: } \Delta = Q_2V^2 + Q_1V + Q_0 \tag{2}$$

$$\text{Assumed response: } \Delta = L_1V + L_0 \tag{3}$$

$$\Delta = r_i \quad \text{when} \quad V = V_i \tag{4}$$

$$\Delta = r_f \quad \text{when} \quad V = V_f \tag{5}$$

$$(Q_2V_f^2 + Q_1V_f + Q_0) - (L_1V_f + L_0) = e \tag{6}$$

Here Δ represents the physical quantity being measured (load or displacement), and e is the maximum deviation of actual response from linearity. It is assumed

TABLE 2—*Extensometer calibration data*
displacement = $(6.10459 \times 10^{-6}) \times (volts^2) + 0.0157787 \times (volts) + 0.301025$.

Volts	Observed Displacement, in.[a]	Calculated Displacement, in.	Residual, in.
−9.59941	0.15000	0.150121	−1.21236E-04
−8.01661	0.17500	0.174926	7.44462E-05
−6.42404	0.20000	0.199914	8.61436E-05
−4.82658	0.22500	0.22501	−9.99868E-06
−3.24377	0.25000	0.249907	9.32962E-05
−1.64631	0.27500	0.275065	−6.49095E-05
−0.0635076	0.30000	0.300023	−2.29478E-05
1.52418	0.32500	0.325089	−8.87513E-05
3.09722	0.35000	0.349954	4.63128E-05
4.68002	0.37500	0.375003	−3.36766E-06
6.25794	0.40000	0.400006	−6.28829E-06
7.83586	0.42500	0.42504	−3.95775E-05
9.40401	0.45000	0.449948	5.20051E-05

[a]Observed displacement values are ±0.00005 in.

TABLE 3—*Extensometer calibration data*
displacement = (2.08413 × 10^{-7}) × (*volts*^{3}) + (6.16422 × 10^{-6}) × (*volts*^{2}) + 0.0157656 × (*volts*) + 0.301024.

Volts	Observed Displacement, in.[a]	Calculated Displacement, in.	Residual, in.
−9.59941	0.15000	0.150067	−6.67423E-05
−8.01661	0.17500	0.174926	7.43866E-05
−6.42404	0.20000	0.199944	5.61923E-05
−4.82658	0.22500	0.22505	−4.97550E-05
−3.24377	0.25000	0.249941	5.87404E-05
−1.64631	0.27500	0.275084	−8.42214E-05
−0.0635076	0.30000	0.300022	−2.22921E-05
1.52418	0.32500	0.325068	−6.81579E-05
3.09722	0.35000	0.349918	8.16584E-05
4.68002	0.37500	0.374963	3.68357E-05
6.25794	0.40000	0.399976	2.38419E-05
7.83586	0.42500	0.425039	−3.92795E-05
9.40401	0.45000	0.450002	−1.78814E-06

[a]Observed displacement values are ±0.00005 in.

in the above model that the maximum deviation occurs at the extremes of the transducer working range, as suggested by the results in Table 1.

Values for the coefficients in the above model for any range in physical quantity (load or displacement) or any degree of nonlinearity can be obtained in the following way. Assuming that L_1 and L_0 are obtained from the actual calibration data of the transducer (as calculated from Eq 2), using a linear regression analysis, then the linear and quadratic equation coefficients can be related by the expressions

$$L_1 = Q_2 f(V) + Q_1 \tag{7}$$

$$L_0 = Q_2 g(V) + Q_0 \tag{8}$$

Here $f(V)$ and $g(V)$ are functions of the transducer output voltage alone, and as such are independent of the range in physical quantity or degree of nonlinearity of the transducer. Substituting these expressions into Eq 6 and collecting terms yields

$$Q_2 = e/[V_f^2 - V_f f(V) + g(V)] \tag{9}$$

Evaluating Eq 2 at $\Delta = r_i$ and $\Delta = r_f$, and subtracting the resulting equation yields

$$Q_1 = [(r_f - r_i) - Q_2 (V_f^2 - V_i^2)]/(V_f - V_i) \tag{10}$$

Finally, from Eq 2

$$Q_0 = r_f - Q_2 V_f^2 - Q_1 V_f \tag{11}$$

Values for the coefficients Q_2, Q_1, Q_0, L_1, and L_0 for various conditions are shown in Table 4. Only extensometer nonlinearity was modeled since load transducers are typically quite linear over the range of loads encountered in a J test. Condition 1 in Table 4 was run using input parameters from the data in Table 1 as a check of the accuracy with which the model predicts observed transducer behavior. For both the linear and quadratic equations, the predicted coefficients and those calculated from the actual data agree quite well. Conditions 2 through 5 were run to provide an analytical description of increasingly nonlinear extensometer response.

Nonlinearity is however not the only source of error between the actual load or displacement and that predicted by the transducer calibration equation. Systematic calibration errors (such as might be caused by a shift in transducer sensitivity) can also occur and be superimposed on the errors caused by nonlinearity. Systematic errors effectively cause a shift in the coefficients of the calibration equation. Therefore, the combined effect of nonlinearity and systematic inaccuracy can be modeled by shifting the coefficients of the linear equation by some amount, while allowing the coefficients of the quadratic equation to retain their true (accurate) values. Algebraically, the expression

$$P \quad \text{or} \quad \delta = (L_1 + \epsilon_{L1})V + (L_0 + \epsilon_{L2}) \tag{12}$$

can be used to account for systematic calibration errors.

Crack Length Measurement Accuracy

In the unloading compliance single-specimen J-test technique, crack lengths are calculated from the specimen compliance measured as the ratio of the change in displacement to change in load during partial (elastic) unloadings of the specimen at various points throughout the test [*1*]. Specifically, for the compact fracture specimen [*2*]

$$a/w = 1.000196 - 4.06319\,(U_{LL}) + 11.242\,(U_{LL})^2 - 106.043\,(U_{LL})^3 + 464.335\,(U_{LL})^4 - 650.677\,(U_{LL})^5 \tag{13}$$

where

$$U_{LL} = 1/[(EBC)^{1/2} + 1] \tag{14}$$

Consequently, any error in the measurement of the change in load or displacement during the unloadings, or any error in the specimen width, thickness, or Young's

TABLE 4—*Calibration data predicted by model.*

Input					Output				
Initial Displacement	Final Displacement	Initial, V	Final, V	% Deviation from Linearity	$Q_2 \times 10^{-6}$	Q_1	Q_0	L_1	L_0
0.15	0.45	−9.59941	+9.40401	0.13	6.66667	0.0157866	0.300928	0.0157853	0.30115
0.15	0.45	−10	+10	0	0	0.015	0.3	0.015	0.3
0.15	0.45	−10	+10	0.1	4.73684	0.015	0.299526	0.015	0.2997
0.15	0.45	−10	+10	0.2	9.47368	0.015	0.299053	0.015	0.2994
0.15	0.45	−10	+10	0.3	14.2105	0.015	0.298579	0.015	0.2991

modulus measurement will ultimately create an error in the calculated crack length.

To analyze the sensitivity of the crack length calculation to systematic errors in these parameters, let $\bar{C} = EBC$ denote the true specimen compliance normalized for specimen thickness and elastic modulus, and let $\bar{C}^e$ denote the normalized compliance in which some error has been introduced. If a^e is the erroneous crack length, then

$$a^e/w = w^e/w \quad \text{function} \quad (U_{LL}) \tag{15}$$

where

$$U_{LL} = (\sqrt{\bar{C}^e} + 1)^{-1} \tag{16}$$

$$\bar{C}^e = \bar{C}\,(1 + \epsilon_E/E)\,(1 + \epsilon_B/B)\,(1 + \epsilon_C/C) \tag{17}$$

The quantities ϵ_E/E, ϵ_B/B, and ϵ_C/C are the fractional errors in modulus, thickness, and compliance, respectively. The errors in modulus and thickness must be determined from an analysis of the techniques used in making those measurements. However, since the compliance is determined from measurements of load and displacement during the J test, the fractional error in compliance can be related to errors in the load and displacement measurements during the unloadings. To do this, let

$$C + \epsilon_C = (\Delta\delta + \epsilon_\delta)/(\Delta P + \epsilon_P) \tag{18}$$

represent the measured specimen compliance in which some error has been introduced because of errors ϵ_δ and ϵ_P. Then for small errors

$$\epsilon_C/C = \epsilon_\delta/\Delta\delta - \epsilon_P/\Delta P \tag{19}$$

where C is the true compliance calculated from $\Delta\delta$ and ΔP. Since the load transducer is assumed to be perfectly linear, any error ϵ_P is due solely to a systematic error in the calibration. Therefore

$$\epsilon_P/\Delta P = [(L_1 + \epsilon_{L1} - L_1)/L_1\Delta V]\,\Delta V = \epsilon_{L1}/L_1 \tag{20}$$

which is the fractional difference between the real and assumed load transducer calibration coefficients. The quantity $\epsilon_\delta/\Delta\delta$ is slightly more complicated since it must include both the effect of systematic calibration errors as well as any local error that might exist between the actual change in displacement and that

predicted by a linear calibration equation. However, assuming that the displacement transducer is linear at least over the range of an unloading (which, since the unloadings are so small, will be true except for cases of extreme nonlinearity) then

$$\Delta\delta = (2Q_2V + Q_1)\Delta V \tag{21}$$

$$\epsilon_\delta = (L_1 + \epsilon_{L1} - 2Q_2V - Q_1)\Delta V \tag{22}$$

$$\epsilon_\delta/\Delta\delta = [(L_1 + \epsilon_{L1})/(2Q_2V + Q_1)] - 1 \tag{23}$$

where V is the absolute output voltage of the extensometer at the time of the unloading.

Errors in crack length calculated using the above model are shown in Figs. 1 and 2 as a function of the true instantaneous crack length. Figure 1 shows the crack length errors for a test in which the crack grows from $a/w = 0.5$ to

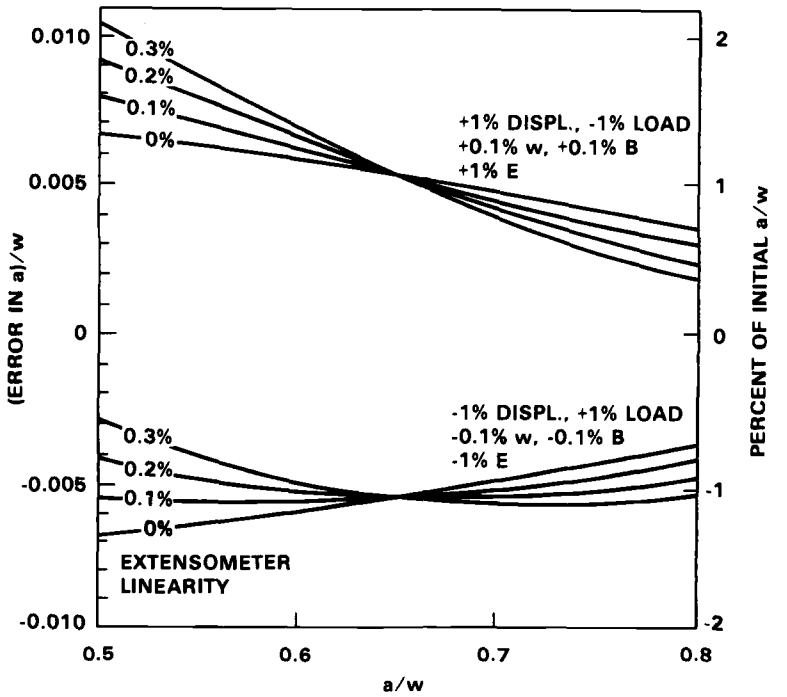

FIG. 1—*Error in unloading compliance crack length measurement normalized with respect to true specimen width for* $0.5 \leq a/w \leq 0.8$.

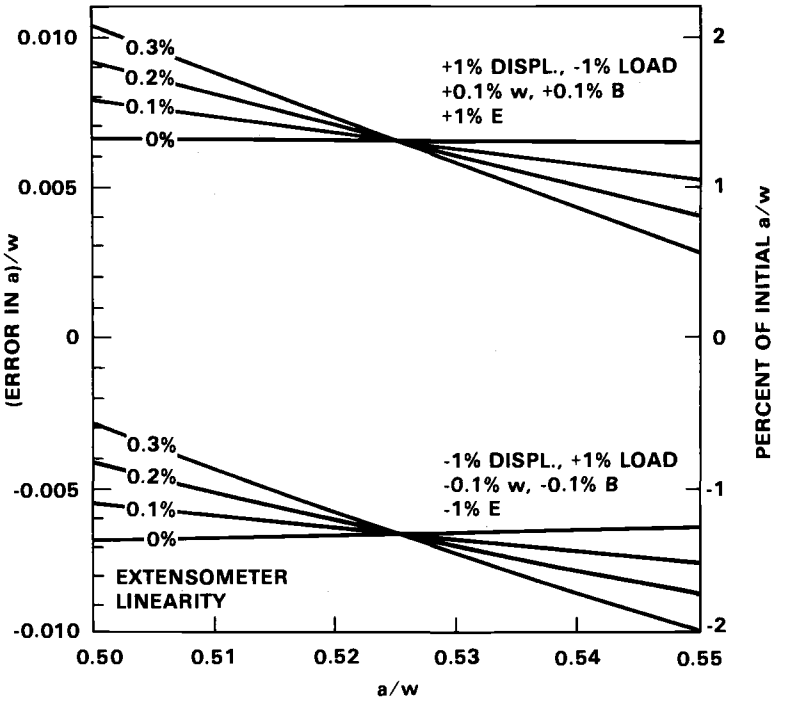

FIG. 2—*Error in unloading compliance crack length measurement normalized with respect to true specimen width for* $0.5 \leq a/w \leq 0.55$.

$a/w = 0.8$, while Fig. 2 shows the expected errors for a test with crack extension from $a/w = 0.5$ to $a/w = 0.55$. In both cases, it is assumed that the entire extensometer range is needed to produce the crack extension indicated, and that crack extension occurs uniformly with changes in displacement. The systematic errors in width, thickness, modulus, and transducer calibration were chosen in accordance with the specifications of ASTM (E 813) where applicable, or according to experience when the standard specified no tolerance in accuracy. In addition, the deviation from linearity of the extensometer calibration data was varied from 0 to 0.3% of range to investigate the effect of nonlinearity on the crack length calculation. In all cases, the polarity of the errors was chosen to produce the greatest errors in crack length. The cases where errors cancel was not considered.

Results of the single-specimen J test generally consist of a plot of J values versus crack extension from the initial crack length. Therefore, it is necessary to know how test parameter errors affect errors in crack extension as well as in absolute crack length. This information can be obtained by replotting the curves in Figs. 1 and 2, as shown in Figs. 3 and 4. In these figures, the error in crack extension is defined as the difference between the true (no error) crack extension and that calculated using the inaccurate absolute crack lengths.

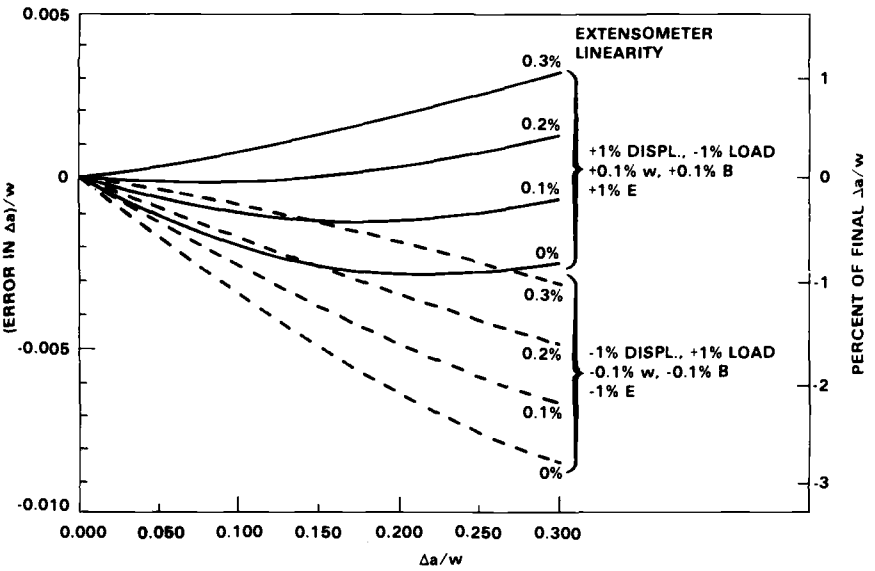

FIG. 3—*Error in unloading compliance crack extension measurement normalized with respect to true specimen width for crack extension* $\leq 0.3w$.

J Calculation and *J*-Resistance Curve Accuracy

As with crack length, J values cannot be measured directly but must be calculated from other test data. The following equation is currently used to calculate J [3] (ASTM E 813)

$$J_{i+1} = [J_i + (\eta_i A_{i,i+1}/b_i B)] \{1 - [(\gamma_i/b_i)(a_{i+1} - a_i)]\} \tag{24}$$

where

$$\eta_i = 2 + 0.522\, b_i/w \tag{25}$$

$$\gamma_i = 1 + 0.76\, b_i/w \tag{26}$$

and $A_{i,i+1}$ is the area under the load-displacement curve between lines of constant displacement at points i and $i + 1$ (generally taken to be two successive unloadings). In an automated procedure, this area term is calculated using a numerical integration technique on load and displacement data obtained from the transducers on the specimen

$$A_{i,i+1} = (\delta_{n+1} - \delta_n)(P_{n+1} + P_n)/2 \tag{27}$$

Consequently, errors can be introduced into the J expression through the specimen width and thickness values as well as through the crack length and area calculations.

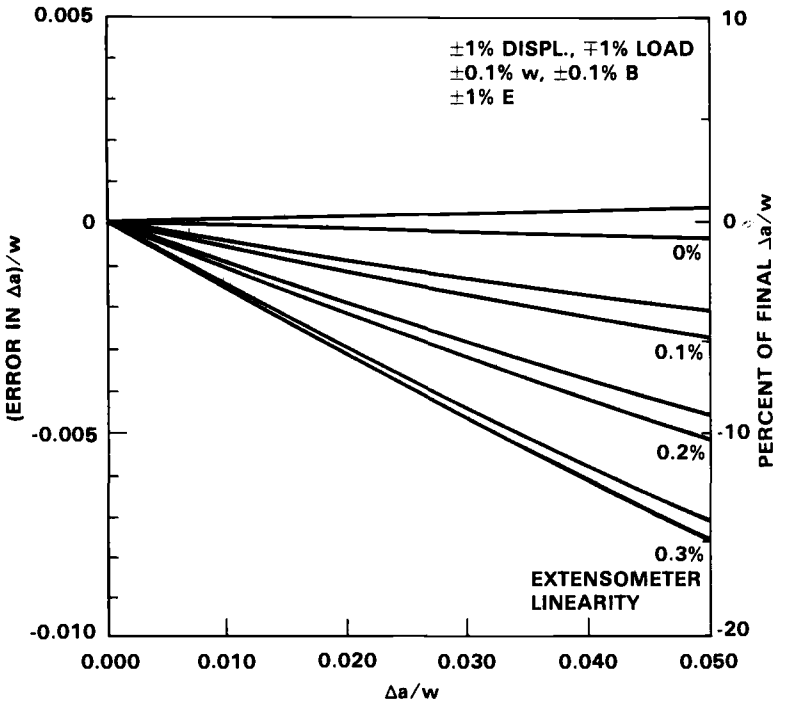

FIG. 4—*Error in unloading compliance crack extension measurement normalized with respect to true specimen width for crack extension* ≤ 0.05w.

To analyze the sensitivity of the J calculation to errors in input data, let J_{i+1} denote the true (no error) J value calculated at unload $i + 1$, and let $J_{i+1}{}^{e}$ denote the value calculated using erroneous width, thickness, area, and crack length values. For generality, it is desirable to write the error in J as some fraction of the true J value so that no assumptions regarding the actual load-displacement curve or the specimen size are required. Therefore, let the J values be nondimensionalized as follows

$$J_{i+1} = J_{i+1}wB/A_{i,i+1}, \bar{J}_{i+1}{}^{e} = J_{i+1}{}^{e}w^{e}B^{e}/A_{i,i+1} \tag{28}$$

Further, to simplify the analysis assume that the test is conducted in such a way that the area increments between successive unloadings remain constant throughout the test (such as might be the case for a low strain hardening material). Then $A_{i,i+1} = A_{i-1,i}$, and it is possible to write

$$\bar{J}_{i+1} = J_{i+1}\,(wB/A_{i,i+1})$$

$$= \{\bar{J}_{i} + [2/(1 - a/w)] + 0.522\} \tag{29}$$

$$\{1 - [1/(1 - a/w) + 0.76]\,[(a_{i+1} - a_{i})/w]\}$$

Following the same logic

$$\bar{J}_{i+1}^{e} = \{\bar{J}_i^{e} + [2/(1 - a^e/w^e) + 0.522]\,(A_{i,i+1}^{e}/A_{i,i+1})\} \{1 - [1/(1 - a^e/w^e) + 0.76]\,[(a_{i+1}^{e} - a_i^e)/w^e]\} \tag{30}$$

Therefore, the fractional error in J can be defined as

$$(J_{i+1} - J_{i+1}^{e})/J_{max} = (\bar{J}_{i+1} - \bar{J}_{i+1}^{e})/\bar{J}_{max}\,(w/w^e)\,(B/B^e) \tag{31}$$

which can be evaluated without knowledge of the specimen size or area under the load-displacement curve.

It is not particularly useful, however, to consider errors in the J calculation in isolation. Rather, since the J-R curve (consisting of a plot of J values as a function of crack extension) is the principle test result, a more meaningful estimate of the sensitivity of the unloading compliance J-test procedure to errors in input parameters can be obtained by considering the effect of errors in the J and crack extension calculations simultaneously. A reasonable way to do this is to define the error in J as the vertical separation of a J-R curve generated using erroneous data from that generated without error. Errors in J (expressed as a percentage of the maximum J value attained in the test) calculated in this way are plotted in Figs. 5 through 6 as a function of crack extension. Figure 5 shows the percentage error in J for a test in which the crack was grown from $a/w = 0.5$ to $a/w = 0.8$, while a test with crack extension from $a/w = 0.5$ to $a/w = 0.55$ is analyzed in Fig. 6. In all cases, only extensometer nonlinearity was considered, this nonlinearity being described by the model developed in the first section. The errors caused by transducer nonlinearity and systematic inaccuracy were applied both to the crack length calculation (as described in the previous section) and to the area term defined previously. It was assumed that the entire extensometer range was needed to reach the maximum J value in each case, and that crack length increased uniformly with displacement. Consequently, each crack length and area term was calculated at a different absolute displacement and was subject to a different calibration error as before. The magnitudes of the errors used in this analysis were identical to those in the analysis of the crack length calculation, with the polarities again chosen to produce the greatest error in J.

J_{Ic} Calculation Sensitivity

ASTM E 813 defines J_{Ic} as the point of intersection of a line fit to data immediately after the onset of tearing and the theoretical blunting line described by the equation $J = 2\,\sigma_f \Delta a$. This definition, while not particularly useful in identifying the J value at the actual initiation of crack growth, does provide a good engineering estimate of material toughness by taking into account both the difficulty in initiating a crack as well as the resistance to further growth im-

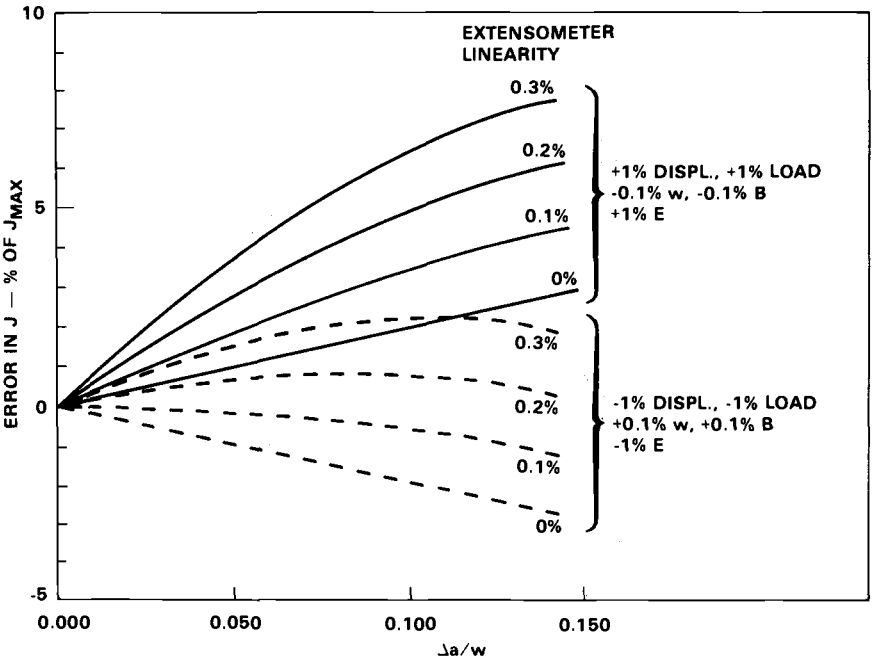

FIG. 5—*Error in J calculated as difference between true* J-R *curve and* J-R *curve generated using erroneous parameters shown as a function of crack extension for* $\Delta a \leq 0.15w$.

mediately after initiation. However, because of the nonlinearity often observed in *J*-resistance curves and because of the fact that both the multiple-specimen and unloading compliance single-specimen *J*-test techniques generate discrete data for use in calculating J_{Ic}, the ASTM J_{Ic} definition is susceptible to several errors not previously discussed.

Effect of Data Spacing

A *J*-resistance curve generated using the elastic unloading compliance single-specimen *J*-test technique is shown in Fig. 7. The points eligible for use in calculating J_{Ic} according to ASTM E 813 are shown as triangles and are labeled 1 through 8. Using this set of data, J_{Ic} is calculated to be 285 kJ/m^2 (1630 in. · lb/in.^{2}). If, however, the test had been conducted in such a way that only points 2, 4, 6, and 8 of the original set of points had been generated, a J_{Ic} value of 273 kJ/m^2 (1560 in. · lb/in.^{2}) would have been obtained, corresponding to a −4.3% deviation from the original calculation. On the other hand, if only points 1, 3, 5, and 7 had been generated then a J_{Ic} value of 301 kJ/m^2 (1720 in. · lb/in.^{2}) would have been obtained, corresponding to a +5.5% deviation from the original calculation. All three calculations are valid according to the standard, the only difference between them being the relative placement of the data points along the (nonlinear) *J-R* curve. Consequently, all other parameters

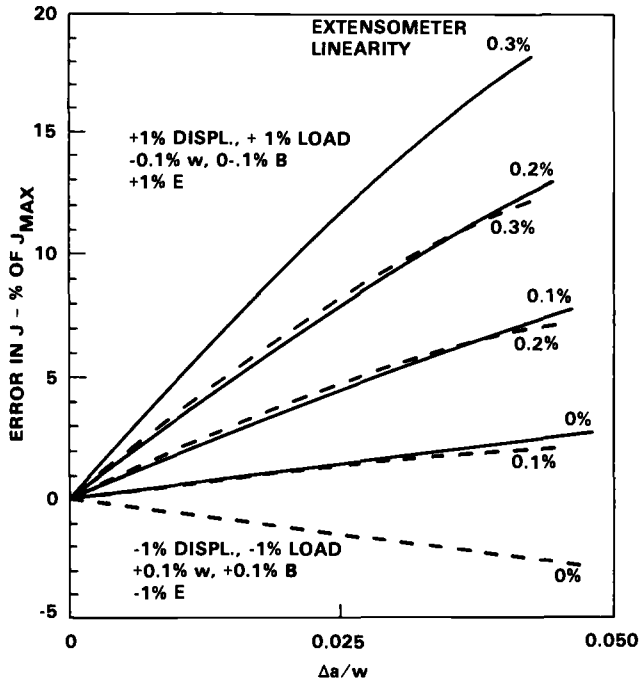

FIG. 6—*Error in* J *calculated as difference between true* J-R *curve and* J-R *curve generated using erroneous parameters shown as a function of crack extension for* $\Delta a \leq 0.05w$.

being equal, the J_{Ic} calculation is sensitive to the spacing of the J-Δa data points for materials that exhibit nonlinear J-R curves.

Position of Blunting Line

In the unloading compliance single-specimen J-test technique, an offset often exists between the crack length measurements made during the test and the initial crack length measurement used to calculate crack extension. Such an offset causes a shift of the J-Δa data away from proper placement relative to the theoretical blunting line, and if not corrected will produce an error in J_{Ic} equal to

$$\epsilon J_{Ic} = 2\,\sigma_f S/[(2\,\sigma_f - 1)/J'] \tag{32}$$

where S is the amount of shift, and J' is the slope of the J-R curve in the region used in the J_{Ic} calculation. For the data shown in Fig. 7 (J' = 230 MPa [33 366 in. · lb/in.^{3}], σ_f = 595 MPa [86.4 ksi]), a shift of 0.0254 mm (0.001 in.) creates an error in J_{Ic} of 7.25 kJ/m^2 (41.4 in. · lb/in.^{2}), corresponding to a 2.5% deviation from the original calculation. If, in addition, the shift is sufficient to cause a different set of points to satisfy the eligibility criteria of the standard then J' will change as well, and the variation in J_{Ic} will be even greater. Con-

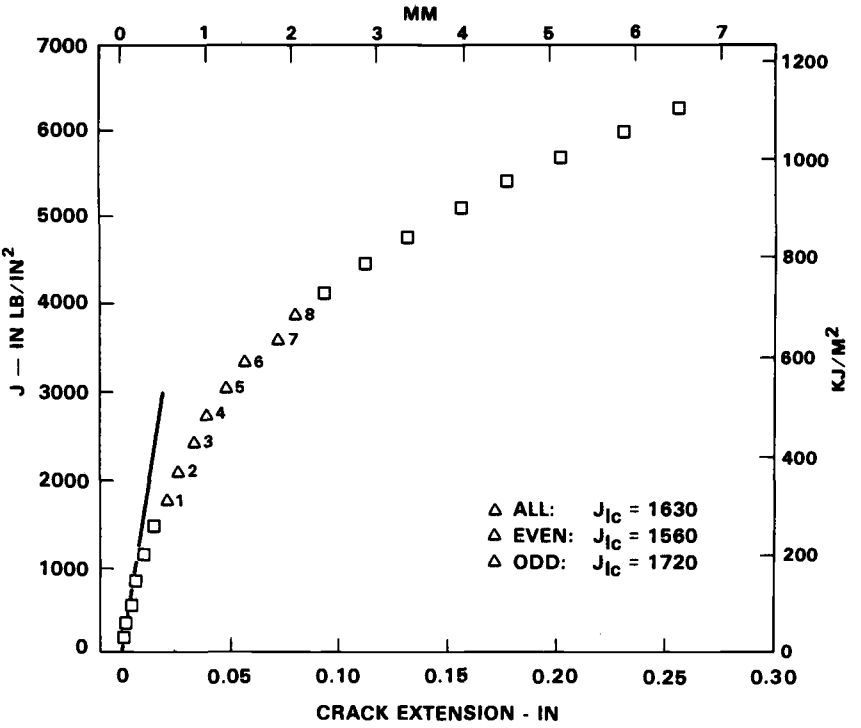

FIG. 7—*Material* J-R *curve, with* J_{Ic} *values calculated according to ASTM E 813 using various combinations of the data points shown as triangles.*

sequently, the J_{Ic} calculation is quite sensitive to the alignment of the test data relative to the theoretical blunting line.

Flow Stress Accuracy

Since J_{Ic} is defined as the intersection of a line fit to data on the *J-R* curve and the line $J = 2\sigma_f \Delta a$, any error in the flow stress will create a corresponding error in J_{Ic}. Specifically

$$J_{Ic}/J_{Ic}^{e} = (\sigma_f/\sigma_f^{e}) \{1 + [2'(\epsilon_\sigma/\sigma_f)/(2 - J'/\sigma_f)]\} \tag{33}$$

where J_{Ic}^{e} is the result of the calculation performed using a flow stress value with an error ϵ_σ, and J' is the slope of the *J-R* curve. It should be observed from the above expression that the error in J_{Ic} is greatest when the ratio of the slope of the *J-R* curve to the flow stress is greatest. Therefore, letting $J'/\sigma_f = 1$ (the maximum value allowed by ASTM E 813), the maximum fractional error in J_{Ic} can be written as

$$1 - (J_{Ic}/J_{Ic}^{e}) = 1 - [1/(1 + \epsilon_\sigma/\sigma_f)] \tag{34}$$

Simplifying terms and ignoring the products of errors, the fractional error in J_{Ic} caused by errors in flow stress can be written as

$$1 - (J_{Ic}/J_{Ic}^{e}) \leq 1 - \sigma_f^e/\sigma_f \tag{35}$$

Discussion

Because the accuracy of the J-test final results are strongly dependent on how errors were accumulated during the test, it is not possible to discuss the significance of every combination of errors on every type of J test. However, the particular cases studied here are representative of the results from a variety of materials commonly tested, and some general comments can be made:

1. The crack length calculation is relatively insensitive to errors in specimen dimensions and transducer calibration in the magnitudes allowed by the ASTM J_{Ic} standard. The maximum error in a/w for the test conditions allowed by the standard occurred at $a/w = 0.5$ and was estimated to be $+0.008$, corresponding to a 4.1% error in compliance. Relaxing the required maximum deviation from linearity from 0.1 to 0.3% of range for the extensometer increased the maximum error in a/w to only $+0.010$, suggesting the insensitivity of the crack length calculation to extensometer linearity.

2. Because of the nonlinearity of the compliance calibration equation for the compact fracture specimen, errors in the crack length calculation do not remain constant but vary throughout the test. This creates an error in the calculation of crack extension during the test, the magnitude of which is dependent on the total amount of crack extension. For $\Delta a/w = 0.3$, the error is less than 3% of the total crack extension for the test parameter errors tolerated by the standard, and is relatively insensitive to moderate decreases in the linearity of the extensometer (Fig. 3). However, for $\Delta a/w = 0.05$, the error in crack extension is approximately 5% of the total crack extension for the same errors in input parameters, and increases to almost 15% of the total crack extension when the linearity requirement on the extensometer is relaxed (Fig. 4).

3. For a test with total crack extension of $\Delta a/w = 0.15$, the errors in J were estimated by this model to vary from -3 to $+4$% of the maximum J value for various combinations of the test parameter errors allowed by the standard but were relatively insensitive to extensometer nonlinearity. For $\Delta a/w = 0.05$, the errors in J were estimated to vary from -3 to $+7$% of the maximum J value for various combinations of errors allowed by the standard and were found to reach 15% of the maximum J for a case where the maximum deviation from linearity of the extensometer calibration data was relaxed to 0.3% of range. These trends are consistent with the effect of the investigated errors on calculated crack extension.

4. Despite the effect of these errors on the shape of the J-R curve, it is likely

that their effect on J_{Ic} is small. It has been observed that the ASTM J_{Ic} value corresponds roughly to the J value at a crack extension within the interval $\Delta a = 0.127$ to 2.54 mm (0.005 to 0.010 in.). As can be seen in Figs. 5 and 6, the error in J at these crack extensions is quite small and is in fact less than the variability caused by differences in data placement onthe J-R curve or to the offset of data from the blunting line.

5. Since errors in flow stress create equal fractional errors in J_{Ic}, the J_{Ic} calculation can be considered to be relatively insensitive to the errors in flow stress encountered in normal experimental measurements.

6. Since variability in J_{Ic} is so strongly affected by data placement and the manner in which a test is performed, it is clear that as many data points should be obtained on the J-R curve in the region used in the J_{Ic} calculation as is experimentally feasible. In particular, a sufficient number of points should be obtained in the region of crack-tip blunting to allow the determination of an experimental blunting line, which can be used to precisely align the J-R curve data with the theoretical blunting line used in the J_{Ic} calculation. In addition, a sufficient number of data points should be obtained between the exclusion lines defined by the standard so that the line fit to the data represents a true average of the actual material behavior within that region. Although the exact number of data points required to accomplish this depends on many factors (including the amount of scatter in the individual data points), it has been the experience of the authors that at least six to eight data points (as opposed to the four points required by the J_{Ic} standard) should be obtained in each of the regions defined above to avoid undue uncertainty in the J_{Ic} calculation.

7. Alternatively, to desensitize the J_{Ic} calculation to the location of data on the J-R curve when data are sparse, the actual data can be curve fit and J_{Ic} values calculated as the intersection of the theoretical blunting line, and a line fit to closely spaced data obtained from the equation. An equation of the form

$$J = C_4 (C_3 + \Delta a)^{C_2} + C_1 \Delta a + C_0 \tag{36}$$

has been found to provide an excellent fit to most J-R curves since it simultaneously describes the initial nonlinear portion of the curves (often represented by a power law function) as well as the flattening of the J-R curves at larger crack extensions. Curves fit to the J-R curve shown in Fig. 7 as well as to the set of even points and set of odd points from that J-R curve are shown in Fig. 8. A J_{Ic} value of 296 kJ/m^2 (1690 in. · lb/in.^{2}) was calculated using data from the curve fit to the entire J-R curve, while values of 292 kJ/m^2 (1670 in. · lb/in.^{2}) (-1.2% difference) and 298 kJ/m^2 (1700 in. · lb/in.^{2}) ($+0.6\%$ difference) were obtained from the curves fit to the even and odd data points, respectively. In each case, data obtained from the equation were subject to the same validity criteria as the actual test data so that only the source of data for use in the J_{Ic} calculation and not the method of calculating J_{Ic} was changed.

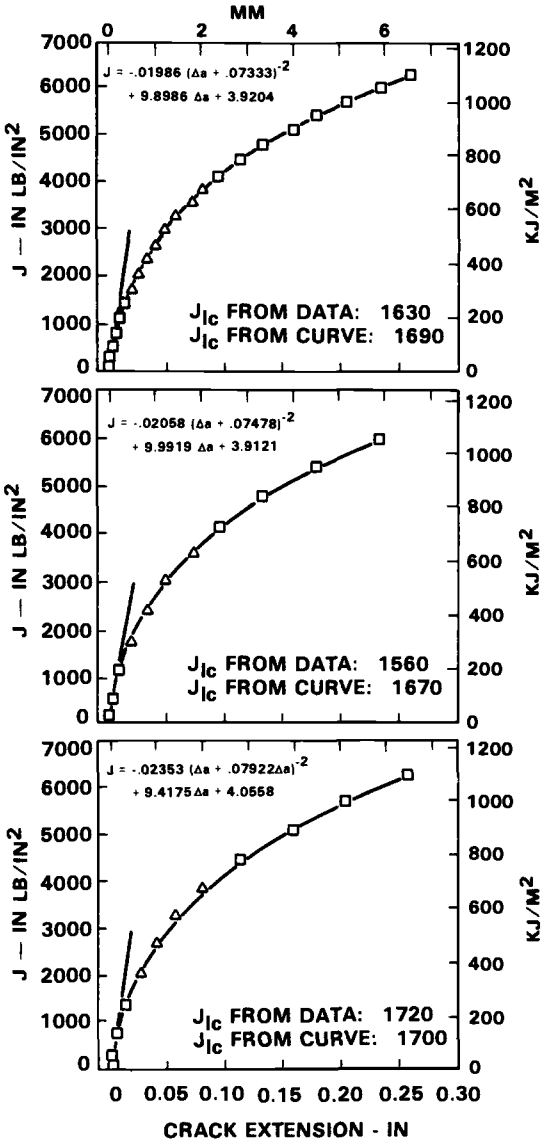

FIG. 8—*Material* J-R *curve, showing actual* J-Δa *data as well as curves fit to the data.* J_{Ic} *values calculated using the actual data as well as data obtained from the equations. Top view shows analysis applied to entire set of data; center view shows analysis applied to even numbered points from original set; bottom view shows analysis applied to odd numbered points from original set.*

Conclusions

It has been the goal of this study to suggest one method for determining the sensitivity of the unloading compliance J-test procedure to errors in test parameters, and to analytically investigate the degree of variability in the final results of tests conducted according to the J_{Ic} and proposed J-R curve test procedures. This has not been done to directly challenge either of the procedures, but rather to provide information that may be useful in determining the significance of deviations from the procedures. In this light, several conclusions can be drawn.

1. The J-R curve and calculated J_{Ic} value are relatively insensitive to the errors in test parameters allowed by ASTM E 813 as modeled in this study. Slight decreases in the linearity of the extensometer (often the most difficult specification in the standard to meet) appear to be insignificant except when testing extremely tough materials (for example, materials that exhibit little crack extension for large changes in load-line displacement). For this reason, however, no changes to the accuracy specifications are recommended.

2. The J_{Ic} calculation is sensitive to the location of J-Δa data points along the (nonlinear) J-R curve, as well as to the position of the J-Δa data relative to the theoretical blunting line.

3. Because of the sensitivity of the J_{Ic} calculation to the location and spacing of data points on the J-R curve, it is recommended that as many data points as possible be obtained in the region of crack blunting and between the exclusion lines defined by the standard. It is the experience of the authors that six to eight data points should be obtained within each of these regions whenever possible. Alternatively, the J_{Ic} calculation can be desensitized to the location of data along the J-R curve when data are sparse by curve fitting the actual data and using closely spaced points obtained from the resulting equation in the J_{Ic} calculation.

References

[1] Van Der Sluys, W. A. and Futato, R. J., "Computer-Controlled Single Specimen J-Test," *Elastic-Plastic Fracture: Second Symposium, Volume II—Fracture Resistance Curves and Engineering Applications, ASTM STP 803*, American Society for Testing and Materials, Philadelphia, pp. II-464–II-482.

[2] Saxena, A. and Hudak, S. J., Jr., "Review and Extension of Compliance Information for Common Crack Growth Specimens," Paper 77-9E7-AFCGR-P1, Westinghouse Scientific, Pittsburgh, PA, May 1977.

[3] Albrecht, P., Andrews, W. R., Gudas, J. P., Joyce, J. A., Loss, F. J., McCabe, D. E., Schmidt, D. W., and Van Der Sluys, W. A., "Tentative Procedure for Determining the Plane Strain J_I-R Curve," *Journal of Testing and Evaluation*, Vol. 10, No. 6, Nov. 1982, pp. 245–251.

Thomas Hollstein,[1] *Johann G. Blauel,*[1] *and Bert Voss*[1]

On the Determination of Elastic-Plastic Fracture Material Parameters: A Comparison of Different Test Methods

REFERENCE: Hollstein, T., Blauel, J. G., and Voss, B., **"On the Determination of Elastic-Plastic Fracture Material Parameters: A Comparison of Different Test Methods,"** *Elastic-Plastic Fracture Test Methods: The User's Experience, ASTM STP 856,* E. T. Wessel and F. J. Loss, Eds., American Society for Testing and Materials, 1984, pp. 104–116.

ABSTRACT: *J*-initiation values and *J*-resistance curves are the most promising candidates for the characterization of fracture resistance of materials used in the transition and upper shelf toughness region. Though their use for prediction of initiation of crack growth and of ductile tearing instability was successfully demonstrated in evaluations of large-scale tests, there still remain several problems concerning the determination of initiation values and generation of *J*-resistance curves. This paper reports on results of investigations conducted on different materials with different specimen types. It covers the comparison of different methods for initiation detection and *J*-resistance curve determination and the influence of side grooves and specimen dimensions. For both the measurement of *J*-initiation values J_i and *J* resistance J_R, the DC potential drop technique, the partial unloading compliance technique, and the multiple specimen interrupted loading procedure were used on compact specimens with dimensions ranging from B = 12 5 to 100 mm. The tests were carried out in a temperature range of 25 to 600°C (77 to 1112°F). The generated *J*-resistance curves agree very well, but slightly different values of crack initiation were determined. The definition of initiation of crack growth is discussed.

KEY WORDS: fractures (materials), crack initiation, crack propagation, fracture tests, fracture toughness, elastic-plastic fracture, J integral, specimen size, fracture mechanics

Critical *J* values for onset of crack growth and *J* based crack growth resistance curves are the most promising candidates for elastic-plastic material characterization and ductile failure assessment. Besides the multiple-specimen interrupted loading method as used in the ASTM Test for J_{Ic}, a Measure of Fracture Toughness (E 813), single-specimen procedures have become available and they form the basis of a tentative test procedure for determining material resistance curves $J_R = J(\Delta a)$ [*1*].

For all these methods the crack driving parameter J is determined in the same

[1]Senior scientist, head of metallic materials group, and senior scientist, respectively, Fraunhofer-Institut für Werkstoffmechanik, Wöhlerstr. 11, D-7800 Freiburg, West Germany.

way from the force-displacement diagram. What is different is the way the increments of crack length are determined. Results from using the change of electrical resistance (direct current potential drop [DCPD]) and of elastic compliance (partial unloading compliance [PUC]) for stable crack growth evaluation are compared here to direct measurements on the fracture surfaces of series of separate specimens. Some new results for different materials and temperatures up to 600°C (1112°F) are presented in the following together with a discussion of measurement requirements, advantages, and deficiencies of these three methods concerning J_R curves and initiation values. The reliability and accuracy of the results of either one of these methods are a necessary basis of ongoing research on the problem of a unique, that is, a geometry independent, material characterization and of transferability of the results to structures.

Multiple-Specimen Method

According to ASTM E 813, J is evaluated from the work done on the cracked specimen, and the crack lengths are derived from direct measurements on the fracture surfaces of a series of separate specimens. Each specimen delivers only one $J/\Delta a$-point of the whole J_R curve (Fig. 1). The stable crack growth increments include the crack-tip stretch zone, and a nine-point average over the

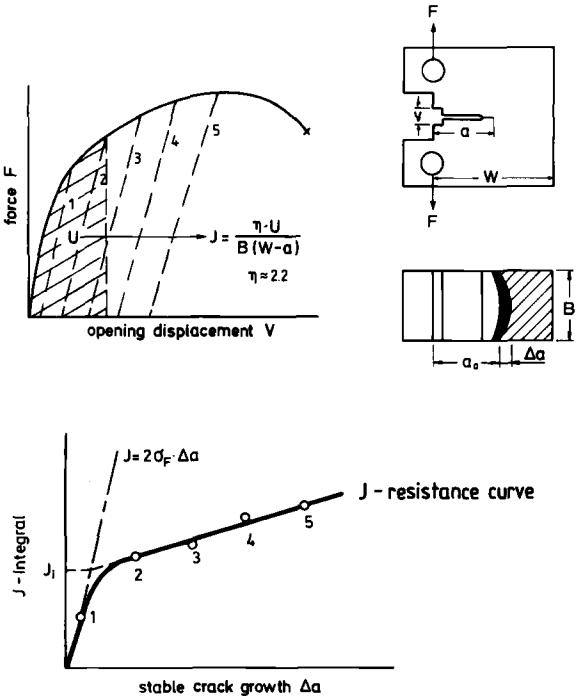

FIG. 1—*Principle of multiple-specimen interrupted loading method.*

specimen thickness is used. Intersection of a straight line fit with a formal blunting line $J = 2\Delta a\ \sigma_f$ delivers J_{Ic}, but the initiation value J_i for first physical crack growth (after a full stretch zone has developed) can be much smaller (Fig. 2).

Partial Unloading Compliance Method

Instead of using the interrupted loading technique the increasing crack length can be inferred from successive measurements of the elastic compliance $C = \Delta V / \Delta F$ of the specimen that is derived from small superimposed unloadings ($\Delta F \approx 0.1\,F$) and known functions $a = f$(elastic compliance C, Young's modulus E, and specimen geometry) (Fig. 3). Meeting the standard conditions of ASTM E 813 for the number of data points (unloadings) and appropriate data grouping a J_{Ic} value is determined by extrapolation, which in a technical sense characterizes initiation for each specimen; additional statistical information about material variation is then gained by testing several specimens.

The major problems with the partial unloading compliance method are the requirements of a very high accuracy, stability, and linearity of all components of the measurement and data aquisition system and of a low friction loading device. The system used here was developed in the Institut für Werkstoffmechanik (IWM) and is described in Refs *2* and *3*, and in the accompanying paper by Voss and Mayville.[2] Figures 4 and 5 demonstrate good performance of the system up to a temperature of 300°C (572°F) by low scatter of the first data

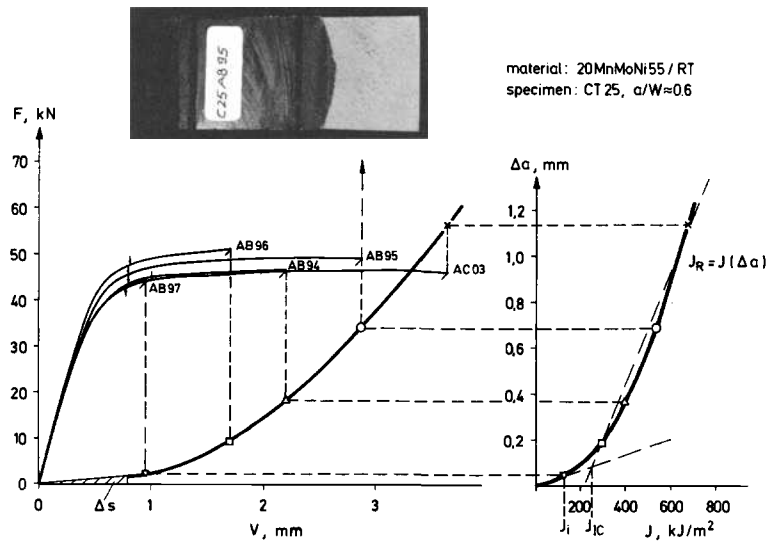

FIG. 2—*Determination of initiation toughness from interrupted loading test series; stretch zone width* Δs *from scanning electron microscope measurements on the fracture surfaces.*

[2]Voss, B. and Mayville, R. A., in this publication, pp. 117–130

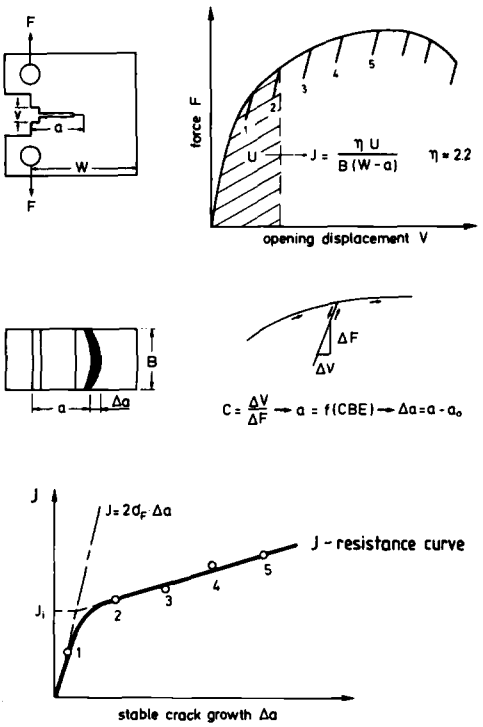

FIG. 3—*Principle of single-specimen J_R-curve testing by the method of partial unloading compliance (PUC).*

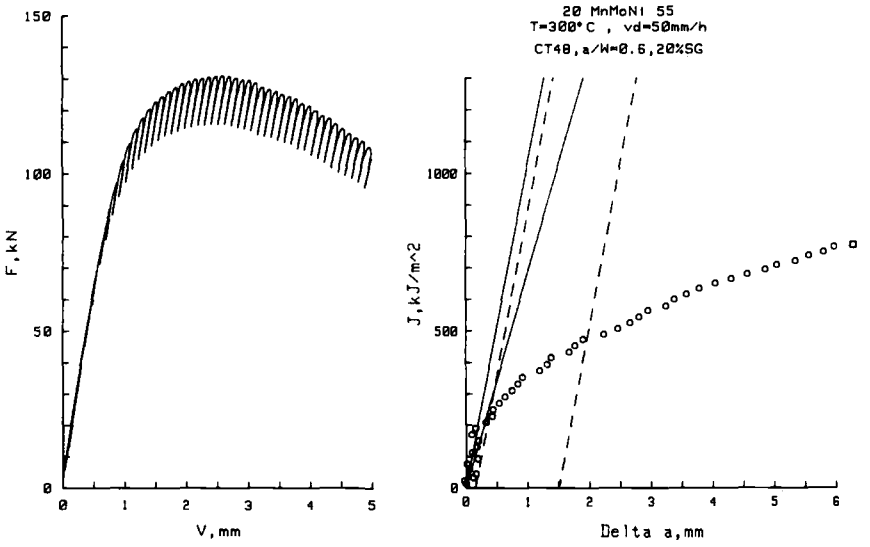

FIG. 4—*Force* F *versus opening displacement* V *diagram and corresponding* J_R *curve determined by the PUC method; square marks* Δa *measured on the fracture surface.*

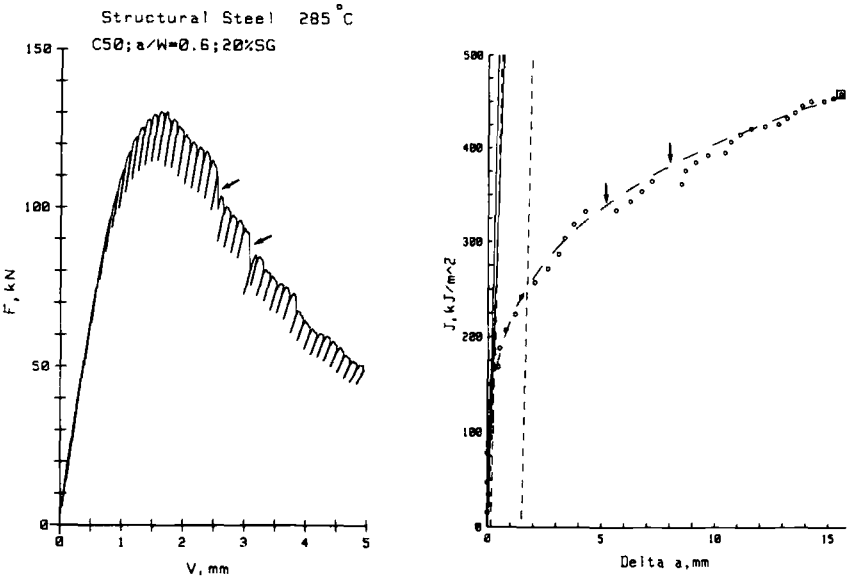

FIG. 5—*Force* F *versus opening displacement* V *and corresponding* J_R *curve for a CT 50 specimen tested at 285°C (545°F); square marks* Δa *measured on the fracture surface.*

points along the blunting line and by close agreement of predicted and measured final crack lengths. The Δa-steps marked by arrows in Fig. 5 are not due to experimental scatter but are related to load drops occurring beyond the limits of valid Δa measurements according to Ref *1*.

Potential Drop Method

The principle of the direct current potential drop method as used by IWM for compact specimens is shown in Fig. 6 [*4*]. A constant direct current is fed into the specimen in the plane of loading, and the potential drop ϕ is measured at two contact pins across the crack. ϕ changes when the specimen is loaded and especially when the crack grows. At onset of stable crack growth a more or less distinct change of the shape of the ϕ-V curve is found and the further change of ϕ is proportional to the crack growth (typically 12 $mm^2/\mu V$ for 2 A and CT25). In this way critical values of force and displacement and of J for onset of crack growth can be evaluated. In addition a complete J_R curve can be determined by linear interpolation between the base line values of ϕ and J for the loaded crack of initial length a_o and the values ϕ_m and J_m for the final crack length $a_o + \Delta a$ at termination of the experiment (Fig. 6). The base line is constructed by extrapolation of the linear part of the ϕ-V curve in the elastic regime.

Figure 7 shows as an example of a force/potential-displacement diagram together with the fracture surface of a 300°C (572°F) test of a 50-mm thick compact specimen of the German reactor pressure vessel steel 20 MnMoNi 5 5

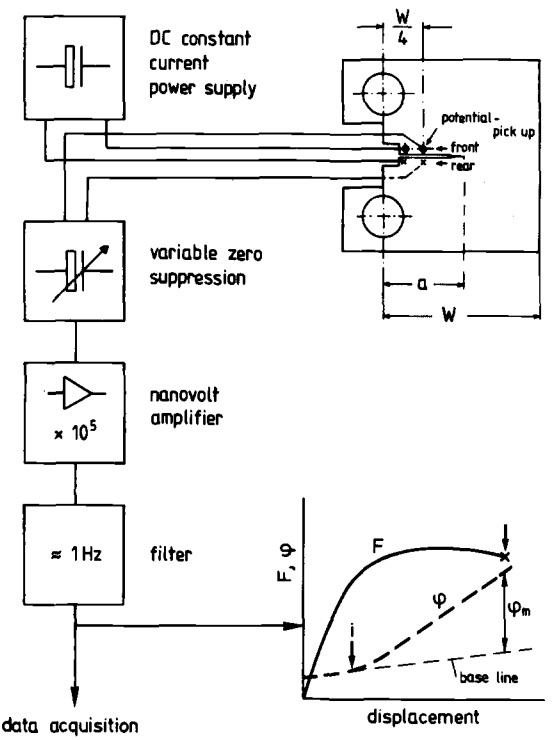

FIG. 6—*Principle of setup used in the Institut für Werkstoffmechanik (IWM) for direct current potential drop (DCPD) measurement.*

(Unified Numbering System [UNI] U 12 539). In Fig. 8 the corresponding continuous J (Δa) curve is shown together with additional PD results evaluated in the same way. The final points of the interrupted loading tests (filled symbols in Fig. 8) confirm the primary J_R curves. The crack extension by crack-tip blunting has not been taken into account here. Some material scatter is indicated by the different tests.

The J_{Ic} value defined according to ASTM E 813 by an extrapolation to $\Delta a = 0$ of the regression line through at least four data points between $0.15 \leq \Delta a \leq 1.5$ mm yields $J_{Ic} = 151$ kJ/m^2. This value is about 25% higher than the J_i value calculated for the displacement at "i" in Fig. 7 ($J_i \simeq 120$ kJ/m^2), which is well confirmed by the first interrupted loading point. Using a power law fit according to Loss et al [5] through the "valid" interrupted loading data, one finds $J_{Ic}^{Loss} = 174$ kJ/m^2.

Figure 9 gives some additional insight into the influence of experimentation and evaluation. In this example initiation is uncertain between $0.5 \leqslant V_i \leqslant 0.7$ from the ϕ/V curve resulting in a variation of the PD critical value $43 \leqslant J_i \leqslant 81$ kJ/m^2; for a more precise determination of J_i testing of an additonal specimen to very little crack growth is therefore recommended. But the uncertainty of the point of initiation has only little influence on the resulting J_R curve and

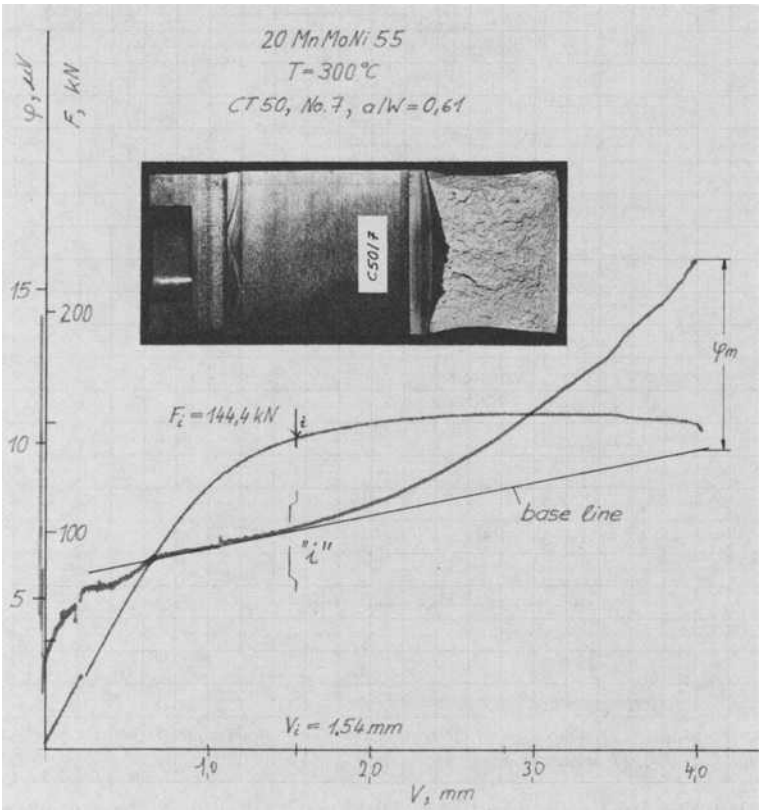

FIG. 7—*Original force/potential-displacement record for Test 7, CT 50 specimen of steel 20 MnMoNi 5 5 at 300°C (572°F).*

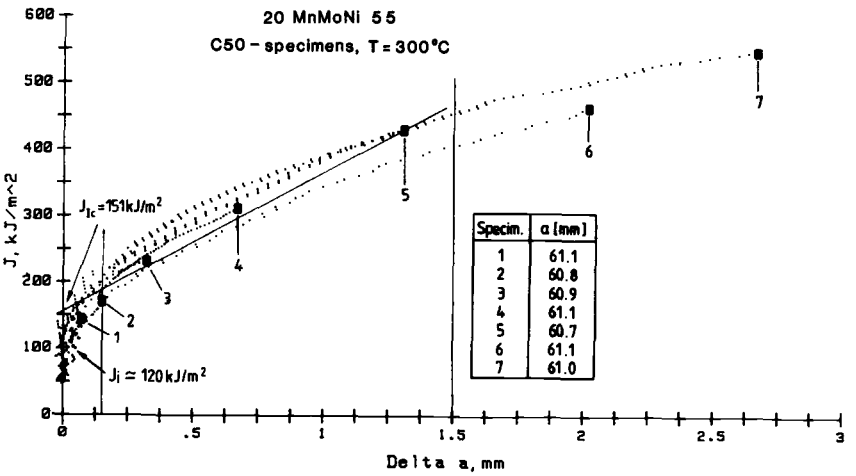

FIG. 8—J_R*-curve data from an interrupted loading test series together with a potential drop evaluation; CT 50 specimens of steel 20 MnMoNi 5 5 tested at 300°C (572°F).*

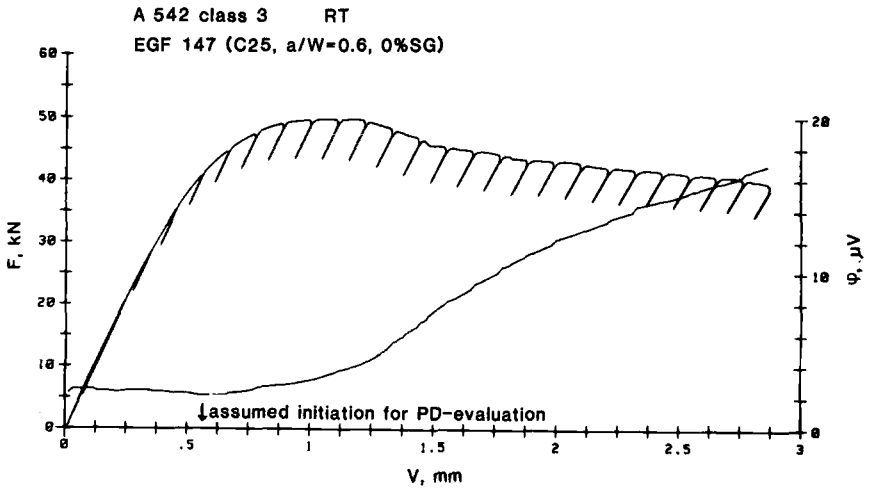

FIG. 9—F/ϕ *versus* V *diagram of simultaneous partial unloading and potential measurement.*

the ASTM J_{Ic} evaluated from it; in this example only a negligible variation of $143 \leqslant J_{Ic} \leqslant 150$ kJ/m^2 results.

Comparison of PUC and DCPD Methods

Figures 9 and 10 show results from a partial unloading experiment with simultaneous measurement of potential drop (for clarity the ϕ data during unloadings have been omitted). For this comparison the calibration of potential

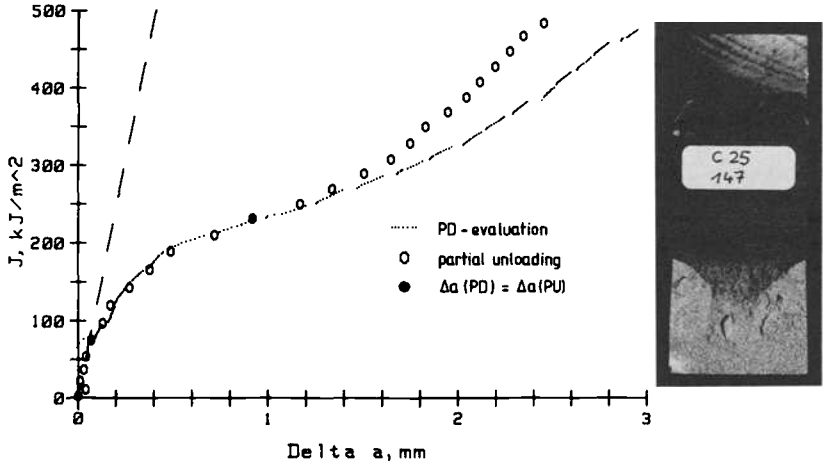

FIG. 10—J_R*-curve evaluation from Fig. 9;* Δa *for DCPD adjusted at the two marked partial unloadings; the fracture surface of the nonside-grooved specimen shows pronounced tunnelling.*

was adjusted to the crack lengths measured by the sixth and thirteenth unloading, which are marked in Fig. 10. For this special choice (though somewhat arbitrary) both resulting J (Δa) curves are a good agreement for small amounts of crack growth. But for $\Delta a > 1.5$ mm the slopes of both curves increase, and they deviate from each other. Both predictions of final crack growth underestimate the measurement $\Delta a = 3.9$ mm on the fracture surface by different amounts. It seems reasonable to relate the increase in slope with the onset of pronounced tunnelling, which is visible on the fractured specimen (Fig. 10) having no side grooves. This is supported by analytical and experimental results of Prij [*6*] and Prantl [*7*] showing that for tunnelled cracks the crack length will in general be underestimated by the compliance function of Ref *1*. Specifically in Ref *6* for a similar geometry as for the specimen in Fig. 10 an error of about 40% is found for the crack length, and this is almost exactly the difference found here between PUC prediction and fracture surface measurement. Thus it may be concluded that the PUC and the DCPD method both underestimate the growth of tunnelling cracks, but by slightly different amounts. To avoid problems like these in defining a correct effective crack length, it is recommended, as in Ref *1*, to use appropriately side-grooved specimens.

The temperature range of application of the PUC and the DCPD method can be extended to investigate creep phenomena. Figure 11 as an example shows results of two short-time creep tests at constant load and at constant displacement rate, respectively, with good agreement of measured crack growth rates from both methods [*8*].

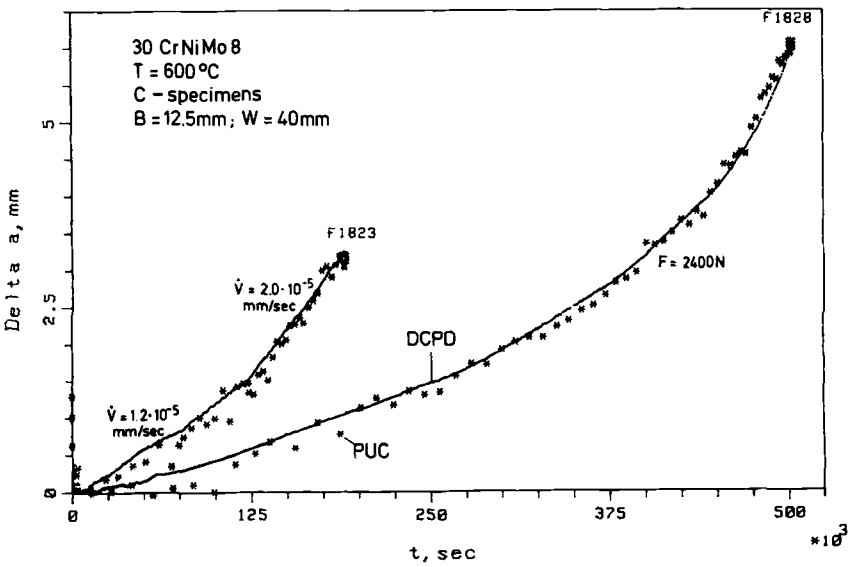

FIG. 11—*600°C (1112°F) short-time creep tests with crack growth* Δa *measured by DCPD and PUC method* [8].

Application to Material Characterization

The experimental methods discussed above were used to better define the ductile fracture properties of a specific melt of the reactor pressure vessel steel 20 MnMoNi 5 5. From the results in Figs. 12 through 15 a discussion of the influences of different measurement procedures as well as specimen geometry, relative crack length, and test temperature is possible.

Figure 12 shows J_R curves measured at 80°C (176°F) with different specimen sizes. It demonstrates good overall reproducibility of the J_R curves and no significant size effect for the valid side-grooved specimens. All $J(\Delta a)$ points of each specimen may be well approximated by a power law fit as proposed in Ref *6* for an alternative J_{Ic} extrapolation. Mainly because of the slight differences for small Δa values the fitted curves are slightly different, resulting in lower J_{Ic} values for the compact specimens (CT) 25 mm thick. Only the 12.5-mm thick

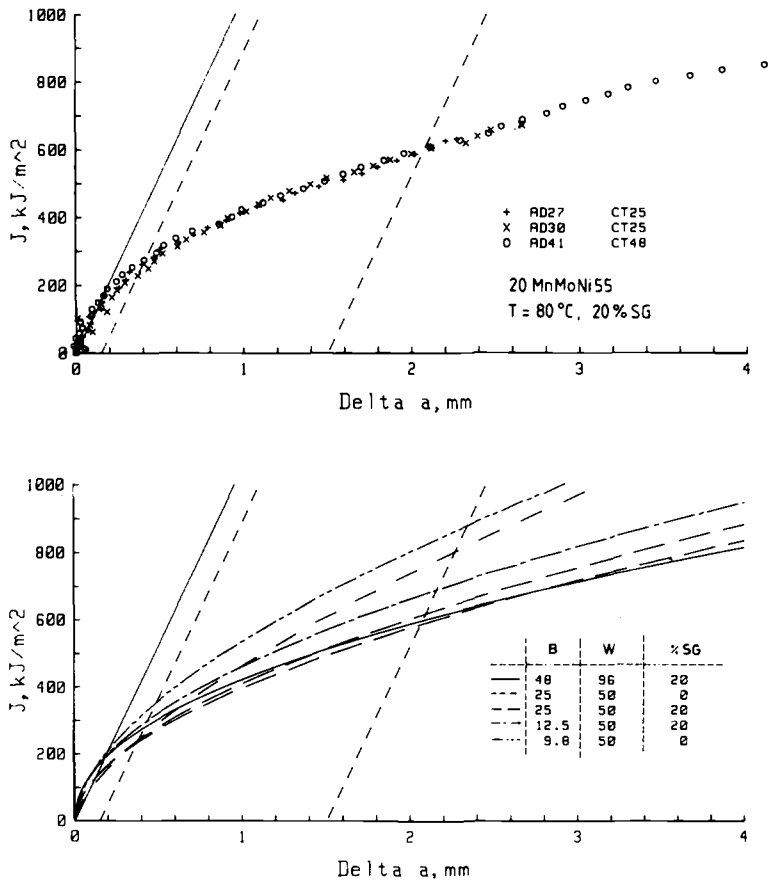

FIG. 12—J *versus* Δa *measured by PUC method for different compact specimens of the steel 20 MnMoNi 5 5 at 80°C (176°F).*

specimen shows a tendency for a steeper J_R curve, being invalid however because of not meeting the thickness requirements of Ref *1*. On the other hand the specimens without side grooves deliver significantly steeper J_R curves compared to the 20% side-grooved specimens.

In Fig. 13 results measured at 150°C with specimens of different thicknesses with and without side grooves are compared. The scatter bands of the interrupted loading tests and of the partial unloading tests for nonside-grooved specimens are in good agreement. The J_R curves measured with 20% side-grooved specimens by the partial unloading method are significantly lower.

In Fig. 14 results measured at 300°C with interrupted loading, potential drop, and partial unloading methods are compared. They show good agreement independent of the testing method and specimen thickness. Even 20% side grooving seems to have no influence on the crack growth resistance for this test temperature for the thicknesses tested, although the side-grooved specimens showed homogeneous crack growth over the full thickness instead of pronounced tunnelling in the smooth specimens. The lower of the PUC curves is also shown in Fig. 4.

Conclusions

Different procedures can be used to determine material parameters J_i, J_{Ic}, and J crack growth resistance curves for the characterization of crack initiation and

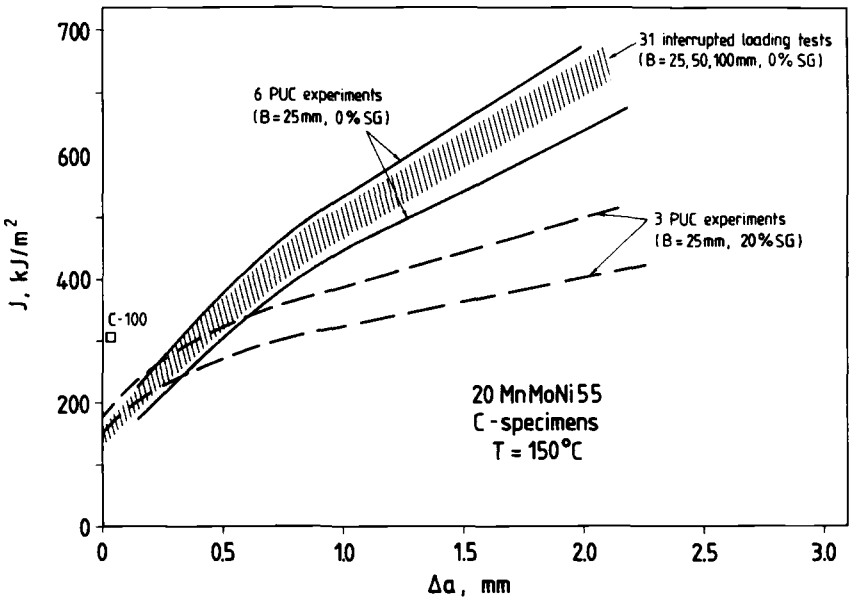

FIG. 13—*Comparison of partial unloading and interrupted loading/potential drop results at 150°C (302°F).*

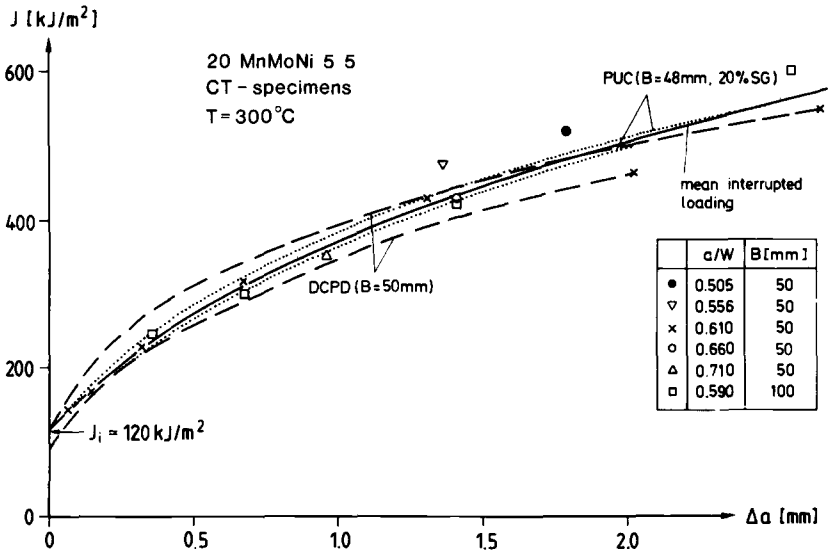

FIG. 14—J_R *curves from different methods; material: 20 MnMoNi 5 5; CT specimens with and without side grooves (SG); test temperature 300°C (572°F).*

stable crack growth. Single-specimen procedures are superior to multiple-specimen techniques because of the reduced expenditure and improved information.

With the method of partial unloading for each single specimen a complete J_R (Δa) curve can be derived, the quality of which may be assessed by comparing the predicted initial and final crack lengths with those measured on the fracture surface. Testing of several specimens of the same kind in principle delivers equivalent J_R curves. Therefore additional information is gained about the material scatter. J_{Ic} may be determined as a technical inititation parameter following the ASTM extrapolation procedure. Determination of onset of stable crack growth requires an additional specimen unloaded just beyond initiation.

The potential drop method allows for the evaluation of a continuous J_R (Δa) curve if initiation is given (at least approximately). There remains some uncertainty with this point of initiation because the physical sources of the change of potential under loading are not well understood. Therefore J_i should be confirmed by testing one additional specimen with very little crack growth. The J_{Ic} extrapolation is less sensitive to the uncertainty in J_i.

Both methods discussed underestimate crack growth compared to the area mean value if pronounced tunnelling occurs, as often seen in smooth specimens. To avoid errors by this effect testing of side-grooved specimens is recommended.

As shown by the results for the steel 20 MnMoNi 5 5 at different temperatures, equivalent results are derived from potential drop, partial unloading compliance, and interrupted loading tests.

References

[1] Albrecht, P., Andrews, W. R., Gudas, J. P., Joyce, J. A., Loss, F. J., McCabe, D. E., Schmidt, D. W., and Van Der Sluys, W. A., "Tentative Test Procedure for Determining the Plain Strain J_i-R Curve," *Journal of Testing and Evaluation*, Vol. 10, No. 6, Nov. 1982, pp. 245–251.

[2] Voss, B. and Blauel, J. G., *Proceedings of the 4th ECF-Conference*, Vol. 1, K. L. Maurer, and F. E. Matzer, Eds. Engineering Materials Advisory Services, Ltd., Warley, United Kingdom, 1982, pp. 47–56.

[3] Voss, B., "On the Problem of 'Negative Crack Growth' and 'Load Relaxation' in Single Specimen Partial Unloading Compliance Tests," *Proceedings of CSNI Workshop on Test Methods for Ductile Fracture*, Nuclear Energy Agency, Organization for Economic Cooperation and Development, Paris, 1983, pp. 54–60.

[4] Kloss, G., "Rechnergestützte J-R-Kurvenbestimmung nach dem Potentialverfahren," Vorträge der 13. Sitzung des Arbeitskreises Bruchvorgänge, Hannover, Deutscher Verband für Materialprüfung, Berlin, 1981, pp. 336–349.

[5] Loss, F. J., Menke, B. H., Gray, R. A., Jr., and Hawthorne, J. R., "J-R-Curve Characterization of Irradiated Nuclear Pressure Vessel Steels," *Proceedings of the U.S. Nuclear Regulatory Commission*, CSNI Specialists Meeting on Plastic Tearing Instability, NUREG/CP-0010, CSNI Report 39, U.S. Nuclear Regulatory Commission, Washington, DC, 1979, pp. 202–315.

[6] Prij, J., "Some Finite Element Results of CTS Specimen," *Proceedings of CSNI Workshop on Test Methods For Ductile Fracture*, Nuclear Energy Agency, Organization for Economic Cooperation and Development, Paris, 1983, pp. 176–180.

[7] Prantl, G., "Assessment of Crack Extension by Different Methods," *Proceedings of CSNI Workshop on Test Methods for Ductile Fracture*, Nuclear Energy Agency, Organization for Economic Cooperation and Development, Paris, 1983, pp. 115–122.

[8] Hollstein, T. and Voss, B., "Hochtemperatur-Riβwiderstand und Kriechriβwachstum—Untersuchungen mit dem Gleichstrompotential—und dem Teilentlastungsverfahren," Vorträge der 15. Sitzung des Arbeitskreises Bruchvorgänge, Darmstadt, Deutscher Verband für Materialprüfung, Berlin, 1983, pp. 45–55.

Bert Voss[1] *and Ronald A. Mayville*[2]

The Use of the Partial Unloading Compliance Method for the Determination of J_I-R Curves and J_{Ic}

REFERENCE: Voss, B. and Mayville, R. A., **"The Use of the Partial Unloading Compliance Method for the Determination of J_I-R Curves and J_{Ic},"** *Elastic-Plastic Fracture Test Methods: The User's Experience, ASTM STP 856*, E. T. Wessel and F. J. Loss, Eds., American Society for Testing and Materials, 1985, pp. 117–130.

ABSTRACT: A computerized testing system was developed and utilized to determine J_I-R curves and J_{Ic} by the partial unloading compliance method according to the ASTM Test for J_{Ic}, a Measure of Fracture Toughness (E 813) and the tentative test procedure for determining the plane strain J_I-R curve. Based on testing experience with different materials in the temperature range from -196 to > 300°C some problems of the standard procedure concerning, for example, mechanical loading, data evaluation, and validity requirements, are discussed and some alternatives are proposed.

KEY WORDS: fracture (materials), crack propagation, fracture tests, fracture mechanics, elastic plastic, J integral, tests, ductile fracture, resistance curve, loading grips

On the basis of the ASTM Test for J_{Ic}, a Measure of Fracture Toughness (E 813) and the tentative test procedure for determining the plane strain J_I-R curve [*1*] a computerized testing system using the partial unloading compliance method was developed. The system was successfully used for determining J-R curves especially for ferritic steels and aluminum alloys in the temperature range from -196°C (-320°F) to more than 300°C (572°F). Some problems of the testing and data evaluation procedure, especially their consequences for the determination of the initiation parameter J_{Ic}, will be discussed.

Procedure

Testing System

Figure 1 shows schematically the testing system as developed in the Institut für Werkstoffmechanik and first described by Mayville and Blauel [*2*]. The

[1]Senior scientist, Fraunhofer-Institut für Werkstoffmechanik, Wöhlerstr. 11, D-7800 Freiburg, West Germany.

[2] Senior scientist, Arthur D. Little, Inc., Acorn Park, Cambridge, MA 02140.

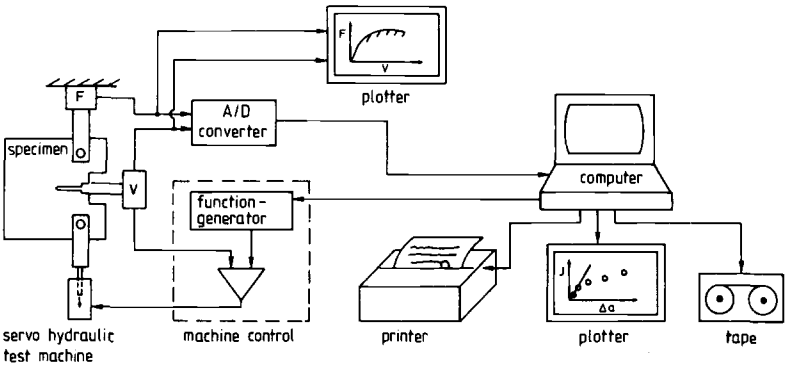

FIG. 1—*Schematic of computerized automatic test system with on-line evaluation.*

specimen is loaded by a servo hydraulic or screw driven testing machine with closed loop control. For normal strain control experiments the load-line displacement V is measured by a clip gage between blades in the load line, and the signal is fed to the servo control amplifier. The same signal together with the load signal is fed to the A/D converters, digitizing with an integration time of 20 ms and a resolution of 1 in 100 000. These data are read by a desktop computer and evaluated for control of the test according to test parameters predefined or determined from measured values of the actual test. The computer controls functions of the analog ramp generator of the testing machine (load, unload, hold, and displacement velocity) and of the data aquisition system. All the data are evaluated on-line and stored on a mass storage for a post-test reevaluation. The area under the load F versus load-line displacement V curve is numerically integrated by a trapezoidal rule to calculate J values with and without crack growth correction according to Ref *1* and ASTM E 813. Crack growth is derived from unloading compliance by the functions given in Ref *1*. Compliances are calculated separately for unloading and reloading by linear regression through the F-V data points excluding only a few points at the upper and lower ends of the unloading paths. About 25 points are used for the regression, yielding correlation coefficients of 0.9999 to 0.999999 at room temperature, decreasing to 0.999 and even 0.99 for low- and high-temperature experiments. But, as will be discussed later, a better measure for the accuracy of the crack length measurement seems to be the difference of the crack lengths calculated from the unloading and reloading compliance.

During the test, in addition to the analog plot of F versus V the computer delivers a printed record of the main steps and a plot of the resulting J versus crack growth Δa points. This information allows one to decide whether changes of predefined test parameters are necessary. The computer code is written in BASIC, and the computer allows the operator to change variables from the keyboard without interrupting the program. This flexibility may be important, for example, to meet the requirements of ASTM E 813 for a valid J_{Ic} test if an unknown material has to be tested. On the other hand, normal tests may be run

automatically from start to final unloading of the specimen. This feature is especially important to realize complete and reproducible control of relatively fast experiments and in order to save manpower during very slow tests. This automatic system has been successfully used for tests with about 40 unloadings with an overall testing time between 20 min and 16 h.

At the end of each test preliminary results are documented by printed lists including J_{Ic} and a plot of the J-R curve. Stored data may be plotted and re-evaluated by post processing programs.

Specimens

All results discussed here were measured with compact specimens (CT) shaped according to ASTM E 813 normally with relative crack lengths $a/W \approx 0.6$ and 20% side grooves. In particular, pinhole diameters of $0.25W$ and appropriate pins were used instead of the reduced diameter proposed in Ref *1*. Thickness B normally equalled $W/2$, but some specimens had reduced thicknesses of $W/4 \leq B < W/2$.

Experimental Results and Discussion

Apparent Negative Crack Growth

Figure 2 shows J-R curves from two different steel specimens. The upper curve shows apparent negative crack growth, well known to sometimes arise in

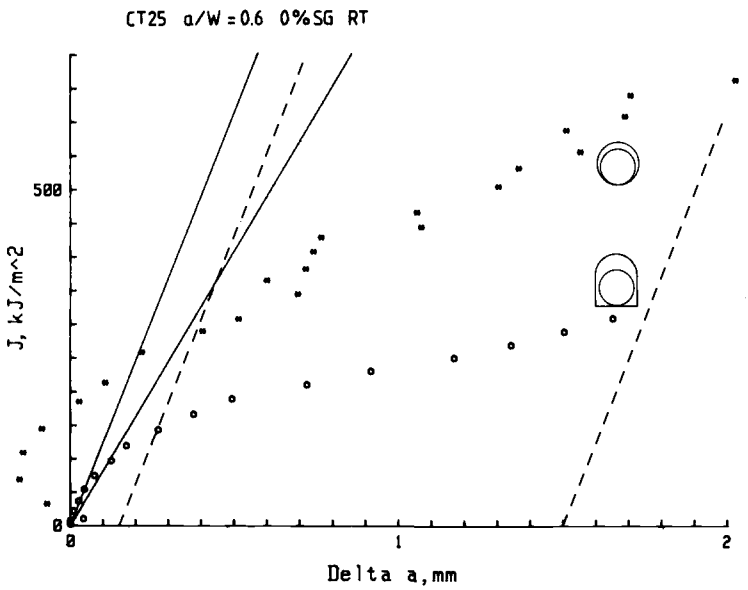

FIG. 2—*Qualitatively different* J-R *curves (for different steels) measured: with round clevis holes—negative crack growth and with flat bottom holes—no negative crack growth.*

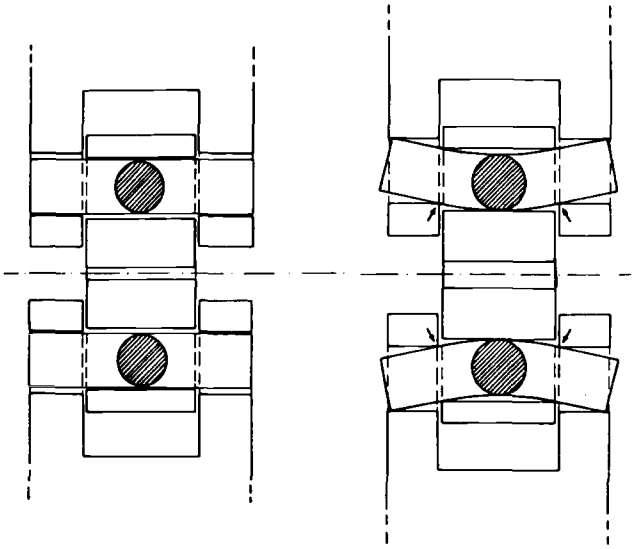

FIG. 3—*Front view of CT specimen loaded in standard clevises. Arrows mark areas with risk of plastic indentation.*

partial unloading compliance tests, and the lower one does not show negative crack growth. The reason for the apparent negative crack growth is the geometry of the clevis hole [*3*].

ASTM E 813 proposes flat bottom holes or roller bearings in the clevises for pin loading of compact specimens to avoid friction effects. Roller bearings (now omitted in Ref *1*) are difficult to handle and have some problems at elevated test temperatures. Use of insufficiently operating flat bottom holes instead may result in negative crack growth. Figure 3 shows a front view of a compact specimen loaded by a clevis with flat bottom holes according to ASTM E 813 (schematically). By loading the specimen the pins bend and may cause plastic

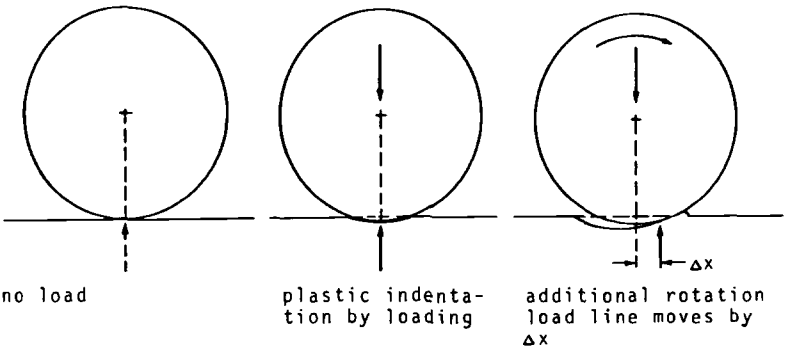

FIG. 4—*Contact area of bolt and clevis hole, schematically.*

deformation of the flat surfaces of the clevises in the regions marked by arrows. Figure 4 shows side views of the contact area of pins and clevis without load, with plastic indentation by vertical loading and the effect of additional rotation of the loading pin, which is necessary to maintain mechanical equilibrium while the crack is opened by loading.

Figure 5 models this situation by loading the specimen (radius of the holes r_s) by a pin (radius r_b) rolling on a circular surface of the clevis hole (radius r_c). For this idealized geometry the effect on the measured compliance may be quantified [3].

At a displacement V measured in the load-line position each half of the specimen near the load line is tilted relative to the crack plane by an angle α_s. Assuming a rotation center in front of the crack tip (crack length a) on the ligament (size b) at a distance ϵb ($\epsilon \approx 0.3$), α_s is approximately given by

$$\alpha_s \approx \tan \alpha_s = V/[2(a + \epsilon b)] \tag{1}$$

Because of this rotation of the pinhole region of the specimen the lines of contact of the pin to the specimen and the clevis, respectively, must move towards the crack tip by a distance Δx quantified below. The assumed load line for compliance evaluation and crack length calculation passes through the center of

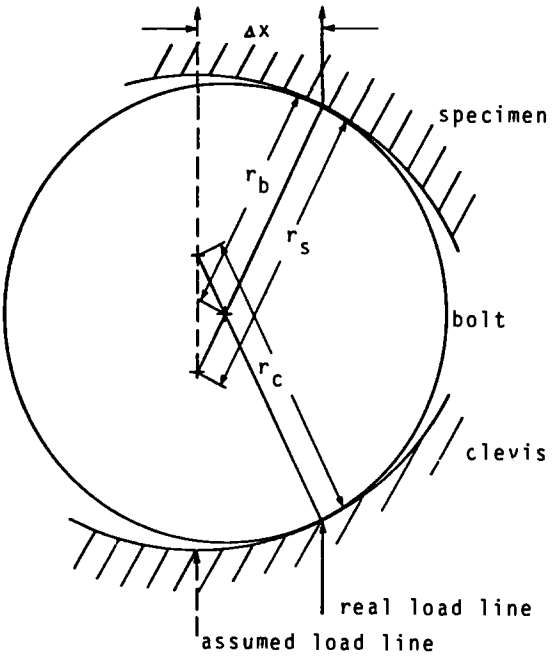

FIG. 5—*Force is measured in the real load line displaced by* Δx *relative to the assumed load line through the center of the specimen hole.*

the pinhole in the specimen (dashed arrows in Fig. 5). But the real load line is at a distance Δx towards the crack tip and the measured force F_m, or a difference ΔF_m during a partial unloading will be greater compared to the assumed load-line position. This causes an underestimation of the compliance and of the crack length and consequently results in negative Δa values before real crack growth.

Assuming free rolling of the contacting surfaces without any slip Δx is given by

$$\Delta x = r_s \sin \{\alpha_s [r_s/(r_s + r_c - 2 r_b)]\} \tag{2}$$

and the measured compliance C_m may be corrected for this error by

$$C_{corr} = C_m [(a + \epsilon b)/(a + \epsilon b - \Delta x)] \tag{3}$$

In practice the correction by Eq 3 normally will not be applicable because r_c ($\approx r_b$) will be an unknown and not constant if caused by plastic indentation. But for reasonable assumptions (CT specimen, B = 25 mm [1 in.] $W = 2B$; r_s = 6.25 mm [0.25 in.], $r_c = r_b$ = 6 mm [0.24 in.]) the consequences of this effect are demonstrated in Fig. 6 using data of a real experiment without negative crack growth and introducing the error by the inverse of Eq 3. This results in a shape of the new J (Δa) curve and Δa_{min} = −0.25 mm (−0.01 in.) similar to Fig. 2. For the three *J-R* curves depicted in Fig. 6 by different symbols, the regression lines to determine J_{Ic} according to ASTM E 813 are also given. Obviously with negative crack growth simulated by this model the value of J_{Ic} = 173 kJ/m^2 (990 in.-lb/in.^{2}) is greater than the original value, J_{Ic} = 122 kJ/m^2 (700 in.-lb/in.^{2}). But even correcting for the effect of negative Δa by shifting all points to

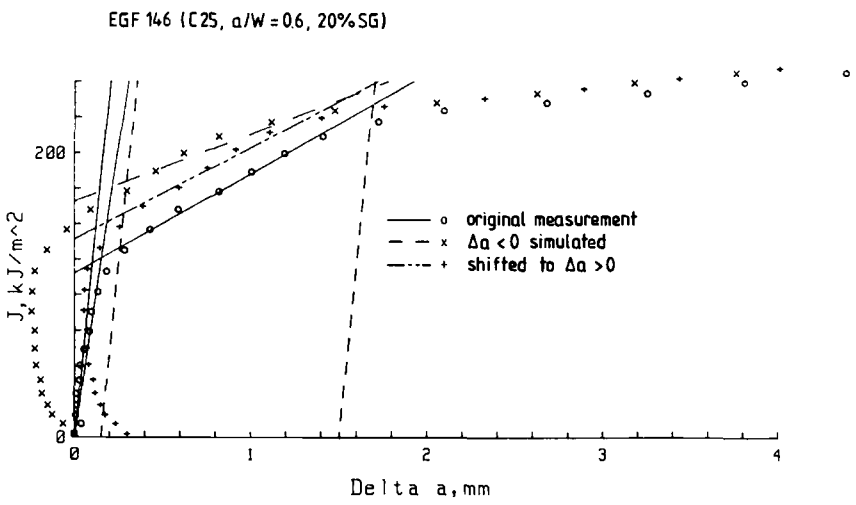

FIG. 6—*Simulation of negative crack growth by the inverse of Eq 3, influence on the extrapolated* J_{Ic}.

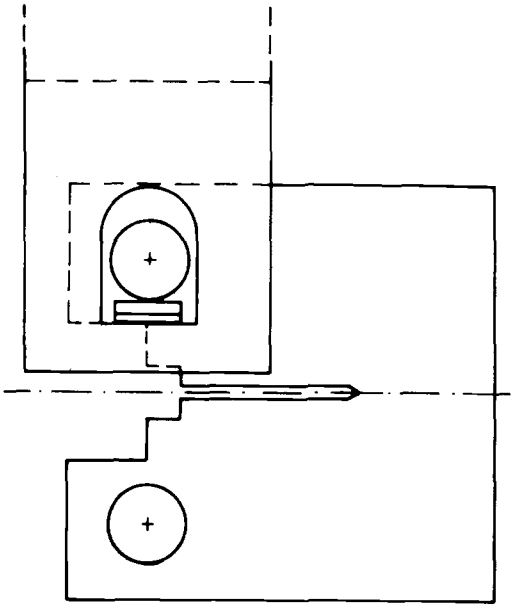

FIG. 7—*Alternative clevis design, side view (schematically).*

positive Δa values with the most negative point on the blunting line results in J_{Ic} = 147 kJ/m^2 (840 in.-lb/in.^{2}) being greater than the correct one. So apparent negative crack growth may result in nonconservative J_{Ic} estimations.

For a flat bottom hole without indentation $1/r_c = 0$, and Eq 2 results in $\Delta x = 0$, that is, negative crack growth is not predicted by this model. To decrease the risk of indentation, special grips were developed and successfully tested [*3*]. They are shown schematically in Figs. 7 and 8. Hardened inserts allow for tilting of the flat bottom planes if the loading pins are bending. So line loads are applied instead of point loads (arrows in Fig. 3) thereby decreasing pressure and consequently minimizing the risk of plastic deformation. Figure 9 shows the performance of this clevis type at room temperature. J-Δa points of three similar specimens follow the blunting line with a scatter of about ± 0.01 mm (±0.0004 in.). Figure 10 shows a J-R curve measured at 300°C (572°F). Scatter of the Δa measurements is increased for reasons discussed later, but there is no significant apparent negative crack growth. Even creep crack growth measurements at 600°C (1112°F) with clevises of this type resulted in acceptably low scatter [*4*].

A minor improvement of the compliance measurement was attained by using very stiff knife edges (pencil sharpener blades) with the edge of one of the knife edges cut so that the clip gage contacts it over a width of only 1 mm (0.04 in.). Then the position and orientation of the clip gage are less sensitive to misalignment of the blades, such as what might occur by nonsymmetric deformation of the specimen.

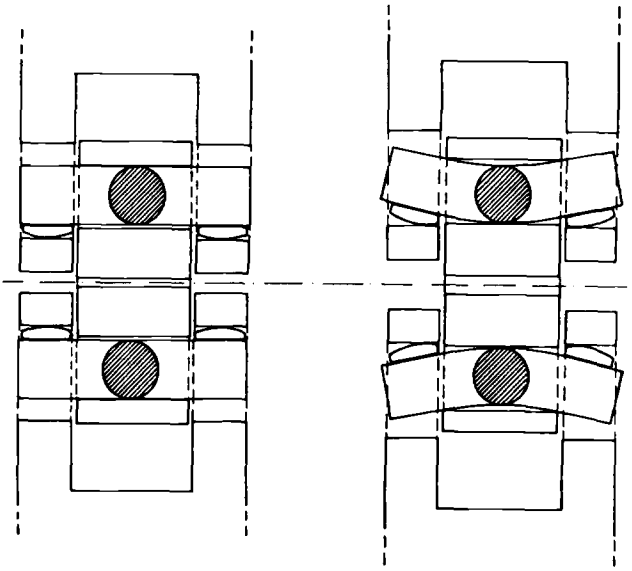

FIG. 8—*Front view of CT specimen loaded in alternative clevises. Curved hardened plates allow for bending of the loading bolt.*

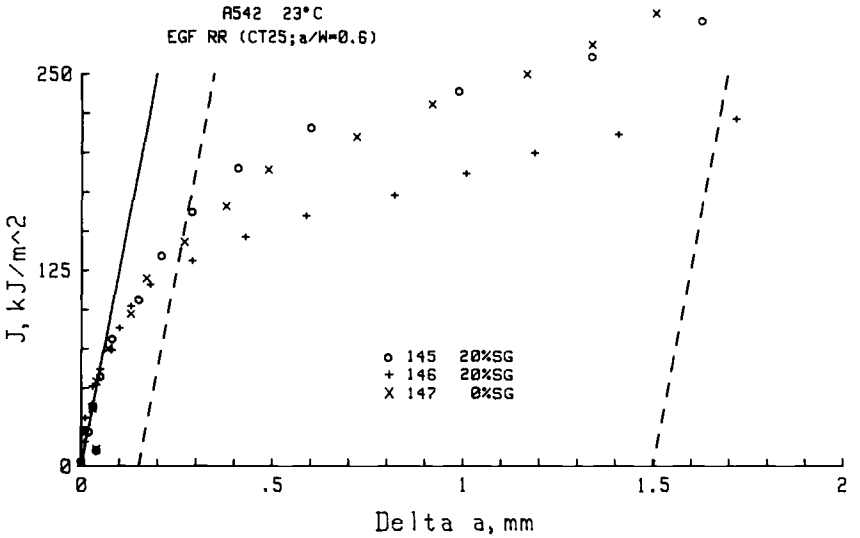

FIG. 9—*Three* J-R *curves measured with the clevis type of Figs. 7 and 8 showing low scatter and good reproducibility before crack initiation.*

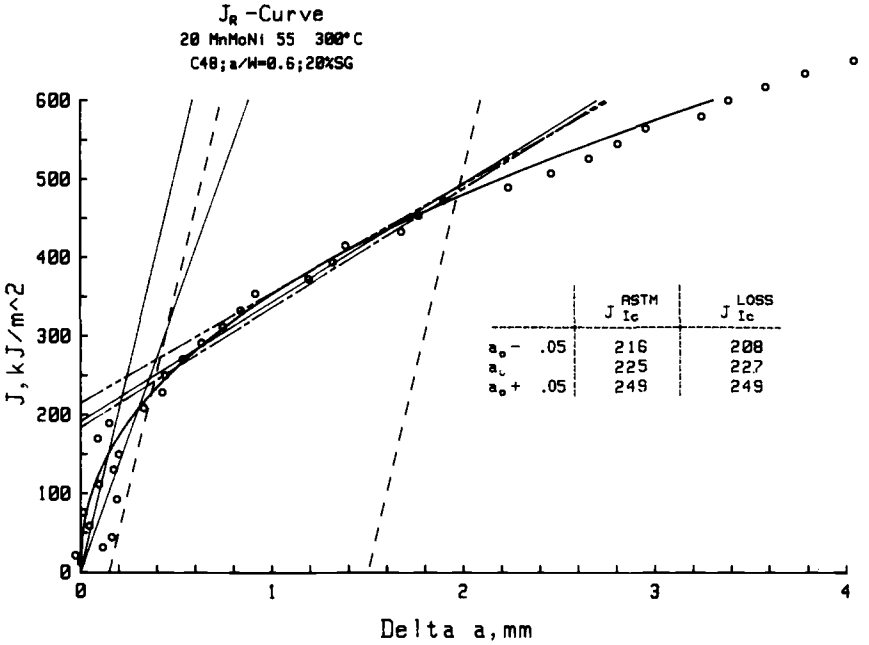

FIG. 10—*Influence of an uncertainty of ±0.05 mm in initial crack length measurement* (a_o) *on* J_{Ic} *determined according to ASTM E 813 and Loss* [6].

Load Relaxation Effects

Time dependent effects in the specimen may cause problems for the crack length determination from the compliance measured in partial unloadings [*3*], particularly during tests at elevated temperatures (for example, range of service temperature of light water reactors 300°C [572°F]).

Figure 11 shows part of a load versus displacement diagram measured at 300°C (572°F; steel 20 Mn Mo Ni 55 [Unified Classification System (UNI) K12539] CT specimen B = 48 mm [1.9 in.] = $W/2$) with load drops of about 5% during constant displacement control up to 3-min duration. Although the nearly exponential load drop, as visible in the load versus time diagram of Fig. 11, did not reach a nearly constant level during this time, the crack lengths could be estimated from the compliances. The differences in crack lengths calculated from unloading and reloading compliances showed an (apparent) crack growth of 0 to 0.4 mm (0.016 in.) during the unloading cycles. In spite of these differences the final crack length estimated from the last compliance measurement of this test agreed with the heat tint measurement within 0.2 mm (0.008 in.).

Even without the 3-min relaxation time, reasonable J-R curves can be measured. Figure 12 shows one of several unloadings without relaxation, followed immediately by a second unloading in a test with a displacement velocity of about 1 mm/min (0.04 in./min; specimen size and material as Fig. 11). The

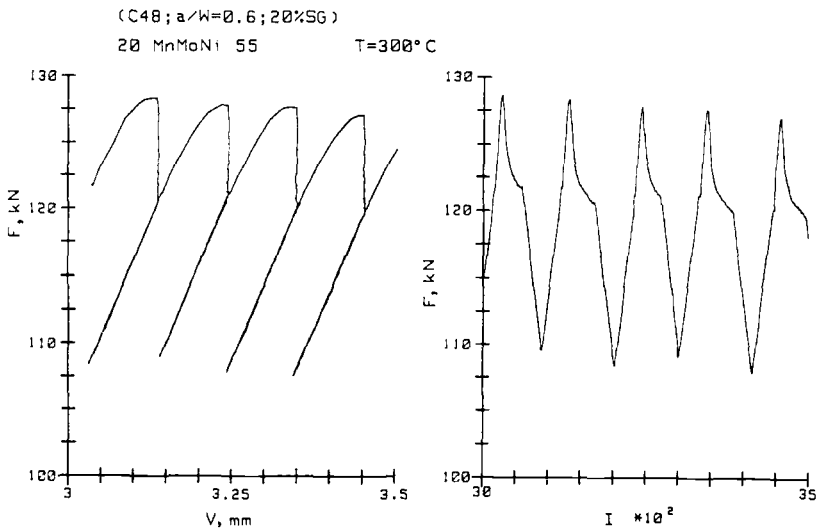

FIG. 11—*Load dropping exponentially with time in constant displacement control followed by linear elastic unloading* (I *is proportional to time with different factors for loading, relaxation, and partial unloading*).

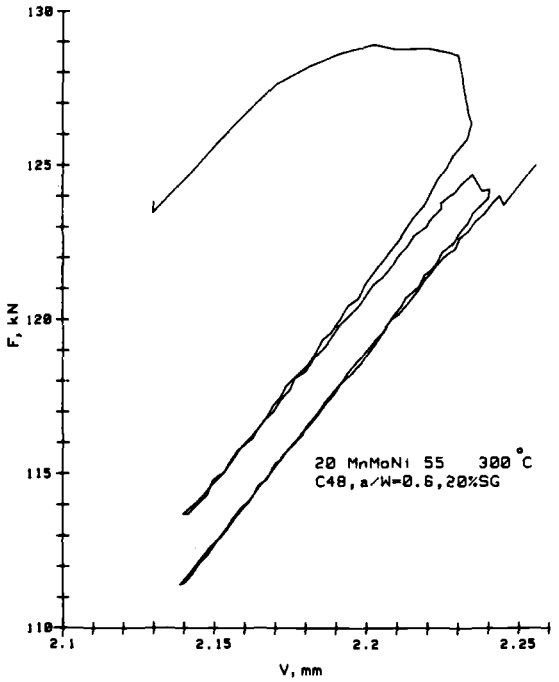

FIG. 12—*Superposition of elastic unloading and time dependent load drop in partial unloadings without prior load relaxation period.*

differences of the estimated crack lengths from the unloading and reloading paths were 1.6 mm (0.06 in.) for the first cycle and 0.45 mm (0.018 in.) for the second one. This is caused by the curvature, visible in Fig. 12 especially for the first cycle. The difference of the mean values for these two cycles was only 0.24 mm (0.01 in.) and for several pairs of unloadings in the range of 0.02 to 0.29 mm (0.0008 to 0.012 in.). This is comparable to the difference of 0.2 mm (0.008 in.) found between the crack length derived from the last single-cycle unloading and the heat tint measurement for this test.

Waiting for constant load before partial unloading frequently takes the most time of the whole experiment even if the relaxation time is limited. Waiting time may be decreased by unloading the specimen by a few percent of actual load before relaxation, but then the total load drop (elastic part plus additional relaxation) may be even greater than that shown in Fig. 11.

Superposition of elastic unloading and time dependent relaxation effects may be a reason for apparent negative crack growth or other errors. Therefore if appreciable differences of unloading and reloading compliances are found the regression data points should be carefully analyzed.

Definition of the Point $\Delta a = 0$

All tests at high temperature discussed here were run with the specimen and the clip gage contained in a closed chamber heated by circulating air causing vibrations of the clip gage. This resulted in scatter of the F-V measurements as visible in Fig. 12 causing some more scatter of the compliances and the derived crack lengths (Fig. 10 [5]) than found at room temperature (Fig. 9).

ASTM E 813 excludes points left of the 0.15-mm exclusion line from the regression for J_{Ic} determination thereby excluding part of the error resulting from scatter of small Δa values. But a comparable uncertainty of the definition of the point $\Delta a = 0$ should be considered. To evaluate J_{Ic} from the J-Δa points of Fig. 10, the point $\Delta a = 0$ is assumed to be uncertain by ± 0.05 mm (0.002 in.), which is less than $\pm 0.1\%$ of the measured crack length. J_{Ic} is calculated from a linear regression according to ASTM E 813 and from a power law fit according to the alternative method proposed by Loss et al [6]. Both methods deliver comparable results, but they are changed by the small uncertainty of a_o by nearly $\pm 10\%$ of the original value as given in the table of Fig. 10.

This demonstrates that the accuracy, at which one can expect to measure the "true" J_{Ic}, is limited by the accuracy and scatter of the crack lengths derived from the first partial unloadings of a test. On the other hand, if the J-R curve is used to derive a J-T diagram [7] as used for instability analysis, only the correlation of J and dJ/da is needed, and the accuracy of a_o is less important.

Data Grouping Condition

To avoid errors in J_{Ic} determined by regression through clustered data points, ASTM E 813 sets some requirements for valid data. Figure 13 shows a $J(\Delta a)$ curve well defined by 40 points, measured with a CT specimen with $B = 14$

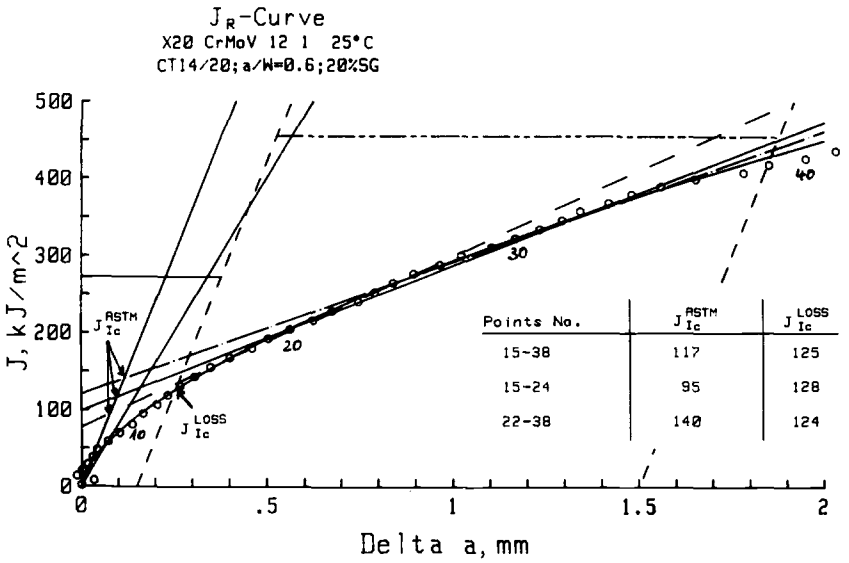

FIG. 13—*Influence of valid selections of regression points on* J_{Ic} *determined according to ASTM E 813 and Loss* [6] *(see Table 1).*

mm (0.55 in.) and $W = 40$ mm (1.58 in.) for a 12% chromium steel. J_{Ic} according to ASTM E 813 (denoted by "ASTM") and according to the alternative power law method [6] (denoted by "Loss") are given in Table 1. The valid points of this experiment are 15 to 38 yielding the "correct" values of 117 and 125 kJ/m^2, respectively. Other limited sets of data selected from all valid points could also be valid according to the data grouping condition. Limiting cases are the sets 15 to 24 and 22 to 38 resulting in valid ASTM J_{Ic}-values about ±20% different from the original one. Adding only the extreme point near to the opposite exclusion line (15 and 38, respectively) to these sets diminishes these differences. Taking only three equidistant points out of the clustered group plus the extreme point at the opposite exclusion line, four points just meeting the minimum

TABLE 1—J_{Ic} *according to ASTM 813 and Loss* [6] *by regression through valid data groups selected from the* J-R *curve of Fig. 13.*

Selected Valid Points	Number of Points	J_{Ic}^{ASTM}, kJ/m^2	J_{Ic}^{Loss}, kJ/m^2
15 to 38	24	117	125
15 to 24	10	95	128
22 to 38	17	140	124
15 to 24; 38	11	118	128
15; 22 to 38	18	127	126
15, 19, 24; 38	4	118	128
15; 22, 30, 38	4	117	128

requirement of ASTM E 813, then results in the original J_{Ic}. Of course this is no argument for taking only four valid points because material scatter was excluded by just taking a single specimen, and experimental scatter was small in this case. Instead the following is concluded.

1. Even without influence of material scatter J_{Ic} extrapolation may be less accurate if clustered data just satisfying the data grouping condition are used for the regression.
2. At least one data point near to the exclusion line away from the cluster should be required.
3. Data points should be nearly equidistant.
4. More than four valid data points should be required for the single-specimen test, to get information about the experimental scatter that occurs in a test.
5. At least two single-specimen tests should be required.
6. More than four valid specimens should be required for multiple-specimen tests especially if material scatter is evident.

The alternative regression procedure based on a power law fit [*6*] (last column of Table 1) has shown that J_{Ic} for different materials is less sensitive to the special choice of regression points if the curvature of the $J(\Delta a)$ curve is accounted for. This alternative method would not be useful in general for the evaluation of multiple-specimen tests because the curvature can be hidden by material scatter.

Conclusions

Apparent negative crack growth as a possible source of error in determining J_{Ic} from partial unloading compliance experiments may be caused by insufficient operation of flat bottom holes. This may result in nonconservative J_{Ic} values as demonstrated by a quantitative estimation of the effect for a special model. An alternative clevis design is presented that decreases the risk of plastic deformation of the clevises and essentially eliminates this problem, even for high-temperature applications.

Particularly during tests at elevated temperature load, relaxation effects may cause errors in compliance measurements. Waiting for a nearly constant load for a few minutes will increase the quality of crack length determination. The difference between compliances calculated for unloading and reloading is a useful measure for the technical quality of the data.

Depending on the scatter of results from the experiment, the point $\Delta a = 0$ is defined with some uncertainty thus influencing the accuracy of J_{Ic}. For other evaluations, for example, full J-R-curve development, this error is less important.

The conditions of ASTM E 813 to validate J_Q as J_{Ic} for clustered data points are not sufficient. A wider spread and perhaps more than four valid data points should be required.

References

[1] Albrecht, P., Andrews, W. R., Gudas, J. P., Joyce, J. A., Loss, F. J., McCabe, D. E., Schmidt, D. W., and Van Der Sluys, W. A., *Journal of Testing and Evaluation*, Vol. 10, No. 6, Nov. 1982, pp. 245–251.

[2] Mayville, R. A. and Blauel, J. G., "Die Methode der partiellen Entlastung zur Ermittlung von Riβwiderstandskuven," Vorträge der 12. Sitzung des Arbeitskreises Bruchvorgänge, Freiburg 1980, Deutscher Verband für Materialprüfung, Berlin, pp. 383–384.

[3] Voss, B., "On the Problem of 'Negative Crack Growth' and 'Load Relaxation' in Single Specimen Partial Unloading Compliance Tests," in *Ductile Fracture Test Methods, Proceedings of a CSNI Workshop*, Nuclear Energy Agency, Organization for Economic Cooperation and Development, Paris, 1983, pp. 54–60.

[4] Hollstein, T. and Voss, B., "Hochtemperatur-Riβwiderstand und Kriechriβwachstum-Untersuchungen mit dem Gleichstrompotential-und dem Teilentlastungsverfahren," Vorträge der 15. Sitzung des Arbeitskreises Bruchvorgänge, Darmstadt, Deutscher Verband für Materialprüfung, Berlin, 1983, pp. 45–55.

[5] Voss, B. and Blauel, J. G., *Proceedings of the 4th ECF-Conference*, Vol. 1, K. L. Maurer and F. E. Matzer, Eds., Engineering Materials Advisory Services Ltd., Warley, United Kingdom, 1982, pp. 47–56.

[6] Loss, F. J., Menke, B. H., Gray, R. A., Jr., and Hawthorne, J. R., "*J-R*-Curve Characterization of Irradiated Nuclear Pressure Vessel Steels," *Washington University Proceedings of US NRC CSNI Specialist's Meeting on Plastic Tearing Instability*, Report NUREG/CP-0070, Nuclear Regulatory Commission, Washington, DC, 1980.

[7] Paris, P. C., "A Method of Application of Elastic-Plastic Fracture Mechanics to Nuclear Vessel Analysis," in *Resolution of the Task A 11: Reactor Vessel Material Toughness Safety Issue*, Report NUREG 0744, Vol. 1, Johnson R., Nuclear Regulatory Commission, Washington, DC, 1982.

Jean Bernard[1] *and G. Verzeletti*[1]

Elastic-Plastic Fracture Toughness Characteristics of Irradiated 316H Stainless Steel

REFERENCE: Bernard, J. and Verzeletti, G., **"Elastic-Plastic Fracture Toughness Characteristics of Irradiated 316H Stainless Steel,"** *Elastic-Plastic Fracture Test Methods: The User's Experience, ASTM STP 856*, E. T. Wessel and F. J. Loss, Eds., American Society for Testing and Materials, 1985, pp. 131–149.

ABSTRACT: In the frame of an irradiation program of American Iron and Steel Institute (AISI) 316H (Unified Numbering System [UNS] S31 400) stainless steel at fast fluences ($E > 0.1$ MeV) ranging from 0.1 to 2 *dpa*, the fracture toughness of the steel was measured, using the J parameter, at 0, 0.1, and 0.3 *dpa* at 350 and 550°C. A dimensional analysis has been used to derive J resistance curves as well as J_{Ic} values for the base material and its welds. The specimens used were three-point bend (3PB) specimens, 20 mm high by 15 mm thick by 80 mm effective span. A noteworthy result concerning the base material is the lowering at 550°C and 0.1 *dpa* of dJ/da by about 50% and of J_{Ic} by about 35%. The other dJ/da and J_{Ic} values were not significantly altered at 550°C. Apart from this case, generally low degradation of base metal properties is found at both temperatures between the nonirradiated and the irradiated material.

The weld material exhibits significantly lower initiation toughness and tearings moduli in the preirradiation and post-irradiation conditions, but these fracture mechanics (FM) characteristics are practically unaltered at both temperatures and at the above mentioned fluence levels. The heat-affected zone (HAZ) material was also studied. It was found that all J-Δa values were bounded on the upper side by the base material at 350°C and on the lower side by the welded material at 550°C for corresponding fluence levels.

KEY WORDS: austenitic stainless steels, cracks, irradiation, welded joints, heat affected zone, J integral, crack extension, R curve

The evaluation of neutron damage to American Iron and Steel Institute (AISI) 316H (Unified Numbering System [UNS] S31 400) steel in terms of fracture toughness characteristics is needed for safety assessments of liquid metal fast breeder reactor (LMFBR) primary circuit components. To this end, irradiations covering the 0.1, 0.3, 1, and 2 displacements per atom (dpa) fast fluences ($E > 0.1$ MeV) have been planned. The results obtained so far concern the nonirradiated material and the 0.1 and 0.3 dpa irradiations. AISI 316H base metal, weld metal, and heat-affected zone (HAZ) material have been examined. Tests were conducted at 350 and 550°C on plane-sided three-point bend (3PB)

[1] Senior scientists, Applied Mechanics Division, Commission of European Communities, Joint Research Centre—Ispra Establishment, 21020 Ispra (Va), Italy.

TABLE 1—*Chemical composition of the investigated steel in weight percent.*

Carbon	Silicon	Manganese	Phosphorus	Sulfur	Chromium	Nickel	Molybdenum	Cobalt	Titanium	Niobium	Copper	Boron	Vanadium	Nitrogen
							BASE MATERIAL							
0.056	0.34	1.61	≤0.02	0.009	15.2	12.1	2.44	0.06	≤0.005	≤0.005	0.22	0.00097	0.087	0.082
							WELD MATERIAL							
0.051	0.43	2.25	≤0.02	0.009	16.0	8.9	2.36	0.06	≤0.005	≤0.005	0.17	0.00088	0.08	0.082

specimens. Various routes were followed to determine the J fracture mechanics parameter at incipient crack growth and under stable tearing. Candidate methods were the potential drop direct current method and a dimensional analysis, together with deformation theory of plasticity concepts. Reasonably accurate crack growth predictions were obtained using the latter approach, and this method was used to compute J resistance curves. Both methods yielded J_{I_c} values that corresponded in a satisfactory manner.

Materials and Specimen Preparation

The specimens were cut from a 316H stainless steel plate in accordance with ASTM Specification for Heat-Resisting Chromium and Chromium-Nickel Stainless Steel Plate, Sheet and Strip for Fusion-Welded Unfired Pressure Vessels (A 240). The material is in the fully annealed condition (½ h at 1080°C and quenched in water). Two strips were cut from the plate and butt-welded together following the metal-inert-gas (MIG) procedure. No annealing of the welded assemblage was done. The chemical composition of the steel is listed in Table 1. The mechanical properties of the nonirradiated steel appear in Table 2. They are based on the average of three to seven tension test results. The tension test specimen used is shown in Fig. 1. The longitudinal axis of the specimen is parallel to the plate rolling direction. The dimensions of the 3PB specimens used in this program appear in Fig. 1. The nominal a_0/W ratio is 0.55 where a_0 is the initial crack length and W the height of the 3PB specimens. Following standard designation the specimens are of the L-S type. Three types of specimen are distinguished according to the material into which the crack propagates, that is, base material (B specimens), weld material (W specimens) and HAZ material (HAZ specimens).

Precracking

Precracking of the specimens up to a nominal $a_0/W = 0.55$ value was achieved by operating the servohydraulic machine in amplitude control of the load-point displacement (20-Hz sinusoidal wave); the load amplitude $P = P_{max} - P_{min}$ varies in such a way that the amplitude of the specimen deflection at the load

TABLE 2—*Mechanical properties of the nonirradiated steel.*

Material	Temperature, °C	Yield Strength, MPa	Ultimate Tensile Strength, MPa	Uniform Elongation, %
Base	20	240[a]	570[a]	65[a]
Base	350	133	483	36
Base	550	105	440	35
Weld	350	300	445	16
Weld	550	250	382	14

[a]Result obtained in one test on a diameter ϕ 4 mm tension specimen, gage length was 20 mm.

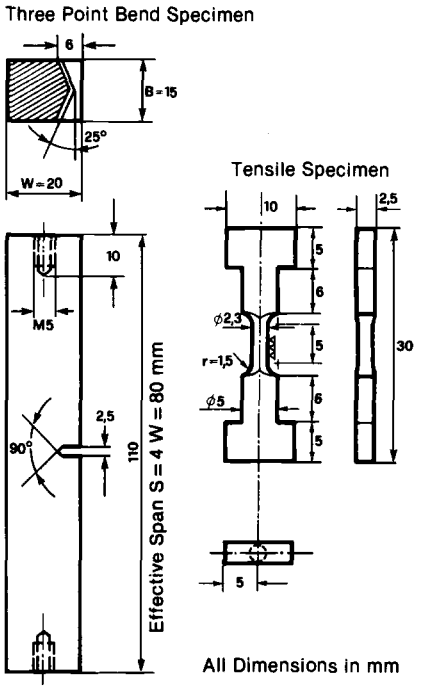

FIG. 1—*Dimensions of 3PB and tension specimens.*

point is kept constant by an electronic device. This technique results in a smoothly decreasing load as the crack grows and a slowly decreasing stress intensity factor ΔK applied to the specimen. The system allows a precise automatic arrest of the machine when the ΔP value reaches a predetermined minimum value. During fatigue precracking, P_{min} was held constant at 0.5 kN. P_{max} was controlled so that its value would remain within the limits set by the British Draft for Development Publication Methods for Crack Opening Displacement Testing (DD:1972). Following the above described methodology, this condition is satisfied from $a_0/W = 0.48$ onward as shown in Fig. 2. In this figure, K_f is the maximum allowable fatigue stress intensity at the crack tip. $K_f \leq 0.63\sigma_y B^{1/2}$ where $B = 15$ mm and σ_y was taken as the average of the yield and the ultimate tensile stress. The base material having the lowest σ_y of 405 MPa has determined the maximum loads that were applied for all three materials (B, W, and HAZ).

Irradiation

The irradiation was performed in the high flux reactor (HFR) of the Joint Research Centre (JRC) Petten (Netherlands) Establishment. The neutron spectrum in the irradiated positions is given in Fig. 3. The neutron metrology is given in Table 3. It may be observed that the weld material sustained a fast fluence of about 0.15 dpa instead of 0.1 dpa, which had been planned. The

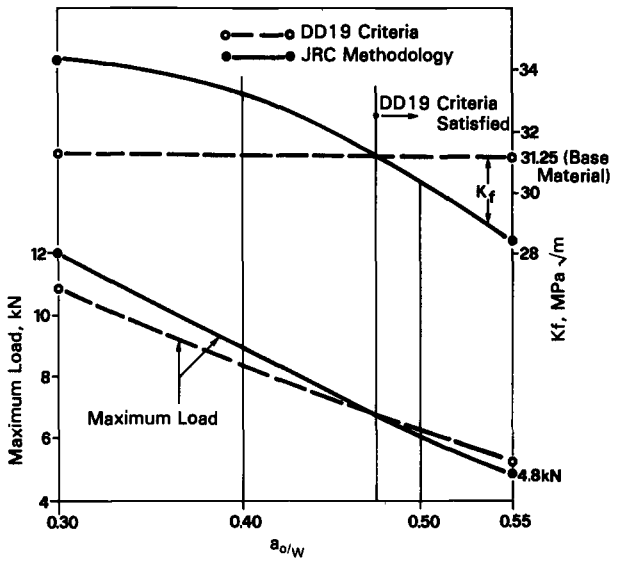

FIG. 2—*Applied maximum load during precracking.*

variation in fluence is about ±20% in a series of four specimens. The axial variation in the temperature of the sodium contained in the HFR capsules was at the most 50°C. The heat generation did not exceed 2.5 W/g corresponding to a temperature gradient of about 30°C between center and surface of the specimens.

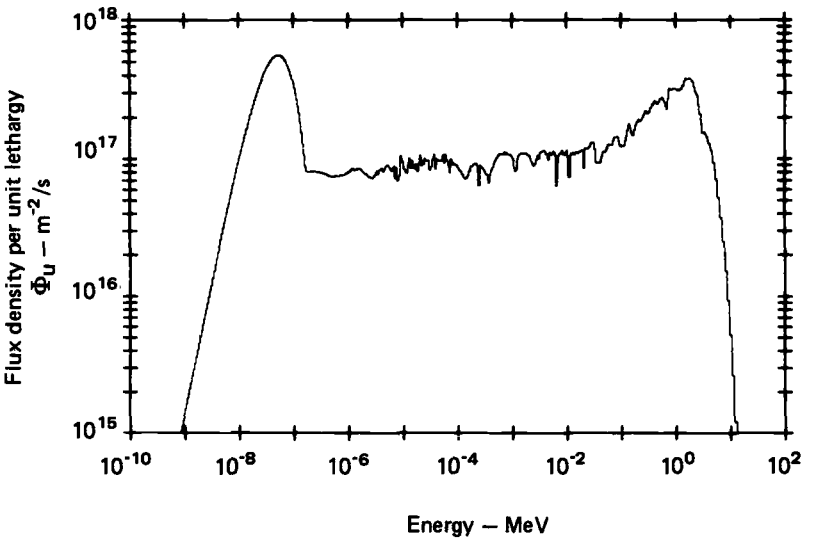

FIG. 3—*Neutron spectrum in the irradiated positions.*

TABLE 3—*Test matrix.*

Material and Number of Specimens	Temperature, °C	Fast Fluence Minimum and Maximum dpa	Aging in Sodium, days
B-4	350	0×10^{-2}	26
B-3	350	0	78
B-2	550	0	26
B-4	550	0	78
B-4	350	8.4 to 10.5	26
B-3	550	7.6 to 9.9	26
B-4	350	19 to 29	78
B-4	550	24 to 33	78
W-4	350	0	26
W-4	350	0	78
W-3	550	0	26
W-4	550	0	78
W-4	350	14.6 to 18.7	26
W-4	550	13.0 to 17.9	26
W-4	350	19.0 to 27.0	78
W-4	550	21.0 to 28.0	78
HAZ-4	350	0	26
HAZ-4	350	0	78
HAZ-2	550	0	26
HAZ-4	550	0	78
HAZ-4	350	10.3 to 12.9	26
HAZ-4	550	11.1 to 13.1	26
HAZ-4	350	34.0 to 48.0	78
HAZ-4	550	34.0 to 38.0	78

Test Matrix

The test results available for analysis are given in Table 3. The 26 and 78 days aging in sodium autoclaves corresponds to the duration of the 0.1 and 0.3 dpa irradiation in HFR, respectively.

Procedure

Testing Rigs—The hot cell installation includes a 50-kN Instron® machine equipped with an electric furnace for tests in air at 350 and 550°C. The temperature at which tests are run in the hot cell corresponds to the temperature at which the specimens are sustained during irradiation. The crosshead velocity varies from 0.5 to 2.5 mm/min. Two spring-loaded rods are brought in contact with the specimen central loading pin, on either side of the specimen. They actuate the central plungers of two linear variable differential transformers (LVDT) mounted outside the furnace. The bodies of the LVDT are fixed, in a diametrically opposite position, to a tube extending from the center of the specimen bearing plate. Two simultaneous measurements of load-line displacements are obtained. These, however, include additional deformations, which are not relevant to the ones being sought, that is, relative to the cracked specimen exclusively. They

originate essentially from the deformation of the rollers, the deformation of the roller bearing plates, and the indentation of the specimens where they are in contact with the rollers. To address this problem, geometrical similar uncracked specimens, made of the reference AISI 316H material, are loaded in the test rig, and averaged calibration curves at 350 and 550°C are obtained that relate the nonrelevant load-line displacements to the current applied load. At any load attained during a test carried out on the cracked specimens, the corresponding value of the nonrelevant deformation is subtracted from the one derived from the averaged LVDT measurements. This is automatically taken care of by the data reduction procedure. The load-line displacements used in the J computation thus correspond to the cracked body deformations only, and the obtained J values do not include the deformation energy contribution of the uncracked specimen.

As far as data acquisition is concerned, the servohydraulic machine is directly connected to a Hewlett-Packard (HP) 1000 data acquisition system that records in digital form the applied force, two displacements, the average of which corresponds to the load-point displacement as well as two potentiometric signals indicating crack growth initiation. The system picks up signals at equispaced time intervals of about $T/1500$-s duration where T is the time needed to carry out the bending test. T is of the order of 300 s at the most. The nonirradiated specimens have been tested in a similar rig, using a 60-kN Schenck® machine and an on-line data acquisition system.

Detection of Initiation of Stable Crack Growth—The DC potential drop method has been considered for its applicability in adverse conditions of high temperature (up to 550°C) and remote control operation possibilities needed for the irradiated materials testing. A DC 40-A stabilized current source is introduced at the end faces of the 3PB specimens. The potential drop is measured between two points located near the crack tip on diagonally opposite sides of the specimens. Two pairs of pickup points are installed (see Fig. 4). The specimens are insulated from the testing machine. During the monotonic loading of a precracked specimen, the potential drop versus load point displacement is recorded. In these diagrams it is possible to distinguish an initial part where the behavior is random,

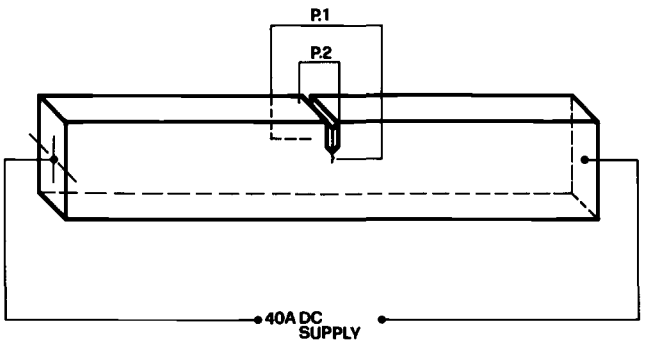

FIG. 4—*Location of potential drop direct current pickup points.*

a second region where the diagram assumes the form of a straight line, and a third curved region. The point where a transition is observed between the second and the third region is considered to represent the initiation of stable crack growth according to the British Draft for Development DD:1972 document. Preliminary tests were run on 3PB specimens of identical configuration as the subject research specimens, and consistent indications of incipient crack growth were obtained using this technique. There was a strong incentive to use the potential drop method for crack growth evaluation as well, but crack extensions could be ambiguously derived from the third curved region characteristics and as far as this specific problem is concerned, the method was discarded.

Measurement of Initial and Final Crack Length—Up to incipient crack growth, the initial ligament is $b_0 = W - a_0$ where a_0 is the initial crack length. The initial fatigue crack size and the final crack extension were defined using the nine-points average after crack marking by heat tinting at 550°C for several minutes. The specimen halves were separated after each test by fatigue cracking and sawing of the remaining ligament. Crack extension measurements were inclusive of the stretch zone. The measurements were made using a Zeiss® microscope with a sixfold magnification factor. More refined crack extension measurements were carried out by taking photographs of the cracked zones of the specimens using a magnification factor of 20. Subsequently, the photographs have been analysed on a TEKTRONIX® 4956 digital table having a resolution of 0.1 mm. About 1000 pairs of coordinates have been introduced for both the fatigue and the final crack fronts. From these data, the crack advances are then computed. In this case, where the initial crack fronts were practically straight and the extended fronts were very regular, both methods yielded within very narrow limits identical results; therefore the nine-point average procedure was subsequently used.

Crack Extension Calculation

From dimensional analysis applied to the case of pure bending of a small remaining ligament, it has been shown [*1*] that the relationship between angular displacement θ_c and bending moment per unit thickness M is

$$\theta_c = f(M/b^2) \tag{1}$$

where b is the remaining ligament size. The function f depends only on the material monotonic stress-strain properties. It can be observed that the only significant geometrical parameter entering the form (Eq 1) is the ligament size; that is, the ratio b/W is not relevant in the case of pure bending. By virtue of the deformation theory definition [*2*]

$$J = \int_0^P (\partial\Delta/\partial a)_P dP \tag{2}$$

where Δ is the load point displacement through which the applied load P works. In the case of bending Eq 2 equates to

$$J(a, \theta_c) = -\int_0^M (\partial\theta_c/\partial b)_M dM \tag{3}$$

where $b = W - a$ and W is the width of the 3PB specimen. From Eqs 3 and 1 and on the assumption that the material is history independent, the following expression for J (referred to as J_D) is derived [*1*]

$$J_D = 2\int_0^{\theta_c} (M/b)d\,\theta_c - \int_{a_0}^{a} (J_D/b)da \tag{4}$$

Inverting the form (Eq 1) leads to

$$M/b^2 = F(\theta_c) \tag{5}$$

or

$$M = b^2F(\theta_c) \tag{6}$$

where $F(\theta_c)$ is referred to as the material "key curve." It is possible, in theory, to determine the $F(\theta_c)$ function using specimens having ligaments of relatively smaller lengths than the one encountered in the frame of this research. The specific difficulties inherent to irradiated materials are such that the problem had to be addressed in a different way. Considering Eq 6 and in the case of 3PB specimens, one may write

$$0.25\,PS = b^2F(\theta_c) \tag{7}$$

where S is the specimen span set at 80 mm.

It is convenient to carry the analysis further considering only the significant parameters from Eq 7. A function

$$C(\theta_c) = (4/S)F(\theta_c) \tag{8}$$

is introduced. Since S is constant throughout the tests, $C(\theta_c)$ differs from $F(\theta_c)$ by a scaling factor $4/S$, which was constant in all of our tests. The $C(\theta_c)$ function is directly related to the $F(\theta_c)$ function and has consequently the same characteristic of being, in theory, unique for a series of tests characterized by a material, the temperature, and the fluence. From Eqs 7 and 8 follows

$$P = b^2C(\theta_c) \tag{9}$$

Following an analogous rationale, a function $C'(\theta_c)$ is defined as follows

$$P = b_o^2C'(\theta_c) \tag{10}$$

The $C'(\theta_c)$ function is known from the experimental load-load line displacement measurements, the angular displacement θ_c being proportional to the load-line displacement Δ since

$$\theta_c = 4\Delta/S \tag{11}$$

In Fig. 5, a typical $C'(\theta_c)$ function is schematically represented by a curve in a normalized load-angular displacement record of the test corresponding to the major crack advance. The subscript 4 is arbitrarily ascribed to the parameters characterizing this specific test. For this $C'(\theta_c)_4$ curve we define

$(b_0)_4$ = initial ligament length,
$(P_f)_4$ = applied load at the end of the test, and
$(\theta_{cf})_4$ = angular displacement at the end of the test.

In addition $(\Delta a_{of})_4$ corresponding to the total crack growth is measured at the end of the test.

In Fig. 5, the point having coordinates

$$(P_f)_4/(b_f)_4^2, \qquad (\theta_{cf})_4$$

where $(b_f)_4 = (b_0)_4 - (\Delta a_{of})_4$ is the final ligament length, corresponds to the end of Test 4 conditions. This point defines one value $C(\theta_{cf})_4$ of the $C(\theta_c)$ function as defined by Eq 9 since $(P_f)_4 = (b_f)_4^2 C(\theta_{cf})_4$.

In Fig. 6, a $C'(\theta_c)_4$ curve is represented schematically as well as the $(P_f)_i/$

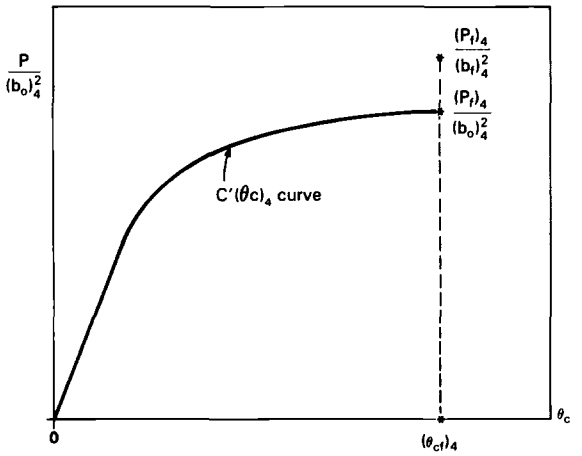

FIG. 5—*Normalized load—angular displacement record of test corresponding to the major crack extension.*

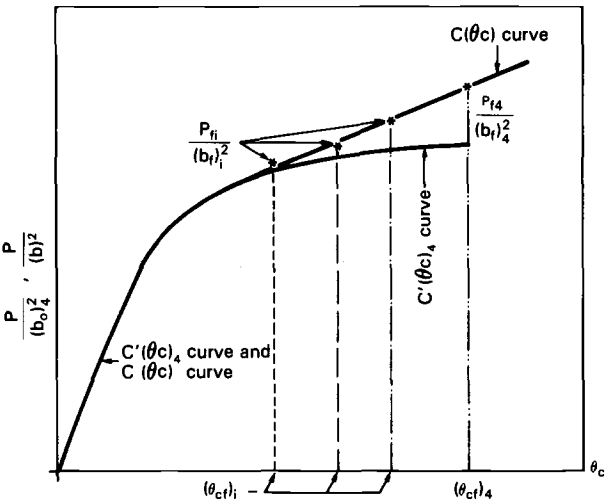

FIG. 6—*Normalized load—angular displacement record using all results.*

$(b_f)_i^2$, $(\theta_{cf})_i$ points ($i = 1 \ldots 4$) corresponding to the four (at the most) ends of the test conditions of the tests run in a specific case. As already observed, these points lie on the $C(\theta_c)$ curve defined by Eq 9. It has been verified for all cases concerning the base material and weld material, which are described in Table 3, that the four (at the most) $(P_f)_i/(b_f)_i^2$, $(\theta_{cf})_i$ points line up in a most satisfactory manner on a tangent to the $C'(\theta_c)_4$ curve. Thus the $C(\theta_c)$ function is adequately represented by a straight line (elastic deformation), a curve, and a straight line tangent to the curved part (Fig. 6). By the straightforward data reduction procedure, the tangent, in any test, to the $C'(\theta_c)$ curve that passes through an imposed $P_f/(b_f)^2$, θ_{cf} end of a test point, is defined. With this procedure, the single-specimen method (allowing one *J-R* curve per specimen) is applied as follows. From Eqs 9 and 10

$$b_i = b_o \sqrt{C'_i/C_i} \tag{12}$$

and the current crack growth

$$(\Delta a_o)_i = b_o[1 - \sqrt{(C'_i/C_i)}] \tag{13}$$

where the subscript refers to the specific point where b_i and $(\Delta a_o)_i$ are evaluated.

An incremental extension of the crack length $a_{i+1} - a_i$ follows directly from Eq 13

$$a_{i+1} - a_i = b_o(\sqrt{C'_i/C_i} - \sqrt{C'_{i+1}/C_{i+1}}) \tag{14}$$

J Calculation

The J value was calculated from the relationship applicable to plane-sided 3PB specimens [*3*]

$$J_{i+1} = [J_i + (2/b_i) \cdot (A_{i,i+1}/B)] \left\{1 - \left[\frac{(a_{i+1} - a_i)}{b_i}\right]\right\} \quad (15)$$

where $A_{i,i+1}$ = area under the load versus load-line displacement record between lines of constant displacement at points i and $i + 1$. This area does not include the uncracked body energy. The values to be introduced in Formula 15 are

b_i from Formula 12,
$a_{i+1} - a_i$ from Formula 14, and
B = 15 mm.

Formula 15 used at the point where incipient crack growth is detected by the potential drop technique yields a J_{I_c} value referred to as $(J_{I_c})_{PD}$ in Table 4.

Results

J_{I_c} *Values and J Resistance Curves for the Base and the Weld Metal*—The study of the J resistance curves of the base and the weld metal indicated that, as expected, there were no effects of aging in sodium for the nonirradiated metals. The 16 specific cases concerning the base and the weld metal can thus be reduced to twelve cases, which are described in the first columns of Table 4. The average J_{I_c} values yielded by the potential drop method and referred to as $(J_{I_c})_{PD}$, are found to correspond to averaged values of J resistance curves ordinates at $\Delta a = 0$ for the weld metal and at some offset Δa ranging from 50 to 150 μm for the base metal (see Table 4). In addition, the J_{I_c} values taken on the J resistance curves at the tabulated Δa and referred to as $(J_{I_c})_{DA}$ in Table 4 have a spread of ±6 to ±24% for all results, inferior to the ±8 to ±46% (this maximum value corresponding to the last case of Table 4, discarding it, the maximum is ±26%) of the $(J_{I_c})_{PD}$ values, suggesting a better reproducibility of the results using the key curve approach. Since with this approach growing Δa values are found onward from the point of tangency between the $C(\theta_c)$ and the $C'(\theta_c)$ curves, it may be inferred that the case of the weld metal corresponds to a negligibly small stretch zone width, whereas the Δa values for all base metal cases suggest some amount of stretching before actual stable crack growth.

Finally, the variation in dJ/da in all cases tabulated in Table 4 was found to be practically nil in most cases and reached a maximum of ±20% in the case of the nonirradiated weld material at 350°C.

It is interesting to observe that the lowest spread in J_{I_c} values and dJ/da values concerns the irradiated material. In order to give an insight on the neutron damage sustained by the base and the weld metals, average resistance curves were computed and plotted. In Figs. 7 through 10 such averaged curves are presented in

TABLE 4—$(J_{Ic})_{DA}$ *from dimensional analysis versus* $(J_{Ic})_{PD}$ *from potential drop technique.*

Material and Number of Specimens	Temperature, °C	Fast Fluence dpa Minimum and Maximum	$(J_{Ic})_{PD}$, kJ/m²	$(J_{Ic})_{DA}$, kJ/m²	Δa Offset, μm
B-7	350	0×10^{-2}	230 to 280	230 to 280[a]	80
B-6	550	0	170 to 250	180 to 240[a]	80
B-4	350	8.4 to 10.5	240 to 300	260 to 300[a]	120
B-3	550	7.6 to 10.9	100 to 140	100 to 130	50
B-4	350	19 to 29	210 to 300	250 to 280[a]	120
B-4	550	24 to 33	240 to 280	230 to 280[a]	150
W-8	350	0	38 to 62	38 to 62	0
W-7	550	0	30 to 50	45 to 55	0
W-4	350	14.6 to 18.7	41 to 52	44 to 55	0
W-4	550	13.0 to 17.9	43 to 45	54 to 58	0
W-4	350	19.0 to 27.0	44 to 75	40 to 60	0
W-4	550	21.0 to 28.0	20 to 54	44 to 52	0

[a]The J integral capacity [3] of 139 kJ/m² for the base material at 350°C and of 123 kJ/m² for the base material at 550°C is exceeded in these cases.

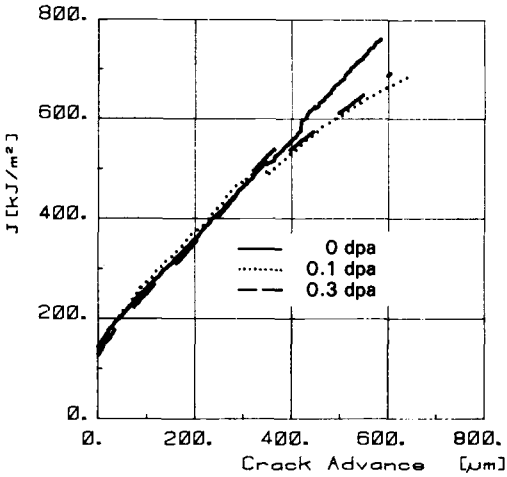

FIG. 7—*Averaged J-resistance curves for the base metal at 350°C.*

groups of three curves corresponding to one material, a temperature and the three nominal fluences. The data reduction procedure followed consists simply in averaging, at the current Δa value, the J values of the i resistance curves where i = number of specimens in any specific case as reported in Table 4. As Δa increases, a decreasing number of curves are averaged as final crack lengths are attained in succession. Logically, steps in the averaged curves may thus appear in these particular points.

Since trends in material behavior were considered of primordial importance rather than highly precise absolute values, no smoothing of the averaged resistance curves was done. From these figures it may be concluded that, as far as the base metal is concerned, it appears (see Fig. 8) that at 550°C and 0.1 *dpa*

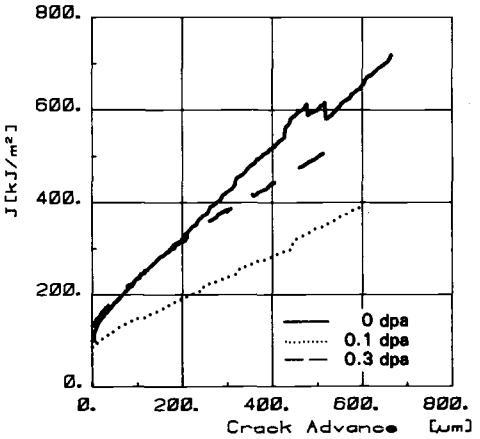

FIG. 8—*Averaged J-resistance curves for the base metal at 550°C.*

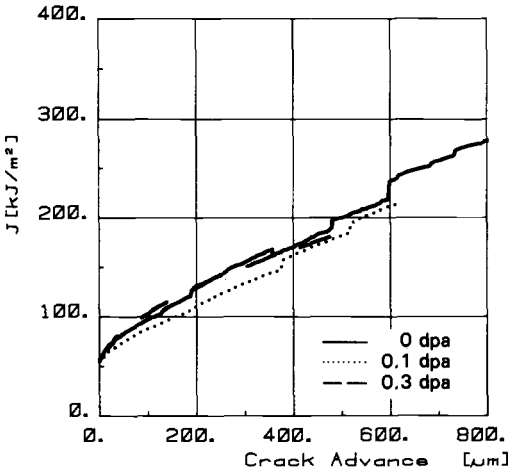

FIG. 9—*Averaged J-resistance curves for the weld metal at 350°C.*

irradiation, the J_{1_c} value drops by 35% and the dJ/da value by 50% relative to those values at 0 dpa. A generally low degradation of the base metal properties is found in the other cases at both temperatures between the nonirradiated and the irradiated metal.

As far as the weld metal is concerned, it exhibits significantly inferior fracture toughness and J resistance curve slopes in the preirradiation and post-irradiation conditions but is not very significantly altered at both temperatures and all fluence levels.

Finally, and in order to illustrate the efficacy of the key curve approach, groups of four (at the most) resistance curves corresponding to four specific

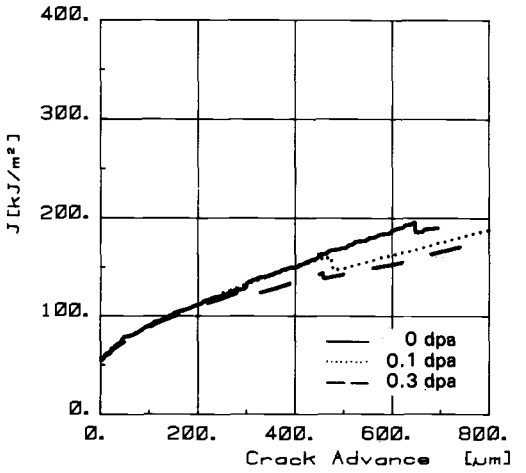

FIG. 10—*Averaged J-resistance curves for the weld metal at 550°C.*

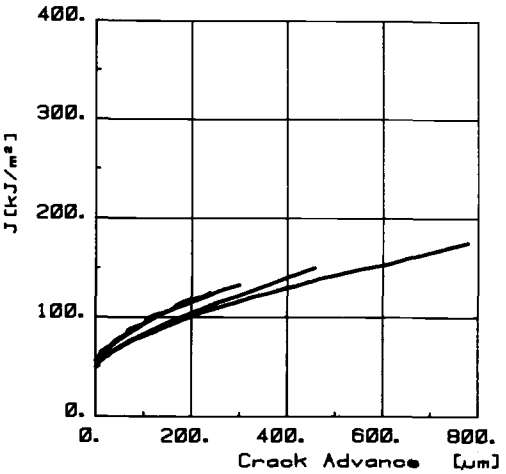

FIG. 11—*J-resistance curves for weld metal at 550°C and 0.3* dpa.

cases from Table 3, taken at random, are presented in Figs. 11 through 14. It can be seen that the resistance curves of the greatest crack extension case match the lower crack extension results in a satisfactory manner.

Test Results of HAZ Material

The widely spread HAZ results lie practically within the base material at 350°C and the weld material at 550°C for both the nonirradiated and the irradiated case. Typical results appear in Fig. 15. These are not unexpected results considering that in the case of the HAZ material, the crack front actually "cuts" through all three materials, B, W and HAZ, in some random way because of

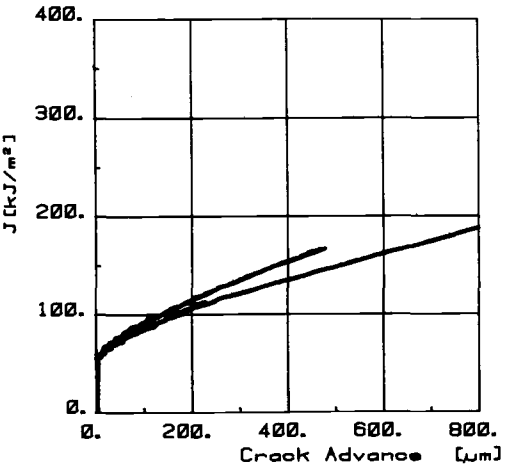

FIG. 12—*J-resistance curves for weld metal at 550°C and 0.1* dpa.

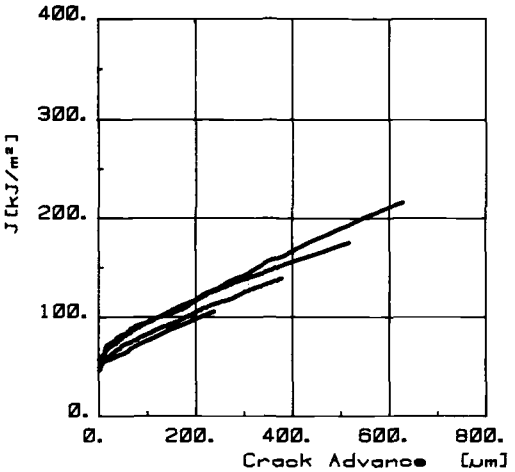

FIG. 13—*J-resistance curves for weld metal at 350°C and 0.1* dpa.

the fact that the HAZ is in fact extremely narrow and the B-W interface is somewhat warped. On the basis of these observations it has been decided to exclude the HAZ material from future irradiation tests.

Conclusions

In the case of the relatively small 3PB specimens studied, for which the J controlled crack growth is about 700 μm, it is shown how a dimensional analysis (together with the deformation theory of plasticity) enables the derivation of J resistance curves for materials having distinctly different load displacement diagrams such as the base and the weld material. In fact the crack extensions Δa,

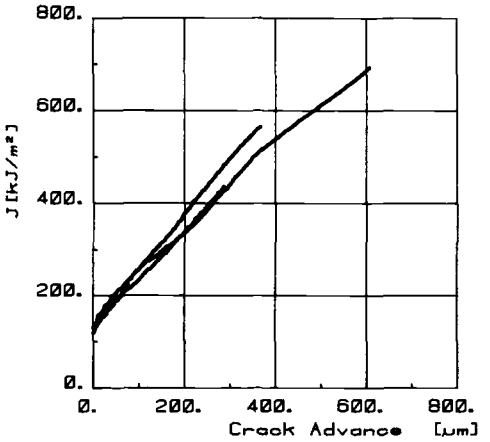

FIG. 14—*J-resistance curves for base metal at 350°C and 0.3* dpa.

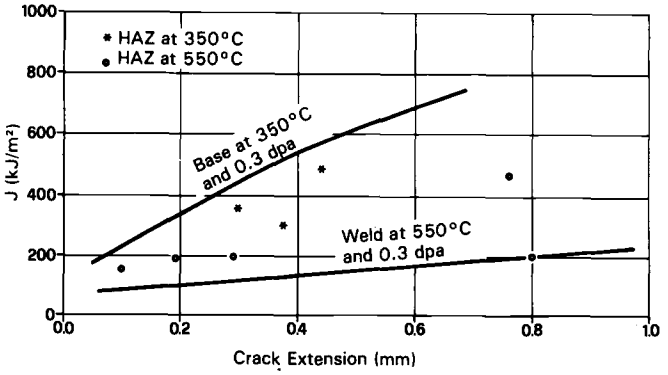

FIG. 15—*HAZ, results at 0.3* dpa *nominal fluence.*

inferred using this procedure on the test covering the longest crack advance, are corroborated in a satisfactory manner by the heat tinting values of Δa found in three (at the most) accompanying tests. The method should thus be suitable when a small number of 3PB specimens is available, as is obviously the case in irradiation studies. Future work will benefit from a recently [*4*] introduced new formulation of the J integral, referred to as J_M, which allows analysis of crack growth up to 30% of the ligament under bending loads. The results presented here, covering crack growths of about 7% are in no significant way different if the analysis follows either the J_D or the J_M route. The importance of increased out-of-plane constraint will be tackled on 20% side-grooved specimens that are submitted to a 0.3-*dpa* nominal fluence. As far as the J_{Ic} values are concerned, they correlate reasonably well with the potential drop defined specimens when taken on the J resistance curve at some Δa offset value of about 100 μm for all base material tests and at zero offset for the welded material. Because of the difficulties encountered when applying the ASTM Test for J_{Ic}, A Measure of Toughness (E 813), particularly with respect to the definition of the stretch zone width in high toughness material, such as the AISI 316H steel, a defect assessment procedure aiming at the determination of J_{Ic} on the crack growth resistance curves at some offset Δa has recently been evolving. One of the conclusions of this work is that such a procedure is valid, even in the case of the weld material since the relatively low dJ/da value found for this material will lead to a reasonably small overestimation of J_{Ic} at about 100 μm of Δa with respect to the tabulated values. It appears from Table 4 that there is less spread in the results derived from dimensional analysis than in the *PDdc* results indicating an overall better reproducibility of the procedure.

To fully endorse this analysis as applied to 3PB specimens, tests on differently sized ligaments will be carried out on nonirradiated material. As such, the method has effectively shown trends in fracture toughness characteristics of AISI 316H steel, a major objective in this work. Even results where the specimen has exceeded its J integral capacity are considered useful. Since no crack tunneling

problems have been encountered, it has not been imperative to use side-grooved specimens, though the 0.3 *dpa* fluence tests will be repeated on 20% side-grooved specimens of identical overall configuration as those used up to now. An interesting result, so far, is the decrease in J_{I_c} and dJ/da values encountered in the 0.1 dpa irradiation at 550°C for the base material, with respect to the values at the 0 and 0.3 *dpa* fluence level, at the same temperature. Finally, it may be observed that the width of 20 mm of the L-S type specimen is relevant to the wall thickness of some of the LMFBR's primary circuit components such as the containment vessel wall.

Acknowledgments

The authors wish to thank the following persons: Messrs. Manzotti and Tognoli, Applied Mechanics Division, JRC-Ispra, who performed the calibrations and the measurements; Messrs. Piatti and Weir, Materials Division, JRC-Ispra, for the metallographic analysis.

References

[*1*] Hutchinson, J. W. and Paris, P. C., "The Stability Analysis of *J*-Controlled Crack Growth," *Elastic-Plastic Fracture, STP 668*, American Society for Testing and Materials, Philadelphia, 1979, pp. 37–64.

[*2*] Rice, J. R., "Mathematical Analysis in the Mechanics of Fracture," *Fracture*, Vol. II, Academic Press, Oshkosh, WI, 1968.

[*3*] Albrecht, P., Andrews, W. R., Gudas, J. P., Joyce, J. A., Loss, F. L., McCabe, D. E., Schmidt, D. W., and Van Der Sluys, W. A., "Tentative Test Procedure for Determining the Plane Strain J_I-R Curve," *Journal of Testing and Evaluation*, Vol. 10, No. 6, Nov. 1982, pp. 245–251.

[*4*] Ernst, H., "Material Resistance and Instability Beyond *J*-Controlled Crack Growth," *Elastic-Plastic Fracture: Second Symposium Volume I Inelastic Crack Analysis, STP 803*, American Society for Testing and Materials, Philadelphia, 1983, pp. I-191–I-123.

Marie T. Miglin,[1] *W. Alan Van Der Sluys,*[1] *Robert J. Futato,*[1] *and Henry A. Domian*[1]

Effects of Strain Aging in the Unloading Compliance *J* Test

REFERENCE: Miglin, M. T., Van Der Sluys, W. A., Futato, R. J., and Domian, H. A., **"Effects of Strain Aging in the Unloading Compliance *J* Test,"** *Elastic-Plastic Fracture Test Methods, The User's Experience, ASTM STP 856*, E. T. Wessel and F. J. Loss, Eds., American Society for Testing and Materials, 1985, pp. 150–165.

ABSTRACT: The behaviors of two heats of SA 515 Grade 70 in the unloading compliance *J* test were compared. Tensile properties were measured for both heats of material; one heat was found to be susceptible to dynamic strain aging. This heat also exhibited a steeper drop in the slope of the J_I-R curve with increasing temperature, and serrated flow during the high-temperature *J* tests. The magnitude of the serrations varied during each test and with changes in loading displacement rate. Comparison with data from other carbon steels and weld metals showed that a large J_{Ic} drop with increasing temperature was associated with a large drop in ductility. *J* tests of strain-aging susceptible materials also showed a marked decrease in load drop from relaxation and peaks in load upon reloading at temperatures at the lower end of the temperature range of dynamic strain aging.

KEY WORDS: strain aging, steels, tensile properties, unloading compliance, ductile fracture, toughness

A comparison of unloading compliance J_{Ic} results from several carbon steels and various weld metals collected over the past several years has shown a decrease in J_{Ic} with increasing temperature up to the highest test temperature of 288°C (550°F), or a minimum in J_{Ic} below this temperature. Some of the *J*-test load-displacement traces were serrated, and the resulting J_{Ic} values were unusually low. It was suspected that dynamic strain-aging embrittlement was occurring during tests that exhibited serrated load-displacement curves, and that the test parameters might be influencing the magnitude of this effect and thus the J_{Ic} values.

Examples of unloading compliance load-displacement curves in the presence and absence of serrations are shown in Fig. 1. The shielded metal arc (SMA) weld metal trace at 121°C (250°F) on the left in Fig. 1 also exhibits a reload peak after each unloading increment and a small load drop caused by relaxation. These anomalies are present to a lesser extent in the traces from the gas tungsten

[1]Research metallurgist, technical advisor, research metallurgist, and supervisor, respectively, Babcock & Wilcox, a McDermott Company, Alliance, OH 44601.

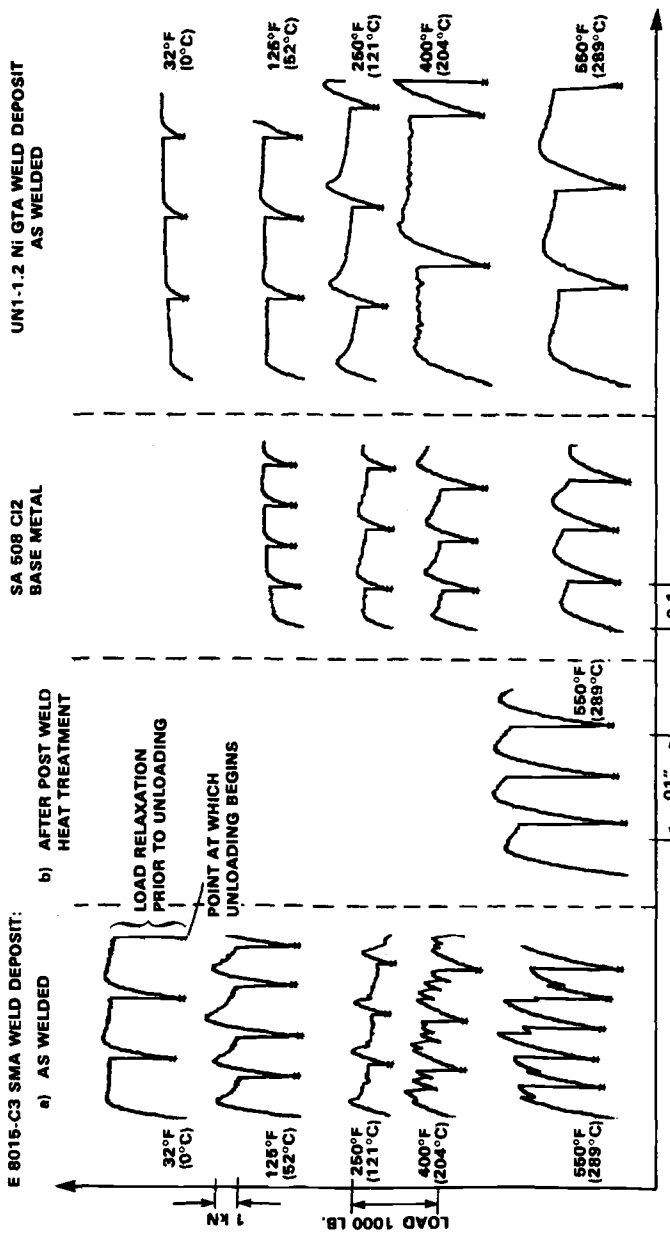

FIG. 1—*Portions of unloading compliance traces at several test temperatures. Loading displacement rate = 0.3 mm/s (0.0002 in./s)* [1]. Left: *E 8015-C3 SMA weld deposit (a) as welded and (b) after post weld heat treatment.* Center: *SA 508 Class two 76.2-mm (3-in.) thick forged plate.* Right: *UN 1-1.2 nitrogen GTA weld deposit, as welded.*

arc (GTA) weld at the right and are almost completely absent from the SA 508 base metal traces and post-weld heat-treated trace in the center of Fig. 1. Anomalies in the unloading compliance trace as illustrated in Fig. 1 are associated with reduced values of J_{Ic}. Figure 2 shows a 70% drop in J_{Ic} for the SMA weld with the serrated load-displacement traces shown in Fig. 1 and a lesser drop for the GTA weld [*1*].

Dynamic strain aging in carbon steels is caused by the interaction between dislocations and interstitial solutes (nitrogen and carbon) or solute pairs consisting of one interstitial and one substitutional solute atom (such as manganese-carbon and manganese-nitrogen) [*2*]. The characteristic serrated stress-strain behavior has been attributed to the repeated breakaway and repinning of dislocations by solute atmospheres [*3*]. The occurrence of dynamic strain aging depends upon the rate of solute diffusion and the dislocation velocity, which depend upon temperature and strain rate. Keh et al have illustrated the temperature and strain-rate dependence of dynamic strain-aging graphically, as shown in Fig. 3 [*4*]. Other indications of dynamic strain aging are a maximum in flow stress with temperature and strain rate, reduction in ductility, and rapid strain hardening [*2,4*].

The ductile fracture resistance J_{Ic} of a given material often varies inversely

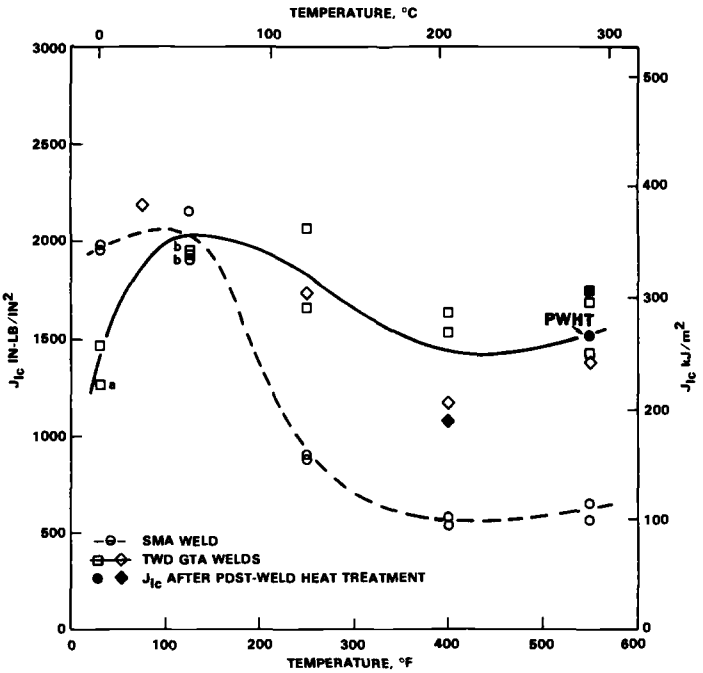

a VIOLATES ASTM DATA SPACING CRITERIA
b CALCULATED FROM A CURVE FIT TO $J_T R$ PLOT

FIG. 2—*Temperature dependence of* J_{Ic} *for weld metals of Fig. 1* [1].

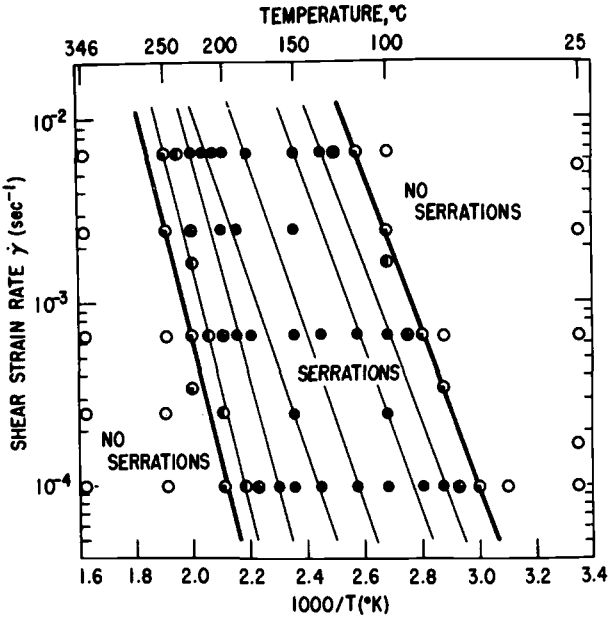

FIG. 3—*Temperature and strain rate regime for serrated flow in 0.03% carbon steel* [4].

with flow strength and may therefore also exhibit a minimum with temperature and strain rate in the presence of dynamic strain aging. The study described in the following paragraphs was initiated to determine the effect of variations in unloading compliance J-test parameters on J_{Ic} in a material that exhibits serrated load-displacement traces and to assess the validity of the dynamic strain aging explanation of the serrations. It was also an attempt to identify a tensile parameter that would reliably predict a loss in toughness from dynamic strain aging. Tension tests were conducted to determine material susceptibility to serrated flow, and unloading compliance J tests were performed at various loading rates and temperatures to identify the effects of these two variables on measured fracture toughness. Subsequent work under this program will include additional unloading compliance test variables, and microstructural and fractographic information.

Experimental Procedures

Two heats of pressure vessel steel, SA 515 Grade 70, were chosen as test materials. The compositions, heat treatments, and nil-ductility temperatures (NDT) for these heats are listed in Table 1. Tension tests were conducted at several temperatures ranging from room temperature to 316°C (600°F) and at crosshead speeds of 1.3, 0.13, and 0.013 mm/min (0.05, 0.005, and 0.0005 in./min). Tests were performed on a Materials Testing System (MTS) servohydraulic test machine, which was interfaced with a Programmable Data Processor (PDP) 11/34 minicomputer to allow computer control of specimen loading and comput-

TABLE 1—*Composition, heat treatment, and NDT of SA 515 Grade 70 steel.*

	Composition, weight %							Heat Treatment		
Heat	Carbon	Manganese	Phosphorus	Sulfur	Silicon	Aluminum	Nitrogen (Uncombined)	Austenitize	Stress-Relieve	NDT
645	0.29	0.72	0.009	0.015	0.23	<0.005	0.004	1525°F (829°C), 1½ h air cool	1125°F (607°C), 3 h air cool	10°F (−12°C)
649	0.26	0.76	0.008	0.023	0.18	<0.005	0.003	1650°F (899°C), 3½ h air cool	1200°F (649°C), 3½ h cool 15°F (8°C)/h to 600°F (316°C) air cool	20°F (−7°C)

erized data acquisition and analysis. Temperature control was achieved by enclosing the specimen in a box furnace and mounting thermocouples at three positions along the reduced section.

Unloading compliance J tests were performed according to the procedure outlined in ASTM Test for J_{Ic}, a Measure of Fracture Toughness (E 813) and Ref *5* at temperatures ranging from room temperature to 204°C (400°F). An MTS servohydraulic test machine was used in conjunction with the previously mentioned minicomputer for control of testing, data acquisition, and analysis. Specimen temperature was maintained by a box furnace and monitored by a thermocouple mounted on the specimen at a sufficient distance ahead of the crack tip to allow for crack growth. The displacement rate during loading was kept constant at 1.5 mm/min (0.06 in./min) except where otherwise indicated below. Unloading displacement rate was 0.3 mm/min (0.012 in./min) in all cases. Before each unloading, the load was allowed to relax until the rate of load relaxation was less than 0.3% of the unloading rate. Displacement was monitored by a displacement gage mounted on knife edges at the load line. Figure 4 is a diagram of the specimen. For details of the computerized single specimen J-test facility see Ref *6*.

An attempt was made to identify the loading displacement rate that would produce the maximum serration height in an unloading compliance trace at 204°C (400°F) in Heat 645 material. A specimen from which a J_I-R curve had already been obtained was tested further for this purpose. The loading displacement rate was varied from reload to reload to maximize the serration height, and the loading displacement rate that produced the largest serration height was applied to an identical specimen at 204°C (400°F) from the onset of testing. However, only very small serrations were visible at the beginning of this test, and when the

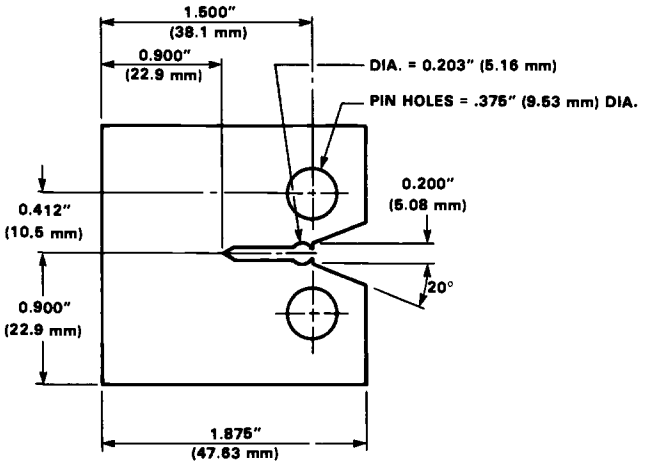

FIG. 4—*3/4 T (19-mm thick) compact tension specimen side-grooved (not shown) to a depth of 10% per side.*

loading rate was increased, the serration height increased. Because a fixed loading rate corresponding to maximal serration intensity was not successfully defined, loading rates for the remaining tests in this series were chosen at random to span two orders of magnitude.

Results

Heat 645 material exhibited serrated flow in all tension tests conducted at 121 and 204°C (250 and 400 F) and in unloading compliance J tests at the latter temperature.[2] The serrations were similar in appearance and magnitude to those of the GTA weld deposit at 204°C (400°F) shown at the right side of Fig. 1. The results of the tension tests are shown graphically in Figs. 5 and 6. The yield strength of Heat 649 material, which flowed without serrations, decreased almost linearly with increasing temperature, while that of Heat 645 material ceased to decline above 121°C (250°F). The ultimate strength of the latter material reached a maximum at 204°C (400°F) while that of Heat 649 material exhibited a shallow minimum at this temperature. The variations in test temperature had a much larger effect than the crosshead speed on measured strengths.

The ductility, measured as percentage reduction in area, of Heat 649 material, deviated by less than 10% over the range of test conditions. However, that of Heat 645 material declined by approximately 20% with increasing test temper-

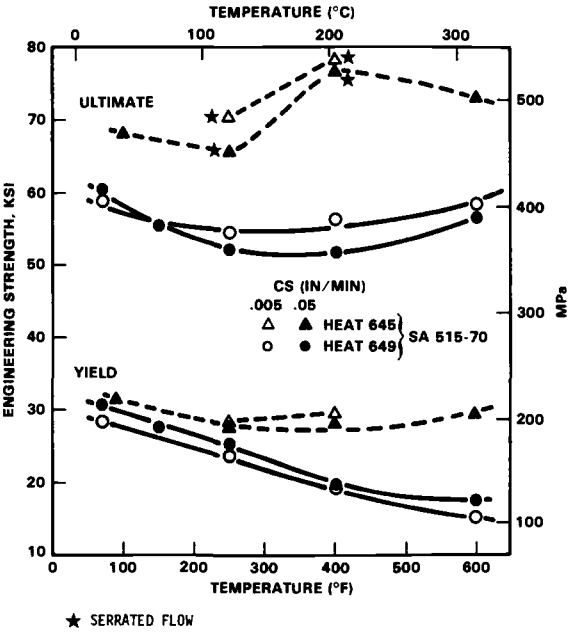

FIG. 5—*Temperature dependence of 0.2% offset yield strength and ultimate strength for two heats of SA 515 Grade 70.*

[2]Unloading compliance J tests of this heat were performed only at 65 and 204°C (150 and 400°F).

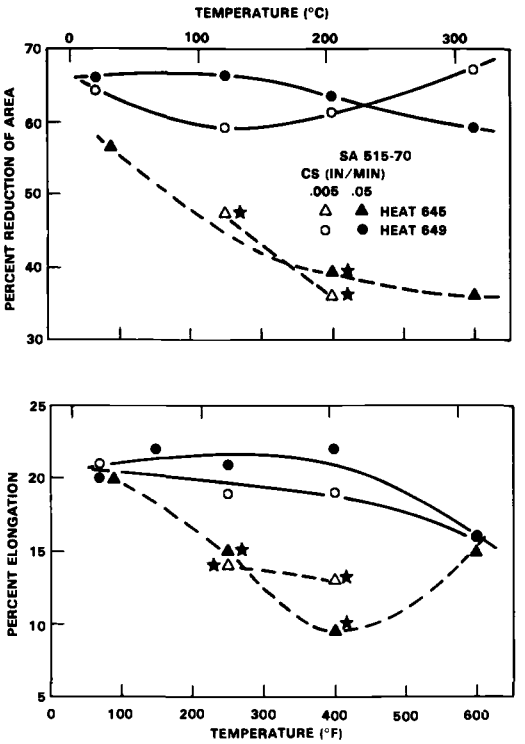

FIG. 6—*Percent uniform elongation and reduction of area for two heats of SA 515 Grade 70 as in Fig. 5.*

ature from 32 to 316°C (90 to 600°F). The uniform elongation was also fairly constant for Heat 649 material while that of 645 material reached a minimum at 204°C (400°F). Again, variations in test temperature had a larger effect than the crosshead speed on measured properties.

J values were calculated using an expression that corrected for the effect of crack extension on the measured load versus displacement curve (ASTM E 813). Valid ASTM E 813 J_{Ic} values could not be obtained for most of the specimens because the criterion

$$B, b \geq 25\, J / \tfrac{1}{2}(S_y + S_{ult}) \tag{1}$$

where

B = net thickness of specimen,
b = initial uncracked ligament length,
S_y = yield strength, and
S_{ult} = ultimate strength.

was violated (ASTM E 813).

The J_I-R curves are shown in Figs. 7 and 8. The slope of the J_I-R curve beyond the crack-tip blunting region declined monotonically with increasing test temperature for Heat 649 material. The same span of test temperatures produced a greater decrease in J_I-R curve slope in Heat 645 material. Variation in loading displacement rate at 204°C (400°F) over two orders of magnitude produced a small change in J_I-R curve position as shown in Fig. 8, but as for the tension test, the temperature dependence was stronger. However, there was a definite difference in serration height among the 204°C (400°F) tests. The loading displacement rate of 1.5 mm/min (0.06 in./min) produced more intense serrations than either of the other two loading displacement rates.

Discussion

The tension test results for SA 515 show evidence of dynamic strain aging, but the magnitude of the effect differs between the two heats that were studied. The stress-relieving heat treatment given Heat 649 is more effective in immobilizing nitrogen by silicon than is the heat treatment given Heat 645 [7]. The most obvious indication of dynamic strain aging is the presence of serrations on the tensile curves of Heat 645 material at 121 and 204°C (250 and 400°F). Other indications are the reduced ductility at these temperatures and the rise in ultimate strength with temperature above 121°C (250°F). The relatively rapid strain-hardening rate of Heat 645 material at 204°C (400°F), another characteristic of dynamic strain aging, is indicated by the high ultimate strength and small uniform elongation at this temperature. The variations in crosshead speed had a much

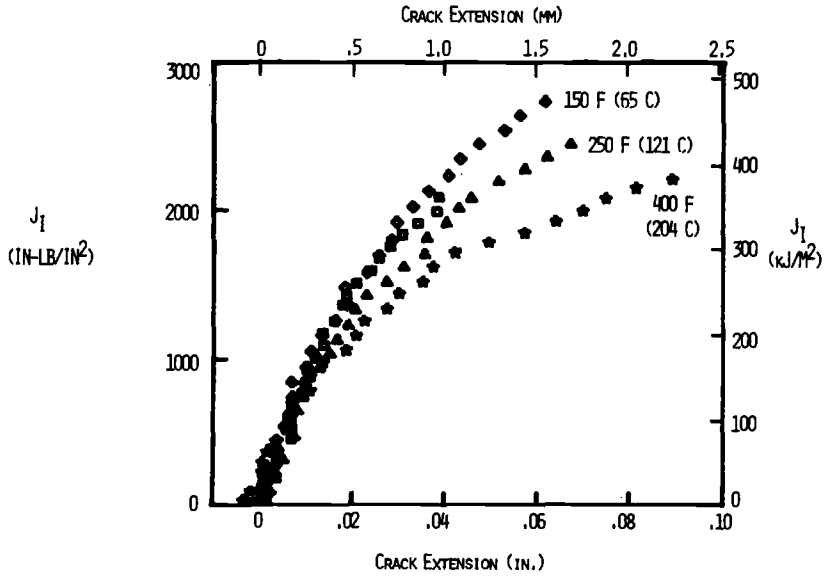

FIG. 7—J_I-R *curves for SA 515 Grade 70, Heat 649. Loading displacement rate = 1.5 mm/min (0.06 in./min).*

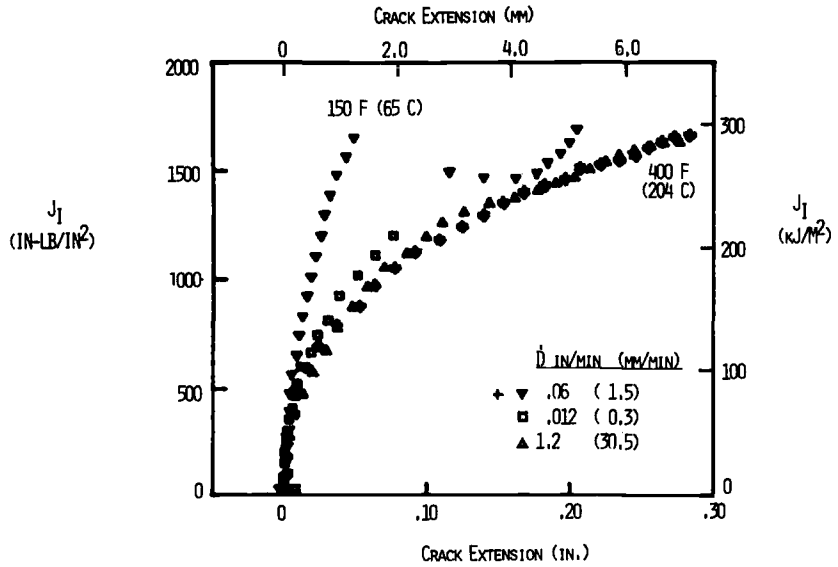

FIG. 8—J_I-R *curves for SA 515 Grade 70, Heat 645.* D = *loading displacement rate. The discontinuity in the* J_I-Δa *curve at 65°C (150°F) represents unstable crack extension.*

smaller effect on measured tensile properties than the temperature variation. The greater temperature sensitivity is illustrated in Fig. 3, which shows that the serrated flow regime in 0.03% carbon steel spans a temperature range of only 200°C and a strain rate range of at least two orders of magnitude [*4*].

The relatively large drop in the J_I-R curves of Heat 645 material with temperature is probably a result of dynamic strain aging occurring during the higher temperature tests. The small dependence of J_I-R curve position on loading rate at 204°C (400°F) may be a result of differences in the intensity of dynamic strain aging, which was evidenced by differences in serration height between the tests. However, control specimens will be tested to ascertain the effects of loading rate variations in the absence of strain aging.

The inability to define a fixed loading displacement rate corresponding to maximal serration intensity may result from a variable plastic-zone strain rate or a growing dislocation density during each test. The occurrence of dynamic strain aging depends upon attainment of a critical dislocation velocity, which is related to dislocation density and strain rate through the expression [*3*]

$$\dot{\epsilon} = \rho b v \tag{2}$$

where

$\dot{\epsilon}$ = strain rate,
ρ = mobile dislocation density,
b = Burger's vector, and
v = dislocation velocity.

Because work hardening in the plastic zone is accompanied by an increasing dislocation density, Eq 2 predicts that the strain rate associated with the critical dislocation velocity decreases during the unloading compliance J test. Although the loading displacement rate may be constant, this does not necessarily fix the average strain rate in the plastic zone. Either a variable strain rate or dislocation density may explain the rapid increase and subsequent attenuation of serration amplitude that was typical of unloading compliance traces obtained at constant loading displacement rate under dynamic strain aging conditions.

The results of this program were compared with data from other carbon steels and several weld metals in an attempt to identify a tensile property that might be a reliable indicator of dynamic strain aging susceptibility. Unloading compliance J_{Ic} results for three carbon steels are shown in Fig. 9; additional background information is given in Table 2. The temperature dependence of the tensile properties of SA 106 (Fig. 10) is very similar to that of Heat 645 SA 515 of this program. Both a rise in ultimate strength and decrease in reduction of area occur in the approximate temperature range of the J_{Ic} drop. Complete tensile data were not available for the SA 508 and SA 516, and the J_{Ic} data are included only for breadth.

Tension and unloading compliance test results from several submerged arc weld metals showed that a drop in ductility with temperature was accompanied by a drop in J_{Ic}[3] (Figs. 11 and 12). In contrast to the results of this program, there was no clear correlation between dynamic strain aging susceptibility and

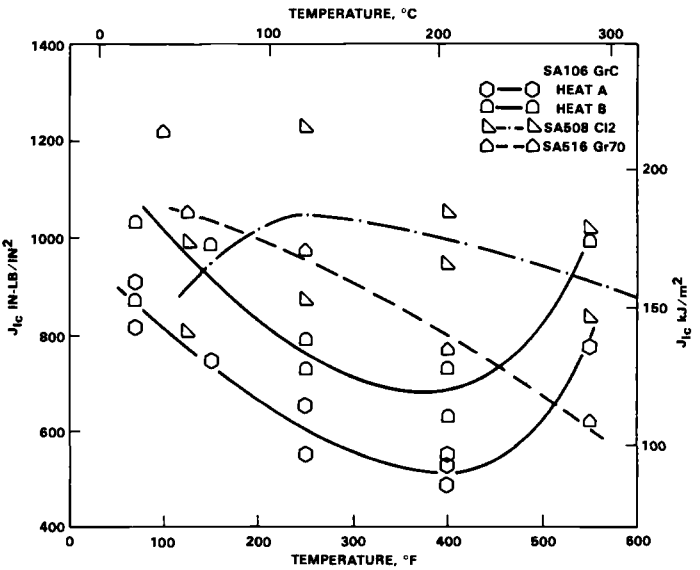

FIG. 9—*Temperature dependence of* J_{Ic} *for three carbon steels (Ref* 1 *to* 8 *and ASTM E 813).*

[3]Van Der Sluys, W. A. Emanuelson, R. H., and Futato, R. J., this publication, pp. 68–83.

TABLE 2—*Composition, heat treatment, and mechanical properties of SA 106 Grade C, SA 516 Grade 70, and SA 508 Class 2* [1,8].

Material	Composition, weight %					Heat Treatment			Nil-Ductility Temperature, °F (°C)	Room Temperature Tensile Properties, ksi (MPa)		% Reduction of Area
	Carbon	Manganese	Phosphorus	Sulfur	Silicon	Austenitize	Temper	Stress-Relieve		0.2% Yield Strength	Ultimate Strength	
SA 106 Grade C												
Heat A	0.28	0.87	0.012	0.025	0.19	1600 to 1650°F (871 to 899°C), 2½ h water quench	1100 to 1150°F (593 to 621°C), 4 h air cool	1100 to 1150°F (593 to 621°C), 3½ h furnace cool	−20 (−28)	46.7 (322)	78.9 (543)	53.1
Heat B	0.31	0.91	0.012	0.015	0.11	1600 to 1650°F (871 to 899°C), 2½ h water quench	1100 to 1150°F (593 to 621°C), 4 h air cool	1100 to 1150°F (593 to 621°C), 3½ h furnace cool	−10 (−23)	45.8 (316)	79.4 (547)	56.0
SA 516 Grade 70	0.28	0.98	0.010	0.026	0.20	1650°F (899°C), 4 h air cool	...	1150°F (621°C), 48 h furnace cool	0 (−17)	44.8 (308)	69.5 (479)	53.6
SA 508 Class 2	.....not available.....					1598 to 1670°F (870 to 910°C), 5 h water quench	1202 to 1238°F (650 to 670°C), 6¼ h air cool	1125°F (607°C), 50 h furnace cool	not available	73.7 (507)	97.2 (669)	73.2

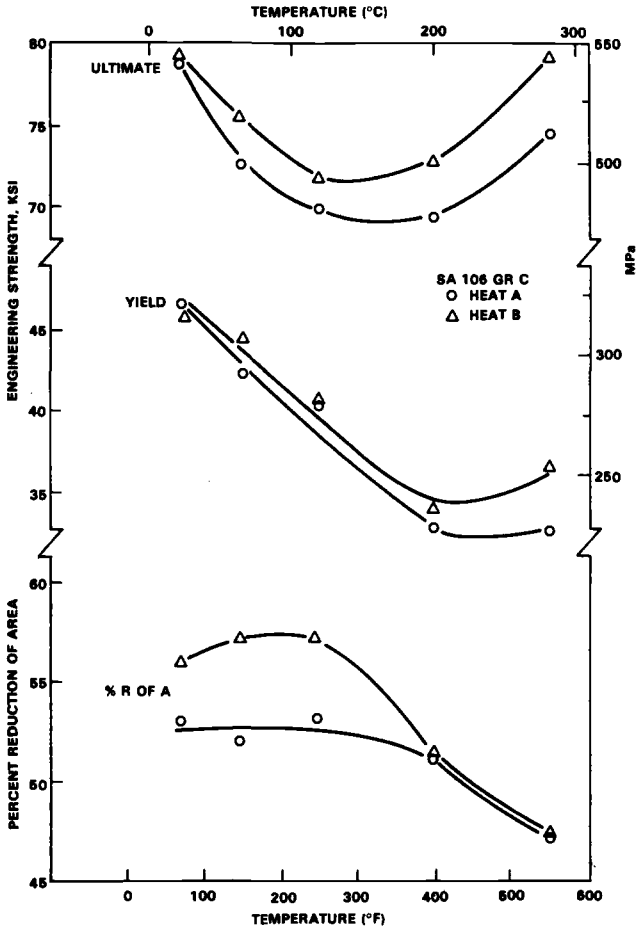

FIG. 10—*Temperature dependence of tensile properties of two heats of SA 106 Grade C* [8].

ultimate tensile strength. Tensile properties of the GTA and SMA weld metals discussed above are shown in Fig. 13. Comparison with the J_{Ic} results in Fig. 2 again shows that the material with the larger J_{Ic} drop with temperature—in this case, the SMA weld—also has a larger drop in ductility and sharper rise in ultimate tensile strength.

Comparison of unloading compliance traces of tests in which dynamic strain aging occurred revealed two other anomalies in addition to serrated flow. The load drop during load relaxation reached a minimum at temperatures just below the temperature range of serrated flow, as seen in Fig. 1. This is probably because of dislocation pinning by interstitial solutes during relaxation, which could restrict the amount of elastic strain converted into plastic strain.

At maximum load and beyond, a peak in load occurred after each unload in the temperature vicinity of the load-relaxation minimum in strain-aging susceptible material. In Fig. 1, these reload peaks are seen at 121°C (250°F) on both

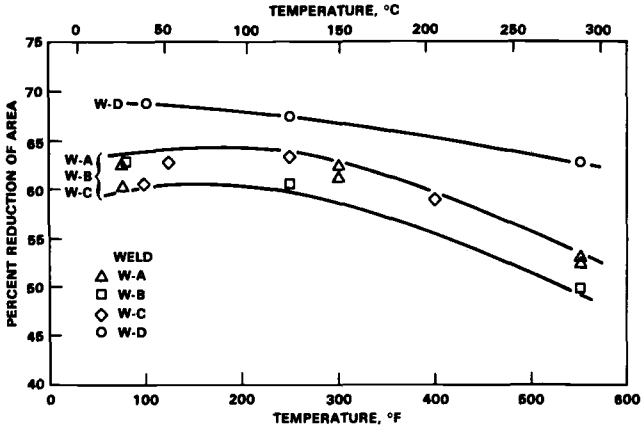

FIG. 11—*Variation of ductility with temperature for four submerged arc welds.*[3]

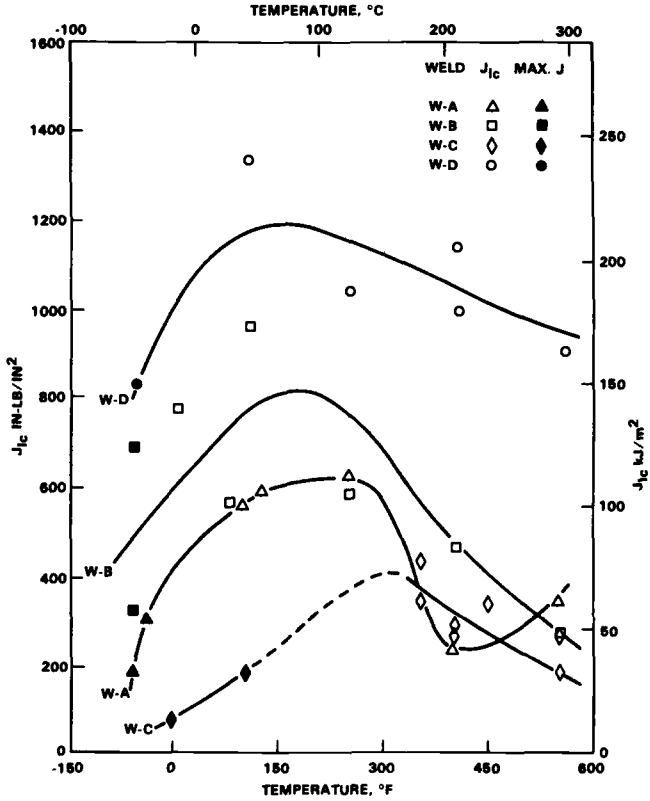

FIG. 12—*Temperature dependence of* J_{Ic} *for the four submerged arc welds of Fig. 11.*[3]

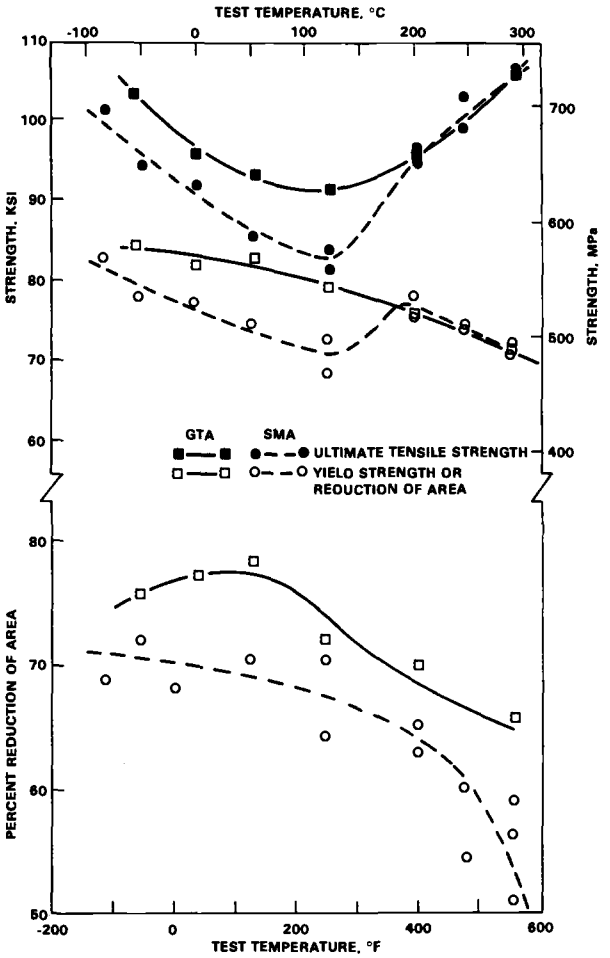

FIG. 13—*Temperature dependence of tensile properties for the two weld metals of Figs. 1 and 2* [1].

SMA and GTA unloading compliance traces. They are probably a result of static strain aging during load relaxation and unloading, which would explain their occurrence at temperatures near the load relaxation minimum. It is interesting to note that the reload peak height of the SMA weld metal is approximately equal to that of the GTA weld metal, although the J_{Ic} value for the former is much lower at this temperature. This suggests that reload peak height alone may have a smaller effect on the magnitude of J_{Ic} than serrated flow.

Conclusions

1. The presence of dynamic strain aging during J testing in one heat of SA 515-70 at 121 and 204°C (250 and 400°F) was evidenced by serrated flow,

reduced ductility, and rapid strain hardening. Another heat with lower nitrogen content exhibited no serrated flow under the same test conditions.

2. The strain-aging susceptible heat of SA 515-70 showed a greater drop in J_I-R curve slope with increasing temperature than the nonstrain-aging heat.

3. In unloading compliance J tests that exhibited serrated flow, the intensity of serrations varied between tests with different loading displacement rates. The intensity also varied within each test, with serrations appearing in the vicinity of maximum load, quickly reaching a maximum, and then decreasing over the duration of the test.

4. For SA 515-70, SA 106C, and several weld metals, a drop in J_{Ic} with increasing temperature was sometimes associated with an increase in tensile strength with temperature and always accompanied by a loss in ductility.

5. Other anomalies in the unloading compliance J test associated with strain aging are a minimum in load drop caused by relaxation and the appearance of reload peaks at a temperature corresponding to the low-temperature end of the temperature range of dynamic strain aging. The presence of serrated flow is associated with a greater drop in J_{Ic} than the presence of reload peaks alone.

Acknowledgments

We wish to gratefully acknowledge the assistance of J. L. Korosy with the experimental work and of D. L. Babbo and P. J. Rozich in preparing the final manuscript. We also wish to thank the Electric Power Research Institute for use of the data in Ref *1*.

References

[*1*] Feldstein, J. G., Bloom, J. M., and Van Der Sluys, W. A., "Repair Welding of Heavy Section Steel Nozzles," EPRI Report NP-3614, Vol. 1, Electric Power Research Institute, Palo Alto, CA, July 1984.

[*2*] Li, C. C. and Leslie, W. C., *Metallurgical Transactions*, Vol. 9A, Dec. 1978, pp. 1765–1775.

[*3*] Hirth, J. P. and Lothe, J., *Theory of Dislocations*, 1st ed., McGraw-Hill, New York, 1968, pp. 621–623.

[*4*] Keh, A. S., Nakada, Y., and Leslie, W. C., *Dislocation Dynamics*, McGraw-Hill, New York, 1968, pp. 381–408.

[*5*] Albrecht, P., Andrews, W. R., Gudas, J. P., Joyce, J. A., Loss, F. L., McCabe, D. E., Schmidt, D. W., and Van Der Sluys, W. A., "Tentative Test Procedure for Determining the Plane Strain J_I-R Curve," *Journal of Testing and Evaluation*, Vol. 10, No. 6, Nov. 1982, pp. 245–251.

[*6*] Van Der Sluys, W. A. and Futato, "Computer-Controlled Single-Specimen J-Test," *Elastic-Plastic Fracture Second Symposium: Volume II Fracture Resistance Curves and Engineering Application, STP 803*, American Society for Testing and Materials, Philadelphia, 1983, pp. II-464–II-482.

[*7*] Leslie, W. C., The University of Michigan, Ann Arbor, MI, June 1983, private communication.

[*8*] Fortner, E., Babcock and Wilcox, McDermott Co., Alliance, OH, 1982, unpublished research.

Gregory P. Gibson[1] *and Stephen G. Druce*[1]

Some Observations on *J-R* Curves

REFERENCE: Gibson, G. P. and Druce, S. G., **"Some Observations on *J-R* Curves,"** *Elastic-Plastic Fracture Test Methods: The User's Experience, ASTM STP 856*, E. T. Wessel and F. J. Loss, Eds., American Society for Testing and Materials, 1985, pp. 166–182.

ABSTRACT: The effect of specimen size and geometry on the onset of ductile tearing (J_i, δ_i) and the initial slope of $J(dJ/da)$ and crack opening displacement $d\delta/da$ resistance curves has been investigated for a carbon-manganese steel. The results indicate that in plane sided specimens a thickness in excess of that specified in ASTM Test for J_{Ic}, a Measure of Fracture Toughness (E 813) is required to achieve a lower bound, or plane strain, J_i value. However, the resultant decrease in J_i is relatively small. Side-grooving was found to be very effective in promoting plane strain conditions in subsized specimens. The initial tearing resistance was found to be markedly influenced by specimen thickness and degree of side-grooving, and the results indicate that achieving plane strain conditions in the proximity of the crack tip does not ensure a unique *J-R* curve in side-grooved specimens.

J_{Ic} values obtained using ASTM E 813 were found to overestimate the "true" J_i values for a carbon-manganese steel and a pressure vessel steel. This arises from the linear representation of the *R* curve and the assumed blunting line behavior A power law equation was found to give a statistically better fit to the J-Δa data, particularly in high toughness materials. The need for an engineering or working definition of ductile crack initiation for structural assessment has been acknowledged, and an alternative to the ASTM E 813 procedure suggested, based on the *J* value at 0.2 mm of crack extension.

KEY WORDS: elastic-plastic properties, ductility, steels, elastic-plastic fracture, *J* integral fracture mechanics, crack opening displacement, stable crack growth, ductile crack initiation

There is considerable interest in the use of *J*-integral crack growth resistance data in component integrity assessments defining the onset of stable and unstable ductile crack extension [*1*,*2*]. To ensure conservative predictions, it is necessary that the materials *J-R* curve is adequately representative of the constraint experienced by a defect in the structure. Conventionally, this is achieved using specimens of dimensions sufficient to promote plane strain conditions in the proximity of the crack tip. The first part of the paper reports an experimental investigation of the effects of varying specimen size and geometry on resultant *R* curves. The results are discussed in terms of the size requirements for plane strain behavior and whether obtaining plane strain conditions is sufficient to

[1]Higher scientific officer and senior scientific officer, respectively, AERE Harwell, Materials Physics and Metallurgy Division, Building 338, Oxfordshire OX11 ORA, England.

ensure lower bound *R* curve behavior. The second part of the paper discusses the problems of analyzing *J-R* curves to derive "initiation" toughness values at the onset of crack growth.

Experimental Procedure

The effects of specimen size and geometry on *R* curves were studied using a carbon-manganese steel, BS4360 43A. *J-R* curves from ASTM A508 Class 3 (Unified Numbering System [UNS] K12042) and ASTM A542 (UNS K21590) steels are used to investigate suitable equations to model the initial shape of the *R* curve. Carbon-manganese steel specimens, all with the same orientation, were mostly of the compact geometry type, with independently varying width, thickness, and degree of side-grooving. In addition, one size of single-edge notched three-and four-point bend specimens were tested.

The *J* values for compact and three-point bend specimens were calculated in accordance with the ASTM Test for J_{Ic}, a Measure of Fracture Toughness (E 813). In the case of the four-point bend geometry the *J* integral was calculated using the method described in Ref *3*. All the *J* values were corrected for crack growth using the method given in Ref *4*. A multi-specimen technique was used to determine the initial part of the *J-R* curve up to 2- to 3-mm crack extension. Values of "initiation" toughness were derived according to the ASTM E 813 procedure and are subsequently described as J_{Ic} values.

A modification to the *J* integral has been recently suggested by Ernst [*5*]. Although this modification has not been used in this work, it is noted that it would have a negligible effect on any of the reported initiation toughness values. The initial slope of the *R* curve is also not expected to be affected significantly as the amount of ductile crack extension Δa is small.

Measurements of critical stretch zone width (SZW_c) were taken parallel to the crack plane on broken specimens using a scanning electron microscope (SEM). SZW_c measured in the central region of the specimen, together with the blunting line relationship between *J* and SZW before crack initiation, can be used to determine initiation *J* values [*6*]. For the carbon-manganese steel the blunting line relationship was experimentally determined as

$$J = 2.2\ \sigma_f\ SZW \tag{1}$$

where σ_f = flow stress. J_i is the "initiation" *J* value as defined using Eq 1 and the SZW_c.

Silicone-rubber crack impressions were obtained from a number of specimens while at load, using the infiltration technique described in Ref *7*. Briefly, this involves injecting a catalytically hardenable silicone-rubber fluid into the crack. Once set, the specimen is unloaded, cooled in liquid nitrogen, and broken apart. The silicone-rubber cast is removed, sectioned, and examined in the SEM. From the impressions, direct measurements of the crack opening displacement δ at the

original crack tip were taken. From plots of δ versus fibrous crack extension (total crack extension minus critical SZW), the δ at crack initiation δ_i and the slope of the δ resistance curve $d\delta/da$ were obtained.

Results

Figure 1 gives δ_i and $d\delta/da$ (plus and minus standard errors) along with the SZW_c (plus and minus standard deviation) measured from 13-mm-thick 26-mm-wide compact geometry specimens with various amounts of side-grooving. It can be seen that the trends exhibited by δ_i and SZW_c are in good agreement, which gives confidence in the use of SZW_c to quantify the effect of specimen size on J_i.

Figures 2 through 7 show for the various specimen sizes and geometries (1) J_i as calculated from SZW_c and the blunting line, (2) J_{Ic} in accordance with ASTM E 813, and (3) dJ/da calculated over the Δa range between the two offsets given in ASTM E 813. It can be seen from the figures that J_{Ic} calculated in accordance with ASTM E 813 is consistently larger than J_i calculated from SZW_c. The errors associated with J_i values determined from SZW_c are generally much smaller than errors in J_{Ic} values as determined from the ASTM E 813 procedure. Therefore, in this report J_i values from SZW_c will be used to evaluate the effects of specimen size on initiation toughness.

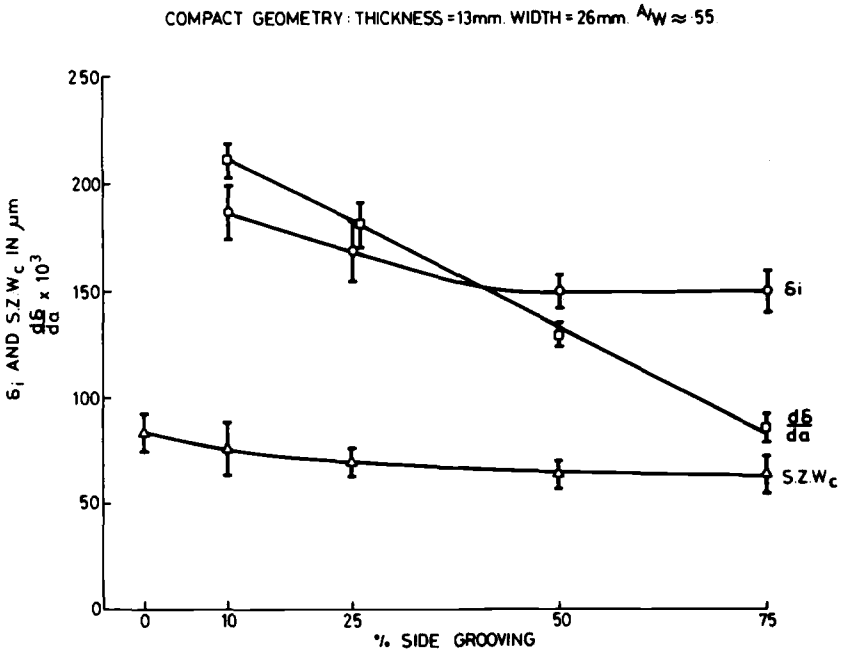

FIG. 1—*Effect of side grooving on* δ_i *and* SZW_c, *and* δ *crack growth resistance* dδ/da.

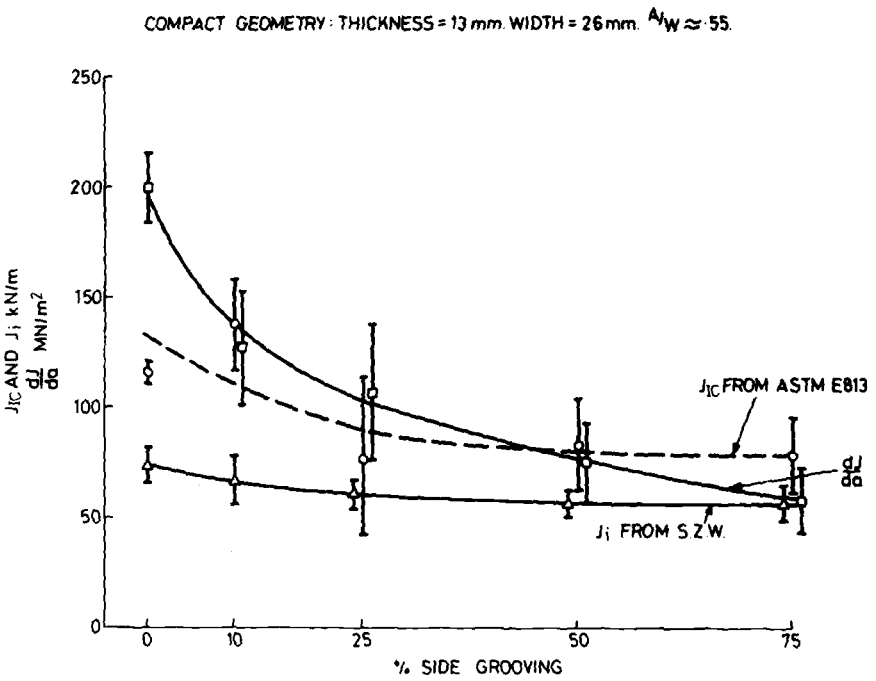

FIG. 2—*Effect of side grooving on* J_{Ic} *determined from ASTM E 813,* J_i *determined from SZW, and the J integral crack growth resistance* dJ/da.

All but two of the specimen types meet the size requirements for plane strain J_{Ic} values given in ASTM E 813, the two invalid specimens being the 13-mm-thick 26-mm-wide 50 and 75% side-grooved specimens. However, as shown by Fig. 2, side-grooving up to 25% lowers J_i and J_{Ic}, and therefore it seems unreasonable to use the net thickness for evaluating the thickness criterion, as required by E 813, since this suggests that side-grooving is detrimental for obtaining high constraint. If the gross thickness is used instead, which suggests that side-grooving is neither an advantage nor a disadvantage, all the specimens would meet the size requirements.

Figures 1 and 2 show the effects of increasing depth of side-grooving for 13-mm-thick 26-mm-wide compact specimens. After between 25 to 50% side-grooving, both J_i and δ_i decrease about 30% to a minimum plateau value, which is assumed to be that for plane strain conditions.

Figure 3 shows a similar effect of side-grooving on J_i and dJ/da for 25-mm-thick 50-mm-wide compact specimens.

Figure 4 shows the effect of varying width for compact specimens of constant thickness equal to 13 mm. Both J_i and dJ/da show little or no systematic variation with increasing width over the range measured.

Figures 5 and 6 show the effect of thickness with constant width and proportionally increasing width, respectively. J_i decreases by about 30% with in-

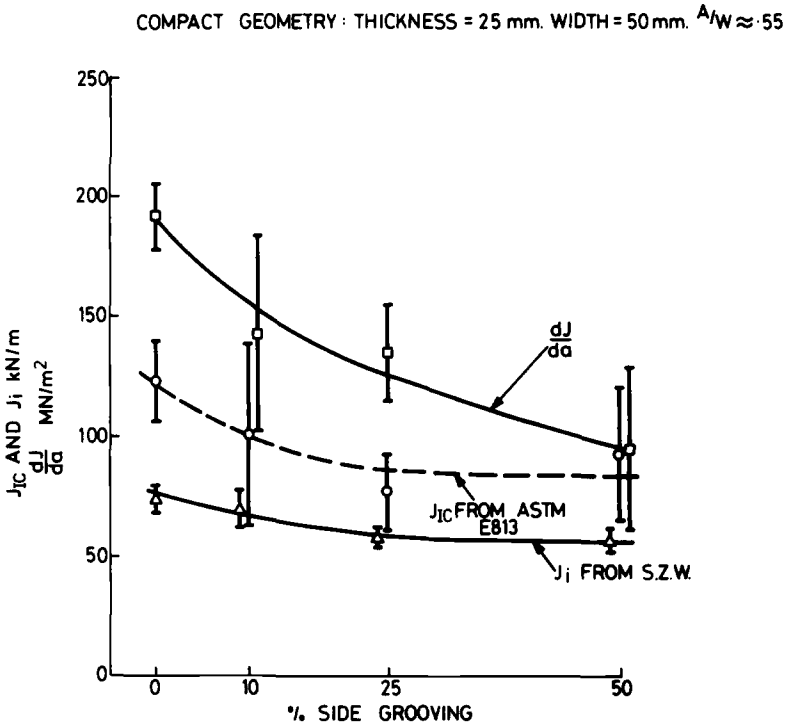

FIG. 3—*Effect of side grooving on* J_{Ic} *determined from ASTM E 813,* J_i *determined from SZW, and the* J *integral crack growth resistance* dJ/da.

creasing thickness from 13 to 50 mm. Comparing Figs. 5 and 6 with Figs. 2 and 3, it appears that the J_i value for a specimen of between 37.5 to 50 mm thick is equal to the minimum plateau J_i value found after 25 to 50% side-grooving in 13- and 25-mm-thick specimens. dJ/da is shown to decrease markedly with increasing thickness.

Figure 7 shows the effect of specimen geometry for similar sized specimens. J_i and dJ/da values are the same for the single-edge notched three- and four-point bend and compact specimens.

Discussion

Specimen Size Effects

Effect on Crack Initiation—The results in Figs. 2 to 6 show that over the range investigated, J_i is unaffected by varying specimen width but is mildly affected by variation in specimen thickness and depth of side-grooving.

Figures 5 and 6 show that in the absence of side-grooves a thickness of between 37.5 and 50 mm is required to achieve the lower bound plateau value, assumed

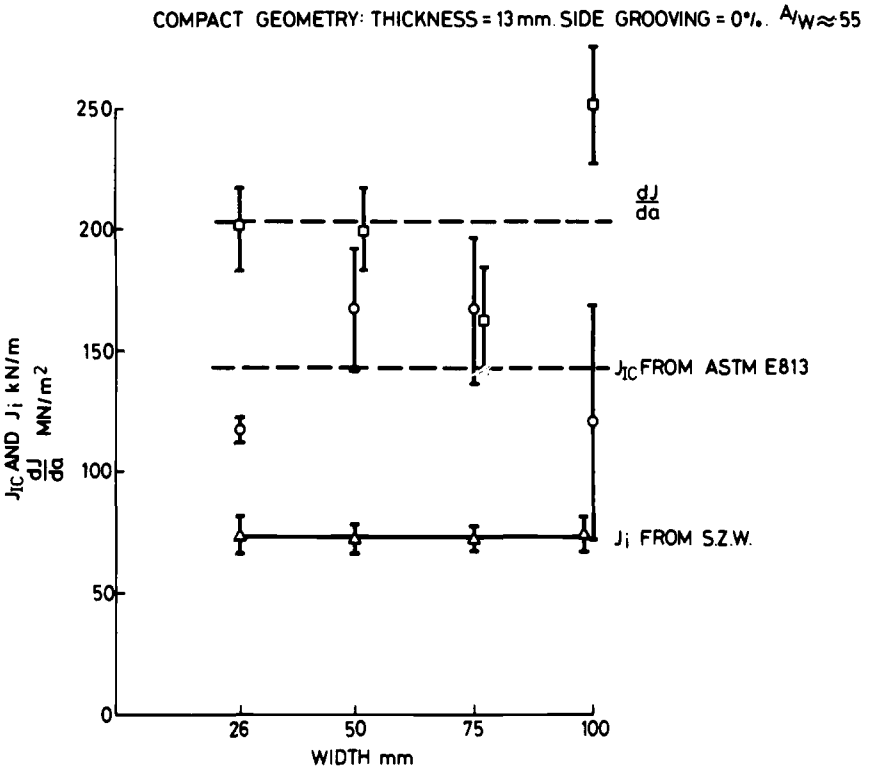

FIG. 4—*Effect of width on* J_{Ic} *determined from ASTM E 813,* J_i *determined from* SZW_c*, and the* J *integral crack growth resistance* dJ/da.

to be that for plane strain conditions. This yields a plane strain specimen thickness requirement of

$$\text{specimen thickness, } B > \alpha\ (J_i/\sigma_f) \tag{2}$$

where $270 < \alpha < 360$. However, it should be noted that the J_i value from the 13-mm-thick specimen (that is, $90\ J_i/\sigma_f$) was only 1.3 × plateau value J_i value.

Figures 2 and 3 show that the plane strain J_i value can be obtained in specimens <37.5 mm thick when suitably side-grooved. For 13- and 25-mm-thick specimens, side-grooving 25 to 50% of the gross thickness is sufficient. A similar result may also occur with even smaller specimens. On the basis of results so far obtained, a conservative estimate of the thickness requirement for plane strain conditions with 25 to 50% side-grooving, expressed in terms of the gross thickness B_g, would be

$$B_g > 90\ J_i/\sigma_f \tag{3}$$

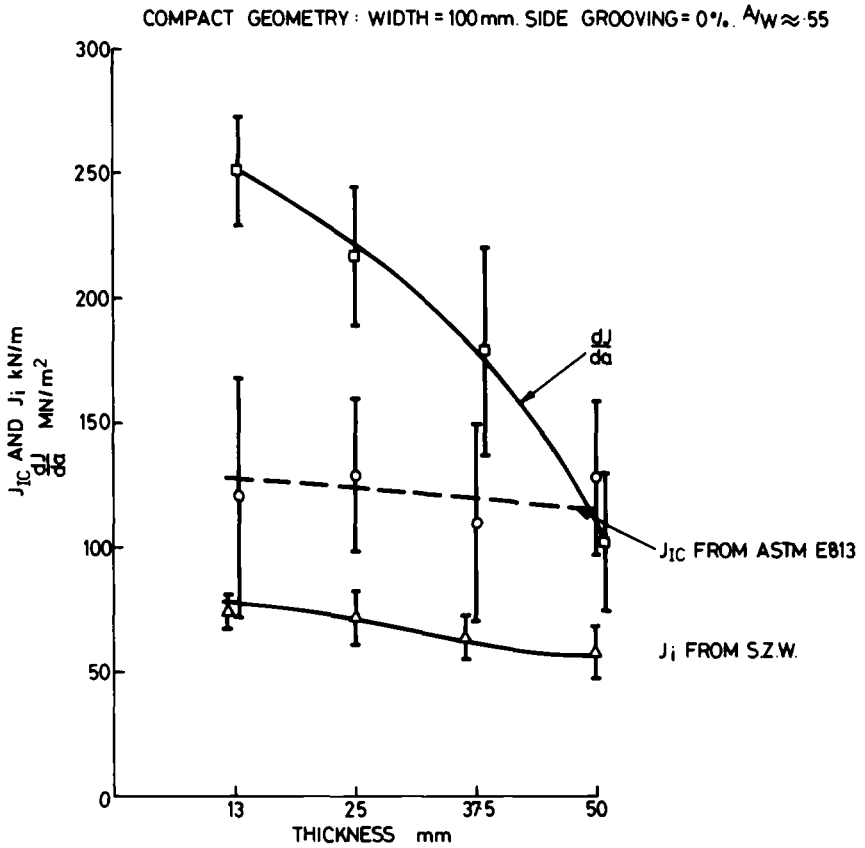

FIG. 5—*Effect of thickness on* J_{Ic} *determined from ASTM E 813,* J_i *determined from SZW$_c$, and the J integral crack growth resistance* dJ/da.

Clearly, side-grooving is very beneficial to obtain plane strain constraint when testing small specimens, and the authors feel that testing standards should acknowledge and encourage their use.

Figure 4 shows there is little or no effect of width on J_i over the entire range tested, suggesting that even smaller specimens would be required in order to determine the minimum ligament size requirement. From the smallest ligament tested, a conservative estimate of the ligament size requirement for plane strain conditions would be

$$\text{ligament, } b > 70\, J_i/\sigma_f \tag{4}$$

Figure 7 shows that J_i is the same for compact, three- and four-point bend geometries for the same specimen thickness and width, indicating that these geometries have the same specimen size requirements for plane strain conditions.

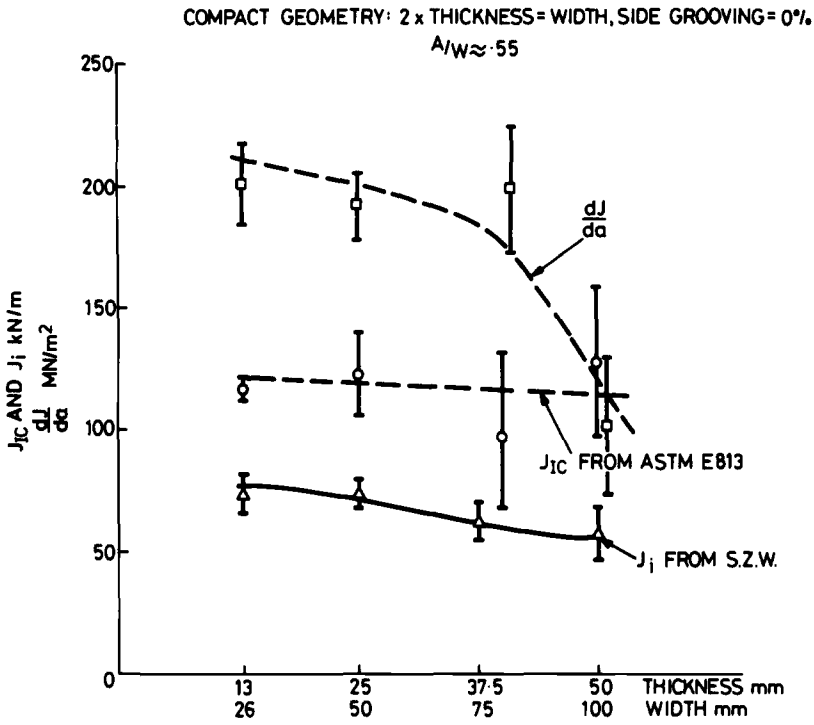

FIG. 6—*Effect of standard specimen size on* J_{Ic} *determined from ASTM E 813,* J_i *determined from SZW, and the* J *integral crack growth resistance* dJ/da.

This suggests that geometries with similar high plastic constraint result in similar crack-tip constraint.

The size requirements given in Eq 2, 3, and 4 are considerably larger than given in ASTM E 813. In the case of Eq 3 and 4 this may be because they are conservative estimates. However, this is not the case for the thickness criterion for nonside-grooved specimens (Eq 2). There are a number of possible reasons for the discrepancy. The first is that for carbon-manganese steel the J_{Ic} determined from ASTM E 813 can typically overestimate the J_i by a factor of two, thus making the thickness and also the ligament criteria appear less stringent. The second is that changing thickness only mildly affected J_i, and because there is often large scatter associated with J_{Ic}, markedly subsized specimens may appear adequate. The third possibility is that the ASTM E 813 size requirement has mainly been verified on high-toughness or high-strength materials. Therefore, there could be a real difference in the size requirement for this material compared to other materials, suggesting the J_i/σ_f is not a suitable scaling factor.

Effects on Crack Growth Resistance—In this section the effects of specimen size and geometry on crack growth resistance are interpreted in terms of crack-tip constraint and deformation remote from the crack tip.

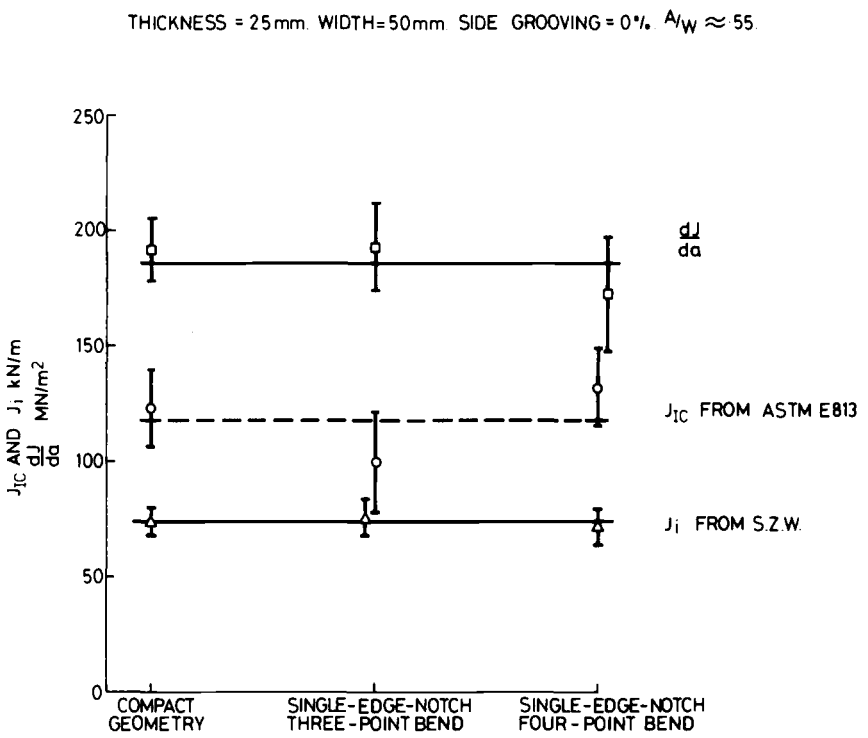

FIG. 7—*Effect of specimen geometry on* J_{Ic} *determined from ASTM E 813,* J_i *determined from* SZW_c, *and the* J *integral crack growth resistance,* dJ/da.

Figures 2 and 3 indicate a marked effect of side-grooving in decreasing *dJ/da*. The fracture surfaces show that the shear lip is removed by side-grooving 10% or more and that the through thickness contraction is zero for >50% side-grooving. In plane sided specimens crack growth occurs preferentially in the central region, whereas side-grooving up to 25% straightens the crack front. In deeply side-grooved specimens some leading of the crack front occurs locally at the side-groove notch radii. Irrespective of the degree of side-grooving, crack initiation occurred after net-section yielding. One possible explanation for the observed side-groove effect is that the *J* calculation formulae, which are only given in ASTM E 813 for side-grooving up to 25%, are not appropriate for deeper side-grooves. This question is addressed by the authors in detail elsewhere [*8*]. It is found that although some correction is necessary, the trends of Figs. 2 and 3 remain unchanged. Furthermore, additional support is given by the corresponding trend in $d\delta/da$ (Fig. 1) directly determined from crack-tip impressions.

An explanation for this behavior based on the combined effects of side-grooving on crack-tip constraint and the plastic hinge point is proposed as follows. Figure 8 schematically illustrates the plastic hinge construction. After initiation

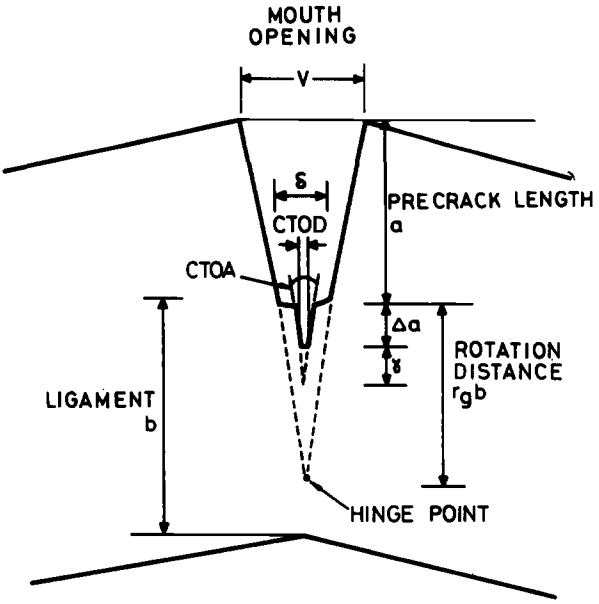

FIG. 8—*Schematic sketch illustrating the hinge point construction during crack growth.*

the increases in mouth opening displacement dV and crack opening displacement $d\delta$ above their respective initiation values V_i and δ_i are related by

$$d\delta = (r_g b\, dV)/(r_g b + a) \tag{5}$$

$r_g b$ defining the hinge point position during growth. Similarly, the crack opening displacement at the tip of the growing crack (crack-tip opening displacement [CTOD]) and crack-tip opening angle (CTOA) are related by the distance γ such that

$$\text{CTOA} = 2 \tan^{-1} (\text{CTOD}/2\gamma) \tag{6}$$

As there is essentially only elastic deformation behind the crack tip $r_g b$ is directly proportional to γ. For the carbon-manganese steel used in this study, the CTOA has been shown [7] to acquire a constant value after about 1.5 mm of crack growth that is related to $d\delta/da$ by

$$\text{CTOA} = 2 \tan^{-1} (d\delta/2da) \text{ for } \Delta a \geq 1.5 \text{ mm} \tag{7}$$

Table 1 gives values of the rotation distance $r_g b$, calculated from Eq 5 using measurements from the infiltration casts and mouth opening gage, for 13-mm-thick 26-mm-wide compact specimens with 10 to 75% side-grooving. It can be

TABLE 1—*Experimentally derived values of* dV/da *and* $r_g b$ *for compact geometry, width 26 mm, thickness 13 mm,* a/W ≃ 0.55, *and various amounts of side-grooving.*

Side-Grooving,%	*dV/da*, ± Standard Error	$r_g b$, mm ± Standard Error
10	1.03 ± 0.25	3.7 ± 1.3
25	0.84 ± 0.14	4.2 ± 1.0
50	0.55 ± 0.09	4.6 ± 1.0
75	0.31 ± 0.05	6.2 ± 1.5

seen from Table 1 that there is little or no increase in $r_g b$, and hence γ, for up to 50% side-grooving. It has been shown elsewhere that both δ_i and CTOD are affected by constraint [7]. Therefore, up to 25 to 50% side-grooving where δ_i is decreasing, and by implication the crack-tip constraint is increasing, CTOD would also be expected to decrease. Decreasing CTOD, with γ remaining constant, leads to a reduction in CTOA (Eq 6), which in turn from Eq 7, means a decrease in crack opening resistance $d\delta/da$. This results in a smaller change in area under the load versus mouth opening displacement curve with crack extension and hence a decrease in dJ/da. Side-grooving in excess of 25 to 50% does not further reduce δ_i, and by implication the crack-tip constraint and CTOD are not further affected. However, above 50% side-grooving Table 1 shows $r_g b$, and hence γ, to significantly increase, and therefore from Eq 6 and 7, $d\delta/da$ and dJ/da continue to decrease with increasing side-grooving. It is thought probable that the increase in the rotation distance from the crack tip $r_g b$, with deep side-grooves is resultant from a change in plastic hinge behavior induced by preventing yielding outside of the side-groove plane.

Figure 4 shows there is little or no consistent variation in dJ/da with increasing specimen width at a constant thickness. This is in agreement with the constant value of J_i observed and suggests that the crack-tip constraint and rotation factor r_g are constant for a small amount of crack growth with changing ligament size.

Figures 5 and 6 show that dJ/da significantly decreases with increasing specimen thickness for either a constant width or a proportionally increasing width. Decreasing dJ/da suggests that $d\delta/da$ is decreasing, and therefore from Eq 7. CTOA is also decreasing. From Eq 6 this would be consistent with a decreasing CTOD and nearly constant or slightly increasing γ value. A decreasing CTOD would be anticipated as J_i is also decreasing, so indicating increasing crack-tip constraint. If the specimen thickness was further increased above the maximum tested, then the CTOD would be expected to remain constant since the J_i has already achieved a minimum plateau value. Furthermore, since the specimen is essentially under plane strain conditions, the size and shape of the plastic zone is not expected to alter with increasing thickness, and so γ is expected to remain constant. Therefore CTOA, $d\delta/da$, and dJ/da are expected to remain constant, and the dJ/da value for the 50-mm-thick specimen is expected to be the plane strain value for nonside-grooved specimens. There is close agreement between

this dJ/da value and that for between 25 to 50% side-grooving, which further supports the use of moderate side-grooving to obtain plane strain *J-R* curve data from significantly smaller specimens. However, it should be noted that achieving plane strain crack-tip constraint does not ensure a unique *J-R* curve and that near field conditions are not related to far field conditions in heavily side-grooved specimens.

Figure 7 shows the same dJ/da values for the single-edge notched three- and four-point bend and compact geometries of the same specimen thickness and width. This is consistent with the above discussion since all three geometries are essentially deep-notched bending configurations.

dJ/da and $d\delta/da$ are measures of the specimen response away from the crack tip. The effect of specimen size and geometry on dJ/da and $d\delta/da$ has been explained in terms of local crack-tip constraint (near field conditions) and remote plastic deformation behavior (far field conditions). For J and δ to control crack growth, the near field conditions need to relate to the far field conditions. In all but the case of deep side-grooves it appears that this requirement has been met. Two conditions have been proposed to ensure J control growth [*9*]. The first is that the crack extension be limited to 6% of the ligament. J values for crack extensions up to 11% of the ligament were used to calculate dJ/da for the 75% side-grooved specimens. However, the trends of $d\delta/da$ and dJ/da are still apparent when crack extension only up to 6% of the ligament is considered. The second condition is that $\omega(b/J \times dJ/da)$ is much greater than unity and a value of ten has been suggested [*9*]. ω was four at the largest J value used to calculate dJ/da for the 75% side-grooved specimens. It may be argued therefore that this ω value is insufficient. However, the restriction of the formation of the plastic hinge by very deep side-grooves is not a phenomenon unique to small specimens and will occur in specimens with a much larger ligament size. Therefore, satisfying the ω criterion and the crack extension limit would not ensure J controlled crack growth in the case of deep side-grooves. Clearly the conditions imposed by heavily side-grooved specimens are very severe and may not be representative of many defected structures. However, these results do indicate that accurate integrity assessment requires data relevant to the overall level of constraint imposed by the structure.

Much of the discussion, interpretation, and prediction given in this section relies on direct measurement of crack-tip profiles. Crack profile data are presently incomplete, and the discussion has on occasions used results indirectly inferred from other measurements. Confirmation awaits the direct measurement of CTOA and CTOD values from crack profiles currently being undertaken.

J-R *Curve Fitting and Defining "Initiation"* J *Values*

As noted previously, the J_{Ic} values derived according to ASTM E 813 are larger than the J_i values from SZW_c, particularly when dJ/da is large. This is well illustrated by the results in Table 2 determined for a highly tearing-resistant

TABLE 2—*ASTM A508 Class 3 at 290°C, J_i values determined from various procedures.*

Procedure	"Initiation" J, $10^2 \times$ kN/m
Using ASTM E 813	3.9
Using ASTM E 813 but with $4\sigma_f$ blunting line	3.2
From SZW_c and blunting line	1.8

material, ASTM A508 Class 3 steel. The blunting line equation used to determine J_i from SZW is given by [*6*]

$$J = 4\sigma_f \, SZW \tag{8}$$

Part of the reason for the difference between J_{Ic} and J_i is that the $2\sigma_f$ blunting line used in the ASTM E 813 J_{Ic} procedure overestimates the degree of blunting. Using Eq 8 as a more reasonable estimate of the blunting line for this material reduces the difference between the two approaches (see Table 2). However, there is still a significant difference, and this is due to the nonlinear nature of the *J-R* curves, particularly at small crack extensions. This has been noted by other authors (Ref *10*, for example). Fitting a linear line to a nonlinear curve also results in a considerable variability in J_{Ic} depending on the distribution of data points, particularly when there are only a few, even when the ASTM E 813 position criterion has been satisfied. These deficiencies suggest there is a need to represent the nonlinear *J-R* curve more accurately.

A wide range of equations were tested to see how well they modelled a multi-specimen *J-R* curve for the ASTM A508 Class 3 material. The equations were fitted using a least-squares procedure to regress crack extension upon J, for 21 data points over a range of crack extensions from 0.5 to 2.3 mm. The accuracy of the fit was determined by the variance, that is, the sum of residual squares divided by the number of degrees of freedom. A lower variance shows that the equation is modelling the shape of the *J-R* curve with greater statistical significance. Table 3 gives the sum of residual squares together with the variance for the more accurate equations tested, together with the linear equation for reference. The linear analysis obtained using data between the ASTM E 813 exclusion limits is also given. However, in this case, the variance has been calculated over a smaller Δa range and therefore cannot be directly compared to the other reported values. Also given in Table 3 are the J_i values obtained by substituting into the various equations the SZW_c measured for this material. The most accurately fitting equations are those based on a power law. The best overall fit was obtained using a power law with a constant offset. The reduction in the sum of residual squares for this equation compared to the simple power law would not be statistically significant if only four to five data points were available as is often the case with multi-specimen testing. Thus, for general use the simple power law equation is therefore recommended to model the shape of the *J-R* curve for high-toughness materials.

TABLE 3—*Sum of residual squares, variance values, J at SZW$_c$ for various functions, fitting A508 C = 3 data, and regressing crack extension upon J.*

Function	Sum of Residual Squares, $\Sigma_{(Y_i-Y)^2}$	Variance $\Sigma_{(Y_i-Y)-2}$/Number, Degrees of Freedom	J_i, J at SZW$_c$, $10^2 \times$ kN/m
Linear – all data points			
$\Delta a = AJ + B$	0.152	0.008	3.0
Linear – ASTM valid data			
$\Delta a = AJ + B$	0.065	0.0034	2.7
Power law			
$\Delta a = AJ^B$	0.0391	0.0021	1.1
Power law + free linear			
$\Delta a = AJ^B + CJ$	0.0388	0.0022	1.0
Power law + fixed linear			
$\Delta a = AJ^B + J/4\sigma_f$	0.0430	0.0023	1.5
Power law + constant offset			
$\Delta a = AJ^B + C$	0.0327	0.0018	0.0
Second order polynomial			
$\Delta a = A + BJ + CJ^2$	0.0399	0.0022	1.6

Table 3 shows that defining initiation as the power law value of J at the SZW$_c$ value of Δa can result in apparently very low toughness values. This is not a surprising result when one considers the crack-tip processes occurring during loading. On initial loading the crack tip will begin to blunt, so forming an incipient stretch zone. At an early stage of loading voids will begin to form and at favorable sites along the crack front, link to the crack tip. Regions of high inclusion density will provide local crack growth, while other regions of the crack front are still blunting. This uneven crack initiation results in a gradual departure from the blunting line that is being modelled by the power law at small crack extensions. Hence the value of the power law fit at the average value of SZW$_c$ (measured in the central region of the specimen) will be somewhat less than the extrapolated blunting line at the same crack extension, which we consider to be the best estimate of true ductile initiation.

Figures 2 and 3 show that as the degree of side-grooving increases and dJ/da decreases, the difference between J_i from SZW$_c$ and J_{Ic} from ASTM E 813 decreases. This is because the nonlinearity in the *J-R* curve decreased as dJ/da decreases. This raises the question of whether the power law equation always gives a statistically better fit than the linear equation. Figure 9 gives the *J-R* curve for an ASTM A542 material, which is an example of a curve exhibiting a high J_i and low dJ/da value. Table 4 gives the variance values for linear and power law equations. It can be seen from Table 4 that both equations fit the data equally well. However, Fig. 9 shows that the power law fit significantly underestimates the J values at low crack extensions and can therefore underestimate initiation toughness. In general, the equation providing the best fit should be used to define the *J-R* curve, combined with some statistical assessment of the accuracy of the fit such as confidence limits.

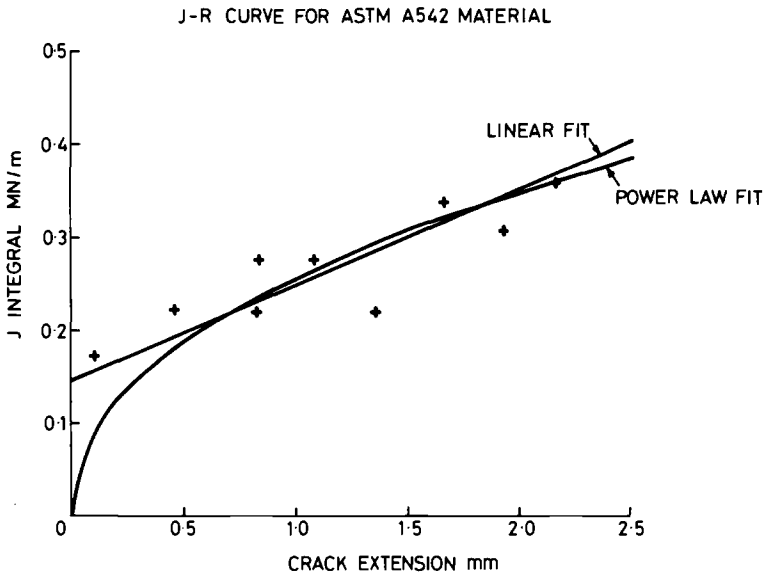

FIG. 9—*J-crack extension plot showing the linear and power law fits to the experimental data for a ASTM A542 material.*

For an initiation concept that is acceptable for use in design and general integrity assessment, an engineering or working definition is required rather than a strictly purist approach. Such a definition must be (1) unambiguous, that is, explicitly state how much crack extension is included at the "initiation" event, (2) experimentally detectable with high precision, and (3) characterize the onset of macroscopic ductile crack growth in an engineering sense.

It has been suggested by the present authors [*11*] that a definition based on the J value at a prescribed amount of crack extension satisfies Conditions 1 and 2. For low and medium strength steels a crack extension of 0.2 mm was proposed as a workable definition. For adequate precision it is important that at least one data point lies close to this value, that is, in the range $\Delta a = 0.15$ to 0.25 mm. Defining initiation in this way is somewhat analogous to the engineering solution of using a proof stress for defining the yield condition in materials not exhibiting a distinct yield point.

The third requirement necessitates an engineering assessment of the relevance of the onset of macroscopic ductile crack growth to the defect tolerance of

TABLE 4—*ASTM A542 tested at 20°C. Variance values for linear and power law fit to all data points.*

Equation Used	Variance
Power law	0.134
Linear	0.129

structures. This cannot be answered by considering *J-R* testing techniques alone, but must be evaluated in conjunction with particular assessment procedures, comparing predicted behavior with a wide variety of experimental and structural experience. We have suggested 0.2 mm of crack extension might be a workable definition, and clearly other definitions might be equally acceptable. However, a detailed appraisal is not within the range of the present paper.

Conclusions

The effect of specimen size and geometry on the onset of crack initiation and small amounts of crack growth has been studied in a carbon-manganese steel. The results show the following.

1. J_i is mildly dependent on the specimen thickness and degree of side-grooving but not on specimen width in the compact specimen geometry. Compact, single-edge notched three- and four-point bend geometries of the same thickness and width give the same value of J_i.

2. The ASTM E 813 thickness size requirement for plane strain condition in plane sided specimens was found insufficient. The resultant degree of overestimation in J_i is small ($\simeq$30%) and is of the same order as statistical scatter arising from conventional multi-specimen J_{Ic} testing. Side-grooving specimens 25 to 50% of the gross thickness considerably reduced the plane strain thickness size requirement.

3. In compact specimens, material crack growth resistance dJ/da, was found to be markedly dependent on specimen thickness and degree of side-grooving but insensitive to variations in specimen width. Compact and bend geometries of the same thickness and width gave the same value for dJ/da. With increasing depth of side-grooves, beyond that required for plane strain crack conditions, dJ/da and $d\delta/da$ continue to decrease, indicating that this condition is not a sufficient condition for a geometry independent R curve.

4. J_{Ic} derived from the testing procedure of ASTM E 813 overestimates J at the onset of ductile crack growth because of errors in the assumed blunting line and the use of linear regression to the J-Δa data. The degree of overestimation is more severe in highly tearing resistant materials. A power law equation usually provides a statistically improved fit to the data. A working or engineering definition for the "onset of macroscopic ductile crack growth" is required for practical application to structural integrity assessment. The J value at 0.2 mm total crack extension is proposed as an alternative to the ASTM E 813 J_{Ic} definition.

Acknowledgments

The authors acknowledge the support of Professor C. E. Turner and Dr. J. A. Hudson for useful discussions, Mr. J. H. Worth for experimental advice, Mr. G. Jordan for making some SZW measurements and Mr. A. R. Curtis for advice on data fitting and error analysis.

References

[1] Paris, P. C., Tada, H., Zahoor, A., and Ernst, H., "Instability of Tearing Mode of Elastic-Plastic Crack Growth," *Elastic-Plastic Fracture, STP 668*, American Society for Testing and Materials, Philadelphia, 1979, pp. 5–36.

[2] Hutchinson, J. W. and Paris, P. C., "The Theory of Stability Analysis of *J*-Controlled Crack Growth," *Elastic-Plastic Fracture, STP 668*, American Society for Testing and Materials, Philadelphia, 1979, pp. 37–64.

[3] Clarke, G. A., Landes, J. D., and Begley, J. A., "Results of an ASTM Cooperative Test Program on the J_{Ic} Determination of HY130 Steel," *Journal of Testing and Evaluation*, Vol. 8, No. 5, Sept. 1980, pp. 221–232.

[4] ASTM Committee E-24 draft document, "The Determination of the Elastic-Plastic Toughness Parameter J_{Ic}," American Society for Testing and Materials, Philadelphia, Sept. 1979.

[5] Ernst, H. A., "Material Resistance and Instability Beyond *J*-Controlled Crack Growth," *Elastic-Plastic Fracture Second Symposium, Volume I: Inelastic Crack Analysis, STP 803*, American Society for Testing and Materials, Philadelphia, 1983, pp. I-191–I-213.

[6] Kobayashi, H., Nakamura, H., and Nakazawa, H., *Fourth International Conference on Pressure Vessel Technology*, Institute of Mechanical Engineering, London, 1980, pp. 251–256.

[7] Gibson, G. P., and Druce, S. G., "A Study of Elastic-Plastic Fracture Parameters Through the Thickness of Fracture Toughness Specimens Using Silicone-Rubber Crack Impressions," Report AERE-R10815, AERE Harwell, Oxon, England, Feb. 1983.

[8] Gibson, G. P., Wilmshurst, M., and Druce, S. G., "An Experimental Evaluation of the *J* Integral in 50% Side-Grooved Compact Geometry Specimens," Report AERE R11202, AERE Harwell, Oxon, England, 1984.

[9] Shih, C. F., German, M. D., and Kumar, V., "An Engineering Approach for Examining Crack Growth and Stability in Flawed Structures," General Electric Report 80CRD205, Sept. 1980.

[10] Carlson, K. W. and Williams, J. A., "A More Basic Approach to the Analysis of Multiple-Specimen R-Curves for Determination of J_c," *Fracture Mechanics—Proceedings of the Thirteenth National Symposium on Fracture Mechanics, STP 743*, American Society for Testing and Materials, Philadelphia, 1981, pp. 503–524.

[11] Druce, S. G., Gibson, G. P., and Belcher, W., *Proceedings of a CSNI Workshop on* "Ductile Fracture Test Methods," Organization for Economic Cooperation and Development, Paris, 1982, pp. 250–262.

Martin I. de Vries[1] *and Bark Schaap*[1]

Experimental Observations of Ductile Crack Growth in Type 304 Stainless Steel

REFERENCE: de Vries, M. I. and Schaap, B., **"Experimental Observations of Ductile Crack Growth in Type 304 Stainless Steel,"** *Elastic-Plastic Fracture Test Methods: The User's Experience, ASTM STP 856*, E. T. Wessel and F. J. Loss, Eds., American Society for Testing and Materials, 1985, pp. 183–195.

ABSTRACT: J-integral fracture toughness tests were performed at room temperature on small compact tension (1/2TCT) specimens of stainless steel Type 304 (Unified Numbering System [UNS] S30400). The ductile crack growth resistance curve was measured with the multi-specimen heat tinting method and automatically recorded using the potential drop (PD) technique and an optical system. The first parts of the curves were different for each method, however, for larger Δa values the curves were nearly the same. Profile measurements of the stretch zone showed blunting to be best represented by the formula $J = 3.5\sigma_f \Delta a$. There was no distinct separation between the blunting and stable crack growth phenomena. A continuous process of alternating crack-tip stretching and ductile crack extension was observed from the very beginning up to final crack extension (about 3 mm). Ductile initiation (formation of first dimples) was measured at about 300 kJ · m^{-2} (J_i) and "onset of stable crack growth" was measured at about 750 kJ · m^{-2} (J_Q).

KEY WORDS: crack initiation, stainless steels, temperature, J-integral test, multi-specimen method, single-specimen test, optical crack extension recording, potential drop technique, crack-tip stretch, crack extension

The austenitic stainless steels are important nuclear construction materials, particularly for elevated temperature applications in advanced reactors (LMFBR, MFR), of which many structural components are exposed to neutron irradiation during their lifetime. At the Netherlands Energy Research Foundation the mechanical properties of irradiated stainless steels have been extensively measured for more than ten years now. Large numbers of tensile, creep, high- and low-cycle fatigue and fatigue crack propagation specimens have been irradiated and tested at temperatures ranging from 300 to 1000 K [*1–3*].

Recently 1/2TCT specimens have been irradiated for fracture toughness experiments at elevated temperatures. To characterize the elastic-plastic fracture behavior of the irradiated stainless steel, the standard linear-elastic plane-strain

[1]Research scientist and technician, respectively, Netherlands Energy Research Foundation ECN, Materials Department, Westerduinweg 3, P.O. Box 1, 1775 ZG Petten, Netherlands.

fracture toughness K_{1c} test technique is not applicable. Therefore, nonconventional test methods, based on the widely accepted elastic-plastic parameter J-integral, have to be used. In this report the results of preliminary tests at room temperature, with a small number of unirradiated specimens, are presented. The experiments were aimed at the evaluation of the experimental equipment and of the measuring techniques before the testing of the irradiated specimens.

Experimental Procedure

The CT specimens (30.0 by 28.8 by 12.0 mm) were made from 20-mm-thick plates of a fully austenitic Type 304 stainless steel. The tensile properties of the material are listed in Table 1.

The specimens were located in the plates with the notch parallel to the rolling direction (T-L orientation). The length of the mechanical notch was 10 mm. The specimens were deeply precracked to crack length versus the specimen width a/W of 0.6 at final load range ΔP of 2.7 kN with a R ratio of 0.1.

The fatigue precracking and the fracture toughness tests were performed on a servo-hydraulic testing machine adapted for remote handling. The 1251 Instron for the testing of the irradiated specimens is installed in a lead cell. The electronic equipment for test control and data measurements is installed outside the lead cell.

The load is measured with a ±20-kN load cell. The displacement is measured with a ±5-mm displacement transducer. The load-line displacement is derived from the relative displacement of the clevices. For the application at elevated temperatures, the clevis displacement is transmitted by an extension rod to the transducer outside the furnace near the bottom of the lower pull rod.

For continuous observation of the crack two optical systems are installed in the lead cell. Both sides of the specimen are monitored with microscope cameras and recorded on video tape driven by a signal from the function generator of the testing machine. At elevated temperatures the crack is observed through two small quartz windows in the furnace walls, positioned opposite each other.

The optical facilities are used for crack length measurements and for observation of the crack-tip phenomena, such as plasticity and crack branching. The fatigue crack is measured on the polished surfaces of the specimen. When there is severe scaling or plasticity around the crack, the crack tip is obscured and no reliable measurements can be made with the direct observation method. However,

Table 1—*Room temperature tensile properties of the Type 304 stainless steel.*

0.2 Yield, MPa	Ultimate Tensile Strength, MPa	Flow[a] Stress, MPa	Elongation, %	Reduction in Area, %
230	580	400	65	75

[a]Flow stress σ_f: $(\sigma_{ys} + \sigma_{uts})/2$.

by means of "through-lightening" of the opened crack an indirect "bright-shadow" of the crack tip can be observed. This technique is used for the optical measurements of ductile crack growth.

A minicomputer controlled direct current potential drop (PD) system has been developed for fully automatic crack length measurements [*4*]. Crack length and the corresponding number of cycles or load and displacement are sampled by the microprocessor and stored on magnetic tape. The data processing system provides tables of the data and graphical output. The J values are calculated using the incremental J_{i+1} relationship given by Ernst et al [*5*]. Additionally, the analogue signals are recorded with conventional equipment for instantaneous manual test control.

The PD signal is converted into crack extension values using the fatigue crack calibration data with a sensitivity of 55 μV/mm. Tensile loading is applied immediately after fatigue precracking, starting without interruption from the mean level of the last fatigue load cycle. This procedure results in a continuously increasing (no minimum!) PD signal.

In Fig. 1 the PD data are compared with the photographically measured values of the final crack extension marked by heat tinting at 800 K. For the larger crack extension values the PD data are within the ASTM Test for J_{Ic}, a Measure of Fracture Toughness (E 813) acceptance limits (15%). The relatively large misfit at low Δa values is due to plasticity effects giving local thickness reductions up to 20%. To obtain a better correlation with the optical data, the PD data can easily be corrected for plasticity contributions. For instance, a correction of 0.15-mm offset value takes into account 20% local thickness reduction at the end of the macroscopic blunting. With this simplified correction, all PD data are within the ASTM E 813 acceptance limits.

There are only limited results of J-type tests on stainless steel in the open

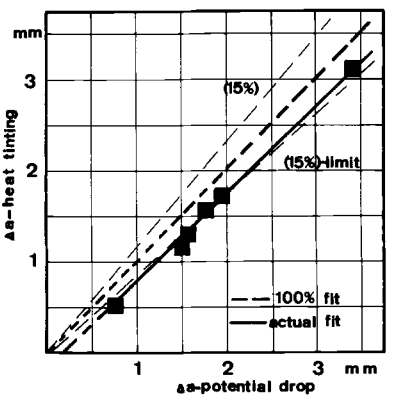

FIG. 1—*Comparison of crack extension values measured with the potential drop method and the heat-tinting technique.*

literature [*6–9*]. Bamford [*6*] and Tobler [*8*] use the theoretical "blunting line" formula to represent apparent crack growth caused by blunting

$$J = 2\sigma_f \Delta a \tag{1}$$

with σ_f being the average of the 0.2% offset tensile yield strength and the ultimate tensile strength. Balladon [*10*] has used experimental blunting lines that appear to be close to the line

$$J = 4\sigma_f \Delta a \tag{2}$$

Apparently, there is some uncertainty if $2\sigma_f$ is the best blunting coefficient for stainless steels [*9,10*]. To clarify this point, we have measured the stretch zone dimensions at a magnification of 200, using a contourograph. From the stretch zone profile curves, stretch-zone dimensions (length Δa and height δ) are measured as indicated in the schematic presentation of Fig. 2. Each specimen was characterized with nine measurements, equally spaced over the fracture surface at distances of 1.2 mm in the thickness direction.

The fracture surfaces of the tested specimens were, after heat-tinting and fatigue post cracking to failure, observed with a scanning electron microscope and an optical stereo microscope. The crack extension values were measured from the photographic pictures at a magnification of 10. The data are based on the weighted nine points averaging method.

Results and Discussion

Crack growth resistance J-Δa curves of stainless steel Type (Unified Numbering System [UNS] S30400) (304) are measured at room temperature with three different crack measuring techniques: multi-specimen heat-tinting, single-specimen "continuous optical," and the single-specimen potential-drop method.

Multi-Specimen Heat-Tinting

With this method final crack extension values are measured on the fracture surfaces of the broken specimens. Inspection of the heat-tinted fracture surfaces

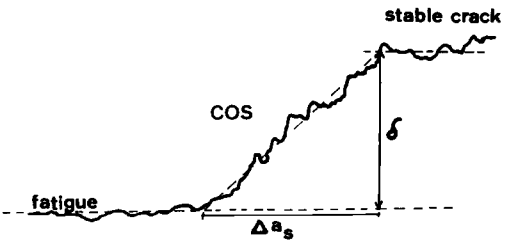

FIG. 2—*Schematic presentation of the stretch zone profile and the dimensions measured with the Perthograph.*

showed crack extension over the full thickness of the specimens (Figs. 3*a* and *b*). For small Δa values the crack extension at the outer surfaces was even about twice as much as at the middle of the specimen (Fig. 3*a*). This is the opposite of the crack-tunneling effect usually observed in pressure vessel steels.

Heat-tinting primarily marked the dimpled fracture; the photographs did not show a separation between stretch zone and ductile crack extension by dimple fracture. An attempt was made to measure the stretch zone, using the high reflectivity of this area. However, this caused overestimation of the stretch zone, as shown in Fig. 4*b*.

Fractographic observations with the scanning electron microscope (SEM) also showed no distinct separation between crack-tip stretch and ductile (dimpled) fracture (Fig. 5). Even the specimen tested to the low J value of 400 kJ $\cdot$ m^{-2} showed a combination of dimples and stretch (Fig. 6).

Comparison of the SEM crack measurements with the heat-tinting data showed a slight underestimation of the crack extension by the latter method. This is attributed to the contribution from the end of the fatigue crack that is also partly stretched and thus included in the SEM measurements.

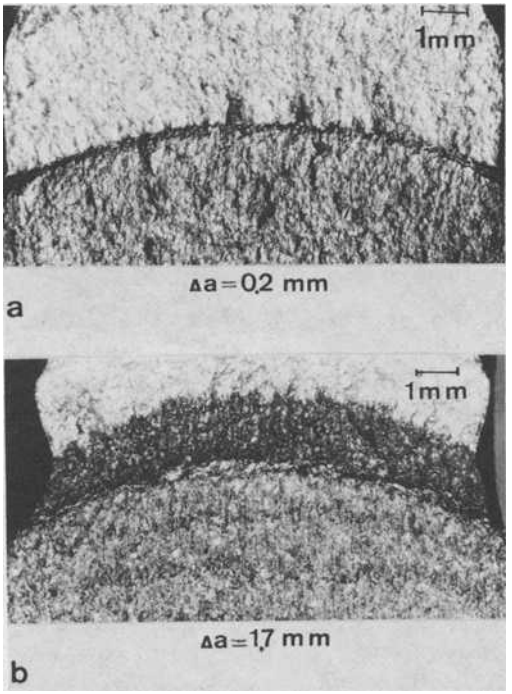

FIG. 3—*Fracture surfaces showing ductile crack extension (dark zone by heat tinting) over the full thickness of the specimens.*

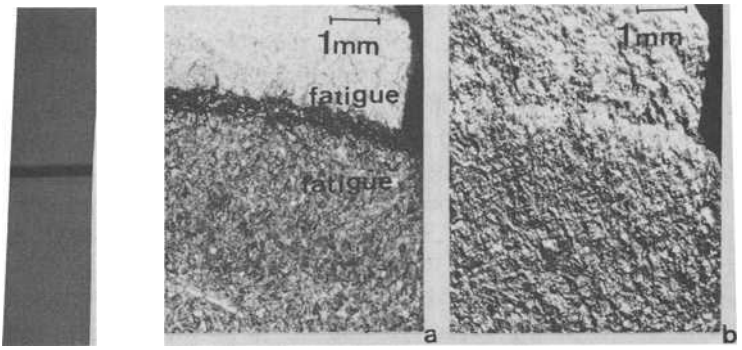

FIG. 4—*Fracture surface as observed with different illuminations of the specimen, showing overestimation of the crack-tip stretch caused by high reflectivity of the stretch zone.*

Single-Specimen Optical

The applicability of this technique was favored by the phenomenon of crack extension over the full thickness of the specimens. The video records showed a continuous process of alternating crack-tip blunting and ductile crack extension. This was observed from the very beginning of the fracture toughness test up to the largest applied crack extension of 3 mm. Pictures of the crack-tip at the beginning and the end of a fracture toughness test, taken from the monitor during replay of the video tape are shown in Figs. 7 and 8, respectively. The crack-tip opening displacement (CTOD) significantly changes, but the crack-tip phenomena remain the same. The Δa values are measured along the fracture surface, thus representing crack extension in the direction of the original fatigue crack, as indicated by the black arrows in Fig. 8*a*.

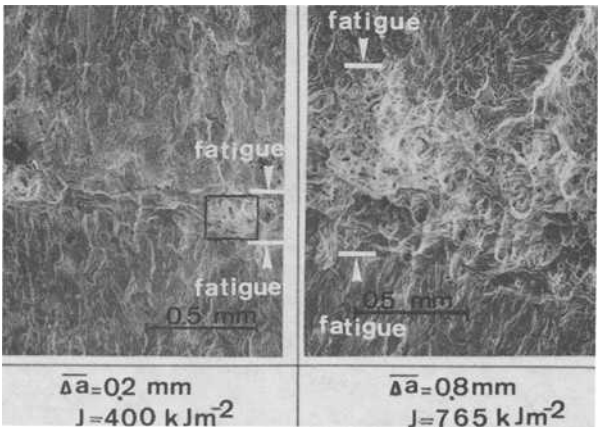

FIG. 5—*Fracture surfaces as observed with SEM showing no distinct separation between stretch zone and ductile crack extension.*

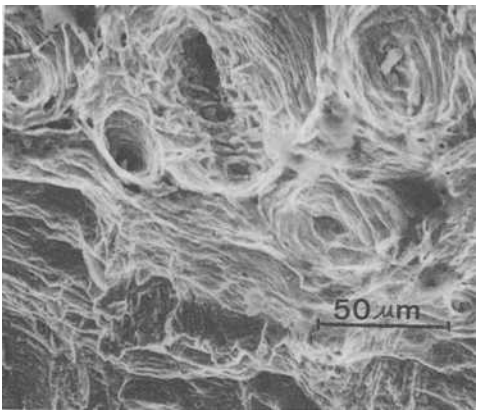

FIG. 6—*Detail of Fig. 5a showing a combination of stretch and dimples for a specimen tested up to* $J = 400\ kJ \cdot m^{-2}$.

Single-Specimen Potential Drop

The PD technique does not discriminate between crack-tip plasticity and crack extension. Proper application of this technique results in a continuously increasing PD signal. A minimum, sometimes interpreted as the moment of crack initiation, was not observed. At low Δa values the PD data overestimate the crack length with more than 15% because of the relatively large contribution from the plasticity. However, at larger Δa values, when macroscopic blunting is completed, the PD data satisfy the 15% criterium of ASTM E 813. In Fig. 9 a plot of the load versus deflection is shown together with the Δa-deflection

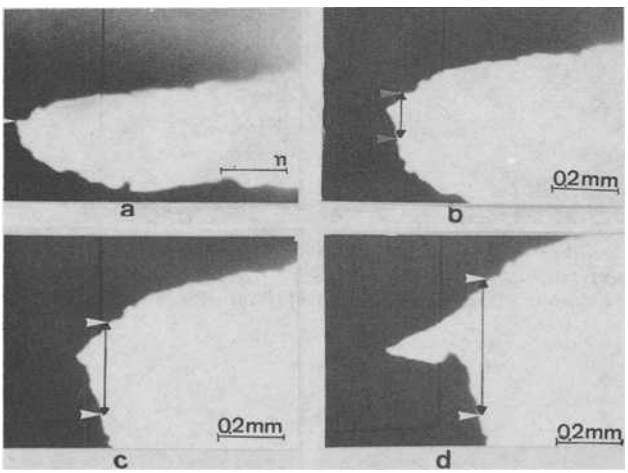

FIG. 7—*Optical observations during the very beginning of a fracture toughness test, showing* (a) *crack opening,* (b) *and* (c) *crack-tip stretching, and* (d) *first crack extension.*

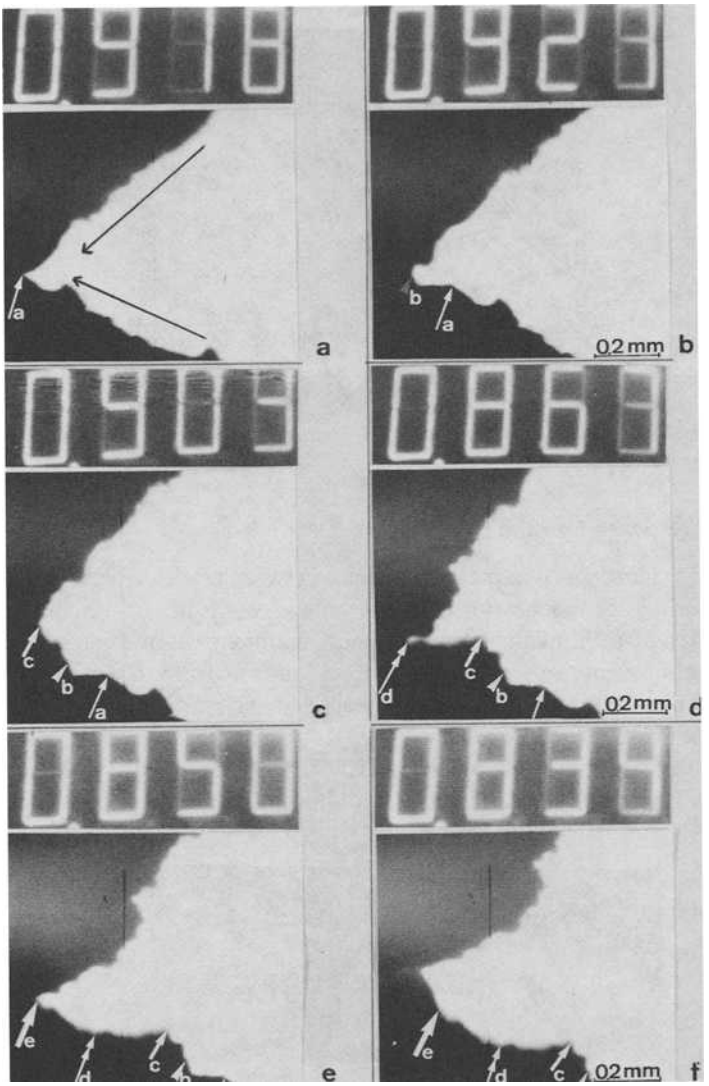

FIG. 8—*Optical observations of the crack tip during the latter stage of a fracture toughness test showing sequences of crack extension and crack-tip stretch. Also shown corresponding load values (MN)* (a) *and* (b) *before* P_{max}, *and* (c), (d), (e), *and* (f) *after* P_{max}.

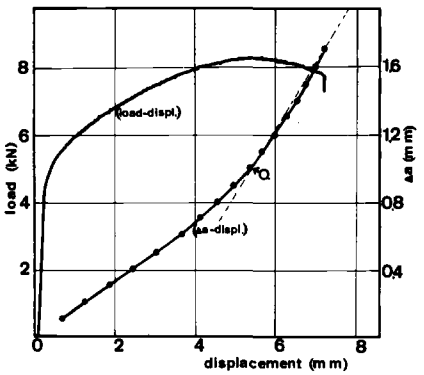

FIG. 9—*Load-deflection diagram with corresponding crack-extension curve showing slope change at Q.*

curve. A significant slope change (indicated by an arrow and the letter Q) can be seen at about 1-mm crack extension.

Stretch Zone Profile Measurements

The irregular profiles of the stretch zone, as recorded with the Perthograph, reflect alternating stretch and dimple fracture. Results of the dimension measurements are plotted in Figs. 10 and 11, showing J-Δa and J-δ plots, respectively. Within the scatter bands, given by the extreme values of the nine measurements on one specimen, the blunting coefficient ranges from $2\sigma_f$ to $4\sigma_f$. Apparent crack growth caused by blunting is best represented by the formula based on the means of the measurements for Fig. 11

$$J = 3.5\sigma_f \tag{3}$$

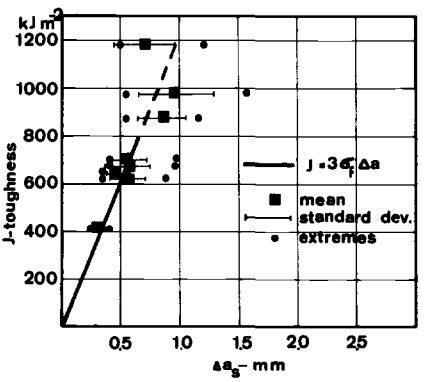

FIG. 10—*Results of stretch zone measurements with the Perthograph showing a blunting coefficient of* $3\sigma_f$.

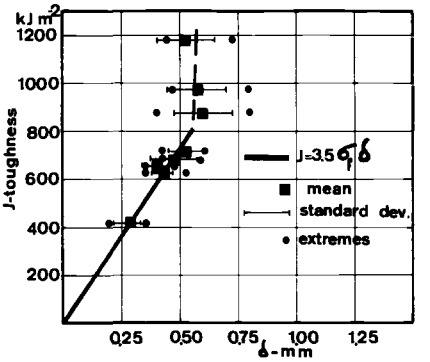

FIG. 11—*Results of stretch zone measurements with the Perthograph showing a blunting coefficient of* $3.5\sigma_f$.

Figure 11 clearly shows a maximum of crack-tip stretch at J of about 800 kJ · m^{-2}. This end of blunting (onset of stable crack growth) is not so significant in Fig. 10 because of additional stretch of the end of the fatigue crack that is included in the Δa measurements.

Crack Growth Resistance Curves

Resistance curves for the three different methods are shown in Figs. 12 through 14. The slopes of the first parts of the curves are different. At larger Δa values the "stable crack growth curves" are nearly the same, and consequently the J_a values are measured at the same value of about 750 kJ · m^{-2}. This "end of blunting" was also indicated by the slope change of the PD versus displacement curve.

The resistance curves are analyzed according to the ASTM E 813 procedure, using blunting coefficients of $4\sigma_f$ in Fig. 12 and 2σ in Figs. 13 and 14. We have drawn the parallel exclusion lines at offset-values of Δa = 0.15 mm and

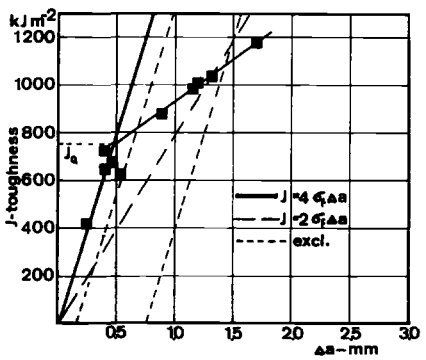

FIG. 12—*Multi-specimen heat tinting* J-Δa *curve.*

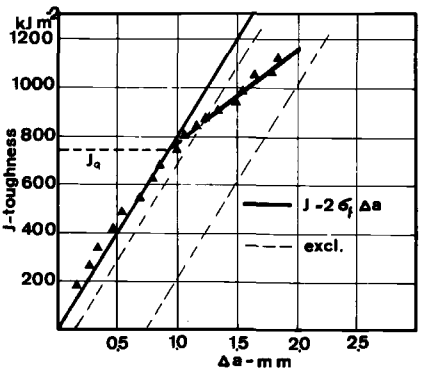

FIG. 13—*Single-specimen optical* J-R *curve.*

Δa = $^{1.5}/_{2}$ mm, the latter being equivalent to about 6% of the original ligament length b_o.

When the single-specimen curves are analyzed with a blunting coefficient of $3.5\sigma_f$, based on the actual measured stretch zone dimensions, many low Δa data fall between the exclusion lines. In that case the extrapolated regression lines intercept the blunting line at J of about 300 kJ · m^{-2}. This value corresponds to the first crack extension on the outer surfaces as measured with the optical technique. From extrapolation of the SEM observations, first dimple formation can be expected at the same J value of 300 kJ · m^{-2}.

Both single-specimen methods overestimate the mean crack extension caused by additional contributions from local phenomena during the early stage of the fracture toughness test. The optical method measures the crack extension at the outer surfaces, which is originally larger than the mean crack extension, and the PD method measures additional crack-tip plasticity (local thickness reduction) during the macroscopical blunting.

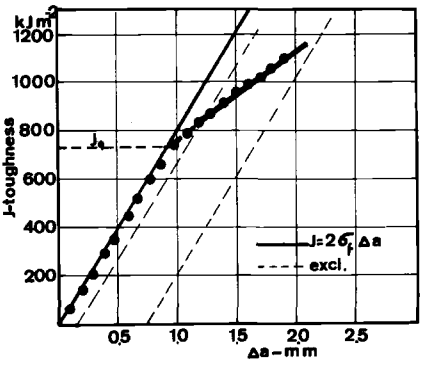

FIG. 14—*Single-specimen potential drop* J-R *curve.*

Summary and Conclusions

A blunting coefficient of $3.5\sigma_f$ is observed from measurements of the actual stretch-zone dimensions. There is no distinct separation between "blunting" and "ductile crack growth;" crack extension is observed to be a continuous process of alternating stretch and ductile dimple fracture.

Initiation (first dimple fracture) is observed at about J_i of 300 $kJ \cdot M^{-2}$. The heat-tinting method slightly underestimates mean crack extension because of the gradual transition of the original crack tip from fatigue crack into stretch zone. The optical and the PD-method overestimate the mean crack extension because of crack extension at the outer surfaces and plasticity effects, respectively.

The "end of blunting" (onset of stable crack growth) J_Q value is consistently measured at about 750 kJ $\cdot$ m^{-2} with the three different methods. The onset of stable crack growth is also indicated by a slope change of the PD displacement curve.

It is concluded that consistent J_Q values can be measured with the three different methods. This J_Q value represents the end of the macroscopic crack-tip blunting. Ductile crack growth in the form of dimple fracture is initiated at lower J values of about 300 kJ $\cdot$ m^{-2}.

References

[1] Vries, M. I. de, "Effects of Temperature and Strain Rate on the Low Cycle Fatigue Properties of Neutron Irradiated Stainless Steel DIN 1.4948," in *Effects of Radiation on Materials: Eleventh Conference, STP 782,* H. R. Brager and J. S. Perrin, Eds., American Society for Testing and Materials, Philadelphia, 1982, pp. 665–689.

[2] deVries, M. I., "Fatigue Crack Growth of Low-Fluence Neutron Irradiated Stainless Steel DIN 1.4948," in *Effects of Radiation on Materials: Eleventh Conference, STP 782,* H. R. Brager and J. S. Perrin, Eds., American Society for Testing and Materials, Philadelphia, 1982, pp. 720–734.

[3] Schaaf, B. van der, "Low Dose Irradiation Effects on Heat-to-Heat Variation of Type 304 Stainless Steel Creep and Tensile Properties," *Effects of Radiation on Materials: Eleventh Conference, STP 782,* H. R. Brager and J. S. Perrin, Eds., American Society for Testing and Materials, Philadelphia, 1982, pp. 597–618.

[4] Tjoa, G. L., Broek, F. P. van der, and Schaap, B. A. J., "Automated Test Methods for Fatigue Crack Growth and Fracture Toughness Tests on Irradiated Stainless Steels at High Temperatures," *Automated Test Methods for Fracture and Fatigue Crack Growth, STP 877,* American Society for Testing and Materials, Philadelphia, 1985.

[5] Ernst, H. A., Paris, P. C., and Landes, J. D., "Estimations on J-Integral and Tearing Modulus T from a Single Specimen Test Record," *Fracture Mechanics: Thirteenth Conference, STP 743,* Richard Roberts, Ed., American Society for Testing and Materials, Philadelphia, 1981, pp. 476–502.

[6] Bamford, W. H. and Bush, A. J., "Fracture Behavior of Stainless Steel," *Elastic-Plastic Fracture, STP 668,* J. D. Landes, J. A. Begley, and G. A. Clarke, Eds., American Society for Testing and Materials, Philadelphia, 1979, pp. 553–577.

[7] Dufresne, J., Henry, B., and Larsson, H., "Fracture Toughness of Irradiated AISI 304 and 316L Stainless Steels," *Effects of Radiation on Structural Materials, STP 683,* J. A. Sprague and D. Kramer, Eds., American Society for Testing and Materials, Philadelphia, 1979, pp. 511–528.

[8] Tobler, R. L., Read, D. T., and Reed, R. P., "Strength/Toughness Relationship for Interstitially Strengthened AISI 304 Stainless Steels at 4 K Temperature," *Fracture Mechanics,*

Thirteenth Conference, STP 743, Richard Roberts, Ed., American Society for Testing and Materials, Philadelphia, 1981, pp. 250–268.

[*9*] Janssen, G. T. M., Eikoff, J. van der, and Rongen, H. J. M. van, "Prediction of Ductile Crack Growth in the Austenitic Steel WN 1.4948 at Ambient and Elevated Temperature," *Transactions of the 6th International Conference on Structural Mechanics in Reactor Technology,* Vol. L, Paper L 5/2, Paris, 17–21 August, 1981.

[*10*] Balladon, P., "*J-R* Curves of Austenitic Stainless Steels—Comparison of Unloading Compliance and Interrupted Test Methods," *Ductile Fracture Test Methods, Proceeding of a CSNI Workshop, Paris, 1–3 December 1982,* Frank Loss and Peter Oliver, Eds., OECD Nuclear Energy Agency, Paris, 1983.

A. R. Rosenfield[1] *and D. K. Shetty*[1]

Cleavage Fracture of Steel in the Ductile-Brittle Transition Region

REFERENCE: Rosenfield, A. R. and Shetty, D. K., **"Cleavage Fracture of Steel in the Ductile-Brittle Transition Region,"** *Elastic-Plastic Fracture Test Methods: The User's Experience, ASTM STP 856*, E. T. Wessel and F. J. Loss, Eds., American Society for Testing and Materials, 1985, pp. 196–209.

ABSTRACT: Fracture-toughness experiments on ASTM A508 (Unified Numbering System [UNS] K13502) steel within the ductile-brittle transition region are a combination of both ductile and brittle behaviors, leading to severe data scatter. Both crack blunting and dimpled rupture are terminated by unstable cleavage. At a lower test temperature, cleavage during blunting predominates, whereas at a higher test temperature, cleavage tends to occur after some stable crack growth. It is suggested that this behavior results from the existence of a distribution of "trigger" sites in the microstructure (for example, inclusions and carbides). Methods for eliminating the dimpled-rupture contribution to the test record are discussed and are shown to be useful for predicting large-specimen behavior.

KEY WORDS: steels, ductile brittle transition, cleavage. fracture toughness, microstructural effects, data scatter, cleavage fracture

Nomenclature

- G_R Elastic component of J_R
- J_{Ic} Path-independent integral
- J_R Value of path-independent integral after some stable crack growth. J_R values reported in this paper are those calculated at the onset of cleavage.
- K Stress intensity
- K_{Ic} Plane strain fracture toughness
- K_Q Toughness associated with crack initiation
- N Ramberg-Osgood work-hardening exponent
- X_o Separation of cleavage-initiating particle and crack tip
- λ Separation of cleavage initiating particle and fatigue precrack
- σ_f^* Critical normal cleavage fracture stress
- σ_y Yield strength
- 1T Compact specimen size (ASTM Test for J_{Ic}, a Measure of Fracture Toughness)

[1]Research leader and principal research scientist, respectively, Physical Metallurgy Section, Battelle-Columbus, Columbus, OH 43201.

Introduction

This paper is concerned with problems encountered in measuring the fracture toughness of steel in the ductile-brittle transition range. We mainly discuss situations where the load/displacement curve departs significantly from linearity, but where stable crack growth is interrupted by a cleavage instability before the second exclusion line (for example, Fig. 1). Under these circumstances, neither K_{Ic} nor J_{Ic} can be measured by standard ASTM procedures. A second factor, which compounds the problem, is the large scatter in K_{Ic} that is often reported within the transition region [*1–3*].

Serious difficulties arise from these observations; the origin of the scatter needs to be explained and lower-bound toughness for use in a safety analysis needs to be specified. This paper focuses on a phenomenological description of crack initiation within the transition region. The data are discussed within the framework of current understanding of the transition, particularly the question of the microstructural mechanisms of cleavage failure.

Micromechanism of Cleavage

The idea that local plastic deformation is a necessary condition for cleavage failure of steel dates back at least to Low [*4*] who showed that the cleavage strengths of unnotched specimens in tension are equal to their yield strengths in compression. McMahon and Cohen [*5*] then observed that the critical event leading to cleavage is the slip-induced fracture of brittle second-phase particles. This event is the basis of the micromodel of Smith [*6*], which stated the fracture

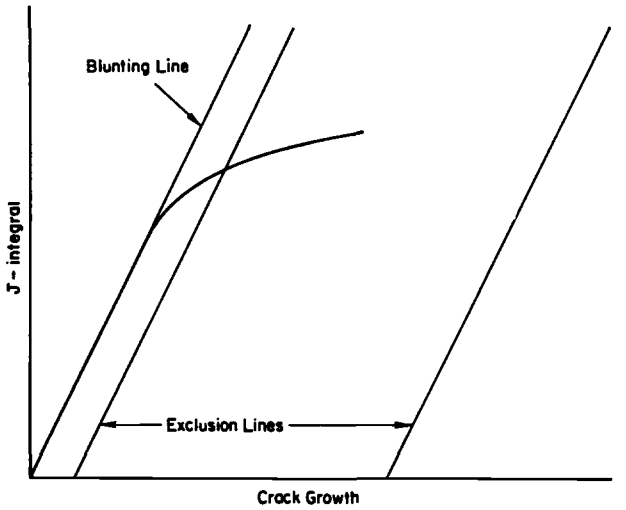

FIG. 1—*Schematic J_R curve. Terminology of ASTM E 813 is used.*

criterion in terms of microstructural dimensions, the yield strength, and a critical normal stress σ_f^*. A number of authors, most recently Curry [7], have measured σ_f^* by finding where yielding and cleavage are coincident in the bending of notched bars. It is now generally agreed that σ_f^* is approximately temperature-independent but is strongly affected by microstructure [8].

This line of research culminated in the theory of Ritchie et al [9] (generally called RKR). They hypothesized that K_{Ic} corresponds to the stress intensity at which the maximum tensile stress reaches σ_f^* at a critical distance ahead of the crack X_o. In the context of the earlier research, discussed above, X_o is the location of the particle whose slip-induced cracking triggers unstable cleavage fracture. RKR arbitrarily set X_o equal to two ferrite grain diameters, and this value seems to be roughly correct for a low-alloy quenched-and-tempered steel [10]. However, when applying the RKR equation to their data on mild steel, Curry and Knott [11] concluded that X_o was independent of grain size, except for the largest grain size studied. This finding, of course, does not invalidate the basic premise of RKR, particularly the idea that cleavage instability occurs by the linkage to the dominant crack to a microcrack ahead of it.

There appear to be very few direct measurements of X_o. One exception is our earlier fractographic research on a low-alloy quenched-and-tempered steel [12,13]. Although the number of specimens was limited, the cleavage origin invariably was located ahead of the fatigue precrack, in agreement with RKR. There were two other observations of interest:

1. The value of X_o was not constant, but varied widely among nominally identical specimens. There was also some indication that X_o increased with increasing temperature [13].
2. Under the testing conditions used, some stable crack growth, via the dimpled-rupture mechanism, occurred before final cleavage instability [12,13].

Other direct evidence bearing on cleavage initiation is due to Khan et al [14] who used more highly alloyed steels. By a combination of acoustic emission and fractography, they also detected the formation of a number of stable cleavage microcracks before final instability. Note that they were working at a temperature where dimpled rupture did not occur before cleavage.

Probabilistic Theories

Our evidence that X_o is a broadly scattered quantity [13] suggests that cleavage-crack extension must be treated as a probabilistic phenomenon. The extreme scatter in K_{Ic} [1–3] reinforces this argument.

Probabilistic theories of cleavage fracture can be evaluated using the experimental result [15–17]

$$K_{Ic}\,\sigma_y^{\alpha} = \text{constant} \tag{1}$$

where K_{Ic} is the mean fracture toughness and σ_y is the yield strength at the temperature and loading rate of interest; α is discussed below. In the model of Hahn et al [*15*], it was argued that the mechanism associated with Eq 1 is the generation of a critical density of ferrite or carbide microcracks within the crack-tip plastic zone, and that the form of the equation is consistent with Weibull weakest link statistics.

Pineau [*17*] later reported an analysis in which Weibull's expression for survival probability was combined with an elastic-plastic stress distribution. Equation 1 resulted from his analysis, with α being related to the Weibull shape factor m. Evans [*18*] combined the same elements into a somewhat different analysis. His result also can be put into the form of Eq 1, with α being a function of the Ramberg-Osgood work-hardening exponent N.

Another statistical model, that of Curry and Knott [*19,20*], is based on a deduction that the cleavage-initiating carbide particles in spheroidized steels are in the upper fifth percentile of the size distribution. The particle-size distribution enters explicitly into Wallin's [*21*] model, which reduces to Eq 1.

Lower-Bound Toughness Estimates

The experiments reported in this paper were undertaken as part of a program to determine "lower-bound" toughnesses of reactor pressure-vessel steels. The specific motivation was to obtain small-specimen K_{Ic} values to match those of very large cylinders ($\sim$1.0 m outside diameter [OD], 150 mm wall thickness, and 1.2 m height) that had undergone severe thermal shock [*22*]. Typically, small-specimen data are extremely scattered, with a factor of two spread in apparent K_{Ic} values not unusual [*1–3,21–23*]. Furthermore the cylinder data are at the lower end of the small-specimen scatter band [*22*]. Two semiempirical remedies to this problem have been somewhat successful:

1. Calculating a value of K_{Ic} for the small specimen from the instability load and crack length by using an elastic K solution [*12,13*]. This procedure is based on the assumption that only the elastic energy stored in a specimen is available to drive a cleavage crack.
2. Essentially subtracting the effective-plastic-zone size from the crack length [*24*]. This procedure was developed to account for the loss of constraint in thin specimens.

The data reported in this paper are examined in light of both of these corrections.

Procedure

Compact specimens of lT dimensions with 25% side grooves were machined from ASTM A508 (Unified Numbering System [UNI] K13502) steel used in the Oak Ridge National Laboratory (ORNL) experiment TSE-6 [*22*] and were loaded monotonically to failure. Six specimens were tested under nominally identical

conditions to provide a means for estimating the data scatter. Tests were done at room temperature and at 82 or 83°C. The displacement rate at the load points was either 550 or 760 mm/s. These high rates were used to promote "lower-bound" behavior by exploiting the negative slope of the toughness/loading rate curve [*23,25*]. If the load/displacement curves were perfectly linear, the failure times would be on the order of 10^{-3} s for K_{Ic} values of 100 MPa·m$^{1/2}$. Because nonlinearities developed caused by plasticity and, in some cases, stable crack growth, actual failure times were in the range from 2.5×10^{-3} to 12×10^{-3} s. One of the specimens failed just as the load/displacement curve reached zero slope, whereas the others failed while the load was rising. Previous unloading-compliance measurements [*12*] on a similar steel showed that when stable crack growth occurs it proceeds by the dimpled-rupture mechanism and that instability is associated with conversion to cleavage fracture. In the present experiments, only the load, the displacement to instability, and the length of dimpled rupture on the fracture surface were measured. The value of J at instability was calculated from the relations in ASTM Test for J_{Ic}, a Measure of Fracture Toughness (E 813), and is denoted J_R. Estimates of the elastic component of J_R, denoted G_R, were obtained using the methods mentioned earlier [*12,24*]. All specimens were examined fractographically using the scanning electron microscope in order to measure X_o for each specimen. These results have been reported separately [*26*] and will be summarized below.

Results

The toughness data are given in Table 1. The amount of stable crack growth before conversion to cleavage was significantly different for the two test temperatures. The room-temperature data exhibited what might be characterized as lower-transition behavior, in that no crack extension by the dimpled-rupture mechanism was visible to the naked eye, while the high-temperature data reflected stable crack growth. At each temperature, there was one exception to this general behavior.

Lower-Transition Behavior

As is seen in Table 1, all but one of the room-temperature specimens failed during blunting. The specimen that exhibited a very small amount of stable crack growth also had by far the highest toughness. Even considering only the remaining specimens, there still was considerable scatter in the data. However the lowest toughness values were on the order of those observed for the large, thermally shocked ORNL cylinders [*22*], which is indicated by the scatter band in Fig. 2. From the viewpoint of using small-scale tests to predict large-scale behavior, this result is encouraging.

In Ref *26*, fractographic examination was used to locate the microstructural features associated with cleavage instability for the specimens listed in Table 1. Tear ridges and river markings were used to trace the fracture path back to its

TABLE 1—*Small-specimen crack-initiation data for steel from ORNL Experiment TSE6.*

Specimen	Test Temperature, °C	Loading Rate, mm/s	Stable Crack Growth, mm	Crack-Growth Resistance, MJ/m²		
				J_R	G_R[a]	G_R[b]
90-2	22	760	0.05	0.140	0.071	0.099
86-1	22	760	0	0.032	0.028	0.020
101	21	550	0	0.077	0.051	0.051
102	21	550	0	0.046	0.037	0.025
103	21	550	0	0.058	0.043	0.021
104	21	550	0	0.031	0.027	0.014
90-1	83	760	0.6 to 0.7	0.330	0.104	0.133
105	82	550	0.7	0.372	0.111	0.119
106	82	550	0.8	0.372	0.111	0.124
107	82	550	0.3	0.239	0.091	0.122
108	82	550	0	0.074	0.051	0.039
109	82	550	0.08	0.204	0.085	0.074

[a]Estimated using the Merkle method [*24*].
[b]Estimated using the Seidle method [*12,13*].

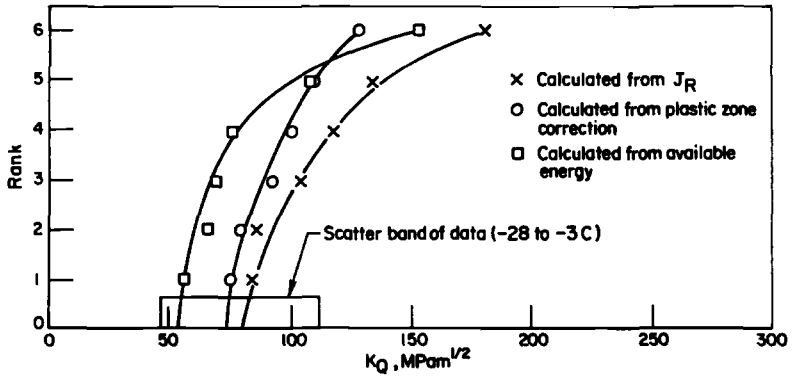

FIG. 2—*Cumulative distribution of high-rate crack-initiation data at 22°C (TSE6 steel, 1T specimens). Scatter band covers ORNL thermal-shock data.*

origins. Both grain-boundary carbides and manganese sulfide inclusions were thus located. Additional grain-boundary origins were found for which no second-phase particle was observed. In the room-temperature series, low values of toughness were associated with origins located at the tip of the stretch zone [*26*]. In these same experiments, intermediate toughnesses were associated with apparent multiple origins, all but one of which were located ahead of the stretch zone. As was noted above, the highest toughness corresponded to a specimen in which some stable crack growth occurred. In addition, the cleavage origin in that specimen was some distance ahead of the ductile crack. Fractography could not determine, however, if the manganese sulfide inclusions initiate cleavage cracks in ferrite grains by the same mechanism as do the grain-boundary carbides, that is, slip-induced microcracking in the carbide followed by unstable extension of the microcracks into the adjacent ferrite grains. The manganese sulfide inclusion shown in Fig. 3*b*, for example, did not show clear evidence of microcracking.

Upper-Transition Behavior

Figure 4 is a plot of the higher temperature toughness data of Table 1. The points on the J_R curve are the values of J at which stable crack growth became unstable. Thus, the curve labelled J_R is similar to a standard multispecimen crack-growth-resistance curve, the difference being that the fractographic measurement of crack growth excludes the blunting component. For this reason, exclusion lines on Fig. 4 would be vertical. Note that the J_R curve intersects the ordinate axis well above the data point for the specimen with no stable crack growth. A similar observation has been reported by Lott [*27*], who found that cleavage can occur either on the blunting line or on the stable-growth part of the J_R curve. More seriously, the present data with stable crack growth significantly overestimate the large-specimen result [*22*].

Figure 4 also shows values of G_R, the estimated elastic component of J_R. The

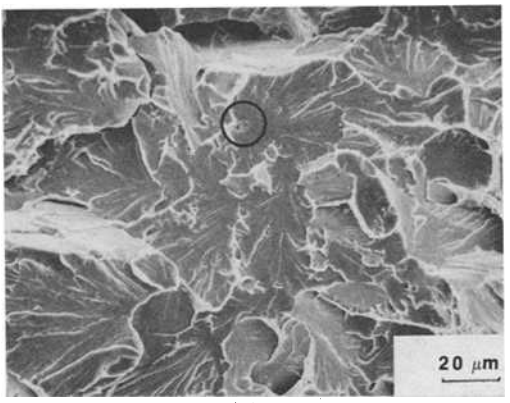

(a)

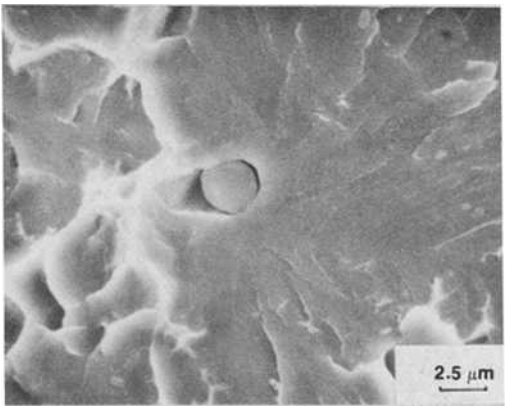

(b)

FIG. 3—*Coplanar cleavage facets at Cleavage Origin A in* (a) *Specimen 90-1 and* (b) *cleavage-initiating manganese sulfide inclusion.*

G_R curve is much flatter than the J_R curve and does extrapolate back much closer to the large-specimen toughness value.

The most important point about Fig. 3 is that it indicates the existence of two values of fracture toughness for this steel when tested in the transition regime: a J_{Ic} level associated with dimpled rupture and a lower level of J_{Ic} associated with cleavage. The engineering value of J_{Ic} should be that associated with cleavage. However, the scatter in this quantity complicates its measurement and may lead to the erroneous conclusion that the higher dimpled-rupture value is the appropriate one. To understand this point, consider how these data would be analyzed in the absence of Specimen 108 (J_R value of 0.074 and zero stable crack growth). If that specimen had not been tested, the multiple-specimen J_R curve of Fig. 3 could have been extrapolated to 0.16 MJ/m^2, which would be considered a J_{Ic} value consistent with ASTM E 813. However, this ductile-

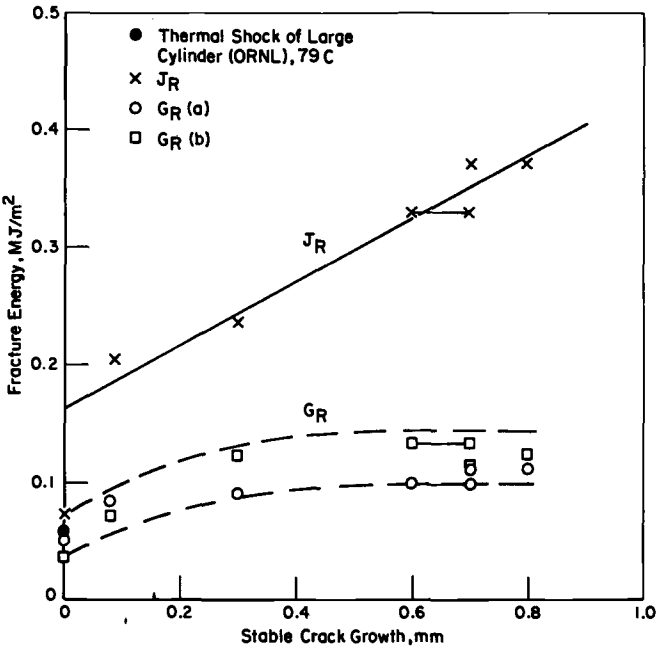

FIG. 4—*Crack-Growth-Resistance curves at 82 to 83°C. The elastic component of J was estimated using* (a) *the plastic zone correction and* (b) *the available energy method.*

rupture J_{Ic} value lies considerably above the large-specimen cleavage value. In effect, the small-specimen data excluding Specimen 108 are not representative of large-specimen behavior because of the difference in failure mechanisms at the onset of crack growth.

Figure 5 relates the toughness and fracture appearance of the higher temperature specimens. In the figure, the abscissa is the amount of stable crack growth, and the ordinate is the distance that the cleavage origin was ahead of the stable crack. The numbers within the data points are the associated fracture-toughness values expressed as K_R in MPa·m$^{1/2}$. One specimen (K_R = 276 MPa·m$^{1/2}$) exhibited two origins, both of which are plotted, while two other specimens had identical K_R values of 293 MPa·m$^{1/2}$. There appears to be a clear linear relation between crack growth and origin location ($X_o \approx 5/4\ \Delta a$). If we define $\lambda = \Delta a + X_o$ as the distance between the fatigue precrack and the cleavage origin, $\Delta a \approx 4/9\ \lambda$. Thus, the amount of stable crack growth is slightly less than half of the precrack/origin separation. The physical reason underlying this observation is not clear. A monotonic relation between Δa and X_o is intuitively expected from the general concept of statistical sampling of "weak spots" by the stress field of the stable crack. It is not obvious, however, that this relation should be linear. Examination of the figure also reinforces the result of Fig. 2 that a large increase in toughness is associated with modest separations of 100 to 200 μm.

Figure 6 shows the fracture surface of Specimen 90-1. At least two cleavage

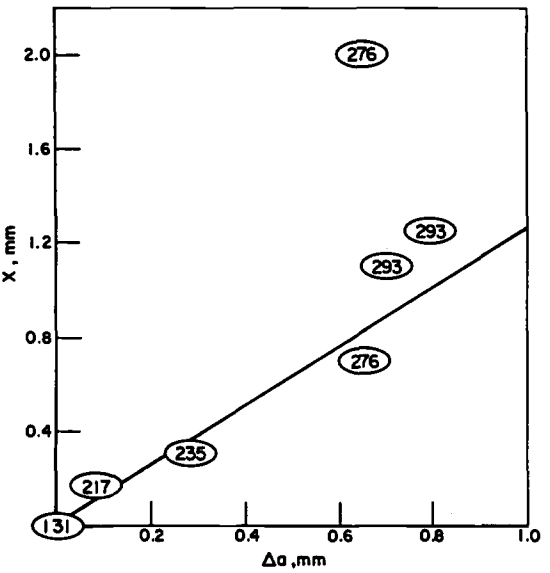

FIG. 5—*Relation between the amount of stable crack growth and the location of the microstructural feature that triggered cleavage. The numbers in the data points are the stress-intensity values at the onset of cleavage fracture calculated from* J_R. *Test temperature = 82 to 83°C.*

origins could be located in that specimen, and those locations are outlined by the circles in Fig. 5. Closer examination of the cleavage-origin locations showed that manganese sulfide inclusions triggered the cleavage fracture. Figure 6 shows the manganese sulfide inclusion found at Origin Site A. Energy-dispersive X-ray analysis performed on the inclusion confirmed that it was manganese sulfide.

Discussion

Both the lower and higher temperature data indicate that cleavage fracture in ASTM A508 steel needs to be analyzed in statistical terms. The reason appears to be that microstructural sites that can trigger unstable cleavage are relatively widely spaced. At the higher temperature investigated here, the sites were sufficiently widely spaced that some stable crack extension had to occur before such a site could be activated. Milne and Curry [*25*] suggest that cleavage after stable crack growth occurs when the temperature is raised and the yield strength is decreased; because the maximum tensile stress ahead of the crack is some small multiple of the yield strength, it becomes increasingly more difficult to reach σ_f^* at higher temperatures. Conversely, at lower temperatures, values of σ_f^* are reached more readily.

The new results in this paper are consistent with the idea that there is a distribution of σ_f^* values within the steel. For example, a low value of σ_f^* would be associated with an unusually large particle or a large ferrite grain favorably

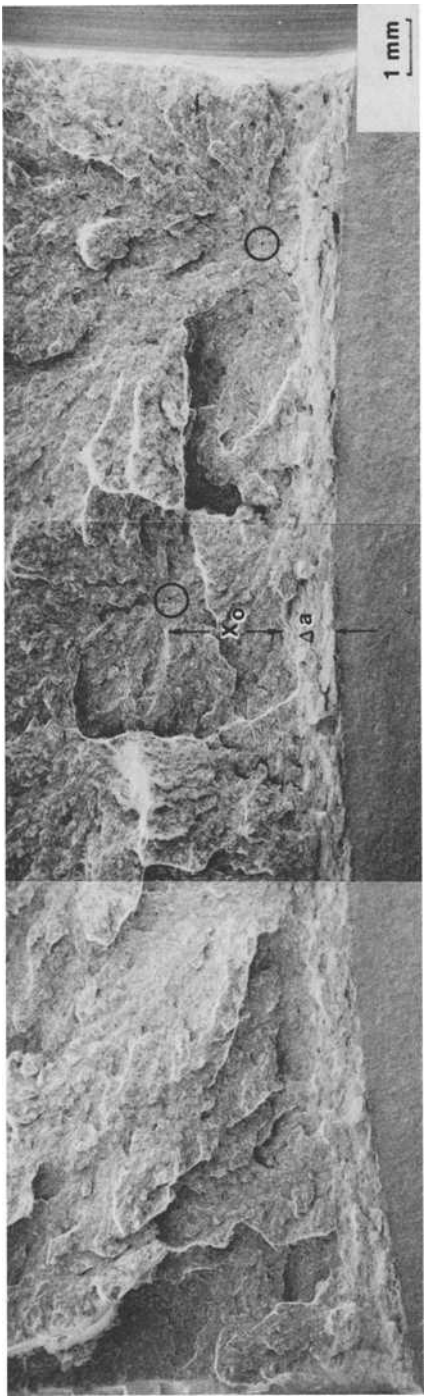

FIG. 6—*Fracture surface of 1T compact Specimen 90-1. Circles outline two independent cleavage origins. Note the definitions of* X_o *and* Δa.

oriented for cleavage with respect to the imposed stress system or both. Thus, the steel microstructure can be viewed as a collection of Weibull weak spots that are sampled by the stress field of the main crack. At low temperatures, the sampling is efficient because of the high local values of hydrostatic stresses, cleavage failure is triggered readily, and the value of K_{Ic} is low. At higher temperatures, the local hydrostatic stresses are not so high, the sampling is less efficient, and cleavage-crack initiation is relatively difficult. Several quantitative models consistent with this picture have been reported recently [*18,28,29*].

The view that the scatter in K_{Ic} in the transition region reflects a weak-spot distribution was introduced by Landes and Shaffer [*1*]. They noted that both the mean and the scatter in K_{Ic} decreased with increasing specimen size. This is consistent with the Weibull theory, inasmuch as large specimens are expected to contain more weak spots than do small specimens. Microstructural studies [*19,21*] link these weak spots to the upper tail of the particle-size distribution. The comparisons between large cylinders and lT specimens in Fig. 2 and, especially, Fig. 6 reinforce this view.

Finally, there is a question of specifying K_{Ic} for cleavage failure after stable crack growth. Several authors [*23,30*] argue that the level of K_I has to be increased through stable crack growth to reach a level high enough to trigger cleavage. Accordingly, they view the instability point on the J_R curve as equal to J_{Ic} for cleavage. The problem with this argument is that it suggests that J_{Ic} (or K_{Ic}) for cleavage is higher than J_{Ic} for dimpled rupture, which seems unlikely on thermodynamic grounds [*13*]. The present authors have taken the view that the value of J_R at which cleavage is triggered is more than sufficient to activate the local weak spot in question. The data presented here and earlier [*12,13*] as well as Merkle's analysis [*24*], suggest that the K_{Ic} value just sufficient to trigger cleavage is obtained through factoring out the plasticity contribution from the load/displacement curve [*12,24*]. Although the theoretical basis for these corrections is not strong, they do seem to provide a practical means for estimating structural behavior using reasonably few small-size specimens.

Conclusions

Measurement of K_{Ic} in the ductile/brittle transition region of steel is complicated by the differing nature of the two micromechanisms involved. Results presented here, and in earlier papers, suggest that cleavage fracture requires the formation of microcracks at special sites and their subsequent propagation. The activation strengths of these sites appear to have a broad distribution, and they appear to be scattered throughout the microstructure. In accord with statistical fracture theory, the toughnesses of large specimens lies at the lower end of the range of toughnesses of small specimens. Detailed fractographic studies combined with factoring-out complications caused by the intervention of dimpled rupture can aid in overcoming the problem of predicting large-specimen behavior from small-specimen data.

Acknowledgments

This research is being supported by the Heavy Section Steel Technology Program under Union Carbide Corporation-Nuclear Division, (UCC-ND) Subcontract 85X-17624C. The authors are grateful to C. E. Pugh and G. D. Whitman (ORNL) and to M. Vagins (Nuclear Research Commission) for their continuing advice and encouragement. Expert experimental assistance was provided by P. N. Mincer.

References

[1] Landes, J. and Shaffer, D. H., "Statistical Characterization of Fracture in the Transition Region," *Fracture Mechanics: Proceedings of the Twelfth National Symposium on Fracture Mechanics, STP 700*, American Society for Testing and Materials, Philadelphia, 1980, pp. 368–382.

[2] Andrews, W. R., Kumar, V., and Little, M. M., "Small-Specimen Brittle-Fracture Toughness Testing," *Fracture Mechanics: Proceedings of the Thirteenth National Symposium on Fracture Mechanics, STP 743*, American Society for Testing and Materials, Philadelphia, 1981, pp. 576–598.

[3] Iwadate, T., Tanaka, Y., Ono, S.-I., and Watanabe, J., "An Analysis of Elastic-Plastic Fracture Toughness Behavior for J_{Ic} Measurement in the Transition Region," *Elastic-Plastic Fracture: Second Symposium, Volume II Fracture Resistance Curves and Engineering Applications, STP 803*, American Society for Testing and Materials, Philadelphia, 1983, pp. II-531–II-561.

[4] Low, J. R., Jr., "The Fracture of Metals," *Progress in Material Science*, Vol. 12, 1963, pp. 1–96.

[5] McMahon, C. J., Jr. and Cohen, M., "The Fracture of Polycrystalline Iron," *Proceedings of the Ist International Conference on Fracture*, Vol. 2, The Japanese Society for Strength and Fracture of Materials, Sendai, Japan, 1965, pp. 779–812.

[6] Smith, E., "The Nucleation and Growth of Cleavage Microcracks in Mild Steel," *Physical Basis of Yield and Fracture*, Institute of Physics and Physical Society, London, 1966, p. 36.

[7] Curry, D. A., "Influence of Hydrostatic Tension on Cleavage Fracture of Bainitic Pressure Vessel Steel," *Metal Science*, Vol. 16, 1982, pp. 435–440.

[8] Curry, D. A., "Cleavage Micromechanisms of Crack Extension in Steels," *Metal Science*, Vol. 14, 1980, pp. 319–326.

[9] Ritchie, R. O., Knott, J. F., and Rice, J. R., "On the Relationship Between Critical Tensile Stress and Fracture Toughness in Mild Steel," *Journal of the Mechanics and Physics of Solids*, Vol. 21, 1973, pp. 395–410.

[10] Ritchie, R. O., Server, W. L., and Wullaert, R. A., "Critical Fracture Stress and Fracture Strain Models for the Prediction of Lower and Upper Shelf Toughness in Nuclear Pressure Vessel Steels," *Metallurgical Transactions*, Vol. 10A, 1979, pp. 1557–1570.

[11] Curry, D. A. and Knott, J. F., "The Relationship Between Fracture Toughness and Microstructure in the Cleavage Fracture of Mild Steel," *Metal Science*, Vol. 10, 1976, pp. 1–6.

[12] Rosenfield, A. R. and Shetty, D. K., "Lower-Bound Fracture Toughness of a Reactor-Pressure-Vessel Steel," *Engineering Fracture Mechanics*, Vol. 14, 1981, pp. 833–842.

[13] Rosenfield, A. R. and Shetty, D. K., "Cleavage Fracture of Steel in the Upper Ductile-Brittle Transition Region," *Engineering Fracture Mechanics*, Vol. 17, 1983, pp. 461–470.

[14] Khan, M. A., Shoji, T., and Takahashi, H., "Acoustic Emission from Cleavage Microcracking in Alloy Steels," *Metal Science*, Vol. 16, 1982, pp. 118–126.

[15] Hahn, G. T., Hoagland, R. G., and Rosenfield, A. R., "Variation of K_{Ic} with Temperature and Loading Rate," *Metallurgical Transactions*, Vol. 2, 1971, pp. 537–541.

[16] Kotilainen, H., "Temperature Dependence of the Fracture Toughness and the Cleavage Fracture Strength of a Pressure Vessel Steel," *Fracture Mechanics: Proceedings of the Twelfth National Symposium on Fracture Mechanics, STP 700*, American Society of Testing and Materials, Philadelphia, 1980, pp. 352–367.

[17] Pineau, A., "Review of Fracture Micromechanisms and a Local Approach to Predicting Crack

Resistance in Low Strength Steels," *Advances in Fracture Research*, Vol. 2, D. Francois, Ed., Pergamon, Oxford, 1981, pp. 553–577.

[*18*] Evans, A. G., "Statistical Aspects of Cleavage Fracture in Steel," *Metallurgical Transactions*, Vol. 14*A*, 1983, pp. 1349–1355.

[*19*] Curry, D. A. and Knott, J. F., "Effects of Microstructure on Cleavage Fracture Stress in Steel," *Metal Science*, Vol. 12, 1978, pp. 511–514.

[*20*] Curry, D. A., "Comparison Between Two Models of Cleavage Fracture," *Metal Science*, Vol. 14, 1980, pp. 78–80.

[*21*] Wallin, K., Saario, T., and Torronen, K., "A Statistical Model for Carbide-Induced Brittle Fracture in Steel," *Metal Science*, Vol. 18, 1984, pp. 13–16.

[*22*] Cheverton, R. D., Canonico, D. A., Iskander, S. K., Bolt, S. E., Holz, P. P., Nanstad, R. K., and Stelzman, W. J., "Fracture Mechanics Data Deduced from Thermal Shock and Related Experiments with LWR Pressure Vessel Material," *Transactions of the American Society of Mechanical Engineers, Journal Pressure Vessel Technology*, Vol. 105, 1983, pp. 102–110.

[*23*] Milne, I. and Curry, D. A., "Ductile Crack Growth Analysis Within the Ductile-Brittle Transition Regime: Predicting the Permissible Extent of Ductile Crack Growth," Central Electricity Generating Board Report RD/L/2209N81, Leatherhead, Surry, United Kingdom, 1982.

[*24*] Merkle, J. G., "An Approximate Method of Elastic-Plastic Fracture Analysis for Nozzle Corner Cracks," *Elastic-Plastic Fracture, STP 668*, American Society for Testing and Materials, Philadelphia, 1979, pp. 674–702.

[*25*] Crosley, P. B. and Ripling, E. J.,"Plane Strain Crack Arrest Characterization of Steels," *Transactions of the American Society of Mechanical Engineers*, Vol. 97J, 1975, pp. 291–298.

[*26*] Rosenfield, A. R., Shetty, D. K., and Skidmore, A. J., "Fractographic Observation of Cleavage Initiation in the Ductile-Brittle Transition Region of a Reactor-Pressure-Vessel Steel," *Metallurgical Transactions A*, Vol. 14A, 1983, pp. 1934–1937.

[*27*] Lott, R. G., Shogan, R., Marshall, C. W., Mincer, P. N., Landow, M. P., and Rosenfield, A. R., "Unirradiated Testing," Section 3.1 of Semiannual Progress Report No. 6 to Electric Power Research Institute, "Development of a Crack-Arrest-Toughness Data Bank for Irradiated RPV Materials," by T. W. Mager and C. W. Marschall, Palo Alto, CA, March 1982.

[*28*] Beremin, F. M., "A Local Criterion for Cleavage Fracture of a Nuclear Pressure Vessel Steel," *Metallurgical Transactions A*, Vol. 14A, 1983, pp. 2277–2287.

[*29*] Wallin, K., "The Scatter in K_{Ic}-Results," *Engineering Fracture Mechanics, Fracture Mechanics: Fifteenth Symposium, STP 833*, American Society for Testing and Materials, Philadelphia, 1984, pp. 378–392.

[*30*] Landes, J. D. and McCabe, D. E., "Effect of Section Size on the Transition Temperature Behavior of Structural Steels," Vol. 19, 1984, pp. 1085–1093.

Ted L. Anderson,[1] *Harry I. McHenry,*[2] *and Michael G. Dawes*[1]

Elastic-Plastic Fracture Toughness Tests with Single-Edge Notched Bend Specimens

REFERENCE: Anderson, T. L., McHenry, H. I., and Dawes, M. G., **"Elastic-Plastic Fracture Toughness Tests with Single-Edge Notched Bend Specimens,"** *Elastic-Plastic Fracture Test Methods: The User's Experience, ASTM STP 856*, E. T. Wessel and F. J. Loss, Eds., American Society for Testing and Materials, 1985, pp. 210–229.

ABSTRACT: Fracture toughness tests have been performed on five geometries of single-edge notched bend (SENB) specimens machined from a 25.4-mm (1.0-in.) thick plate of ABS Grade EH36 steel, a normalized carbon-manganese steel. Critical values of the J integral and the crack-tip opening displacement (CTOD) were measured as a function of temperature. Test temperatures, which ranged from −196 to 25°C, covered the entire ductile-to-brittle transition range. On the upper shelf, critical values of J and CTOD at the onset of stable crack growth were insensitive to specimen geometry. However, in the ductile-to-brittle transition region, where fracture occurred by unstable cleavage, fracture toughness decreased with increasing specimen thickness and crack length. This effect of geometry on fracture toughness in the transition region is attributed to changes in crack-tip region constraint with geometry.

Various aspects of the SENB fracture toughness test have been examined. Experimental results indicate that both J and CTOD can be accurately measured with a single clip gage. Work hardening caused the ratio of J to CTOD to increase with strain. The m factor, which relates J to CTOD and flow stress, was directly proportional to the notch constraint factor. The η factor, which is a dimensionless constant used to relate the J integral to energy absorbed by the specimen, was independent of crack length for SENB specimens of ABS EH36 steel with a/W ranging from 0.19 to 0.75. The rotational factor r_p was not a strong function of temperature or specimen geometry in the material studied.

KEY WORDS: ductile brittle transition, mechanical properties, toughness, carbon steels, crack propagation, carbon-manganese steels, crack-tip opening displacement, elastic-plastic fracture, J integral

Structural steels undergo a transition from fully ductile to fully brittle behavior as temperature is decreased. Lower shelf (brittle) fracture behavior can be quantified by K_{Ic}, and upper shelf (ductile) fracture resistance can be described in terms of J_{Ic}. Both J_{Ic} and K_{Ic} are material properties that are independent of the geometry of the test specimen or structure. Fracture in the ductile-to-brittle

[1] Senior research engineer and principal research engineer, The Welding Institute, Abington Hall, Abington, Cambridge, England CB1 7AL.

[2] Metallurgist, Fracture and Deformation Division, National Bureau of Standards, Boulder, CO 80303.

transition region usually occurs by unstable cleavage, but extensive plastic flow at the crack tip can occur before failure. This crack-tip plasticity invalidates a description of the fracture resistance in terms of K_{Ic}. Thus, fracture in the transition region must be addressed with elastic-plastic analyses. However, the J_{Ic} test method as defined in ASTM Test for J_{Ic}, a Measure of Fracture Toughness (E 813) is only valid for upper shelf behavior. The crack-tip opening displacement (CTOD) test in accordance with British Standard (BS) Methods for Crack Opening Displacement (COD) Testing (BS 5762) is the only standardized test that covers all fracture behaviors that can occur between the extremes associated with the K_{Ic} and J_{Ic} tests. Recently, Dawes [*1*] has proposed a J equivalent of the CTOD test. This would give the same continuity in J-based tests as in CTOD based tests.

Contrary to common assumptions, there is not, at present, a geometry-independent fracture toughness parameter for the ductile-to-brittle transition region of steels. Data of various investigators indicate that critical values of J and CTOD in the transition region are affected by the geometry of the fracture specimens [*2–11*]. Larger specimens tend to induce a greater degree of stress triaxiality near the crack tip, thereby limiting plastic flow. This constraint of plastic flow is believed to be responsible for shifting the ductile-to-brittle transition to higher temperatures.

This paper presents experimental data that show the effect of geometry of single-edge notched bend (SENB) specimens on critical J and CTOD values in the ductile-to-brittle transition region. In addition, various aspects of elastic-plastic fracture toughness tests with SENB specimens are analyzed. The topics discussed include: relationships between J and CTOD, measurement of both J and CTOD with a single clip gage, and detecting the onset of tearing in an SENB specimen.

The major advantage of the SENB specimen (see Fig. 1) over the compact tension (CT) specimen is its relatively low machining cost. Also, the SENB specimen has lower load requirements than a CT specimen with the same ligament dimensions. An SENB specimen with the desired notch location and orientation can be more readily machined out of a welded plate and therefore it is better suited to fracture toughness testing of weldments. Also, one can make simultaneous measurements of J and CTOD during a fracture test with an SENB specimen; there is presently no standardized test method for measuring the CTOD of a CT specimen.

Test Material

The test material was a 25.4-mm (1.0-in.) thick plate of ABS Grade EH36 steel, a 350-MPa (51-ksi) yield strength carbon-manganese steel whose chemical composition is given in Table 1. The steel was in the normalized condition and had particularly uniform properties because of sulfide shape control.

The tensile properties of the normalized steel were determined from round

TABLE 1—*Chemical composition of the ABS Grade EH36 steel (weight percent).*

Carbon	Manganese	Phosphorus	Sulfur	Silicon	Copper	Nickel	Chromium	Molybdenum	Iron
0.12	1.39	0.015	0.006	0.380	0.05	0.03	0.05	0.007	balance

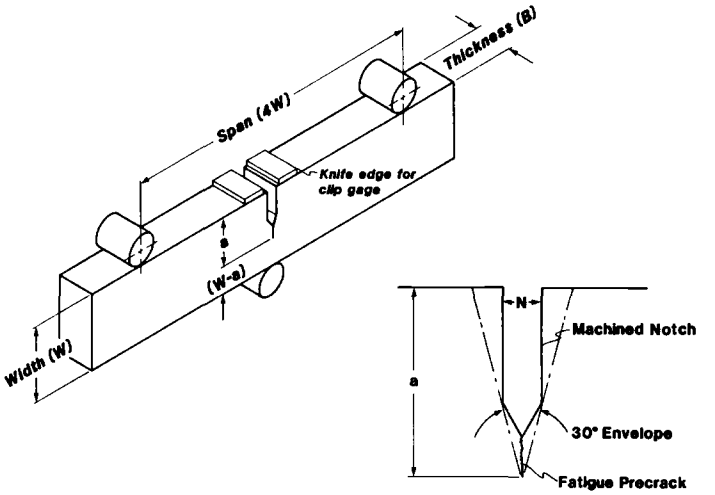

FIG. 1—*Three-point bend specimen used to obtain fracture toughness test results.*

tension specimens (6.35 mm diameter and 31.75-mm gage length) with the tensile axis parallel to the rolling direction. These specimens were tested at various temperatures ranging from −196 to 25°C. All tension tests were performed in a screw-driven tension test machine at a crosshead speed of 0.2 cm/min. All testing and measurement procedures conformed to the guidelines of ASTM Tension Testing of Metallic Materials (E 8).

The tensile properties as a function of temperature are shown in Fig. 2. The data followed the expected trends with a minimal amount of scatter. Both the yield strength and the ultimate tensile strength increased markedly with decreasing temperature. All flow curves exhibited an upper and lower yield point, which

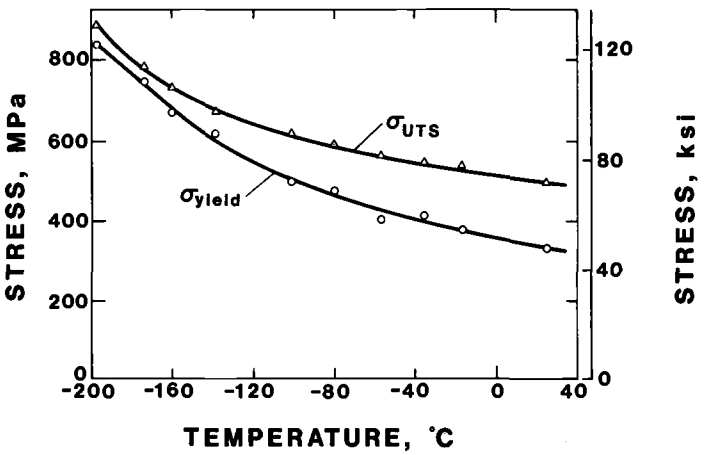

FIG. 2—*Tensile properties of ABS Grade EH36 steel as a function of temperature.*

TABLE 2—*Test matrix for fracture toughness tests on SENB specimens.*[a]

a/W	*B* = 12.7 mm	*B* = 25.4 mm	*B* = 38.1 mm
0.2	X	X	X
0.5		X	
0.75		X	

[a] *W* = 25.4 mm (1.0 in.).

is characteristic of low-carbon steels. The yield strength (as plotted in Fig. 2) was defined as the upper yield point; this definition was used to conform to the specifications of ASTM E 8.

Experimental Procedure

The ductile-to-brittle transition curves have been established as a function of constraint in SENB specimens. Notch constraint was varied by varying the crack-length/width ratio *a/W* and the specimen thickness *B*. The fracture toughness test matrix is shown in Table 2. The specimens were machined with the notch orientation shown in Fig. 3.

All specimens were fatigue precracked at room temperature according to the specifications in BS 5762 for COD testing. The tests were performed in displacement control on a 100-kN servohydraulic test machine. The displacement rate in all tests was 0.80 mm/min. The mouth-opening displacement and the load-line displacement were measured simultaneously during the test by two clip gages. The load-line displacement was measured by the comparison bar technique developed by Dawes [*12*]. The load and the two displacements were recorded on a two-pen *X-Y* plotter. The test instrumentation was wired to a minicomputer through an analog-to-digital converter. The load, crosshead displacement, and both clip-gage displacements were recorded by the computer at approximately 0.3-s intervals and stored on a magnetic disk. The computer typically collected and stored around 500 sets of data in a 3- to 5-min bend test.

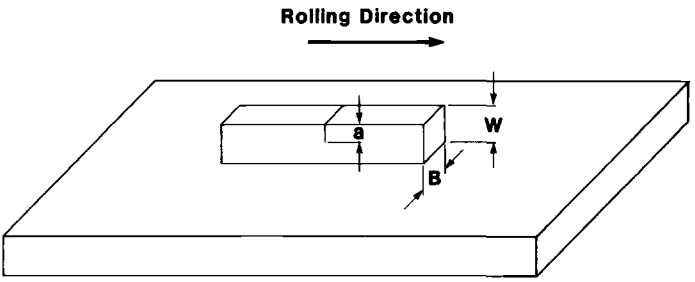

FIG. 3—*Orientation of SENB specimens with respect to the rolling direction. Charpy impact specimens were also prepared with this orientation.*

Low temperatures were attained by attaching a box to the lower crosshead and filling it with either liquid nitrogen or an alcohol and dry ice mixture. Intermediate temperatures (between −196 and −70°C) were attained by pouring liquid nitrogen into the box to a level below the specimen. The specimen was cooled by heat transfer through the test fixture and by the vapor coming off of the boiling nitrogen below the specimen. The actual specimen temperature was measured by a thermocouple implanted in the specimen.

In each test, fracture toughness was measured by the two elastic-plastic fracture parameters, J and CTOD. Figure 4 shows the notation used for critical values of CTOD (BS 5762). The notation depends on the nature of the fracture event, that is, whether the crack extension is brittle or ductile, and whether or not unstable cleavage is preceded by stable crack growth. A similar notation is used for reported critical values of the J integral [*2*] (see Fig. 5).

CTOD was computed from the following relationship

$$\delta = \delta_e + \delta_p = (K^2/2\sigma_0 E) + \{[r_p(W - a)\, V_p]/[r_p(W - a) + a + z]\} \quad (1)$$

where

V_p = plastic component of the mouth-opening displacement,
z = knife edge thickness,
r_p = rotational factor,
σ_0 = yield stress,
K = stress intensity factor, and
E = Young's modulus.

This equation separates CTOD into elastic and plastic components δ_e and δ_p. BS 5762 suggests that a value of 0.4 be assumed for r_p in Eq 1. However, a more precise value for the rotational factor can be calculated if the plastic components of load-line displacement and mouth-opening displacement (q_p and V_p, respectively) are known [*13*]

$$r_p = [1/(W - a)]\, \{(V_p W/q_p)\, [1 - (q_p/16\, W)] - (a + z)\} \quad (2)$$

The average value of r_p was found to be ~0.5 for this specimen material (see Results and Discussion section). This value was used in Eq 1 for all CTOD calculations.

ASTM E 813 recommends that the following equation be used to estimate the J integral for an SENB specimen

$$J = 2U/[B(W - a)] \quad (3)$$

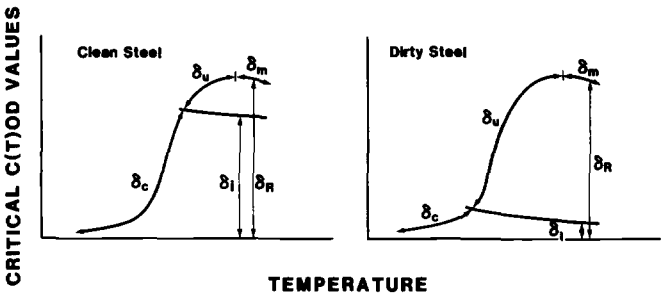

δ_c = Unstable cleavage-no prior slow crack growth
δ_u = Unstable cleavage-with prior slow crack growth
δ_m = Plastic collapse or tearing instability
δ_i = Onset of slow stable crack growth
δ_R = Resistance curve value

FIG. 4—*Notation for critical CTOD values (BS 5762).*

where U is the area under the load/load-line displacement curve. However, J can also be estimated from an equation derived by Sumpter and Turner [*14*]

$$J = (K^2/E') + [2U_p^v/B(W - a)]\{W/[r_p(W - a) + a + z]\}$$

where U_p^v is the area under the load/mouth-opening displacement curve. Both Eqs 3 and 4 were used to compute values of J.

The method used to detect the onset of stable crack growth was the double

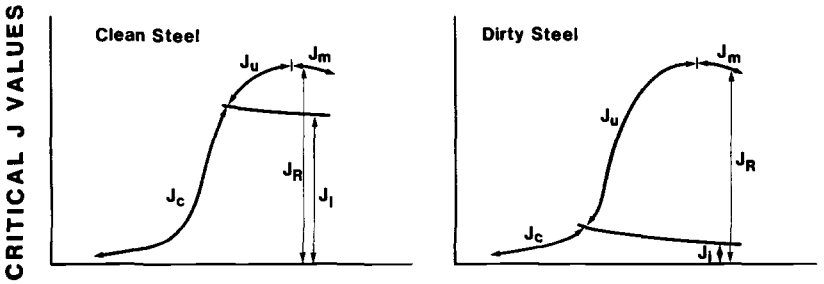

J_c = Unstable cleavage-no prior slow crack growth
J_u = Unstable cleavage-with prior slow crack growth
J_m = Plastic collapse or tearing instability
J_i = Onset of slow stable crack growth
= J_{Ic} when certain conditions are met
J_R = Resistance curve value

FIG. 5—*Notation for critical* J *values* [1].

displacement method. Both the mouth-opening displacements V and the load-line displacements q from each test were stored on a magnetic disk. The derivatives dq/dV and d^2q/dV^2 were computed and plotted against V. The critical displacement was inferred from these plots. This method is further described below.

Results and Discussion

Cleavage Fracture Toughness

The fracture toughness data for the lower shelf and transition region are summarized in Figs. 6 through 9. The critical values of CTOD and J along with the critical fracture event for each specimen are reported; δ_c and J_c are defined at the occurrence of unstable cleavage without prior stable crack growth. When cleavage is preceded by stable crack growth, δ_u and J_u are measured at the point of instability.

Figures 6 and 7 show that the ductile-to-brittle transition curves shift approximately 30°C as the specimen thickness increases from 13 to 38 mm. The thickest specimen produces the greatest of crack-tip region constraint; constraint is the restriction of plastic flow by the surrounding elastic material. Constraint causes a triaxial stress state and raises the flow stress near the crack tip. This increase in flow stress tends to promote cleavage fracture (that is, shift the transition curve to the right) since it is easier to reach the fracture stress.

Note that the thickest specimens (B = 38.1 mm) had slightly deeper cracks than the other two specimen geometries shown in Figs. 6 and 7. The deeper cracks were necessary to prevent the load on the thick specimens from exceeding

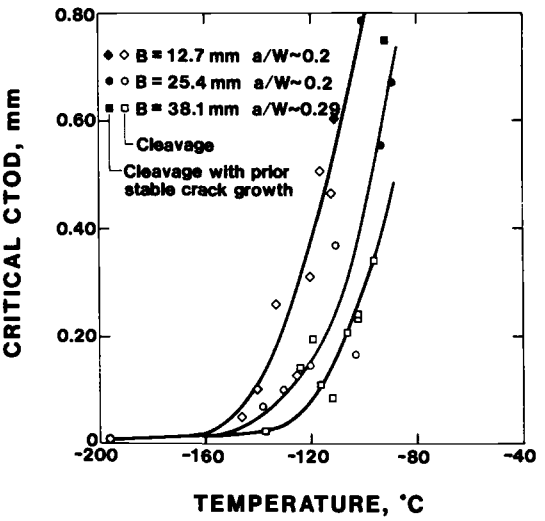

FIG. 6—*Critical CTOD for cleavage as a function of temperature and specimen thickness for ABS Grade EH36 steel.* W = *25.4 mm (1.0 in.).*

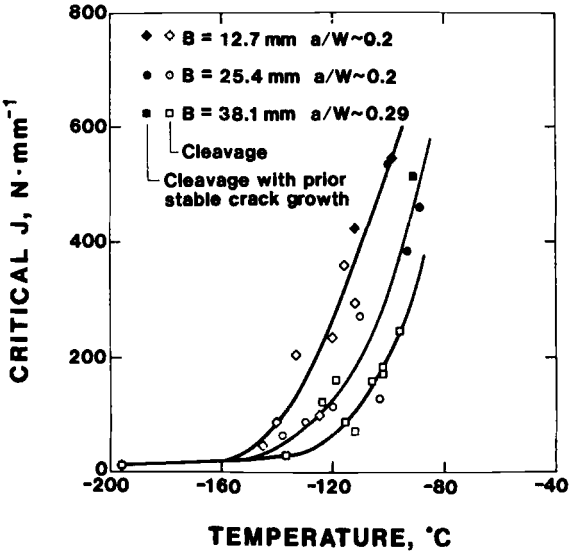

FIG. 7—*Critical J for cleavage as a function of temperature and specimen thickness for ABS Grade EH36 steel.* W = *25.4 mm (1.0 in.).*

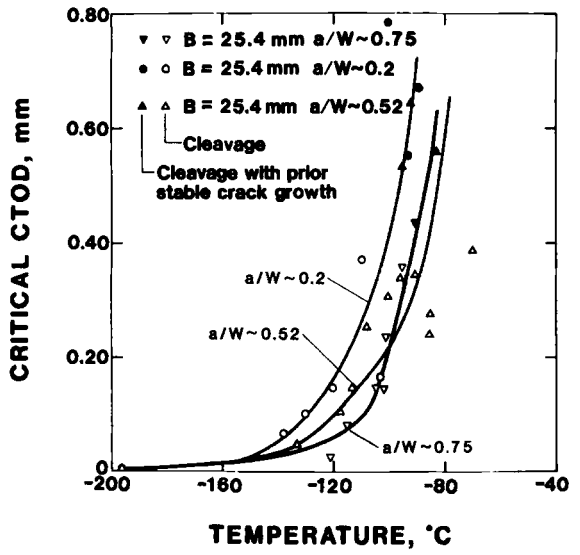

FIG. 8—*Critical CTOD for cleavage as a function of temperature and crack length for ABS Grade EH36 steel.* W = *25.4 mm (1.0 in.).*

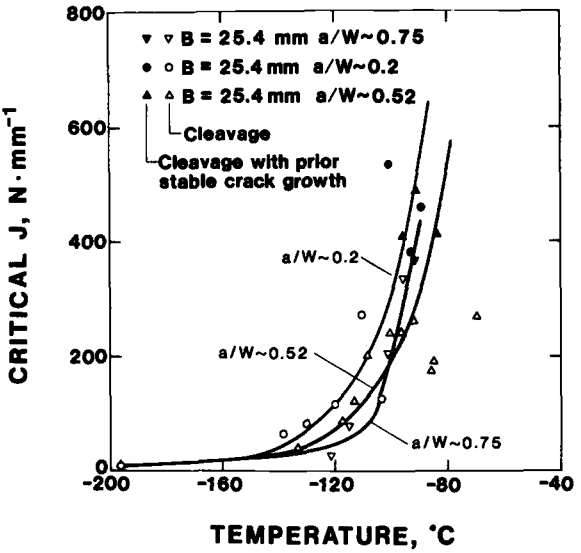

FIG. 9—*Critical* J *for cleavage as a function of temperature and crack length for ABS Grade EH36 steel.* W = *25.4 (1.0 in.).*

the capacity of the test machine. These deeper cracks probably contributed to the shift in the transition curve to higher temperatures.

The influence of crack length on the ductile-to-brittle transition curve is shown in Figs. 8 and 9. The curves in Figs. 8 and 9 tend to shift to higher temperatures with increasing crack length. Deeper notched specimens (that is, shorter ligament length) apparently have more crack-tip constraint. The data for the deep-notched geometry ($a/W \sim 0.75$) behave in an unusual manner. The curve fitted to these data (Figs. 8 and 9) crosses the curve representing the $a/W \sim 0.5$ data. At low values of δ_c and J_c, where the plastic zone is relatively small, the deep notched geometry has more constraint than the $a/W \sim 0.5$ geometry. At higher temperatures (and higher δ_c and J_c values), the plastic zone at fracture is on the order of the size of the ligament in the deep notched geometry. The constraint is relaxed as the plastic zone approaches a free surface.

In general, the transition shifts to higher temperatures with an increasing thickness-to-ligament ratio $B/(W - a)$. For the five SENB geometries used in this investigation, $B/(W - a)$ varied from 0.62 to 4.0; this corresponds to approximately a 40°C shift in the ductile-to-brittle transition.

The effect of ligament length on the slip patterns in SENB specimens was investigated. Two specimens were coated on one side with a photoelastic material that, when viewed with polarized light, changes color with strain. Black and white photographs of the multicolor strain patterns on two SENB specimens at net-section yield are shown in Fig. 10 The slip lines on both specimens emanate from the crack tip at initial angles of approximately 45° from the crack plane. These slip lines are then deflected inward by the bending stresses. At the neutral

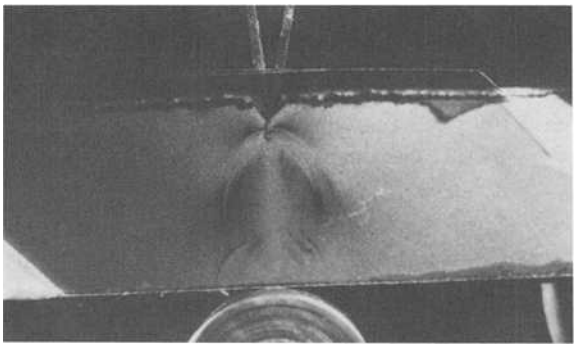

a

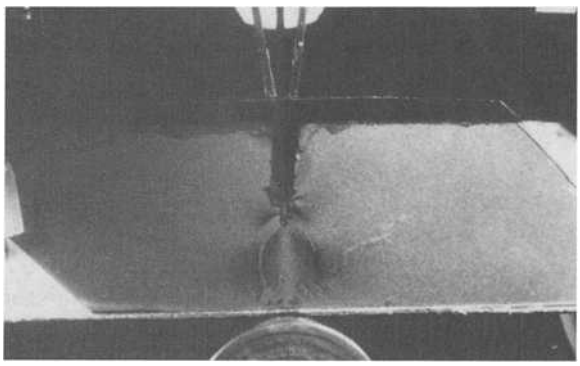

b

FIG. 10—*Photoelastic strain patterns for SENB specimens:* (a) a/W ~ *0.2 and* (b) a/W ~ *0.5.*

axis the normal stress changes sign; the portion of the ligament below the hinge point is in compression. In the deep notched specimen (Fig. 10*b*), the hinge point is closer to the crack tip. The compressive stress field near the crack tip tends to produce additional constraint. As ligament length decreases, the compressive stress field moves closer to the crack tip and constraint increases. As stated before, for very short ligaments constraint can be relaxed by plastic flow to the nearest free surface.

Increasing geometrical constraint causes the load at net-section yield to increase. This elevation of yield load can be quantified by the notch constraint factor L, which is defined by the limit load expression for SENB specimens

$$P_y = [L\sigma_0(W - a)^2B]/4W \tag{5}$$

where P_y is the load at net-section yield. In the absence of a crack, $L = 1$.

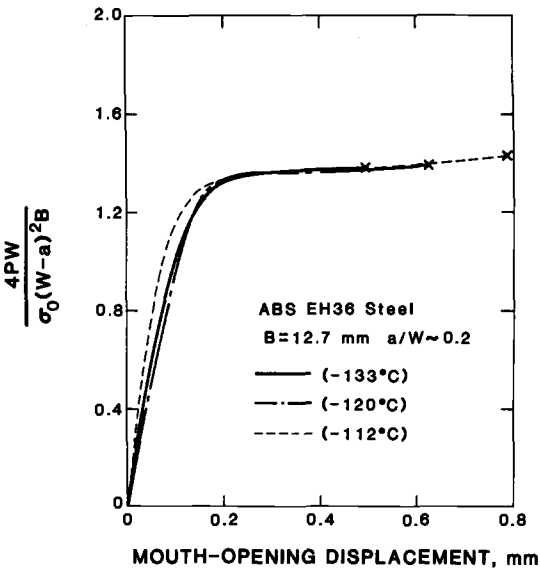

FIG. 11—*Nondimensional load versus displacement curves at various temperatures for a constant SENB specimen geometry.*

Dimensionless load is plotted versus mouth-opening displacement in Figs. 11 and 12. Dimensionless load (that is, load normalized for yield stress and ligament dimensions) is defined on the ordinates of Figs. 11 and 12 and is equal to L when $P = P_y$. The curves in Fig. 11, which are for a constant geometry at various temperatures, form a single curve because load is normalized for yield stress. Figure 12 shows that dimensionless load is elevated when crack length, specimen thickness, or both are increased. The curves in Fig. 12 support the hypothesis that the observed shifts in the ductile-to-brittle transition curves (Figs. 6 through 9) are caused by increases in stress triaxiality.

Upper Shelf (Initiation) Toughness

During a fracture test with an SENB specimen, the load-line displacement q was continuously plotted against crack-mouth opening displacement V. After net-section yield, the q versus V plot is a nearly straight line. However, as the crack grows this line gradually decreases in slope because the center of rotation moves during crack growth. Figure 13 is a plot of the first derivative of q with respect to V plotted against V. The behavior at the far left of this plot represents the transition from elastic to plastic deformation. During plastic deformation, the first derivative remains relatively constant and then increases sharply. At $V = 1.48$ mm there is a sharp drop in the first derivative. This behavior is characteristic of fracture tests where tearing was observed. Observation of fracture surfaces of specimens that fractured before and immediately following the onset of tearing and the corresponding derivative plots indicate that the sharp

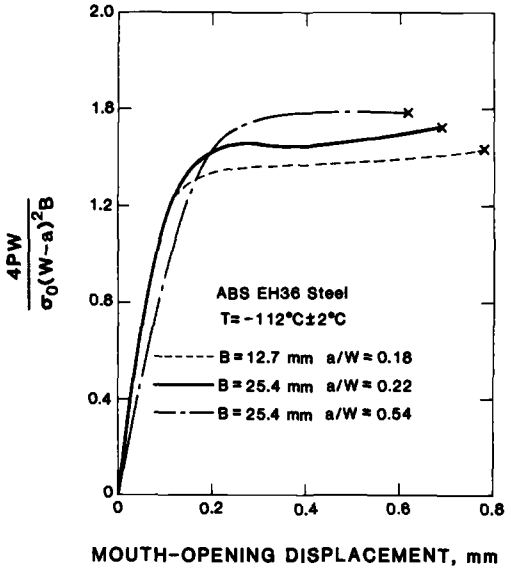

FIG. 12—*Nondimensional load versus displacement curves as a function of SENB specimen geometry.*

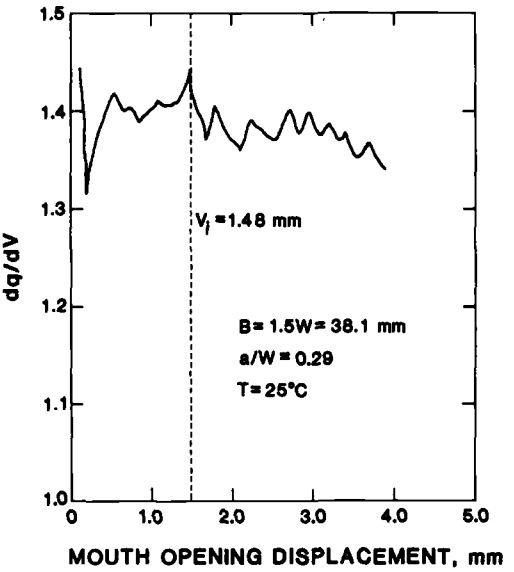

FIG. 13—*Derivative of* q *with respect to* V. *A sharp drop in the first derivative generally indicates tearing.*

drop in the first derivative coincides with incipient tearing. At higher displacements the curve has a zigzag shape, which is believed to be associated with successive increments of crack growth.

Figure 13 is typical of the first derivative plots from fracture tests in which tearing was observed. The spike in the curve, which was taken as the point of incipient tearing, is slightly more pronounced than the other spikes. Often the initiation point is ill defined because of the uncertainty of which spike corresponds to the onset of stable crack growth.

The critical displacement V_i and the corresponding area under the curve were used to compute δ_i and J_i from Eqs 1 and 3. Figures 14 and 15 show values of δ_i and J_i, respectively, for the five SENB specimen geometries. Both J_i and δ_i are apparently independent of geometry, and δ_i is approximately independent of temperature. J_i increases slightly with decreasing temperature because the area under a load-displacement curve at a constant displacement increases with increasing flow stress. Because of the uncertainty in this technique, the point of incipient crack growth is often not well defined, contributing to the scatter seen in Figs. 14 and 15.

The Rotational Factor

The rotational factor r_p is defined as the distance from the crack tip to the hinge point divided by the ligament length. The rotational factor was previously defined in Eq 2, where r_p is expressed as a function of specimen dimensions and the plastic components of mouth-opening V_p and load-line q_p displacements [*13*].

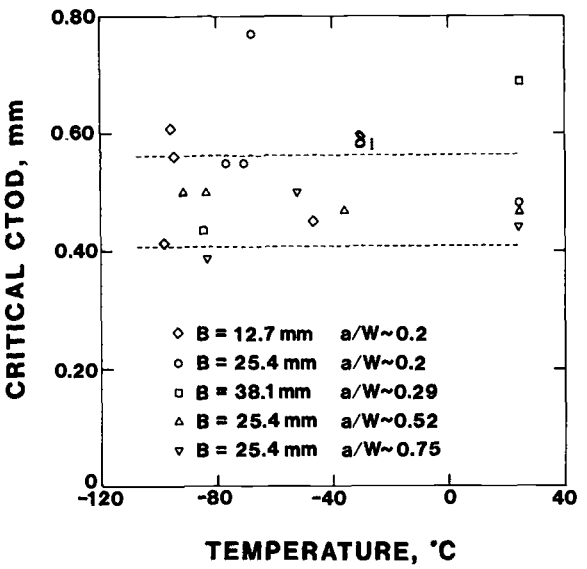

FIG. 14—*Critical CTOD for the onset of tearing as a function of temperature and SENB specimen geometry for ABS Grade EH36 steel.* W = *25.4 mm (1.0 in.).*

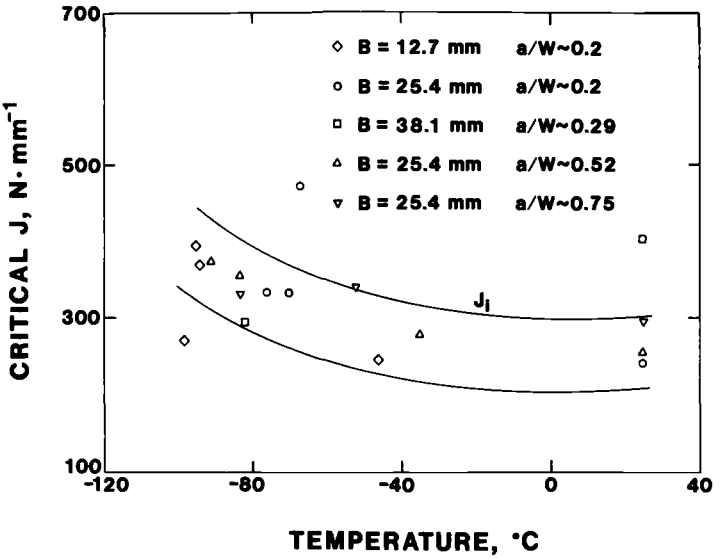

FIG. 15—*Critical J for the onset of tearing as a function of temperature and SENB specimen geometry for ABS Grade EH36 steel.* W = *25.4 mm (1.0 in.).*

Equation 2 was derived assuming the SENB specimen deforms in pure bending about a hinge point; the specimen halves are assumed to remain rigid.

The rotational factor was measured for five geometries of ABS EH36 steel SENB specimens at various temperatures. Figure 16 shows that r_p is insensitive to geometry and test temperature for this material. The mean value of the data in Fig. 16 is 0.522; the standard deviation is 0.030.

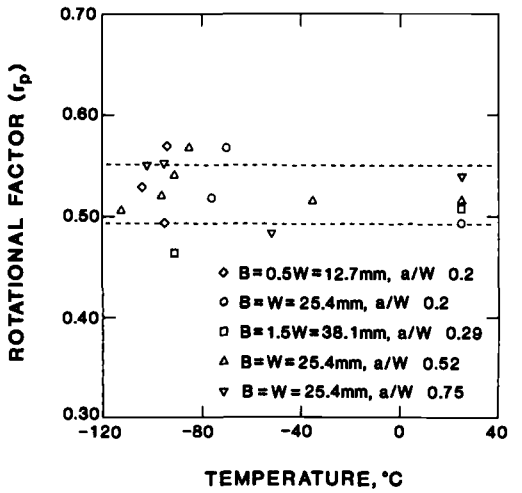

FIG. 16—*Plastic rotational factor as a function of SENB specimen geometry and temperature for ABS Grade EH36 steel.*

Equation 6 can be used to determine the sensitivity of CTOD measurements to variations in r_p [*14*]

$$[d(\delta_p/V_p)]/dr_p = [(a + z)(W - a)]/[r_p(W - a) + a + z]^2 \quad (6)$$

Using $r_p = 0.5$, $W = 25.4$ mm, $a = 12.7$ mm, and $z = 1.3$ mm, the above derivative is equal to 0.43. The value of r_p recommended by BS 5762 is 0.4, or 20% below the nominal value of 0.5 for this specimen material. If 0.4 is used in Eq 1, a 14% error in the computed CTOD value would occur. It is therefore important to have a reasonably accurate estimate of r_p for a given material; the standard value (0.4) is apparently not adequate for all materials.

Estimation of J *from CMOD*

For deep-notched SENB specimens, the J-integral is usually estimated from Eq 3. The value of J can also be estimated from the load versus mouth-opening displacement curve using Eq 4. Equation 4 is based on the Sumpter and Turner [*14*] equation, although they approximated the plastic area under the P/V curve by

$$U_p^v \cong P_L V_p \quad (7)$$

where P_L is the limit load.

The J-integral was calculated for a number of tests using Eqs 3 and 4, and the agreement is very good. Figure 17 shows a comparison of estimates from the two equations. The data represent a single specimen at various displacements. The differences between the two J estimates for this particular specimen range from 0.5 to 1.5%.

The value of r_p used in Eq 4 to generate Fig. 17 was measured from the same

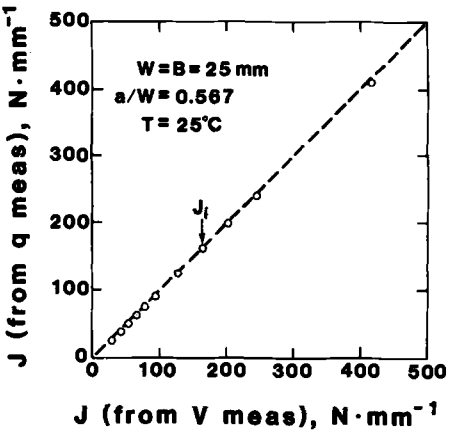

FIG. 17—*Comparison of* J *estimates from Eqs 3 and 4.*

specimen using Eq 2. The excellent agreement between Eqs 3 and 4, as shown in Fig. 17, is evidence that the simple hinge mechanism is an adequate model to describe the plastic deformation of an SENB specimen. Figure 17 also shows that the J integral can be accurately measured from the mouth-opening displacement if r_p is known. Thus, it is possible to measure both J and CTOD from an SENB specimen with a single clip gage.

Relationships Between J *and CTOD*

Under conditions of small-scale yielding, the relationship between J and CTOD can be estimated by

$$J = m\sigma_0\delta \tag{8}$$

where m is a dimensionless constant that relates J to CTOD and yield stress; $m = 1$ for plane stress and $m = 2$ for plane strain. The value of m for large-scale yielding should lie between 1.0 and 2.0.

The plastic term in Eq 4 is similar to the equation for the plastic CTOD

$$\delta_p = [r_p(W - a)V_p]/[r_p(W - a) + a + z] \tag{9}$$

From Eqs 4 and 9 one can obtain a simple equation for the ratio of the plastic J to the plastic CTOD

$$J_p/\delta_p = 2U_p^vW/[V_pBr_p(W - a)^2] \tag{10}$$

Equation 10 has been incorporated into a computer program that plots J_p/δ_p as a function of mouth-opening displacement. A typical plot is shown in Fig. 18. The ratio J_p/δ_p increases with displacement because of work hardening. The work hardening can be accounted for by replacing the yield stress in Eq 8 with a nominal flow stress

$$J_p = m_p\sigma_{\text{flow}}\delta_p \tag{11}$$

The nominal flow stress can be estimated by

$$\sigma_{\text{flow}} = (\bar{P}/P_y)\,\sigma_0 \tag{12}$$

where P is the average load defined as

$$\bar{P} = U_p^v/V_p \tag{13}$$

and P_y is the load at yield defined previously in Eq 5. Combining Eqs 5 and 10 through 13 yields the following relationship for m_p

$$m_p = L/2r_p \tag{14}$$

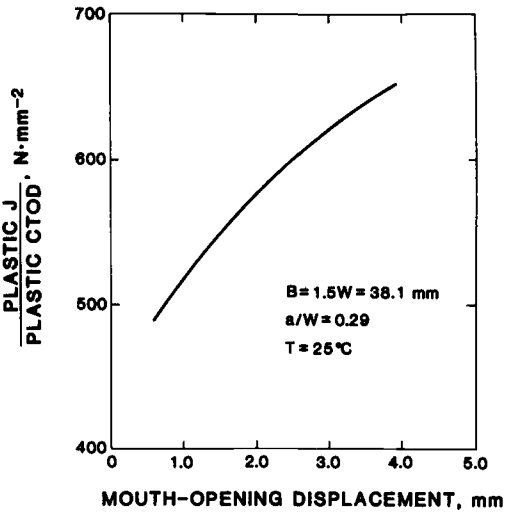

FIG. 18—*The ratio of the plastic components of J and CTOD as a function of displacement.*

For the ABS Grade EH36 steel, $r_p \cong 0.5$; therefore, $m_p \cong L$ (the notch constraint factor). Thus, the relationship between plastic components of J and CTOD (Eq 11) depends on the geometrical constraint of the specimen and the flow properties of the material.

The η Factor

The η factor is a dimensionless constant that relates J to energy divided by ligament area. It is used in a more general form of Eq 3

$$J = \eta U/B(W - a) \tag{15}$$

where $\eta \cong 2$ for deep notched SENB specimens. The above equation can be divided into elastic and plastic components [*14*]

$$J = [\eta_e U_e/B(W - a)] + [\eta_p U_p/B(W - a)]$$
$$= (K^2/E') + [\eta_p U_p/B(W - a)] \tag{16}$$

The elastic η factor η_e can be derived from the elastic compliance and stress intensity coefficient. The solid line in Fig. 19 is a plot of η_e versus notch depth [*15*].

Since J can be defined as the negative of the spatial derivative of work, the plastic η factor η_p or the overall η factor η_0 can be computed as follows

$$J = \eta_0 U/B(W - a) = (-1/B)\,(dU/da) \tag{17}$$

hence

$$\eta_0 = -[(W - a)/U]\,(dU/da) \tag{18}$$

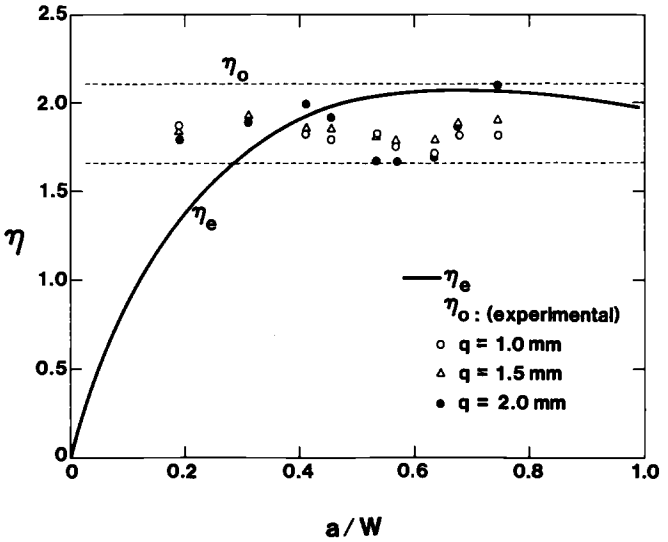

FIG. 19—*The overall* η *factor* η_0 *as a function of* a/W *and displacement. The elastic* η *factor curve* [15] *is superimposed for comparison.*

A series of SENB specimens with notch depths ranging from $a/W = 0.19$ to 0.75 were tested at room temperature. The area under the load versus load-line displacement curve U was measured for each specimen at displacements of 1.0, 1.5, and 2.0 mm. These values of U were then plotted versus crack length, and dU/da was measured for various crack lengths by drawing tangents to the U versus a curves and computing the slopes; η_0 was then computed as a function of crack length. The results are plotted in Fig. 19. According to Fig. 19, η_0 is relatively independent of crack length down to $a/W = 0.19$ for the ABS EH36 steel. It therefore seems reasonable to use a value of $\eta_0 = 1.8 - 2.0$ for all J measurements from SENB specimens, the present material, with $a/W \geq 0.2$. A variation of 0.10 in η_0 corresponds to approximately a 5% error in the measured value of J.

Summary and Conclusions

The fracture toughness (critical J and CTOD) of structural steels in the ductile-to-brittle transition region is dependent on size and geometry. The transition can be shifted to higher temperatures by increasing the thickness or decreasing the ligament length of SENB specimens, or both. These transition shifts are attributed to increases in crack-tip region constraint that elevate the flow stress locally. This elevation of the flow stress tends to promote cleavage fracture since it is easier to reach the fracture stress. Fracture toughness in the transition region is geometry dependent; one cannot safely predict the fracture behavior of a large structure from the toughness of a small specimen.

The rotational factor r_p in SENB specimens is insensitive to geometry and temperature for ABS EH36 steel. Significant errors in CTOD may result if the standard r_p value (0.4) is used for all materials. Both J and CTOD can be measured from an SENB specimen with a single clip gage at the crack mouth. The relationship between J and CTOD is a function of specimen geometry. The η factor is approximately equal to 1.85 for ABS EH36 steel SENB specimens with a/W ranging from 0.19 to 0.75.

Acknowledgments

This research was funded by the U.S. Department of Interior Minerals Management Service. The contract monitor was Mr. John B. Gregory.

References

[1] Dawes, M. G., *The Welding Institute Research Bulletin*, Vol. 23, No. 2, Feb. 1982, p. 50.
[2] Dawes, M. G., "Elastic-Plastic Fracture Toughness Based on the COD and J-Contour Integral Concepts," *Elastic-Plastic Fracture, STP 668*, American Society for Testing and Materials, Philadelphia, 1979, pp. 306–333.
[3] Stuber, A. B., Ph.D. thesis, University of Kansas, Lawrence, KS, 1980.
[4] Ritchie, R. O., Smith, R. F., and Knott, J. F., *Metal Science*, Vol. 9, 1975, p. 485.
[5] Penelon, A., Bassim, M. N., and Dorlot, J. M., "Variation of Fracture Toughness with Specimen Geometry and Loading Conditions in Welded Low Alloy Steels," *Fracture Mechanics—Proceedings of the Eleventh National Symposium on Fracture Mechanics: Part 1, STP 677*, American Society for Testing and Materials, Philadelphia, 1979, pp. 449–462.
[6] Milne, I., *Materials Science Engineering*, Vol. 30, No. 3, Nov. 1977, p. 243.
[7] Chell, G. G. and Spink, G. M., *Engineering Fracture Mechanics*, Vol. 9, No. 1, 1977, p. 101.
[8] Milne, I. and Worthington, P. J., *Materials Science Engineering*, Vol. 26, 1976, p. 185.
[9] Chell, G. G. and Davidson, A., *Materials Science Engineering*, Vol. 24, 1976, p. 45.
[10] Chell, G. G. and Gates, R. S., *International Journal of Fracture*, Vol. 14, No. 2, April 1978, p. 223.
[11] deCastro, P. M. S. T., Sprurrier, J., and Hancock, P., "An Experimental Study of the Crack Length/Specimen Width (a/W) Ratio Dependence of the Crack Opening Displacement (COD) Test Using Small-Scale Specimens," *Fracture Mechanics—Proceedings of the Eleventh National Symposium on Fracture Mechanics: Part 1, STP 677*, American Society for Testing and Materials, Philadelphia, 1979, pp. 486–497.
[12] Dawes, M. G., *The Welding Institute Research Bulletin*, Vol. 7, No. 7, July 1976, p. 185.
[13] Lin, I.-H., Anderson, T. L., deWit, R., and Dawes, M. G., *International Journal of Fracture*, Vol. 20, 1982, p. R3.
[14] Sumpter, J. D. G. and Turner, C. E., "Method for Laboratory Determination of J_c," *Cracks and Fracture—Proceedings of the Ninth National Symposium on Fracture Mechanics, STP 601*, American Society for Testing and Materials, Philadelphia, 1976, pp. 3–18.
[15] Towers, O. L., *Tests for Fracture Toughness and Fatigue Assessment: A Compilation of Stress Intensity Compliance and Elastic η Factors*, The Welding Institute, Cambridge, England, 1984.

Gerald W. Wellman[1] *and Stanley T. Rolfe*[2]

Engineering Aspects of Crack-Tip Opening Displacement Fracture Toughness Testing

REFERENCE: Wellman, G. W. and Rolfe, S. T., **"Engineering Aspects of Crack-Tip Opening Displacement Fracture Toughness Testing,"** *Elastic-Plastic Fracture Test Methods: The User's Experience, ASTM STP 856*, American Society for Testing and Materials, E. T. Wessel and F. J. Loss, Eds., American Society for Testing and Materials, 1985, pp. 230–262.

ABSTRACT: An investigation of the crack-tip opening displacement (CTOD) fracture behavior of four pressure vessel steels and one ship steel has been conducted. The purpose of the investigation was to determine the fracture behavior of the steels, to study the effects of CTOD testing variables, to examine various methods of evaluating test records, and to study the relationships among several fracture toughness parameters. The five steels studied, A508, A533, A516, A517, and A131, (Unified Numbering System [UNS] K12766, K12539, K02700, K11856, and K02102) had yield strengths from 240 to 750 MPa. In addition, three specimen sizes of the A533 and A516 steels were studied.

The CTOD fracture parameter provides a relatively simple method of extending fracture mechanics concepts from plane-strain linear elastic behavior to elastic-plastic behavior. Plane-strain linear elastic fracture toughness values (K_{Ic} as defined in ASTM Test Method for Plane-Strain Fracture Toughness of Metallic Materials E 399) can be obtained only at extremely low temperatures and large specimen sizes for the steels investigated. J_{Ic} (as defined in ASTM Test Method for J_{Ic}, a Measure of Fracture Toughness E 813) toughness values are currently applicable only to stable, fibrous tearing behavior. Thus, there is a large temperature region between the K_{Ic} and J_{Ic} toughness parameters where neither J nor K test results will meet their respective J_{Ic} or K_{Ic} test specifications. The CTOD fracture toughness parameter covers this temperature region between K_{Ic} and J_{Ic} as well as covering both the regions where K_{Ic} and J_{Ic} are valid. Thus the CTOD test method can be used throughout the entire service temperature range for pressure vessel and structural steel applications.

For the low to moderate strength steels tested, the macroscopic failure surface appearance changed from all brittle to a fibrous thumbnail initiation at a relatively consistent CTOD value. The change in appearance, which takes place between the lower and upper shelf, must occur at a much lower CTOD value for the high strength A517 steel. Correlations among Charpy V-notch (CVN), CTOD, J, and K_c values are presented. Generally it was not possible to obtain linear elastic plane-strain critical stress intensity factor K_{Ic} values for the specimen sizes studied, hence the use of K_c values. The results of the correlations increased with increasing temperature as expected.

Using the preferred specimen geometry of thickness t by depth $2t$, there is a definite size effect in CTOD testing. On the upper shelf (fibrous tearing failure) a smaller specimen

[1]Member of technical staff, Sandia National Laboratories, Division 6322, Albuquerque, NM 87185.

[2]Professor, Department of Civil Engineering, University of Kansas, Lawrence, KS 66045.

will give a smaller apparent toughness. In the lower transition region (brittle failure) the size effect is less clear. A smaller specimen (1/2*t* by *t*) will give a larger apparent toughness using average CTOD values, but there is no apparent size effect when the lowest CTOD test values are compared. Until this size effect is clarified, the British Standard requirement that the test specimen be the full thickness of the structure of interest is appropriate.

An extensive CTOD study of five structural steels has shown that this test method can be used to predict the elastic-plastic fracture toughness over the entire test temperature range, and that the results can be correlated with other fracture toughness test results such as CVN, *J*, and *K*.

KEY WORDS: steels, fracture mechanics, fracture tests, cracks, crack-tip opening displacement (CTOD), elastic-plastic fracture mechanics, strains

For many years linear elastic fracture mechanics (LEFM) has been the primary method used to analyze the fracture behavior of flawed structural components. Using LEFM, the stress intensity factor in the structure K_I is compared to the critical stress intensity factor K_{Ic} measured in a laboratory specimen. However, for most low to moderate strength structural steels, K_{Ic} is impractical if not impossible to measure. Even if K_{Ic} is measured, the test specimen generally must be so thick and the test temperature must be so low that these K_{Ic} values have little or no relation to actual service conditions. However, failures occasionally do occur in actual structures. Therefore, there is a need to extend the general concepts of LEFM to describe material behavior beyond the LEFM region into the elastic-plastic regime.

Currently, there are several elastic-plastic fracture mechanics approaches under extensive study, including the *R* curve, *J* integral, the crack-tip opening displacement (CTOD), and the tearing modulus. Because of the growing use of the CTOD approach to material toughness specifications in actual structures (for example, the Alaska pipeline, North Sea offshore rigs, liquefied natural gas storage tanks, and so forth) and because of the limited research in the United States on the use of this approach, an investigation of the CTOD behavior of pressure vessel and structural steels as well as the significance of CTOD values was conducted.

A summary of the current status of CTOD testing and design application along with the major problems existing in this area was reviewed in 1980 by Harrison [*1*]. As noted by Harrison, the background development of the CTOD fracture parameter and test method has occurred over the past 20 years [*2–5*]. This work has culminated in a British Standard (BS) for CTOD testing Methods for Crack Opening Displacement Testing (BS 5762:1979).

The use of CTOD in design or analysis is not as well developed as the testing procedure. Several problems still exist. The decision as to which CTOD test value is appropriate is a question that generates much controversy. For materials and temperatures that exhibit a brittle failure with no prior macroscopic fibrous tearing, there is only one critical CTOD value, that is, the value at the initiation of the fracture. The load displacement curve for this type behavior is shown in Fig. 1*a*. However, for materials that exhibit the formation of a fibrous "thumb-

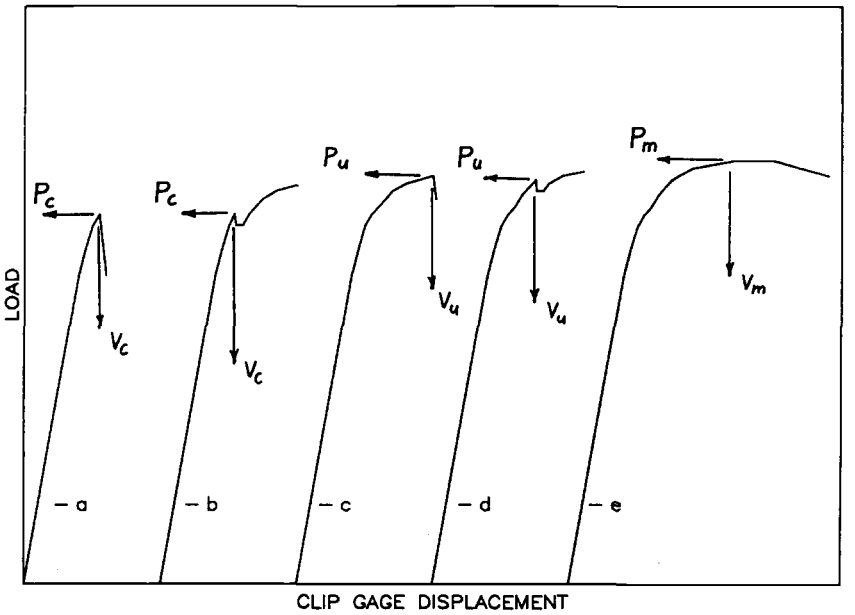

FIG. 1—*Schematic CTOD load—clip-gage displacement records.*

nail" at failure initiation, the question arises whether the initiation of the fibrous tearing or the beginning of the unstable event is the critical CTOD value. Figure 1*c* shows the load displacement curve for this type behavior. The other curves in Fig. 1 are described later. There is no consensus on this controversy in the literature [*3,6,7*]. BS 5762:1979 leaves this question to be decided by agreement between the manufacturer and purchaser. In practice, for low-strength structural steels, if the material is tough enough that failure initiation is by ductile fibrous tearing, fracture is often not the controlling failure mechanism.

Data scatter is inherent in fracture toughness testing in the elastic-plastic regime and particularly so in the transition region. There is no consensus as to the proper method of statistical treatment of CTOD data. At present, use of the lowest test value attained is often specified and may be the best treatment of this problem [*1*]. This problem of data scatter is not limited to the CTOD test but is true for all other elastic-plastic fracture parameters. Testing of weldments increases the data scatter.

The purpose of this paper is to present the basic CTOD data that will be used in the development of a comprehensive failure prediction method and to discuss the test variables that affect the CTOD test results. Also of interest is the determination of the practical aspects of performing a CTOD test. This includes the effects of temperature failure mechanism changes, and specimen size on critical CTOD values, as well as the details of test record interpretation. Finally, the relationships among critical CTOD values and the results of other toughness

testing methods are investigated and related to the more familiar LEFM critical stress intensity factor K_c.

Materials

Five steels were studied during this investigation. They included a typical low-strength ferrite-pearlite steel with a yield strength of 240 MPa, a moderate strength spheroidized steel with a yield strength of 490 MPa, and a high-strength quenched and tempered martensite steel with a yield strength of 750 MPa. Four of the five steels, A516, A533, A508, and A517 (Unified Numbering System [UNS] K02700, K12539, K12766, and K11856) can be considered as primarily pressure vessel steels. The fifth steel, A131 (UNS K02102) is a ship steel included to broaden the applicability of this study. The A516 and A517 steels are typical of steels sold under these ASTM designations. The A508 and A533 steels are from the Heavy Section Steel Technology (HSST) Program at Oak Ridge National Laboratory. The unique thermo-mechanical processing of these steels, resulting in a spheroidized microstructure, makes them atypical of steels normally produced under this specification. The A131 steel is from the Ingram Barge that exhibited a brittle fracture in 1972. The room temperature mechanical properties of the steels are shown in Table 1 and the chemical compositions in Table 2.

A508 Steel

The A508 Class 2 steel came from forging prolongations of the full-scale (152 mm thick) HSST vessels V1 and V2 [*8*]. A total of seven 102-mm thick compact tension specimens were machined from each vessel prolongation and tested at Westinghouse Electric Corporation [*9*]. Twenty three-point bend specimens (25 by 50 by 200 mm) that were not full thickness were obtained from the top 38 mm, above the loading holes, of five of these compact tension specimens. The flaw propagation direction was the radial direction (specimen orientation C-R)[3] in the original vessel.

The HSST data indicate only a minor variation in properties among the inside diameter, the middle, and the outside diameter surface. The outside surface had the highest strength, the middle had the lowest strength, and the inside surface had a slightly higher strength than the middle. The maximum variation in yield strength was about 10%. Because this through thickness variation was minimal, the properties were assumed constant throughout the cross section. The Charpy V-notch (CVN) temperature transition curve is shown in Fig. 2.

A533 Steel

The A533 Grade B Class 1 steel also was obtained from the HSST program. In this case the steel was from a prolongation of the 152-mm thick vessel V-8

[3]The first letter designates the direction normal to the crack plane and the second letter the direction of the expected crack propagation.

TABLE 1—*Mechanical properties.*[a]

Steel[b]	Yield Strength, MPa	Tensile Strength, MPa	Elongation in 2 in., %	Reduction in Area, %	Ultimate Strain, in./in.
A508					
ORNL	480	620			
KU	487	624	28	70	0.13
A533					
ORNL	450	586			
KU	427	586	28	77	0.213
A516					
Mill	313	492			
KU	266	459	38	72	0.2281
A517					
Mill	745	824			
KU	742	809	23	68	0.0885
A131					
KU	261	471	52	73	0.2176

[a]1 in. = 25.4 mm.
[b]ORNL is Oak Ridge National Laboratory and KU is Kansas University.

TABLE 2—*Chemical analysis.*

Steel	Carbon	Manganese	Phosphorus	Sulfur	Silicon	Nickel	Chromium	Molybdenum	Vanadium
A508 Class 2	0.26	0.75	0.01	0.014	0.26	0.81	0.45	0.61	0.05
A533 Grade B	0.20	1.23	0.015	0.017	0.26	0.49	...	0.52	0.05
A516	0.23	1.15	0.009	0.022	0.25	...	...	...	...
A517 Grade F	0.18	0.84	0.010	0.013	0.212	0.93	0.607	0.456	0.042
A131 Grade B	0.16	1.01	0.009	0.010	0.070	...	...	...	...

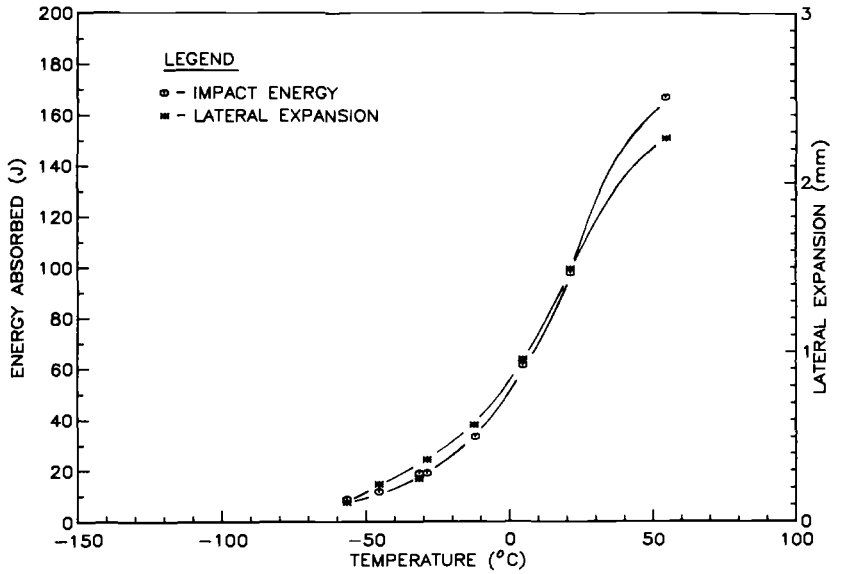

FIG. 2—*Charpy V-notch impact test results for A508 steel.*

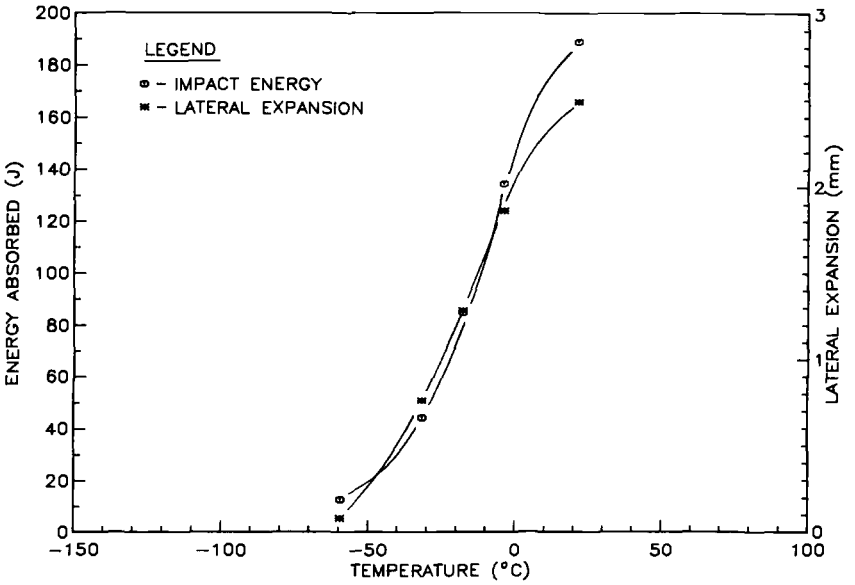

FIG. 3—*Charpy V-notch impact test results for A533 steel.*

[*10*]. Three sizes of specimens were obtained from an arc shaped piece. Eight specimens (38 by 76 by 304 mm) that were not full thickness were taken near the inside diameter. Twenty-four specimens (25 by 50 by 200 mm) were taken near the outside diameter. Sixteen specimens (12.5 by 25 by 100 mm) were machined from the broken ends of the 38- by 76- by 304-mm specimens. Specimens were tested such that the flaw propagation was in the vessel radial direction (specimen orientation C-R). The Charpy V-notch temperature transition curve is shown in Fig. 3.

A516 Steel

The A516-70 steel in this study came from a 44-mm thick straight rolled plate [*11*]. Three sizes of specimens (40 by 80 by 305 mm, 25 by 50 by 200 mm, and 12.5 by 25 by 100 mm) were machined and tested perpendicular to the rolling direction (specimen orientation L-T). The Charpy V-notch temperature transition curve is shown in Fig. 4.

A517 Steel

The A517 steel is from a 25-mm straight-rolled quenched and tempered plate [*12*]. Testing was carried out on 25- by 50- by 200-mm specimens in the L-T direction. The Charpy V-notch temperature transition curve is shown in Fig. 5.

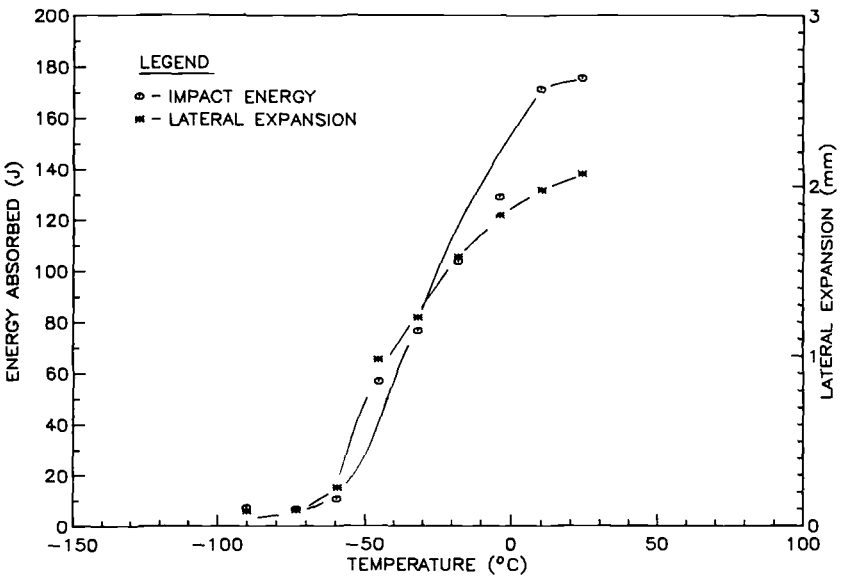

FIG. 4—*Charpy V-notch impact test results for A516 steel.*

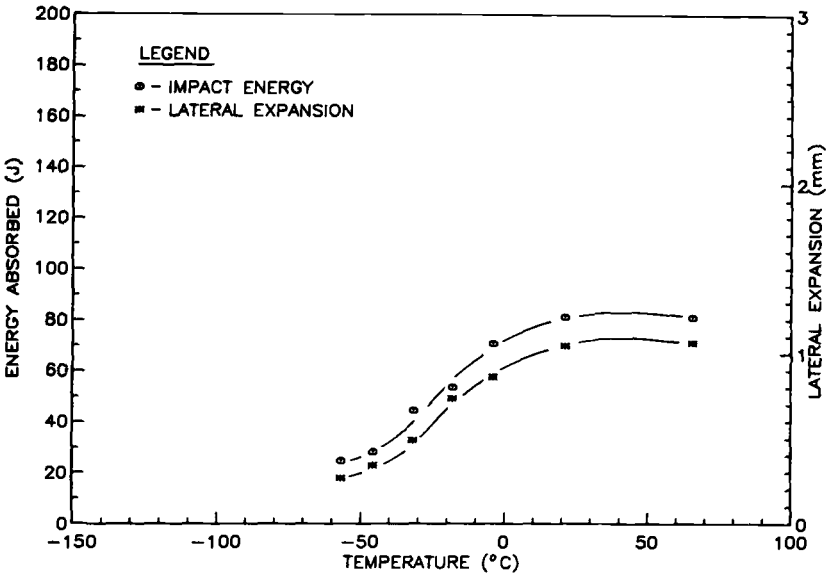

FIG. 5—*Charpy V-notch impact test results for A517 steel.*

A131 Steel

The A131 Grade B (ABS-B) ship steel came from a 25-mm thick hull plate from the Ingram Barge (IOS 3301 Barge) that failed in a brittle manner in 1972. Specimens (25 by 50 by 200 mm) were machined from this plate. The rolling direction was not specifically known but was estimated from the banding of the microstructure. Testing was in the suspected L-T orientation. The Charpy V-notch temperature transition curve is shown in Fig. 6.

CTOD Test Procedure

Before the publication of a standard CTOD test method in 1979, British Standard Methods for Crack Opening Displacement Testing (BS 5762:1979), CTOD tests for this project were conducted according to the British Standards Institution Draft for Development DD 19. After 1979, CTOD testing was conducted according to BS 5762:1979. Test preparation, specimen machining, fatigue cracking, and equipment calibration are similar to those in ASTM Test Method for Plane-Strain Fracture Toughness of Metallic Materials (E 399) and British Standard Methods of Test for Plane-Strain Fracture Toughness (K_{Ic}) of Metallic Materials (BS 5447:1977).

The three-point bend specimen was used exclusively, and only those results from the preferred geometry (B by W-2B by S-8B, as shown in Fig. 7) are reported. A 200-kN universal closed-loop testing machine was used for both fatigue cracking and the final ramp load to failure. Knife edges for the clip-gage

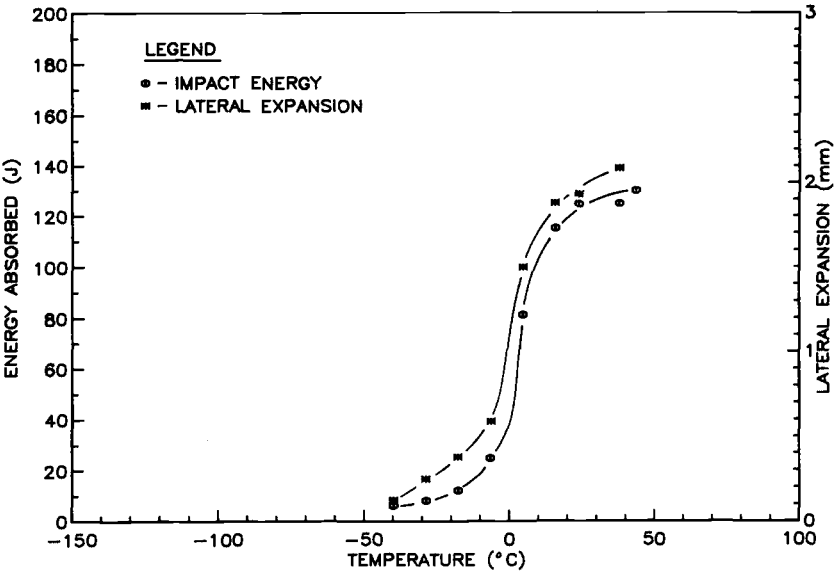

FIG. 6—*Charpy V-notch impact test results for A131 steel.*

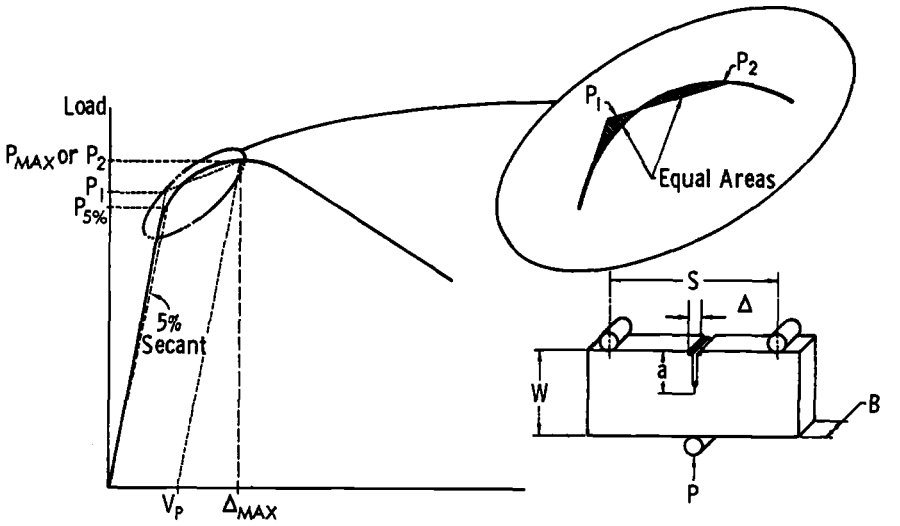

FIG. 7—*Schematic CTOD record showing required measurements.*

were machined into the specimens in every case. Load and clip-gage displacement were transmitted directly from the test machine signal conditioners to an *X-Y* plotter. In addition, load-line displacement was measured using a linear variable displacement transducer (LVDT). A second *X-Y* plotter recorded load versus load-line displacement. Because the LVDT was mounted such that the displacement between the test machine bed and the load cell was measured, the displacements of the test machine crosshead, test fixtures, load cell, and specimen plasticity under the loading rollers were included in the load-line displacement measurement. Therefore the accuracy of the load-line displacement measurement was not as good as the accuracy of the clip-gage displacement measurement. Despite these known inaccuracies, many of which are inherent in measuring load-line displacement on a three-point bend specimen, this mounting location was used because it provided considerable convenience and stability.

Low- and high-temperature testing was carried out within a heat transfer tank mounted on the hydraulic actuator. This arrangement permitted specimens to be held for approximately 20 min at the test temperature and then tested without removing them from the heat transfer fluid. For low-temperature testing, alcohol was used as the heat transfer medium. Below −73°C, liquid nitrogen was circulated through copper coils within the alcohol. Above −73°C, solid carbon dioxide was used to reduce the temperature. For temperatures greater than ambient, a 50-50 mixture of water and a commercial automotive antifreeze was used as the heat transfer fluid. A submersible electric resistance heating element was used to achieve the test temperature. For both cooling and heating, an electric stirrer was used to minimize any thermal gradients, and two thermometers were used to measure the temperature.

The first attainment of a local maximum load was used to analyze the load clip-gage displacement curves. This definition of the critical point is shown for several types of load clip-gage displacement curves in Fig. 1. In the case of a local instability (Fig. 1*b*), where the crack propagates in a brittle manner for a short distance followed by arrest and a subsequent rise in load, the critical values are the load and displacement occurring at the initiation of the local instability.

Critical CTOD values are reported according to the type of failure. Brittle initiation and propagation failures are reported as δ_c values (Fig. 1*a* and *b*). Failures showing a ductile fibrous thumbnail followed by a brittle cleavage or mixed mode propagation are reported as δ_u values (Fig. 1*c* and *d*). For upper-shelf ductile failures (fibrous tearing initiation and propagation) the CTOD values are reported as δ_m values (Fig. 1*e*).

BS 5762:1979 provides the following formula for analyzing the load-clip gage displacement record to obtain the critical CTOD value

$$\delta = \{[K^2 (1-\nu^2)]/(2 \sigma_{ys} E)\} + \{[0.4 (W-a) V_p]/(0.4 W + 0.6 a)\} \quad (1)$$

where the variables used in this and subsequent equations are described in the Appendix and Fig. 7.

This formula is based on an elastic and a plastic component of CTOD and implies the existence of a rotation point below the crack tip. For δ_c and δ_m critical CTOD values, the crack length is taken as the end of the fatigue crack. For δ_u type failures, the end of the fibrous thumbnail was used for the crack length. This usage causes some confusion and perhaps even some degree of contradiction regarding δ_u and δ_m values. From a practical standpoint, for the testing in this study, the use of the ductile thumbnail or fatigue crack caused only minor change (less than 10%) in the critical CTOD value. This usage follows BS 5762:1979 procedure.

The J-integral value at maximum load (not to be confused with J_{Ic}) was also calculated. An analysis by Dawes [*13*], using the load clip-gage displacement can be used to calculate the J integral as follows

$$J = K^2/E + [(P_1 + P_2)/B\,(w\text{-}a)]\,\{W\,V_P/[a + 0.4\,(W\text{-}a)]\} \qquad (2)$$

The more familiar formula by Rice [*14*] using the area under the load-line displacement record was also used

$$J = 2\,A/(W\text{-}a)\,B \qquad (3)$$

where A is the area under the load-line displacement record.

CTOD Test Results

CTOD test results are presented as a function of testing temperature as shown schematically in Fig. 8. The results of CTOD testing of five materials and three specimen sizes are shown in Figs. 9 through 17. All the CTOD temperature transition curves have roughly the same shape, and for the purpose of description these transition curves can be divided into four regions: (1) lower shelf, (2) lower transition, (3) upper transition, and (4) upper shelf.

The lower shelf region is characterized by little or no change in toughness with changes in temperature. All fracture surfaces show brittle behavior both for initiation and propagation. Behavior is nearly linear elastic and K_{Ic} can be used to describe the behavior throughout most of this region. As shown in Fig. 8, the lower shelf region lies approximately 150°C below the nil ductility testing temperature (NDT) for the steels studied. None of the test results shown in Figs. 9 through 17 are "valid" K_{Ic} test results according to ASTM E 399. The only "valid" K_{Ic} test was achieved for the high-strength A517 steel at −200°C. Thus all the data shown in Figs. 9 through 17 should be considered to lie above the lower shelf.

The lower transition region is characterized by a brittle fracture with no visible evidence of prior stable cracking. The toughness increases steadily with increasing temperature from near the linear elastic K_{Ic} values (calculated as 0.005- to 0.013-mm CTOD) to the toughness at the initiation of a fibrous thumbnail visible

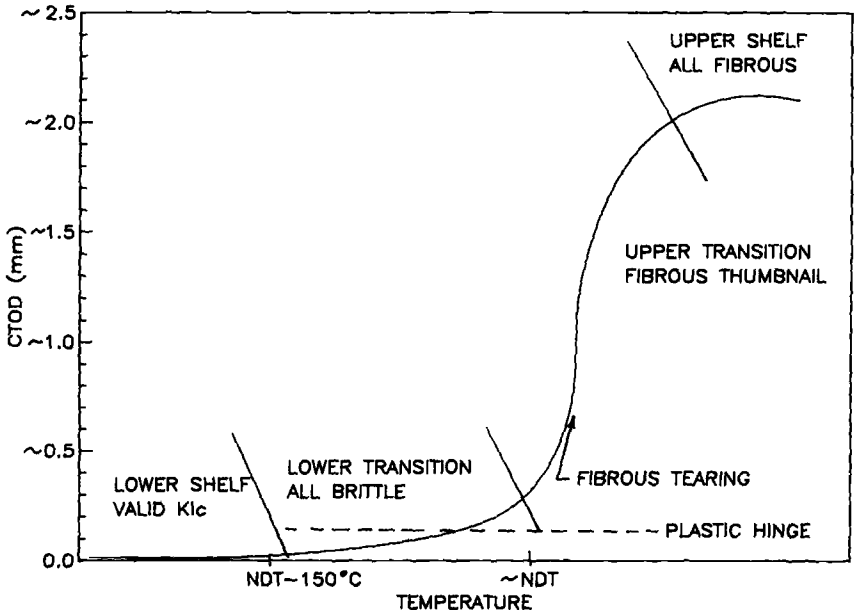

FIG. 8—*Schematic CTOD—temperature transition curve.*

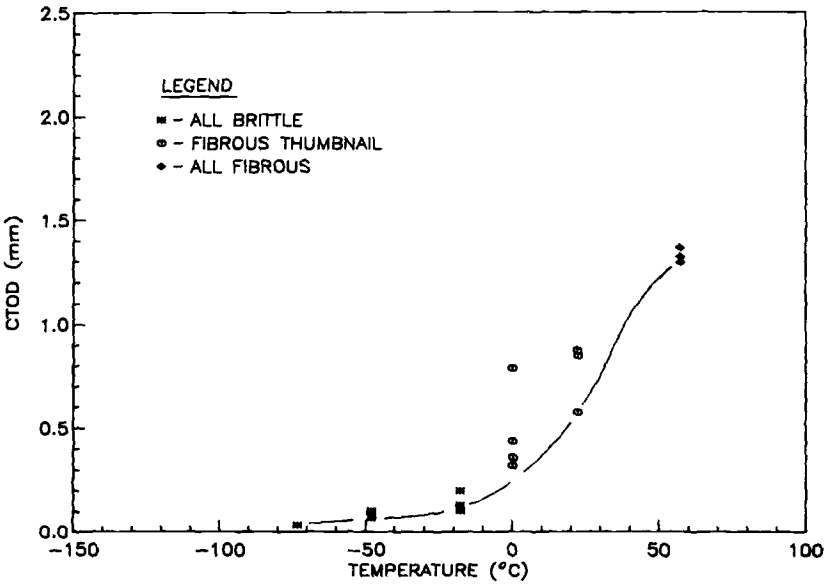

FIG. 9—*CTOD temperature transition curve A508 steel specimen size (25 by 50 by 200 mm).*

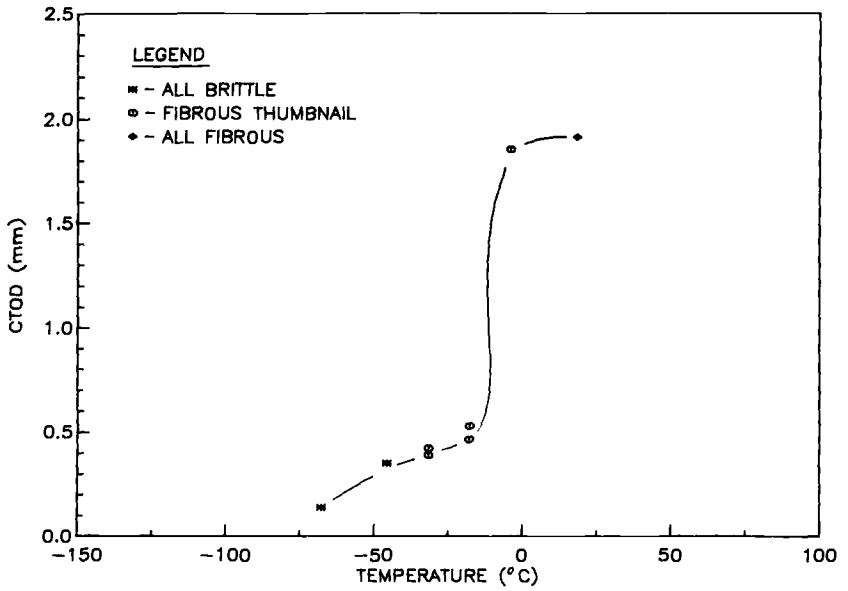

FIG. 10—*CTOD temperature transition curve A533 steel specimen size (38 by 76 by 305 mm).*

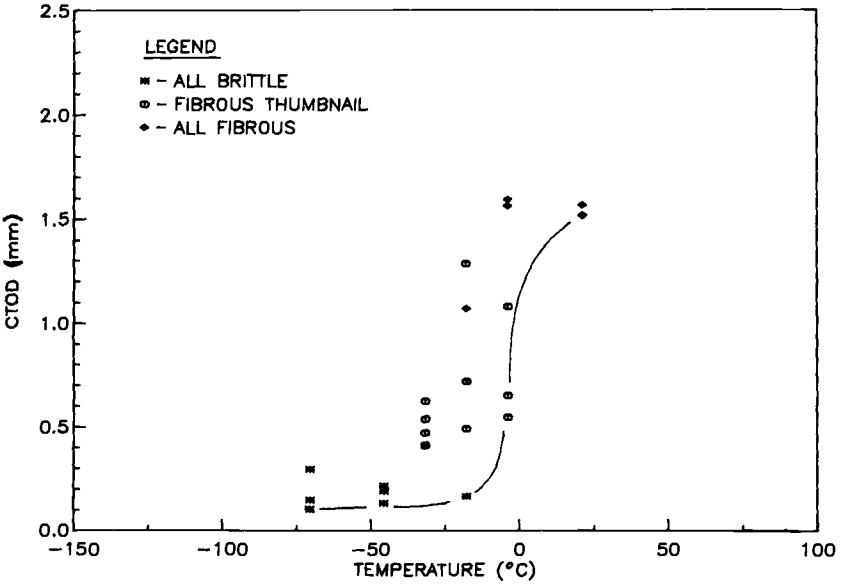

FIG. 11—*CTOD temperature transition curve A533 steel specimen size (25 by 50 by 200 mm).*

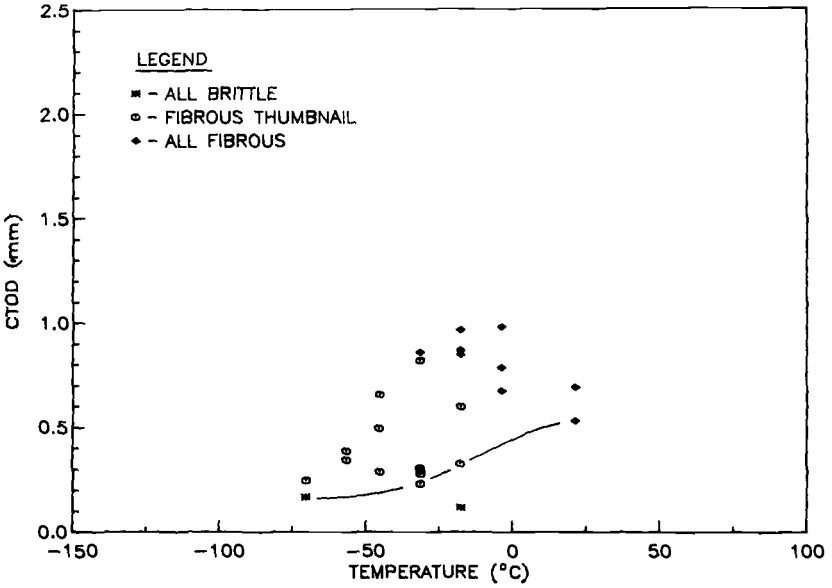

FIG. 12—*CTOD temperature transition curve A533 steel specimen size (12.5 by 25 by 100 mm).*

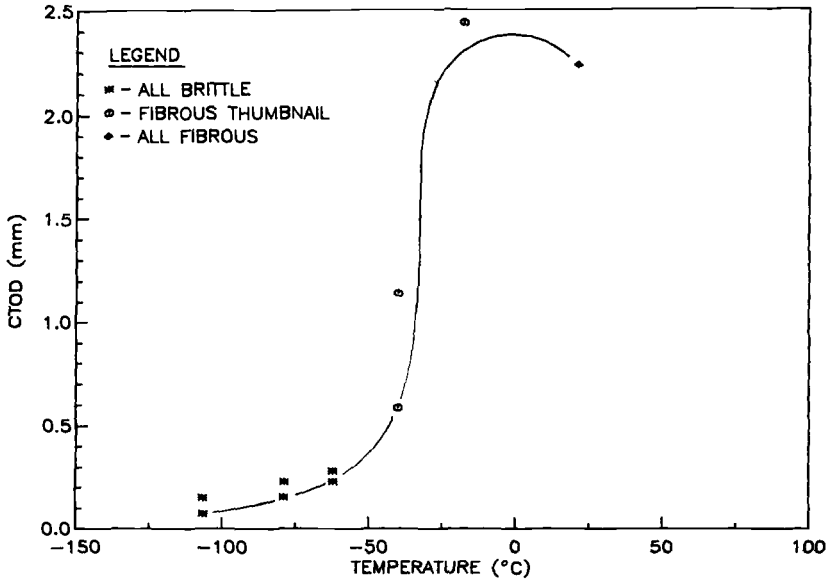

FIG. 13—*CTOD temperature transition curve A516 steel specimen size (40 by 80 by 305 mm).*

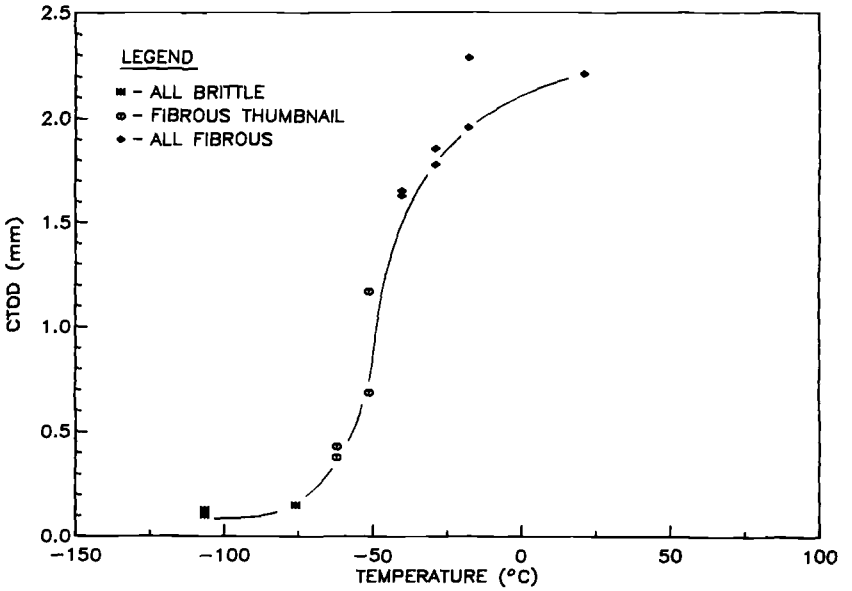

FIG. 14—*CTOD temperature transition curve A516 steel specimen size (25 by 50 by 200 mm).*

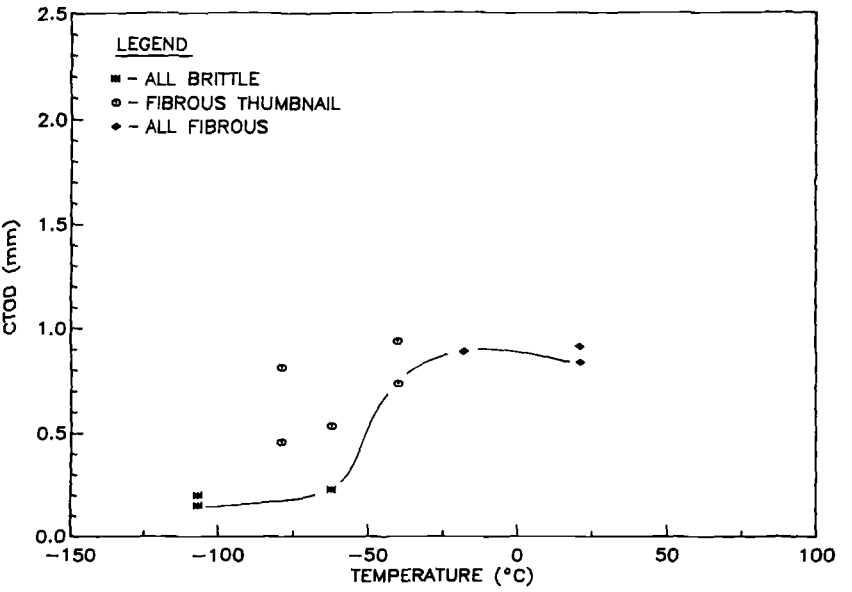

FIG. 15—*CTOD temperature transition curve A516 steel specimen size (12.5 by 25 by 100 mm).*

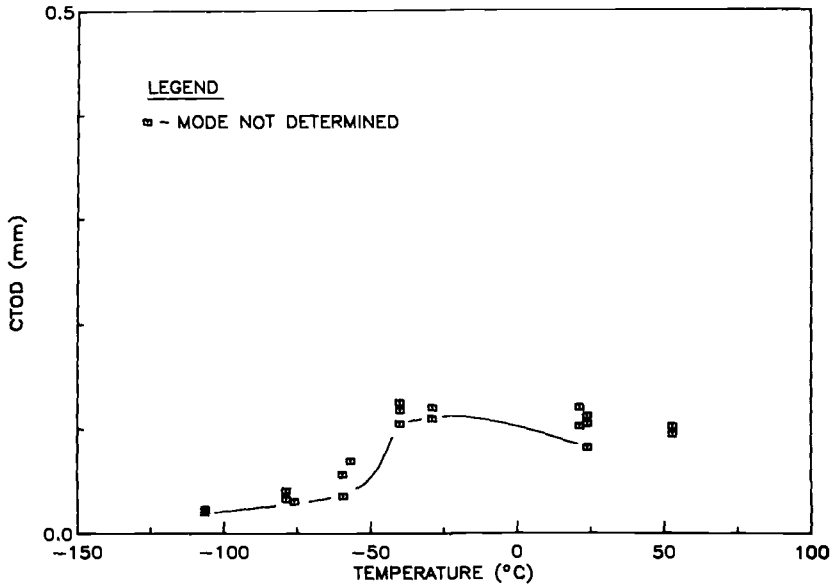

FIG. 16—*CTOD temperature transition curve A517 steel specimen size (25 by 50 by 200 mm).*

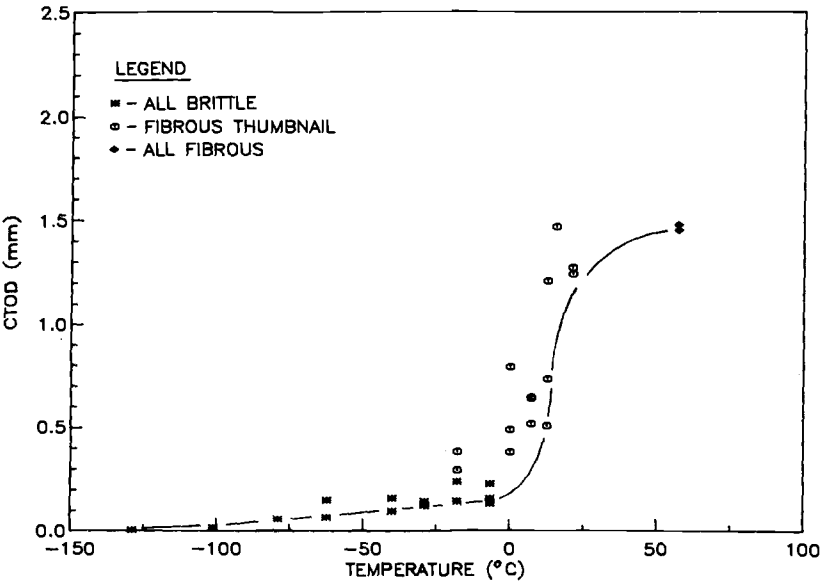

FIG. 17—*CTOD temperature transition curve A131 steel specimen size (25 by 50 by 200 mm).*

to the naked eye (about 0.25 mm for all steels studied except the A517 steel). This toughness increase takes place over a temperature range of 100 to 150°C. Finite-element analysis [*15*] shows that within this range (at about 0.05 to 0.18 mm with variations caused by yield strength and specimen size) a plastic hinge develops in the three-point bend test specimen. The development of a plastic hinge demonstrates that the lower transition region is definitely a region of elastic-plastic fracture behavior. Because K_{Ic} measures linear elastic plane-strain behavior, and J_{Ic} measures the initiation of stable cracking, CTOD is the only fracture parameter currently applicable in this lower transition region. This observation has significant implications for the usefulness of the CTOD parameter because the service temperatures of most structures are in the lower transition region.

In the upper transition region, the failure initiates by stable ductile tearing recognizable by a coarse fibrous "thumbnail" detectable by unaided visual observation of the fracture surface. This ductile "thumbnail" initiation is followed by a fast brittle propagation. The change from the brittle fracture of the lower transition region to the visible fibrous thumbnail of the upper transition region occurs at approximately 0.25 mm for all steels and specimen sizes studied except the A517 steel.

The upper shelf region is characterized by fibrous ductile tearing over the entire surface. The exact location of the start of the upper shelf is somewhat ambiguous because of the data scatter in the upper transition region. This ambiguity is avoided if the upper shelf is arbitrarily defined to start at the temperature at which all specimens show 100% fibrous tearing failures.

In the case of the A517, a high-strength quenched and tempered steel, it is very difficult to determine the difference between brittle and ductile failures by visual observation. This difficulty is analogous to that encountered in determining the percent shear for Charpy V-notch impact specimens of high-strength steels. The general shape of the A517 steel CTOD temperature transition curve is the same as that of the lower strength steels discussed above, but at lower values. Because the A517 steel has an upper shelf at about 0.1 mm, the change from lower to upper transition regions occurs at about 0.05 to 0.075 mm, unlike the 0.25 mm for the other four steels. As shown by finite-element analysis, this 0.05- to 0.075-mm CTOD value occurs before the development of a plastic hinge for the 25- by 50- by 200-mm A517 specimen [*15*].

Three specimen sizes of two steels, A533 and A516, were tested. On the upper shelf, there is a clear effect of specimen size. The larger specimens yield a higher CTOD value and a higher apparent toughness. In the upper transition region, the data scatter is severe. CTOD values varied from upper shelf values (a function of specimen size) to the maximum lower transition region values (about 0.25 mm) at the same temperature. In the lower transition region, there is no consistent effect of specimen size on the lowest values of the CTOD test data. However, the smaller test specimens exhibit more data scatter than do the larger specimens. Therefore, if average CTOD values are used, there is an

apparent increase in toughness with a decrease in specimen size in the lower transition region. No valid K_{Ic} results were obtained for the A533 and A516 steels in this study even at −200°C. However, the intent of ASTM E 399 is to eliminate specimen size effects. Therefore, it is expected that there would be no size effect on the lower shelf.

The effect of specimen size on the critical CTOD value needs further study. However, specimen size effect appears to depend upon the location on the temperature transition curve where the testing is being conducted. Therefore, as required in the British Standard, CTOD testing should use full thickness specimens. In addition, when testing small specimens, even if they are the full thickness of the structure under investigation, more tests will be required to achieve a statistically valid population than will be required for larger specimens because there is more scatter in the test results for the smaller specimens.

Correlation of Various Fracture Parameters

The correlation between stress intensity factor K and two commonly used elastic-plastic fracture parameters (J and CTOD) have been investigated. Two correlations with CVN (Barsom-Rolfe two stage and Robert's lower bound) were also investigated. These two correlations are described in the Pressure Vessel Research Committee (PVRC) interpretive report by Roberts and Newton [*16*]. The correlations were applied to all five steels, A517, A508, A533, A516, and A131, and to the three specimen sizes tested of A533 and A516. The results are presented in Figs. 18 through 26. A discussion of the correlations follows.

J *Integral*

The equations used to estimate K from J are

$$K = \sqrt{J E} \quad \text{plane-stress} \tag{4}$$

$$K = \sqrt{J E/(1 - \nu^2)} \quad \text{plane-strain} \tag{5}$$

These correlations are only strictly valid for linear elastic conditions where J is equivalent to the energy release rate G. In this region, with the proper restrictions on specimen size, it is proper to use the expression

$$K_{Ic} = \sqrt{J_{Ic}^{E}/(1 - \nu^2)} \quad \text{plane-strain} \tag{6}$$

The J values used herein are not the results of J_{Ic} testing. Because the J values are based on maximum load regardless of prior plasticity or crack extension, and because the correlations with K are strictly valid only for linear elasticity, the K values are not described as K_{Ic} values. However, they may be regarded as an estimate of toughness for the particular specimen geometry tested, a K_c value. For this report, the plane-strain correlation was used. However, there is

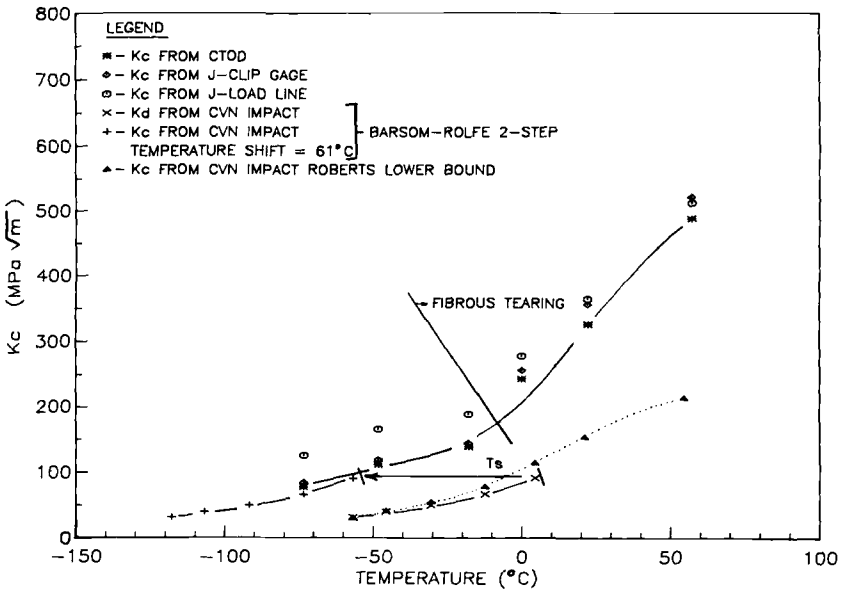

FIG. 18—K_c-*CVN-CTOD-J correlations for A508 steel specimen size (25 by 50 by 200 mm) lower bound values.*

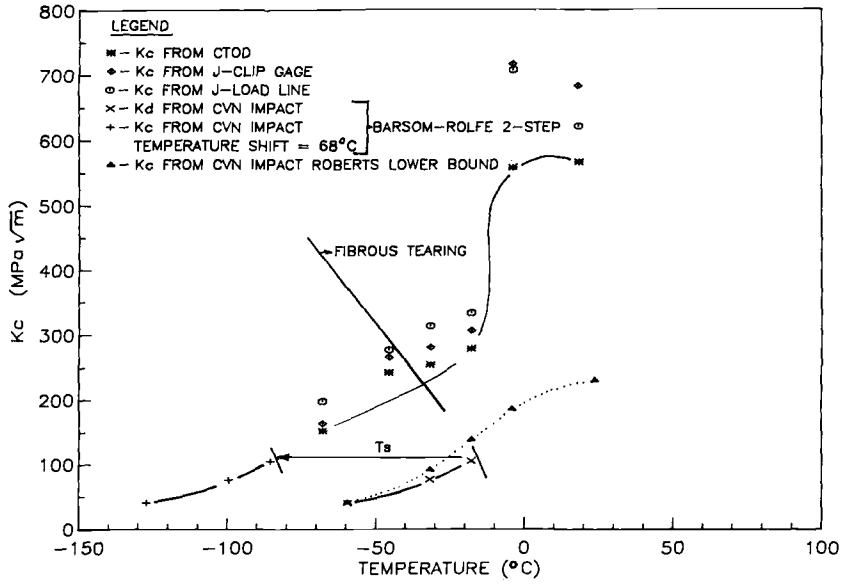

FIG. 19—K_c-*CVN-CTOD-J correlations for A533 steel specimen size (38 by 76 by 305 mm) lower bound values.*

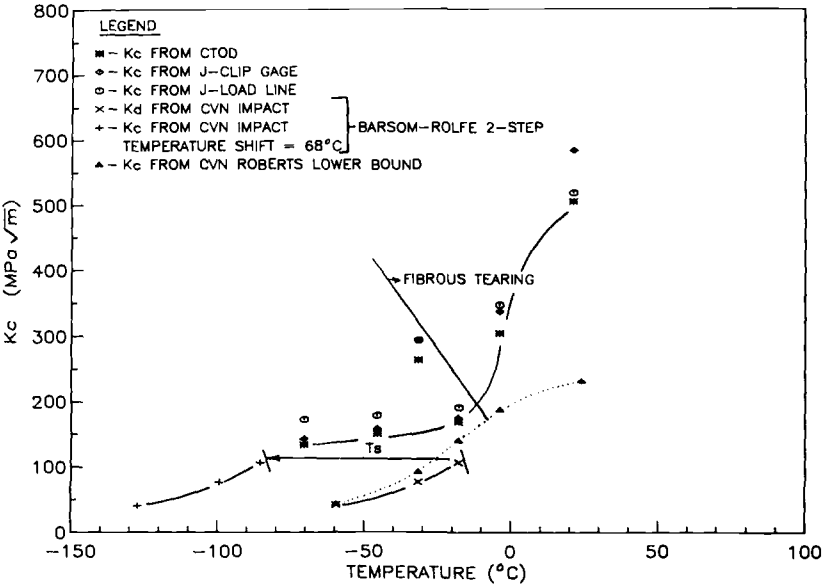

FIG. 20—K_c-*CVN-CTOD-J correlations for A533 steel specimen size (25 by 50 by 200 mm) lower bound values.*

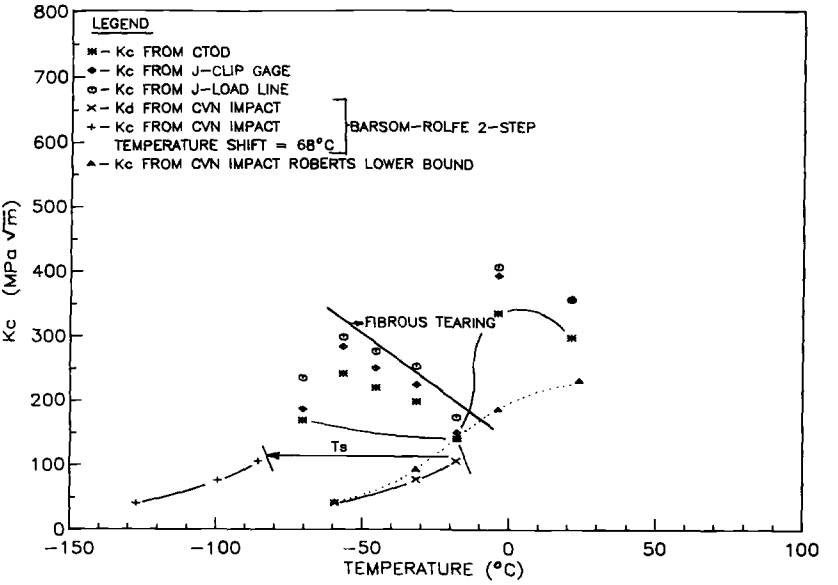

FIG. 21—K_c-*CVN-CTOD-J correlations for A533 steel specimen size (12.5 by 25 by 100 mm) lower bound values.*

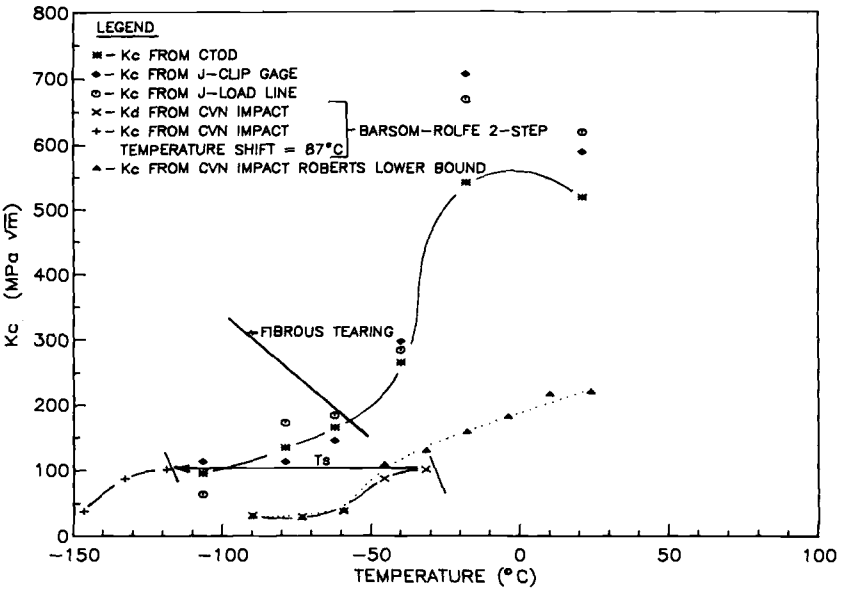

FIG. 22—K_c-*CVN-CTOD-J correlations for A516 steel specimen size (40 by 80 by 305 mm).*

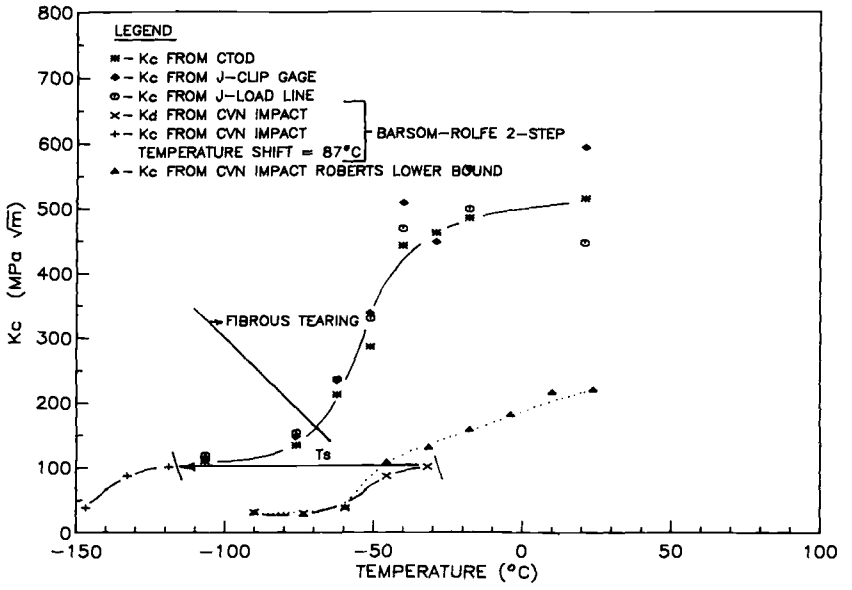

FIG. 23—K_c-*CVN-CTOD-J correlations for A516 steel specimen size (25 by 50 by 200 mm) lower bound values.*

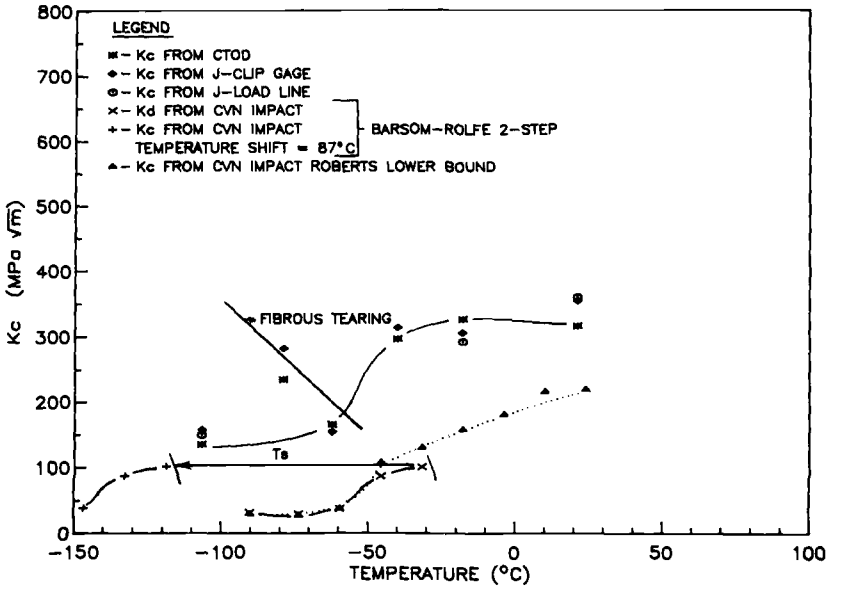

FIG. 24—K_c-*CVN-CTOD-J correlations for A516 steel specimen size (12.5 by 25 by 100 mm) lower bound values.*

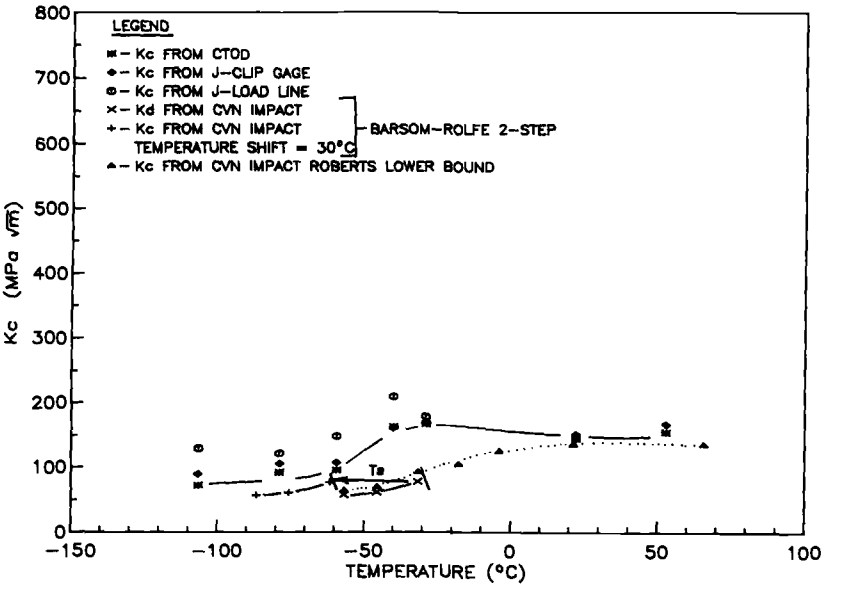

FIG. 25—K_c-*CVN-CTOD-J correlations for A517 steel specimen size (25 by 50 by 200 mm) lower bound values.*

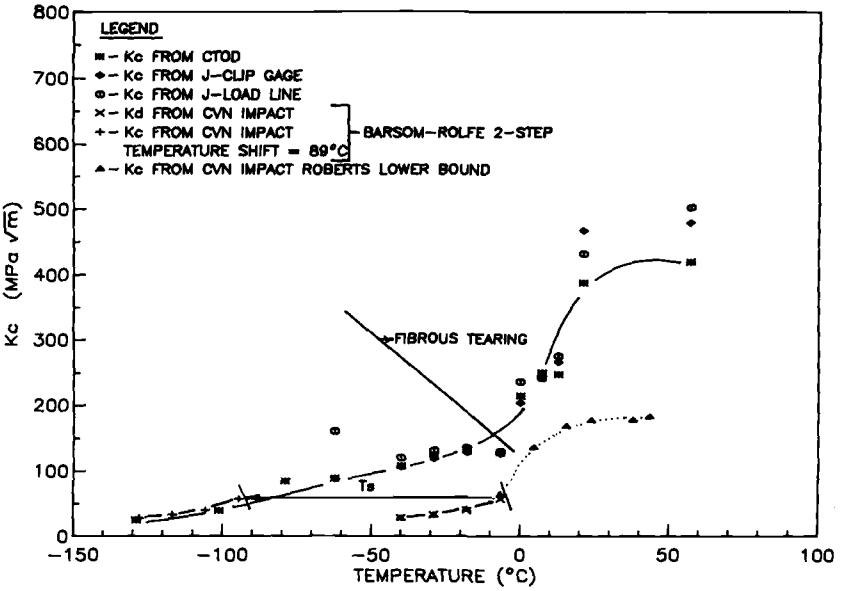

FIG. 26—K_c-*CVN-CTOD-J correlations for A131 steel specimen size (25 by 50 by 200 mm) lower bound values.*

only a 5% difference in results for plane strain versus plane stress. Thus it is insignificant which correlation (Eq 4 or Eq 5) is used.

CTOD

The equation used to estimate K from CTOD is

$$K = \sqrt{m E \sigma_{ys} \delta} \tag{7}$$

The parameter m is described as a constraint factor that varies from 1 to 2 based on the degree of through thickness constraint. The use of the correlations for CTOD and J described above (Eqs 4 and 7) implies that CTOD can be correlated with J by the following

$$J = m \sigma_{ys} \delta \tag{8}$$

A two-dimensional finite-element analysis of three-point bend specimens performed at the University of Kansas [*15*] provides additional insight into the correlation of CTOD with J. For all cases analyzed, all five materials and all three specimen sizes, analytically computed J and CTOD are linearly related over the entire range of performance from linear elasticity to the limit load. This implies that, for two-dimensional analysis, CTOD and J are equivalent parameters. In addition, for the range of materials and specimen sizes investigated,

the finite-element analysis [*15*] provided a consistent correlation of CTOD with J using the flow stress instead of the yield stress and using $m = 1.6$ for plane strain and $m = 1.2$ for plane stress as follows

$$\sigma_{flow} = \sigma_{ys} + \sigma_{ult}/2 \tag{9}$$

$$J = 1.2\ \sigma_{flow}\ \delta \quad \text{plane-stress} \tag{10}$$

$$J = 1.6\ \sigma_{flow}\ \delta \text{ plane-strain} \tag{11}$$

In order to maintain consistency with the correlations from J to K, which used the plane-strain Eq 5, the correlation data presented in Figs. 18 to 26 use a modification of Eq 7 applied to the lowest CTOD test values

$$K = \sqrt{1.6\ E\ \sigma_{flow}\ \delta} \tag{12}$$

Charpy V-Notch

Two separate correlations of Charpy V-notch with K_c were investigated. The Barsom-Rolfe correlation requires two steps [*17*]. The first step involves estimation of the dynamic fracture toughness curve K_d from the Charpy V-notch impact energy absorption results as shown below

$$K_d = \sqrt{5\ E\ (\text{CVN})},\ \text{psi} \cdot \text{in.}^{1/2},\ \text{psi, ft-lb} \tag{13a}$$

$$K_d = \sqrt{0.64\ E\ (\text{CVN})},\ \text{MPa} \cdot \text{mm}^{1/2},\ \text{MPa, J} \tag{13b}$$

The second step depends on the assumption that in the transition zone (defined as extending from the lower shelf CVN values to a CVN value in ft-lb of one half the yield strength in ksi), the static K_c and dynamic K_d transition curves have a similar shape and are separated by a constant temperature difference. This temperature shift can be related to the room temperature yield strength by

$$Ts = 215 - 1.5\ \sigma_{ys},\ ^\circ\text{F, ksi} \tag{14a}$$

$$Ts = 119 - 0.12\ \sigma_{ys},\ ^\circ\text{C, MPa} \tag{14b}$$

Thus K_c at temperature $T - Ts$ is equal to K_d at temperature T. This correlation is only applicable for CVN values from the lower shelf to about half way up the transition curve.

The Robert's lower bound CVN correlation was also investigated. As the name implies, this correlation is very conservative and should be used only where such conservatism does not impose excessive restrictions on design or material selection. The formulae for this correlation are

$$K_c = 9.35\ (\text{CVN})^{0.63},\ \text{ksi} \cdot \text{in}^{1/2},\ \text{ft-lb} \tag{15a}$$

$$K_c = 8.47\ (\text{CVN})^{0.63},\ \text{MPa} \cdot \text{m}^{1/2},\ \text{J} \tag{15b}$$

Results of Correlations

The results of correlations among K_c, CVN, CTOD, and J are shown in Figs. 18 through 26. Both steps of the Barsom-Rolfe two stage correlation (CVN to K_d then the temperature shift to K_c) are shown. Robert's lower bound correlation for static K_c values is similar to the CVN versus K_{Id} (dynamic) curve of the Barsom-Rolfe two stage correlation.

The low to moderate yield strength steels (A131, A516, A533, and A508) exhibit a typical slow rise in toughness with increasing temperature from the lower shelf through the lower transition region. These steels then undergo a rapid toughness increase (the upper transition region), which is characterized by the development of a ductile fibrous thumbnail on the fracture surface. In the lower transition region, the Barsom-Rolfe CVN versus K_c correlation yields essentially the same results as the CTOD versus K_c and the J versus K_c correlations. This fact increases the confidence in all the correlations except Robert's lower bound, which by intention is a conservative lower bound curve. In the upper transition region and upper shelf, specimen size effects dominate the material behavior. Thus, after the initiation of stable cracking, the correlations may not be meaningful even though the trend appears to be reasonable.

The high-strength steel (A517) behaves in a manner somewhat different from the lower strength steels. Because of the higher yield strength, there is a much smaller loading rate shift. Also because of the higher yield strength, the determination of a fibrous thumbnail on the failure surface is much more difficult for the A517 steel than for the lower yield strength steels. This is analogous to the difficulty encountered in fracture appearance rating Charpy V-notch specimens of high-strength steel. However, the general appearance of the temperature transition curve, with a lower shelf, a lower and upper transition region, and an upper shelf, is maintained but at much lower toughness levels.

Conclusions

An investigation of the CTOD behavior of four pressure vessel steels and one ship steel to develop the material behavior, define the effects of test variables, establish the practical aspects of CTOD testing, and study the relationships among several toughness parameters resulted in the following conclusions.

1. The CTOD fracture parameter provides a method to extend fracture mechanics concepts from plane-strain linear elastic behavior to elastic-plastic behavior. The CTOD test method is well established as a British Standard (BS 5762:1979). The CTOD test is the only standardized fracture mechanics type test method that can be used in the region between plane-strain linear elastic (K_{Ic} per ASTM E 399) behavior and ductile tearing initiation (J_{Ic} per ASTM Test for J_{Ic}, a Measure of Fracture Toughness [E 813]) behavior.

2. For all the low to moderate yield strength steels tested, macroscopic stable crack growth (defined as a "thumbnail" with a coarse fibrous texture visible without aid on the fracture surface) apparently starts at about the same CTOD

value, regardless of yield strength or specimen size. For the high-strength A517 steel, fibrous tearing starts at a much lower CTOD value.

3. The correlations relating CVN, CTOD, J, and K_c values yield consistent results within the ranges of applicability. The results presented in this report, in terms of the familiar stress intensity factor K_c, can easily be presented in terms of any other parameter. Because of the inability to achieve a valid K_{Ic} value, the absolute accuracy of the correlations cannot be verified. It is clear, however, that the toughness values increase with increasing temperature as expected. At temperatures above the onset of macroscopic fibrous tearing, the accuracy and applicability of these correlations is questionable. However, at these temperatures, the toughness generally is high enough that fracture is no longer of primary concern.

4. The limited study of size effects in CTOD testing showed a decrease in the upper shelf toughness with a decrease in specimen size. This was the expected effect. Specimen size effects in other regions of the temperature transition curve were not clearly established particularly when the lowest test values were considered. Another effect as important as that listed above was the increase in the data scatter with decreasing specimen size. Because of this scatter, it is necessary to increase the number of tests as the specimen size decreases in order to determine the bounds on possible material behavior. It also appears to be prudent to use the lowest test value attained for design use until actual service experience dictates a more appropriate value. Finally, until the effect of specimen size is fully understood, the requirement in Methods for Crack Opening Displacement Testing (BS 5762:1979), that the thickness of the test specimen be the full thickness of the structure of interest, appears fully warranted.

In summary, a body of CTOD test data for five structural steels using three specimen sizes has been developed over a range of temperatures. Practical aspects of CTOD testing, including test record analysis, fracture surface categorization, specimen size effect, and experimental techniques, have been discussed. Because K_{Ic} measures linear elastic plane-strain behavior and the J_{Ic} measures the initiation of stable cracking, CTOD is the only fracture mechanics parameter currently applicable in the lower transition region. Finally, correlations among CVN, CTOD, and J-integral toughness were investigated, and the results were used to estimate the nonplane-strain stress intensity factor K_c.

Acknowledgments

The authors would like to express appreciation to Dr. A. K. Shoemaker, Chairman, Subcommittee on Failure Modes in Pressure Vessel Materials—Pressure Vessel Research Committee, Welding Research Council (WRC). This work was cooperatively funded by WRC and American Iron and Steel Institute (AISI). The steels tested were provided by S. Steel, Bethelehem Steel, Oak Ridge National Laboratory, and the U.S. Coast Guard. This support is gratefully acknowledged.

APPENDIX

Explanation of Variables

$$K_{5\%} = (P_{5\%}\, S/B\, W^{1.5})\, f(a/w) \quad \text{ASTM E 399}$$

$$\delta = [K^2\,(1 - \nu^2)/2\,\sigma_{ys}\, E] + \{[0.4(W - a)\, V_p]/(0.4\, W + 0.6\, a)\} \quad \text{BS 5762:1979}$$

$$J = (K^2/E) + [(P_1 + P_2)B/(W - a)]\,\{V_p/[a + 0.4(W - a)]\} \quad \text{Dawes 1977 [13]}$$

where

a	=	crack length
B	=	specimen thickness
W	=	specimen depth
E	=	modulus of elasticity
ν	=	Poisson's ratio
$K_{5\%}$	=	K_Q stress intensity factor at 5% secant offset load
$P_{5\%}$	=	5% secant offset load
P_1	=	shown on Fig. 7
P_2	=	maximum load
V_P	=	plastic component of clip-gage displacement
K	=	stress intensity factor at maximum load
S	=	loading span

References

[1] Harrison, J. D., "The State of the Art in Crack Tip Opening Displacement (CTOD) Testing and Analysis," *Metal Construction*, Vol. 12, No. 9–11, Sept.-Nov. 1980, pp. 415–418, 420–422, 524–529, 600–605.

[2] Wells, A. A., "Unstable Crack Propagation in Metals: Cleavage and Fast Fracture," *Proceedings of Crack Propagation Symposium*, Vol. 1, Cranfield, England, 1961, pp. 210–230.

[3] Burdekin, F. M. and Stone, D. E. W., "The Crack Opening Displacement Approach to Fracture Mechanics in Yielding Materials," *Journal of Strain Analysis*, Vol. 1, No. 2, Jan. 1966, pp. 145–153.

[4] Ingham, T., Egan, G. R., Elliot, D., and Harrison, T. C., "The Effect of Geometry on the Interpretation of COD Test Data," *Practical Application of Fracture Mechanics to Pressure Vessel Technology*, Vol. C54, London, England, 1971.

[5] Dawes, M. G., "The Application of Fracture Mechanics to Brittle Fracture in Steel and Weld Metals," Ph.D. thesis (Council for National Academic Awards), The Welding Institute, Abington, Cambridge, England, 1976.

[6] Harrison, T. and Fearnbough, G., "The Influence of Specimen Dimensions on Measurements of the Ductile Crack Opening Displacements," Gas Council Engineering Research Station, Newcastle upon Tyne, England, 1979.

[7] Barr, R. R., Elliot, D., Terry, P., Walker, E. F., "The Measurement of COD and Its Application to Defect Significance," *Metal Construction*, Vol. 7, No. 12, Dec. 1975, pp. 604–610.

[8] Derby, R. W., Merkle, T. G., Robinson, G. C., Whittman, G. D., and Witt, F. J., "Test of 6-Inch-Thick Pressure Vessels, Series 1: Intermediate Test Vessels V-1 and V-2," HSST Program, Feb. 1974, ORNL-4895.

[9] Mager, T. R., Yanichko, ZS. E., and Singer, L. R., "Fracture Toughness Characterization of HSST Intermediate Pressure Vessel Material," Westinghouse Nuclear Energy Systems HSST Program Report 38, WCAP-8456, Dec. 1974.

[10] Bryan, R. H., Canonico, D. A., Holz, P. P., Iskander, S. K., Merkle, J. G., Smith, J. E., and Stelzman, W. J., "Test of 10-Inch-Thick Pressure Vessels. Series 3: Intermediate Test Vessel V-8," Dec. 1979, ORNL/NUREG-58, HSST Program.

[11] Stuber, A. B., "A Study of Crack Growth Behavior and Specimen Size Effects in the Crack

Tip Opening Displacement Test," Ph.D. thesis, University of Kansas, Lawrence, KS, Sept. 1980.

[12] Blom, R. C., "Final Report on Testing of the A517 Material," M.S. thesis, University of Kansas, Lawrence, KS, June 1980.

[13] Dawes, M. G., "Elastic-Plastic Fracture Toughness Based on COD and J-Integral Concepts," The Welding Institute, Cambridge, England, 1977.

[14] Rice, J. R., "A Path Independent Integral and the Approximate Analysis of Strain Concentration by Notches and Cracks," *Journal of Applied Mechanics, Transactions American Society of Mechanical Engineers*, Vol. 5, Series E, June 1968, pp. 379–386.

[15] Wellman, G. W., Rolfe, S. T., and Dodds, R. H., "Two and Three Dimensional Finite Element Analysis of Standard Three-Point Bend Specimens," *Fracture Mechanics: Sixteenth Symposium, STP 868*, American Society for Testing and Material, Philadelphia, 1985.

[16] Roberts, R. and Newton, C., "Interpretive Report on Small-Scale Test Correlations with K_{Ic} Data," *Welding Research Council Bulletin 265*, New York, Feb. 1981.

[17] Barsom, J. M. and Rolfe, S. T., "Correlations Between K_{Ic} and Charpy V-Notch Test Results in the Transition-Temperature Range," *Impact Testing of Materials, ASTM STP 466*, American Society for Testing and Materials, Philadelphia, 1970, pp. 281–302.

DISCUSSION

M. G. Dawes (written discussion)—This paper draws attention to the fact that the ductile to brittle transition temperature range in steels can include a temperature band of several hundred degrees for which it is not possible to obtain a valid ASTM test result, that is, for the available section thickness, the temperatures are either too high to obtain a valid K_{Ic} (ASTM Test for Plane-Strain Fracture Toughness of Metallic Materials [E 399]) value or too low to obtain a valid J_{Ic} (ASTM E 813) value. Within this temperature range, the authors chose to characterize the fracture toughness using the CTOD test (BS 5762 or draft ASTM E24-08-05 method) or a full J equivalent. The latter test was first proposed by the writer at the ASTM Subcommittee E24.08 on Elastic-Plastic and Fully Plastic Fracture Mechanics Terminology meeting in Nov. 1980, but it has not yet been published in the open literature. In view of this, and the increasing awareness of the need for a ubiquitious elastic-plastic fracture mechanics test, the proposal is reiterated below.

The proposal is based on the following premises.

1. From an experimental viewpoint at least, the crack-tip opening displacement (CTOD) and the J contour integral are equally useful for quantifying resistance to the onset of crack extension under elastic-plastic loading conditions.
2. All fracture events are inherently valid, and to deny this is to place artificial restraints on the use of potentially valuable test data.

The proposed test would be complementary to the existing J_{Ic} test and would cover all the different fracture behaviors that can occur between the extremes

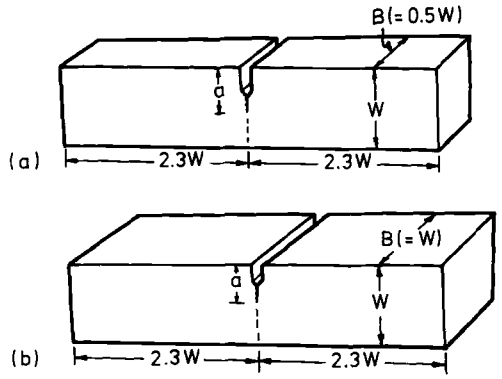

FIG. 27—*Proportional dimensions for bend test pieces, half loading span = 2W (after BS 5762):* (a) *preferred, 0145 < a/W < 0.55; and* (b) *subsidiary, a/W value by agreement between manufacturer and purchaser.*

associated with K_{Ic} tests and R-curve tests. This would give the same continuity in J based tests as is seen in CTOD based tests. Furthermore, there is now evidence by Shih [*1*] to show that we are approaching more accurate theoretical relationships between CTOD and J, so that any fracture behavior described in terms of CTOD should have a recognized equivalent in terms of J.

In considering this proposal it will be helpful to review the background and philosophy for the fracture behaviors covered by the CTOD test, and also the very limited extent to which these are covered by the J_{Ic} test.[1]

The CTOD test was developed to quantify resistance to the onset of crack extension in structures where experience has shown that the material yield strengths, section thicknesses, crack sizes, loading rates, and temperatures can result in brittle fractures at nominal stresses less than yield, but with amounts of crack-tip region plasticity that invalidate a description of resistance to crack extension in terms of K_{Ic}. These situations commonly occur in structural materials at ambient temperatures, especially in ferritic steels. In the case of steels it is often not recognized that the onset of cleavage fracture, even without prior stable crack growth, can occur with widely different amounts of crack-tip region plasticity, including net section yielding.

This background led to the philosophy of full thickness CTOD tests at the temperatures and loading rates in the structures of interest, combined with the use of the same specimen types and instrumentation as used in the ASTM E 399 and BS 5447 K_{Ic} tests. The only case for limiting the specimen thickness is when $B > 2.5\ (K_{Ic}/\sigma_Y)^2$, that is, when geometry independent plane strain fracture toughness values occur.

The full thickness preferred geometry test specimens (see Fig. 27*a*) are used to obtain lower bound critical CTOD values. However, by agreement between

[1]The ASTM E 813 J_{Ic} test is designed to give a geometry independent estimate of resistance to the onset of slow stable crack extension.

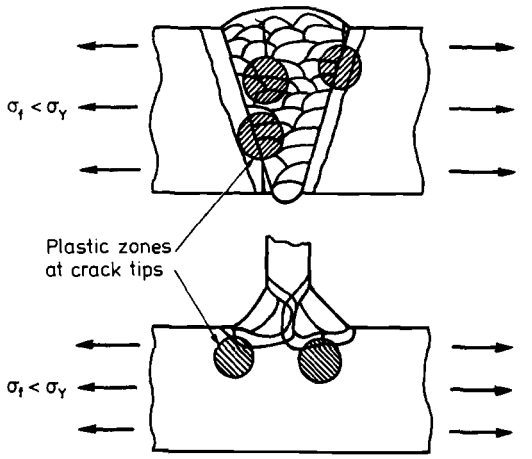

FIG. 28—*Shallow cracks in welds. Many brittle fractures in welded steel structures occur by cleavage, without prior slow stable crack growth, under conditions that invalidate linear-elastic fracture mechanics analyses.*

the parties involved, the subsidiary (Fig. 27*b*) full section thickness square test specimens can be used to match more closely the fracture toughness associated with shallow cracks that have their tips in discrete microstructures, such as those in welds (Fig. 28). This dispensation for shallow cracks is extremely important, since the lower bound values of fracture toughness are often unduly restrictive when applied to as-welded structures. For example, in the ductile/brittle tran-

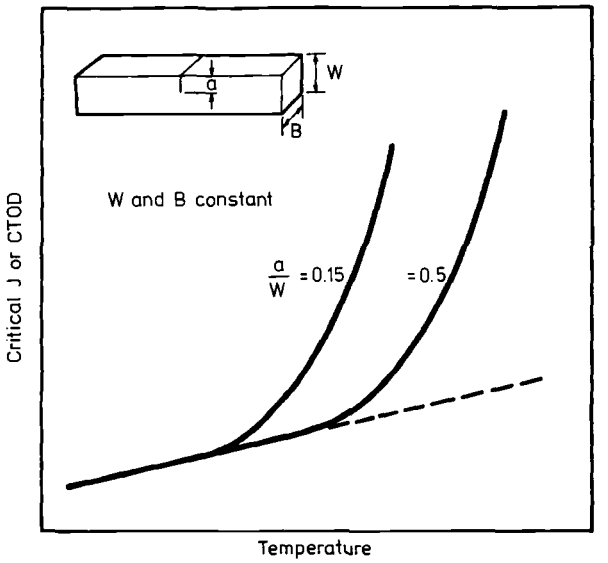

FIG. 29—*Influence of notch depth on critical* J *and CTOD values.*

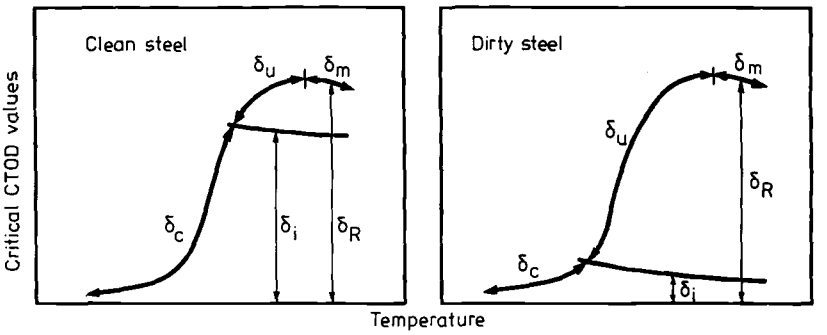

FIG. 30—*Notation for different fracture events in CTOD tests:* δ_c = *unstable cleavage—no prior slow crack growth;* δ_u = *unstable cleavage—with prior slow crack growth;* δ_m = *plastic collapse or tearing instability;* δ_i = *onset of slow stable crack growth; and* δ_R = *resistance curve value.*

sition temperature ranges for some steels, the more realistic measures of fracture toughness for shallow cracks may represent critical crack sizes that are more than double the values associated with lower bound measurements of fracture toughness (Fig. 29), which could have serious implications concerning available nondestructive examination (NDE) capabilities.

All the advantages associated with the aforementioned geometry dependent critical CTOD values can be realized in the proposed equivalent *J* tests by simply interpreting the CTOD test results in terms of *J*. This can be achieved by introducing an equivalent fracture notation (Figs. 30 and 31) and estimating the critical *J* values from the standard load versus notch mouth opening displacement records, for instance, by using the procedures put forward by Sumpter and Turner [*2*] and by Dawes [*3*]. As indicated in Fig. 31, there will be some situations where the values of J_I will satisfy the requirements for the ASTM E 813 J_{Ic} test and others where acceptable, but geometry dependent J_I values may be obtained from the subsidiary geometry test specimens.

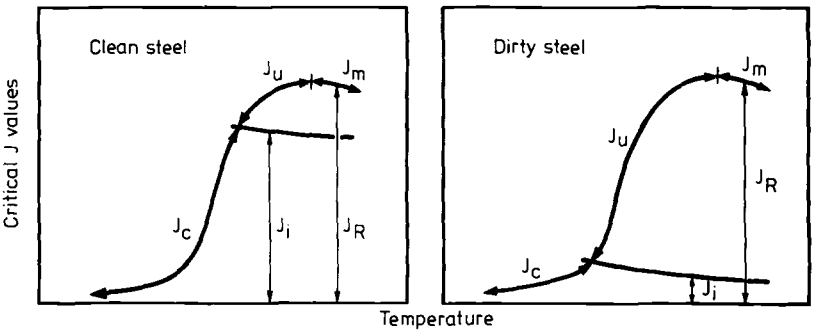

FIG. 31—*Proposed notation for different fracture events in* J *tests:* J_c = *unstable cleavage—no prior slow crack growth;* J_u = *unstable cleavage—with prior slow crack growth;* J_m = *plastic collapse or tearing instability;* J_i = *onset of slow stable crack growth* = J_{Ic} *when certain conditions are met; and* J_R *resistance curve value.*

References

[1] Shih, C. F., "Relationships Between the J-integral and the Crack Opening Displacement for Stationary and Extending Cracks," *Journal of the Mechanics and Physics of Solids*, Vol. 29, No. 4, Aug. 1981, pp. 305–326.

[2] Sumpter, J. D. E. and Turner, C. E., "Method for Laboratory Determination of J_c," *Cracks and Fracture, STP 601*, American Society for Testing and Materials, Philadelphia, 1976, pp. 8–18.

[3] Dawes, M. G., "Elastic-Plastic Fracture Toughness Based on the COD and J-Contour Integral Concepts," *Elastic-Plastic Fracture, STP 668*, American Society for Testing and Materials, Philadelphia, 1979, pp. 307–333.

Allen L. Hiser[1] *and Frank J. Loss*[1]

Alternative Displacement Procedures for *J-R* Curve Determination

REFERENCE: Hiser, A. L. and Loss, F. J., **"Alternative Displacement Procedures for *J-R* Curve Determination,"** *Elastic-Plastic Fracture Test Methods: The User's Experience, ASTM STP 856*, E. T. Wessel and F. J. Loss, Eds., American Society for Testing and Materials, 1985, pp. 263–277.

ABSTRACT: This investigation evaluates alternative displacement techniques with the single-specimen compliance (SSC) procedure, which do not require the commonly used load-line displacement measurements in a compact toughness (CT) specimen to determine the *J-R* curve. The two techniques studied are a double clip gage technique involving both crack-mouth displacement and load-line displacement at the edges of the specimen and a technique that requires only crack-mouth displacement. *J-R* curves developed using these techniques are compared to *J-R* curves developed with the normal load-line based deflections. In addition, results of a round-robin program using the SSC procedure are discussed in terms of validating the double clip gage technique. *J-R* curves developed from crack-mouth displacements on the J-integral specimen from ASTM Test for J_{Ic}, a Measure of Fracture Toughness (E 813) suggest that the ASTM Test Method for Plane-Strain Fracture Toughness of Metallic Materials (E 399) specimen design can be used for both linear-elastic (for example, K_{Ic}) and elastic-plastic (for example, *J-R* curve) toughness assessments. This fact can be of particular value in the testing of reactor surveillance specimens that may not have been machined to permit load-line displacement measurements.

KEY WORDS: fracture tests, displacement, elasticity, *J-R* curve, elastic-plastic fracture, single-specimen compliance procedure, double clip gage technique, nuclear pressure vessel steel

Assessment of structural integrity requires knowledge of the fracture toughness of the materials used in the structure. For elastic-plastic behavior, the *J-R* curve is a widely used method to characterize fracture toughness. The *J-R* curve is composed of values of J integral and crack growth as determined experimentally, usually with a compact toughness (CT) specimen or a bend specimen.

Experimental determination of the *J-R* curve requires displacement measurement at the points of load application V_{LP}. Because of the practical difficulty of this requirement, displacements are usually measured at the load line V_{LL} under the assumption that the latter is an adequate approximation to V_{LP}. With CT specimens of the ASTM Test Method for Plane-Strain Fracture Toughness of

[1]Engineer and technical director, respectively, Materials Engineering Associates, Inc., 9700-B George Palmer Highway, Lanham, MD 20706.

Metallic Materials (E 399) design, V_{LL} measurements have required an enlargement of the notch region of the specimen and an increase in the spacing between the loading pinholes to permit the placement of a displacement gage on the load line (Fig. 1). However, increasing the pinhole spacing reduces the ligament between the hole and the top or bottom of the specimen, possibly creating local yielding problems on small specimens (<25 mm thick). Additionally, compact specimens in reactor surveillance capsules or test reactor irradiations may not have the modified notch, thereby restricting their current use to K_{Ic} determinations, involving crack mouth displacement V_M measurement. Therefore, a procedure to develop *J-R* curves from standard CT specimens would prove to be extremely advantageous.

One instance in which load-line displacement measurements were not possible was in the testing of the 0.5T- and 0.8T-CT specimens used in the Nuclear Regulatory Commission (NRC) Heavy Section Steel Technology (HSST) program on irradiated low upper-shelf welds. These specimens were machined with integral seats on the load line for clip gage mounting, but these seats were

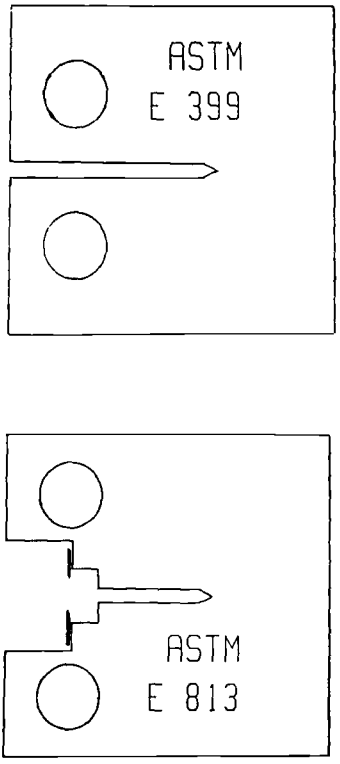

FIG. 1—*Comparison between the recommended ASTM E 399 compact specimen and the J-modified compact specimen. With the ASTM E 813 specimen, the larger pinhole spacing can cause yielding problems at the edge of the specimen.*

insufficient for accurate displacement measurement. Additionally, the irradiated specimens could not be modified for mounting of razor blades on the load line, as is commonly done in experimental determinations of J. To alleviate these problems, the authors modified the technique at the Naval Research Laboratory (NRL) for J-R curve testing. This technique uses two clip gages to record displacements at alternative locations, that is, crack mouth displacement V_M and load-line displacement at the specimen edges $V_{LL'}$ (Fig. 2). This method has been termed the "double clip gage technique" where V_M is used for crack length prediction via the compliance procedure, while $V_{LL'}$ is used to determine the specimen energy input necessary for the calculation of J. The apparatus used

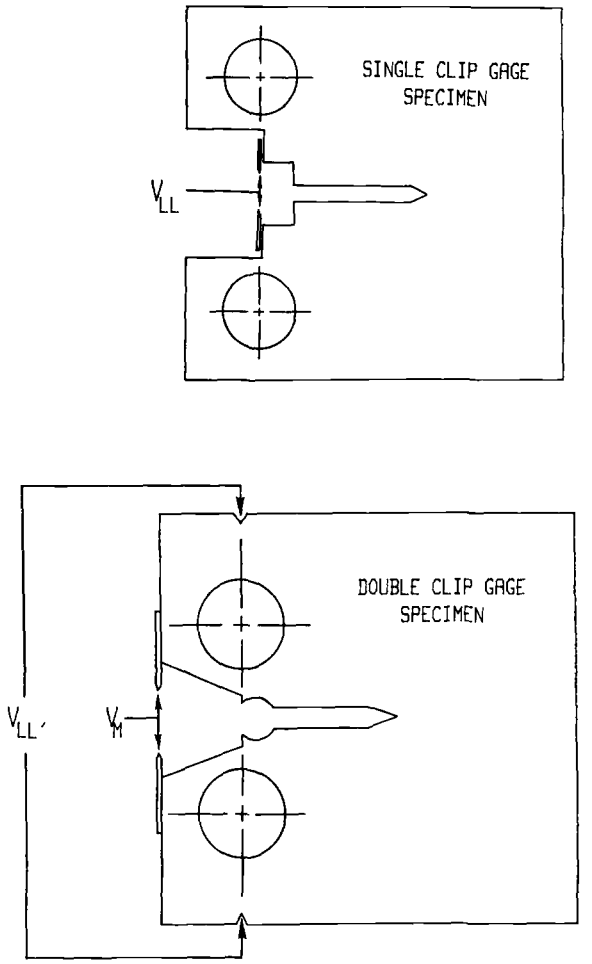

FIG. 2—*Comparison between displacement measurement points using the double clip gage technique and the single clip gage method. With the double clip gage technique,* V_M *is used for crack length prediction via unloading compliance while* $V_{LL'}$ *is used for* J *calculations.*

for the "double clip gage technique" is identical to that suggested in the ASTM tentative *J-R* curve test procedure. The clip gages used are from standard technology.

To validate this new technique, a round-robin program using 0.5T-CT specimens having 20% side-grooves was undertaken to define the "prototype" *J-R* curve for a given steel. The round-robin testing involved the single-specimen compliance (SSC) technique, which requires measurement of the load-line displacement between the pins V_{LL}. A successful comparison of these results with those from the double clip gage technique was required to qualify the latter procedure for testing of the HSST specimens.

Since the completion of this round robin, studies of elastic loading in CT specimens by Newman [*1*] and Orange [*2*] have suggested that it is not necessary to modify CT specimens for V_{LL} determination. Instead, they have proposed that V_M provides an approximation to V_{LP} that is even better than V_{LL}. However, verification of this hypothesis for experimental elastic-plastic loading is required.

Double Clip Gage Qualification Round Robin

Test Procedures

The round robin conducted to validate the double clip gage technique used 0.5T-CT specimens (12.7 mm thick) cut from a single piece of A 533-B (Unified Numbering System [UNI] K12539) Class 2 steel plate. These specimens were then precracked and side grooved by 20% before distribution to the participants.

The SSC procedure was used in the *J-R* curve development, as presented in Ref *3*. Participants were invited to submit results conducted using a single load-line mounted clip gage. The specimen used in these tests consisted of a modified ASTM E 399 specimen with an enlarged notch and increased pinhole spacing, as shown in Fig. 2 (top).

Double clip gage tests were conducted with a specimen design similar to that to be tested under the NRC HSST low upper-shelf welds program, as shown in Fig. 2 (bottom). These specimens are similar to the ASTM E 399 design, except that the notch was slightly enlarged. Only NRL conducted both double clip gage tests and single clip gage tests.

Data Analysis Procedures

Analysis of the test data took several forms. The first was to check each test result against the validity requirements from the tentative *J-R* curve test procedure [*3*]. The second step was to determine critical *J-R* curve parameters, specifically the crack growth initiation value of J (J_{Ic}) and the average value of tearing modulus T_{avg}. To determine these values, the *J-R* data points between the 0.15- and 1.5- mm exclusion lines, as defined by the ASTM Test for J_{Ic}, a Measure of Fracture Toughness (E 813), were curve fit to a power law expression as given by

$$J = C\,(\Delta a)^N \tag{1}$$

where Δa is the crack growth measured by unloading compliance, and C and N are parameters determined through regression analysis. As an alternative procedure to ASTM E 813, J_{Ic} in this paper is taken as that formulated by Loss and his coworkers [*4*], that is, as the J value at the intersection of this power law expression with the 0.15-mm exclusion line. T_{avg} is expressed by

$$T_{avg} = (E/\sigma_Y^2)\,(dJ/da) \tag{2}$$

where dJ/da is the average slope of the J-R curve between the exclusion lines, as determined by a closed form regression fit of the power law expression to a linear equation.

The final step in the analysis procedure was to divide the bank of data into three groups, labeled "NRL Single Clip Gage," "NRL Double Clip Gage," and "Other Laboratories". The J-R curves and the averaged parameters J_{Ic} and T_{avg} would then highlight any bias of data generated at the NRL in comparison to other single clip gage data as well as any bias caused by the double clip gage technique.

Round-Robin Results

Eight laboratories participated in the round-robin program (Table 1). Considerable scatter was evident in the single clip gage results partly because of material inhomogeneity as well as problems in test technique. A repetition of the round robin at this time would probably give a smaller degree of scatter caused by improved procedures now used by many of the participants.

All of the digital J-Δa data were put into permanent computer storage to facilitate analysis. Table 2 lists the validity criteria from Ref *3*, along with the percentage of tests meeting each requirement. The two criteria most frequently violated are for final crack length prediction error and for data spacing between the secant line and Δa_{max} $(0.1b_o)$. With these 12.7-mm thick specimens, Δa_{max} was ~1.27 mm, giving a very narrow region in which to place the required ten

TABLE 1—*Round-robin participants.*

Participants	Location
Babcock & Wilcox	Alliance, OH
CISE[a]	Milano, Italy
David Taylor NSRDC[b]	Annapolis, MD
Del Research	Hellertown, PA
IWM[c]	Freiburg, Federal Republic of Germany
U.S. Naval Academy	Annapolis, MD
U.S. Naval Research Laboratory	Washington, DC
Westinghouse R&D Center	Pittsburgh, PA

[a]CISE is Centro Informazioni Studi Esperienze.
[b]NSRDC is Naval Ship Research and Development Center.
[c]IWM is Institut für Werkstoffmechanik.

TABLE 2—J-R *Curve validity criteria* [3].

Code	Criterion	Percent Compliance
1	Final crack length prediction error (Section 8.7.3)[a] $\lvert\Delta a_p - \Delta a_m\rvert < 0.15\Delta a_{max}$ where $\Delta a_{max} = \text{MIN}[0.1\ b_0, \Delta a_m]$	37
2	Initial unload scatter $< 0.002W$ (Section 8.3.1)	65
3	Initial crack length straightness (Section 8.7.1)	94
4	Crack extension uniformity (Section 8.7.2)	70
5	10 data points between secant line and $0.1b_0$ (Section 8.4.1)	24
6	3 data points between $\Delta a = 0$ and secant line (Section 8.4.1)	73

[a]Refers to section in Ref *3*.

data points. Additionally, the predicted crack extension had to be within 0.19 mm of the measured crack extension to be valid. This is a fairly difficult task, as evidenced by the low percentage of tests that met this criterion. Indeed, fully 86% of the tests met the more lenient crack extension prediction requirements in the ASTM E 813 J_{Ic} test, while only 37% could meet the tentative *J-R* curve standard requirement.

A summary of average J_{Ic} and T_{avg} values for each of the groups is provided in Table 3. From Table 3, the T_{avg} values are extremely close, with a maximum deviation in the round-robin groups of 6%. However, the J_{Ic} values differ by up to 16%.

Figure 3 illustrates all of the single clip gage results, including the NRL data. Also shown is a band chosen to represent the data. This band compares well with the 95% interval from the HY-130 *J-R* curve round robin [5]. The average J_{Ic} value for the NRL single clip gage data is 16% less than the J_{Ic} value for the non-NRL data, while the T_{avg} values are virtually identical.

A comparison of the NRL double clip gage results with the band of single clip gage data is shown in Fig. 4. The data fit well within the band, with a slight bias towards the lower boundary of the band near the 0.15-mm exclusion line. The J_{Ic} and T_{avg} values for this data are 8 and 6% lower than the non-NRL single clip gage results, respectively. These values are 10% higher and 4% lower than the NRL single clip gage values, respectively. Based upon the excellent corre-

TABLE 3—*Average results of* J_{Ic} *and* T_{avg}.

Participants	J_{Ic}, kJ/m^2	T_{avg}
Other laboratories	185	53
NRL single clip gage	155	52
NRL double clip gage	171	50

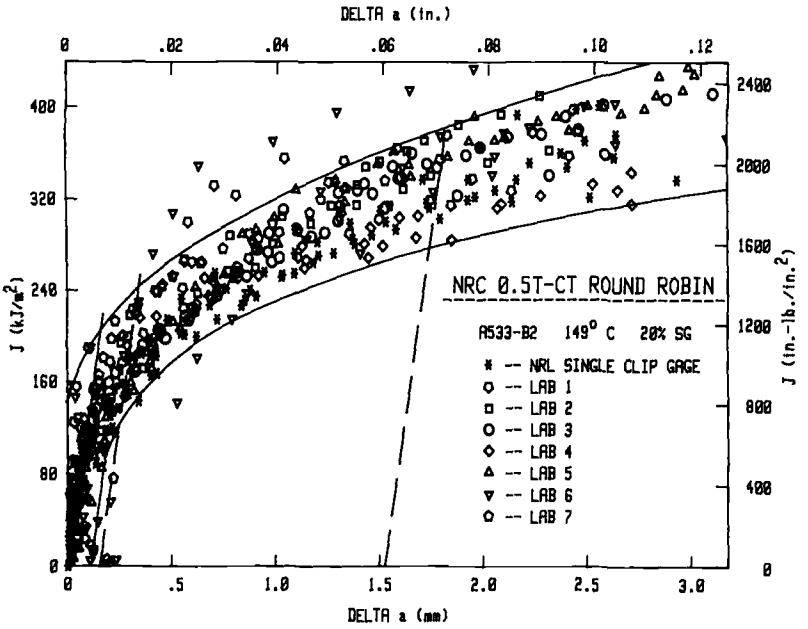

FIG. 3—*Summary of the single clip gage data from the round robin. The band shown will be used to compare with other sets of data.*

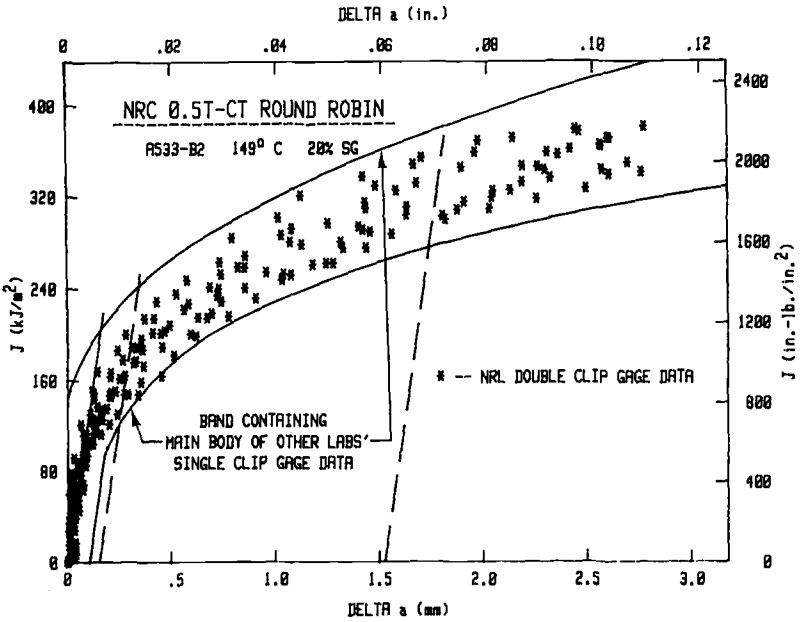

FIG. 4—*Comparison between NRL double clip gage data and the band from Fig. 3. The double clip gage data are to the center of the band, except for a slight bias towards the lower boundary near the 0.15 mm exclusion line.*

spondence of the double clip gage data with the single clip gage data, the double clip gage technique is considered suitable for testing of the HSST specimens.

Elastic-Plastic Displacement Relationships for Compact Specimens

Background

The currently accepted practices for determining plane strain fracture toughness K_{Ic} and the plane strain J_I-R curve use different displacement measurement points, and hence different specimens. This difference has resulted from the requirement of researchers to measure load-line V_{LL} (in place of load-point) displacement for J-R curve determination, while K_{Ic} determinations only require crack-mouth displacement V_M. To reconcile these two test techniques, several investigators have proposed using crack-mouth displacement in place of load-line displacement for J-R curve development. In 1975, Neale [*6*] suggested a factor of 0.77 to relate crack-mouth displacement to load-pin displacement. These results were from an elastic-plastic finite-element study. More recently, Newman [*1*] and Orange [*2*] have proposed using V_M as a replacement for load-point displacement from finite-element studies of elastic loading. The factor suggested by Orange is 0.773. Using basic geometry, Landes [*7*] suggested a simplistic relation between V_M and V_{LL}, based on a/W and axis of rotation ratio r. The value of r was dependent on material strength and whether the loading was elastic or plastic. Assuming full plasticity and an intermediate strength material (that is, $r = 0.33$), the Landes relation yields values from 0.727 at $a/W = 0.5$ to 0.769 at $a/W = 0.75$. Despite these numerical solutions, no experimental work has been conducted to verify if crack-mouth displacement can indeed be used to replace either load-line or load-point displacement for elastic-plastic loading.

By combining these theoretical studies with experimental results from the HSST irradiated low upper-shelf welds program using the double clip gage procedure, conclusions can be reached as to the feasibility of relating crack-mouth displacement to load-line displacement. In addition, several suggestions can be made as to a proper technique to relate these displacements. Using the resulting technique, these crack-mouth J-R curves can be compared to load-line J-R curves for two steels.

Results and Discussion

Using the double clip gage technique, simultaneous values of crack-mouth V_M and load-line prime $V_{LL'}$ displacement were measured (Fig. 2, bottom). To establish a relationship between V_M and $V_{LL'}$ for elastic-plastic loading, these quantities were compared for several specimens (irradiated and nonirradiated) of A 508 (UNI K13502) weld deposit from the HSST low upper-shelf welds program. As an example, Fig. 5 shows typical behavior of these two displacements. While the relationship is of a quadratic form, a linear fit to the data also may be considered acceptable. Additionally, while Fig. 5 shows results from 0.8T-CT

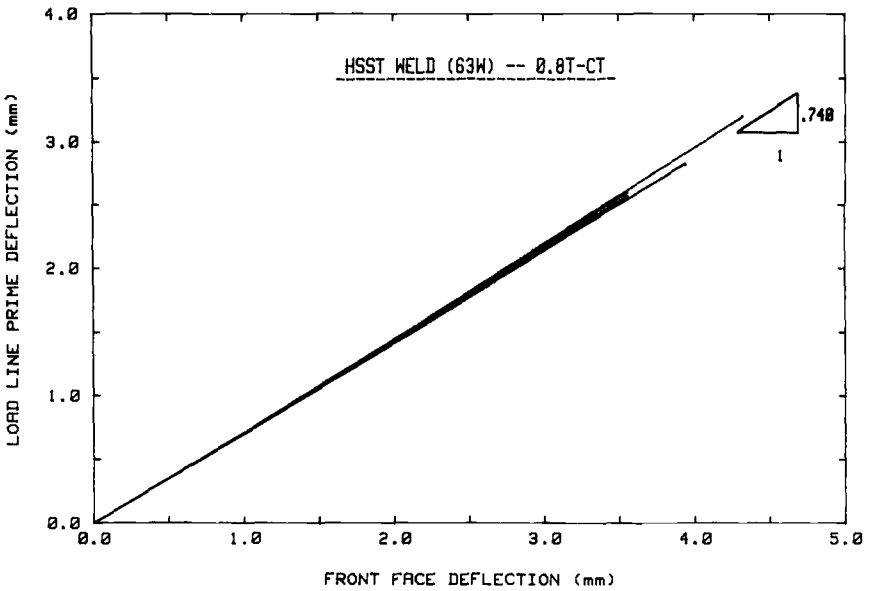

FIG. 5—*Typical comparison between* V_M *and* $V_{LL'}$ *for one of the seven HSST welds. Similar behavior has been seen for the other six HSST welds.*

tests, the 0.5T-CT results are virtually identical. Almost no bias was found in these results because of temperature (range from 75 to 288°C) or irradiation.

The nonlinear relationship between $V_{LL'}$ and V_M as a function of relative crack length a/W is more clearly illustrated in Fig. 6. The symbols shown are from five tests. The points are from differentiating the quadratic equation relating V_M to $V_{LL'}$ (that is, $dV_{LL'}/dV_M$), and then evaluating the differential at intervals of V_M as a/W increases. The sharp increase in ratio at the beginning of each data set is indicative of the change in loading from elastic to plastic. Also shown in this figure is the elastic displacement ratio $V_{LL'}/V_M$ computed by Newman for the standard CT specimen. In this case, the enlarged notch (Fig. 2, bottom) was not modelled. From the experiment results, the average value of displacement ratio was found to be 0.740. Crack-mouth displacement can be "corrected back to the load line" by multiplying with this 0.740 ratio. This value was fairly constant with temperature (75 to 288°C), specimen size (0.5T-and 0.8T-CT) and irradiation.

By taking all of the data in a form similar to Fig. 6 and fitting it to a straight line, the following relationship was established

$$V_{LL'}/V_M = 0.1807\ (a/W) + 0.6385 \tag{3}$$

Remarkably, Eq 3 is within 1% of the Landes equation (with $r = 0.33$) for a/W from 0.4 to 0.8.

A summary of the elastic displacement ratios determined by Newman for the

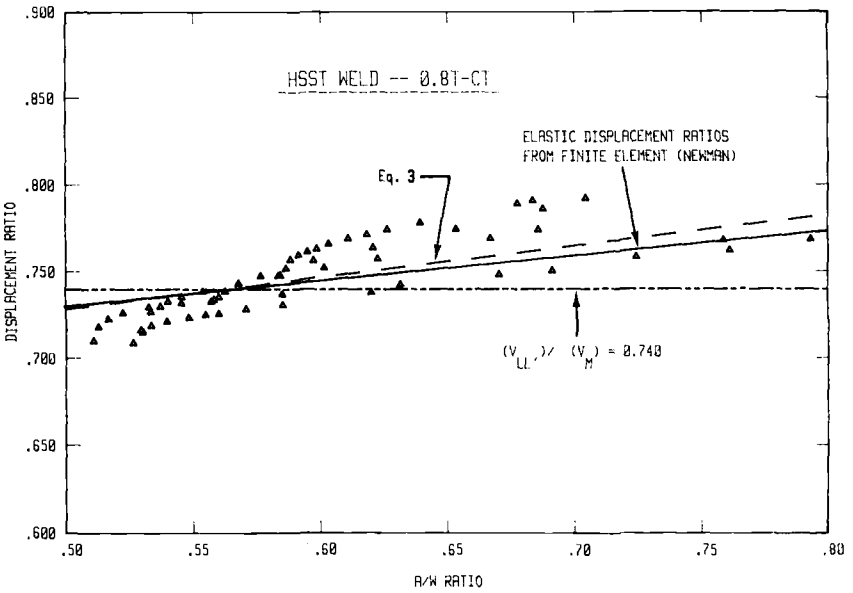

FIG. 6—*Displacement ratio as a function of relative crack length* a/W. *An average value of this ratio and a linear expression are compared to the finite-element results* [1].

standard CT specimen is given in Fig. 7. The value of 0.740 crosses Newman's appropriate data at $\sim a/W = 0.57$, indicating that the finite-element results closely match elastic-plastic behavior. From this figure, it is readily apparent that the relationship between load point and load line *LP/LL* is more nonlinear than the relationship between load point and crack mouth *LP/M*, indicating that crack mouth should be more accurate with just a constant factor. As well, load-line prime and load-line deflection appear to differ by from 8% to about 1% between a/W of 0.5 and 0.75 from this figure, while from the round-robin results these two appear almost to be equal (Fig. 4). Surprisingly, Eq 3 matches almost identically the appropriate finite-element data.

The potential use of this procedure is illustrated in Figs. 8 and 9. These specimens were tested using the double clip gage procedure, yielding the "combination" data. The "crack mouth" data are determined using a factor of 0.740 to correct the J values. Figure 8 compares the combination data and the crack-mouth data. This comparison is the maximum deviation seen for these test results. Figure 9 is a more typical comparison. Included here is a *J-R* curve determined using only the load-line prime data. This comparison shows how close the agreement typically is. Table 4 compares J_{Ic} and T_{avg} results from several tests included in this program. The *J-R* curve based on crack-mouth displacement that has been corrected back to the load line appears to give a consistently good result. Surprisingly, the constant factor (0.740) and Eq 3 give virtually identical J_{Ic} and T_{avg} values.

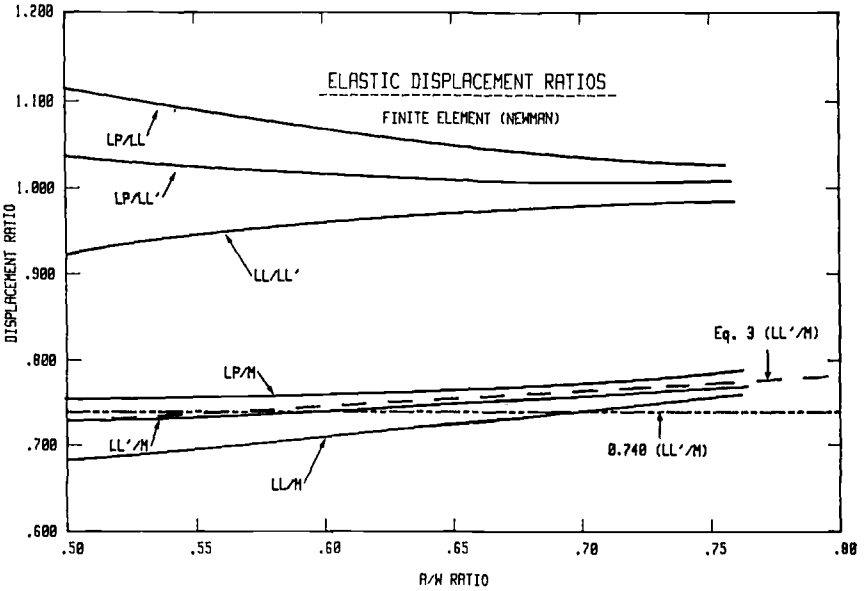

FIG. 7—*Elastic displacement ratios for the standard CT computed by Newman [1]. Also shown is the factor 0.740 and the linear expression (Eq 3).*

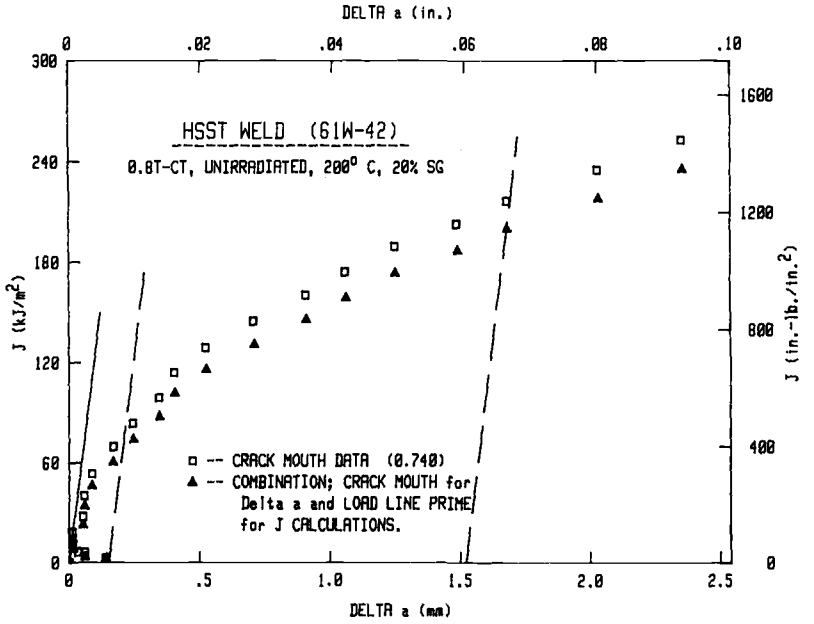

FIG. 8—J-R *curves computed from* V_M *and* $V_{LL'}$. *This is the largest deviation between these sets of data from any of the HSST tests.*

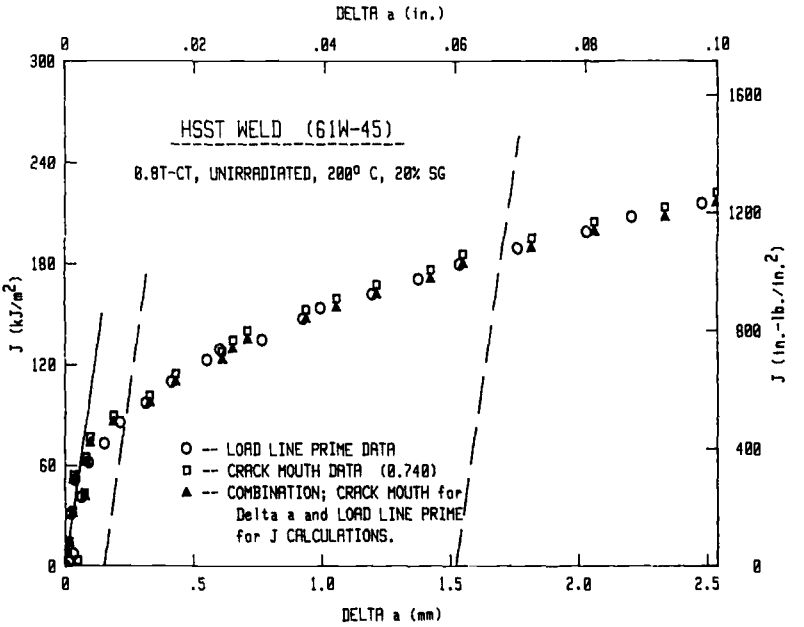

FIG. 9—J-R *curves computed from* V_M *and* $V_{LL'}$. *This is typical of the agreement seen from the HSST tests.*

TABLE 4—*Comparisons of* J_{Ic} *and* T_{avg} *computed from different displacement locations.*

Data Types	J_{Ic}, kJ/m²	Change, %	T_{avg}	Change, %
	SPECIMEN 61W-42			
Combination	69	...	45	...
Crack mouth (0.740)	81	+17	47	+4
Crack mouth (Eq 3)	81	+17	46	+2
	SPECIMEN 61W-45			
Combination	90	...	50	...
Crack mouth (0.740)	95	+6	50	0
Crack mouth (Eq 3)	95	+6	49	−2
Load-line prime	91	+1	51	2
	SPECIMEN 63W-173			
Combination	101	...	76	...
Crack mouth (0.740)	105	+4	78	+3
Crack mouth (Eq 3)	106	+5	79	+4
	SPECIMEN 66W-121			
Combination	92	...	49	...
Crack mouth (0.740)	90	−2	48	−2
Crack mouth (Eq 3)	93	+1	47	−4

A final comparison using this procedure is given in Table 5. Here, eight 1.6T-CT specimens were tested at two different temperatures. Two clip gages were mounted to these specimens, one on the load line as is typical, and the other on the crack mouth. The load-line data were used to compute the standard *J-R* curve, while the crack-mouth data were normalized by a factor of 0.740 to obtain a *J-R* curve. Values for J_{Ic} and T_{avg} are evaluated for each curve, and then the value from the *J-R* curve computed using crack-mouth displacement is divided by the load-line *J-R* curve value to determine the amount of change. The J_{Ic} values are increased by an average of 8% and a maximum of 16% while the T_{avg} values had a range of ±5% from the load-line values. Figure 10 shows the most deviation from the load-line data, while Fig. 11 shows a typical comparison. Figure 11 also shows the crack-mouth data determined using Eq 3. These data are virtually colinear with the 0.740 data, implying that the constant factor of 0.740 provides similar results as the incremental equation.

Summary and Conclusions

The *J-R* curve is normally computed based upon load-line displacements determined with a modified CT specimen of the ASTM E 399 design. This paper has investigated the use of displacements measured at other locations on the specimen, for example, crack-mouth opening V_M and load-line displacement at the edges of the specimen $V_{LL'}$ as alternative displacements with which to compute the *J-R* curve. The rationale behind this work was the need to characterize the *J-R* curves of irradiated specimens for which it was not possible to determine a conventional load-line displacement. A double clip gage technique was used to circumvent this difficulty. This technique was validated through a round-robin test program.

A theoretical basis for the use of V_M and $V_{LL'}$ in the *J-R*-curve determinations is given by the work of Newman and Orange for elastic loading. However,

TABLE 5—*Ratio of* J-R-*curve parameters for crack-mouth* J-R-*curve values as compared to load-line* J-R-*curve values.*

J_{Ic}, MEA/ASTM[a]	T_{avg}
A 508-2 FORGING (54°C)[b]	
1.04/1.14	1.05
1.14/1.16	0.97
1.11/1.14	0.95
1.02/1.03	0.99
A 533-B PLATE (90°C)[b]	
1.13/1.11	0.97
1.05/1.06	1.00
1.07/1.03	1.00
1.06/1.07	1.03

[a] J_{Ic} as defined by Materials Engineering Associates, Inc. (MEA) and ASTM E 813, respectively.
[b] 1.6T-CT tests.

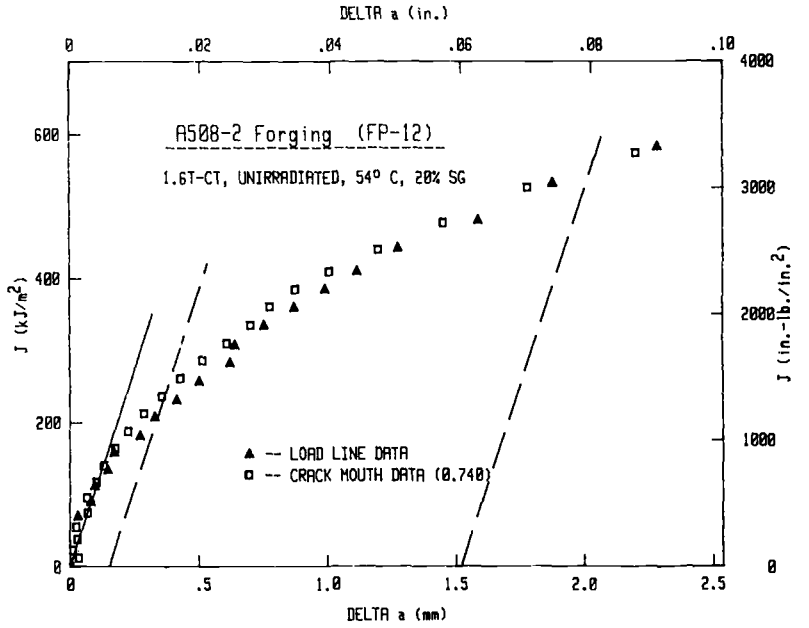

FIG. 10—*Comparison of* J-R *curves from crack-mouth data and from load-line data. This is the most deviation between the two data sets.*

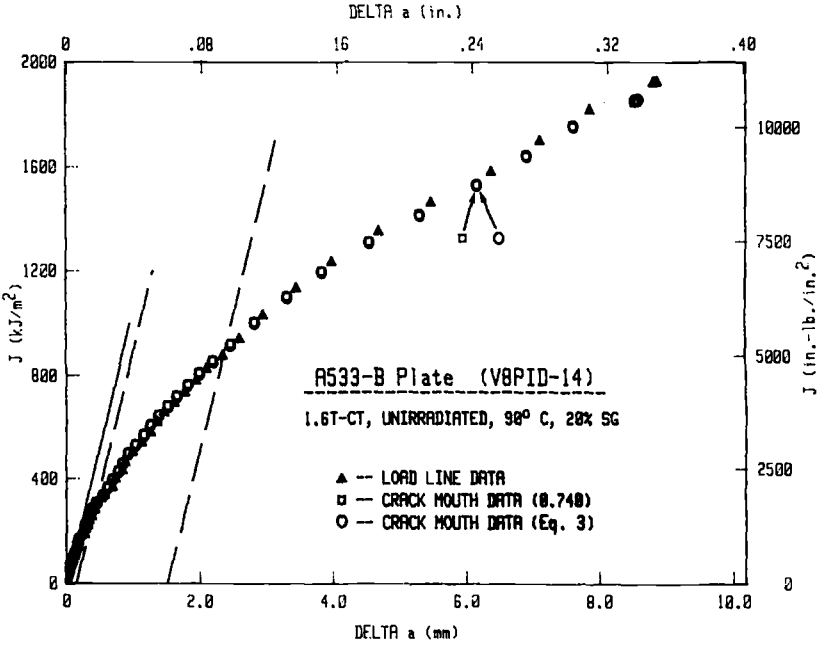

FIG. 11—*Comparison of* J-R *curves from crack-mouth data and from load-line data. This is typical of the agreement seen from these eight tests.*

experimental determinations are required to verify these theoretical projections for specimens subjected to plastic deformations. The results of this program provide this verification and suggest that the modified CT specimens used for *J-R* curve testing may not be necessary. Instead a single specimen of the ASTM E 399 design may be used for *J-R* curve determinations as well as for plane strain fracture toughness K_{Ic} measurements.

This study yields the following conclusions for the materials investigated.

- Load-line displacement can be related to other displacements on the compact specimen through displacement ratios.
- Load-line displacement is not mandatory to determine a *J-R* curve.
- Crack-mouth data can give a *J-R* curve equivalent to that determined from load-line displacements.
- A constant factor of 0.740 is equivalent to a linear incremental technique in relating crack-mouth displacement to load-line displacement, in terms of the *J-R* curve that is computed from these displacements.
- The ASTM E 399 compact specimen, using crack-mouth displacement, can be used for both K_{Ic} and *J-R* curve determinations.

Acknowledgements

The authors wish to thank M. Vagins, Office of Nuclear Regulatory Research, Division of Engineering Technology, Nuclear Regulatory Commission for his support of this work.

References

[1] Newman, J. C., Jr., "Stress Intensity Factors and Crack-Opening Displacements for Round Compact Specimens," Technical Memorandum TM-80174, National Aeronautics and Space Administration, Hamptom, VA, 1979.

[2] Orange, T. W., "Crack Displacements for J_I Testing with Compact Specimens," *International Journal of Fracture*, Vol. 19, No. 3, July 1982, pp. R59–R61.

[3] Albrecht, P., Andrews, W. R., Gudas, J. P., Joyce, J. A., Loss, F. J., McCabe, D. E., Schmidt, D. W., and Van Der Sluys, W. A., "Tentative Test Procedures for Determining the Plane Stain J_I-*R* Curve," *Journal of Testing and Evaluation*, Vol. 10, No. 6, Nov. 1982, pp. 245–251.

[4] Loss, F. J., Menke, B. H, Gray, R. A., Jr., Hawthorne, J. R., and Watson, H. E., "*J-R* Curve Characterization of A533-B Weld Metal with Irradiation and Post Irradiation Annealing," *Effects Of Radiation On Materials: Proceeding of the Tenth International Conference, STP 725*, American Society for Testing and Materials, Philadelphia, 1981, pp. 76–91.

[5] Gudas, J. P. and Davis, D. A., "Evaluation of the Tentative J_I-R Curve Testing Procedure by Round Robin Tests of HY 130 Steel," *Journal of Testing and Evaluation*, Vol. 10, No. 6, Nov. 1982, pp. 252–262.

[6] Neale, B. K., "A Proposed Materials Test Piece Design to Derive the Plane Strain Fracture Toughness," Central Electricity Generating Board Report RD/B/N3421, Gloucestershire, United Kingdom, June 1975.

[7] Landes, J. D., "*J* Calculation from Front Face Displacement Measurements on a Compact Specimen," *International Journal of Fracture*, Vol. 16, No. 4, Aug. 1980, pp. R183–R186.

B. Faucher[1] *and W. R. Tyson*[1]

A Comparison of Crack-Mouth Opening and Load-Line Displacement for J-Integral Evaluation Using Bend Specimens

REFERENCE: Faucher, B. and Tyson, W. R., **"A Comparison of Crack-Mouth Opening and Load-Line Displacement for J-Integral Evaluation Using Bend Specimens,"** *Elastic-Plastic Fracture Test Methods: The User's Experience, ASTM STP 856,* E. T. Wessel and F. J. Loss, Eds., American Society for Testing and Materials, 1985, pp. 278–293.

ABSTRACT: The measurement of the displacement at the crack mouth of three-point bend specimens is compared to the measurement of load-line displacement for crack-length and J-integral evaluation. For crack-length determination by the unloading technique, the correction that must be made when using a clip gage mounted on knife edges is derived from load-line and crack-mouth opening displacements expressed as a function of crack length. Experimental results with tough steels show excellent agreement between the crack lengths determined by the two types of displacement measurements. The J integral can be evaluated using either method. The agreement between the two methods of J evaluation depends essentially on the evaluation of crack length. It is concluded that the J integral may be measured easily with a clip gage mounted at the crack mouth of three-point bend specimens.

KEY WORDS: pressure vessels, unloading, modulus of elasticity, pressure vessel steel, three-point bend test, unloading technique, crack-mouth opening, crack-length evaluation, J integral

The critical value of the J integral at the initiation of crack growth J_{Ic} is one of the major parameters characterizing the fracture toughness of materials. It is particularly suited to tough materials for which the measurement of the plane strain fracture toughness K_{Ic} would require prohibitively thick specimens. The conventional method for determination of J_{Ic}, ASTM Test for J_{Ic}, a Measure of Fracture Toughness (E 813), requires at least four specimens to evaluate J as a function of crack extension. To determine J_{Ic} with a single specimen, various techniques have been used to measure the crack advance during the test. The technique used herein—the unloading technique—is described in the appendix

[1] Research scientist and section head of Engineering and Metal Physics Section, respectively, CANMET, Physical Metallurgy Research Laboratories, 568 Booth St., Ottawa, Ontario, Canada K1A OG1.

of ASTM E 813 and uses the same instrumentation as that necessary to measure J. Crack lengths are evaluated during the test from compliances measured during partial unloadings, and J values are obtained from the load versus load-line displacement record. The load-line displacement can be measured directly on a slightly modified compact tension specimen with the same clip gage as for other fracture mechanics tests. For bend specimens, the load-line displacement is usually monitored by a special transducer. However, J values may also be obtained from a load versus crack-mouth opening displacement (CMOD) test record [*1,3*]. Furthermore, it has been recently reported [*4,5*] that crack extension can be determined from CMOD during partial unloadings. The measurement of the displacement at the crack-mouth of three-point bend specimens is compared in this report to the measurement of load-line displacement for crack-length and J-integral evaluation.

Experimental Details

Two experimental heats of 2¼ Cr-1 molybdenum pressure vessel steels were used. The compositions are given in Table 1. Steel A was of low phosphorus content and Steel D was rare earth treated. After air melting and rolling, the steels were austenitized at 925°C for 1 h, then water quenched. They were subsequently annealed at 675°C for 1½ h and then water cooled. This heat treatment was selected to obtain tough properties at room temperature. The lower toughness of Steel D, shown with other room temperature properties in Table 2, results from a higher inclusion content [*6*].

Tests were carried out at room temperature on four different types of specimens: standard 10-mm Charpy V-notch (CVN), standard 10 × 20 mm^2 three-point bend (3PB), and both of the above types with 25% side grooves. The specimens were cut in the L-T orientation, and machined according to standard specifications except for the envelope of the starter notches being slightly larger than allowed. In compensation, the machined slots of the 3PB specimens were limited to 5 mm depth, and the specimens were precracked to an initial crack length of about 12 mm. Similarly, the CVN specimens were precracked from the end of the V notch at a depth of 2 mm to an initial crack length of about 6 mm. During the last 2 mm of crack growth, the load was reduced in accordance with ASTM E 813.

The specimens were tested in an Instron® testing machine using the jig shown in Fig. 1. The load P was recorded as a function of both the load-line displacement Δ and the crack-mouth opening displacement V on two X-Y recorders. The load was obtained from the Instron load cell amplifier, Δ was monitored with a linear variable differential transformer (LVDT) of 0.72 V/mm sensitivity, and V was monitored with an Instron clip gage connected to a Budd® strain indicator. The sensitivity of the V measuring system was 0.23 V/mm for the P-V records and was increased to 1.97 V/mm for the unloading measurements. At the beginning of each test, the specimens were cycled three times between 10 and 40% of their

TABLE 1—*Composition of steels in percent by weight.*

Steels	Carbon	Manganese	Silicon	Sulfur	Phosphorus	Chromium	Molybdenum	Tin	Aluminum	Nickel	Vanadium	Cerium	Lanthanum
A	0.12	0.47	0.37	0.005	0.005	2.33	1.01	0.001	0.033	<0.01	<0.005	. . .	. . .
D	0.12	0.53	0.48	0.002	0.039	2.29	0.98	0.001	0.038	<0.01	<0.005	0.115	0.057

TABLE 2—*Mechanical properties of steels at room temperature.*

Steels	Yield Stress, MPa	Tensile Strength, MPa	Elongation, %	Reduction of Area, %	Charpy Energy, J
A	643	743	25	67	190
D	607	714	25	66	110

limit load to determine the initial crack length; then the load was applied at a constant crosshead speed of 0.25 mm/min. This procedure allowed the maximum load to be reached in about 2 min. Before reaching the maximum load, at least one unloading sequence was performed; after attaining maximum load, several unloading sequences were performed during the remainder of the test. Before each unloading, the crosshead was stopped for about 1 min. Some relaxation was observed; then the load was dropped to 90% of its value just before the unloading compliance measurement was made. Voltage suppressions allowed the signals to be amplified during the unloadings to enable slope measurements to be made from the linear plots of (1) load versus load-line displacement and (2) load versus CMOD. Typical records are shown in Fig. 2. The overall accuracy of the measured slopes has been evaluated from the scatter in the calibration at 2% for the P-Δ line and at 4% for the P-V line. The larger uncertainty for the P-V line results from nonlinearities in the strain gage amplifier. The extraneous displacement caused by the elastic deformation of the machine and the indentation

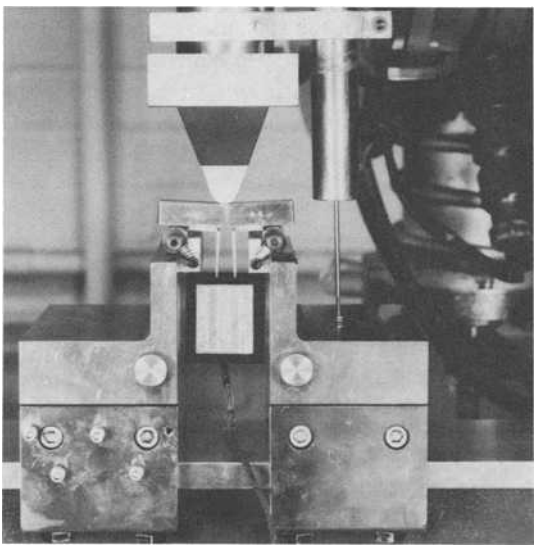

FIG. 1—*Details of the jig used to measure both load-line displacement and crack-mouth opening displacement on three-point bend specimens.*

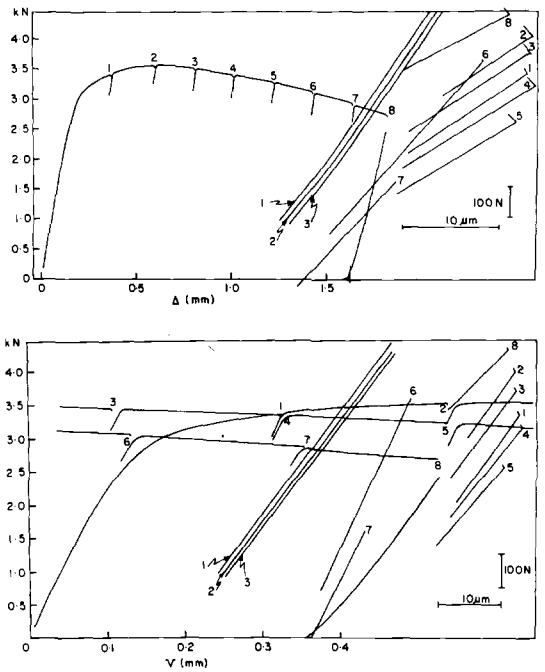

FIG. 2—*Typical records of load versus* (a) *load-line displacement and* (b) *crack-mouth opening displacement, showing the main record, three initial unloadings, and eight partial unloadings.*

of the specimen at the roller contacts was measured directly by loading one of the arms that was not deformed of the specimen to the same load levels as that experienced during the test but with a span equal to the diameter of the rolls. The elastic deformation from bending in this case was negligible. After completion of the test, the specimens were heat tinted and broken at a low temperature. The initial and final crack lengths were then determined by the nine-point average technique.

Determination of Crack Length

Analysis of the Literature

Several authors [*7–10*] have expressed the compliance of bend specimens as a function of crack length. The load-line displacement Δ is usually partitioned into an elastic component Δ_e and a component from the presence of the crack Δ_c as

$$\Delta = \Delta_e + \Delta_c$$

Δ_e is obtained from the theory of elasticity by

$$\Delta_e = \{[(1 - n^2)P]/EB\}\,(S/4W)\,[(S/W)^2 + 3(1 + \nu)]$$

where P is the applied load, S, W, and B are the span, the width, and the thickness of the sample, respectively, ν is Poisson's ratio, E is Young's modulus for the material, and n is equal to zero in plane stress and to ν in plane strain. For a standard 3PB specimen ($S = 4W$), with $\nu = 0.3$, the nondimensional compliance C is obtained as

$$C = EB(\Delta/P) = C_e + C_c \tag{1}$$

with

$$C_e = 19.9(1 - n^2) \tag{2}$$

Tada [7] gives

$$C_c = 24(1 - n^2)\,[(a/W)/(1 - a/W)]^2\,[5.58 - 19.57a/W + 36.82(a/W)^2 - 34.94(a/W)^3 + 12.77(a/W)^4] \tag{3a}$$

where a is the crack length. The expression of Bucci et al [8] is

$$C_c = 32(1 - n^2)\,[4.21(a/W)^2 - 8.89(a/W)^3 + 36.9(a/W)^4 - 83.6(a/W)^5 + 174.3(a/W)^6 - 284.8(a/W)^7 + 387.6(a/W)^8 - 322.8(a/W)^9 + 149.8(a/W)^{10}] \tag{3b}$$

while Adams and Munro [9] give intermediate values. Estimates of crack length from Eqs 3a or 3b with Eqs 1 and 2 may differ by up to 0.015 W, that is, about 3% for crack sizes in the range from 0.3 to 0.8 W. The difference becomes more apparent by plotting $C(1 - a/W)^2$ as a function of a/W as shown in Fig. 3.

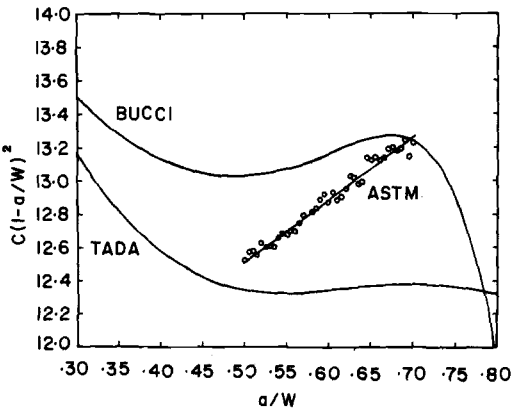

FIG. 3—*Comparison of various expressions of compliance as a function of crack length from Refs 7, 8, and ASTM E 813.*

The figure also suggests that, in the crack size range from 0.45 to 0.75 W, the compliance may be well approximated by a relation

$$C = A/[1 - (a/W)]^2 \tag{4}$$

where the constant A is 13.13 and 12.36 for Bucci and Tada's relations, respectively. Equation 4 is consistent with the expression proposed to evaluate crack advance [*5,11*] in 3PB specimens

$$da = (b/2)(dC/C) \tag{5}$$

where $b = W - a$, within the range of a/w from 0.45 to 0.75. The compliances for 3PB specimens given in the Annex of ASTM E 813 have been plotted in Fig. 3. They do not fit Eq 4 but may be better expressed as

$$C = 10.652[1 + 0.35(a/W)]/[1 - (a/W)]^2$$

or

$$C = 10.834 \exp[0.2894(a/W)]/[1 - (a/W)]^2$$

If the ASTM values describe accurately the compliance as a function of crack length, then Eq 5 for the evaluation of crack advance becomes

$$da = [(2/b) + (0.2894/W)]^{-1}(dC/C)$$

Because of the differences in crack length obtained from compliance by using the different relations shown, it appears that Eq 4 would be an accurate enough relationship and one easy to handle most purposes in the crack size range from 0.45 to 0.75 W.

Crack size can also be evaluated from V, the crack-mouth opening displacement. V has been expressed as a function of crack length by Tada et al [*7*]; for standard 3PB specimens

$$EB(V/P) = 24(1 - n^2)(a/W)\{0.76 - 2.28(a/W) + 3.87(a/W)^2 - 2.04(a/W)^3 + \{(0.66/[1 - (a/W)]^2\} \tag{6}$$

Equation 6 has been compared to Eq 1 with Eqs 2 and 3a for the full range of crack lengths. It has been found that in the crack size range from $0.2W$ to $0.7W$ the load-line compliance and CMOD are linearly related. For 0.005 step increases of a/W, the relation under plane strain is obtained from the least squares method as

$$C = 15.2 + 1.05\, EB(V/P) \tag{7}$$

and under plane stress as

$$C = 16.7 + 1.05\,EB(V/P)$$

Using Eq 3b instead of Eq 3a the plane strain relation becomes

$$C = 15.0 + 1.14\,EB(V/P) \tag{8}$$

Measurements of CMOD are therefore equivalent to measurements of compliance, and they can be used to determine crack length by the unloading technique. CMOD measurements will be only about 10% less sensitive than compliance measurements.

The linear relation between compliance and CMOD allows a determination of the correction to be made when the CMOD is measured with knife edges. Referring to Fig. 4 and assuming that during small elastic unloadings the top surface of the specimen rotates with respect to a fixed point at a distance x from the surface, the geometry gives

$$(V/2x) = V_{meas}/[2(x + z)] \cong (\Delta/2W)$$

where V_{meas} is the value of V measured at the knife edge location. Hence

$$V_{meas} \cong V + (z/W)\Delta$$

Using Eq 7, one obtains

$$EB(V/P) = \{[EB(V/P)]_{meas} - 15.2(z/W)\}/[1 + 1.05(z/W)] \tag{9}$$

For example, for the Charpy specimens that were tested, $z = 0.16W$, and the correction is

$$EB(V/P) = 0.856[EB(V/P)]_{meas} - 2.1$$

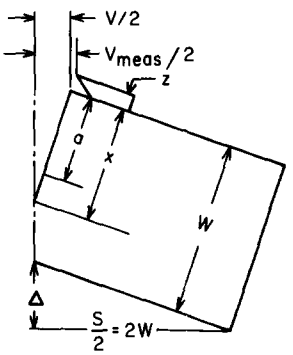

FIG. 4—*Geometry of the 3PB specimen.*

TABLE 3—*Comparison of initial* a_o *and final* a_f *crack lengths obtained from physical measurements and from calculations.*

	Measured		Calculated From			
			Compliance		CMOD	
Specimen	a_o/W	a_f/W	a_o/W	a_f/W	a_o/W	a_f/W
A-20	0.587	0.643	0.599	0.617	0.606	0.636
A-24	0.590	0.641	0.601	0.619	0.601	0.629
A-8″	0.596	0.640	0.619	0.645	0.620	0.649
A-18″	0.586	0.658	0.607	0.655	0.608	0.660
D-2	0.555	0.633	0.568	0.609	0.573	0.624
D-34	0.625	0.663	0.633	0.648	0.634	0.651
D-18″	0.620	0.660	0.642	0.672	0.638	0.668
D-30″	0.589	0.689	0.608	0.687	0.605	0.685
A-B1	0.604	0.630	0.615	0.641	0.621	0.649
A-B3	0.595	0.618	0.615	0.624	0.608	0.624
A-B8″	0.600	0.641	0.614	0.651	0.618	0.651
A-B13″	0.609	0.635	0.616	0.641	0.621	0.639
D-B8	0.595	0.633	0.617	0.637	0.611	0.637
D-B17	0.593	0.666	0.600	0.653	0.606	. . .
D-B5″	0.605	0.662	0.612	0.661	0.615	0.655
D-B7″	0.609	0.698	0.623	0.704	0.620	0.698

"Side-grooved specimen. The first letter refers to the type of steel, and "*B*" identifies a 3PB specimen.

If Eq 8 was used instead of Eq 7, the correction would be

$$EB(V/P) = 0.846[EB(V/P)]_{meas} - 2.0$$

The difference between the two corrections is only 1% of the measured values.

Finally, combining Eqs 5 and 7, the crack advance may be expressed as a function of change in CMOD as

$$da = (b/2)[d(EB\ V/P)/(14.5 + EB\ V/P)]$$

Experimental Measurement of Crack Length

Crack lengths evaluated by the unloading technique can be compared with their physical measurement only at the beginning and the end of a test. This comparison is shown in Table 3 for each test. The accuracy of physical crack lengths is $\pm 0.002\ W$ for Charpy size specimens and $\pm 0.001\ W$ for 3PB specimens. The crack length values have been calculated with Tada's plane strain Eqs 3a and 6. The uncertainty of the corrected V and Δ is only about 5%, which from Eq 5 gives an uncertainty for "a" of approximately $0.01\ W$.

On average, the initial-crack length calculated from load-line compliance with Tada's relation is found to be 2.4% larger than the measured value. The calculated final-crack length is however found to be 0.6% lower than the measured value. Compliances are plotted as a function of crack lengths in Fig. 5, together with Tada's and Bucci's plane strain relations. It is seen that the experimental values follow these relations closely, except for some of the specimens without side grooves.

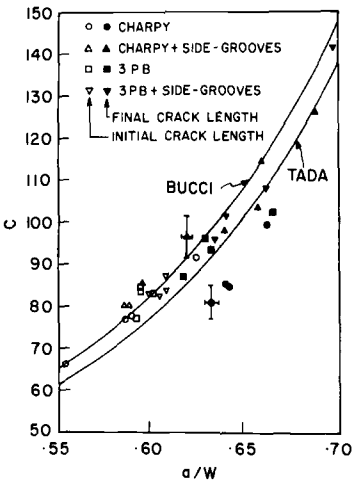

FIG. 5—*Comparison of measured compliance with Bucci's and Tada's plane strain expressions for various crack lengths.*

TABLE 4—*Comparison of measured and calculated crack extension.*

Specimen	Measured, mm	Compliance		CMOD	
		Calculated, mm	Difference, %	Calculated, mm	Difference, %
A-20	0.56	0.18	−68	0.30	−46
A-24	0.51	0.18	−65	0.28	−45
A-8[a]	0.44	0.26	−41	0.29	−34
A-18[a]	0.72	0.48	−33	0.52	−28
D-2	0.78	0.41	−47	0.51	−35
D-34	0.38	0.15	−61	0.17	−55
D-18[a]	0.40	0.30	−25	0.30	−25
D-30[a]	1.00	0.79	−21	0.80	−20
A-B1	0.52	0.52	0	0.56	+8
A-B3	0.47	0.16	−66	0.32	−32
A-B8[a]	0.82	0.80	−2	0.66	−20
A-B13[a]	0.52	0.50	−4	0.56	+8
D-B8	0.76	0.40	−47	0.52	−32
D-B17	1.45	1.06	−27	. . .	. . .
D-B5[a]	1.14	0.98	−14	0.80	−30
D-B7[a]	1.78	1.62	−9	1.58	−11

[a]Side-grooved specimen. The first letter refers to the type of steel, and "*B*" identifies a 3PB specimen.

The initial crack lengths calculated from CMOD with Tada's Eq 6 are also found to be 2.6% larger on average than the measured values. Because the calculated final-crack lengths are on average equal to the measured values, the calculated crack extension may be significantly smaller than the measured one. The differences in crack extension shown in Table 4 indicate that, on average, the unloading technique gives reasonable values only with side-grooved 3PB specimens. This result is in agreement with previously published data [*12*].

Compliance and CMOD data are compared in Fig. 6 together with Eqs 7 and 8. The experimental points come from several tests, and they show excellent agreement with the linear relation of Eq 7, especially for the side-grooved specimens.

J evaluation

The J integral may be evaluated directly from the load versus load-line displacement curve in accordance with the ASTM E 813. When evaluated from CMOD [*1,3*], the *J* integral is divided into an elastic and a plastic component as

$$J = J_e + J_p$$

The elastic component J_e is equal to the crack-extension force G and is expressed by

$$J_e = G = (K^2/E)(1 - n^2) \tag{10}$$

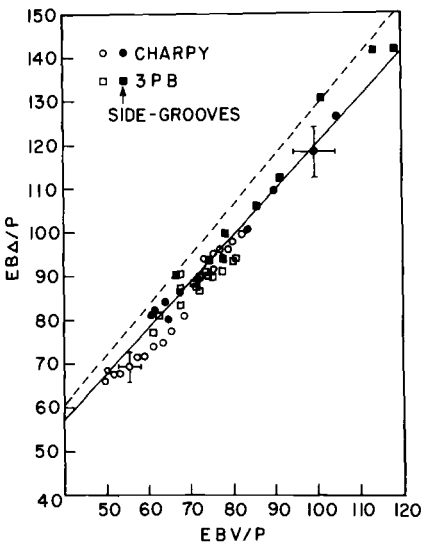

FIG. 6—*Comparison of load-line and crack-mouth opening displacements with Eq 7 (continuous line) and Eq 8 (dashed line).*

J_c can thus be evaluated from the standard formula for the stress intensity factor K by

$$J_c = [Y^2P^2(1 - n^2)]/(EB_e^2W) \tag{11}$$

where Y is a function of a/W, and B_e is the effective thickness for side-grooved specimens [5].

When there is no crack growth, J may be evaluated from

$$J = 2U/Bb \tag{12}$$

where U is the area under the load-displacement curve. Thus, in the elastic case

$$J_c = (P/B)(\Delta/b)$$

Because $J_c = G$, and expressing G [13] by

$$G = (P^2/2B)[d(\Delta/P)/da]$$

it follows that

$$[d(\Delta/P)/(\Delta/P) = 2da/(W - a)$$

hence

$$C = EB(\Delta/P) = A/[1 - (a/W)]^2$$

It has been shown that this relation, Eq 4, is approximately verified in the crack-length range of interest.

The plastic component of J, J_p, is calculated from Eq 12 by considering the plastic displacement Δ_p only. To obtain Δ_p from the plastic CMOD V_p, it is assumed that the specimen deforms around a plastic hinge located at a distance $r_p(W - a)$ from the crack tip. The geometry (Fig. 4) gives

$$V_p/\Delta_p = (z/W) + (a/W) + r_p[1 - (a/W)] \tag{13}$$

The values of Δ_p calculated from measurements of V_p, using Eq 13 with $r_p = 0.4$, were 6% larger than the values measured directly from the load-line displacement. This difference was however typically ~0.05 mm, which is of the order of the experimental uncertainties. For a ≈0.6 W, an increase of r_p from 0.4 to 0.5 would decrease the calculated Δ_p by 4%, and a 10% increase in the crack length would cause the same 4% decrease of Δ_p. It should be noted that the calculated values of Δ_p were obtained after normalizing the crack length to the measured value.

The increase of J between two consecutive unloading points may then be

determined using Eqs 11 to 13, and corrections can be made for crack-length increase as indicated in ASTM E 813 for J_p. If the crack length is determined at two points, i and $i + 1$, then

$$J_{i+1} = (J_e)_{i+1} + (J_p)_{i+1} \tag{14a}$$

where

$$(J_p)_{i+1} = \{(J_p)_i + [2\,A_{i,i+1}/(B_N b_i)]\}(b_{i+1}/b_i) \tag{14b}$$

$A_{i,i+1}$ is the area under the P-versus Δ_p curve from point i to $(i + 1)$, and B_N is the nominal thickness of the specimen. $A_{i,i+1}$ may be approximated as

$$\begin{aligned} A_{i,i+1} &= [(P_i + P_{i+1})/2][(\Delta_p)_{i+1} - (\Delta_p)_i] \\ &= [(P_i + P_{i+1})/2]W[V_{p,i+1}/(z + a_{i+1} + r_p b_{i+1})] \\ &\quad - [V_{p,i}/(z + a_i + r_p b_i)] \end{aligned} \tag{14c}$$

where use has been made of Eq 13. Comparisons of the J versus Δa relationships determined from load-line displacement by the standard method and determined from CMOD measurements using Eq 14 are shown in Fig. 7 for Test A-B8. This test satisfied the ASTM E 813 requirements except for the ligament that becomes too short. The disqualified data points have nevertheless been used to determine the linear regression line of J upon Δa. As shown in Fig. 7, J_c, a critical value of J, is then obtained according to the standard method. The average values obtained after normalization of the crack extension are also plotted in Fig. 7. The J_c values differ only by 10%, but there is 40% difference between the slopes. These differences result essentially from variations in the evaluation of crack lengths. The highest values are obtained for the CMOD because it gave the smallest values of crack extension in this particular example.

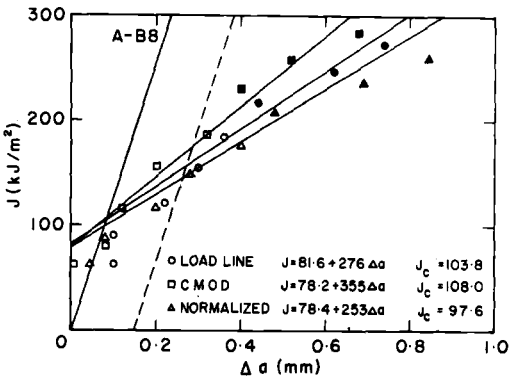

FIG. 7—*Comparison of the variation of* J *as a function of crack extension obtained from measurements of compliance, CMOD, and with normalized crack lengths. Filled-in data points, for which* $b < 25\ J/\sigma_y$, *have been used to obtain least square lines and a critical value* J_c *similarly to the standard procedure.*

Discussion and Conclusion

Tests on various types of specimens have shown that the measurement of CMOD during unloading gives crack lengths that are comparable to those obtained from the measurement of compliance. The crack lengths calculated by both unloading techniques are however shorter than the measured physical crack lengths. This is particularly noticeable with thin specimens where side grooves have been used [*5,12*] to obtain good correlation between calculated and measured crack lengths.

The J integral is readily evaluated from CMOD measurements with the concept of a center of rotation. For the geometry used, values of J are not very sensitive to the actual position of this center of rotation, but depend quite significantly on the estimation of crack length. To characterize the tearing stability of materials, it has been proposed [*14*] to use a "tearing modulus" T defined as

$$T = (dJ/da)(E/\sigma_y^2)$$

where σ_y is the yield stress. The tearing modulus is even more sensitive to the crack-length values than J, and it might be useful to normalize the calculated crack lengths to those measured after the test. Figure 7 compares various measurements obtained from one test sequence on a single specimen. The difference in the data comes essentially from the evaluation of crack length that affects both values of Δa and J, Δa directly, and J through Eq 14 or one similar. This indicates that the large scatter in J_I-R curve found in a round-robin test program [*15*] results mainly from difficulties in evaluating the crack length.

The use of load-line displacement to measure J, requires an additional test to obtain the extraneous displacements. On the contrary, true CMOD values are obtained directly with the correction given by Eq 9. It is therefore more convenient to use the CMOD rather than the load-line displacement in J evaluation with 3PB specimens. This becomes especially useful under severe testing conditions, such as low temperatures, or with irradiated samples.

Acknowledgments

The help of the technical staff and the encouragement from Physical Metallurgy Research Laboratories (PMRL) during the preparation of this report is gratefully acknowledged. Special thanks are due to R. F. Knight for providing the sample plates and to C. Trinque for his invaluable assistance in the experimental work.

References

[*1*] Sumpter, J. D. G. and Turner, C. E., "Method for Laboratory Determination of J_c," *Cracks and Fracture, STP 601*, American Society for Testing and Materials, Philadelphia, 1976, pp. 3–18.

[*2*] Dawes, M. G., "A Re-assessment of J Estimation Procedures," *International Journal of Pressure Vessel and Piping*, Vol. 6, No. 3, May 1978, pp. 165–176; also "Elastic-Plastic

Fracture Toughness Based on the COD and *J*-Contour Integral Concepts," *Elastic-Plastic Fracture, STP 668*, American Society for Testing and Materials, Philadelphia, 1979, pp. 306–333.

[3] You-Gu Xiao and Guo-Hao Huang, "On the Compatibility Between J-Integral and Crack Opening Displacement," *Engineering Fracture Mechanics*, Vol. 16, No. 1, 1982, pp. 83–94.

[4] Joyce, J. A., Hasson, D. F., and Crowe, C. R., "Computer Data Acquisition Monitoring of Stress Corrosion Cracking of Depleted Uranium Cantilever Beam Specimens," *Journal of Testing and Evaluation*, Vol. 8, No. 6, Nov. 1980, pp. 293–300.

[5] Albrecht, P., Andrews, W. R., Gudas, J. P., Joyce, J. A., Loss, F. J., McCabe, D. E., Schmidt, D. W., and VanDerSluys, W. A., "Tentative Test Procedure for Determining the Plane Strain J_I-R Curve," *Journal of Testing and Evaluation*, Vol. 10, No. 6, Nov. 1982, pp. 245–251.

[6] Knight, R. F., Tyson, W. R., and Sproule, G. I., "Reduction of Temper Embrittlement of 2¼Cr-1Mo Steels by Rare Earth Additions," to be published in *Metals Technology*.

[7] Tada, H., Paris, P. C., and Irwin, G. R., *The Stress Analysis of Cracks Handbook*, Del Research Corporation, PA, 1973.

[8] Bucci, R. J., Paris, P. C., Landes, J. D., and Rice, J. R., "*J* Integral Estimation Procedures," *Fracture Toughness*, STP 514, American Society for Testing and Materials, Philadelphia, 1972, pp. 40–69.

[9] Adams, N. J. I. and Munro, H. G., "A Single Test Method for Evaluation of the J Integral as a Fracture Parameter," *Engineering Fracture Mechanics*, Vol. 6, 1974, pp. 119–132.

[10] Duggan, T. V., Proctor, M. W., and Spence, L. J., "Stress Intensity Calibrations and Compliance Functions for Fracture Toughness and Crack Propagation Test Specimens," *International Journal of Fatigue*, Vol. 1, Jan. 1979, pp. 37–47.

[11] Clarke, G. A., "Single-Specimen Tests for J_{ic} Determination—Revisited," *Fracture Mechanics: Proceedings of the Thirteenth National Symposium on Fracture Mechanics, STP 743*, American Society for Testing and Materials, Philadelphia, 1981, pp. 553–575.

[12] Gudas, J. P., et al, "A Summary of Recent Investigations of Compact Specimen Geometry Effects on the J_I-R Curve of High-Strength Steels," Report NUREG/CR-1813, U.S. Nuclear Regulatory Commission, 1980.

[13] Bucci, R. J., Paris, P. C., Landes, J. D., and Rice, J. R., "*J* Integral Estimation Procedures," *Fracture Toughness, STP 514*, American Society for Testing and Materials, Philadelphia, 1972, pp. 63–68 (Appendices).

[14] Paris, P. C., Tada, H., Zahoor, A., and Ernst, H., "The Theory of Instability of the Tearing Mode of Elastic-Plastic Crack Growth," *Elastic-Plastic Fracture, STP 668*, American Society for Testing and Materials, Philadelphia, 1979, pp. 5–36.

[15] Gudas, J. P. and Davis, D. A., "Evaluation of the Tentative J_I-R Curve Testing Procedure by Round-Robin Tests of HY130 Steel," *Journal of Testing and Evaluation*, Vol. 10, No. 6, Nov. 1982, pp. 252–262.

H. Kagawa,[1] *T. Fujita,*[1] *T. Akiyama,*[1] *and N. Urabe*[1]

Determination of J_{Ic} Values by the Double Clip-on Gage Compliance Method

REFERENCE: Kagawa, H., Fujita, T., Akiyama, T., and Urabe, N., **"Determination of J_{Ic} Values by the Double Clip-on Gage Compliance Method,"** *Elastic-Plastic Fracture Test Methods: The User's Experience, ASTM STP 856*, E. T. Wessel and F. J. Loss, Eds., American Society for Testing and Materials, 1985, pp. 294–307.

ABSTRACT: As one of the candidates for the single-specimen method to determine the J_{IC} value, the double clip-on gage compliance method (DCGC) was introduced. This technique is based on the concept of the rotational factor of the compact tension specimen. According to the DCGC method, the J_{Ic} value can be determined by using only two clip-on gages on a compact tension specimen under monotonic loading. To examine the usefulness of the DCGC method, J_{Ic} values of several kinds of steel were determined by the DCGC method and were compared with J_{Ic} values obtained by the multiple specimen method described in ASTM and Japan Society of Mechanical Engineers (JSME) standards. The relationship between J_{Ic} values by the DCGC method and by the multiple-specimen method was discussed, and the industrial utility of the DCGC method was verified.

KEY WORDS: fracture tests, tension tests, crack initiation, fracture toughness testing, ductile fracture, J integral, single specimen method, rotational factor, compact tension specimen

J_{Ic} is one of the typical criteria to estimate the initiation toughness of ductile cracks. Recently, ASTM and the Japan Society of Mechanical Engineers (JSME) have standardized the test method to determine the J_{Ic} value in ASTM Test Method for J_{Ic}, a Measure of Fracture Toughness (E 813) and JSME Standard Method of Test for Elastic-Plastic Fracture Toughness J_{Ic} (S 001), respectively. In ASTM E 813, the *R*-curve method is considered to be a typical multiple-specimen method that requires measurement of the ductile crack length at equally spaced nine points in each specimen where more than four specimens are needed. In JSME S 001, the *R*-curve method and stretched zone width method are recommended and required measurement of the ductile crack length and stretched zone width at three points in each specimen or both, and more than five specimens are needed.

[1]Research engineers, Fracture Engineering Laboratory, Technical Research Center, Nippon Kokan K. K., Kawasaki, Japan 210.

On the other hand, lots of single-specimen methods to determine the J_{Ic} value have also been proposed. These are the unloading compliance method, acoustic emission method, ultrasonic method, electro-potential drop method, and others. These identify the ductile crack initiation by means of each technique. But these single-specimen methods seem to have some defects such as an effect of unloading on J_{Ic} value, elevation of temperature at the crack tip caused by electric current, and so on.

In this report, we introduce the double clip-on gage compliance (DCGC) method to determine the J_{Ic} value, which is based on the concept of the rotational factor of the compact tension specimen. The DCGC method needs only two clip-on gages contacted on a single specimen without any expensive equipment. Also, some of the advantages of the method are discussed.

Description of the DCGC Method

According to the slip line field analysis on the perfectly plastic-rigid body, the compact tension specimen as well as the three-point bending specimen rotate themselves around the center of rotation, after being yielded. Referring to Fig. 1, the distance between the center of rotation and the crack tip is written as follows

$$a = r\,(W - a_0) \tag{1}$$

where W is the specimen width, a_0 is the initial fatigue crack length, and r is the rotational factor. Let V_1 and V_2 be the distance between the crack surfaces on the load line, at the middle point between the load line and the crack tip,

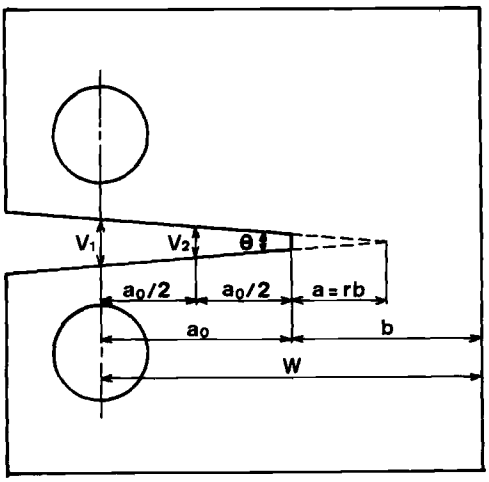

FIG. 1—*Assumed crack configuration.*

respectively. Because of the geometrical relationship, V_1 and V_2 can be described as follows

$$V_1 = (a_0 + a)\theta \tag{2}$$

$$V_2 = (\tfrac{1}{2}a_0 + a)\theta \tag{3}$$

where θ is the angle between the crack surfaces. Taking the derivative of V_2 with respect to V_1, we get Eq 4

$$dV_2/dV_1 = [(\tfrac{1}{2}a_0 + a)d\theta + \theta da]/[(a_0 + a)d\theta + \theta da] \tag{4}$$

Now the changes in dV_2/dV_1 because of the crack-tip blunting, the ductile crack initiation, and the crack growth are considered as Stages I, II, and III in Fig. 2, respectively. The first inflexion point (the boundary of the Stage I and II) and the second inflexion point (the boundary of the Stage II and III) in the dV_2/dV_1 versus V_1 curve correspond to the general yielding and the initiation of the ductile crack, respectively. In Stage I, the crack tip blunts off; therefore the center of rotation moves away from the crack tip. When the specimen is generally yielded (Stage II), a is constant since the specimen rotates itself around the center of rotation. Thus, dV_2/dV_1 is a constant value until the ductile crack initiates. After the ductile crack initiation (Stage III), the center of rotation again moves forward.

Consequently, the ductile crack initiation is identified as the location where dV_2/dV_1 begins to increase from the constant value. This process is also shown schematically in Fig. 2. Therefore, according to the DCGC method, the initiation point can be caught by observing the change in the value of dV_2/dV_1.

Shiratori and Miyoshi [*1*] have obtained the rotational factor r of the compact tension specimen under plane strain conditions

$$r = -(W/b - 1) + [(W/b - 1)^2 + 2r_0(W/b - \tfrac{1}{2})]^{0.5} \tag{5}$$

where $b = W - a_0$ is the ligament length, and r_0 is the rotational factor, which is 0.370 under pure bending conditions. On the other hand, Merkle and Corten [*2*] have solved the same problem neglecting the plastic constraint; their equation can thus be considered the solution under the plane stress condition. In the latter case, the rotational factor is given by substituting $r_0 = 0.5$ into Eq 5. For the 1-in. thick compact specimen (1TCT) ($a_0 = b = 25$ mm and $W = 50$ mm), the value of the rotational factor is 0.452 under plane strain conditions and 0.581 under plane stress conditions, respectively. Substituting these values into Eq 1 and then into Eq 4, Eq 6 can be obtained

$$dV_2/dV_1 = \begin{cases} 0.656, \text{ plane strain condition} \\ 0.684, \text{ plane stress condition} \end{cases} \tag{6}$$

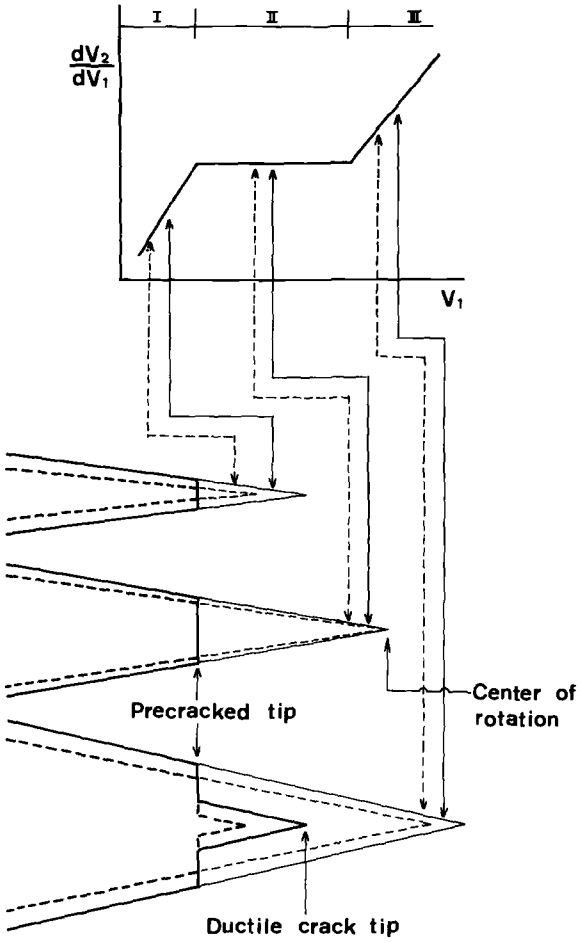

FIG. 2—*Assumed three stages of crack growth.*

According to the experimental results by McCabe [*3*], r is about 0.25 for extremely high strength steels whose tensile strength is greater than 800 MPa. Even in this case, the value of dV_2/dV_1 is equal to 0.60 under plane strain conditions. These values correspond to the plateau of dV_2/dV_1 in Fig. 2.

Examination of the DCGC Method by FEM Analysis

In order to examine the adequacy of the DCGC model proposed in the previous section, the elastic-plastic finite-element analyses (FEM) in plane strain conditions were carried out using the ADINA code. The material constitutive behavior is modeled as an isotropic hardening [*4*] together with the Mises yield condition. The stress-strain relation is approximated by a bilinear curve where yield strength is 700 MN/m^2 and the modulus of strain hardening is 1400 MN/m^2.

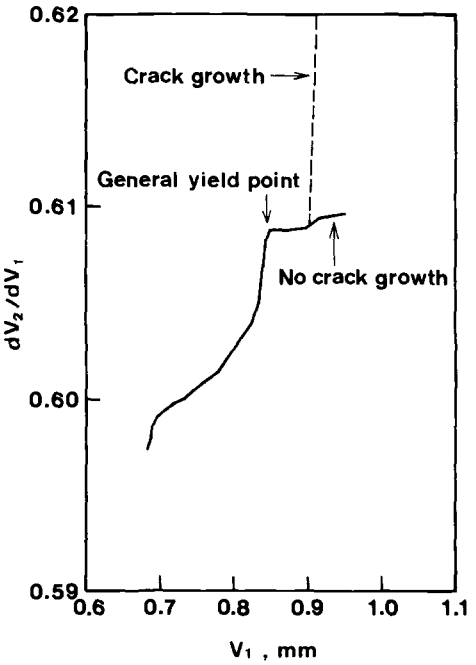

FIG. 3—dV_2/dV_1 *versus* V_1 *curve obtained by finite-element calculation.*

The calculations were carried out on both cases for the ductile crack growth and for no crack growth. Since ADINA has the element birth and death option, the ductile crack growth can be simulated by eliminating the stiff truss elements arranged at the nodes along the ligament on the plane of symmetry. Each truss element was eliminated at the appropriate point of V_1 after the specimen was generally yielded.

Figure 3 shows the dV_2/dV_1 versus V_1 curve obtained by the finite-element calculations. The solid line corresponds to the case of no ductile crack growth. The value of dV_2/dV_1 first increases with an increase of the V_1 value, approaching constant value at the general yield. The general yield was assumed to occur at the moment when Gaussian points, whose effective stress reached the yield

TABLE 1—*Chemical compositions.*

Steel	Carbon	Silicon	Manganese	Phosphorus	Sulfur	Nickel
1	0.10	0.24	1.22	0.019	0.007	. . .
2	0.11	0.32	1.61	0.014	0.008	0.02
3	0.14	0.25	1.30	0.024	0.004	. . .
4	0.04	0.22	0.45	0.009	0.003	9.17
5	0.05	0.29	0.64	0.003	0.001	9.15
6	0.06	0.26	0.44	0.002	0.001	9.20

TABLE 2—*Mechanical properties.*

Steel	Yield Strength, MN/m^2	Ultimate Tensile Strength, MN/m^2	Elongation to Rupture, %	Charpy Shelf Energy, J
1	377	505	38	157
2	466	597	25	108
3	451	589	27	190
4	725	755	42	323
5	666	725	25	255
6	666	715	31	314

strength, were linked up in the ligament. After that the dV_2/dV_1 kept a constant value of about 0.61. On the other hand, the dotted line in Fig. 3 designates the dV_2/dV_1 versus V_1 relation for ductile crack growth. It can be seen from Fig. 3 that the relationship between dV_2/dV_1 and V_1 with or without the crack extension shows definitely different behavior. Therefore, the finite-element analysis encourages the proposed DCGC method to include the ability to evaluate the J_{Ic} and also the *J-R* curve.

Experimental Procedures

The materials examined were six types of steel whose chemical compositions and mechanical properties are listed in Table 1 and Table 2, respectively. Figure 4 shows the specimen geometry and configuration. The thickness of specimens was 25.4 mm except for that of Steel 1, which had a thickness of 20 mm. Specimens were machined as the T-L orientation described in ASTM Test Method for Plane-Strain Fracture Toughness of Metallic Materials (E 399). In order to make the ductile crack front straight, side grooves were machined on each specimen except for Steel 3, which had depths of 10% of the thickness. Fur-

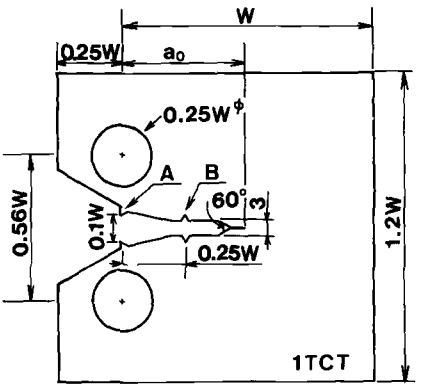

FIG. 4—*Specimen geometry and configuration.*

thermore, specimens without side grooves were also prepared for the case of Steel 2 and 6, in order to examine the effect of the shape of the ductile crack front on the J_{Ic} value by the DCGC method.

Experiments were carried out at room temperature on a 200-kN capacity screw driven type displacement control testing machine. The rate of load line displacement was kept constant at 0.5 mm/min. During the test, the displacements V_1 and V_2 and the load P were measured. V_1 and V_2 were measured by two clip-on gages, and P was measured by a load cell. These data were fed to a pen recorder as a P versus V_1 curve and a V_2 versus V_1 curve, which were converted into J versus V_1 and dV_2/dV_1 versus V_1 curves by using a personal computer system. J values were calculated according to Eq 7 described in ASTM E 813 and JSME S 001 for the compact tension specimen

$$J = (A/Bb)\cdot f(a_0/W) \tag{7}$$

where A is the area under the load versus load line displacement V_1 record in energy units, B is the specimen thickness, and $f(a_0/W)$ is a dimensionless coefficient value. For the calculation of the J value on specimens with side grooves, breadth at the minimum cross section was used for convenience sake. Figure 5 shows the layout of the experimental setup. Examples of P versus V_1 and V_2 versus V_1 curves, and J versus V_1 and dV_2/dV_1 versus V_1 curves are shown in Figs. 6 and 7, respectively.

On the other hand, the J_{Ic} values were also determined on the same specimens by the R-curve methods according to JSME S 001 and ASTM E 813. In the JSME method, the ductile crack length is measured as the average value of crack length measured at 3/8, 4/8, and 5/8 thickness of the specimen. Furthermore, the blunting line is drawn using the experimental data, and the R-curve is also drawn

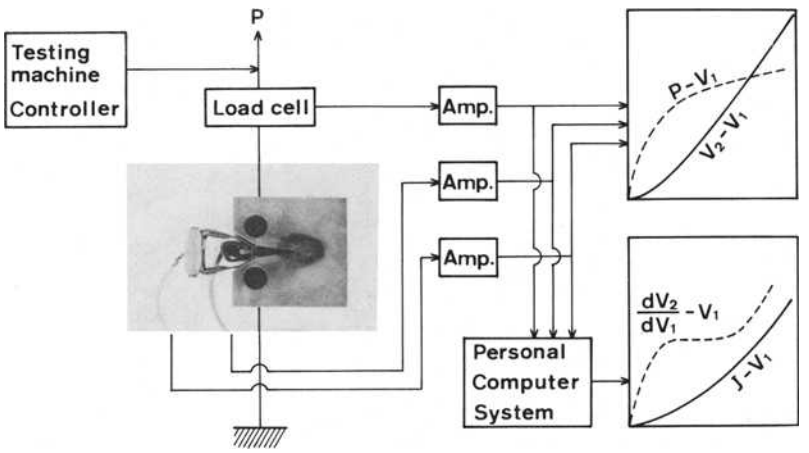

FIG. 5—*Layout of experimental setup.*

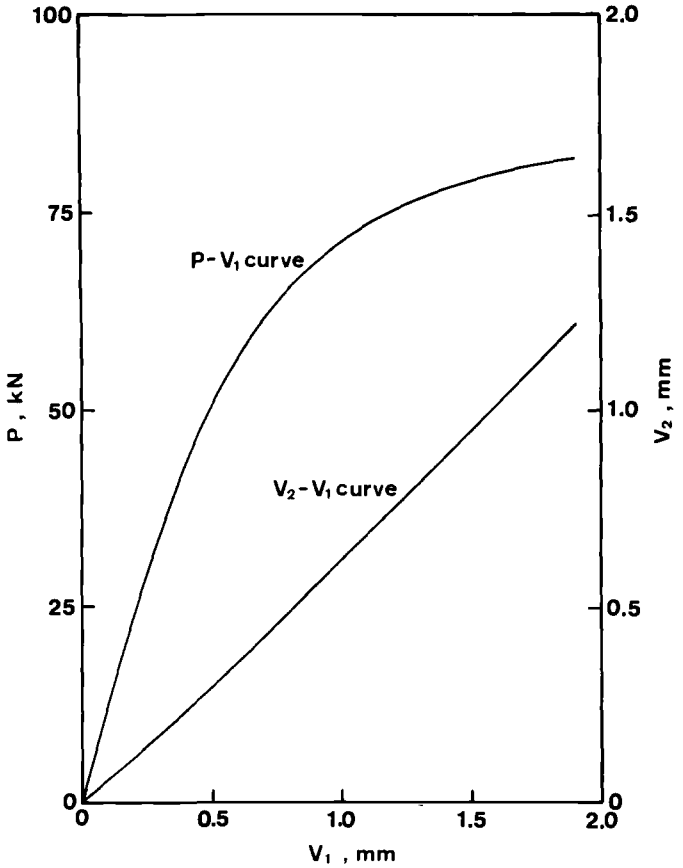

FIG. 6—*Example of* P *versus* V_1 *and* V_2 *versus* V_1 *curves.*

using the data measured on the specimens whose ductile crack lengths are in the range between 0.1 and 1.0 mm.

Experimental Results

According to the present model, the J value corresponding to the second inflexion point in the dV_2/dV_1 versus V_1 curve is the J_{Ic}; so the J_{Ic} value can be determined by carrying out the treatment shown as broken line in Fig. 7. All of the J_{Ic} values determined by the DCGC method are listed in Table 3, in which the J_{Ic} values on the specimens with side grooves are distinguished by the symbol, SG, from those of the standard specimens. In Table 3, J_{Ic} values obtained by the multiple specimen method described in the JSME method and the ASTM method are also listed. J_{Ic} values by JSME method and DCGC method coincided fairly well with each other. However, J_{Ic} obtained by the ASTM method rather differed from that by the JSME method for Steel 3 while they were almost

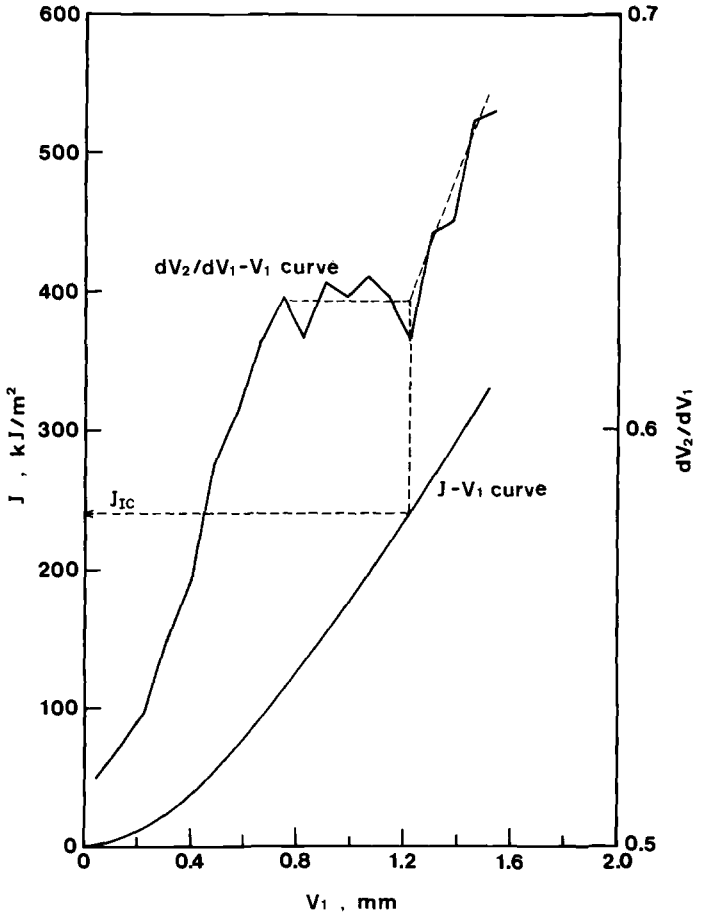

FIG. 7—*Example of* J *versus* V_1 *and* dV_2/dV_1 *versus* V_1 *curves.*

equivalent for Steel 2. In this study, specimens were unloaded at a relatively early point compared with maximum load point; therefore in many cases, the J-Δa points needed to determine the R-curve according to ASTM E 813 were not obtained. Examples of R-curves for Steels 2 and 3 determined by ASTM E 813 and JSME S 001 are shown in Figs. 8 and 9, respectively. The reason for the large discrepancy between the ASTM J_{Ic} and the JSME J_{Ic} is due to large differences in the blunting lines and R-curves.

Examples of the fractured surfaces are shown in Fig. 10. The ductile crack front is fairly uniform in the side grooved CT specimen if it is compared with that of the specimen without side grooves. Nevertheless, J_{Ic} values on side grooved specimens and those on specimens without side grooves coincide well with each other, within 5% error. Therefore, it seems that the shape of ductile crack front affects slightly the J_{Ic} values by the DCGC method.

TABLE 3—J_{Ic} *values by the DCGC method and multiple-specimen methods.*

Steel	J_{Ic} (ASTM), kJ/m²	J_{Ic} (JSME), kJ/m²	J_{Ic} (DCGC), kJ/m²	
			Mean	Standard Deviation
1 (SG)	. . .	180	230	12
2 (SG)	130	120	160	0
2	160	120	150	15
3	400	250	280	32
4 (SG)	. . .	260	240	57
5 (SG)	. . .	200	250	28
6 (SG)	. . .	250	250	78
6	. . .	240	260	0

Discussion and Further Work

Shiratori and Miyoshi [5] have also obtained the general yield load P_{GY} as follows

$$P_{GY} = 2kbB(2.706\{-(w/b - 1) + [(w/b - 1)^2 + 0.740(w/b - \tfrac{1}{2}]^{0.5}\} - 1) \quad (8)$$

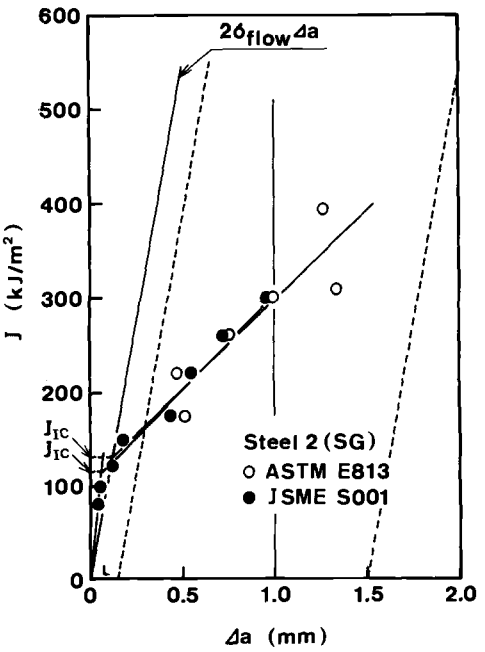

FIG. 8—R *curves determined by ASTM E 813 and JSME S 001 for Steel 2 (SG).*

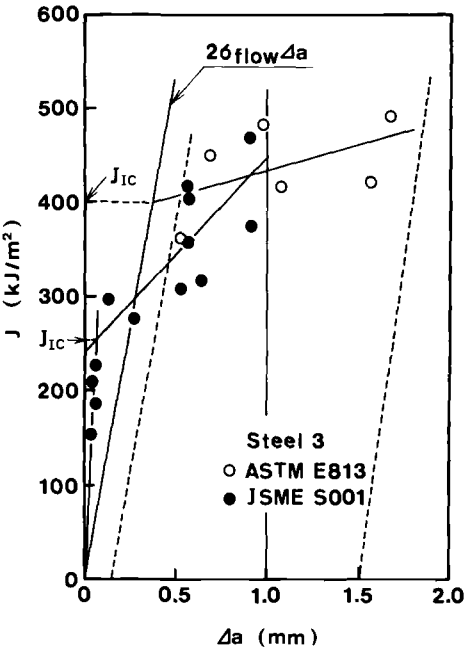

FIG. 9—R *curves determined by ASTM E 813 and JSME S 001 for Steel 3.*

based on the results of the slip line field analysis. In Eq 8, k is the shear yield stress. The J value corresponding to the first inflexion point in the dV_2/dV_1 versus V_1 curve (Fig. 7) and the J value calculated from the load versus load line displacement up to the P_{GY} according to Eq 8 coincided well with each other. The value of the plateau in the dV_2/dV_1 versus V_1 curve always was about 0.65. This test result agrees well with the predictions by the slip line field analysis on the perfectly plastic-rigid body (plane strain case of Eq 6) and by the elastic-plastic finite-element analysis.

All of the J_{Ic} values listed in Table 3 clear the restriction condition of

$$a_0, B \geq 25J/\sigma_y \tag{9}$$

The J_{Ic} values determined by the DCGC method for each material distribute in a relatively small range, and the standard deviations are less than about 10% of the mean values except for two cases.

Figure 11 shows the comparison between the mean of the J_{Ic} values by the DCGC method and the J_{Ic} value by the multiple-specimen method of the JSME standard. The J_{Ic} values by both methods coincide well with each other, within a -10 to $+40\%$ error, while this method seems to have a tendency to give a smaller J_{Ic} value compared with that obtained by the ASTM standard.

In this paper, the DCGC method was applied to the six kinds of steel listed in Table 2. Thus, the DCGC method seems to have enough reproducibility and

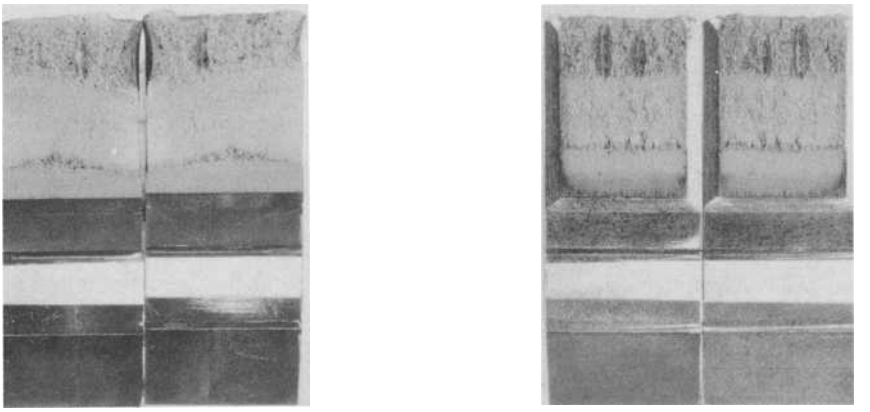

FIG. 10—*Examples of fractured surfaces.* Left—*on the standard specimen.* Right—*on the specimen with side grooves.*

accuracy to determine the J_{Ic} values for materials whose tensile strength is larger than about 500 MN/m^2. This method was also applied to mild steel whose tensile strength was about 400 MN/m^2. In this case, the obvious plateau could not be obtained in dV_2/dV_1 versus V_1 curves. Because of the micrographic observations, many dimples were observed in stretched zone for this steel. In other words, the ductile crack had been initiated at the crack tip during the process of blunting.

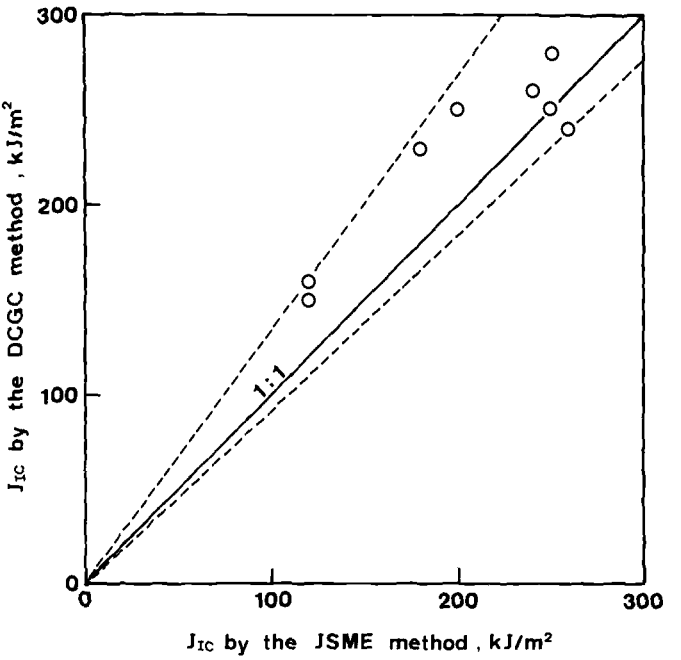

FIG. 11—*Comparison between J_{Ic} values by the DCGC method and the JSME method.*

This phenomenon is the main reason why the plateau could not be obtained for this steel.

As predicted by the finite-element analysis, the dV_2/dV_1 is expected to increase in its value beyond the second inflexion point in dV_2/dV_1 versus V_1 curve because of the ductile crack growth. Therefore, the DCGC method has possession of the possibility for a single-specimen method to determine the *J-R* curve. In order to confirm the possibility of the *J-R* curve determination and to prove the assumption that was made previously, that is, the center of rotation moves forward if the ductile crack initiates and grows, the additional experiments were preliminarily performed. A 1TCT specimen was loaded up to the several prescribed load levels, and the change in the crack shape, including the ductile crack, was cast by silicon rubber, and the changes in V_1 and V_2 by means of clip-on gages were recorded at each prescribed load level. Because of the observation of the change in crack shape, it was confirmed that the center of rotation moved toward the backface of the specimen after the ductile crack initiation, while it stands at the same position within the experimental error before the crack initiation. But any useful information could not be obtained about the relationship between V_1 and V_2 during the ductile crack growth because the clip-on gage might not have enough accuracy for this purpose. However, it is possible to obtain the *J-R* curve as well as the J_{Ic} value with only a single specimen, by using two clip-on gages having better accuracy.

Conclusion

The DCGC method to determine the J_{Ic} value was introduced for the single-specimen technique, and some of the advantages of this method were discussed. The main results obtained are as follows.

1. The J_{Ic} values of each material by the DCGC method were distributed in relatively small range.
2. The J_{Ic} values by the DCGC method and those by the JSME method coincided well with each other within a -10 to $+40\%$ error for many steels that show wide ranges of tensile strength.
3. The shape of the ductile crack front does not greatly affect the J_{Ic} values by the DCGC method.
4. The DCGC method needs only two clip-on gages contacted on a single specimen; so this method is considered to be a useful method to determine the J_{Ic} value in an industrial sense.

References

[1] Shiratori, M. and Miyoshi, T., *Fracture Mechanics of Ductile and Tough Materials and Its Applications to Energy Related Structures*, H. W. Liu, T. Kunio, V. Weiss, and H. Okamura, Eds., Martius Nijhoff Publishers, Boston, MA, 1981, pp. 89–98.

[2] Merkle, J. G. and Corten, H. T., *Journal of Pressure Vessel Technology, Transactions of the American Society of Mechanical Engineers*, Vol. 94, No. 4, Nov. 1974, pp. 286–292.

[3] McCabe, D. E., "Determination of R-Curves for Structural Materials by Using Nonlinear Mechanics Methods," *Flaw Growth and Fracture, STP 631*, American Society for Testing and Materials, Philadelphia, 1977, pp. 245–266.

[4] Hill, R., *The Mathematical Theory of Plasticity*, Oxford Press, Glasgow, Scotland, 1950.

[5] Shiratori, M. and Miyoshi, T., *Transactions of the Japan Society of Mechanical Engineers*, Vol. 45, No. 389, June 1979, pp. 50–56.

Wayne R. Andrews[1]

Determining Crack Extension Using a Displacement Based Key-Curve Method

REFERENCE: Andrews, W. R., **"Determining Crack Extension Using a Displacement Based Key-Curve Method,"** *Elastic-Plastic Fracture Test Methods: The User's Experience, ASTM STP 856*, E. T. Wessel and F. J. Loss, Eds., American Society for Testing and Materials, 1985, pp. 308–321.

ABSTRACT: A method for determining crack-growth resistance curves previously proposed by the author is derived from fundamental relationships. Data are presented that further demonstrate the application of the method to materials having a wide range of properties. It is concluded that the use of this method results in obtaining fracture properties not previously measured directly.

KEY WORDS: ductile fracture, tests, crack propagation, crack-growth resistance curves, crack-opening displacement, *J* integral, compact specimen

The concept of characterizing ductile crack growth using a resistance parameter, for example, the *J* integral, has gained acceptance because, to a large extent, of the introduction of single-specimen test techniques for measuring crack growth. Among those in common use are the unloading-compliance [*1*], the electric-potential-drop [2], and the "key-curve" [*3,4*] methods. These methods each have certain advantages and disadvantages that cannot be exhaustively reviewed here. While attempting to apply the unloading compliance method to large (4T) compact specimens, the author saw a need to develop yet another method using available instrumentation [*5*]. The new test method is referred to here as the "Displacement-Based Key-Curve" (DBKC) method.

Interest in the method is continuing because of the derived benefits of simplified test procedures that reduced test time and, at the same time, increased the number of data for *R* curve presentation.

Enthusiasm among other investigators for the DBKC method seemed reserved because of the empirical nature of the formulation and because of the fact that an adjustable parameter is required. Nevertheless, the method has developed into a preferred method at the General Electric (GE) Turbine Technology Laboratory. Recently, a derivation was found that shows the relationship between

[1]Engineer of advanced mechanics of materials, Turbine Technology Laboratory, General Electric Company, Building 55, Room 163, Schenectady, NY 12345.

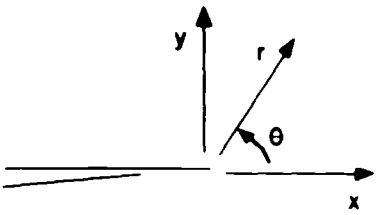

(a) SHARP CRACK

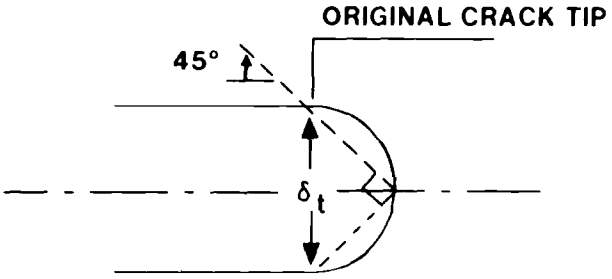

(b) DEFORMED PROFILE

FIG. 1—*An elastic-plastic crack-tip profile showing the defining construction for crack-tip opening displacement.*

the DBKC method and the Rice-Drugan-Sham (RDS) [*6*] model of ductile crack growth, thus answering the need for a theoretical basis.

It is the purpose of this paper to relate the DBKC method to the RDS model and further, to document the application of the method, including typical results from tests of several materials covering a range of strength properties.

Derivation

The J integral and the crack-tip opening displacement have been shown to be viable criteria for ductile crack initiation and crack growth [*7*]. Based on an unambiguous definition proposed for δ_t [*8*] as the separation between the intersection of 45° lines with the crack faces (Fig. 1), an explicit relation between δ_t and J was proposed

$$\delta_t = d_n (J/\sigma_o) \tag{1}$$

where the coefficient d_n is strongly dependent on the strain hardening exponent

n and weakly dependent on the quantity σ_o/E, the flow stress divided by Young's modulus. The application of Eq 1 to a static (nongrowing) crack is widely accepted, but its application to a growing crack is proposed here.

Rice et al [6] and Shih et al [9] have suggested that the crack-opening angle measured near the current crack tip is a viable criterion for continued crack growth. This angle is approximated by the following relationship [6]

$$\delta_c/r_m = [(d_\infty/\sigma_o)\,(dJ/da)] + [(\beta'\sigma_o/E)\ln(eR'/r_m)] \quad (2)$$

The angle is represented by an opening δ_c at a distance r_m from the current tip. The parameter d_∞ corresponds to d_n in Eq 1 for a nonhardening material. β' is a constant and R' is the radius of the zone of intense plasticity.

The objective of what follows is to derive the method for determining crack extension first presented by Andrews and Shih [5] from Eqs 1 and 2. Supporting data are presented.

The Model

The model assumed previously [5] and for this derivation is a geometric construction, Figure 2, which represents the profile of a growing crack. In this model, the original crack tip is located at a distance a_o from the crack mouth.

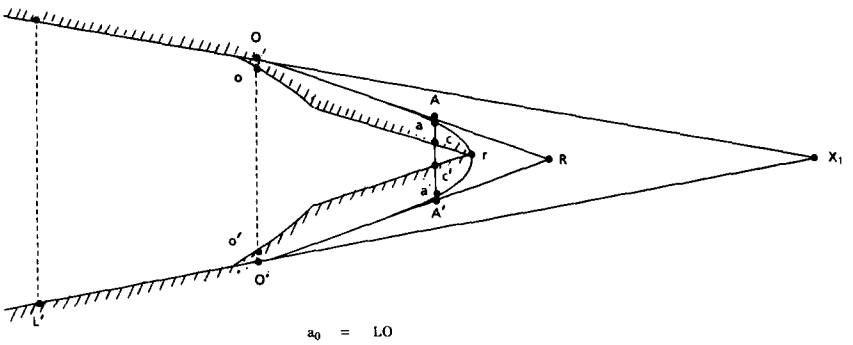

a_0 = LO
a_1 = LA
r_m = $\delta_t/2$ = cr
R = OR
V_L = LL'
X_1 = LX 1
δ_c = CC'
δ_0 = OO'
δ_t = aa'
δ_T = AA'
Δa = OA
$1/\rho$ = ∠(ORO') = ∠(ARA')

FIG. 2—*A growing elastic-plastic crack-tip profile showing additional defining construction.*

As the crack mouth is opened a distance V_L $(L - L')$, the linear extrapolation of the crack faces $LOX1$ from remote locations to the original tip are separated by a distance δ_o $(O - O')$ at the tip. The intersection of $LOX1$ with $L'O'X1$ forms a rotation point located at a distance $L - X1$ from the mouth.

As the crack grows, it opens by an amount dc $(c - c')$ at a distance r_m $(c - r)$ from its tip. As the crack grows, a second center of rotation at R results from the intense plasticity and is located a distance $O - R$ from the original crack tip.

The opening δ_T $(A - A')$ is determined by calculation assuming the value is the same for a growing crack as it would have been had the original crack had a length a_o plus Δa $(L - A)$. The method for calculating δ_T will be given later.

When no crack growth has occurred $(\Delta a = O - A = O)$ δ_T is taken as identical to δ_o. δ_T and δ_t $(a - a')$ are measured at the same distance from the tip, that is, $\delta_t/2$ from the leading edge of the stretched crack front. As the crack begins to grow, however, the real crack profile has an opening δ_c at a distance r_m from the tip. To be consistent with the model for a nongrowing crack, r_m was assigned the value $\delta_t/2$. A virtual (or imaginary) crack-tip profile at the tip of a growing crack is assumed to have openings δ_t and δ_T at $\delta_t/2$ from the crack tip. The values of δ_T and δ_t for a growing crack are assumed to be the same as they would be for a nongrowing crack of the same length and of the same mouth opening. (This is the same as assuming the values are independent of the path taken in displacement-crack-length space.)

Take note that for strain hardening materials, δ_T is larger than δ_t by an amount that depends on material properties (n and σ_o), thus these dimensions are shown separately in Fig. 2. When a rigid perfectly plastic material ($n = \infty$) is considered, δ_T is identical to δ_t. Note also that δ_o is a measurable dimension whereas, in general, δ_T and δ_t are not.

These definitions of δ_o and δ_T allow us to define the distance R as $O - R$. This distance can be thought of as a measure of the length of the wake of intense plastic deformation associated with the growing crack. Furthermore, we note that

$$R = \Delta a + \delta_T \rho \tag{3}$$

Therefore

$$1/\rho = (R - \Delta a)/\delta_T \tag{4}$$

We now turn our attention to the basic relationships (Eqs 1 and 2) to correlate them with the model. Examination of Eqs 1 and 2, differentiating Eq 1 and

using $r_m = \delta_t/2$ leads to the transformation of Eq 2 to be expressed in terms of displacement and length only

$$2\,\delta_c/\delta_t = (d\delta_T/da) + (\beta'\sigma_o/E)\ln(2\,eR'/\delta_t) \tag{5}$$

Note: in deriving Eq 5, use was made of the following relationship. Since

$$\delta_T = d_\infty\,(J/\sigma_o)$$

then

$$d\delta_T/da = (d_\infty/\sigma_o)\,(dJ/da)$$

The left-hand side of Eq 5 cannot be measured directly. It can, however, be transformed to be expressed in values that can be determined. The transformation makes use of the assumed path independence of δ_T. For suitably short amounts of crack growth, the profile in Fig. 2 can be viewed as the result of a two-step process. Step one was to open the mouth to its current value V_L while keeping the crack length constant. At that value of V_L, δ_T will have a value identical to the measurable δ_o. The second step was to allow the crack to grow to its current value while maintaining V_L constant. In the second step, δ_o increased by an amount equal to the opening of the extending crack. That opening is

$$\delta_o - \delta_T|a_o = \Delta a\,(2\,\delta_c/\delta_t) \tag{6}$$

therefore

$$(2\,\delta_c/\delta_t) = (\delta_o - \delta_T|a_o)/\Delta a \tag{7}$$

Substitution of Eq 6 for the left-hand side of Eq 5 and rearranging gives

$$\Delta a = (\delta_o - \delta_T|a_o)/[(\beta'\sigma_o/E)\ln(2\,eR'/\delta_t) + (d\delta_T/da)] \tag{8}$$

This result is the same as originally proposed by Andrews and Shih [5]

$$(\delta_o - \delta_T|a_o)/[(1/\rho) + (d\delta_T/da)] \tag{9}$$

if it is assumed that Eq 10 holds

$$1/\rho = (\beta'\sigma_o/E)\ln(2\,eR'/\delta_t) \tag{10}$$

Application

To use Eq 9, one must first establish δ_T as a function of a and V_L. This relationship forms the "key curve." To develop the key curve, we make use of

the fact mentioned earlier that δ_o and δ_T are identical before any crack growth. An early version of the required key curve was published in Ref *5*. There, it was suggested that a normalization of δ_T by the remaining ligament and V_L by material properties and a function of crack length would establish a function that is independent of crack length for the compact $C(T)$ specimen

$$x = EV_L/[\sigma_o W(2 + a/w)^2] \tag{11}$$

$$y = \delta_T/(W - a_o) \tag{12}$$

where W is specimen width, E is Young's modulus, and σ_o is the flow stress defined by the Ramberg-Osgood stress-strain relationship

$$\epsilon/\epsilon_o = \sigma/\sigma_o + \alpha\,(\sigma/\delta_o)^n \tag{13}$$

An improved function making use of the same normalization parameters is proposed here. The new function is given by Eq 14

$$\delta_T/(W - a_o) = \sigma_o/E\,\{A[X_R\mathrm{Tanh}^{1/n'}(X/X_R{}^{n'})] + 3.38[X - X_R\,\mathrm{Tanh}^{1/n'}\,(X/X_R{}^{n'})]\} \tag{14}$$

In Eq 14, A is a weak function of a_o/W and, since A is associated with the elastic loading of the specimen (the first term represents the elastic term), A can be determined as the value that best produces a calculation of zero crack growth for the initial and elastic loading of the specimen. The value of A is in the range of 1.45 ± 1.0.

The second term of Eq 14 is associated with plastic deformation. The value of XR is 0.5 and of n' is 1.2. The use of the hyperbolic tangent function provides a smooth transition from the elastic region to the plastic region.

For verification purposes, the key curve relationship was compared to results of ADINA finite-element calculations for 4T $C(T)$ specimens [*7,9*] with good results. Equally good results were obtained by comparison with the results of deLorenzi [*10*].

A second term in Eq 9 requiring evaluation is $d\delta_T/da$. This was accomplished in [*5*]

$$d\delta_T/da\,(\delta_T/W - a_o)\,\{(a_o/W - 4)/[2 + (a_o/W)]\} \tag{15}$$

Finally, the term $1/\rho$ is evaluated as an adjustable parameter, assuming it is constant for the entire crack growth process [*6*]. This is accomplished in practice by marking the fracture surface at the last displacement measurement and using the measured crack length and Eq 9 to determine $1/\rho$.

TABLE 1—*Material compositions, weight %.*

Carbon	Manganese	Phosphorus	Sulfur	Copper	Silicon	Nickel	Chromium	Molybdenum	Aluminum	Cobalt	Nitrogen	Tin	Vanadium
							A533-B						
0.20	1.22	0.01	0.016	. . .	0.15	0.65	. . .	0.54	. . .	. . .	. . .	. . .	. . .
							A508-2						
0.20	0.73	0.10	0.008	0.04	0.03	0.73	0.33	0.60	0.006	. . .	. . .	0.001	0.30
							Type 304 Stainless Steel						
0.027	1.62	0.034	0.015	0.31	0.43	10.04	18.3	0.31	. . .	0.15	0.070	. . .	. . .

TABLE 2—*Materials stress-strain properties.*

Specification	Ramberg-Osgood Parameters[a]				
	σ_o, ksi	ϵ_o	n	E, ksi	α
A533-B	60	0.002	9.71	30 000	1.12
A508 Class 2 steel	87	0.0029	11.41	30 000	1.04
A204/304 stainless	24.5	0.00079	8.04	31 000	1.03

[a] $\epsilon/\epsilon_o = \alpha(\sigma/\sigma_o)^n$, ϵ = engineering strain, and σ = engineering stress. Data taken at strains less than 30%. 1 ksi = 6894 kPa.

Experimental Verification

Materials

To evaluate the proposed relationship (Eq 9), materials having a wide range of properties were selected. The materials used were A533-B steel, A508 Class 2 steel, and ASTM A-240 Type 304 stainless steel (Unified Numbering System [UNS] K12539, K12766, and S30400, respectively). The compositions are shown in Table 1. The tensile properties are shown in Table 2. The flow stress σ_o, and the strain-hardening exponent n obtained from analysis of the tensile data are also listed in Table 2.

The A533-B steel was obtained from the remaining and broken halves of specimens used for Electric Power Research Institute (EPRI) Project RP601-2 [*7*].

The A508 Class-2 steel was obtained from the Westinghouse Research Laboratory and came from the center thickness portions of the tube-sheet forging used for EPRI Project RP1238-2 [*11*].

The Type 304 stainless steel was purchased as a 62.6-mm (2½ in.) thick plate from a local distributer.

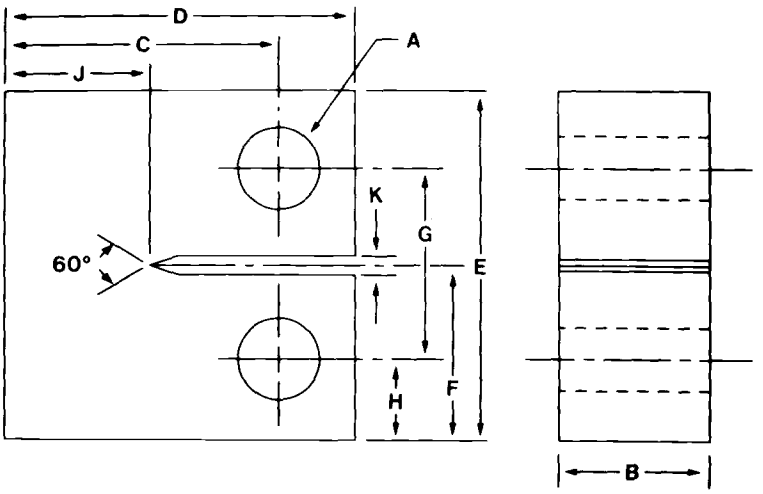

FIG. 3—*Compact specimens used in this study.*

TABLE 3—*Critical dimensions of the compact specimen, mm.*

Size	A	B	C	D	E	F	G	H	J	K
1T	12.70	25.40	50.80	63.50	60.96	30.48	27.94	16.51	29.72	2.54
2T	25.40	50.80	101.60	127.00	121.92	60.96	55.88	33.02	59.44	5.08

Specimens

Compact specimens (Fig. 3 and Table 3) were used for all tests. The 2T size was used for the 304 stainless steel and the A533-B steel while the 1T size was used for the A508 Class-2 steel.

Equipment

The tests were all performed using electrohydraulic servo-controlled test machines controlled by actuator displacement. The displacements were applied at a constant slow rate until the desired final displacement was reached, or until the specimen broke, whichever occurred first.

Displacements were measured at the front V_f and the back V_b of the specimens using strain-gage bridge "clip" gages similar to Test Method for J_{Ic}, a Measure of Fracture Toughness (E 813) and ASTM Test Method for Plane-Strain Fracture Toughness of Metallic Materials (E 399) design. A frame surrounding the spec-

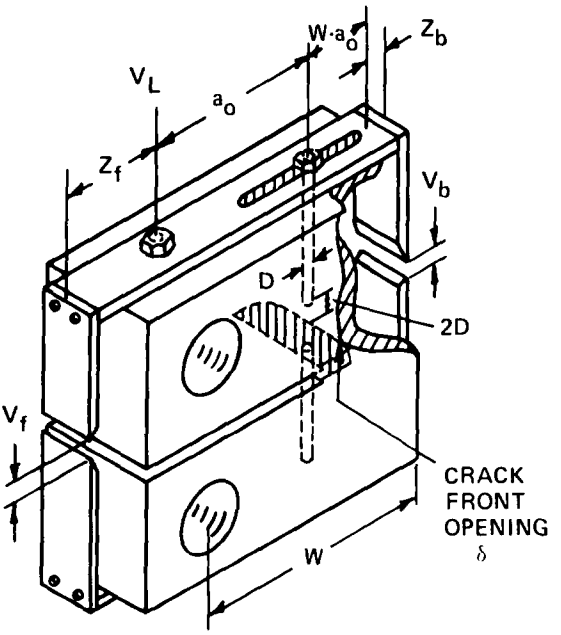

FIG. 4—*The extensometer fixture used in this study.*

imen (Fig. 4) was required by the method. The frame included knife edges front and back. The fixture was attached at the load line with small screws and rested firmly at the bottom of holes drilled above and below the crack faces near the crack tip. With the frame so attached, points of reference were established for inferring displacements at the load line V_L and at the crack tip δ_o. The inferences were accomplished using Eqs 16, 17, and 18 [7]

$$r = \{Z_b + W - a_o - [(V_b/V_f)(Z_f + a_o)]/[(V_b/V_f) + 1]\} \quad (16)$$

$$\delta_o = r\, V_f/(Z_f + a_o + r) \quad (17)$$

$$V_L = (r + a_o)\, V_f/(Z_f + a_o + r) \quad (18)$$

Procedures

During each test, the displacements V_f and V_b were continuously recorded until either a final displacement was reached or the specimen broke, whichever occurred first. Load also was continuously recorded throughout the test.

All data were recorded in digital form and stored on magnetic tape for later reduction using a computer.

At the conclusion of each test, the final crack length a_f was either measured directly on the fracture surface or obtained by heat tinting the crack, breaking open the specimen, and measuring the heat-tinted crack length.

Calculations

Crack Length

The crack lengths were calculated using Eq 9 following the method described in "Application," above.

J *Integral*

The J integral values were calculated from the load and the load-line displacements recorded during each test. J-integral calculations used the incremental formulation of ASTM E 813, which accounts for crack extension. The calculation approximates the deformation-theory definition of J

$$J_{i+1} = \{J_i + (f(a/w)/b)_i\, [(A_{i+1,i})/B_N]\}\, \{1 - (\gamma/b)_i\, (a_{pi+1} - a_{pi})\} \quad (19)$$

where

$\gamma = 1 + 0.76\, (b_i/W)$,
A = area under the load, load-line displacement record,
B_N = specimen net thickness, and
b = uncracked ligament, W-a.

The subscripts i and $i + 1$ indicate functions evaluated in the previous or in the current calculation step. The term $Ai + 1,i$ refers to the area bounded by the actual test record trace and the lines of constant displacement, $(V_L)_i$ and $(V_L)_{i+1}$.

Results and Discussion

To determine the validity of the DBKC crack-growth model, single-specimen R-curves were determined using Eq 9 and compared to multispecimen R curves. These comparisons are presented in Figs. 5 through 7.

Figure 5 presents data for A533-B steel tested at room temperature using 2T compact specimens of varied crack length. Of the three results, Specimens U21 and U5 form one R curve, while Specimen U21 forms a second. The R curve formed by Specimens U1B1 and U5 was further verified by heat-tint results obtained using additional specimens. The cause of the separate R curve resulting for specimen U21 is uncertain.

Figure 6 shows the R curve data obtained for the A508 Class 2 steel. The open points are DBKC crack-extension values while the filled-in data are heat-tint crack-length data from the present investigation. The curve shown represents the data reported by Landes et al [*11*].

Figure 7 shows the R curve obtained for the 304 stainless steel using 2T specimens. The open circles and the small dots are DBKC crack-length results, while the large, filled-in circles are heat-tint results.

Typical values obtained for $1/\rho$ while determining the R curves are shown in Table 4.

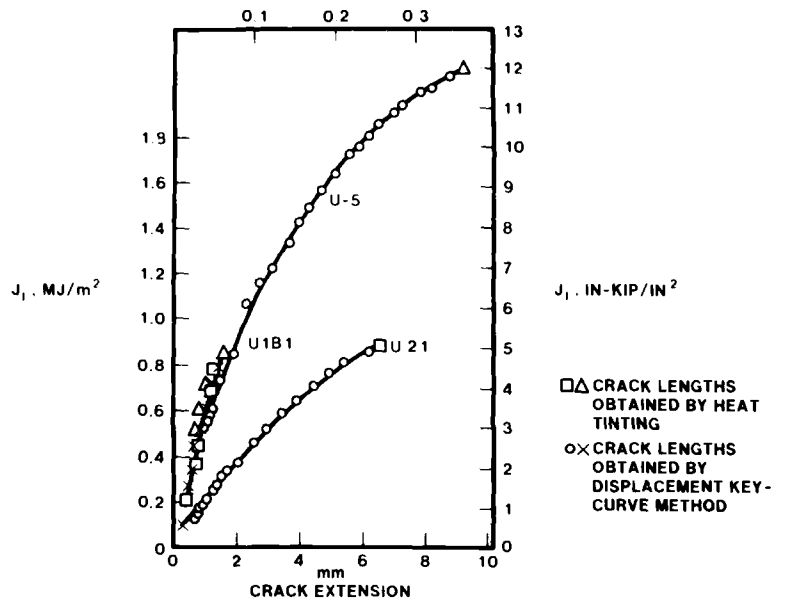

FIG. 5—R *curves for A533-B steel determined using the DBKC method and using the heat-tint method.*

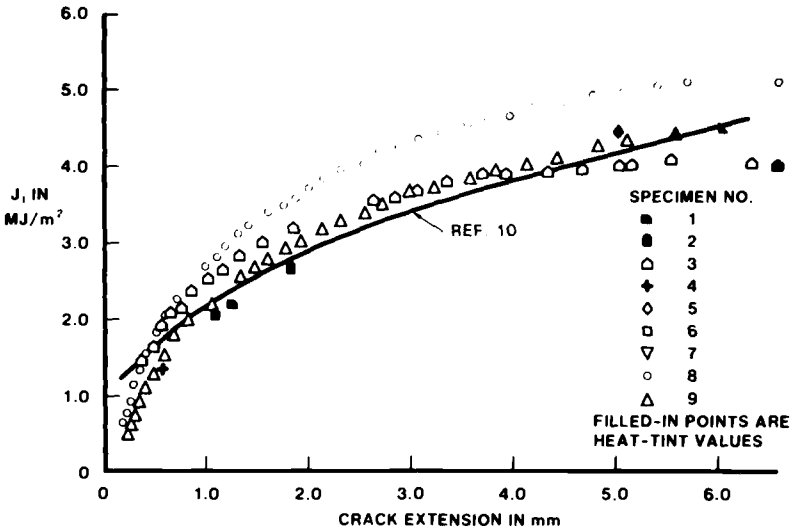

FIG. 6—R *curves A508 Class 2 steel determined using the DBKC method and the heat-tint method. Indicated J values are 10 times the actual value.*

Comparison of the data presented in Figs. 5 through 7 shows good agreement between the two methods. Moreover, the author has obtained equally good agreement in other unpublished work performed by the General Electric Company for materials ranging from 2024T351 aluminum to CrMoV steel. In light of the demonstrated agreement, it can be concluded that the DBKC model for crack extension, Eq 9, is valid for many materials for constant $1/\rho$.

The use of the DBKC method for inferring crack growth has been shown to be a viable laboratory tool. These demonstration tests have shown that the R curves obtained by this method correlated closely with those obtained by heat-

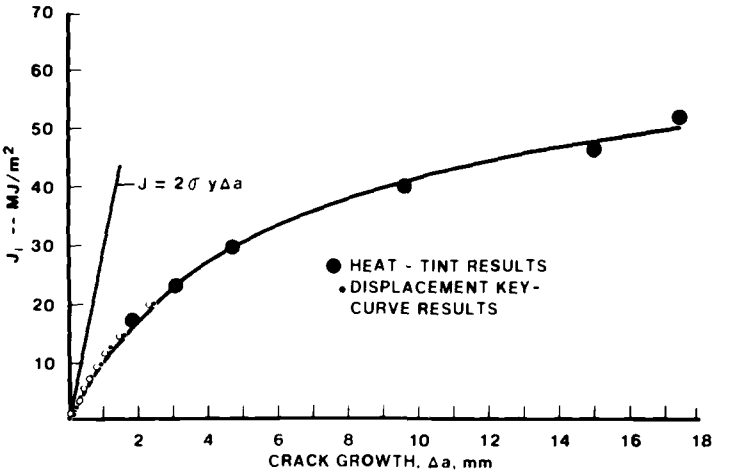

FIG. 7—R *curves for Type 304 stainless steel determined using the DBKC method and the heat-tint method. Indicated J values are 10 times the actual value.*

TABLE 4—*Crack-growth parameters* $1/\rho$ *obtained for the steels tested.*

Steel	$1/\rho$
304 S/S	0.49
A533-B	0.14
A508 Class 2	0.07

tinted specimens. It can also be said that the DBKC method offers a cost effective alternative to either multiple-specimen testing or single-specimen testing requiring multiple unloading. In addition to the cost benefit derived, relatively lower measurement precision is required for displacements. The multiple unloading compliance method requires measurement precision on the order of ten times better than is normally found in industrial laboratories.

The demonstrated effectiveness of the DBKC method and the demonstrated relationship of Eq 9 with basic concepts of elastic-plastic crack growth (Eqs 1 and 2) seem to offer an avenue for obtaining new understanding of crack growth. Fracture parameters previously unmeasured are now open to study.

Conclusions

1. A displacement-based key-curve (DBKC) model for determining crack extension was derived and was shown to result in an accurate and cost effective laboratory method for determining R curves.

2. The assumed constancy of the crack-opening-angle parameter $1/\rho$, which results from the DBKC model, appears justified based on the correlation of single-specimen and multiple-specimen crack-growth data.

3. The relationship of the DBKC model (Eq 9) with the fundamental Rice, Drugan, and Sham model (Eq 2) was derived.

Acknowledgments

The author is grateful to those who have supported this work with their encouragement and critical review, especially Robin Jones and Douglas Norris of EPRI, D. F. Mowbray and A. F. Anderson of GE Co., and C. F. Shih of Brown University. The financial support came primarily from the Electric Power Research Institute under Contract RP1237-8.

References

[*1*] Clarke, G. A. and Andrews, W. R. in *Mechanics of Crack Growth, STP 590,* American Society for Testing and Materials, Philadelphia, 1976, pp. 27–42.

[*2*] Schwalbe, K.-H. and Hellmann, D., *Journal of Testing and Evaluation,* Vol. 9, No. 3, May 1981, pp. 218–221.

[*3*] Ernst, H., Paris, P. C., Rossow, M., and Hutchinson, J. W. in *Fracture Mechanics, Proceedings of the Eleventh National Symposium on Fracture Mechanics, STP 677,* American Society for Testing and Materials, Philadelphia, 1979, pp. 581–599.

[4] Joyce, J. A., Ernst, Hugo, and Paris, P. C. in *Fracture Mechanics, Proceedings of the Twelfth National Symposium on Fracture Mechanics, STP 700,* American Society for Testing and Materials, Philadelphia, 1980, pp. 222–236.

[5] Andrews, W. R. and Shih, C. F. in *Elastic-Plastic Fracture, STP 668,* American Society for Testing and Materials, Philadelphia, 1979, pp. 426–450.

[6] Rice, J. R., Drugan, W. J., and Sham, T-L. in *Fracture Mechanics, Proceedings of the Twelfth National Symposium on Fracture Mechanics, STP 700,* American Society for Testing and Materials, Philadelphia, 1980, pp. 189–221.

[7] Shih, C. F., Andrews, W. R., deLorenzi, H. G., German, M. D., Van Stone, R. H., and Mowbray, D. F., "Methodology for Plastic Fracture," NP1735, Final Report, Contract RP601-2, Electric Power Research Institute, Palo Alto, CA.

[8] Shih, C. F., *Journal of Mechanics and Physics of Solids,* Vol. 29, No. 4, 1981, pp. 305–326.

[9] Shih, C. F., deLorenzi, H. G., and Andrews, W. R., "Studies on Crack Initiation and Stable Crack Growth," *Elastic-Plastic Fracture, STP 668,* American Society for Testing and Materials, Philadelphia, 1979, pp. 65–120.

[10] deLorenzi, H. G., "3-D Elastic Plastic Fracture Mechanics with ADINA," TIS Report CRD242, General Electric Co., Schenectady, NY, Nov. 1980.

[11] Landes, J. D., McCabe, D. E., Ernst, H. A., Wessel, E. T., and Pryle, W. H., "Elastic-Plastic Methodology to Establish R Curves and Instability Criteria," Sixth Semiannual Report, Contract RP1238-2, Electric Power Research Institute, Palo Alto, CA, Aug. 1982.

Takahiro Fujita,[1] *Hiroyuki Kagawa,*[1] *Akihide Yoshitake,*[1] *and Namio Urabe*[1]

J-Integral Values of Steels Tested Under Constant Load

REFERENCE: Fujita, T., Kagawa, H., Yoshitake, A., and Urabe, N., "***J*-Integral Values of Steels Tested Under Constant Load,**" *Elastic-Plastic Fracture Test Methods: The User's Experience, ASTM STP 856*, E. T. Wessel and F. J. Loss, Eds., American Society for Testing and Materials, 1985, pp. 322–337.

ABSTRACT: A stable to unstable transition phenomenon of cracking under constant load was studied. The transition phenomenon was mainly caused by initiation and growth of the ductile crack. When this fracture process was examined by means of *J*-integral resistance (*J-R*) curves, the ductile crack growth under constant load seemed to agree with the *J-R* curve that had been determined by the conventional multiple-specimen method. If J_g is defined as the minimum *J* value that causes the unstable ductile fracture under the constant load, J_g exists between J_i (corresponding to the ductile crack initiation) and J_m (corresponding to the maximum load point in displacement control test). Thus the J_g might be one of the parameters to define the unstable ductile fracture under the constant load condition, though the effect of specimen geometry on J_g is recognized.

KEY WORDS: fracture tests, crack propagation, cracks, fracture toughness testing, ductile fracture, *J* integral, resistance curve, stable crack growth, crack instability, compact tension specimen

Test methods for elastic-plastic fracture toughness have been recently standardized. These are the ASTM Test Method for J_{Ic}, a Measure of Fracture Toughness (E 813), the Japan Society for Mechanical Engineers (JSME) Standard Method for Elastic-Plastic Fracture Toughness J_{Ic} (S 001-1981), British Standard (BS) Methods for Crack Opening Displacement (COD) Testing (5762-1979), and Japan Welding Engineering Society (WES) Method for Crack Tip Opening Displacement (COD) (WES 2805-1980). The most reliable toughness parameters in these tests for elastic-plastic fracture are J_{Ic} and δ_i, which correspond to the ductile crack initiation. And many investigators have shown that these parameters are independent of specimen geometry and thus characteristic of the material.

It seems however that it is too conservative to use the initiation toughness as a design parameter, especially for high toughness materials that develop a large amount of stable crack growth before final unstable fracture. Consequently, crack

[1]Research engineers, Fracture Engineering Laboratory, Technical Research Center, Nippon Kokan K. K., Kawasaki, 210, Japan.

opening displacement at the maximum load δ_m is frequently used as a critical value in the ductile region, even though δ_m is known to depend on specimen geometry. Thus, a suspicion arises in using δ_m as the material's constant. Since the displacement control is an optimistic loading condition for structural materials, it is known that the unstable fracture occurs at lower value than δ_m or J_m under constant load, which is considered as the severest loading condition [*1–4*].

In this study, various empirical examinations were performed to survey the ductile fracture phenomena under constant load conditions. Load and load-line displacement were monitored during the test, while crack length and change in crack shape were measured by means of the copper plating technique and the ultrasonic echo technique, and fracture appearance was observed by optical and scanning electron microscopes. The *J*-integral resistance curve was applied to this fracture process, and the toughness parameter in the ductile region was studied. Also, the effect of specimen geometry on this fracture behavior was investigated by a series of tests varying specimen thickness and ligament length.

Experimental Procedures

The materials tested were four kinds of structural steels whose ultimate tensile strength levels were classified as 800 and 500 MPa. These are similar to ASTM A514 and A441 steel (Unified Numbering System [UNS] K11856 and K12211), respectively. But those steels are designated as A1 and A2 for 800-MPa class and B1 and B2 for 500-MPa class, since the manufacturing processes are different. Their thicknesses and mechanical properties are listed in Table 1. Standard compact specimens were used in this study as shown in Fig. 1, in conformity with the ASTM Method for Plane-Strain Fracture Toughness of Metallic Materials (E 399). In order to investigate the effect of specimen geometry on fracture toughness, crack length to specimen width ratio a/W and specimen thickness were varied in some steels as shown in Table 1. Specimens were then fatigue precracked according to ASTM E 813.

All tests were carried out at room temperature using a 200-kN capacity electrohydraulic testing machine. Load-line displacement was measured by clip gages attached to the loading pins. Ductile crack shape at the starting point of load holding was marked by the copper plating technique, in which copper sulfate aqueous solution is injected into the crack tip and rinsed away with acetone and then blown off by air, so that the copper is deposited immediately on the crack surface. Also, the crack configuration at the instant of stable-unstable transition was revealed by unloading quickly and subsequent fatigue fracturing. Initiation and growth of the ductile crack during the load holding was also observed by the ultrasonic echo technique [*5*], in which the ultrasonic probe is attached on the back face of the specimen and ultrasonic echo responding to the growing crack tip was monitored on cathode-ray tube (CRT). Ductile crack profiles were observed by optical micrograph and scanning electron micrograph in some in-

TABLE 1—*Materials used in this study.*

Steel	Thickness, mm	Yield Strength, MPa	Tensile Strength, MPa	Specimen Thickness	Specimen *a/W*
A1	55	755	814	2T 1T	0.7
A2	55	804	863	1T	0.3, 0.7
B1	55	333	549	2T 1T	0.7
B2	38.1	318	455	½T 1T ½T	0.7

terrupted specimens in order to investigate the fracture process from a viewpoint of micromechanics.

Descriptions of Fracture Behavior

Variation of the load-line displacement with respect to time as to 2T-CT specimens of Steel A1 and ½T-compact tension (CT) specimens of Steel B2 are shown in Figs. 2 and 3, respectively. Arrows indicate the displacement level

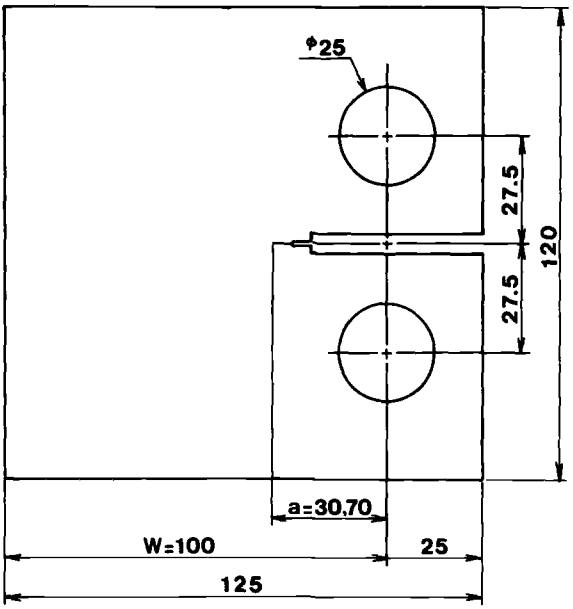

All dimensions in mm.

FIG. 1—*Specimen geometry and configuration.*

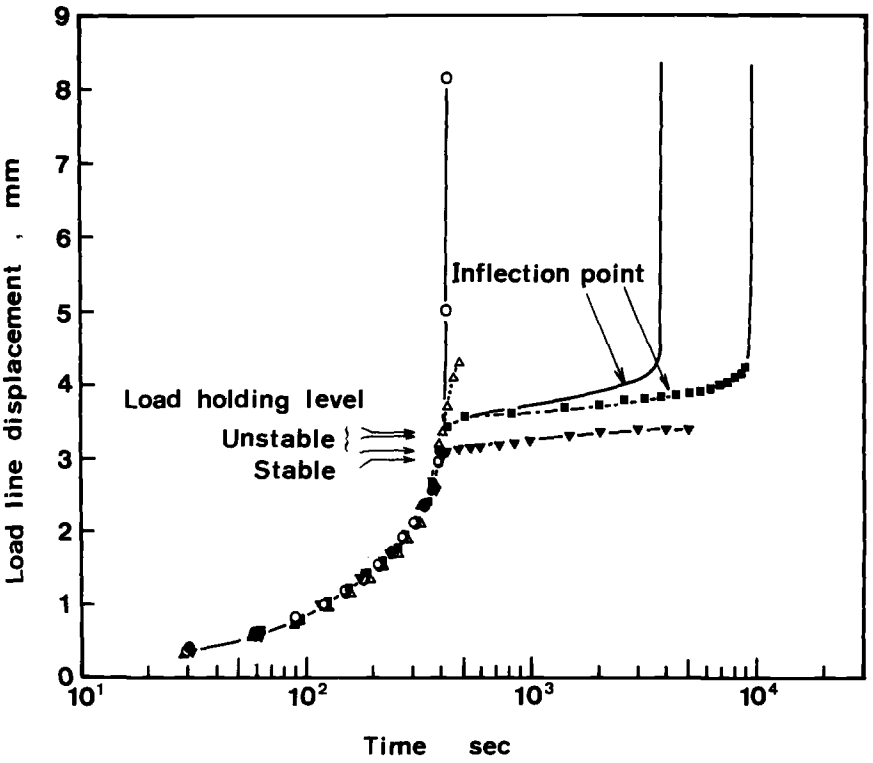

FIG. 2—*Load-line displacement versus time record, 2T-CT specimens of Steel A1.*

at the instance of load holding. The stable crack growth became unstable above a certain value of the load-line displacement. When the load was kept constant above this limit value, the greater the displacement at the instance of load holding, the shorter became the time to failure [*2–4*].

From Figs. 2 and 3, it can be seen that the load versus load-line displacement curve under load holding conditions differs from that of conventional tests in the increase in displacement during the load holding. Tsuru and Garwood [*3*] have defined a "static" load versus load-line displacement curve as that obtained by loading at an infinitely slow rate. Figure 4 shows the comparison between "static" and conventional load versus load-line displacement curves for 2T-CT specimens of Steel A1. Solid marks indicate the results obtained from conventional test methods, which mean monotonic loading by both displacement control and load control without load holding. These fall within the same scatter band designated by oblique lines in Fig. 4. Open marks represent the points of load and load-line displacement after 1-h load holding at each prescribed load level. The increase in load-line displacement is remarkable above 100 kN, and the "static" load versus load-line displacement curve is derived definitely. This problem is again discussed in the following section.

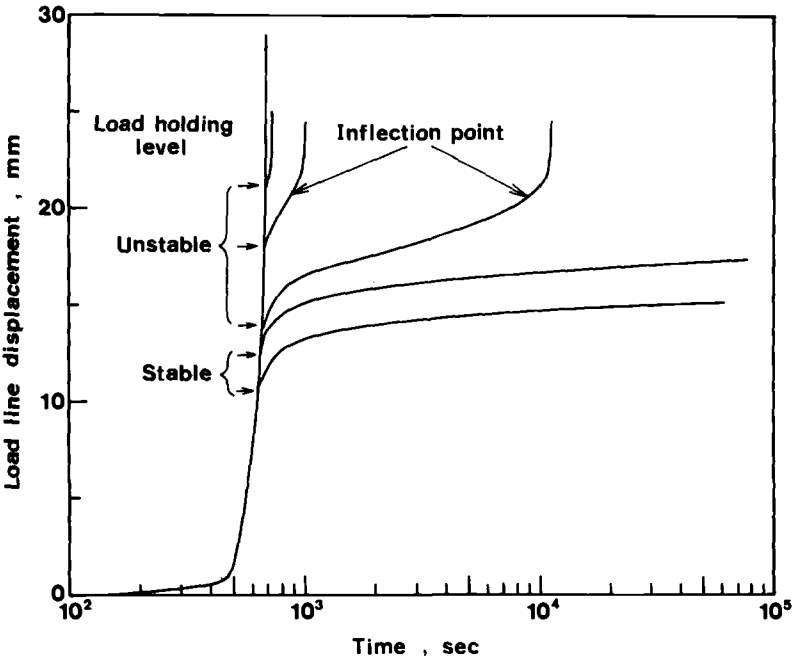

FIG. 3—*Load-line displacement versus time record, ½T-CT specimens of Steel B2.*

Increase in displacement during the load holding, which was expected to be caused only by crack growth, was also observed before the ductile crack initiation. Some phenomenon at the crack tip, such as plastic flow or stress relaxation and so forth, seems to contribute to the increase in displacement before and after crack initiation. In order to confirm this fact, the load was increased by 10 kN in step by step fashion. The increase in load-line displacement during 1-h load holding at each load level is plotted in Fig. 5. The results show that the relationship between the load and the incremental increase in displacement can be approximated by a bilinear curve. Assuming that the cross point of the two lines corresponds to the ductile crack initiation (this is confirmed later), only the plastic flow at the crack tip contributes to the increase in displacement before the initiation point, while above this point the increase in displacement caused by the crack growth contributes to the increase in displacement.

J value corresponding to the cross point is 200 kJ/m^2, if it is calculated from the load versus load-line displacement record, agrees very well with the J_i value obtained from the multiple-specimen technique as shown in Fig. 6. Therefore, this stepwise loading technique seems to have a possibility of application to J_{Ic} test by single specimen.

The change in strain distribution around the crack tip was measured by the strain gages, glued on the specimen surface, during the load holding (less than J_i level). The results are shown in Fig. 7. The broken lines and the solid lines show the equi-strain contours for just after the load hold and for after 1-h load

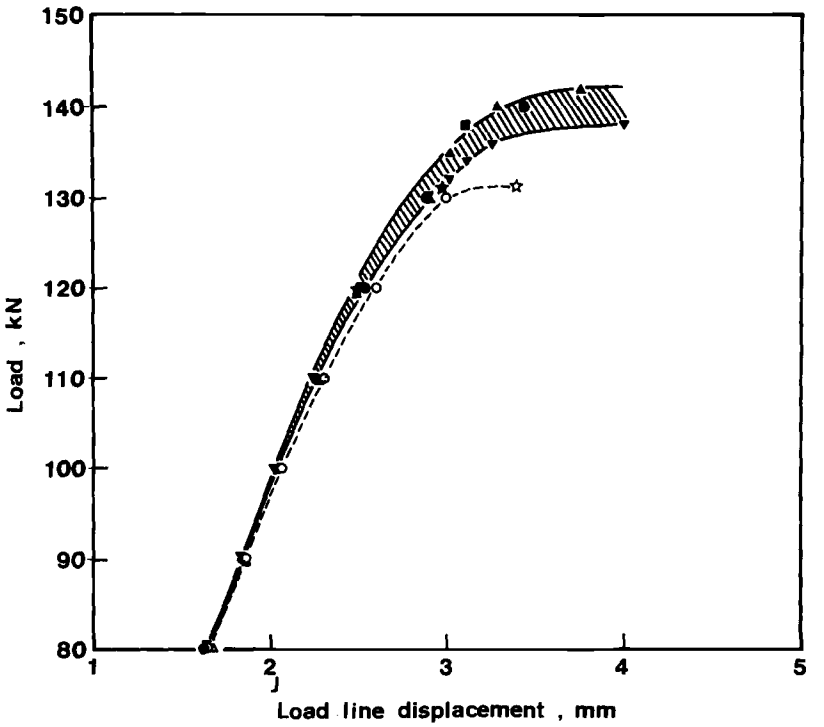

FIG. 4—*Load versus load-line displacement curve (2T-CT specimens of Steel A1).*

holding, respectively. As can be seen from Fig. 7, the highly strained areas were spread out during the load holding. The cross marks in Fig. 7 show the location where the strain gages were glued.

An example of the copper plating technique is shown in Fig. 8 (2T-CT specimen of steel B1). It is evident that the ductile crack has already initiated at the moment of load holding and that the crack grows during the load holding. The shape of ductile crack growth during the load holding does not differ at all from that obtained by the conventional test method (loading to the prescribed level and unloading immediately without load holding). This technique might not affect the fracture process since the duration of applying the copper sulfate aqueous solution was less than a few seconds and the deposited copper film was quite thin.

Figure 9 shows an example of measurement for the crack extension by the ultrasonic echo technique. Figure 9 was obtained by the stepwise loading on 1T-CT specimen of Steel A1, which has a dull machine notch of 0.2-mm radius instead of the fatigue crack. When the load was kept at 204 kN, a small peak appears in front of a large peak that corresponds to the machine notch (Fig. 9*b*). This small peak seems to represent the ductile crack. As the time elapsed, this peak moved away from the large peak of machine notch, which means the ductile

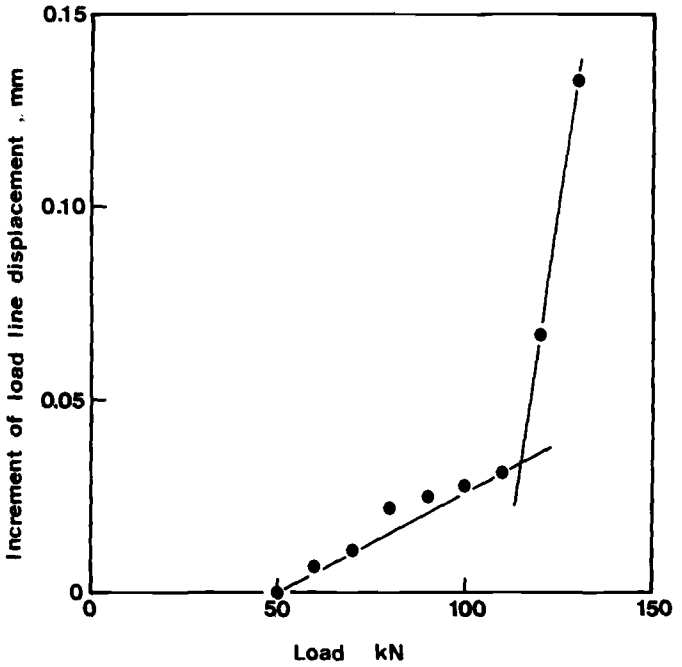

FIG. 5—*Incremental increase in load-line displacement during load holding (2T-CT specimens of Steel A1).*

crack grows under the load holding. The final ductile crack length that can be obtained from the last figure (Fig. 9*d*), taken at the moment of unloading, was 3.6 mm, while the measured crack length on the fracture surface after the test was 3.8 mm.

J-Integral Estimations

Figure 6 shows the *J-R* curve of 2T-CT specimens of Steel A1. *J* values were calculated according to ASTM E 813. Open rhombic marks indicate the results of the conventional multiple-specimen technique under displacement control. In the case of load holding tests, triangular marks and circular marks represent the values at the moment of load holding and after load holding, respectively. In such cases, the cracks ceased to grow. Solid marks instead indicate that the stable-unstable transition took place under the load holding condition. At the locations of the solid circles, the specimens were unloaded after affirming the transition phenomenon. Though the "static" load versus load-line displacement curve was derived in the previous section (Fig. 4), it can be seen from Fig. 6 that the results of load holding tests fall on the same *J-R* curve obtained by the conventional tests. Therefore, it can be concluded that the *J-R* curve is a characteristic of the material and that the ductile crack under load holding condition

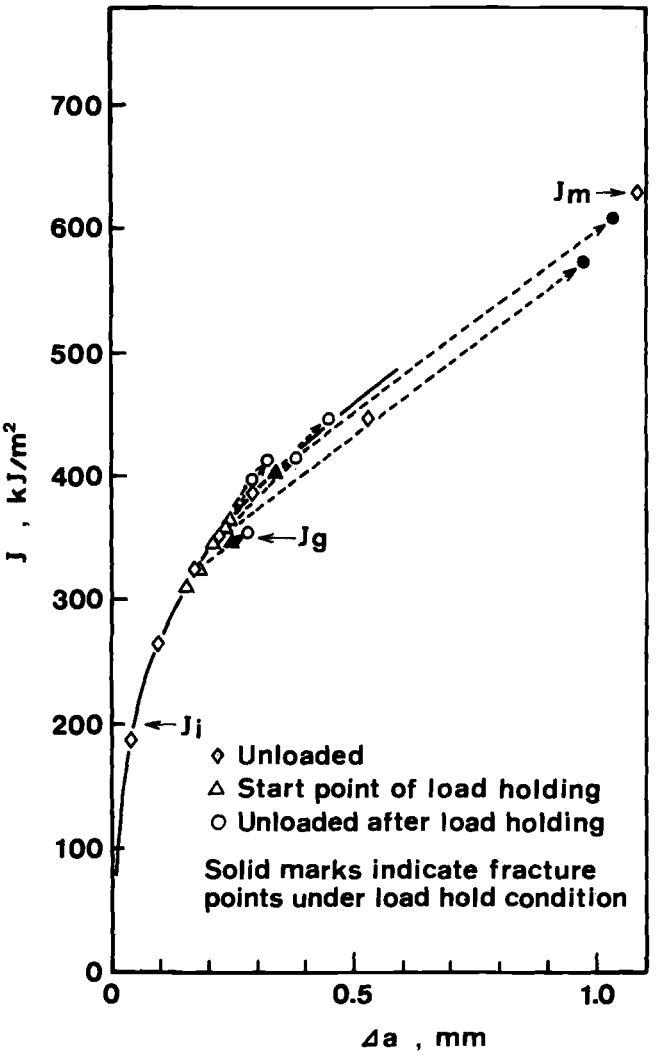

FIG. 6—J-R *curve and comparison between* J_i, J_m, *and* J_g *(2T-CT specimens of Steel A1).*

grows along the *J-R* curve. The difference between the "static" and the conventional load versus load-line displacement originates in the initiation and growth of the ductile crack.

In the conventional displacement-controlled fracture toughness test, the unstable ductile fracture often occurs after the applied load reaches the maximum value. If J_m is defined as the J value corresponding to the maximum load point, J_m has been frequently used as a critical value of materials in such cases. Plotting J_m and corresponding Δa_m (ductile crack length) on Fig. 6, J_m also falls on the same *J-R* curve and the identification of the *J-R* curve is recognized again.

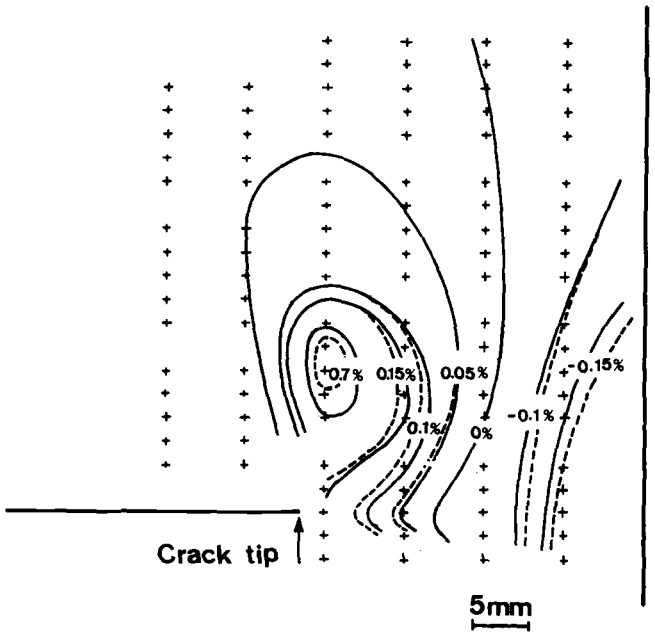

FIG. 7—*Change in strain distribution during load holding (2T-CT specimen of Steel A1).*

Green and Knott [*1*] introduced the parameter δ_g defined as the COD below which failure will not occur under the constant load. Following their definition, when J_g is defined as the minimum J value at the instance of load holding which causes unstable ductile fracture under the load holding condition, J_g exists between J_i and J_m. Since J_m is obtained from the displacement control test which is not severe testing condition for materials, J_m gives an unconservative estimate for structural materials in some cases. On the contrary, J_i is too conservative because J_i corresponds to the ductile crack initiation, and it can not represent the unstable fracture at all. Because J_g is obtained under severest load condition for structures, J_g seems to give a reasonable estimation for the toughness of materials used in the ductile region.

Next, the effect of specimen geometry on J_g was investigated. The results are summarized in Table 2. The maximum J-integral capacity [*6*] for each specimen is shown in Table 3, which is given by the smaller of

$$J_{max} = b\sigma_y/20$$

or

$$J_{max} = B\sigma_y/20$$

where

b = ligament length,
B = specimen thickness, and
σ_y = yield strength.

For high-strength Steels A1 and A2, all the J_g values meet the J_{max} conditions, that is, $J_g < J_{max}$. These values do not exhibit the thickness dependency, while the effect of ligament length is quite remarkable. On the contrary, J_g values depend strongly on the specimen thickness for low-strength Steels B1 and B2. Note that these values considerably exceed J_{max}; that is, the specimen geometry does not satisfy the size requirement as to these kinds of low-strength and high-toughness steels when J_g values are evaluated. It has been pointed out that δ_g decreases as the thickness increases [*1,2*], although a reverse tendency was observed regarding Steel B2. Since this steel contained remarkable nonmetallic inclusions in the mid-thickness region, these inclusion segregations seemed to contribute mainly to the thickness dependency on the J_g of this steel.

Observation on Fractography

Figure 10 shows the ductile crack profiles at the mid-thickness of ½T-CT specimens of Steel B2 at each fracture stage. The *J-R* curve of this specimen is also shown in Fig. 11. Figures 10*a* through *d* correspond to the Points A through D in Fig. 11, respectively. Ductile crack initiation can not be observed at the Point A. At the Point B where ductile crack ceased to grow after load holding, a remarkable ductile crack is recognized and around the crack tip there exists many micro-voids that do not yet coalesce each other. J value at the Point C,

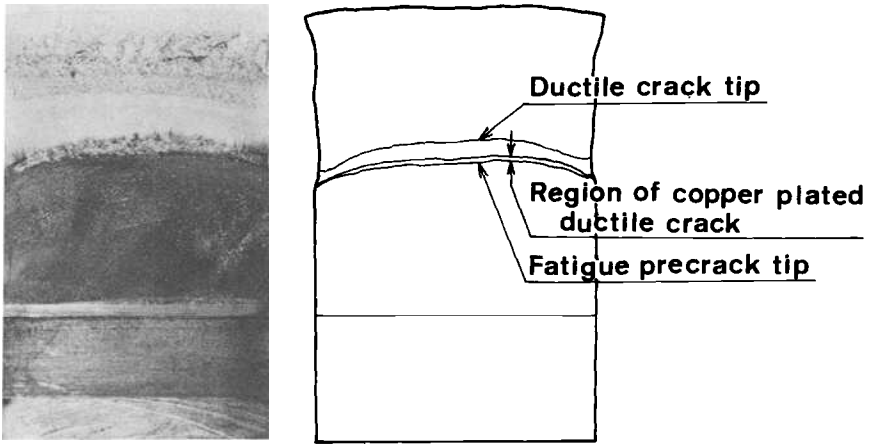

FIG. 8—*Fracture surface subjected to copper plating (2T-CT specimen of Steel B1).*

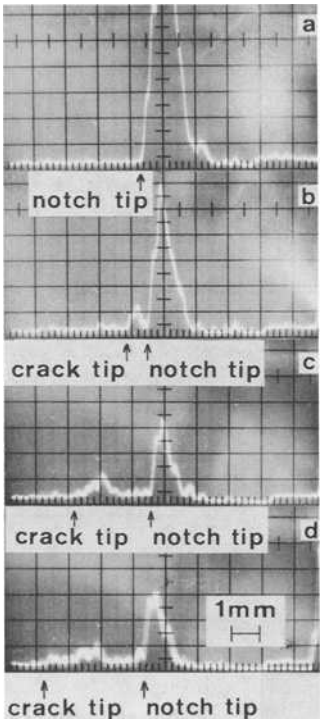

FIG. 9—*Observation on ultrasonic echo during load holding test (1T-CT specimen of Steel A1).*

obtained by unloading without the load holding, exceeds J_g and final fracture should occur if the load were kept constant at this point. Fairly large voids that would coalesce under constant load can be seen around the ductile crack tip. At Point D, specimen was unloaded just before the final fracture during the load holding. Ductile crack growth by coalescence of many voids can be observed. Crack growth behaviors shown in Fig. 10 are almost the same as those in the different thick specimens.

TABLE 2—*Effect of specimen geometry on* J_g.

		a/W	
Steel	Thickness, mm	0.7	0.3
A1	50	340	. . .
	25	370	. . .
A2	25	370	640
B1	50	790	. . .
	25	1320	. . .
B2	38.1	2100	. . .
	25.4	1800	. . .
	12.7	1200	. . .

TABLE 3—*Maximum J-integral capacity* J_{max}.

Steel	Thickness, mm	Ligament, mm	J_{max}, kJ/m²
A1	50	30	1133
	25		944
A2	25	30	1005
		70	
B1	50	30	500
	25		416
B2	38.1	. . .	477
	25.4	30	404
	12.7	. . .	202

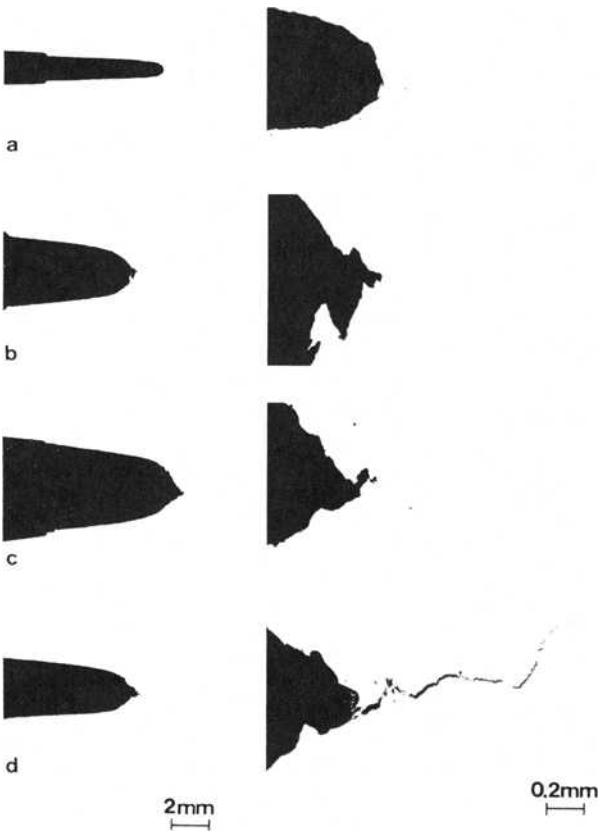

FIG. 10—*Ductile crack profiles at each fracture stage (½T-CT specimens of Steel B2).*

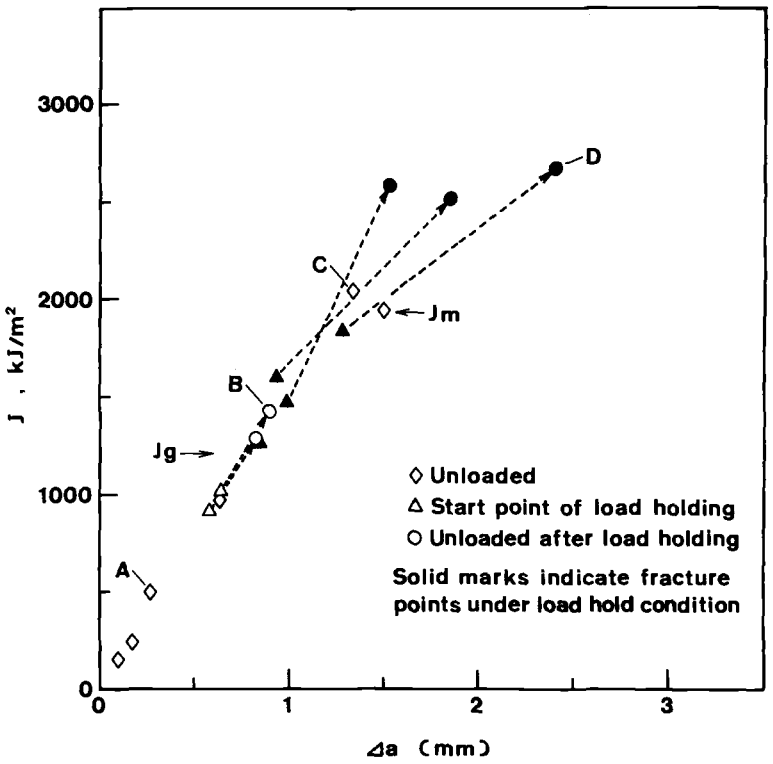

FIG. 11—J-R *curve and crack profile observation points (½T-CT specimens of Steel B2).*

Specimen C (see Figs. 10*c* and 11) was then broken into two pieces by subsequent fatigue cracking, and fracture surfaces were observed by scanning electron micrograph as shown in Fig. 12. As the Steel B2 is very ductile, a fairly large stretched zone appears following the fatigue precrack. A dimpled region can be seen adjoining the stretched zone, which means the ductile crack is caused by void nucleation and coalescence. The fatigue postcracked region is enlarged as shown in Fig. 13. As some large voids (shown by white arrows) are observed on the subsequent fatigue fracture surface, this fact supports the existence of voids ahead of the crack tip, and these voids would contribute to the unstable fracture if the load were kept constant.

Discussion

J_g is defined as the critical J value that represents the stable-unstable fracture transition when the load is kept constant after loading at a usual loading rate. On the other hand, data in Figs. 6 and 11 show that the stable crack arrested and the unstable fracture did not occur even though the load was kept constant below J_g initially but the J value finally exceeded J_g. That is, if the load is kept

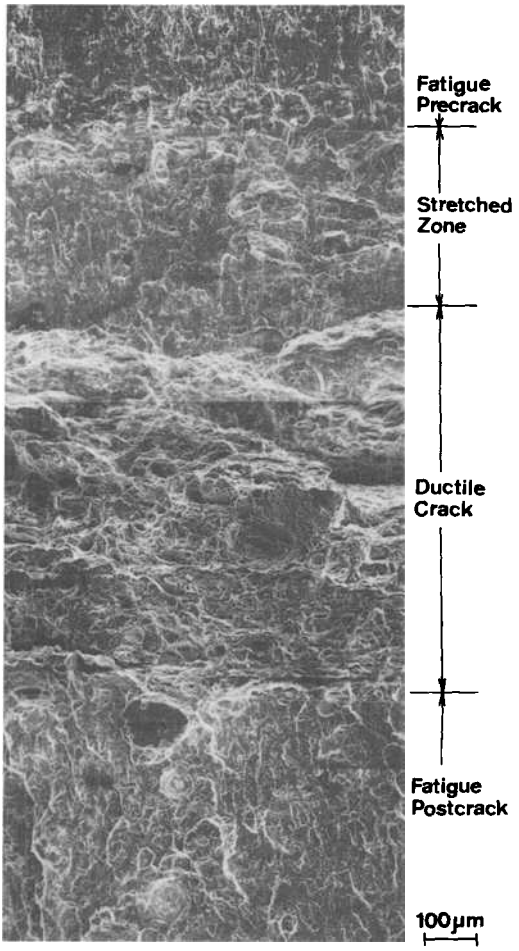

FIG. 12—*Scanning electron micrograph of the fracture surface (½T-CT specimen of Steel B2): overall view of process zone.*

constant after loading at an extremely slow rate, there seems to exist a possibility that the unstable fracture does not occur even if the J value at the start of load holding exceeds J_g. Thus the J_g is considered to depend on the loading history up to the load holding.

As to the J_g values of high-strength Steels A1 and A2, J_{max} condition derived for the specimen size requirement was satisfied sufficiently (see Tables 2 and 3), so that there was no thickness dependency. But the effect of ligament length on J_g was so remarkable. If J_{GY} corresponding to the general yield load is calculated, J_g always exceeds J_{GY} in not only the short ligament specimen ($a/W = 0.7$) but also the long one ($a/W = 0.3$). Therefore, the unstable ductile fracture under constant load seems not to occur in specimens that are not generally

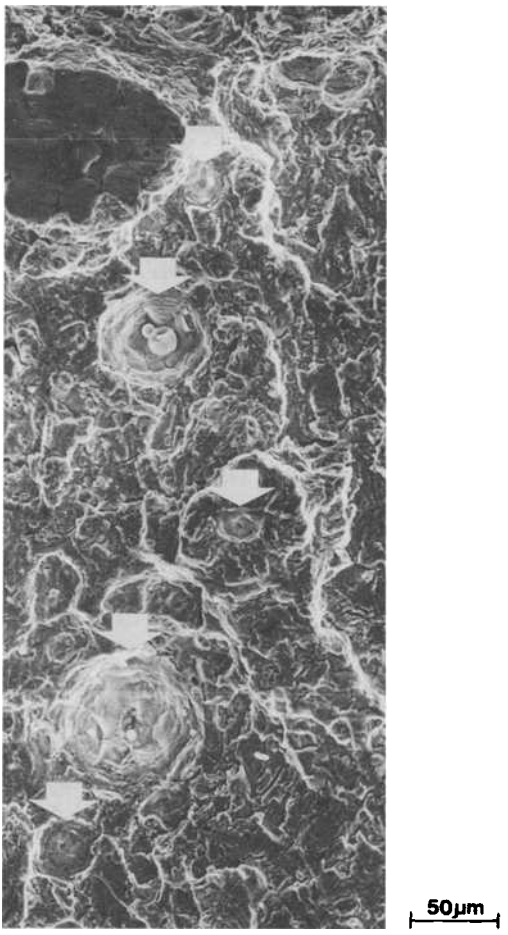

FIG. 13—*Scanning electron micrograph of the fracture surface (½T-CT specimen of Steel B2): closer view of the fatigue post-cracked region.*

yielded, as pointed out by Ingham and Morland [*4*]. Thus, the J_g is considered to depend on the specimen geometry. In order to clarify the meaning of J_g as the critical value, further efforts are needed.

The stable-unstable transition phenomenon of ductile fracture under constant load conditions seems to be described by the inflection point better than by J_g on the load displacement versus time record, as shown in Figs. 2 and 3. The inflection point in Figs. 2 and 3 is indicated corresponding to that determined on the load-line displacement versus normal scale time record. If the J value corresponding to the inflection point is defined as J_g', J_g' values for ½T and ½T specimens of Steel B2 were 3200 and 2100 kJ/m^2, respectively, while J_m values obtained from the displacement controlled tests were 3200 and 1900

kJ/m^2, respectively. A good agreement was thus obtained between J_g' and J_m. Therefore, it seems that J value designating the final collapse is not affected by the loading history although the problem of thickness dependency remains.

Conclusions

Ductile crack growth and unstable fracture under constant load was investigated by some experimental and analytical estimations. The following results are obtained:

1. The increase in load-line displacement and subsequent unstable fracture under constant load is caused by the ductile crack initiation and growth.
2. The ductile crack growth under constant load obeys the J-R curve, which is obtained by the conventional tests.
3. J_g is defined as the minimum value that causes unstable fracture under constant load. J_g seems to depend on specimen geometry (especially on ligament length) and loading history up to the load holding.
4. The ductile crack extension under constant load is caused by the nucleation and coalescence of voids. The fracture process under constant load is not different from the normal ductile fracture mode.

References

[1] Green, G. and Knott, J. F., *Journal of the Mechanics and Physics of Solids,* Vol. 23, No. 3, June 1975, pp. 167–183.
[2] Schulze, H. D., *Transactions of the Fourth International Conference on Structural Mechanics in Reactor Technology,* San Francisco, CA, Paper G 2/5, 1977.
[3] Tsuru, S. and Garwood, S. J., *Proceedings of the Third International Conference on Mechanical Behavior of Materials,* Vol. 3, 1979, pp. 519–528.
[4] Ingham, T. and Morland, E., *Elastic-Plastic Fracture: Second Symposium, Volume I—Inelastic Crack Analysis, STP 803,* American Society for Testing and Materials, Philadelphia, 1983, pp. I-721–I-746.
[5] Hirano, K., Kobayashi, H., and Nakazawa, H., *Proceedings of the Japan Society of Mechanical Engineers,* No. 820-2, Tokyo, Japan, 1982, pp. 1–3.
[6] Albrecht, P., Andrews, W. R., Gudas, J. P., Joyce, J. A., Loss, F. J., McCabe, D. E., Schmidt, D. W., and VanDerSluys, W. A., *Journal of Testing and Evaluation,* Vol. 10, No. 6, Nov. 1982, pp. 245–251.

Karl-Heinz Schwalbe,[1] *Dieter Hellmann,*[1] *Jürgen Heerens,*[1] *Jürgen Knaack,*[1] *and Jens Müller-Roos*[1]

Measurement of Stable Crack Growth Including Detection of Initiation of Growth Using the DC Potential Drop and the Partial Unloading Methods

REFERENCE: Schwalbe, K.-H., Hellmann, D., Heerens, J., Knaack, J., and Müller-Roos, J., **"Measurement of Stable Crack Growth Including Detection of Initiation of Growth Using the DC Potential Drop and the Partial Unloading Methods,"** *Elastic-Plastic Fracture Test Methods: The User's Experience, ASTM STP 856*, E. T. Wessel and F. J. Loss, Eds., American Society for Testing and Materials, 1985, pp. 338–362.

ABSTRACT: The ability of the DC potential drop method and the partial unloading technique to measure crack growth and to detect initiation of crack growth has been investigated using a number of steels and aluminum alloys. It was found that within the range of parameters investigated both of these methods can be recommended for the determination of the R curve; however, since at small amounts of crack growth, the DC potential drop method gave more consistent results, it is therefore considered to be superior. The initiation values J_o of the J integral determined by fractography were compared with J_{Ic} as obtained by current practice. It was found that ductile fracture toughness J_{Ic} is poorly related to initiation or to a specific amount of crack growth. A modification of the J_{Ic} procedure is proposed.

Two contacting arrangements of the DC potential drop method were checked for initiation detection: one indicates initiation by a potential minimum (related to a J value J_{min}), the other by the intersection of the R curve with the blunting line (related to a J value J_{int}).

KEY WORDS: fracture tests, cracks, crack propagation, DC potential drop method, partial unloading technique, initiation of crack growth, fracture toughness J_{Ic}, multiple-specimen method

Nomenclature

- a Crack length
- a_o Fatigue precrack length
- Δa Crack length increment
- B Specimen thickness
- F Applied load

[1]Head of department and research engineers, respectively, GKSS Research Center, 2054 Geesthacht, Federal Republic of Germany.

J J integral
J_{int} J at intersection of initial R curve with blunting line
J_{lin} J at the end of the linear part of the U-F record
J_{min} J at minimum of U-v_g record
J_o J at initiation of crack growth as determined by fractography
J_{Ic} Fracture toughness determined according to ASTM Test for J_{Ic}, a Measure of Fracture Toughness (E 813)
K Stress intensity factor
K_o K at initiation of crack growth
U Potential drop as defined in Fig. 7
U_o U before crack growth
v_g Displacement measured at the specimen's front face
v_{LL} Load-line displacement
W Specimen width
y Half gage span over which U is measured
δ Crack-tip opening displacement
δ_o δ at initiation of crack growth

For monotonically increasing loads two kinds of fracture mechanics properties are determined experimentally:

(1) the initiation of growth of a preexisting crack in terms of stress intensity K_o, J integral J_o, or crack-tip opening displacement (COD) δ_o and
(2) the resistance against crack growth as a function of crack length increase Δa in terms of K_R, J_R, and δ_R.

The determination of these properties requires the accurate measurement of the actual crack length during the course of loading. Although numerous techniques for crack length measurements have been developed (a compilation is given in Ref *1*), only two methods are regularly being used in laboratory practice: the compliance method and the potential drop (PD) method using alternating current (AC) or direct current (DC). If these indirect methods work reliably the multiple-specimen method can be avoided and needs to be used for calibration purposes only.

A simple technique is used in the ASTM Test Method of Plane-Strain Fracture Toughness of Metallic Materials (E 399) for the determination of K_{Ic}. A 5% change of the specimen compliance indicates a nominally 2% increase of crack length. The precrack length is measured microscopically on the fracture surface, and no absolute crack length value is required from the compliance measurement. A shortcoming of this simple technique is that plastic deformations affect the result by an unknown amount. In addition, depending on the specimen size, $\Delta a = 2\%$, means different locations on the R curve, and hence K_{Ic} can be size dependent if there is a rising R curve. The former effect can be avoided by partially unloading the specimen in certain intervals.

Guidance for carrying out the partial unloading procedure (PUL) is given by ASTM Test for J_{Ic}, a Measure of Fracture Toughness (E 813) and Refs 2 and 3. Since unloading occurs elastically even after comprehensive plastic deformation, the unloading trace is a measure of the elastic compliance of the specimen and hence of the actual crack length. But unlike the K_{Ic} procedure the change of crack length is determined quantitatively, which requires very accurate measurement of the compliance. Particularly, any hysteresis effects caused by friction at the loading pins and at the knife edges for the clip gage must be carefully avoided. Thus, although in principle identical instrumentation is used as for a K_{Ic} test (which may make the method attractive), much higher requirements concerning accuracy are needed.

Whereas the partial unloading technique is discontinuous in nature, continuous crack length monitoring is provided by the potential method, which however requires additional expensive instrumentation. Several techniques are in use: AC with varying frequency [4–6] and DC with different positions for current input and potential measurement [1,5,7–11], resulting in different resolution and sensitivity. By experimental or theoretical calibration both the partial unloading and the PD methods are capable of generating crack growth data. A particular problem arises when the initiation of growth has to be detected.

During the course of the present investigation, it turned out that "initiation" is very much a matter of definition. An operational definition of initiation has to comply with the true physical events and with the needs for reproducible experimental determination. A tentative definition will be given in a following section. In current practice three ways of detecting initiation are being used:

1. Measure crack growth Δa as a function of a crack field parameter, K, J, or δ, and extrapolate back to vanishing crack growth to obtain K_o, J_o, or δ_o (Fig. 1*a*). The British Standard (BS) methods for Crack Opening Displacement (COD) Testing (BS 5762:1979) determines the initiation value of δ this way.

2. Since crack growth is often measured including crack-tip blunting (particularly if the crack length is measured by an indirect method), the point of incipient cracking from the blunted crack tip can be found by introducing a blunting line and intersecting it with the extrapolated J-Δa relationship (Fig. 1*b*). This is the procedure adopted by the J_{Ic} test standard (ASTM E 813). In both of these cases the J-Δa or δ-Δa data are represented by a straight-line relationship. This ignores the fact that at its very beginning the R curve is by no means a straight line (Figs. 1*b* and 2).

Therefore, it is more appropriate to represent the R-curve data by a power law [12,13]. The intersection of this power law crack growth curve with either the crack extension line

$$\Delta a = 3/4\ (J/\sigma_F) \tag{1}$$

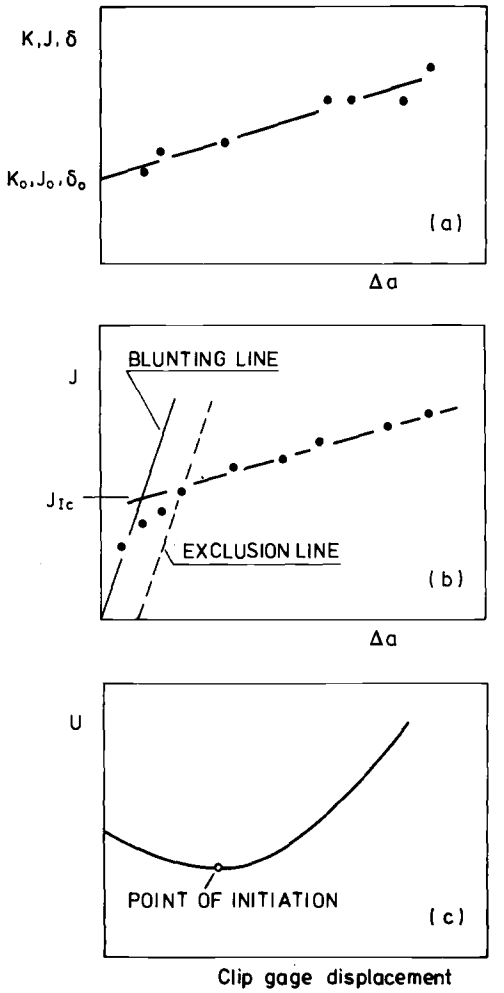

FIG. 1—*Different ways of detecting initiation of crack growth:* (a) *back extrapolation of a crack growth curve to* Δa- → 0, Δa *measured excluding stretch zone;* (b) *intersection of a linearized crack growth curve with the blunting line,* Δa *measured including stretch zone; and* (c) *detection of a potential drop minimum.*

(with σ_F being the flow stress equal to one half the sum of yield strength and tensile strength) or the 0.15-mm exclusion line—whichever yields the highest value—was defined in Ref *12* as the J_{Ic} value and was found to coincide closely with the J_{Ic} value determined after ASTM E 813 (Fig. 2*a*). This proposal has three special properties:

(a) It is based on the actual growth data, which can deviate significantly from the straight-line construction of ASTM E 813.

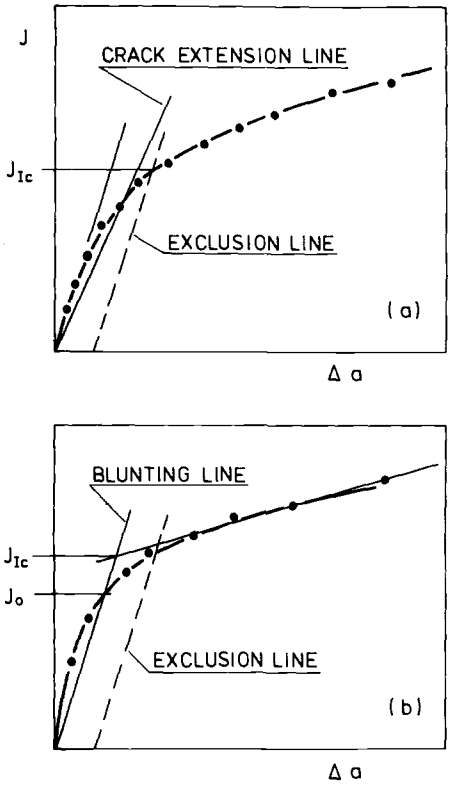

FIG. 2—*Representation of the crack growth curve by a smooth curve,* (Δa *measured including stretch zone*).

(b) It is aimed at defining a critical J at a certain amount of crack growth to avoid the sometimes very large data scatter at the very initiation of growth.

(c) It is capable of determining a well defined J_{Ic} value even if instability occurs so closely to the 0.15-mm exclusion line that no valid J_{Ic} can be derived according to ASTM E 813.

However, it should be kept in mind that the statements made in Ref *12* are based on indirect crack length measurements (unloading compliance technique) and on a single material (A533-B weld deposit).

In order to examine the physical events close to crack growth initiation, it is necessary to make direct fracture surface observations by means of light or electron microscopy. This is the basis of a further proposal [*13*], which is aimed at finding J_o, the true initiation value of J, that is the value of J for $\Delta a \rightarrow 0$. According to Ref *13* this can be done by intersecting the power law crack growth curve with the blunting line (Fig. 2b). The thus determined J value coincides closely with the initiation value J_o determined by fracture surface observations

done with a low-power microscope and is appreciably below the standard J_{Ic} value (Fig. 2b). The first and third of the statements above apply for the second proposal as well. This investigation [*13*] was done on ASTM A533 (Unified Numbering System [UNS] K12539), Grade B, Class 1, heavy section steel technology (HSST) plate 03 steel.

3. The third method consists of searching for a characteristic point on the test record that indicates unequivocally the onset of crack growth. On a potential drop-clip gage displacement U-v_g record such a point can often be detected; it is either a change in slope [*7*] or a minimum on the U-v_g record [*4,6,8,11*] (Fig. 1c).

The work described in the present paper was aimed at further investigation of the relation between J_0 (the initiation value of J) and the standard J_{Ic}. A particular point of interest was the indirect detection of initiation of crack growth (single-specimen method). More specifically, the ability of the DCPD method and the partial unloading technique to determine initiation of crack growth and crack growth was investigated. Another motivation for this work was that the DCPD method as described in Ref *10* and earlier reports has been in use in the authors' lab for a decade; in the meantime, however, the partial unloading technique appeared and additional PD techniques were developed. Thus, the question arose whether our technique is still competitive. The main emphasis was on the DCPD method.

Materials and Test Procedure

Table 1 contains the materials investigated and their tensile properties. All materials were tested in the form of compact tension (CT) specimens, 10 to 25 mm thick; specimen width was 50 or 100 mm. The plan view geometry of the specimens corresponded to the recommendations of ASTM E 813.

All tests satisfied the conditions for valid J_{Ic} values as specified by ASTM E

TABLE 1—*Tensile properties of the materials investigated.*

Material	σ0.2, MPa	UTS, MPa
A 7075-T7351 aluminum	421	504
B 2024-T351 aluminum	317	440
C 2024-FC aluminum[a]	75	217
D A533-B1,1 steel[b]	465	614
E 20MnMoNi55 steel[c]	478	612
F A542 steel[d]	599	715

[a]Furnace cooled condition.

[b]Heavy section steel technology (HSST) plate 03.

[c]Heat KS 11 of the German Forschungsprogramm Kompon enten-Sicherhert (FKS) program, corresponds to A533-B steel.

[d]European Group on Fracture (EGF) round-robin steel.

813. A number of 25-mm-thick wedge-opening load (WOL-X) specimens were made of Material D; this is also indicated on the respective diagram.

Three types of tests were performed:

1. Multiple-specimen tests to determine J_0 by means of scanning electron microscopical (SEM) fracture surface observations. Crack growth (excluding the stretch zone) was measured at equally spaced locations along the crack front whereby at each location seven individual measurements were made as shown in Fig. 3.

2. Computer controlled partial unloading tests were done on Materials C, E,

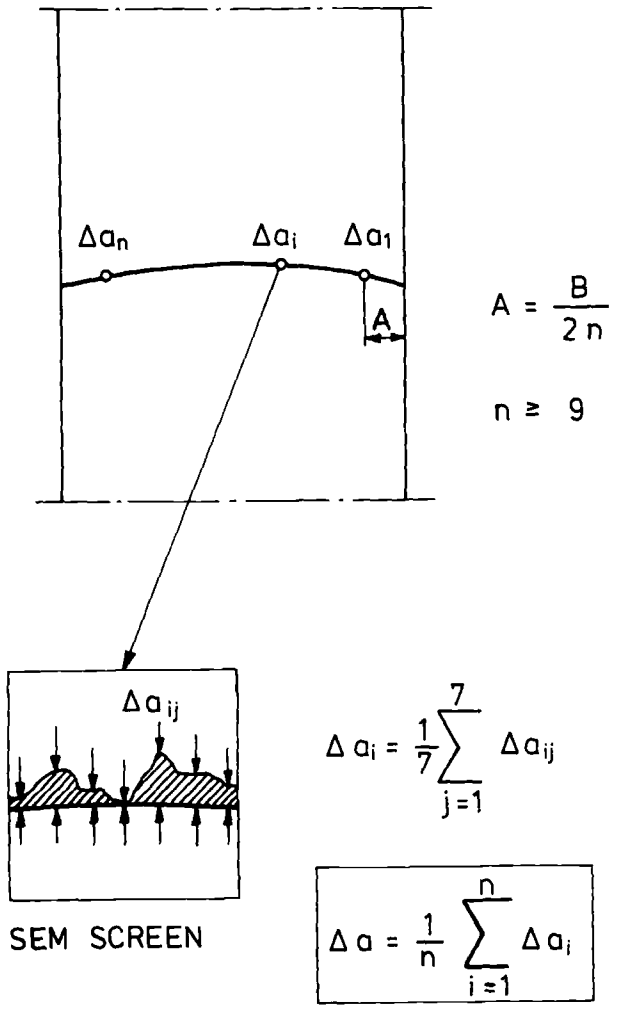

FIG. 3—*Procedure of measuring crack growth in the SEM.*

and F only. Data acquisition and data reduction were done in a fully automated manner (including J_{Ic} determination and check of the criteria of validity) by the computer (HP 9826), which controlled the testing machine.

3. For the DCPD tests the two contacting geometries shown in Fig. 4 were used. Similar contact arrangements were used for the WOL specimens. The current leads were fixed to the specimens using screws; the potential was picked up via small interference pins. A Simac Electronica power supply served as current source, and the potential drop was measured by a Keithley 140-nV meter. The current was adjusted such that a nominal resolution with respect to crack length of roughly 10 to 20 μm was obtained in all tests.

Normally the CT specimens were insulated from the testing machine, that is, insulated loading pins were used and the specimens' side faces were protected by thin Teflon® foils. This practice was applied for the contacting Geometry A in Fig. 4. In addition, the clip gages were insulated so that no short circuit could occur. The CT specimens with contacting Geometry B had noninsulated loading pins since preliminary experiments showed a pronounced potential minimum (Fig. 1*c*) that was suspected to be related to crack initiation. All WOL specimens were insulated with respect to the loading pin and at the side faces whereas the

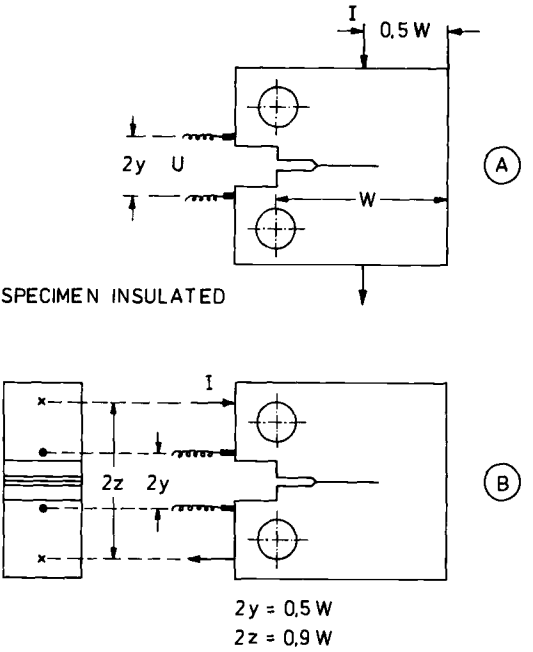

FIG. 4—*Contact geometries used for the DCPD method.*

loading screw was not insulated (for further details of the WOL tests see Ref *11*).

Data Evaluation

J *Integral for CT specimens*

The clip gage displacement values were corrected for rotation [*14*], and the J integral was determined using the relationship given in ASTM E 813, which accounts for crack growth.

J *Integral for WOL specimens*

The J integral for the WOL specimens was calculated according to the recommendations in Ref *8*

$$J = 1.8A/B(W - a) \tag{2}$$

for

$$0.5 \leq a/W \leq 0.6$$

where A is the area under the load $-v_{LL}$ curve; since v_{LL} cannot be measured on a WOL-X specimen it was determined by converting the displacement v_g, measured at the specimen's front face [*8*]

$$v_{LL}/v_g = 0.40\, a/W + 0.44 \tag{3}$$

No crack growth correction was applied to Eq 2 since only initiation values were determined on the WOL specimens.

Crack Length Determination by Unloading Compliance

As mentioned above the evaluation of the unloading compliance tests was carried out fully automatically. For the conversion of the compliance data to crack length, the table in ASTM E 813 was used. In addition, since there are always slight deviations between the measured and calculated crack lengths for the starting point, that is, $a = a_o$ an effective modulus of elasticity was calculated to give coincidence between both values. This effective modulus was then used for data evaluation, a practice that we have used for all our fracture mechanics tests that include compliance measurements irrespective of the specimen type, and which is also referred to in the literature [*12*]. At the end of each test the final crack extension was marked by further fatigue loading and compared with the predicted value.

Crack Length Determination by DCPD

As was demonstrated in Ref *10* the tests on CT specimens with contacting Geometry A (Fig. 4) can be evaluated using the relationship

$$a = (2W/\pi) \cos^{-1} \frac{\cosh (\pi y/2W)}{\cosh \{(U/U_0) \cosh^{-1} [\cosh (\pi y/2W)/\cos (\pi a_0/2W)]\}} \quad (4)$$

which we use as a standard calibration for all our fracture mechanics tests with DCPD measurements. (For the meaning of the symbols see the nomenclature). This calibration formula has a number of advantages:

(1) reasonable resolution and sensitivity,
(2) little effect of misplacement of potential probes [*1*],
(3) application convenient since Eq 4 serves as a calibration function, and
(4) because of its normalized form (U/U_0), Eq. 4 is independent of material, test temperature, current, and size and shape of specimen [*10*].

This last point is of particular convenience when a laboratory has to investigate specimens of various shapes and sizes. Again, as with the partial unloading technique, the final crack extension obtained in each test was compared with the prediction. Figure 5 gives a compilation of these data. All data points fall into an error band of ±10%. This means that Eq 4 does not only represent situations with straight crack fronts; it is also in good accordance with the averaged length of a crack developing a curved front within the range of materials and geometries tested.

During the tests, the potential signal was recorded as a function of load (F-U diagram) and of load-line displacement (U-v_{LL} diagram) (Fig. 6). For contacting Geometry A the crack length was determined from the F-U record as shown in Fig. 7 using the initial linear portion as the U_0 baseline; U_0 is thus defined as the potential drop occurring under load but without crack growth. In some cases the F-U record exhibited only a weakly pronounced linear portion. It was then necessary to define the U_0 baseline as well as possible; an example is shown by Fig. 8. The error in Δa introduced thereby was estimated at about 50 μm. Test records of this kind were not used for initiation detection. The error of 50 μm is of no importance for the macroscopic R curve.

Results

Crack Growth

Figure 9 shows J_R curves obtained on two specimens, whereby the crack length was determined by the partial unloading and by the DCPD techniques, respectively. Similar results were obtained for two side-grooved specimens made

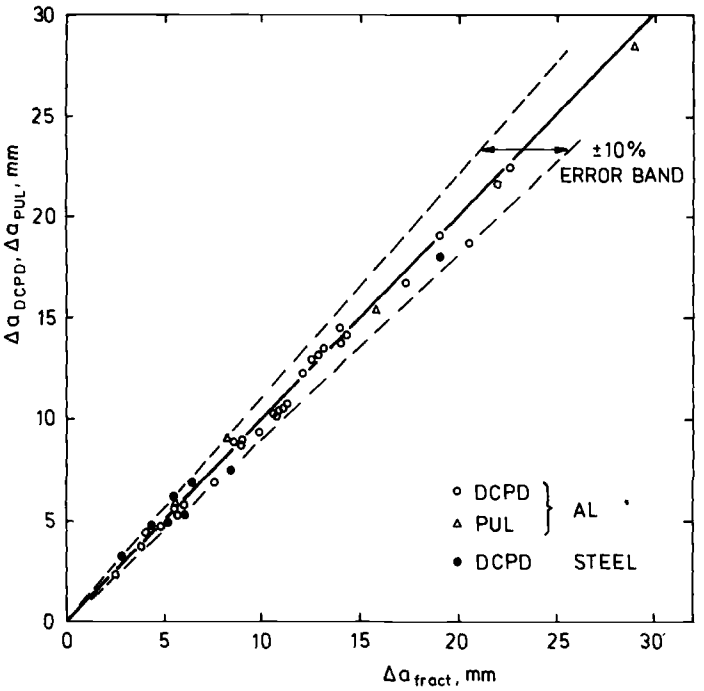

FIG. 5—*Final crack extension values measured on the fracture surface compared with the values predicted by the DCPD and the PUL techniques.*

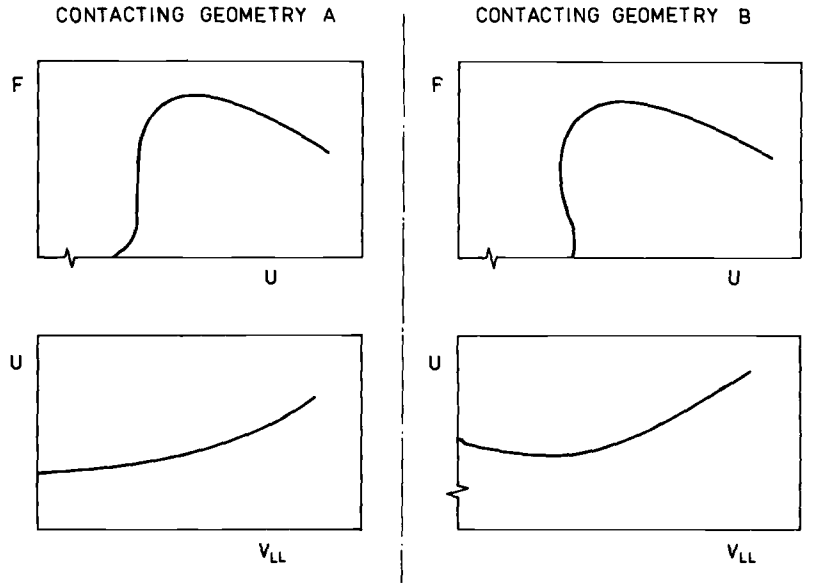

FIG. 6—*Types of test records obtained with the DCPD test.*

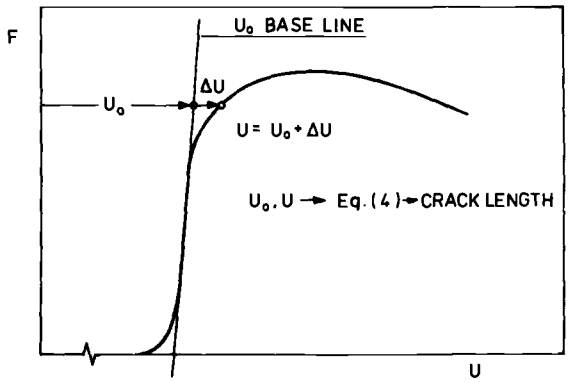

FIG. 7—*For the quantitative determination of crack length by the DCPD method a* U_0 *base line was defined, which provided the* U_0 *values for Eq 4.*

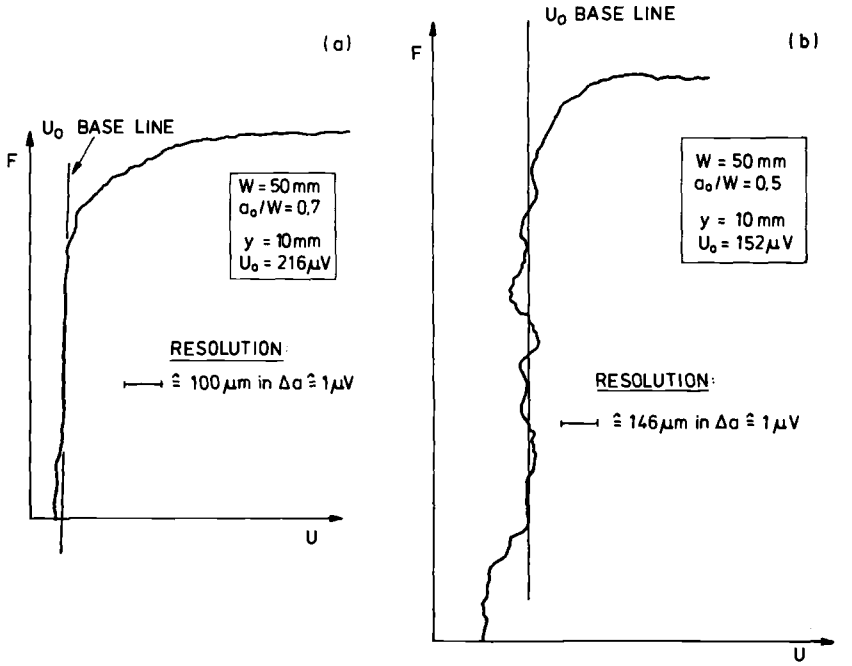

FIG. 8—*Examples for load-potential drop records:* (a) *normal test record and* (b) *poor test record (not used for detection of crack initiation).*

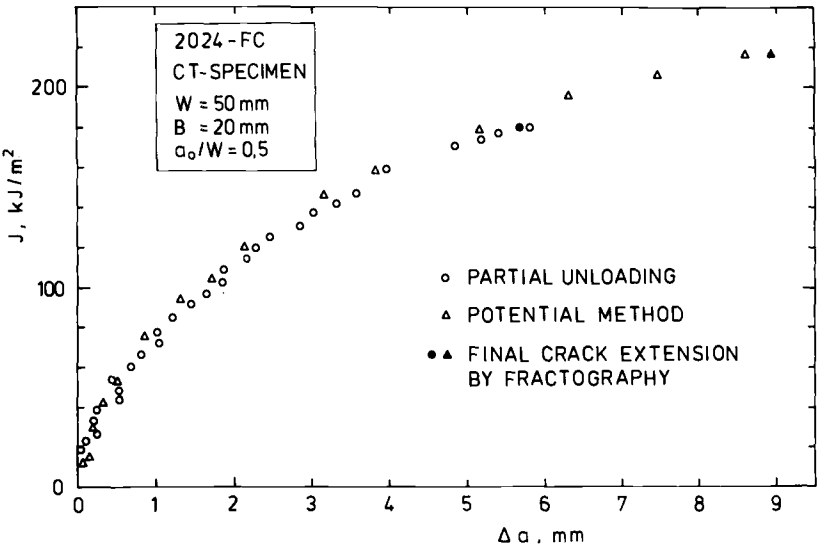

FIG. 9—R *curves obtained on two identical specimens using the DCPD and the partial unloading method, respectively.*

of the same material as those of Fig. 9. As was already expected from Fig. 5 both methods yield identical results.

Crack Initiation

A total of 48 specimens were tested to investigate the initiation behavior. A complete documentation showing the data of each individual specimen will be given in an extended version of the present paper to be published as a GKSS report.

These data will provide the reader with all the information necessary to make a detailed check of the authors' conclusions from the experiments. Because of the limited space the results are presented here in a summarizing form (Table 2). Table 2 contains the following information:

1. J_{Ic} determined according to ASTM E 813.
2. The true initiation point of crack growth J_0 was determined by the multiple-specimen method; the specimens were loaded to different amounts of Δa, unloaded, and subsequently refatigued. Crack growth was then measured in the scanning electron microscope as shown in Fig. 3 ignoring the stretch zone. Some examples are shown in Figs. 10, 11, 14, and 16 together with the crack growth data obtained by the DCPD and PUL techniques. The scatter bands for J_0 shown in some graphs indicate the uncertainty in the back-extrapolation procedure.
3. J values J_{min}, J_{lin}, J_{int}, which were checked as tentative methods to derive

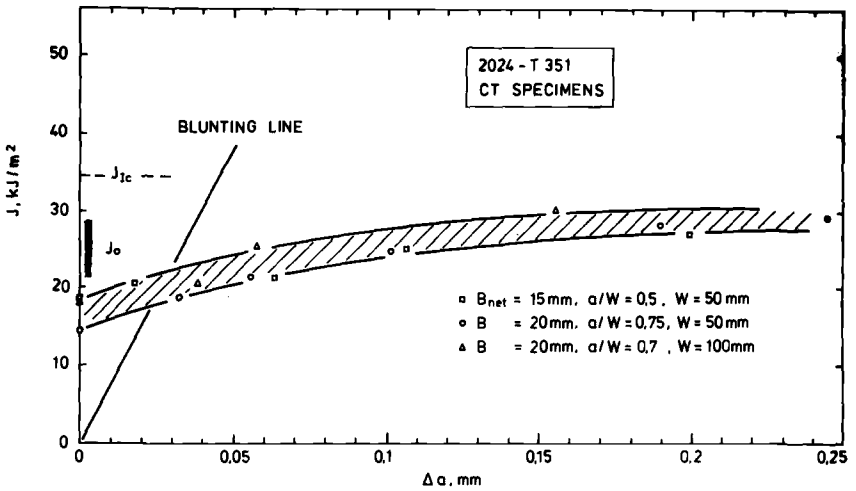

FIG. 10—*Near-initiation crack growth data of aluminum 2024-T351 obtained by the DCPD method.* J_o *was obtained by fractography of 10-mm-thick specimens. This value can be considered as representative of the 20-mm-thick specimens since (as it will be shown in a later report) the origins of the* R *curves are independent of the thickness range considered here.*

initiation from the DCPD method. The detailed explanation will be given in the discussion section.

Some common observations can be made as follows:

1. The value J_o as determined for $\Delta a \rightarrow 0$ is always lower than J_{Ic}.
2. The real crack growth just after initiation ($\Delta a \gtrsim 0.2$ mm) is completely ignored by the J_{Ic} procedure.
3. For small amounts of crack growth the partial unloading technique yields more scatter than the DCPD method (Figs. 11 to 13).

TABLE 2—*Compilation of initiation data with various definitions,* J *values in* kJ/m^2.

Material	J_{Ic}	J_o	J_{Ic}/J_o[a]	J_{min}	J_{lin}	J_{int}
A	33 to 37	25 to 30	1.28	26.3	19.2 to 26.3	23 to 28
B	26.3 to 34.5	21.5 to 28	1.22	. . .	14.6 to 19	18 to 22
C	22 to 35.4	8 to 12	2.87	. . .	6.1 to 9.6	8 to 10
C[b]	17.9	8 to 12	1.79	. . .	9.6	15
D	150	28 to 55	3.6	43.2 to 52.7	16 to 33.1	35 to 50
E	155 to 255[c]	130 to 150	1.44	150[d]	23.5 to 57	110 to 125
F	130	90	1.44	71.5	. . .	105

[a]Average values used.
[b]Side grooved.
[c]When thickness down to 10 mm are considered, J_{Ic} varies from 100 to 265 kJ/m^2 (Figs. 17 to 19).
[d]Two additional tests with ACPD (provided by F. Schmelzer, GKSS) resulted in J_{min} = 125 and 135 kJ/m^2.

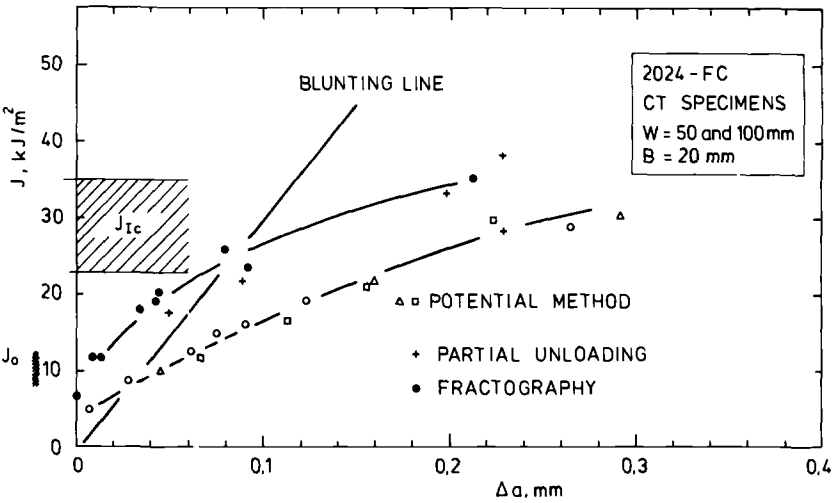

FIG. 11—*Near initiation crack growth data of aluminum 2024-FC for smooth specimens, data close to blunting line.*

4. In the range of microscopical crack growth the DCPD method measures larger amounts of crack growth than is observed on the fracture surface where Δa was measured without the stretch zone.

5. A corresponding statement for the partial unloading technique is not possible since not enough results are available to rule out the scatter observed at small amounts of crack growth.

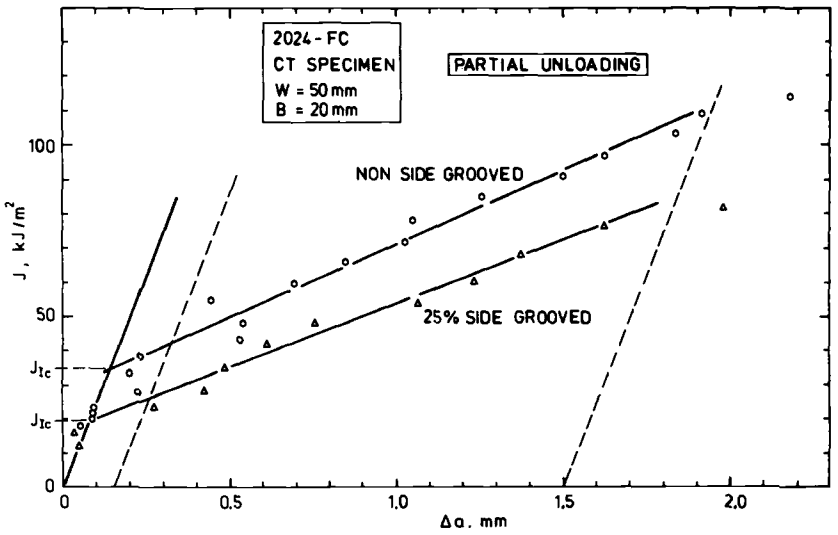

FIG. 12—*Near initiation crack growth data of aluminum 2024-FC for* J_{Ic} *construction based on* R *curves obtained on a side-grooved and a smooth specimen using the partial unloading technique.*

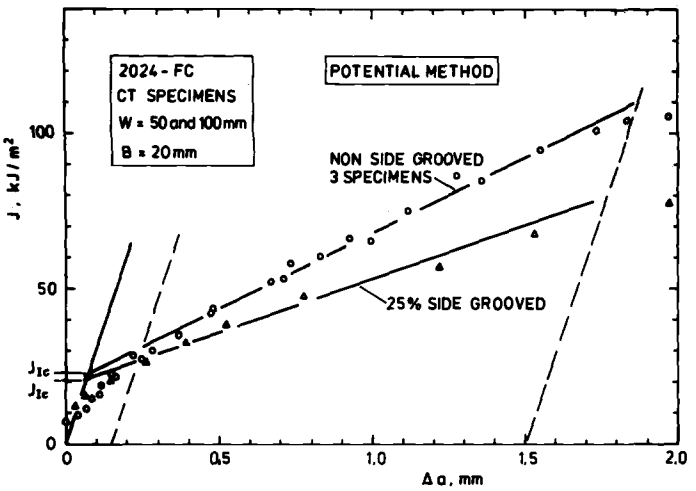

FIG. 13—*Near initiation crack growth data of aluminum 2024-FC using the potential method as in Fig. 12.*

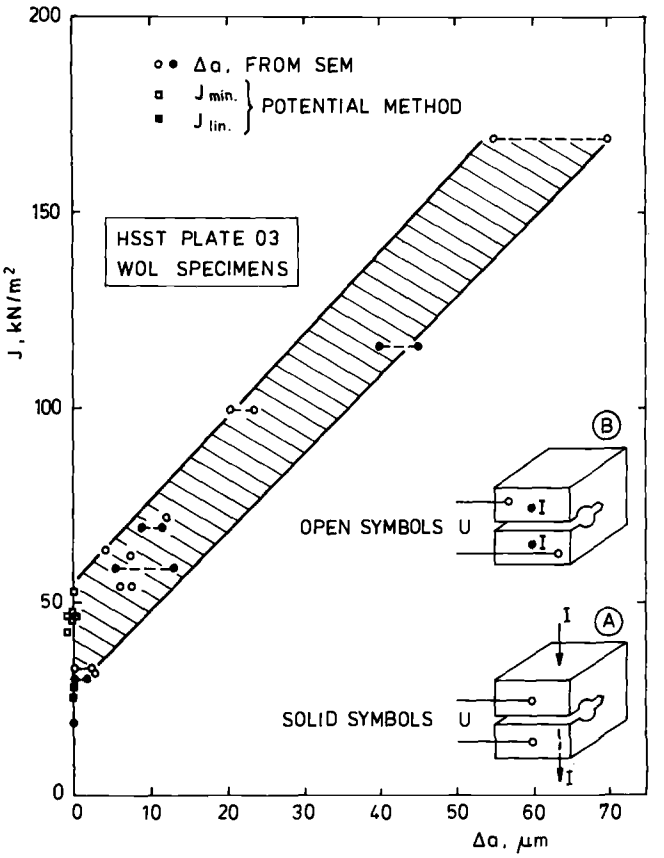

FIG. 14—*Near initiation crack growth data of HSST steel plate 03 for WOL-X specimens for the determination of* J_o.

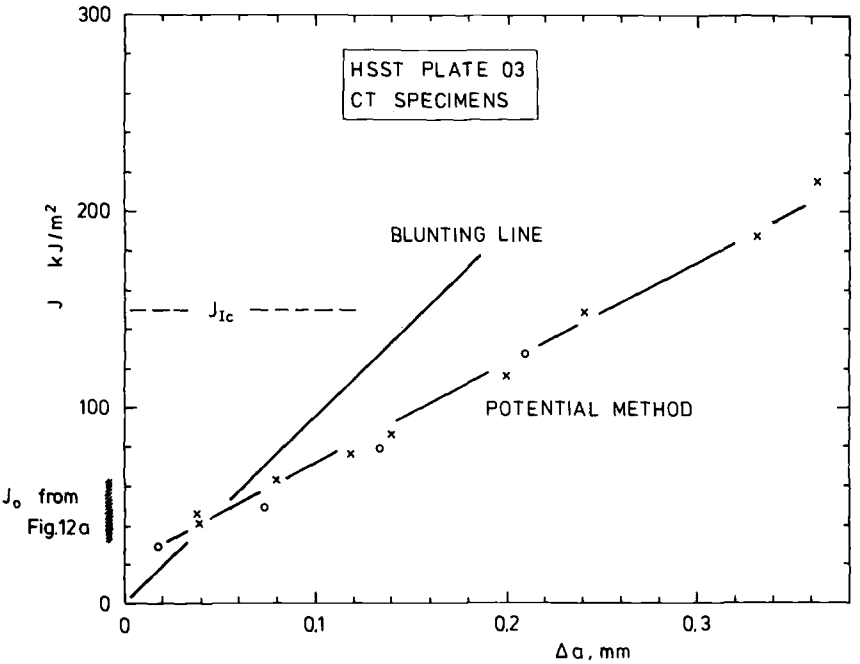

FIG. 15—*Near initiation crack growth data of HSST steel plate 03 for CT specimens.*

6. Side grooving lowers J_{Ic} but not J_0 (Figs. 12 and 13 and Table 2). It can be seen from Figs. 12 and 13 that the R curves of the side-grooved and nonside-grooved specimens tend to emerge from the same origin whereas beyond the first exclusion line they are already split off.

Discussion

Microscopic Crack Growth

At small amounts of crack growth (Δa = some tenths of a millimetre) the DCPD method overestimates crack growth as measured by the SEM (Figs. 11 and 16). The following reasons may account for this effect:

1. The plastic deformation of the specimen's ligament may affect the material's resistivity in such a way that no reliable conversion of potential drop signal to crack length can be achieved [*15*]. However, no significant difference between "as tested specimen calibration points" like in Fig. 5 and saw cut calibrations [*12*] can be observed. Although Fig. 5 was established for macroscopic crack growth, this argument holds also for small amounts of crack growth where less deformation occurred. Thus, we conclude that the order of magnitude of resistivity change has no impact on the crack length calibration.

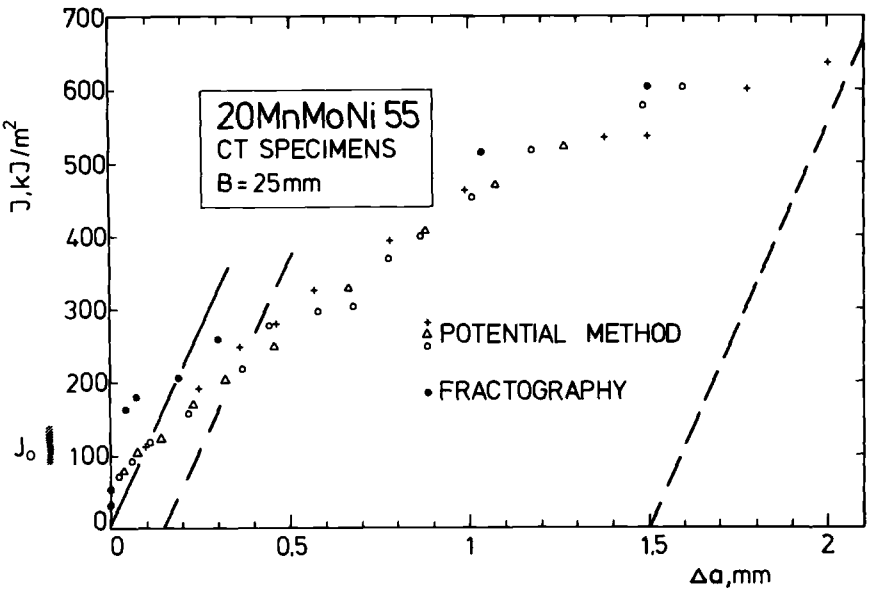

FIG. 16—*Near initiation crack growth data of 20MnMoNi55 steel for three 25-mm-thick CT specimens.*

2. Void formation ahead of the crack tip may increase the material's resistivity. However, no observations of void formation were carried out so that the validity of this argument cannot be checked.

3. As was mentioned above, the fractographical measurements were done ignoring the stretch zone whereas the DCPD method measures crack growth including the stretch zone. It is interesting to note that the DCPD results can roughly be obtained by adding the blunting line to the fractographical data in Figs. 11 and 16. Since the mechanics behind the blunting line are not yet clear, further work on this problem is in progress.

Macroscopic Crack Growth (DCPD Versus Partial Unloading)

According to our results, both of the crack length measurement techniques produce the same macroscopic R curve (Fig. 9). Moreover, the calibration data of Fig. 5 are within a $\pm 10\%$ error band and are thus better than the 15% accuracy required in ASTM E 813 for the partial unloading technique. However, for small amounts of crack growth the scatter of the partial unloading technique (including the scattering of the data points obtained in a single test around the average curve) is bigger than that of the DCPD method (Figs. 11 to 13).

One of the reasons for this observation may be that the DCPD method is continuous in nature whereas the data of the partial unloading test are obtained in a discontinuous process, which may produce variations of the quantity to be

measured. Another point is the compliance measurement. Minute amounts of friction (in the loading and measurement arrangements) and of misplacement of the displacement measuring device can introduce substantial amounts of errors. Thus, although the compliance method is more sensitive than the potential method (see Fig. 8 Ref *1*), its resolution problems (sensitivity to errors of the measurement of the compliance) tend to make it inferior to the electric potential method when small amounts of crack growth are considered. These arguments apply even more in the case of the stiff center cracked tension specimens where much smaller compliances are to be measured [*16*]. Further efforts in friction avoidance (for example, needle bearings in the loading clevises) may improve the situation for the partial unloading method. In addition, side-grooving the specimen leads to more consistent results.

But even so, apart from some exceptions the potential method in the form described above will remain the standard method in our lab, since for *R*-curve determination it is more universal, particularly because of the fact that a single calibration curve (Eq 4) is needed for the commonly used specimen geometries.

In the form described in the present paper the DCPD method is part of a recommended practice for the measurement of *R* curves on center cracked tension specimens [*17,18*].

Determination of Initiation from Fractography

As indicated by Fig. 1*a* existing (BS 5762) and drafted (ASTM Test Method for CTOD Testing) test methods impose a straight line on the crack growth data and determine the initiation point by extrapolation of the straight line to $\Delta a = 0$. The determination of J_{Ic}, which is supposed to be a measure of initiation toughness, uses a similar procedure (Fig. 1*b*). The findings of the present paper show that close to initiation the *R* curve is anything but a straight line. This statement applies for side-grooved specimens also. Moreover, straight-line extrapolations lead to overestimations of initiation. Thus, in the present paper initiation was determined by

(1) measuring crack growth down to very small amounts and
(2) by approximating the data by a smooth curve (which in some cases was linear within a very limited range of crack growth).

The J_0 values thus obtained are listed in Table 2. It should be mentioned that no distinction was made between side-grooved and smooth specimens since the data fell into a common scatterband.

It is sometimes argued that extrapolation to $\Delta a = 0$ leads to unduly conservative values, and initiation should be defined by the achievement of a fully developed crack front. The latter definition may make sense in case of homogeneous materials whereas for inhomogeneous materials local crack growth may be large while at the major part of the crack front the crack has not yet propagated.

Detection of Initiation by the DCPD Method

Potential Minimum—All specimens with contacting Geometry B exhibited a marked potential minimum like that shown in Figs. 1*c* and 6. This minimum was taken to calculate J_{min}, which is listed in Table 2. Although the occurrence of the minimum is not fully understood (it is assumed that the load dependent contact area between pin and specimen provides a less resistant current path with increasing load and that initiation of growth overbalances this effect), it is obvious from Table 2 that the potential minimum is a good indicator of initiation.

End of Linear Portion of F-U *Record*—The J values at the end of the linear portion of the load-potential records for Configuration A were designated as J_{lin}. For the high-strength aluminum alloy 7075-T7351, J_{lin} corresponds approximately to the initiation value J_o (Table 2); that is, in this case the potential drop is essentially a function of crack length only. For all other materials (which are characterized by relatively high ductility) J_{lin} is lower than J_o. The reason is that, as it was discussed above, before initiation because of the high resolution the potential drop responds to crack-tip blunting and thus feigns a small amount of crack growth. This difference is only noticeable on a microscopic scale, of course; it becomes meaningless for the macroscopic R curve.

Alternative Method—In Table 2 an additional J value is listed, which is regarded as candidate initiation value based on the very initial portion of the R curve: J_{int}, the J at the intersection of the blunting line with the potential drop based R curve.

Comparing the various J values of Table 2 it can be concluded that J_{Ic} is very poorly related to initiation. Depending on the material, the J_{Ic}/J_o ratios range from 1.28 to 3.6 (for this calculation the average values for J_o in Table 2 were used). Thus, in terms of crack initiation and very early growth, J_{Ic} is poorly defined and cannot be regarded as an appropriate material characterization. The true initiation toughness is physically much better defined. According to Table 2 it can be determined as follows:

(1) by fractography (multiple-specimen method),
(2) by the DCPD method with contacting Geometry B and taking the potential minimum as the initiation point, and
(3) by an alternative method with similar results that is the determination of the intersection of the initial part of the R curve with the blunting line.

It is noteworthy that these procedures work for a broad range of materials.

Suggested Modifications of J_{IC} Procedure

A specific problem arising with the J_{Ic} procedure is illustrated in Figs. 16 through 19. Specimens made of Material E having thicknesses of 10, 15, 20, and 25 mm and identical width exhibit R curves that are very similar. However,

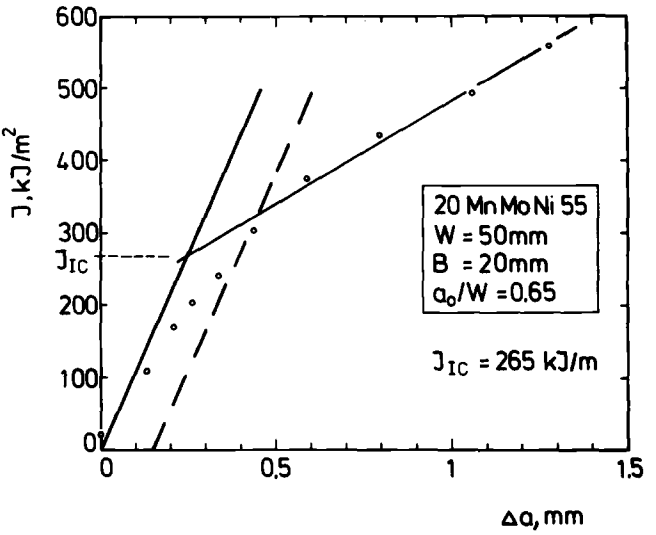

FIG. 17—*Near initiation crack growth data of 20MnMoNi55 steel for a 20-mm-thick CT specimen with* J_{ic} *construction.* R *curves measured by the DCPD method.*

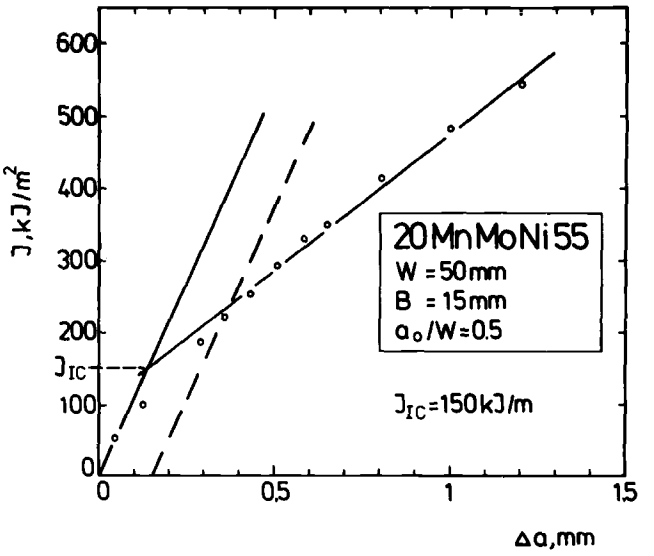

FIG. 18—*Near initiation crack growth data of 20MnMoNi55 steel for a 15-mm-thick steel CT specimen with* J_{ic} *construction.* R *curves measured by the DCPD method.*

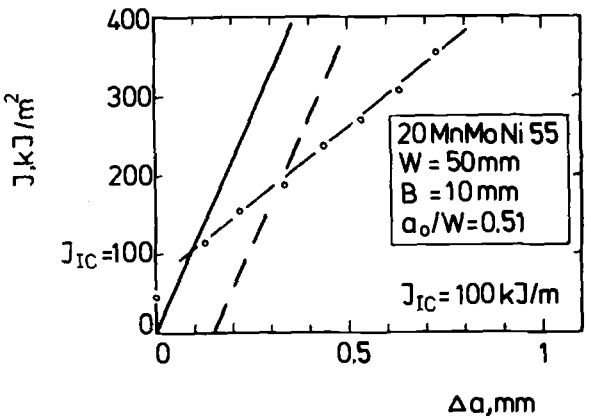

FIG. 19—*Near initiation crack growth data of 20MnMoNi55 steel for a 10-mm-thick CT specimen with* J_{Ic} *construction.* R *curves measured by the DCPD method.*

because of the requirement $B \geqq 15J/\sigma_F$ for a valid data point, the R curves of the different thicknesses terminate at different Δa values.

Thus, the construction of the straight line is based on different ranges of the R curves. Consequently, since the R curves are nonlinear, quite different J_{Ic} values are obtained as indicated in the graphs; J_{Ic} varies by a factor of 2.65. However, all values are valid according to the ASTM E 813 procedure.

To summarize;

(1) J_{Ic} is not related to initiation and

(2) the present construction using a straight line with extrapolation to the blunting line does not produce unequivocal J_{Ic} values for a given material.

This evidence leads us to propose a modification of the J_{Ic} procedure. Such a procedure should avoid a straight-line fit and any extrapolation techniques, thus

1. The straight line must be replaced by a smooth curve representing the real growth behavior close to initiation.

2. This is necessary but not sufficient. We have checked several functions (power laws, polynomials) to fit the data points between the exclusion lines; extrapolation to the blunting line failed to give more consistent results.

3. The initiation toughness J_{Ic} should therefore represent a specified point on the R curve near initiation.

This point should be as close to initiation as possible, ideally the initiation point itself. Possible techniques for the determination are given by J_{int} or J_{min}. On the other hand, when using an indirect measurement technique like DCPD or PUL, the relative error close to initiation can be large. Thus, as a compromise, a

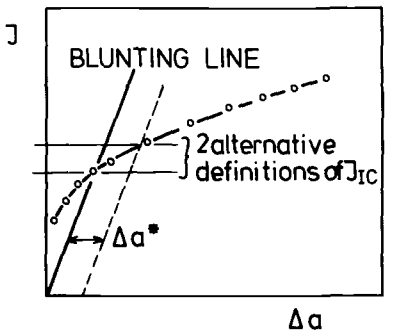

FIG. 20—*Proposed modification of J_{Ic} determination: matching experimental data with smooth curve and taking a specified point on the thus obtained* R *curve.*

modified test standard could allow for a small specified amount Δa^* of crack growth, say 0.1 or 0.2 mm. Consequently, in order to avoid extrapolation procedures experimental data below Δa^* are required. Figure 20 gives a schematic outline of the modified procedure.

Conclusions

1. For macroscopic crack growth the partial unloading and the DCPD techniques yield the same results within the range of materials and specimen sizes investigated, that is, both methods are equally well suitable to determine an *R* curve.

2. The partial unloading technique is inferior to the DCPD method when only small amounts of crack growth are considered, that is, just after initiation.

3. The DCPD method in the form described in the present paper has a number of advantages, the most important of which is the independence of its calibration with respect to test variables such as material, temperature, and specimen size and shape.

4. By special contacting arrangement (contacting Geometry B in Fig. 4) the DCPD method is capable of detecting initiation of crack growth that can be related to a minimum of the clip gage-potential drop record.

5. Contacting Geometry A in Fig. 4 is more suitable for the quantitative determination of crack growth; initiation can be determined by determining the intersection of the initial *R* curve with the blunting line.

6. The reason that the DCPD method with contacting Geometry A indicates a finite amount of growth at initiation is probably the response of the potential drop to crack-tip blunting.

7. J_o, the *J* value at initiation of crack growth as determined by SEM fractography was found to be 1.28 to 3.6 times lower than J_{Ic} as determined by ASTM E 813.

8. J_o seems to be unaltered by side grooving whereas J_{Ic} is lowered.

9. The extrapolation of a straight line fitted to the R-curve data can yield inconsistent results (Figs. 16 through 19).

10. It is suggested to define J_{Ic} for a specified point on the R curve. This point could be the true initiation point or a point with a small amount of crack growth, say 0.1 or 0.2 mm.

Acknowledgment

Part of the work presented in this paper was supported by the German Science Foundation (DFG); this is gratefully acknowledged by the authors.

References

[1] Schwalbe, K.-H., "Test Techniques for Fracture Mechanics Testing," in Advances in Fracture Research, Proceedings of the 5th International Conference on Fracture, D. Francois, Ed., Pergamon Press, Oxford, England, 1982, pp. 1421–1446.

[2] Clarke, G. A., Andrews, W. R., Begley, J. A., Donald, J. K., Embley, G. T., Landes, J. D., McCabe, D. E., and Underwood, J. H., "A Procedure for the Determination of Ductile Fracture Toughness Values Using J Integral Techniques," Journal of Testing and Evaluation, Vol. 7, No. 1, Jan. 1979, pp. 49–56.

[3] Mayville, R. A. and Blauel, J. G., "Die Methode der partiellen Entlastung zur Ermittlung von Riβwiderstandskurven," *Proceedings of the 12th Meeting of Arbeitskreis "Bruchvorgange,"* Deutscher Verband für Materialprüfung, Berlin, 1981.

[4] Marandet, B., Devaux, J. C., and Pellissier-Tanon, A., "Correlation Between General Yielding and Tear Initiation in CT Specimens," Committee for the Safety of Nuclear Installations Specialist Meeting on Tear Instabilities, St. Louis, MO, 1979.

[5] Ingham, T. and Morland, E., The Measurement of Ductile Crack Initiation: a Comparison of Data from Multiple and Single Specimen Methods and Some Considerations of Size Effects," Committee for the Safety of Nuclear Installations Specialist Meeting on Tear Instabilities, St. Louis, MO, 1979.

[6] Okumura, N., Venkatasubramanian, T. V., Unvala, B. A., and Baker, T. J., "Application of the AC Potential Drop Technique to the Determination of R-Curves of Tough Ferritic Steels," *Engineering Fracture Mechanics,* Vol. 14, 1981, pp. 617–625.

[7] McIntyre, P. and Elliott, D., "A Technique for Monitoring Crack Extension During C.O.D. Measurement," British Steel Corporation, Report MG/15/72, 1972.

[8] Hollstein, T. and Blauel, J. A., "Vergleichende Ermittlung von Riβzähigkeitskennwerten mit Hilfe von Kleiunnd Gropproben des Typs WOL-X," Bericht VII/80 des Fraunhofer Instituts für Werkstoffmechanik, Freiburg, West Germany, 1980.

[9] Ritchie, R. O. and Bathe, K. J., "On the Calibration of Electrical Potential Technique for Monitoring Crack Growth Using Finite Element Methods," *International Journal of Fracture,* Vol. 15, No. 1, 1979, pp. 46–55.

[10] Schwalbe, K.-H. and Hellmann, D., "Application of the Electrical Potential Method to Crack Length Measurements Using Johnson's Formula," *Journal of Testing and Evaluation,* Vol. 9, No. 3, May 1981, pp. 218–221.

[11] Schwalbe, K.-H., Heerens, J., and Hellmann, D., "Vorbereitende Arbeiten zur Untersuchung bestrahlter WOL-Proben," GKSS Report 82/3/2, 1982.

[12] Loss, F. J., Ed., "Structural Integrity of Water Reactor Pressure Boundary Components," NUREG/CR-1128, National Research Laboratory Memorandum Report 4122, 1979.

[13] Carlson, K. W. and Williams, J. A., "A More Basic Approach of the Analysis of Multiple-Specimen R-Curves for Determination of J_c," *Fracture Mechanics, Proceedings of the Thirteenth National Symposium on Fracture Mechanics, ASTM STP 743,* American Society for Testing and Materials, Philadelphia, 1981, pp. 503–524.

[*14*] Hawthorne, J. R., Ed., "The NRL-EPRI Research Program (RP 886-2), Evaluation and Prediction of Neutron Embrittlement in Reactor Pressure Vessel Materials, Annual Progress Report for CY 1968," National Research Laboratory, Report 8 327, 1979.

[*15*] Curry, D. A. and Milne, I., "The Detection and Measurement of Crack Growth During Ductile Fracture," Central Electricity Research Laboratories Report RD/L/N64/79, CERL Leatherhead, 1979.

[*16*] Schwalbe, K.-H. and Setz, W., "*R*-Curve and Fracture Toughness of Thin Sheet Materials," *Journal of Testing and Evaluation,* Vol. 9, No. 4, July 1981, pp. 182–194.

[*17*] Schwalbe, K.-H., Setz, W., Schwarmann, L., Geier, W., Wheeler, C., Rooke, D., deKoning, A. W., and Eastarbrook, J., "Application of Fracture Mechanics to Thin-Walled Structures," *Fortschritt-Berichte der VDI-Zeitschriften,* Reihe 18, No. 9, 1980, 114 pp.

[*18*] Wheeler, C., Easterbrook, J., Rooke, D. P., Schwalbe, K.-H., Setz, W., and deKoning, A. W., "Recommendations for the Measurement of *R* Curves Using Centre-Cracked Panels," *Journal of Strain Analysis,* Vol. 17, No. 4, 1982, pp. 205–213.

Kim Wallin,[1] *Timo Saario,*[1] *Pertti Auerkari,*[1] *Heikki Saarelma,*[1] *and Kari Torronen*[1]

Comparison of Potential Drop and Unloading Compliance Methods in Determining Ductile Crack Extension

REFERENCE: Wallin, K., Saario, T., Auerkari, P., Saarelma, H., and Torronen, K., **"Comparison of Potential Drop and Unloading Compliance Methods in Determining Ductile Crack Extension,"** *Elastic-Plastic Fracture Test Methods: The User's Experience, ASTM STP 856,* E. T. Wessel and F. J. Loss, Eds., American Society for Testing and Materials, 1985, pp. 363–374.

ABSTRACT: Two different methods, the unloading compliance and the AC-potential drop method have been applied simultaneously for crack length measurement during ductile crack extension in *J-R* curve determinations. The materials used in the comparison of the two test methods were a pressure vessel steel A533B C1.1 (Unified Numbering System [UNI] K12539), a comparable weldment, and a carbon-manganese steel OX522D weld. Specimen geometries used were 25-mm compact tension (1TCT) and 15-mm three-point bend (3PB), respectively.

The two methods applied give consistent results for the amount of crack extension. However, the location of the potential minimum is dependent upon material, specimen geometry, temperature, frequency and current. This leads to the conclusion that the AC-PD method fails to indicate the initiation of ductile crack extension correctly. Reasons for this are discussed.

KEY WORDS: unloading, alternating current, crack propagation, J_{Ic}, elastic-plastic fracture toughness, unloading compliance, AC-potential drop

Materials fracture toughness in the elastic-plastic (ductile) regime is usually described in terms of a resistance curve based on the J integral determined by the ASTM Test for J_{Ic}, a Measure of Fracture Toughness (E 813). J_R-curves can be cost effectively determined using single-specimen techniques. Crack extension during a single specimen J_R-curve measurement can be detected by either the unloading compliance method or the so-called potential drop methods. There are two types of potential drop methods based on AC or DC [*1*]. In the AC-method a minimum is generally found in the potential. It has been suggested [*2,3*] that this minimum corresponds to the initiation of the ductile crack exten-

[1]Research officer, research officer, head of structural integrity section, research officer, and head of Materials Technology section, respectively, Technical Research Centre of Finland (VTT), Metals Laboratory, Metallimiehenkuja 6, SF-02150 Espoo 15, Finland.

sion. It has however been anticipated [2] that the minimum is somewhat frequency dependent. In this work, an AC-potential drop device was used simultaneously with the unloading compliance method to detect the crack extension during testing. The effects of frequency and temperature on the potential change were studied.

Experimental Procedure

Equipment

The computer interactive testing system used for fracture toughness measurements uses the unloading compliance method on single specimens to determine crack growth resistance curves based on the J-integral concept (J_R-Δa curves) for ductile materials. By means of the J_R-Δa curve, values of the elastic-plastic fracture toughness J_{IC} and the tearing modulus T_{MAT} are routinely determined. Alternatively, similar parameters based on crack-tip opening displacement (CTOD) can be determined as well. For specimens behaving in a nearly linear manner a check for critical stress intensity K_{IC} is made.

The system consists of a microcomputer, a 250-kN servohydraulic testing machine, a data acquisition/control unit, a digital voltmeter, and several auxiliary devices for real time data acquisition as well as for data storage. The block diagram of the system hardware is shown in Fig. 1. The main features of the computer code with its control, analysis, and auxiliary programs are shown in Fig. 2. Both the system hardware and the software are further developments of

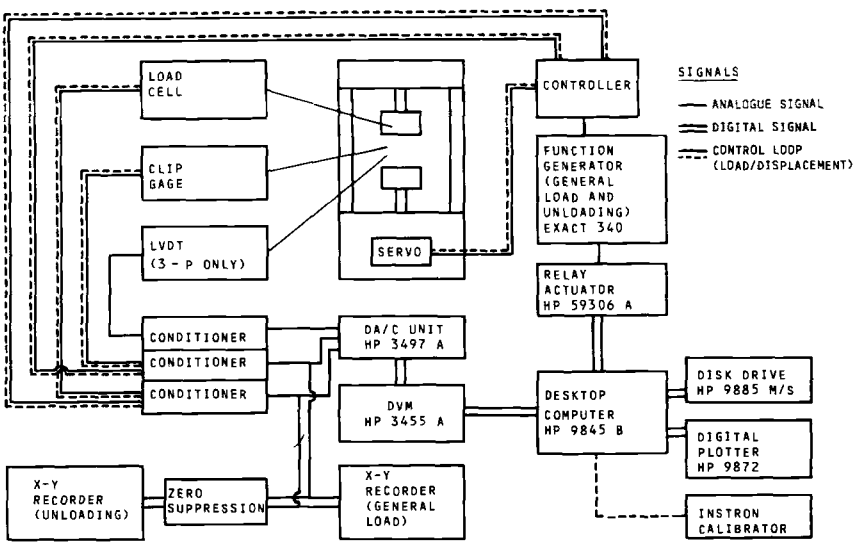

FIG. 1—*Block diagram of the computer interactive testing system used for fracture toughness measurements.*

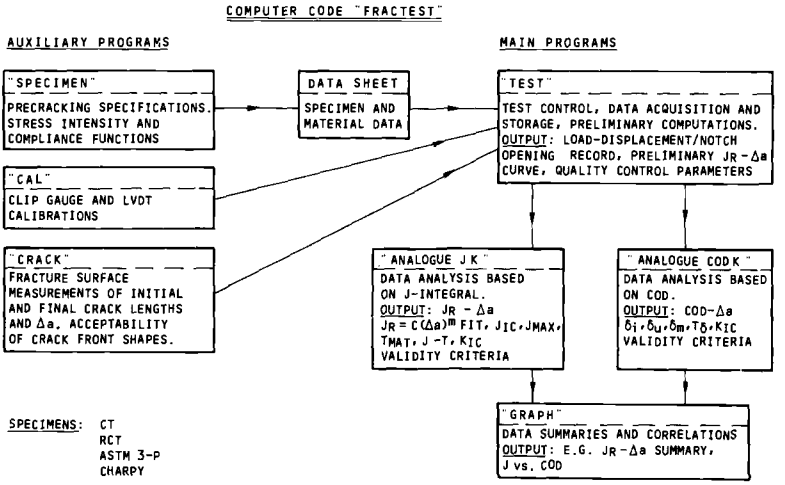

FIG. 2—*Main features of computer code.*

the system originally developed at the Naval Research Laboratory, Washington DC [*4–7*]. The system as a whole meets the requirements of ASTM E 813 for determining elastic-plastic fracture toughness J_{IC}.

The test piece geometries for which the software is available are compact tension (CT), round compact tension (RCT), three-point bend (3PB) and Charpy-sized three-point bend geometries. Using an environmental chamber, CT type specimens up to 2*T* and bend specimens up to 1*T* can be tested at temperatures between −120 and 300°C. Also testing of irradiated specimens up to 1*T* is possible using a parallel system installed in a hot cell.

The potential drop device developed at Technical Research Centre of Finland (VTT) is of AC type with variable phase-locked frequency (10 Hz to 5 kHz) and feed current (1 to 10 A). The device responds to the resistivity changes in the specimen by measuring the potential drop over the crack [*8*]. Because of the design the potential drop device is insensitive to external disturbancies. Potential changes in the range of 1 nV are repeatably detectable. This enables the use of a low current (1 A), which makes the device also suitable for use with small specimens.

Procedure

The tests were performed with two different test geometries (1TCT and 15-mm 3PB), at different temperatures. The materials used were bainitic pressure vessel steel A533B C1.1 (Unified Numbering System [UNS] K12539) and a corresponding weld for the CT specimens, and a carbon-manganese steel OX522D weld for the 3PB specimens.

In the potential drop measurements two currents (1 and 2 A) and two fre-

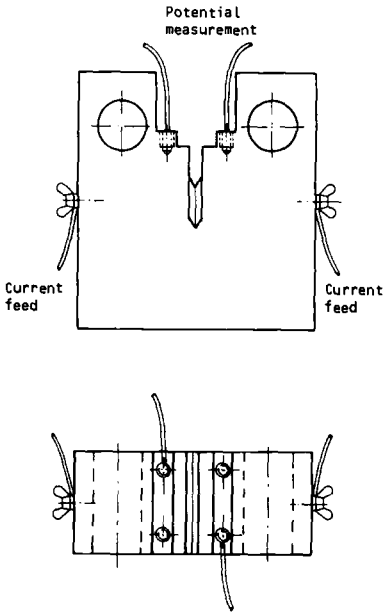

FIG. 3—*Wiring of specimens used in potential drop measurements.*

quencies (54 and 999 Hz) were used. The wiring of the specimens is shown in Figs. 3 and 4. The specimens were electrically insulated from the loading fixtures.

During the test, load, load line displacement, and potential drop were registered on *x-y* plotters with different combinations of variables. The potential change was compared with the crack extension value evaluated using the unloading compliance method.

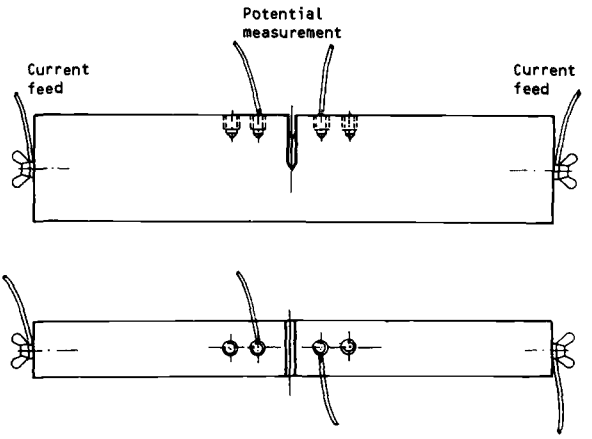

FIG. 4—*Wiring of specimens used in potential drop measurements.*

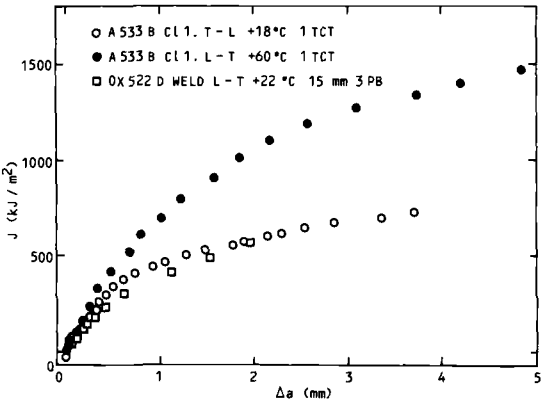

FIG. 5—J-R *curves determined by unloading compliance.*

Results

The *J-R* curves for several cases determined by unloading compliance are shown in Fig. 5. The initial crack length determined by the unloading compliance method is typically within 0.1 mm of the crack length measured directly from the crack surface. The linear regression correlation coefficient based on the complete data, obtained from one unloading cycle, is required to be better than 0.999 and is typically better than 0.9999. If the correlation coefficient is less than 0.999 the result is taken to be invalid.

In Fig. 6 the load-displacement and potential drop-deflection curves are shown for A533B base material in the T-L orientation as defined by ASTM Test for Plane-Strain Fracture Toughness of Metallic Materials (E 399). A 1TCT specimen

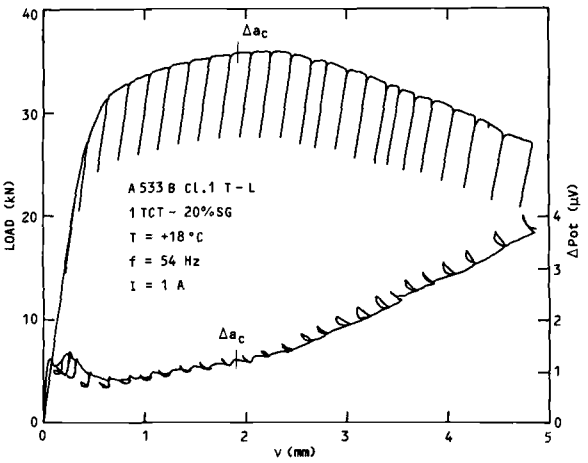

FIG. 6—*Load-displacement and potential drop-deflection curves.*

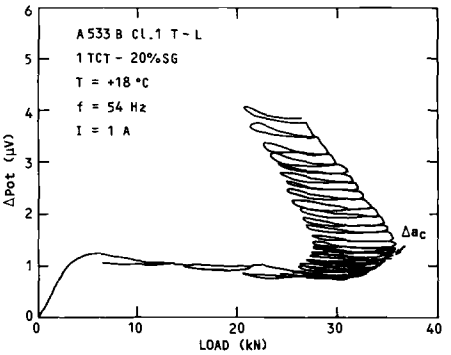

FIG. 7—*Load-potential drop curve corresponding to Fig. 5.*

with 20% side grooving (SG), a frequency of 54 Hz, and a current of 1 A was used. The test was carried out at room temperature. In Fig. 7 the corresponding load-potential drop curve is given. As seen in Fig. 6, the displacement corresponding to J_{IC}, determined according to ASTM E 813, does not coincide with the minimum of the potential change curve. From Fig. 7 it is evident that the load has a strong influence on the level of the potential also in the elastic regime. The same effect is also seen during elastic unloadings in the plastic region. This elastic load dependence is due to the effect of stress on the so called skin depth typical for AC [9].

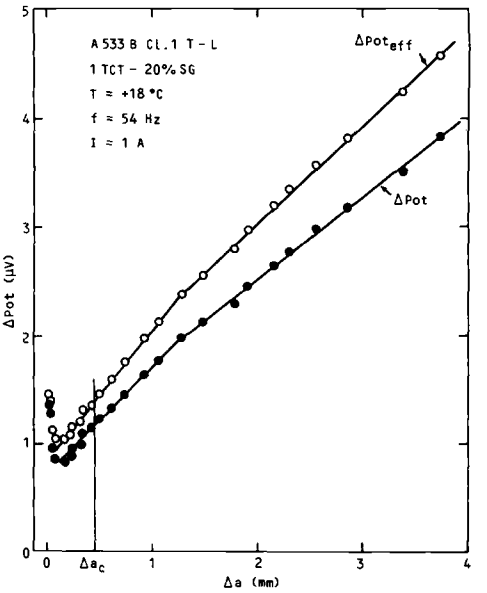

FIG. 8—*Load-displacement-potential drop relationships where the potential change is presented as a function of the crack extension.*

In Fig. 8 the potential change is presented as a function of the crack extension determined from the unloading compliance. During elastic loading, the potential changes almost linearly with changing load [*9,10*]. This enables one to determine the elastic load dependence of the potential $-\partial Pot_e/\partial P$, by determining the slope of the load-potential trace, during an elastic unloading. When the effect of elastic loading $\Delta Pot_e = -P \cdot \partial Pot_e/\partial P$ is extracted from Fig. 6 and subtracted from the measured total potential change ΔPot, the effective potential change $\Delta Pot_{eff} = \Delta Pot - \Delta Pot_e$ is obtained. This effective potential changes relatively linearly as a function of crack extension determined from the loading compliance. The minimum of the ΔPot is shifted towards zero crack extension when taking into account the effects of load on the potential change.

In Fig. 9 the load-displacement and potential drop-deflection curves are shown for the same steel as in Fig. 6, but for a frequency of 999 Hz. Increasing the frequency clearly shifts the potential minimum towards zero displacement. This results in an even more distinct difference in the displacement values corresponding to the potential minimum and J_{IC}, respectively.

The same effect of load correction on the location of the minimum as in Fig. 8 for 54 Hz is also evident in Fig. 10 for 999 Hz.

The effect of temperature is shown in Figs. 11 through 13 for a A533B weld tested at 290°C using 54-Hz frequency and 1-A current. From Fig. 12 it can be seen that the effect of load on the potential is stronger at 290°C than at lower

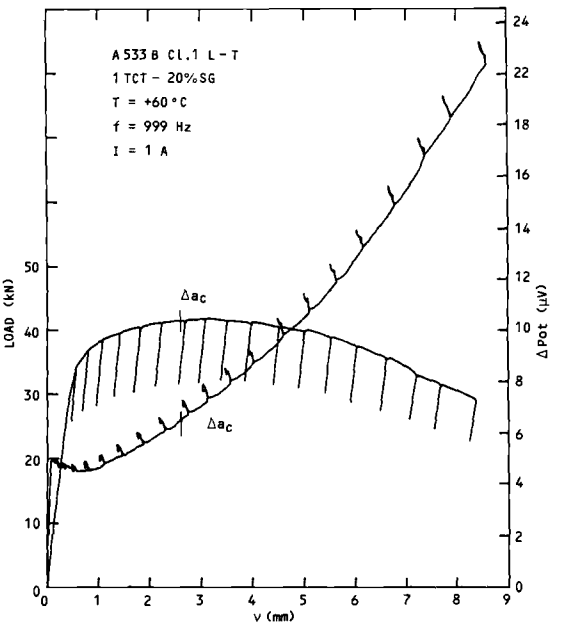

FIG. 9—*Load-displacement-potential drop relationships shown for the same steel as in Fig. 5.*

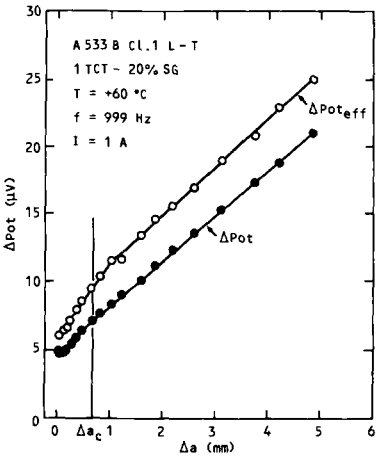

FIG. 10—*Crack extension-potential drop relationship with load correction for 999 Hz.*

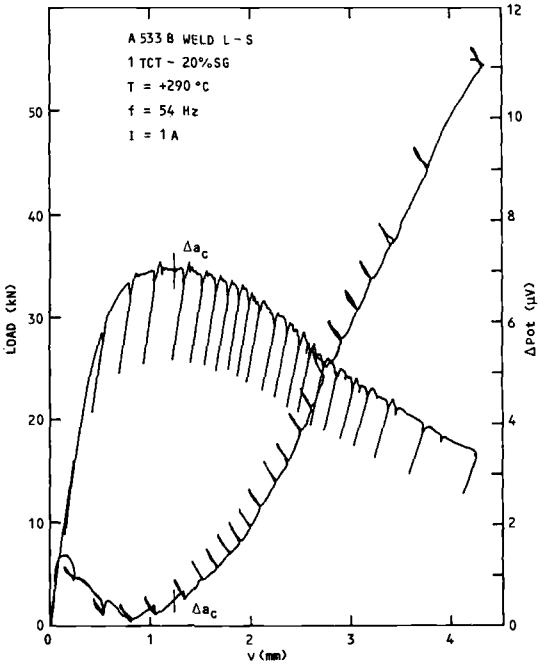

FIG. 11—*Load-displacement-potential drop relationships showing the same effect of load correction as in Fig. 7.*

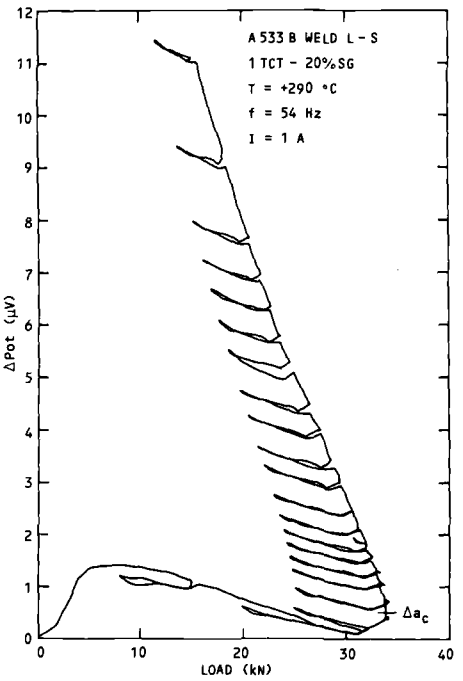

FIG. 12—*Load-displacement-potential drop relationships showing that the effect of load on the potential is stronger at 290°C than at lower temperatures.*

temperatures. Also the total potential change as a function of crack extension is larger as shown in Fig. 13. Figure 14 shows the load-deflection and potential drop-deflection curves for a 15-mm thick 3PB specimen (weld material of a carbon-manganese steel OX522D). A 999-Hz frequency and 1-A current was applied. The minimum is not clearly defined, probably because of poor insulation, but no definite differences caused by differing specimen geometry can be seen. This can also be seen from the potential drop-crack extension dependence in Fig. 15.

Discussion

From the results it is quite evident that the AC-PD method can readily be used to measure crack extension. However, the tests do not show any clear correspondence between the potential minimum and crack initiation, regardless of the frequency and current used. The location of the potential minimum is a function of material, temperature, specimen geometry, frequency, and current. Using the potential minimum, a lower J_{IC} value is obtained than by the unloading compliance technique, and therefore it could be claimed that the PD J_{IC} is the true value because the unloading compliance J_{IC} as determined according to ASTM E 813 allows for some ductile tearing. However, applying the load effect

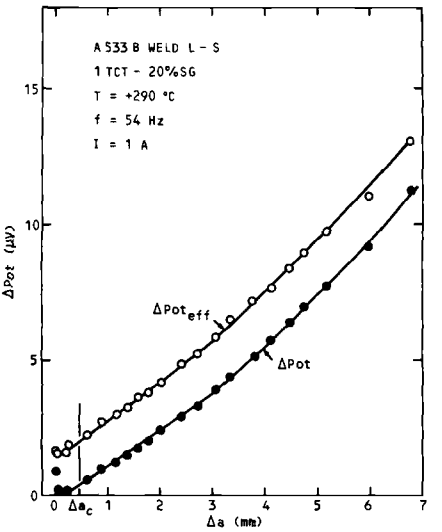

FIG. 13—*Crack extension-potential drop relationship.*

correction on the potential the place of the potential minimum is moved towards zero crack growth. Bearing this in mind, it is quite evident that the location of the potential minimum has no clear dependence upon the initiation of ductile tearing. Therefore the AC-PD method described here cannot be used to detect crack initiation reliably.

An interesting point is that the elastic load dependence of the potential changes as a function of crack extension. This is shown in Fig. 16 for several cases. At first, at some way into the plastic regime, the elastic load dependence of the potential is constant. The value of this constant seems to be depending primarily on the material and temperature, and to some extent on the current used. The

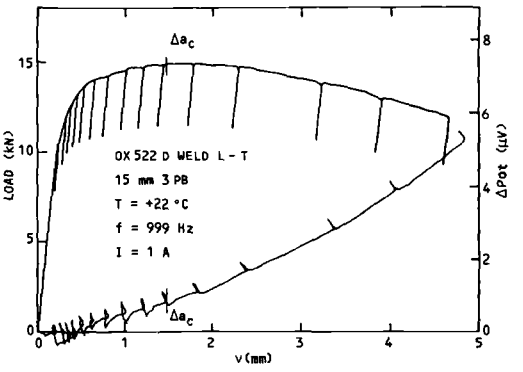

FIG. 14—*Load-deflection-potential drop relationships for a 15-mm thick 3PB specimen.*

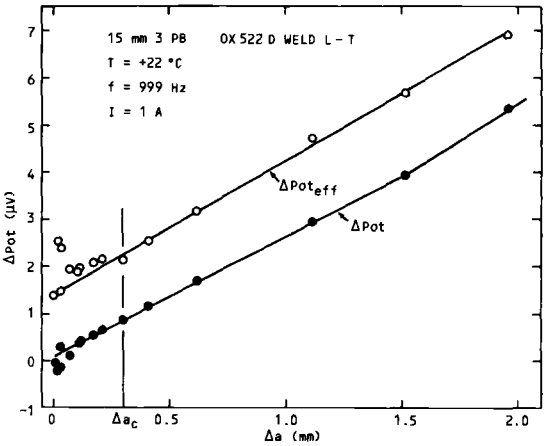

FIG. 15—*Crack extension-potential drop relationship.*

frequency has only a small effect on this value. When moving further into the plastic regime the elastic load dependence of the potential starts to change linearly as a function of crack extension. The amount of this change is primarily dependent on the frequency, the temperature, and current having a minor effect.

The crack extension value where the elastic load dependence of the potential first starts to change does not correspond to the potential minimum on the potential drop-deflection curve. Instead, it corresponds closely to the J_{IC} value determined through unloading compliance as seen from Fig. 16. The value of the load dependence change seems to give the best correlation with the crack initiation determined from the unloading compliance. This would however demand the use of an unloading potential drop method, which would probably be inefficient and somewhat inaccurate.

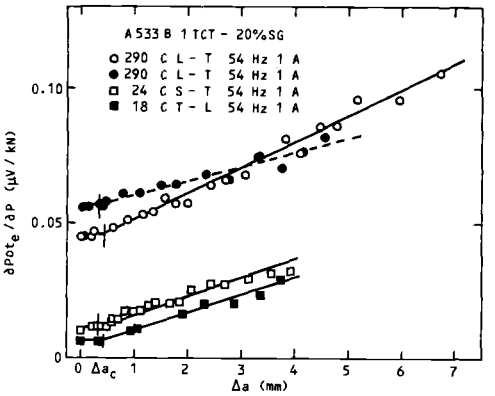

FIG. 16—*Elastic load dependence of potential change.*

Conclusions

In this work the unloading compliance and the AC potential drop methods have beem compared. It is the authors opinion that the AC potential drop method is not suitable for the determination of ductile crack growth initiation but can be readily used to measure crack extension.

Acknowledgments

This work was financed by the Ministry of Trade and Industry and the Technical Research Centre of Finland through the Reliability of Reactor Materials Program.

References

[*1*] Wilkowski, G. M. and Maxey, W. A., "Review and Applications of the Electric Potential Method for Measuring Crack Growth in Specimens, Flawed Pipe, and Pressure Vessels," *Fracture Mechanics Fourteenth Symposium Volume II: Testing and Applications, STP 791,* American Society for Testing and Materials, Philadelphia, 1983, pp. II-266–II-294.

[*2*] Marandet, B. and De Roo, P., "Application of A.C. Potential Drop Method to Prediction of Initiation in Static and Dynamic Testing," *CSNI Principal Working Group 3 Meeting in Paris 1,* Nuclear Energy Agency, Dec., 1983, pp. 75–84.

[*3*] Ingham, T. and Morland, E., "The Measurement of Ductile Crack Initiation: A Comparison of Data from Multiple and Single Specimen Methods and Some Considerations of Size Effects," *CSNI Specialists' Meeting on Plastic Tearing Instability,* USNRC Report NUREG/CP-00100, (CSNI Report No. 39), Washington, DC, U.S. National Research Council, Sept. 1979, pp. 330–358.

[*4*] Valkonen, A. and Saarelma, H., "*J-R*-Curve Determination by Means of the Unloading Compliance Method," Research Reports 30/1981, Technical Research Centre of Finland, Espoo, Finland, 40 pp. plus appendix 6 pp. in Finnish.

[*5*] Saario, T., Wallin, K., Saarelma, H., Valkonen, A., and Torronen, K., "A Computer-Interactive System for Elastic-Plastic Fracture Toughness Testing," *Automated Test Methods for Fracture and Fatigue Crack Growth, STP 877,* American Society for Testing and Materials, Philadelphia, 1984.

[*6*] Loss, F. J., Ed., "Structural Integrity of Water Reactor Pressure Boundary Components—Quarterly Progress Report, April–June 1979," USNRC Report NUREG/CR-0943 (NRL Memorandum Report 4064), U.S. National Research Council, Washington, DC, Sept. 1979.

[*7*] Loss, F. J., Ed., "Structural Integrity of Water Reactor Pressure Boundary Components, Annual Report, Fiscal Year 1979," USNRC Report NUREG/CR-1128, (NRL Memorandum Report 4122), U.S. National Research Council, Washington, DC, Dec. 1979.

[*8*] Wei, R. P. and Brazill, R., "An a.c. Potential System for Crack Length Measurement," *The Measurement of Crack Length and Shape During Fracture and Fatigue,* Engineering Materials Advisory Services Ltd., London, 1980, pp. 190–201.

[*9*] Charlesworth, F. D. W. and Dover, W. D., "Some Aspects of Crack Detection and Sizing Using a.c. Field Measurements," *Advances in Crack Length Measurement,* Engineering Materials Advisory Services Ltd., London, 1982, pp. 253–276.

[*10*] Watt, K. R., "A Consideration of an a.c. Potential Drop Method for Crack Length Measurements," *The Measurement of Crack Length and Shape During Fracture and Fatigue,* Engineering Materials Advisory Services Ltd., London, 1980, pp. 202–221.

Brian K. Neale[1] *and Robert H. Priest*[1]

The Unloading Compliance Method for Crack Length Measurement Using Compact Tension and Precracked Charpy Specimens

REFERENCE: Neale, B. K. and Priest, R. H., **"The Unloading Compliance Method for Crack Length Measurement Using Compact Tension and Precracked Charpy Specimens,"** *Elastic-Plastic Fracture Test Methods: The User's Experience, ASTM STP 856*, E. T. Wessel and F. J. Loss, Eds., American Society for Testing and Materials, Philadelphia, 1985, pp. 375–393.

ABSTRACT: The unloading compliance method has been used to measure crack lengths during the fracture toughness testing of an A508 Class II (Unified Numbering System [UNS] K12766) steel. It is shown that accurate crack length predictions (within ±4%) can be achieved by accounting for the extraneous compliance inherent in the testing fixture. Both precracked Charpy and 25-mm compact tension specimens have been tested over the temperature range −150 to 300°C. From a comparison of the data, an assessment of the capability of precracked Charpy specimens to measure the fracture toughness of pressurized water reactor (PWR) steels is made.

KEY WORDS: fracture tests, steels, unloading, A508 steel, unloading compliance method, extraneous compliance, crack length predictions, fracture toughness, temperature range, compact tension specimen, precracked Charpy specimen, pressurized water reactor (PWR)

The established method of assessing the effect of irradiation on the fracture properties of pressure vessel steels in nuclear reactors is to measure absorbed impact energy levels using Charpy V-notch surveillance specimens. Unfortunately, the impact energy levels give no direct indication of the fracture toughness of the steels, which is required in order to fully assess the structural integrity of the pressure vessels. Although several correlations exist between the fracture toughness and impact energy levels for nonirradiated steels, their accuracy for irradiated steels is less certain. A potentially more reliable method is to measure fracture toughness directly from the surveillance specimens.

Neale [*1*], Neale and Priest [*2,3*], and Pavinich et al [*4*] have successfully developed the unloading compliance method for measuring the fracture toughness

[1] Research officers, Berkeley Nuclear Laboratories, Berkeley, Gloucestershire, England GL 13 9PB.

of irradiated precracked Charpy specimens in three-point bend. The experimental and analytical details required to measure fracture toughness using a precracked Charpy specimen have previously been described [*1*] in a manner that supplements the ASTM Test for J_{IC}, a Measure of Fracture Toughness (E 813). This paper describes the application of the unloading compliance method to compact tension specimens, as used in accelerated irradiation tests and current surveillance programs. Experimental and analytical details are given together with a method for quantifying the extraneous compliance inherent in the testing fixtures [2].

The fracture toughness of steel similar to A508 Class II (Unified Numbering System [UNS] K12766) determined from precracked Charpy specimens is compared with values obtained from compact tension specimens. The comparison has enabled an assessment of the capability of precracked Charpy specimens to measure the fracture toughness of pressurized water reactor (PWR) steels to be made.

Analytical Relationships

The fracture behavior of ductile materials is conveniently characterized in terms of the variation in fracture resistance, as measured by J, with crack growth Δa. This section gives the analytical relationships for evaluating J and Δa from the load and displacement data measured from irradiated compact tension specimens. Because of remote handling considerations in the shielded facility described by Neale and Priest [2], displacements are measured indirectly across the clevices rather than directly from a gage mounted on the test specimen. Consequently, the analytical relationships reflect the need to account for extraneous displacements arising in the loading clevices and pins.

Fracture Resistance J

The fracture resistance J for a compact tension specimen was calculated from the relationship

$$J = \eta U/[B_n(W - a_0)] \tag{1}$$

similar to that of Rice et al [*5*] where a_0 is the initial crack length, W is the specimen width, B_n is the net specimen thickness, and U is the area measured under the load displacement record up to each unloading. The η function given by $\eta = 1.97 + 0.815\,(1 - a_0/W)$ was chosen to fit η values calculated from the plane strain limit load function of Haigh and Richards [*6*] following the procedure given by Neale and Townley [*7*]. This function exceeds the η values given in ASTM E 813 by less than 5% for $0.5 \leq a/W \leq 0.7$.

Values of U are corrected for extraneous displacements following a procedure similar to that described for single-edge notch bend specimens by Neale [*1*].

Crack Length a

For a compact tension specimen, the crack length a at each unloading was evaluated from the relationship

$$E B_e(\delta\Delta/\delta P) = 1752(1 - \nu^2)[0.5(a/W)^2 - 4.177(a/W)^3 + 20.894(a/W)^4 - 69.272(a/W)^5 + 160.75(a/W)^6 - 256.1(a/W)^7 + 67.09(a/W)^8 - 164.8(a/W)^9 + 46.588(a/W)^{10}] - 1.137 \quad (2)$$

where E is Young's modulus at the test temperature, ν is Poisson's ratio, and $\delta\Delta/\delta P$ is the unloading compliance measured along the loading line. Providing $a/W \leq 0.7$, Eq 2 is within 0.7% of the plane strain compliance obtained from numerical results of Newman [*8*], which are widely accepted as the most accurately known results in the literature. These values are more accurate than those quoted in ASTM E 813, which exceed Newman's results by 10% for $0.5 \leq a/W \leq 0.7$. The effective specimen thickness B_e of a side-grooved compact tension specimen of net thickness B_n is given by [*9*]

$$B_e = B - [(B - B_n)^2/B]$$

where B is the specimen thickness.

Values of $\delta\Delta/\delta P$ are corrected for extraneous displacements by subtracting the extraneous compliance calculated from the function given in the next section.

Extraneous Compliance

The unloading compliance method was used to evaluate the extraneous displacements inherent in the testing configuration used by Neale and Priest [*3*]. EN3A and A508 steel compact tension specimens were prepared containing blunt notches spark eroded to a range of depths and were subsequently tested at room temperature. It should be noted that flat bottomed holes were used in the loading clevices in an attempt to reduce frictional effects to a minimum. The extraneous compliance $\delta\Delta_{ext}/\delta P$ was determined by subtracting the analytical compliance given by Eq 2 from the measured unloading compliance. A linear relationship was observed between $P(\delta\Delta_{ext}/\delta P)$ and the load P for both steels, as shown in Fig. 1. These results can be described by the function

$$\delta\Delta_{ext}/\delta P = (1/C_1) + (1/C_2 P) \quad (3)$$

where C_1 is 181 kN · mm^{-1} and C_2 is 20 mm^{-1} for both the EN3A and A508 steel.

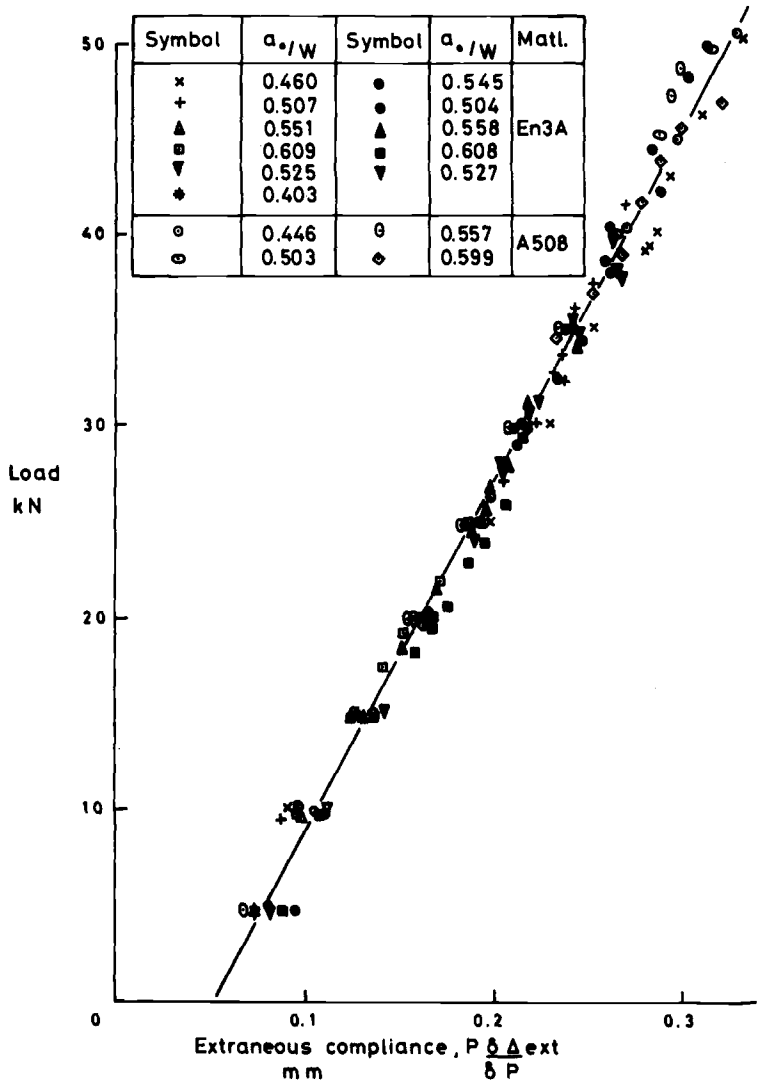

FIG. 1—*Extraneous compliance calibration for 25-mm compact tension specimens.*

The experimental evidence suggests that the value C_1 is associated with elastic displacements in the testing fixture and is therefore independent of the specimen material properties. The value of C_2, the offset in the extraneous compliance, is attributable to the offset arising in the load displacement records caused by the initial interaction of the specimen, loading pins, and clevises during the initial stages of loading.

Experimental Details

Material Characterization

The chemical composition of the steel used in the experimental program, given in Table 1, is similar to that of an A508 Class II steel, though outside the chemical composition requirements given in the American Society of Mechanical Engineers (ASME) Boiler and Pressure Vessel Code (BPVC) Section II, 1977.

The tensile properties measured using specimens prepared in the transverse direction are given in Table 2. The Charpy impact levels measured from standard Charpy specimens machined in the *T-L* orientation are shown in Fig. 2.

It should be noted that while the tensile properties given in Table 2 satisfied the requirements for the steel given in ASME BPVC Section II, 1977, the impact results did not meet the 41-J level required at 4.4°C. In addition, the upper shelf energy level was considerably lower than expected for this type of steel.

Fracture Toughness Specimens

Charpy specimens designated KM1 to KM12 were machined in the *T-L* orientation to the dimensions 10 by 10 by 55 mm. The Charpy specimens were fatigue precracked from the standard 2-mm deep 45° V-notch to give a nominal crack length to specimen width ratio a_0/W of 0.5. A Charpy V-notch profile cutter was used to machine 1-mm deep side grooves in the precracked Charpy specimens. The precracked Charpy specimens were tested in three-point bend at a span to width ratio S/W of four over the temperature range -150 to 300°C using the unloading compliance method as described by Neale [*1*].

In addition, 25-mm compact tension specimens designated KM20 to KM22 were prepared in the *T-L* orientation. These specimens were fatigue precracked to a nominal a_0/W of 0.5. The compact tension specimens were then side grooved to a depth of 2.5 mm and tested using the unloading compliance method.

Results

Precracked Charpy Specimens

The analysis and interpretation of the load-displacement and compliance-displacement test records from precracked Charpy specimens that exhibit stable crack growth have been described by Neale [*1*] for determining the initiation fracture resistance J_q and the tearing resistance dJ/da. Figures 3*a* and *b* show typical load-displacement and compliance-displacement records for specimen KM10, respectively. The extraneous compliance inherent in the three-point bend testing configuration was evaluated from the function given by Neale and Priest [*3*]. Figure 3*c* demonstrates the effect of removing the extraneous compliance from the measured compliance. The resulting fracture resistance J versus crack length a curve is shown in Fig. 4. In addition, definitions of J_q, dJ/da, blunting

TABLE 1—*Chemical composition.*

Element, weight %															
Carbon	Silicon	Manganese	Phosphorus	Sulfur	Chromium	Molybdenum	Nickel	Aluminum	Copper	Vanadium	Niobium	Boron	Titanium	Tin	Arsenic
0.32	0.32	0.85	0.024	0.035	0.46	0.96	1.06	0.039	0.15	0.02	0.022	0.001	0.01	0.025	0.04

TABLE 2—*Mechanical properties.*

Specimen	Temperature, °C	0.2% Proof Stress, MPa	Ultimate Tensile Stress, MPa	Elongation, %	Reduction in Area, %
T1	−100	565	732	26	45
T2	0	455	626	22	45
T3	100	420[a]	560	22	60
T4	200	391	544	18	50

[a]Upper yield stress; Vickers hardness number = 195 VPN_{10}.

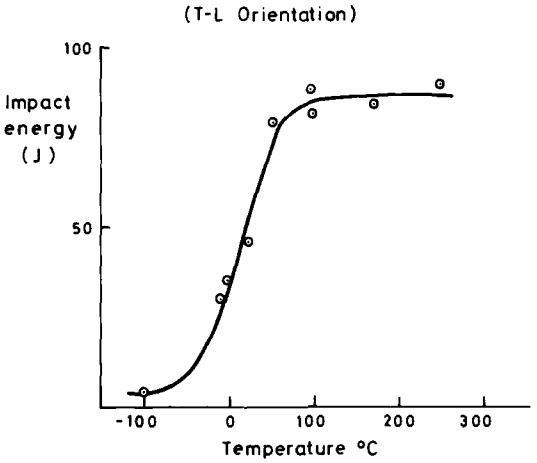

FIG. 2—*Charpy impact energy of A508 Class II steel.*

line, and exclusion line are also included. The intercept of the blunting line with the crack length axis was used to provide an estimate of the initial predicted crack length a_i. The final predicted crack length a_f was determined from the final unloading compliance value.

The initiation fracture toughness K_q was determined from J_q using the relationship

$$K_q = \sqrt{EJ_q/(1 - \nu^2)} \tag{4}$$

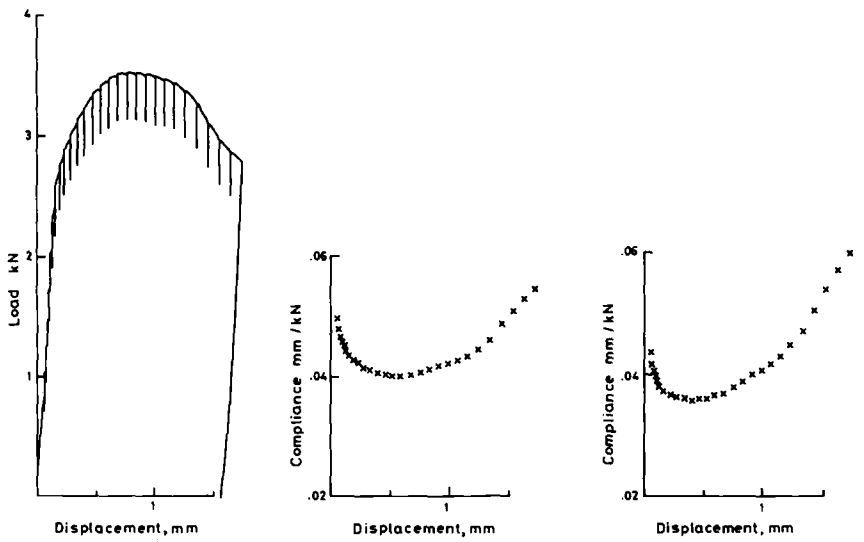

FIG. 3—(a) *Load displacement record for specimen KM10.* (b) *Measured compliance.* (c) *Corrected compliance.*

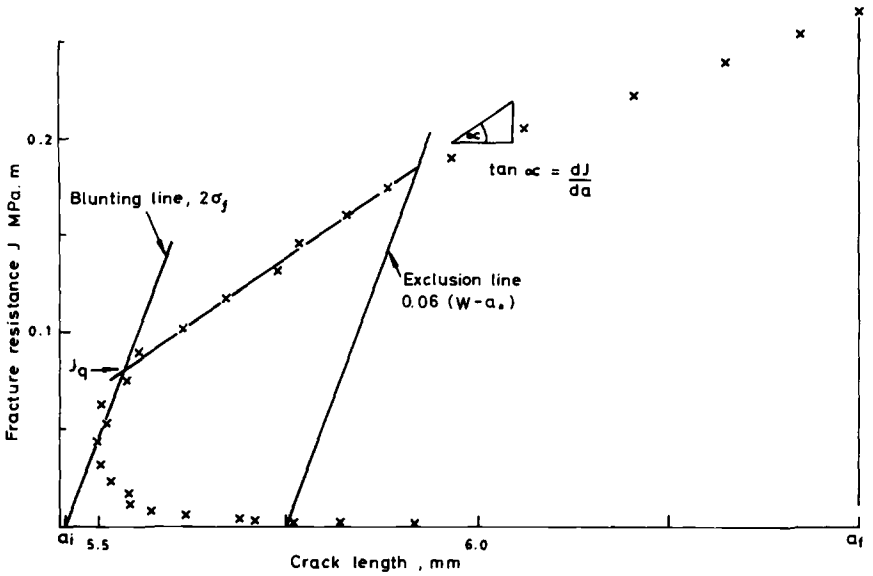

FIG. 4—*Fracture resistance versus unloading compliance estimated crack length for specimen KM10.*

where E is Young's modulus at the test temperature and ν is Poisson's ratio. Values of J_q, dJ/da, and K_q are given as a function of temperature in Table 3. Note that for those specimens that failed in an unstable manner with no evidence of crack growth, J_q was determined at maximum load.

The variation of K_q with temperature is compared in Fig. 5*a* with the upper validity limit calculated from the ASTM E 813 specimen size requirement that

$$W - a_0 \geq (25J_q/\sigma_f) \tag{5}$$

and Eq 4. The flow stress σ_f is given by the mean of the 0.2% proof stress and the ultimate tensile stress. ASTM E 813 suggests that values of K_q below this validity limit may be regarded as a material property independent of test specimen size. Above a temperature of -50°C, an upper shelf fracture toughness K_q of between 129 to 170 MPa·m$^{1/2}$, which is in close agreement with the upper validity limit, is evident. Consequently, all the K_q values may be regarded as material properties and thus be used as conservative estimates of the plane strain fracture toughness K_{Ic}. It is emphasized that the upper shelf fracture toughness values are lower than would normally be expected for this type of steel but are consistent with the relatively low values of upper shelf Charpy impact energy level.

TABLE 3—*Fracture properties of A508 Class II steel determined from precracked Charpy specimens.*[a]

Specimen	Temperature, °C	a_0/W	B_n, mm	J_q, MPa.m	dJ/da, MPa	K_q, MPa.m$^{1/2}$
KM1	−150	0.529	8.08	0.0101	. . .[b]	48.8
KM2	−120	0.548	8.05	0.0365	. . .	92.2
KM3	−80	0.549	8.07	0.0128	. . .	54.3
KM4	−50	0.516	8.02	0.1255	. . .	169.4
KM5	0	0.534	8.10	0.1168	. . .	162.3
KM6	65	0.542	7.96	0.0855	286	137.6
KM7	130	0.534	8.02	0.1120	202	156.0
KM8	200	0.534	8.00	0.0912	142	139.3
KM9	300	0.541	8.07	0.0808	83	129.1
KM10	65	0.545	7.72	0.0800	273	133.2
KM11	−78	0.544	8.09	0.0454	. . .	102.0
KM12	−59	0.528	8.05	0.0884	. . .	142.1

[a] $W = B = 10$ mm.
[b] Unstable fracture is designated by three dots.

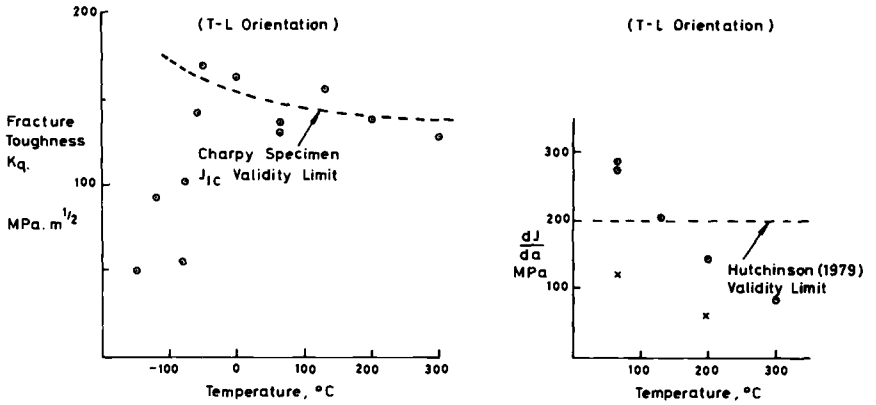

FIG. 5—(a) *Fracture Toughness of A508 Class II steel determined using precracked Charpy specimens.* (b) dJ/da *for A508 Class II steel determined using precracked Charpy specimens.*

The tearing resistances dJ/da are compared in Fig. 5*b* with the Hutchinson validity limit [*10*] expressed as

$$[(W - a_0)/J](dJ/da) > 10 \tag{6}$$

which must be satisfied in order to ensure J-controlled crack growth. Assuming a nominal crack length of 5 mm and J of 0.1 MPa·m, a value of 200 MPa for dJ/da is obtained. Values of dJ/da below this limit should not be regarded as a material property independent of specimen size.

The predicted initial and final crack lengths obtained from the precracked Charpy specimens are compared in Table 4 with the corresponding measured values. The predicted crack lengths and crack growths are within ± 1.6 and ±4.7% of the measured values, respectively. ASTM E 813 requires the predicted crack growth to be within 15% of the measured value.

Compact Tension Specimens

The load-displacement and compliance-displacement test records obtained from the compact tension specimens were analyzed using the relationships given by Eqs 1, 2, and 3. Figures 6*a*, *b*, and *c* show typical load-displacement, compliance-displacement, and corrected compliance-displacement records for specimen KM21, respectively. The resulting fracture resistance J versus crack length a curve is shown in Fig. 7. For consistency, the values of J_q, dJ/da, and K_q given in Table 5 were obtained following a similar procedure to that used for the precracked Charpy specimens. However, for specimen KM20, which failed in an unstable manner with no evidence of crack growth, J_q was determined at maximum load. The data satisfied the validity limits expressed by Eq 5 and 6. Consequently, both the K_q and dJ/da values may be regarded as material properties.

TABLE 4—*Predicted and measured crack lengths using precracked Charpy specimens.*

Specimen	Initial Crack Length, mm		Final Crack Length, mm		Crack Growth, mm	
	Predicted a_i	Measured a_0	Predicted a_f	Measured a_t	Predicted $a_f - a_i$	Measured $a_t - a_0$
KM6	5.500	5.418	5.983	5.905	0.483	0.487
KM7	5.250	5.337	6.063	6.139	0.813	0.802
KM8	5.422	5.335	5.938	5.876	0.516	0.541
KM9	5.468	5.406	6.347	6.315	0.879	0.909
KM10	5.457	5.447	6.500	6.431	1.043	0.984

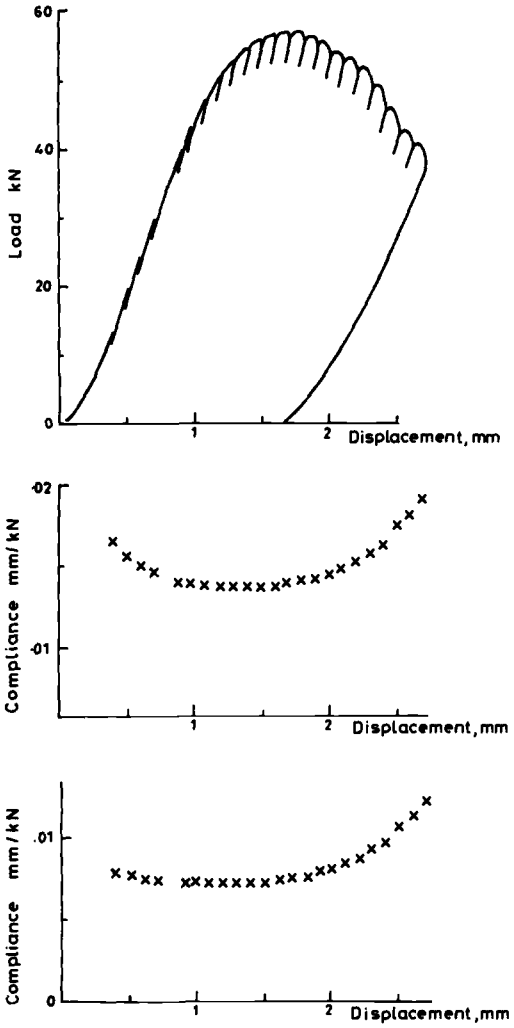

FIG. 6—(a) *Load displacement record for specimen KM21.* (b) *Measured compliance.* (c) *Corrected compliance.*

The predicted initial and final crack lengths are compared in Table 6 with the corresponding measured values. The predicted crack lengths and crack growths are within ±3.3 and ±9.5% of the measured values, respectively.

Discussion

The unloading compliance method has been used to measure the fracture toughness of a steel similar to A508 Class II using precracked Charpy and compact tension specimens. Characterization of the extraneous compliance in-

TABLE 5—*Fracture properties of A508 Class II steel determined from 25-mm compact tension specimens.*[a]

Specimen	Temperature, °C	a_0/W	B_n, mm	J_q, MPa·m	dJ/da, MPa	K_q, MPa·m$^{1/2}$
KM20	−20	0.509	20.26	0.073	. . .[b]	128
KM21	65	0.494	19.78	0.150	107	182
KM22	200	0.497	19.50	0.106	51	151

[a] W = 50 mm and B = 25 mm.
[b] Unstable fracture is designated by three dots.

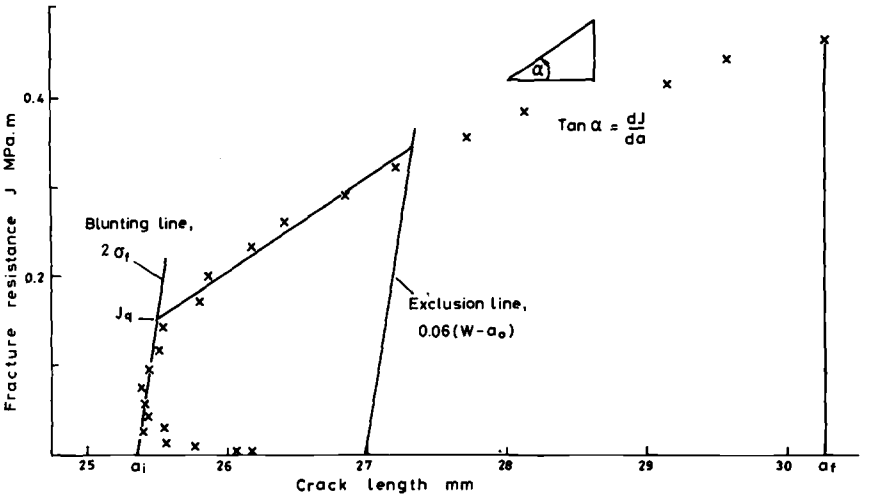

FIG. 7—*Fracture resistance versus unloading compliance estimated crack length for specimen KM21.*

herent in the testing configuration and detailed analyses of the specimen behavior resulted in crack length predictions that were within ±4% of the measured values.

The fracture toughness K_q determined from the 25-mm compact tension specimens is compared in Fig. 8 with the values obtained from the precracked Charpy specimens. Although there are insufficient compact tension specimen data to fully assess the effect of specimen size on the transition behavior, the comparison indicates that on the upper shelf, the Charpy specimen data give a conservative

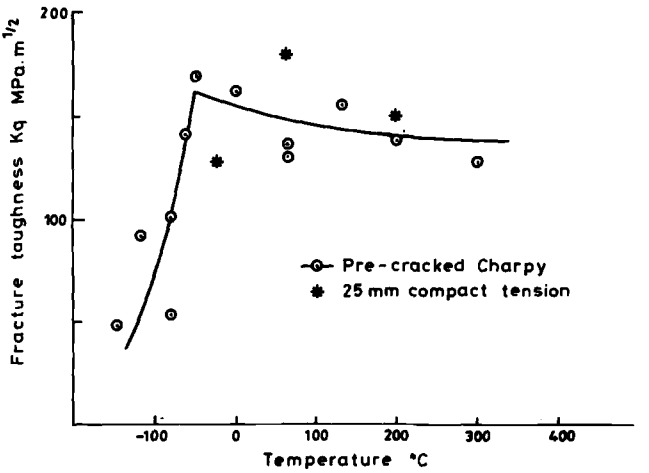

FIG. 8—*Comparison of the fracture toughness determined using precracked Charpy and 25-mm compact tension specimens.*

TABLE 6—*Predicted and measured crack lengths using 25-mm compact tension specimens.*

Specimen	Initial Crack Length, mm		Final Crack Length, mm		Crack Growth, mm	
	Predicted a_i	Measured a_0	Predicted a_f	Measured a_f	Predicted $a_f - a_i$	Measured $a_f - a_0$
KM20	26.290	25.452	. . .[a]	. . .	. . .	. . .
KM21	25.360	24.675	30.283	29.509	4.923	4.834
KM22	25.485	24.845	31.969	32.011	6.484	7.166

[a]Unstable fracture is designated by three dots.

estimate of the larger compact tension specimen data. This result is a direct consequence of the curved shape of the fracture resistance behavior. The construction procedure used to define J_q at the intersection of the blunting line and a least squares fit line drawn through the data from precracked Charpy and compact tension specimens is shown schematically in Fig. 9. Clearly, the J_q value of the smaller Charpy specimen, J_q^S will be a lower estimate of the larger sized compact tension specimen value J_q^L. For example, the value of J_q^S from specimen KM10 was 0.08 MPa·m whereas for specimen KM21, J_q^L was 0.150 MPa·m. However, comparing the fracture resistance curves of these specimens, as shown in Fig. 10, indicates virtually identical behavior, thus demonstrating that the apparent size effect on initiation toughness and tearing resistance arises from the construction procedure used rather than from a real difference in material behavior. An alternative method is to define an engineering value of J_q corresponding to a small amount of crack growth such as 0.2 mm, as recently suggested by Neale et al [*11*]. For the current data this would produce an estimate for J of 0.125 MPa·m for both the precracked Charpy and compact tension specimen.

Although it is envisaged that future reactor surveillance schemes will include compact tension specimens, there may still be a requirement to use Charpy specimens. From the results obtained in the current investigation, it is possible to assess the use of a precracked Charpy specimen for measuring the fracture properties of, for example, PWR pressure vessel steels. To establish the integrity of the vessel under fault conditions, typical values are assumed for J_q and dJ/da of 0.2 MPa·m and 100 MPa, respectively. These values are equivalent to an initiation fracture toughness K_q of approximately 200 MPa·m$^{1/2}$ and a fracture toughness of approximately 300 MPa·m$^{1/2}$ at 2-mm crack growth for a flow

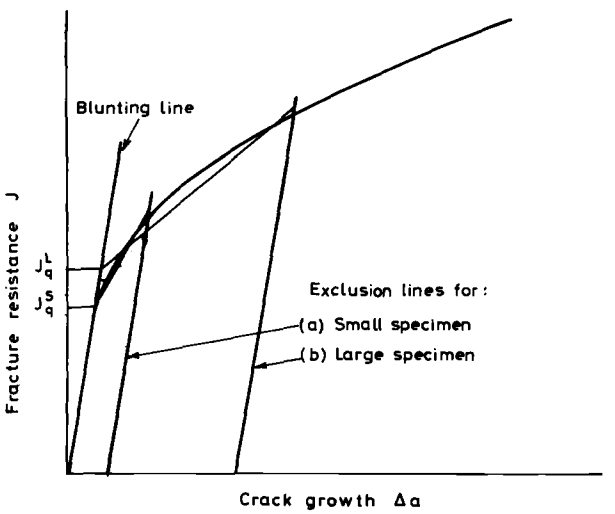

FIG. 9—*Schematic interpretation of* J-Δa *curve for a small and large test specimen.*

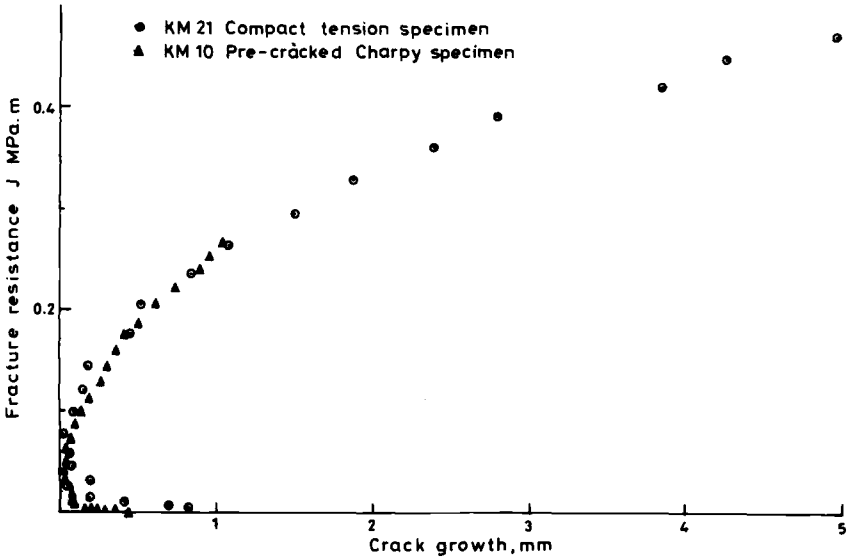

FIG. 10—*The fracture resistance of A508 Class II steel determined from precracked Charpy and compact tension specimens*

stress of 500 MPa. Unfortunately, these fracture toughness values exceed the upper validity limit for a precracked Charpy specimen calculated from the ASTM E 813 test specimen size requirements assuming typical PWR steel tensile properties (Fig. 5*a*). On this basis, it would not be possible to use this size of specimen to demonstrate an initiation toughness of 200 MPa·m$^{1/2}$, nor would it be possible to obtain valid resistance data up to 2-mm crack growth. However, it is encouraging to note the agreement in the fracture resistance behavior determined from these specimens at crack growths well beyond the validity limit with that obtained from a 25-mm compact tension specimen (Fig. 10). Thus, it has to be concluded that while precracked Charpy specimens cannot currently be used to directly measure typical fracture properties of PWR materials, it is acknowledged that improvements in analytical understanding may lead to a change in the future.

Conclusions

For the A508 Class II steel tested here, it was found that

1. With careful characterization of the testing configuration and specimen behavior, the unloading compliance method predicts the initial and final crack lengths to within ±4% of the measured values.

2. On the upper shelf, precracked Charpy specimens analyzed using a technique similar to that described by ASTM E 813 provide a conservative estimate of the fracture toughness as determined from 25-mm compact tension specimens.

3. Currently, the precracked Charpy specimen cannot be used to directly measure the fracture properties of PWR pressure vessel material at crack growths much greater than 1 mm.

Acknowledgments

This paper is published by permission of the Central Electricity Generating Board (CEGB). The assistance of Mr. D. B. Ratcliffe, CEGB Marchwood Engineering Laboratories, who performed the chemical analysis, is gratefully acknowledged.

References

[1] Neale, B. K., "The Determination of J_q the Initiation Elastic-Plastic Toughness Parameter Using Pre-cracked Charpy Specimens," *International Journal of Pressure Vessels and Piping*, Vol. 12, No. 4, 1983, pp. 207–227.

[2] Neale, B. K. and Priest, R. H., "Fracture Toughness Testing of Irradiated Materials," *International Conference on Fracture Toughness Testing—Methods, Interpretation and Application*, The Welding Institute, London, England, 1982.

[3] Neale, B. K. and Priest, R. H., "On the Unloading Compliance Method for Crack Length Measurement," *Engineering Fracture Mechanics*, Vol. 19, No. 3, 1984, pp. 441–448.

[4] Pavinich, W. A., Futato, R. J., Neale, B. K., Lowe, A. L., and Van der Sluys, W. A., "A Single Specimen Method for Determining Upper Shelf Fracture Toughness Shifts Using Precracked Charpy Specimens," *Effects of Radiation on Materials: Proceedings of the Eleventh International Symposium, STP 782*, American Society for Testing and Evaluation, Philadelphia, 1982, pp. 563–581.

[5] Rice, J. R., Paris, P. C., and Merkle, J. G., "Some Further Results of J-integral Analysis and Estimates," *Progress in Flaw Growth and Fracture Toughness Testing, STP 536*, American Society for Testing and Materials, Philadelphia, 1973, pp. 231–245.

[6] Haigh, J. R. and Richards, C. E., "Yield Point Loads and Compliance Functions of Fracture Mechanics Specimens," CEGB Report RD/L/M461, Central Electricity Generating Board, Leatherhead, England, 1974.

[7] Neale, B. K. and Townley, C. H. A., *International Journal of Pressure Vessels and Piping*, Vol. 5, No. 3, 1977, pp. 207–239.

[8] Newman, J. C., Jr., "Stress Analysis of the Compact Specimen Including the Effects of Pin Loading," *Fracture Analysis: Proceedings of the 1973 National Symposium on Fracture Mechanics, Part II, STP 560*, American Society for Testing and Materials, 1974, pp. 105–121.

[9] Shih, C. F., De Lorenzi, H. G., and Andrews, W. R., *International Journal of Fracture*, Vol. 13, No. 4, 1977, pp. 544–548.

[10] Hutchinson, J. W., "Recent Developments in Non-Linear Fracture Mechanics," CSNI Specialists Meeting on Plastic Tearing Instability, St. Louis, MO, U.S. Nuclear Regulatory Commission, Washington, DC, 1979, pp. 16–28.

[11] Neale, B. K., Curry, D. A., Green, G., Haigh, J. R., and Akhurst, K. N., "A Procedure for the Determination of the Fracture Resistance of Ductile Materials," CEGB Report TPRD/B/0495/R84, Central Electricity Generating Board, Leatherhead, England, 1984.

Ad. Bakker[1]

A DC Potential Drop Procedure for Crack Initiation and *R*-Curve Measurements During Ductile Fracture Tests

REFERENCE: Bakker, A., **"A DC Potential Drop Procedure for Crack Initiation and *R*-Curve Measurements During Ductile Fracture Tests,"** *Elastic-Plastic Fracture Test Methods: The User's Experience, ASTM STP 856,* E. T. Wessel and F. J. Loss, Eds., American Society for Testing and Materials, 1985, pp. 394–410.

ABSTRACT: This paper describes the use of a direct current (DC) potential drop technique, a single-specimen technique for the detection of crack growth initiation and subsequent crack growth. From an analysis of the potential drop signal, where the measured signal is divided into parts originating from real physical crack growth and fictitious crack growth caused by deformation of the specimen, a procedure is described to derive both crack initiation and crack growth from the test records of a single specimen. This procedure is then applied to a series of three-point bend (SENB) specimens and the results are compared with the multiple-specimen technique according to the ASTM Test for J_{Ic}, a Measure of Fracture Toughness (E 813). The agreement between the results of both methods is satisfactory. Finally, some possible refinements and further improvements of the method are discussed.

KEY WORDS: fracture tests, crack initiation, crack propagation, tests, fracture mechanics, fracture toughness, elastic-plastic fracture, J integral, potential drop method

The J integral and crack opening displacement (COD) are at present the most widely used parameters for characterization of the ductile fracture resistance of materials. Procedures for their determination are defined in the ASTM Test for J_{Ic}, a Measure of Fracture Toughness (E 813) and British Standard (BS) Methods for Crack Opening Displacement (COD) Testing (BS 5762-79). The aim of these procedures is to find the critical value of the J integral or the crack tip COD δ at the moment of crack growth initiation J_{Ic} and δ_i, respectively. For that purpose multiple-specimen techniques [*1*] are used, where several specimens are loaded to different amounts of stable crack growth, and the initiation value is found by extrapolating these results to zero crack growth (after correcting for apparent

[1]Senior research engineer, Delft University of Technology, Laboratory for Thermal Power Engineering, P.O. Box 5055, 2600 GA DELFT, Netherlands.

growth caused by crack-tip blunting). The relationship between the fracture parameter J or δ and crack growth Δa, the so-called R curve, is assumed linear for the purpose of this extrapolation. The critical value thus derived is in general somewhat higher than the true initiation value, because the real R curve tends to have a convex shape (Fig. 1).

The significant costs in time, labor, and material associated with multiple-specimen techniques form a powerful incentive for the development of procedures to determine the complete R curve from the test records of a single specimen. A further incentive towards such procedures derives from the increasing interest in the post-initiation behavior of materials up to final instability for the purpose of accurate quantification of the margin of safety provided by stable crack growth between the loads at initiation and at instability [*2*,*3*].

One single-specimen technique presently under development is the unloading compliance method, which is based on the change in specimen compliance with crack length [*4*]. An alternative for generating R curves from a single specimen is the potential drop (PD) method, based on the change in electrical resistance of a specimen with crack length and hence independent of the type of loading.

Many applications of the PD method are known from the literature [*5–7*]. Several of these are for crack length monitoring during fatigue tests, but some applications for ductile fracture tests are also known. Most of these focus on the detection of crack growth initiation; though in a few cases it was also attempted to quantify the amount of stable growth. The technique described in this paper is intended both for finding the initiation point and for measuring subsequent stable growth.

Principle and Experimental Setup

The electrical resistance of a cracked body changes with crack length. When a constant current is applied to a specimen, the change in electrical resistance results in a change of the potential drop between two measuring points across

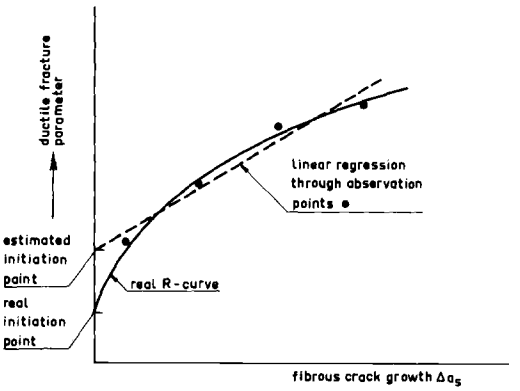

FIG. 1—*Typical linearized and actual* J-R *curve.*

the crack. Provided the change in crack length is the only source of resistance change, the relationship between potential drop and crack length can be determined by experimental calibration or by solving the governing differential equation. A well known example of an analytical calibration relation for direct current through an infinitely long center-notched (CN) strip is that proposed by Johnson [8] (Fig. 2)

$$U/U_o = \{\text{arcosh}\,[\cosh(\pi y/2W)/\cos(\pi a/2W)]\}/\{\text{arcosh}\,[\cosh(\pi y/2W)/\cos(\pi a_o/2W)]\} \quad (1)$$

where

$2y$ = spacing of the potential measuring points,
$2W$ = width of the strip, and
U = potential drop where U_o refers to a reference crack with length $2a_o$.

For symmetry reasons Eq 1 is also applicable to single-edge notched (SEN) and double-edge notched (DEN) strips. Since it is a solution of a two-dimensional differential equation, its applicability is limited to straight cracks. Consequences of sources of resistance change other than a change in crack length are discussed in detail in the next section.

Before application of the potential drop method, decisions are required with respect to

(1) the choice between direct current (DC) and alternating current (AC),
(2) current level,
(3) current input/output locations, and
(4) potential drop measuring locations.

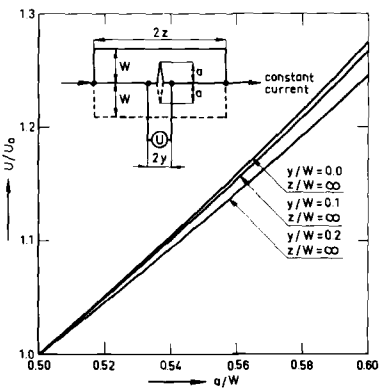

FIG. 2—*Analytical DC calibration for a CN, SEN, and DEN specimen.*

These decisions depend on the required sensitivity and reproducibility and on electronic equipment availability and costs.

Decision 1

Both DC and AC systems are presently under investigation for crack length measuring purposes. The basic difference between DC and AC is that in the first case the current density is (almost) constant through the specimen thickness (except at very high current densities), while for AC the current is carried only by a thin layer near the metal surface. This phenomenon, known as "skin effect," results in a far higher effective resistance for AC, meaning that the same level of sensitivity can be reached with a far lower current. This is of the utmost importance for nil ductility temperature (NDT) field tests on large structures, such as pressure vessels and piping systems. For laboratory tests on relatively small specimens the high current required for DC measurements need not be a disadvantage. On the other hand, the "skin effect" associated with AC presents a distinct disadvantage in R curve testing where the average crack extension over the specimen thickness is required. Therefore a DC system was selected for the present investigation. For detailed discussions on the advantages and disadvantages of both methods the reader is referred to the literature [5].

Decision 2

The sensitivity of the potential drop for a given geometry is directly proportional to the current. With a direct current of 80 A (obtained from a highly stable current source with a maximum of 100 A at 8 V), the signal level U_o was found to be about 0.1 V for the specimen investigated (SENB with $W = 50$ mm, $B = 25$ mm, and $a/W = 0.5 \div 0.6$), yielding a sensitivity of about 0.02-mm crack length/μV potential drop change. Using a microvoltmeter of high accuracy (0.1 μV) and high stability (drift 0.02 μV/°C), this sensitivity is more than adequate for our purpose. Heating of the specimen from the high current was found to be negligible, provided the cross section of the current carrying wires is large enough.

Decision 3

The sensititivy of the potential drop increases as the current carriers are moved closer to the crack (Fig. 3). However, reproducibility decreases rapidly. Since the sensitivity of 0.02 mm/μV mentioned in Decision 2, a theoretical value referring to an infinite strip and uniform current, is adequate for our purpose, the wires were connected to the end faces of the specimen.

Decision 4

With the potential drop measuring points located at the bottom (cracked surface) of the specimen, both sensitivity and reproducibility increase if the mea-

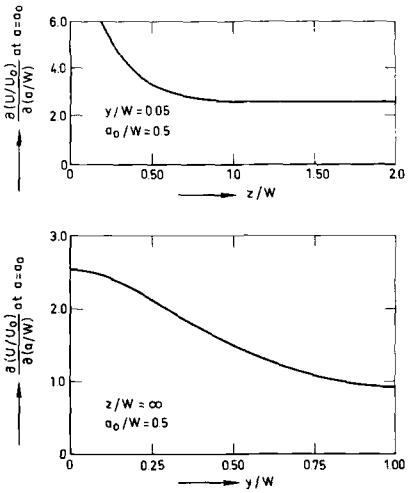

FIG. 3—*Reproducibility and sensitivity versus locations for current carriers* z *and measuring points* y (*see also Fig. 2*).

suring points are moved towards the crack mouth (Fig. 3). Sensitivity can be further increased by moving the measuring points towards the crack tip. This, however, is obtained at the expense of reproducibility, which drops rapidly. Therefore the measuring wires were connected at the bottom at a pitch of $2y$ = 4.5 mm, the closest distance still allowing for a COD clip gage to be mounted at the crack mouth.

A schematic of the complete DC system used is shown in Fig. 4. Many refinements to this simple system have been proposed in the literature, mostly dealing with drift of the equipment. Because of the relatively short duration of ductile fracture tests (±20 min maximum), drift was no problem during the tests described here provided the system was stable at the start of the test. This meant that the system had to be switched on and left idle a few hours before a test. The measuring wires at the specimen had to be thermally insulated to avoid signal variations because of temperature changes.

Signal Analysis

As stated before, the change in potential drop across a crack can be related directly to the change in crack length, provided that the latter forms the only source for the change in electrical resistance of a specimen. During ductile fracture tests (for example, J_I and COD initiation, and R-curve tests), however,

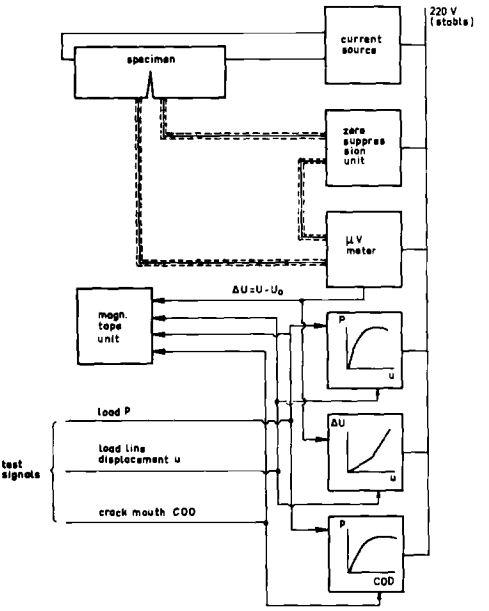

FIG. 4—*DC potential drop measuring system.*

specimens are loaded up to the limit load, in which case there are additional sources of electrical resistance change, namely:

- *Deformation*—Both the specific resistance and the cross-sectional area of the ligament can change because of plastic deformation.
- *Blunting*—The high local deformations at the crack tip result in apparent crack growth before crack growth because separation of the crack faces initiates.
- *Void Growth*—The high local deformations in the small so-called "process" zone ahead of the crack will cause voids to grow, resulting in a change in electrical resistance of this material volume.

All these effects cause an increase in electrical resistance, and hence of the measured potential drop. Some ferritic materials also exhibit a decrease in electrical resistance because of an inverse magnetostriction effect caused by elastic deformation. This effect however can be neglected with respect to the other sources of resistance change, also because elastic stresses do not vary much after the onset of plasticity. From Fig. 2 it follows that the relation between crack length and potential drop is largely linear for relatively small variations in crack length. The electrically effective crack extension can thus be interpreted as the sum of real and apparent crack growths because of the aforementioned phenomena (Fig. 5)

$$\Delta a_{pd} = \Delta a_s + \Delta a_d + \Delta a_b + \Delta a_v \tag{2}$$

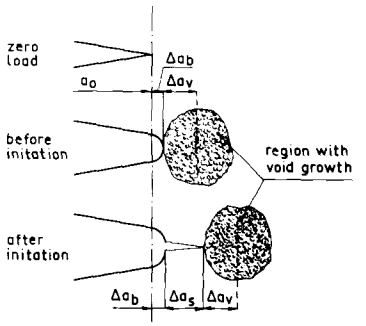

FIG. 5—*Physical and apparent crack extensions.*

where

Δa_{pd} = total apparent crack growth determined from the change in potential drop,
Δa_s = real fibrous crack growth (separation),
Δa_d = apparent crack growth caused by plastic deformation (global),
Δa_b = apparent crack growth caused by crack tip blunting (local), and
Δa_v = apparent crack growth caused by void growth ahead of the crack tip (local).

Before initiation of fibrous crack growth $\Delta a_s = 0$, and Eq 2 becomes at initiation

$$\Delta a_{pd_i} = \Delta a_{b_i} + \Delta a_{d_i} + \Delta a_{v_i} \tag{3}$$

At initiation blunting of the crack tip stops, so Δa_b will remain constant during stable crack growth.

Hence at an arbitrary point after initiation

$$\Delta a_{pd} = \Delta a_s + \Delta a_{b_i} + \Delta a_d + \Delta a_v \tag{4}$$

subtracting Eq 3 from Eq 4 yields for Δa_s

$$\Delta a_s = (\Delta a_{pd} - \Delta a_{pd_i}) - (\Delta a_d - \Delta a_{d_i}) - (\Delta a_v - \Delta a_{v_i}) \tag{5}$$

Several investigators [2,3] have observed that parameters characterizing the local strain intensity at the tip of a growing crack (such as the crack tip opening angle and the local crack tip opening displacement) remain constant. It seems reasonable to infer from this observation that the size of the zone with void growth ahead of the crack tip will also remain constant after initiation, or $(\Delta a_v - \Delta a_{v_i}) = 0$.

The change in apparent crack length caused by global plastic deformation was

investigated by testing some SENB specimens of the same material subsequently used for the actual crack extension tests with a machined notch with root radius $r = 1$ mm. In these tests crack extension initiation could be avoided up to high load line displacements, while it appears reasonable to assume that the influence of void growth was much less than for a sharp crack. Hence one may expect that blunting and plastic deformation were the only sources of resistance change. After the test the measured potential change was translated into a crack growth using the analytical calibration Eq 1, while the average apparent crack growth caused by blunting was measured after the specimen had been sawed apart. It was found that blunting accounted for ±80% of the calculated crack growth, that is, only ±20% of the potential change could be attributed to plastic deformation. The total signal change of the dummy specimen was ±30% of that of a fatigue-notched specimen undergoing crack growth. The total Δa_d thus appeared to be only some 6% of the total signal change for the actual tests, hence it was considered reasonable to neglect the change $(\Delta a_d - \Delta a_{d_i})$ for these tests. Further tests will of course be required before this assumption can be applied to other materials. With this assumption Eq 5 reduces to

$$\Delta a_s = \Delta a_{pd} - \Delta a_{pd_i} \tag{6}$$

The variables of this equation should be plotted against some controlling test variable. The load line displacement appears a logical choice for this purpose, since it increases continuously during any displacement-controlled test.

The moment of true crack extension initiation is marked by two discontinuities, namely, arrest of the stretched zone formation (blunting) and start of fibrous crack growth. This should cause a discontinuity in the potential drop signal. The expected discontinuity has indeed frequently been reported [*9*], but its detection apparently requires some experience from the experimentalist, because the change in slope of potential drop versus load line displacement record is rather small. If one succeeds in thus obtaining the initiation point from the potential drop record, Δa_{pd_i} will be known and Eq 6 then yields the fibrous crack growth for all measuring points subsequent to initiation (Fig. 6).

After interruption of the test, the crack growth can be marked (for example, by heat tinting) before the specimen is broken, preferably at a low temperature to obtain a brittle fracture without further plastic deformation of the ligament. The actual average crack growth through the thickness can then be determined, for example, by the nine-point averaging procedure of ASTM E 813. If the stretched zone is excluded, the measured crack growth can be compared with that predicted from the potential drop signal at the end of the test.

Procedure

All experiments were performed on SENB specimens of mild steel ST52-3 (Data Identification Number [DIN] 17100/66, equivalent to BS 4360 Grade D).

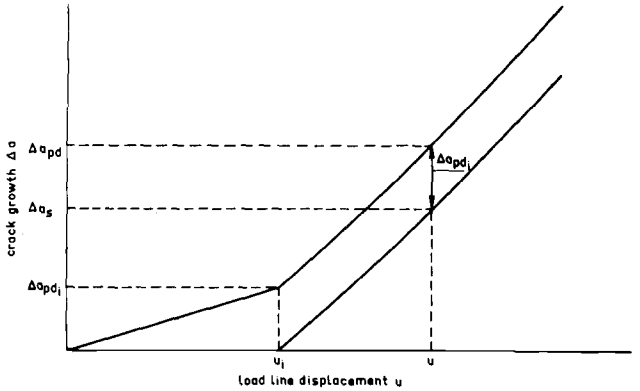

FIG. 6—*Procedures for obtaining crack extensions from potential drop signals.*

Chemical compositional and tensile properties of this material are summarized in Table 1. Nominal specimen dimensions are

$$W = 50 \text{ mm}, B = 25 \text{ mm}, S/W = 4, a_0/W \approx 0.52$$

A total of 18 specimens were tested; of these, nine were fatigue precracked, while the other nine had a spark-eroded precrack with notch root radius r = 0.05 mm.

Load, load-line displacement, crack mouth opening displacement, and potential drop measurements for all specimens were stored on magnetic tape at close intervals (Fig. 4).

The complete procedure for the derivation of R curves from the test results will first be discussed step by step on the basis of the results for one typical specimen (fatigue specimen 4.01).

• Figure 7*a* shows the record of the potential drop signal as a function of load line displacement. Shortly after the start of the test, where the signal is disturbed considerably, which is typical for all tests, the response becomes linear except for some noise on the signal. Then, at the load line displacement indicated in Fig. 7*a*, the slope of the record changes. While this change in slope was typical for all tests, the precise point at which it occurs was sometimes hard to define, as the response after the change in slope is, in general, no longer linear.

TABLE 1—*Chemical composition and tensile properties of ST52-3.*[a]

Cast	Thickness, mm	Manganese	Phosphorus	Sulfur	Carbon	Silicon	Aluminum
1343	30	1.430	0.040	0.023	0.190	0.352	0.035

[a]Yield strength σ_y = 410 MPa, and ultimate tensile strength σ_u = 570 MPa.

As discussed in the previous section, this point is considered to be the moment of crack growth initiation. Later, critical stretched zone measurements on the same material confirmed this [*10*].

- Using the calibration Eq 1, the potential drop signal after initiation is translated to the fibrous crack growth in Δa_s by Eq 6, as shown in Fig. 7*b*.
- The J and crack-tip opening displacement δ at all data points after initiation were determined using the definitions of ASTM E 813 and BS 5762-79, respectively. For the accurate determination of J, the measured load-line displacement was corrected for local deformations near the load application points [*11*]. Using these data points, the J and δ-R curves can be constructed (Fig. 7*c* and *d*); the latter curve being given mainly for the sake of completeness.

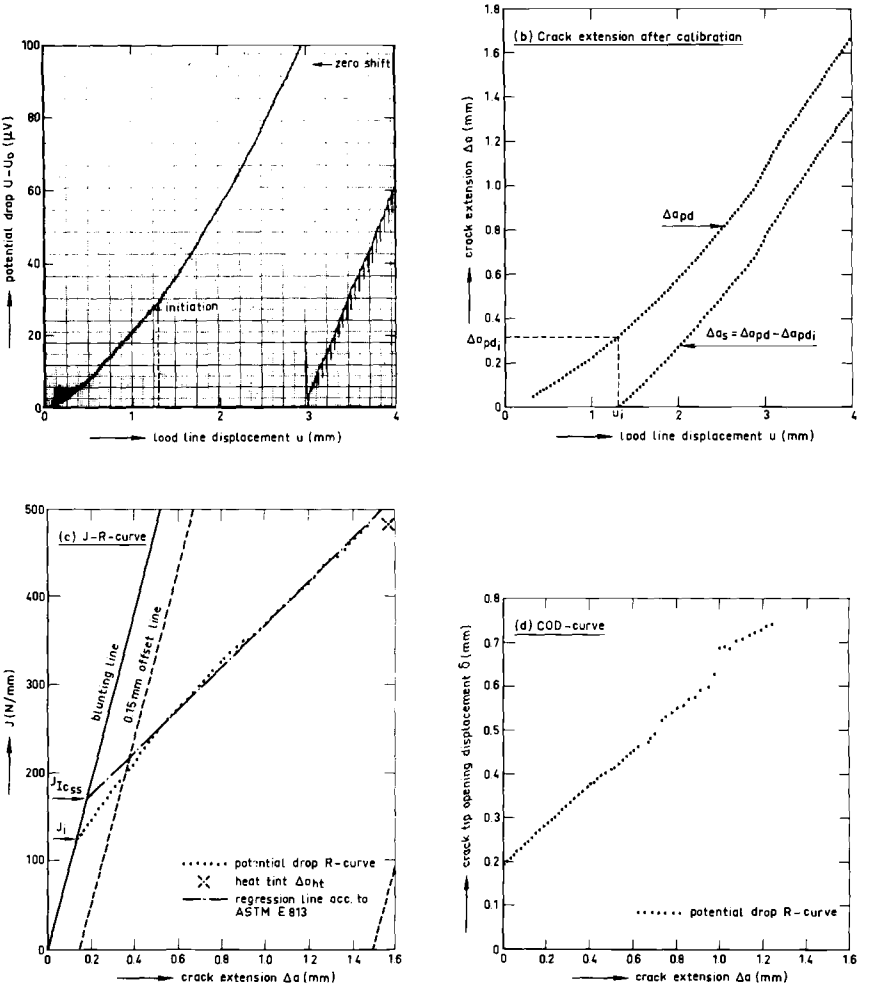

FIG. 7—*Sample determination of* J *and COD* R *curves (specimen 4.01, fatigue precrack).*

For the *J-R* curve, all crack extensions Δa_s were increased by the amount of blunting at the initiation point J_i according to ASTM E 813

$$\Delta a = \Delta a_s + \Delta a_b = \Delta a_s + (J_i/2\sigma_f)$$

The discontinuities in the δ-*R* curve were caused by small relative movements of the COD clip gage with respect to the specimen knife edges. Most probably these were caused by improper mounting of the clip gage, with friction preventing proper initial setting, that is, at the highest prestress of the clip gage. During loading, friction reduces as the prestress decreases with increasing COD, which may cause sudden resettings of the clip gage. The resulting jumps in COD were also observed in the COD versus load-line displacement plot. It is interesting to note here, that they could *not* be found in the load versus COD record as required by BS 5762-79, because they occurred near maximum load, where the variation of load with respect to COD is relatively small.

After completion of the PD tests, each specimen was heat-tinted, broken at low temperature, and had its crack extension (stretched zone plus fibrous growth) measured. The resulting 18 values were grouped according to type of precrack, and the results of each group used to determine a straight *J-R* line by linear regression according to ASTM E 813.

The results for all specimens are summarized in Table 2, and the potential drop and multiple specimen *J-R* curves are given in Figs. 8 and 9.

Discussion

For one specimen it was completely impossible to detect the initiation point from the potential drop record, for some others it was quite difficult.

For large crack extensions, the amount of crack growth is generally underestimated, as was observed for specimen 4.01. This discrepancy cannot be caused by neglecting the deformation effects, as $(\Delta a_d - \Delta a_{d_i}) > 0$ in Eq 5 would increase the difference rather then reduce it. Therefore it is expected to be caused by the calibration. All specimens showed considerable tunneling of the crack growth. For such highly curved crack fronts, the effective PD crack length as determined from Equation 1 may underestimate the average value. This effect might have been avoided by using a side-grooved specimen, which generally exhibits almost uniform crack extension across the thickness. Side grooving may also improve the detectability of the initiation point, because crack growth initiation is then expected to occur simultaneously over a large width of the crack front, whereas for a tunneling crack it gradually spreads from the center of the specimen to the surface.

From Table 2 it is also seen that the J_{Ic} values determined according to ASTM E 813 (intersection point between the blunting line and a linear regression line through all points within the 0.15- and 1.5-mm offset lines) are consistently higher, by a margin of up to 40%, than the single-specimen J_{Ic} results. This is

TABLE 2—*Summary of results.*

Specimen	u_i, mm	Δa_{pd_i}, mm	SZW_i, mm[a]	Δa_e, mm[b]	Δa_{ht}, mm[c]	$(\Delta_{a_e} - \Delta_{a_{ht}})/\Delta a_{ht}$, (−)	J_i, N/mm[d]	$J_{Ic_{ss}}$, N/mm[e]	$J_{Ic_{ms}}$, N/mm[f]	$(J_{Ic_{ss}} - J_{Ic_{ms}})/J_{Ic_{ms}}$, (−)
					FATIGUE PRECRACK					
4.01	1.309	0.139	0.130	1.463	1.568	−0.07	124.8	169.3		−0.13
4.02	1.150	0.290	0.110	1.102	1.203	−0.08	106.0	159.0		−0.19
4.03	1.393	0.340	0.140	0.532	0.518	0.03	134.0	156.0		−0.20
4.05	1.142	0.261	0.106	0.434	0.387	0.12	101.5	119.9		−0.39
4.06	1.232	0.367	0.118	3.331	4.021	−0.17	112.8	176.4	195.8	−0.10
4.08[g]	...	...	...	...	1.528	...	...	...		...
4.10	1.341	0.348	0.132	1.934	2.121	−0.09	126.6	124.6		−0.36
4.11	1.250	0.269	0.120	1.034	0.967	0.07	115.4	123.5		−0.37
4.13[h]	...	...	...	...	1.632	... •	...	...		
					SPARK EROSION PRECRACK					
4.25	1.466	0.228	0.149	0.800	0.804	−0.01	142.8	178.5		−0.19
4.26	1.276	0.228	0.125	0.567	0.605	−0.06	119.2	170.0		−0.23
4.28	1.268	0.176	0.123	1.718	1.865	−0.08	118.5	188.6		−0.15
4.29	1.595	0.255	0.169	1.563	1.583	−0.01	162.1	234.6		+0.06
4.30	1.347	0.210	0.134	1.159	1.353	−0.14	128.9	189.1	221.4	−0.15
4.31	1.257	0.179	0.121	1.898	2.370	−0.20	116.4	216.3		−0.02
4.32	1.576	0.246	0.161	0.373	0.292	0.28	154.1	...		...
4.33	1.416	0.214	0.146	1.298	1.400	−0.07	140.6	204.7		−0.08
4.34	1.500	0.265	0.155	1.328	1.283	0.08	149.0	207.6		−0.06

[a]Stretched zone at initiation SZW_i taken to the blunting at initiation: $SZW_i = J_i/(2\sigma_f)$.
[b]$\Delta a_e = \Delta a_{pd_e} - \Delta a_{pd_i} + SZW_i$.
[c]Average crack extension measurement by heat tinting (including stretched zone) according to ASTM E 813.
[d]Initiation value from potential drop signal.
[e]Single-specimen J_{Ic} determined according to ASTM E 813 from potential drop R curves.
[f]Multiple-specimen J_{Ic} determined according to ASTM E 813.
[g]No initiation detectable on potential drop record.
[h]PD system failure during loading of the specimen.

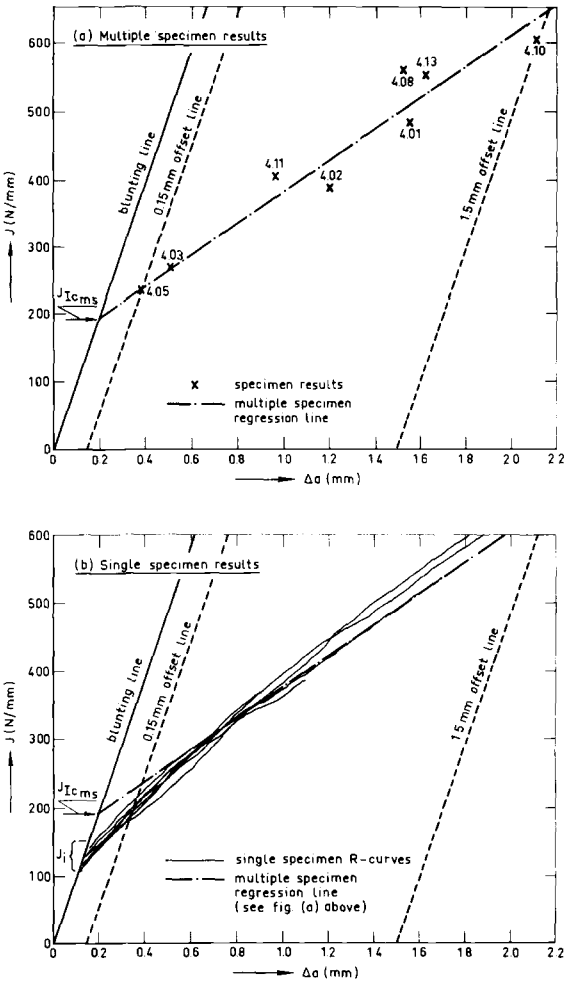

FIG. 8—*Overall comparison between single-specimen PD and multiple-specimen* J-R *curves for specimen with fatigue precrack.*

at least partly due to the fact that the single-specimen R curves have relatively far more data points at low Δa values. However, even if care is taken to have single-specimen R curves, which cover the entire range between the exclusion lines, substantial differences in estimated J_{Ic} values can still be expected because of the rather mild requirements of the ASTM multiple-specimen procedure with respect to both the number of data points (four) and their distribution (clustering paragraph in ASTM E 813).

Qualitatively the potential drop R curves of Figs. 8 and 9 agree well with those reported by the unloading compliance technique, for example, Ref *12*. The difference just noted confirms that application of the regression line values

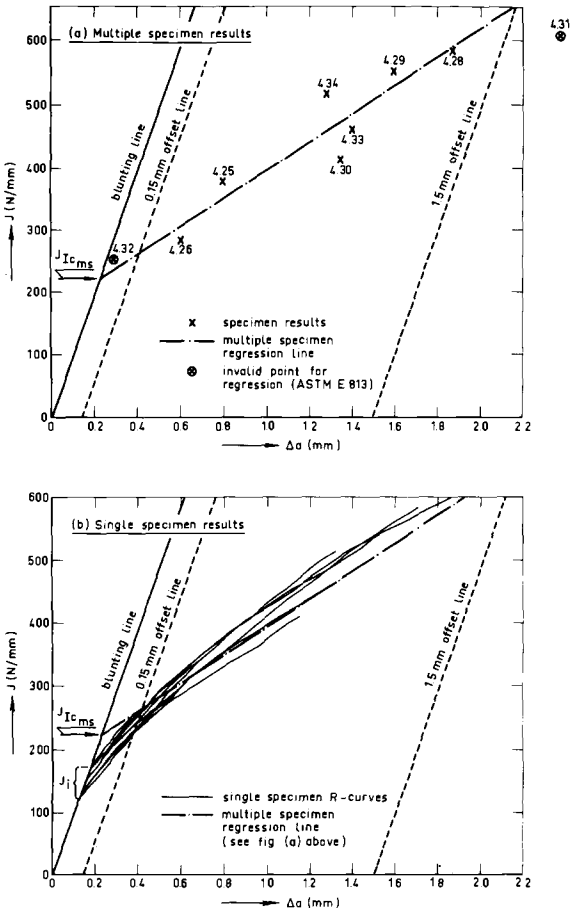

FIG. 9—*Overall comparison between single-specimen PD and multiple-specimen* J-R *curves for specimen with spark erosion precrack.*

for design implies that a small amount of stable growth is accepted. The discrepancies between the crack growth values obtained at the end of the test through heat tinting and from the potential drop signal (Δa_{ht} and Δa_e, respectively) are seen in Table 2 to be generally below 10% and believed to be mainly caused by

(1) calibration errors by violating the conditions for which the calibration Eq 1, is valid, for example, by tunneling of the crack growth and

(2) neglecting the apparent crack growth because of plastic deformation of the ligament.

If in some way, such as by specimen side grooving, the latter effect could be

shown to be the only cause for the discrepancies found, one might adopt an alternative correction procedure based on the measured crack growth at the end of the test to be denoted by Δa_{s_e}.

According to Eq 5 and still assuming $(\Delta a_v - \Delta a_{v_i}) = 0$, the correction for plastic deformation at the end of the test is

$$(\Delta a_{d_e} - \Delta a_{d_i}) = (\Delta a_{pd_e} - \Delta a_{pd_i}) - \Delta a_{s_e} \tag{7}$$

All tests with machined notches with root radius $r = 1$ mm discussed in the signal analysis section exhibited a linear potential drop signal with respect to the load-line displacement. This justifies the assumption that $(\Delta a_d - \Delta a_{d_i})$ varies linearly with the load-line displacement, starting with zero at initiation and growing up to the final value of Eq 7.

Introducing this into Eq 5 yields (Fig. 10)

$$\Delta a_s = \{\Delta a_{pd} - \Delta_{pd_i} - [(u - u_i)/(u_e - u_i)]\}(\Delta a_{pd_e} - \Delta_{pd_i} - \Delta a_{s_e}) \tag{8}$$

Further investigations on possible error sources will be required to verify the applicability of Eq 8. Adoption of this method also implies that the stretched zone is to be subtracted from the measured crack growth to obtain the real, fibrous crack growth to be used in Eq 8.

Conclusions and Recommendations

The PD method as described in this paper gave reasonable results for J_{Ic} (δ_i) and $J(\delta)$-R curves for the two SENB specimen series to which it was applied. For large crack extensions, the PD method underestimated the amount of crack

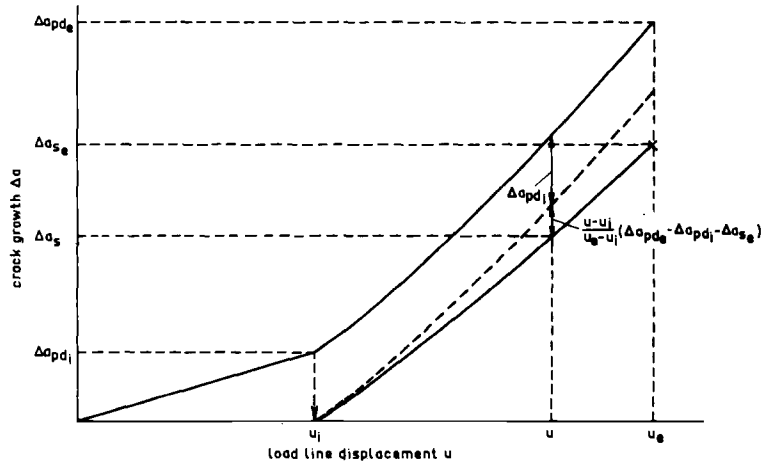

FIG. 10—*Alternative procedure for obtaining crack extensions from potential drop signals.*

growth. Most probably this is caused by tunneling of the crack, resulting in a highly curved crack front for which the effective potential drop crack length is smaller than the average crack length determined according to the nine-point procedure of ASTM E 813. This problem may perhaps be solved by the use of side-grooved specimens.

The detectability of the initiation point may be further improved by recording the potential drop directly as a function of J during the test by on-line integration of the load signal with respect to the load line displacement.

For the tests reported here, potential drop changes caused by gross plasticity and geometrical changes appeared to be negligible. Further tests on other materials are required to verify the general applicability of this finding. Failing this, a correction procedure for the apparent crack growth caused by these phenomena will have to be applied. If side grooving solves the problem of calibration, the alternative method described in the discussion section might offer an approach to deal with the plasticity and geometrical change effects.

Acknowledgments

The work described in this paper was partly sponsored by The Netherlands Ministry of Economic Affairs as part of the cooperative research program, BROS.

The author is indebted to Mr. Franken (former graduate student), Mr. Hartevelt, and Mr. Gerbrands for their care and skill in performing the experiments, and to Mr. De Groot for his contribution to the computer aided data processing and to Professor Latzko for his support and stimulating discussions.

References

[1] Landes, J. D. and Begley, J. A., "Test Results from J-Integral Studies: An Attempt to Establish a J_{Ic} Testing Procedure," *Fracture Analysis, Proceedings of the 1973 National Symposium on Fracture Mechanics, Part II, STP 560*, American Society for Testing and Materials, Philadelphia, 1974, pp. 170–186.

[2] Shih, C. F., Delorenzi, H. G., and Andrews, W. R., "Studies on Crack Initiation and Stable Crack Growth," *Elastic-Plastic Fracture, STP 668*, American Society for Testing and Materials, Philadelphia, 1979, pp. 65–120.

[3] Kanninen, M. F., Rybicki, E. F., Stonesifer, R. B., Broek, D., Rosenfield, A. R., Marschall, C. W., and Hahn, G. T., "Elastic-Plastic Fracture Mechanics for Two-Dimensional Stable Crack Growth and Instability Problems," *Elastic-Plastic Fracture, STP 668*, American Society for Testing and Materials, Philadelphia, 1979, pp. 121–150.

[4] Clark, G. A., Andrews, P. C., Paris, P. C., and Schmidt, D. W., "Single Specimen Tests for J_{Ic} Determination," *Mechanics of Crack Growth, STP 590*, American Society for Testing and Materials, Philadelphia, 1976, pp. 27–42.

[5] Beevers, C. J., Ed., *The Measurement of Crack Length and Shape During Fracture and Fatigue*, EMAS Ltd, Warely (West Midlands), United Kingdom, 1980.

[6] Blauel, J. G., "Experimental Techniques for the Determination of the Initiation of Failure," in *Advances in Elasto-Plastic Fracture Mechanics*, L. H. Larsson, Ed., Applied Science Publishers, Ltd., London, United Kingdom, 1980, pp. 65–90.

[7] Schwalbe, K. H., "Test Techniques," *Proceedings of the 5th International Conference on Fracture (ICF5)*, Program Press, Oxford, United Kingdom, 1981, pp. 1421–1446.

[8] Johnson, H. H., "Calibration of the Electric Potential Method for Studying Slow Crack Growth," Material Research and Standards, Vol. 5, No. 9, 1965, pp. 442–445.

[9] Lowes, J. M., and Fearnehough, G. D., "The Detection of Slow Crack Growth in Crack Opening Displacement Specimens Using an Electrical Potential Method," *Engineering Fracture Mechanics*, Vol. 3, No. 2, 1971, pp. 103–108.

[10] Yin, S. W., Gerbrands, R. A., and Hartevelt, M., "An Investigation of the Blunting Line," *Engineering Fracture Mechanics*, Vol. 18, No. 5, 1983, pp. 1025–1036.

[11] Buzzard, R. J., and Fisher, D. M., "Load Displacement Measurements and Work Determination in Three-Point Bend Tests of Notched or Precracked Specimens," *Journal of Testing and Evaluation*, Vol. 6, No. 1, 1978, pp. 35–39.

[12] Loss, F. J., "Structural Integrity of Water Reactor Pressure Boundary Components," NRL Quarterly Progress Report, April-June 1980, Washington DC, 1981.

Workshop Discussion

Karl-Heinz Schwalbe[1] *and Jürgen Heerens*[1]

Suggestions for a Modification of ASTM E 813*

REFERENCE: Schwalbe, K.-H. and Heerens, J., "**Suggestions for a Modification of ASTM E 813,**" *Elastic-Plastic Fracture Test Methods: The User's Experience, ASTM STP 856,* E. T. Wessel and F. J. Loss, Eds., American Society for Testing and Materials, 1985, pp. 411–416.

ABSTRACT: Some modifications of the present procedure for the determination of J_{Ic} are proposed to ensure better consistency of data. A new blunting line is proposed, which takes advantage of recent theoretical work concerning the crack-tip behavior and which shows good agreement with fractographical data. J_{Ic} is that point on the initial part of the R curve that is determined by the intersection of the R curve with an intercept line parallel to and by an amount Δa^* off the blunting line.

KEY WORDS: crack propagation, fracture tests, toughness, J integral

The present procedure for the determination of J_{Ic} (ASTM Test Method for J_{Ic}, a Measure of Fracture Toughness) fits a straight line through experimental data points between two exclusion lines (Fig. 1). Measurement of crack extension Δa below 0.15 mm are excluded by the lower exclusion line. The intersection of the straight line with the blunting line is defined as J_{Ic}, which is supposed to represent a measure of the material's behavior near initiation. This construction has the following consequences:

- J_{Ic} characterizes a point off the true material behavior since the R curve often exhibits a sharp curvature near initiation.

[1]Head of department and research engineer, respectively, GKSS Research Center Geesthact, 2054 Geethacht, Federal Republic of Germany.

*Note: ASTM Test Method for J_{Ic}, a Measure of Fracture Toughness (E 813).

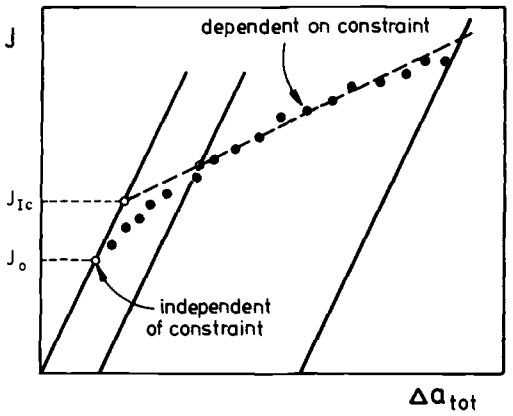

FIG. 1—*Present* J_{Ic} *procedure.*

- J_{Ic} is, by an undefined amount, larger than the true initiation point, J_o, for which $\Delta a \rightarrow 0$.[2]
- J_{Ic} can exhibit a large size effect even if the true material behavior remains unaffected, Fig. 13 in a previous paper.[2] Because of the range of valid data shrinking with decreasing specimen size and the curved shape of the J-Δa data the straight line fit results in increasing slope and hence decreasing J_{Ic} (Fig. 2). As a result of the straight-line fit, the R curve points far beyond initiation control, a quantity J_{Ic} that should represent the material behavior close to initiation.

These drawbacks can be easily avoided by adopting the following modifications: If J_{Ic} is supposed to characterize the material's initiation toughness then, from a fundamental point of view, it should be set equal to the true initiation point J_o, as proposed by the Japanese J_{Ic} test standard.[3] This would have the advantage that the initiation point is largely independent of geometric variables [*1*,*2*] (Fig. 3).

On the other hand, although the determination of J_o as a measure of initiation toughness is desirable from a physical point of view, it seems to be unsuitable for a test standard for the following reasons:

- The determination of a condition for which $\Delta a \rightarrow 0$ is very costly; it requires a scanning electron microscope (SEM) since measurements of very minute amounts of crack growth must be done.
- The meaning of J_o is not well defined for materials that do not behave well.

[2]Schwalbe, K.-H., Hellmann, D., Heerens, J., Knaack, J., and Müller-Roos, J., this publication, pp. 338–362.

[3]Kobayashi, H., Nakamura, H., and Nakazawa, J., this publication, pp. 3–22.

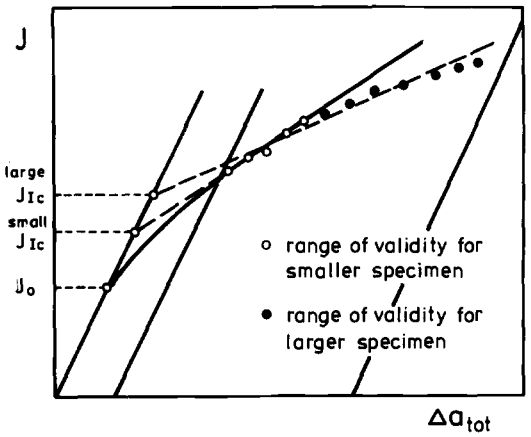

FIG. 2—*Slope change of best-fit straight line caused by different data range, resulting in different* J_{Ic} *values in spite of identical* R *curve data.*

Therefore, it seems reasonable to define initiation toughness at a finite specified amount of crack growth Δa^*, say 0.2 mm. By this compromise, J_{Ic} is defined as a point on the real R curve close enough to initiation that no large size effects are to be expected.

In principle, crack growth can be measured in two ways:

1. Indirect measurements such as the partial unloading technique or the potential drop technique (single specimen methods). In this case Δa_{tot} is measured, that is, ductile tearing plus crack-tip blunting (Fig. 4*a*).
2. Direct measurements on the fracture surface. In this case several specimens are needed to determine the R curve (multiple-specimen method). It is proposed that crack growth should be measured including blunting, as is done by the indirect measurements.

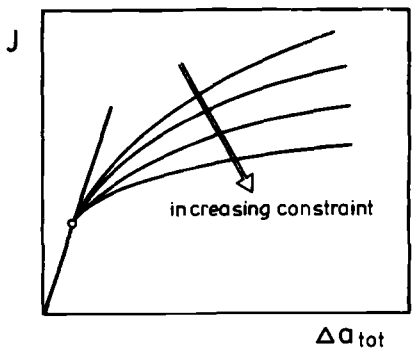

FIG. 3—*Influence of constraint on* R *curve shape,* J_o *remaining constant.*

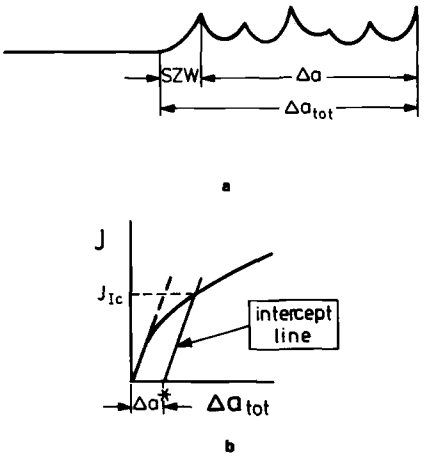

FIG. 4—(a) *Measurement of crack growth with single- and multiple-specimen methods.* (b) *Determination of a modified* J_{Ic} *with single- and multiple-specimen method.*

In any case, J_{Ic} would be the ordinate of the intersection of the R curve with the interception line, which is a straight line parallel to and Δa^* mm off the blunting line (Fig. 4*b*).

It is known that the recommended blunting line $J = 2\sigma_F \Delta a$ is not always strictly representative of the true blunting line. Recent investigations [*3*] show that the formula

$$J = \text{SZW}\ \sigma_0/0.4d_n$$

gives a good prediction of the stretch zone width (SZW) during the blunting phase. σ_0 characterizes the yield strength and *dn* gives the relation between J and δ_t as defined by Shih [*4*]. Thus it should be considered that a blunting line

$$J = \Delta a \sigma_0/0.4d_n$$

gives a better assessment of the true crack-tip blunting than the equation $J = 2\sigma_F \Delta a$.

The use of the single-specimen method is preferable since scatter or systematic variation of material properties in a given piece of material is better reflected by several individual R curves than by data points scattering around an average R curve.

Additional Remarks

Close to the origin of the R curve, the Δa measurements must be sufficiently accurate to ensure that the variability in J_{Ic} is not unduly high (Fig. 5). It is believed that an accuracy of $\pm 0.5\Delta a^*$ or $\pm 10\%$ (whichever is greater) is a reasonable requirement.

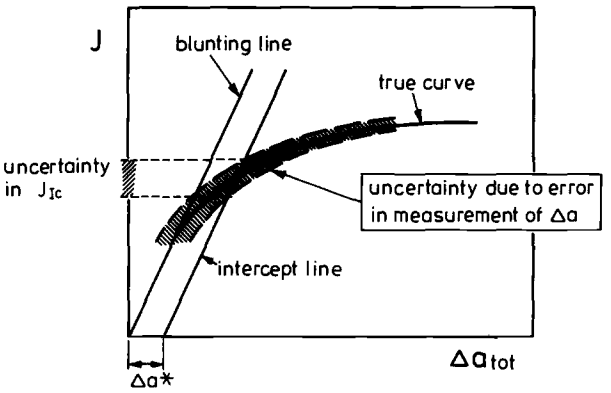

FIG. 5—*Error in J_{Ic} caused by error in measurement of* Δa.

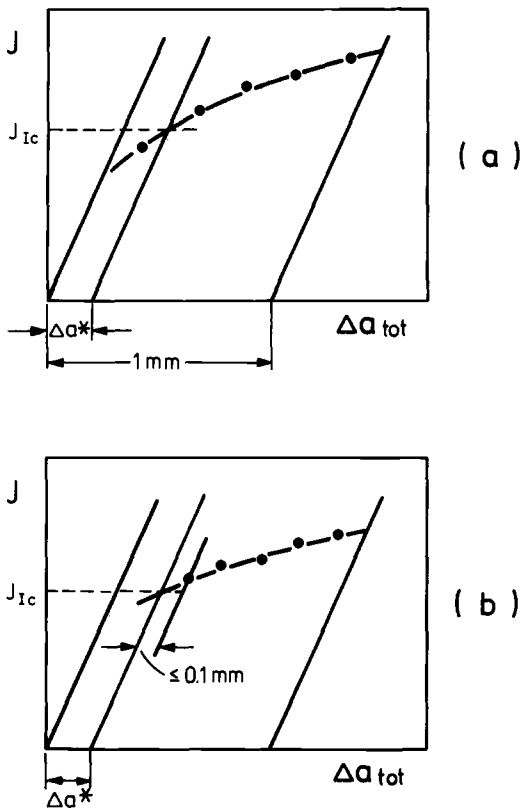

FIG. 6—*Data point requirements for single-specimen method:* (a) *five data points with at least one point left of the intercept line and* (b) *extrapolation allowed if first point is no more than 0.1 mm off the intercept line.*

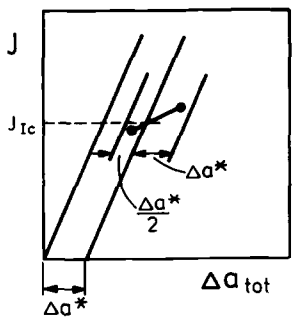

FIG. 7—*Two data points on either side of the intercept line should allow for an estimate of* J_{Ic}.

To determine a valid J_{Ic} value, a minimum amount of data points is necessary that must meet certain requirements. In the case of the single-specimen method, five points taken from the test record are believed to suffice. These should be as evenly distributed as possible over the range shown in Fig. 6*a*. At least one point should be positioned to the left of the intercept line. This specimen must clearly show ductile tearing. If this latter requirement cannot be met an extrapolation of the *R* curve towards the intercept line is allowed if the minimum value of Δa measured is ≤ 0.1 mm off the intercept line (Fig. 6*b*).

Although there is insufficient experience to support the following statement, it should be possible to make a reasonable estimate of J_{Ic} by only two data points if these points lie on either side of the intercept line in the region shown by Fig. 7.

We wish to point out that the comments made previously are being pursued further to substantiate the various statements by as much experimental evidence as possible.

References

[*1*] Schwalbe, K.-H., "Influence of Stress State on Static Crack Growth in AlZnMgCu0.5," *Engineering Fracture Mechanics,* Vol. 9, 1977, pp. 557–583.

[*2*] Schwalbe, K.-H., "Some Properties of Stable Crack Growth," *Engineering Fracture Mechanics,* Vol. 11, 1979, pp. 331–342.

[*3*] Heerens, J. and Schwalbe, K.-H., Gedanken zur Modifizierung des J_{Ic}-Versuches, 16th Annual Meeting of the German Fracture Group, 21–22 Feb. 1984, Karlsruhe, Federal Republic of Germany.

[*4*] Shih, C. F., "Relationship Between the *J*-integral and Crack Opening Displacement for Stationary and Extending Cracks," Report 79CR0075, General Electric, Schenectady, NY, 1979.

Summary

The Symposium on User's Experience with Elastic-Plastic Fracture Toughness Test Methods highlighted the strong worldwide interest in and the associated need for standard test methods for characterizing the fracture behavior of materials in the elastic-plastic behavior regime. The presentations were very successful in terms meeting the primary objectives of assessing the current state of the art, identifying the problems and limitations associated with currently used test methods, describing new experimental techniques and procedures, and highlighting areas requiring further investigation leading to improved methods and procedures. Major points arising from the symposium are as follows.

ASTM E 813-81

The current version of ASTM Test Method for J_{Ic}, a Measurement of Fracture Toughness (E 813-81) has several areas where some modifications and improvements are necessary. The major areas requiring further investigation leading to improvements in the test method involve measurement point definition and all related aspects, specimen size, and geometry considerations; multiple-specimens versus single-specimen techniques; proper calculations of J; equivalency of J_{Ic} with other fracture toughness parameters, that is, crack-tip opening displacement (CTOD); limitations relative to very high toughness materials; and necessary modifications to the present text.

J-R Curves

There is a dire need to be able to characterize a materials resistance to stable, ductile, crack growth (that is, J or CTOD R-curves) over a range of significant amounts of ductile crack extension (greater than that currently permitted in E 813). While there has already been considerable activity in the area of developing a test method for *J-R* curves, as described in ASTM *Journal of Testing and Evaluation*, Vol. 10, No. 6, Nov. 1982, further accelerated effort is needed to develop an ASTM Standard Test Method as rapidly as possible. It is quite apparent that ultimately a single test method for measuring both J_{Ic} and *J-R* curves is desirable. Therefore during the continuing efforts to improve the existing method for J_{Ic} (E 813) and *J-R* curves, appropriate consideration should be given to the feasibility of ultimately developing a single standard test method

that would facilitate the measurement of the complete *J-R* curve including the initiation parameter of J_{Ic}. This new combined method would then supercede the E 813 method.

Ductile to Brittle Transition Region

There is no ASTM fracture mechanics test method that is generally applicable for materials that exhibit a ductile to brittle transition behavior. While ASTM Test Method for Plane Strain Fracture Toughness of Metallic Materials (E 399) is applicable to this ductile to brittle transition temperature region for those cases where the section size of practical interest is sufficient to satisfy the E 399 size requirements, there are however many instances where the section size of practical concern is not adequate to satisfactorily measure K_{Ic}, especially in the upper portions of the transition range. In addition the overall specimen size to satisfy ASTM E 399 requirements for most of the rougher materials of interest is so large as to present severe practical and economical problems in conducting E 399 (K_{Ic}) tests. ASTM E 813 Test Method for J_{Ic} fracture toughness is currently limited to temperature above the ductile to brittle transition region and is therefore not applicable. The symposium emphasized there was a dire need for a new test method for this transaction region, and therefore ASTM Committee E-24 on Fracture Testing should aggressively pursue the rapid development of a suitable new test method for fracture toughness measurements within this transition temperature region. Presentations and discussion at the symposium also suggested that CTOD tests of full section thickness interpreted in terms of equivalent *J* offer some promise as viable test methods for this temperature region.

Commonality of All Fracture Mechanics Test Methods

Ultimately, it appears desirable to have a single test method encompassing all of the pertinent fracture toughness parameter measurements (that is, J_{Ic}, *J-R* curves, CTOD, and K_{Ic}). The consensus of the symposium participants was that the feasibility of developing such a common test method should be given appropriate consideration at this time.

Major Accomplishments of Symposium

The symposium provided a unique opportunity for representatives of several countries to present and discuss their experiences and viewpoints relative to various test methods involving the characterization of the elastic-plastic fracture behavior of materials. This has resulted in a much stronger relationship and increased cooperation and collaboration between ASTM Committee E-24 and overseas groups concerned with elastic-plastic fracture mechanics test methods development, in particular the European group on fracture.

Several key areas where existing methods need modification and improvement were identified. Subsequent to the symposium many participants have provided

specific, detailed, technical suggestions, and recommendation that will substantially enhance and accelerate the preparation of improved ASTM test methods.

The symposium also highlighted the need for new test methods in specific areas, and as a result, ASTM Committee E-24 has taken appropriate action to address these areas.

E. T. Wessel
Westinghouse R&D Center, Pittsburgh, PA 15235, symposium cochairman and coeditor

F. J. Loss
Materials Engineering Associates, Lanham, MD 20706, symposium cochairman and coeditor

Index

ISBN 0-8031-0419-7